AD-A239 194

DOCUMENTATION PAGE

Form Approved
OMB No. 0704-0188

1. AGENCY USE ONLY	2. REPORT DATE	3. REPORT TYPE AND DATES COVERED
	July 1991	Final report 1 - 3 Jul 85

4. TITLE AND SUBTITLE
INTERNATIONAL CONFERENCE POST FAILURE ANALYSIS TECHNIQUES FOR FIBER REINFORCED COMPOSITES

5. FUNDING NUMBERS
PE 62102F
PR 2418
TA 04
WU 31

6. AUTHOR(S)
FRANK FECHEK, COMPILER

7. PERFORMING ORGANIZATION NAME(S) AND ADDRESS(ES)
Stouffers Dayton Plaza Hotel
Dayton, Ohio

8. PERFORMING ORGANIZATION REPORT NUMBER
UDR-TR-91-32

9. SPONSORING/MONITORING AGENCY NAME(S) AND ADDRESS(ES)
Frank Fechek (513) 255-2484
Materials Directorate (WL/MLSE)
Wright Laboratory
Wright-Patterson AFB, Ohio 45433-6543

10. SPONSORING MONITORING AGENCY REPORT NUMBER
WL-TR-91-4074

11. SUPPLEMENTARY NOTES

12a. DISTRIBUTION/AVAILABILITY STATEMENT
Approved for public release; distribution is unlimited.

12b. DISTRIBUTION CODE

13. ABSTRACT (Maximum 200 words)
Although a failure analysis protocos of sequence of analysis techniques has evolved over many years for metal structures, none such exists for high performance composite structures, which technology is relatively young. This First International Conference was convened to assemble technologists working in the fields of composite testing, resin chemistry, inspection and analysis techniques, surface analysis, and structural property prediction and measurement in order to create a foundation of information upon which to construct a protocol for the failure analysis of high performance composites. The Conference Consisted of Five Sessions entitled:—

Con-1 Pg.

14. SUBJECT TERMS

15. NUMBER OF PAGES
488

16. PRICE CODE

17. SECURITY CLASSIFICATION OF REPORT	18. SECURITY CLASSIFICATION OF THIS PAGE	19. SECURITY CLASSIFICATION OF ABSTRACT	20. LIMITATION OF ABSTRACT
Unclassified	Unclassified	Unclassified	unlimited

NSN 7540-01-280-5500

GENERAL INSTRUCTIONS FOR COMPLETING SF 298

The Report Documentation Page (RDP) is used in announcing and cataloging reports. It is important that this information be consistent with the rest of the report, particularly the cover and title page. Instructions for filling in each block of the form follow. It is important to ***stay within the lines*** to meet ***optical scanning requirements***.

Block 1. Agency Use Only *(Leave blank)*.

Block 2. Report Date. Full publication date including day, month, and year, if available (e.g. 1 Jan 88). Must cite at least the year.

Block 3. Type of Report and Dates Covered. State whether report is interim, final, etc. If applicable, enter inclusive report dates (e.g. 10 Jun 87 - 30 Jun 88).

Block 4. Title and Subtitle. A title is taken from the part of the report that provides the most meaningful and complete information. When a report is prepared in more than one volume, repeat the primary title, add volume number, and include subtitle for the specific volume. On classified documents enter the title classification in parentheses.

Block 5. Funding Numbers. To include contract and grant numbers; may include program element number(s), project number(s), task number(s), and work unit number(s). Use the following labels:

C	- Contract	**PR**	- Project
G	- Grant	**TA**	- Task
PE	- Program Element	**WU**	- Work Unit Accession No.

Block 6. Author(s). Name(s) of person(s) responsible for writing the report, performing the research, or credited with the content of the report. If editor or compiler, this should follow the name(s).

Block 7. Performing Organization Name(s) and Address(es). Self-explanatory.

Block 8. Performing Organization Report Number. Enter the unique alphanumeric report number(s) assigned by the organization performing the report.

Block 9. Sponsoring/Monitoring Agency Name(s) and Address(es). Self-explanatory.

Block 10. Sponsoring/Monitoring Agency Report Number. *(If known)*

Block 11. Supplementary Notes Enter information not included elsewhere such as: Prepared in cooperation with . ; Trans. of. , To be published in.... When a report is revised, include a statement whether the new report supersedes or supplements the older report.

Block 12a. Distribution/Availability Statement. Denotes public availability or limitations. Cite any availability to the public. Enter additional limitations or special markings in all capitals (e.g. NOFORN, REL, ITAR).

- **DOD** - See DoDD 5230.24, "Distribution Statements on Technical Documents."
- **DOE** - See authorities.
- **NASA** - See Handbook NHB 2200.2.
- **NTIS** - Leave blank.

Block 12b. Distribution Code.

- **DOD** - Leave blank.
- **DOE** - Enter DOE distribution categories from the Standard Distribution for Unclassified Scientific and Technical Reports.
- **NASA** - Leave blank.
- **NTIS** - Leave blank.

Block 13. Abstract. Include a brief *(Maximum 200 words)* factual summary of the most significant information contained in the report.

Block 14. Subject Terms. Keywords or phrases identifying major subjects in the report.

Block 15. Number of Pages. Enter the total number of pages.

Block 16. Price Code. Enter appropriate price code *(NTIS only)*.

Blocks 17. - 19. Security Classifications. Self-explanatory. Enter U.S. Security Classification in accordance with U.S. Security Regulations (i e , UNCLASSIFIED). If form contains classified information, stamp classification on the top and bottom of the page.

Block 20. Limitation of Abstract. This block must be completed to assign a limitation to the abstract. Enter either UL (unlimited) or SAR (same as report). An entry in this block is necessary if the abstract is to be limited. If blank, the abstract is assumed to be unlimited.

DISCLAIMER NOTICE

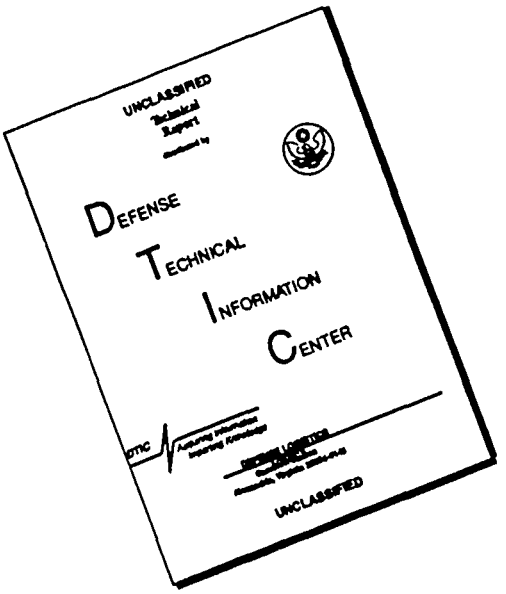

THIS DOCUMENT IS BEST QUALITY AVAILABLE. THE COPY FURNISHED TO DTIC CONTAINED A SIGNIFICANT NUMBER OF PAGES WHICH DO NOT REPRODUCE LEGIBLY.

SECURITY CLASSIFICATION _____

WL-TR-91-4074

INTERNATIONAL CONFERENCE: POST FAILURE ANALYSIS TECHNIQUES FOR FIBER REINFORCED COMPOSITES

Frank Fechek

Stouffers Dayton Plaza Hotel
Dayton, Ohio

July 1991

Final report for period Jul 1985

MATERIALS DIRECTORATE
WRIGHT LABORATORY
AIR FORCE SYSTEMS COMMAND
WRIGHT-PATTERSON AIR FORCE BASE, OHIO 45433-6533

NOTICE

When Government drawings, specifications, or other data are used for any purpose other than in connection with a definitely Government-related procurement, the United States Government incurs no responsibility or any obligation whatsoever. The fact that the government may have formulated or in any way supplied the said drawings, specifications, or other data, is not to be regarded by implication, or otherwise in any manner construed, as licensing the holder, or any other person or corporation; or as conveying any rights or permission to manufacture, use, or sell any patented invention that may in any way be related thereto.

This report is releasable to the National Technical Information Service (NTIS). At NTIS, it will be available to the general public, including foreign nations.

This technical report has been reviewed and is approved for publication.

FRANK FECHEK, Project Engineer
Materials Behavior and Evaluation Grp
Materials Engineering Branch
Systems Support Division

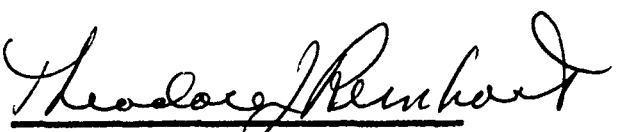

THEODORE J. REINHART, Chief
Materials Engineering Branch
Systems Support Division

FOR THE COMMANDER

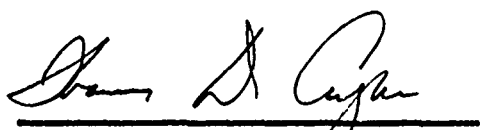

THOMAS D. COOPER, Chief
Systems Support Division
Materials Directorate

If your address has changed, if you wish to be removed from our mailing list, or if the addressee is no longer employed by your organization please notify WL/MLSE , WPAFB, OH 45433-6533 to help us maintain a current mailing list.

Copies of this report should not be returned unless return is required by security considerations, contractual obligations, or notice on a specific document.

PREFACE

High performance fiber reinforced composites are being selected in increasing amounts as structures in the design of each successive military and civilian aircraft. These materials are also finding increased application in land transportation vehicles, space structures, and numerous other applications where high strength and stiffness to weight ratio materials are needed. This increased usage will undoubtedly result in more frequent occurrences of part failure resulting in the need to analyze the failed part and determine the cause of failure. In the case of metallic structures, the analytical techniques and procedures available for determining the cause of failure are quite well developed. The technology for composite structure post-failure analysis is not as mature, however. Although many individuals have applied selected analysis techniques and procedures to failed composite structures, with varying degrees of success, there still remains an absence of a systematic collection of techniques and procedures which are widely accepted for use in conducting a composite post-failure analysis.

In light of the above, the sponsors of this conference considered it timely that an open forum be created which would both facilitate an exchange of ideas by those working with techniques and procedures directly related to the post-failure analysis of composite structures and provide those participants an opportunity to report on the progress of their efforts.

This report contains the text of the papers which were presented at this conference along with a transcript of the question and answer session which constituted the closing session of this meeting.

INDEX

Session I
FAILURE MECHANISMS

FAILURE MECHANICS STUDIES IN COMPOSITES

Wolfe Elber and T. O'Brian
Materials Division
NASA Langley Research Center
Hampton, Virginia

(Paper unavailable)

TESTING UNDER COMPLEX LOADING TO AID ANALYSIS OF FAILURE IN FIBROUS COMPOSITES

A.S. Wronski and T.V. Parry
Engineering Materials Research Group
University of Bradford
Bradford, West Yorkshire, England

TESTING UNDER COMPLEX LOADING TO AID ANALYSIS OF FAILURE IN FIBROUS COMPOSITES

A. S. Wronski, T. V. Parry*

Engineering Materials Research Group, University of Bradford,
W. Yorks. BD7 1DP, England.

ABSTRACT

The mechanisms of failure in axial tension and compression of unidirectional ∿60% volume fraction glass and carbon fibre reinforced epoxy resin composites have been investigated at atmospheric and under superposed hydrostatic pressures extending to 350 MNm^{-2}. Experiments under pressure enable the discrimination between mechanisms operated by tensile and compressive stresses, eg in fibres, on the one hand, and by shear stresses, eg in matrices, on the other.

The atmospheric tensile strengths, σ_t, of the glass and the carbon fibre composites were ∿1.7 GNm^{-2} and ∿2.0 GNm^{-2} respectively, compared to values of ∿1.2 GNm^{-2} and ∿1.5 GNm^{-2} for their respective strengths in compression, σ_c. In tension failure initiated as the debonding between bundles of fibres containing prior curvature at ∿1.2 GNm^{-2} at atmospheric pressure for carbon fibre composite and at ∿0.95 GNm^{-2} for the glass fibre reinforced material. The second stage of failure in both CFRP and GRP was bundle detachment: the growth of (transverse) cracks parallel to the fibre direction under increasing load, leading to the de-coupling of fibre bundles. This process was impeded by the application of pressure and was totally suppressed in CFRP beyond 150 MNm^{-2} and just detectable in GRP at 350 MNm^{-2}. Below these limits load redistribution between fibre bundles, as fibre breaks developed, became increasingly more difficult, resulting in a decrease in composite stress at which the final stage, crack propagation, occurred.

In compression two stages of the failure process could be identified due to their different pressure dependences. Matrix yielding or splitting between regions of maximum curvature of deformed fibre bundles controlled the failure of GRP over the entire pressure range investigated and for CFRP beyond 150 MNm^{-2}. For both materials σ_c increased to ∿2.0 GNm^{-2} at 300 MNm^{-2} superposed pressure. At pressures inferior to 150 MNm^{-2} kink-initiated compression failure in CFRP was controlled by an Euler bundle buckling condition. This is relatively unaffected by pressure and only at higher pressures did matrix yielding become more difficult than bundle buckling, resulting in the strong pressure dependence.

This model has been used to interpret deformation and fracture behaviour of CFRP beams loaded under superposed pressure and the so-called interlaminar shear strength was related to the compressive stress required to satisfy the matrix yielding criterion. It can also predict the compressive strength of woven carbon fibre cloth laminate in which a transition from Euler buckling to matrix yielding controlled failure at atmospheric pressure with decreasing gauge length has been observed.

---

* from 1 September 1985 at the Department of Engineering, University of Durham, England.

INTRODUCTION

Stress-strain and failure characteristics of all materials tend to be obtained using simple stress systems, eg uniaxial tension and compression, torsion and bending. In service, components are generally subjected to complex stress systems, which implies the need, at least in certain circumstances, for biaxial and triaxial testing. If the stress system can be conveniently split into deviatoric and hydrostatic components, mechanical testing under superposed hydrostatic pressure can provide valuable information on the mechanical behaviour of the structure or component. Earliest reported work of this character dates from the nineteenth century and the greatest contribution in the field of high pressure mechanical behaviour of solids has been made by Bridgman[1].

Results of tests under superposed hydrostatic pressure enable the identification or elimination of mechanisms postulated as responsible for particular stages of the failure process, especially if the mechanism can be clearly identified as shear stress or tensile stress-controlled. Let us illustrate the thesis with reference to the trivial case of an isotropic solid under an uniaxial tensile stress, σ_A. The principal stresses are thus:

$$\sigma_1 = \sigma_A$$

$$\sigma_2 = 0$$

$$\sigma_3 = 0$$

and the maximum shear stress:

$$\tau_{max} = \frac{\sigma_1 - \sigma_3}{2} = \frac{\sigma_A}{2}$$

If hydrostatic pressure H is superposed:

$$\sigma_1 = \sigma_A + H$$

$$\sigma_2 = H$$

$$\sigma_3 = H$$

and $$\tau_{max} = \frac{\sigma_A + H - H}{2} = \frac{\sigma_A}{2}$$

ie the shear stress has been unaffected, but the principal stresses have been directly influenced by the application of H. Thus shear stress-operated

mechanisms, such as yielding in metals, are unaffected by H, whereas processes dependent on tensile stress, eg crack propagation, are directly affected as the nett normal stress is reduced to σ_A+H, and has to be increased, by |H| if other conditions are unchanged, for the process to operate.[2] It should be added that no uniformity exists in the literature regarding quoting principal rather than applied or superposed stresses. The present authors use principal and applied, σ_A, stresses and the convention of tensile stresses being positive, thus when σ_A is applied in a hydrostatic environment, H, the maximum principal stress is reduced to σ_A+H.

In our experiments we have conducted tests in uniaxial tension, uniaxial compression and bending using various test specimen geometries. If the applied force is directly determined, the shear stresses are related only to it and specimen geometry as in atmospheric pressure tests, but all the tensile stresses, produced by bending as well as tension, are reduced by |H| and all the compressive stresses increased by |H| when H is superposed on the testing environment.

TESTING UNDER COMPLEX LOADING

Testing under superposed pressure, provided by a suitable fluid, involves adding a pressure cell to a conventional mechanical properties tester or building a suitable straining device inside a pressure cell. Accurate force measurements necessitate the use of internal load cells, specially constructed as pressure affects strain gauges. External load sensing is complicated by friction effects and the requirement to compensate for the "extrusion force" on the tie bar. It can be suppressed by the use of a yoke and dummy rod on which an equal and opposite force to that on the tie bar is exerted by the pressurising fluid (Fig.1).

For all our tests we have used a Hedeby Universal Tester on to the lower crosshead of which was bolted a 3 kilobar (300 MNm^{-2}) Coleraine pressure cell. The yoke and dummy rod arrangement was always used and special jigs were built for tension (Fig.1), compression and bend testing. These have been described in the literature[3-5], but, to illustrate high pressure techniques, testing in 3- and 4-point bending, with spans up to 25mm, will be briefly described.

Compared with the uniaxial test illustrated in Fig.1, the cylindrical yoke assembly is replaced by one of rectangular section through which the load cell

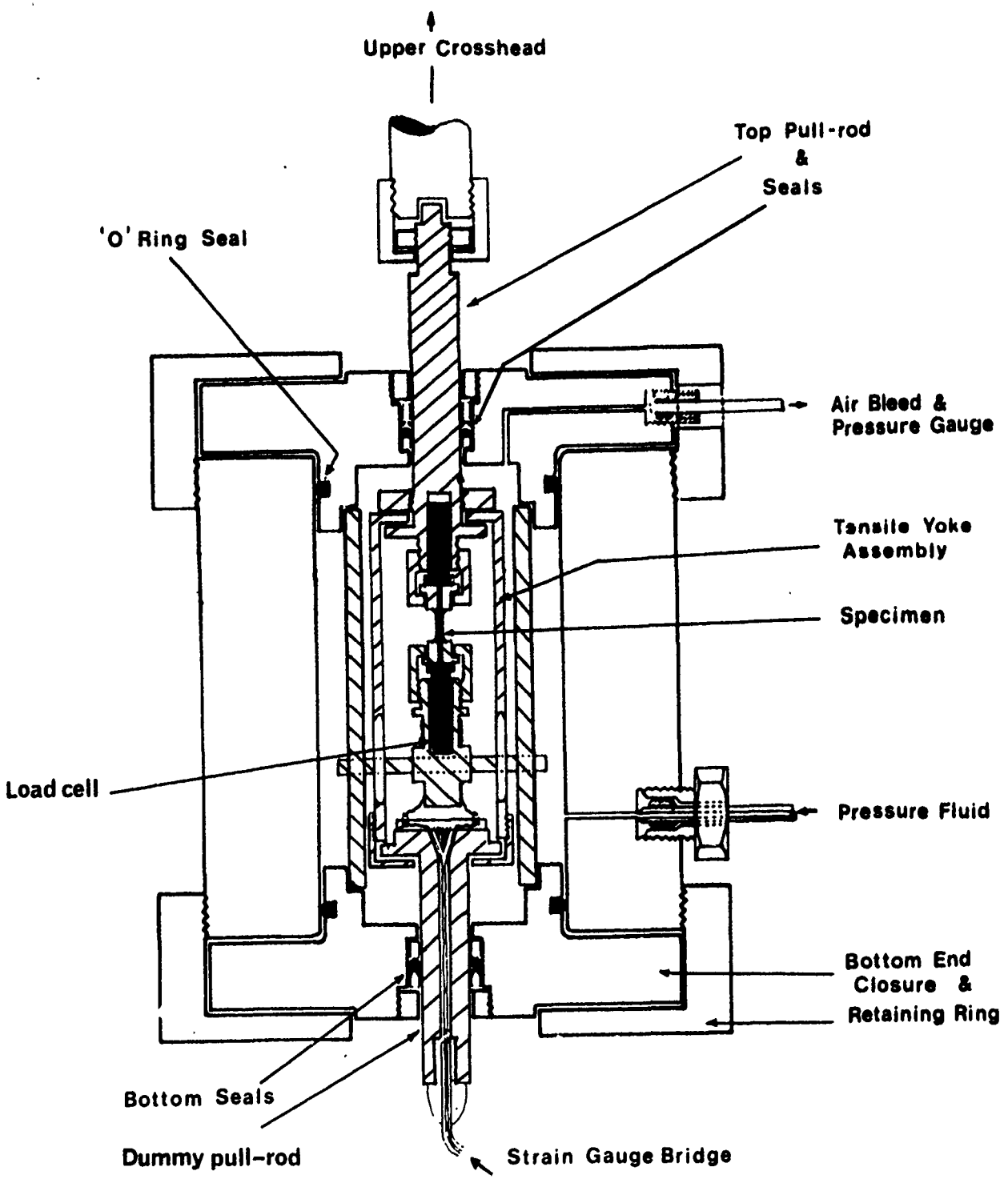

Fig. 1 Block diagram (not to scale) of Coleraine pressure cell. The cylinder is 200mm high and 130mm outside and 575mm inside diameter; pull-rods are 9.50mm in diameter.

and loading roller(s) attachment are connected to the upper pull-rod. The outer cylinder is replaced by a bar of the same length and diameter, but with a machined channel through which the yoke slides (Fig.2). It contains the two supporting rollers and exposes a hole perpendicular to the channel through which the specimen is fitted. An important feature of this arrangement[5] is that bending takes place when the machine operates in the tensile mode, which reduces alignment problems.

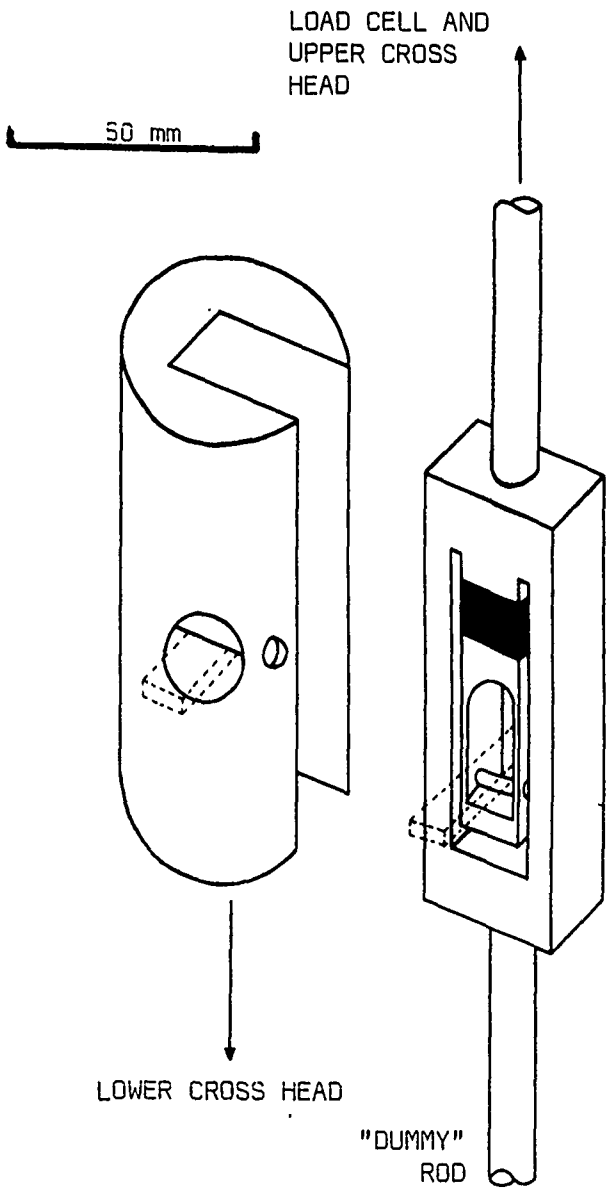

Fig.2. A sketch of the components of the flexural testing jig prior to assembly, insertion of the beam specimen (indicated in relation to the loading rollers in both components) and incorporation into the pressure cell.

The load is measured using an internal resistance load cell; and monitored with the aid of the external (machine) load cell which registers the sum of applied load and frictional forces at the pull and dummy rods.

Liquids are safer as pressurizing media; pentane/isopentane mixtures have been used successfully for pressures superior to 3 GNm^{-2} at ambient temperatures. For lower pressures, to increase safety and minimize leaks, oils, with higher viscosities, are generally employed; we use 'Plexol', a synthetic diester.

ATMOSPHERIC MECHANICAL PROPERTIES

Space and travel within pressure cells are generally limited[5] and therefore miniature specimens are frequently employed. For tensile testing we tend to use round test pieces with gauge diameters in the range 1-2mm. It was not practicable to test under pressure the more recognized designs of compression test pieces and we used a "dog bone" design illustrated in Fig.3(a). To allow comparison, samples of CFRP were made to our and RAE[6] (Fig.3(b)) designs and tested at atmospheric pressure. For a 60% V_f Grafil A-S/epoxide pultrusion[4] the latter specimens failed at 1.30±0.07 GNm^{-2}, whereas the former at 1.33±0.15 GNm^{-2}.

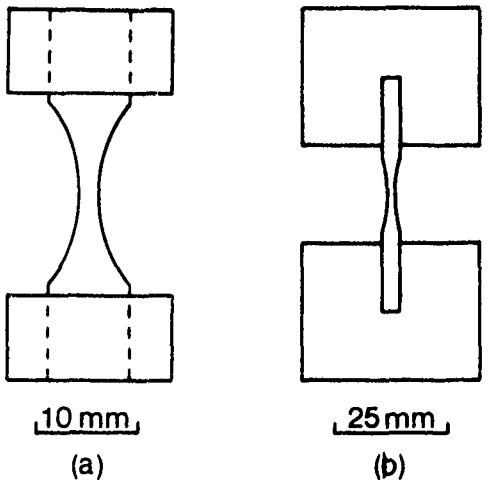

Fig.3. The "dog bone" compressive test specimen used in the pressure tests (a) and the RAE[6]-type compressive (rectangular) specimen (b) also used (only at atmospheric pressure).

The atmospheric compressive strength of our 60% V_f S glass/epoxide pultrusion[7] was 1.15±0.1 GNm^{-2}, somewhat lower than the tensile, about 1.4 GNm^{-2}. Similarly waisted CFRP tensile specimens[8,9] possessing no gauge length of constant cross-section tested at a rate of 0.1mm min^{-1} failed at a stress of 1.99±0.13 GNm^{-2}. It is to be noted that a marked departure from Hookean behaviour[9] took place at loads corresponding to applied tensile stress of 1.20±0.04 GNm^{-2}.

In another series of tests[5,10] on similar, but rectangular section CFRP pultrusions, flexural and "interlaminar shear" strengths were determined using span-to-depth (∿2mm) beam ratios of 5, 15 and 40. Again non-linear deformation preceded failure and "flexural" stresses evaluated using the "strength of materials" formula for span-to-depth ratio of 40 were 1.40±0.04 and 1.57±0.08 GNm^{-2} at the limit of proportionality and peak load, respectively. An increase in acoustic emission rate took place at the limit of proportionality and local damage was detected using optical microscopy at the compression roller contact line at higher stresses. In tests at superposed pressures, beams with span-to-depth ratio of 15, sufficiently short to fit into our pressure cell, gave similar results. When the ratio was reduced to 5, non-Hookean behaviour was also observed at the nominal "interlaminar shear" stress of 62±2 MNm^{-1}, which increased to 88±1 MNm^{-1} at peak load. Tensile strength of this CFRP material was 1.75±0.03 GNm^{-2}, ie somewhat lower than of the round pultrusions.

THEORETICAL BACKGROUND

Tensile strength

It is generally agreed that the tensile strength of unidirectionally aligned continuous fibre composite materials, such as our CFRP and GRP pultrusions, is determined by the breaking strength of the fibres[11-16]. Detailed theories of tensile strength accordingly consider statistical strength distribution in fibres[13] and analyse in detail acoustic activity[12,13]. It is argued that, if the matrix is properly chosen, the fibres will reach their breaking strain before the matrix fails. Rosen's[16] elegant experiments are cited to substantiate the thesis that the role of the matrix is to isolate fibre breaks in a narrow section of the composite due to load transfer into the fibre produced by the shear deformation of the matrix. What is not as frequently referred to, however, is that Rosen's observations were on 6% V_f GRP model lamina (containing ∿100 fibres in all), hardly a high strength composite. It is generally recognised that in high V_f CFRP stress transfer tends to take place by shear, whereas

in GRP by friction. It is noteworthy thus that fibres in failed CFRP tend to be covered with resin, whereas in GRP they are "clean".

Compressive strength.

Theoretical treatments of compressive behaviour again tend to assume perfectly straight, parallel and aligned fibres, perfectly bonded to an ideally elastic matrix[17]. In the more popular models composite strength is postulated to be limited by the strength of the fibres either in compression (acting as columns) or in shear[18,19], by the shear modulus of the matrix (resulting in shear instability[20]) or by a critical matrix stress[21]. The elastic buckling of the fibres, controlled by the matrix shear modulus[20] model appears to have the greatest acceptance, in spite of predicting strength values which are much too high and inability to account for variation of strength with fibre volume fraction[17]. Compressive strength has also been reported to be influenced by fibre-matrix adhesion (controlling interfacial splitting), fibre linearity and local misalignment[22].

Microstructural considerations.

Recently Piggott[17,22] has re-examined the question of compressive strength of composites, pointing out that, as with the theoretical development of models of yield strength of metallic solids, where theoretical strengths of perfect solids are much higher than observed strengths of polycrystalline aggregates, account has to be taken of imperfections, so for composites. One important parameter appears to be fibre straightness and a model based on Swift's analysis[23] has been postulated by Piggott[22]. It has been used and extended by us[7,8] by taking note that another important parameter is the relevant structural unit: ply, tow or lamina. It is suggested that groups of fibres act in unison and the bundle/bundle interface may be more important in determining mechanical properties of soundly manufactured composites, even nominally unidirectionally-aligned as are pultrusions, than the fibre/matrix interface.

Let us postulate that the fibre bundle (tow) has a circular cross-section and its axis assumes a sinusoidal form (noting[17] that using Fourier methods any axis trajectory can be reduced to sine waves). It can also be added that even for initially straight fibres the model has relevance as microbuckling[7] of fibre bundles against the support of the resin matrix may take place before the failure load is reached. If D is the bundle diameter, a the amplitude and λ the wavelength of the sine wave, then the axis displacement[23]:

$$y = a \sin \frac{2\pi x}{\lambda} \qquad \ldots(1)$$

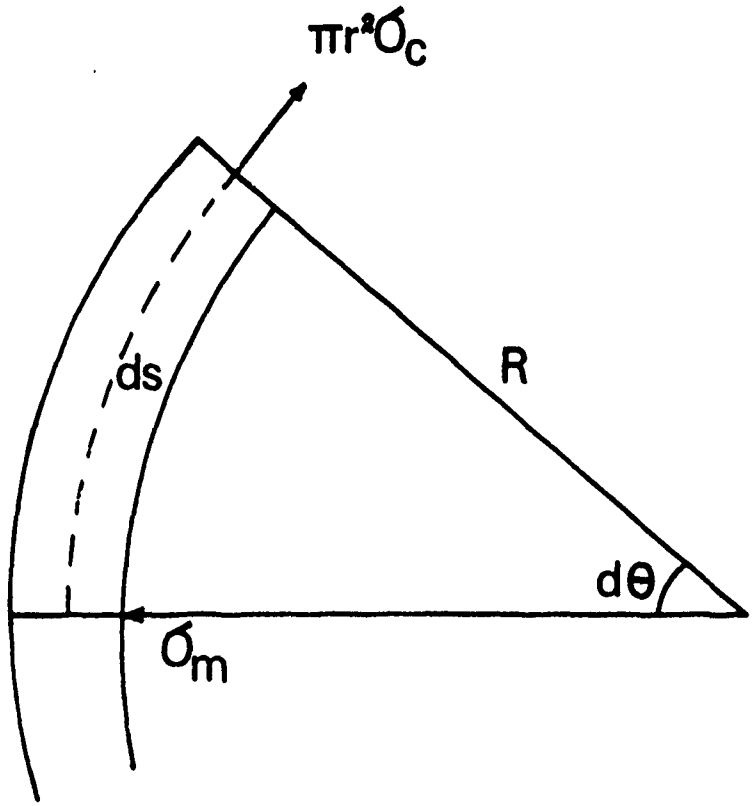

SWIFT: $\pi r^2 \sigma \sin d\theta = \sigma_m 2r\, ds$

Fig.4. Swift model of forces acting on a strained fibre bundle.

The small length of bundle, ds, adjoining the antinode at $x=\lambda/4$ is sketched as Fig.4. The bundle radius of curvature, R, is related to y by:

$$\frac{1}{R} = -\frac{d^2y}{dx^2} = -\left(\frac{2\pi}{\lambda}\right)^2 y \qquad \ldots(2)$$

If the fibre bundle stress is σ_b and σ_y is the stress exerted by the matrix on length ds of the bundle:

$$D\ ds\ \sigma_y = \frac{\pi D^2}{4}\ \sigma_b \quad \sin d\theta \qquad \ldots(3)$$

$$\text{As} \quad \sin d\theta \simeq \frac{ds}{R} \qquad \ldots(4)$$

$$\sigma_b = \frac{4R}{\pi D}\ \sigma_y \qquad \ldots(5)$$

If failure is controlled by this decoupling mechanism, the composite compressive strength will be:

$$\sigma_{c(my)} = \sigma_b = \frac{4R}{\pi D} \sigma_t \qquad \ldots(6)$$

where σ_t is the matrix tensile strength and R the critical bundle radius of curvature (perhaps present prior to loading). Piggott[17,22] postulates support of the matrix on both sides of the fibre (or bundle) and his expression for $\sigma_{c(my)}$ is double of relation (6). In our previous papers[7-9] we also have used Piggott's formula. His analysis further assumes unchanged fibre curvature and postulates the relevant mechanism to be overcoming the yield stress of the resin. Axial compression, however, can cause bending of the fibres until buckling of a surface bundle can overcome the restraint of the matrix, ie R can decrease during compressive loading[7].

Another aspect of this model is its possible application to tensile loading[9]. Transverse (interlaminar) cracking under tensile loading in CFRP[8] has been reported at stresses significantly inferior to the tensile strength. This decoupling can be associated with matrix yielding and bundle detachment in a similar way as axial compression if fibre bundle curvature is already present. Loading now will tend to straighten the fibre bundles against the support of the matrix. The bundle detachment stress would thus be given also by relation (5) and the tensile force would tend to increase R. The bundle, even if partially debonded, would continue to be loaded as it straightened out. The applicability of the same relation (5) for events in the tensile and compressive failure processes would account for the similarities in their strength values, frequently commented upon. The effect of axial force on R would result in lower values for the compressive strength, as generally observed, as R, which appears in the numerator in relation (5), would then tend to decrease. It should also be added that the condition (5) is unlikely to be frequently sufficient for catastrophic tensile failure.

A further relevance of bundles is to the consideration of Euler buckling. Weaver and Williams[18], in interpreting their results on 36% V_f CFRP, suggested that the compressive strength:

$$\sigma_c = \frac{\pi^2 E_f}{(l/K)^2} \qquad \ldots(7)$$

where E_f is the fibre modulus, K, the radius of gyration and l the buckling

length. If, as with Swift's model[23], we substitute a bundle of circular cross-section for the fibre[4], the compressive strength:

$$\sigma_{c(bb)} = \sigma_c = \frac{\pi^2 E_c}{(l/K)^2} \qquad \ldots(8)$$

where E_c is the composite modulus and l and K now refer to the bundle (tow or ply). This model was developed for failure by kinking and thus the composite compressive strength is expected to be the higher of $\sigma_{c(bb)}$ and $\sigma_{c(my)}$ values, both bundle buckling and matrix yielding being necessary processes for compression failure. Bundle detachment is required before buckling (and kinking) can take place, but the relative values of $\sigma_{c(my)}$ and $\sigma_{c(bb)}$ depend on composite properties and the stress system.

EFFECT OF HYDROSTATIC PRESSURE ON MECHANICAL PROPERTIES

(a) Fibres in tension

The authors are unaware of any direct determination of carbon or glass fibre tensile fracture strength under superposed pressure. An indirect study of an unidirectionally aligned carbon fibre/nickel matrix composite[24,25] showed that failure took place at a constant maximum principal tensile stress, σ_1 (ie applied tensile stress, σ_A, increased directly with the superposed pressure). This behaviour is consistent with a critical tensile stress (brittle fracture or cracking) criterion and is postulated, in accordance with experimental evidence, to refer to the behaviour of the fibres. If the critical fibre failure stress was a shear stress, then σ_A would have remained constant, ie σ_1 decreased directly with superposed pressure.

These results are on old, Harwell Type II fibres with a mean tensile strength of $\sim$2.2 GNm^{-2} in 47% V_m of nickel. Work is continuing elsewhere aimed at elucidating the tensile failure mechanisms in individual fibres. We would postulate, nevertheless, that until direct evidence to the contrary, as obtained in eg pressure tests, it should be assumed that failure in tension of glass and carbon fibres is critical tensile (not shear) stress-controlled.

(b) Resins in tension, compression and shear

Tensile, compressive and shear yield strengths of two epoxides were determined under superposed pressures extending to 300 MNm^{-2} in our laboratories[26]. The

data were consistent with a three-parameter (single hexagonal) pyramid yield criterion. The atmospheric tensile yield stresses were 88±3 and 67±3 MNm^{-2} and the compressive 119±1 and 90±3 MNm^{-2} for the two epoxies. This illustrates the phenomenon that, unlike in metallic materials, yielding in polymers depends on the hydrostatic as well as the deviatoric component of stress. The superposed tensile stress for yield, σ_A, increased with pressure, H, by -0.19H in our resins. The fractional increases in tensile yield strengths were 0.28 and 0.22 per 100 MNm^{-2} pressure respectively for the two epoxies; corresponding figures for the superposed compressive yield strengths are 0.27 and 0.20. Fractional increases in the strength of a composite of about 0.25 per 100 MNm^{-2} of superposed pressure would thus correlate with a direct dependence on matrix yielding, ie:

$$\sigma_c(H) = C \sigma_m (H) \qquad ...(9)$$

where C is unaffected by pressure, eg $\frac{4R}{\pi D}$ of relation (6) if R is unaffected by pressure and only the stress for matrix yielding, σ_m, is.

(c) CFRP in tension

Using waisted tensile specimens of pultruded 60% V_f rod we[9] investigated the failure mechanism at superposed hydrostatic pressures up to 300 MNm^{-2}. The maximum principal stress at failure decreased from ∿2.0 at atmospheric pressure (Fig.5) to ∿1.5 GNm^{-2} at H = -200 MNm^{-2}. At higher pressures it remained approximately constant (as for the metal matrix composite in this entire pressure range) indicating that a critical tensile stress-controlled mechanism was operating. The specimen failure surfaces were fairly flat and no damage preceding the catastrophic fracture was detected (Fig.6) in contrast to extensive debonding eg at atmospheric pressure.

At pressures inferior to 200 MNm^{-2} pre-failure damage was detected by optical microscopic examination of the specimen surfaces which appeared to initiate at the commencement of specimen non-Hookean behaviour. Debonding of surface bundles was initiated at atmospheric pressure at a stress of 1.2 GNm^{-2}. Straightening and debond initiation of curved surface bundles was followed by growth of these "interlaminar" cracks, leading to the detachment of curved surface bundles: delamination. The stress for this process increased from ∿1.2 GNm^{-2} at atmospheric to ∿1.5 GNm^{-2} at 150 MNm^{-2} superposed pressure, ie by ∿0.2 per 100 MNm^{-2} pressure, only a little less than the pressure dependence of epoxide-resin yield stress. Delamination was suppressed by transverse (part of the

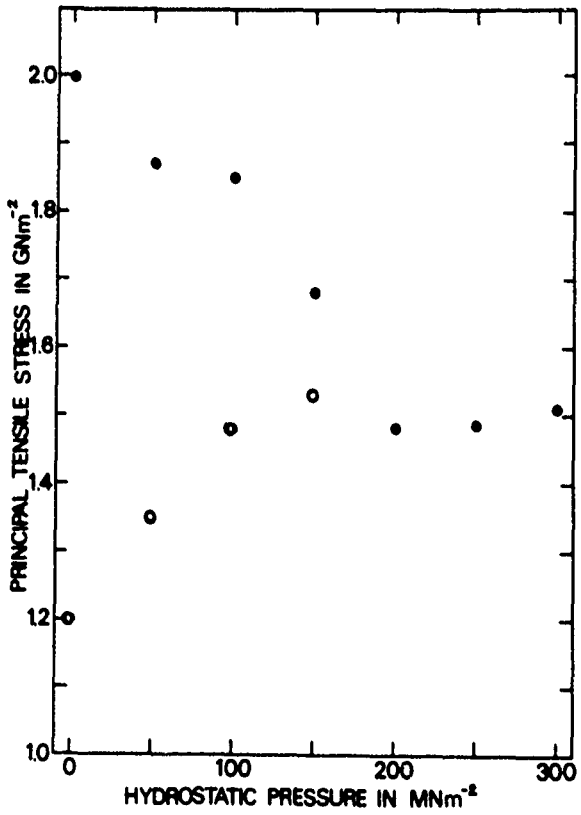

Fig.5. Stresses for fracture (closed symbols) and detection of damage (open symbols) of pultruded CFRP specimens tested in tension under superposed pressure.

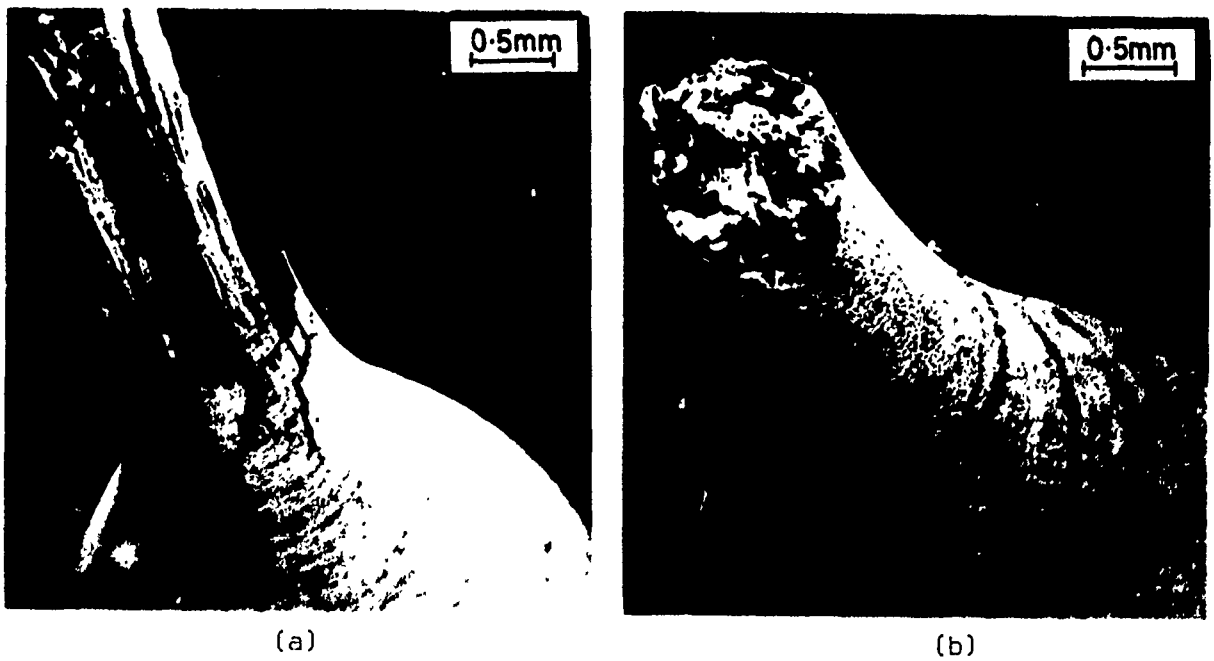

(a) (b)

Fig.6. Scanning electron micrographs of pultruded CFRP tensile specimens which failed at (a) atmospheric pressure and (b) under superposed pressure of 300 MNm^{-2}. Note in (a) decoupled fibre bundles with transverse (interlaminar) cracks continuing into the specimen shoulders in contrast to the fairly flat failure of (b).

hydrostatic) stresses greater than 150 MNm^{-2}. Below this pressure load redistribution between bundles was possible, but increasingly difficult with increase of pressure. Concurrently reduced fibre pull-out (Fig.6) and decreased composite strength (Fig.5) were observed. The critical stage of failure was thus fibre failure throughout the pressure range, but redistribution of stress (from bundle to bundle as well as from fibre to fibre, we would suggest) was increasingly more difficult with increase of pressure and prevented when it reached 200 MNm^{-2}. When no debonding precedes initial fibre failures[9], these fractures resulted in catastrophic composite cracking at $\sim$1.5 GNm^{-2}.

(d) GRP in tension

The failure mechanisms under pressures extending to 350 MNm^{-2} were investigated using specimens of similar design in pultruded $\sim$60% V_f 'S' glass/epoxy resin composite. The maximum principal tensile stress at failure, $\sim$1.7 GNm^{-2}, decreased with increasing pressure to $\sim$1.3 GNm^{-2} at H=-250 MNm^{2} (Fig.7). It remained approximately constant at higher pressures, as had been observed with the metal matrix composite and CFRP, indicating that these failures were controlled by a critical stress-operated mechanism. Again failure surface features in this pressure region were fairly flat although there was some indication (Fig.8) that local damage preceded failure, as more extensively at lower pressures. There was, however, no detectable deviation from the linear load-displacement response at H=-350 MNm^{-2}, whereas it had been observed at all pressures inferior to this value.

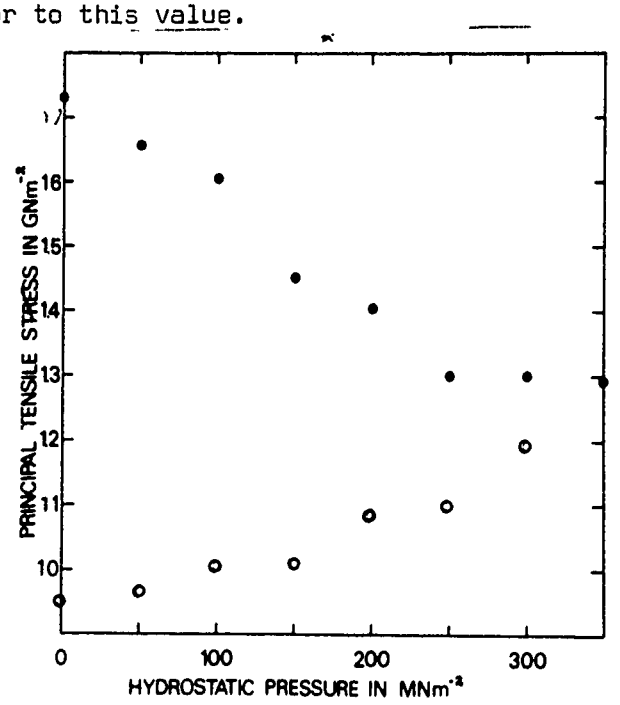

Fig.7. Stresses for fracture (closed symbols) and detection of damage (open symbols) of GRP specimens tested in tension under superposed pressure.

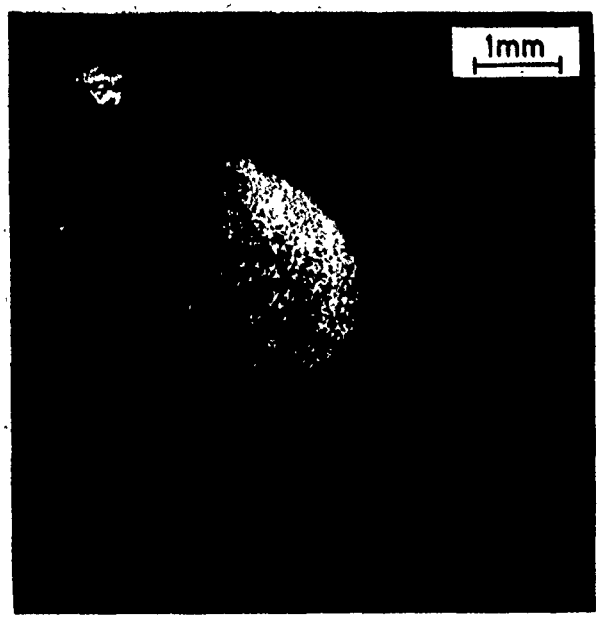

Fig.8. Scanning electron micrograph of a GRP specimen tested in tension under superposed hydrostatic pressure of 350 MNm^{-2}. Note the flat failure surface (as in CFRP, eg Fig.6(b)), but some debonding extending into the specimen shoulders.

Pre-failure damage was identified by optical microscopy and its commencement appeared again to coincide with the departure from Hookean deformation. This process was initiated at a stress of $\sim$0.95 GNm^{-2} at atmospheric pressure, it rose to $\sim$1.2 GNm^{-2} at H=-300 MNm^{-2}, ie by $\sim$0.1 per 100 MNm^{-2} (Fig.7), less than half the pressure dependence of the yield strength of epoxides.

It should be recalled that we have postulated that the first,[8,9] bundle debonding, stage of composite tensile failure process is dependent on local geometry (and can be likened to a stress concentrator in a ductile metal which can be "benign"). Load carrying capacity need not be impaired if stress can be transferred. Glass fibre/resin models invoke friction as the mechanism and this is now postulated to take place between bundles at fibre/matrix interfaces. This is in accord with observation of resin on carbon fibres and "clean" glass fibres in composite failure surfaces (Fig.9). The frictional properties of glass/resin under transverse or hydrostatic compression have not been investigated to the authors' knowledge, but model experiments, eg on steel/epoxy by Bowden[27], indicate the pressure dependence of the frictional stress to be lower than that of the resin yield strength, consistent with our hypothesis.

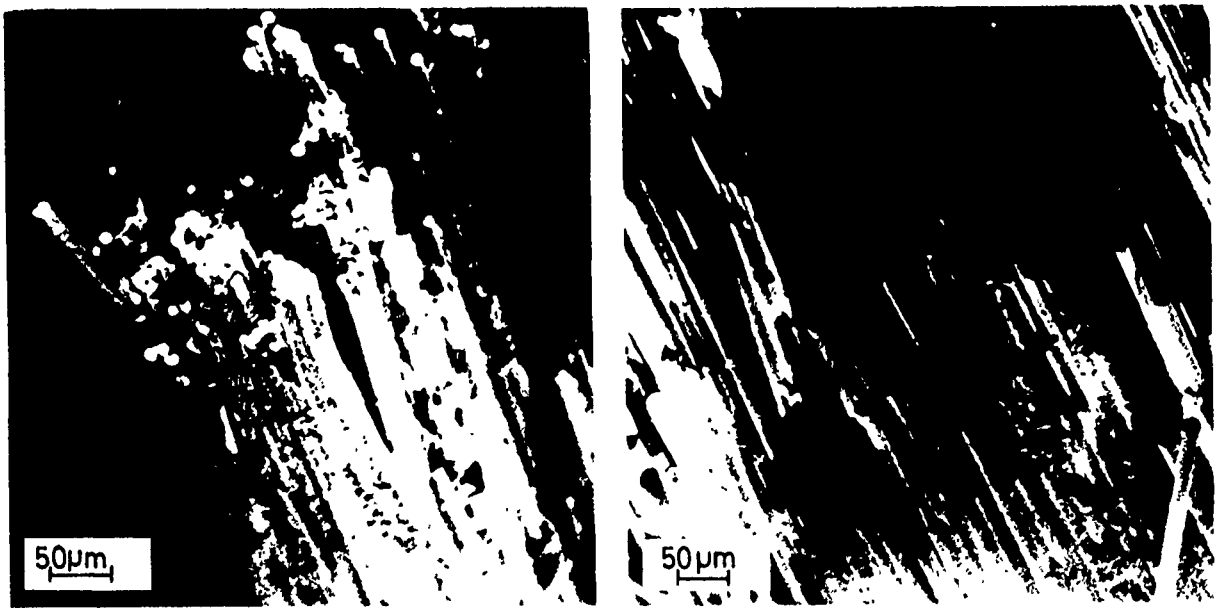

(a) (b)

Fig.9. Scanning electron micrographs of parts of the failure surfaces of tensile specimens of (a) CFRP and (b) GRP. Note the resin adhering to the fibres only in (a).

The critical stage of failure was fibre fracture throughout the pressure range, as for CFRP, but detailed pressure dependence was different. Particularly as fibre/resin detachment was easier (see Figs.6 and 8) in GRP in tension, matrix yielding did not appear to play a major part in the process. Transverse compression has a similar, though smaller, effect on fibre/resin friction to that on resin yielding[27], thus debonding persisted to 350 MNm^{-2} pressure as strength decreased and fracture surfaces approached a flat topography (Fig.8). This reflects greater difficulty of load redistribution between bundles and is associated with strength decrease, as in the case of CFRP (Fig.5).

(e) CFRP in compression

Similar experiments to the tensile were done in compression[4] on 60% Type A carbon fibre/epoxide pultruded bars using "dog bone" specimens (Fig.3(a)) in the pressure range extending to 400 MNm^{-2}. The axial compressive strength was ~1.5 GNm^{-2} at atmospheric pressure and was found to vary strongly with pressure (Fig.10) above 150 MNm^{-2}. Thus mechanisms involving shear-operated failure of the fibres, implying a slope of 1 for pressure dependence, and dependence on the matrix shear modulus which is only weakly pressure dependent, must be discounted, at least for higher pressure data.

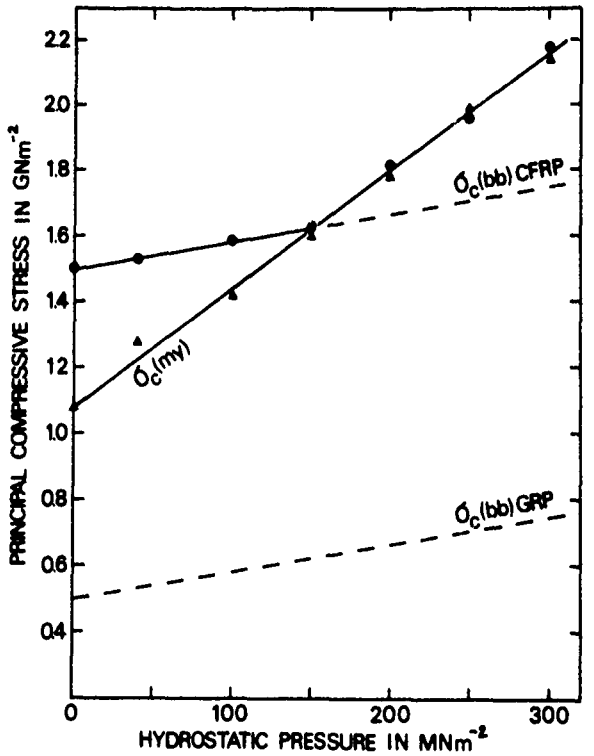

Fig.10. Data on the compressive strengths of pultruded CFRP (●) and GRP (▲) at pressures extending to 300 MNm^{-2}. Plotted are suggested pressure dependences of $\sigma_{c(bb)}$ of CFRP and GRP respectively and of $\sigma_{c(my)}$ for both composites.

It is suggested that there are two segments to the σ_c - H relationship, each corresponding to a necessary stage of the compressive failure process: matrix yielding and bundle buckling. At atmospheric pressure and in tests up to 150 MNm^{-2} pressure the initiation of failure was associated with transverse cracking (splitting) which was followed by kinking, implying that kinking required the higher stress. Using[4] relation (8) and a bundle diameter of 0.43 mm, buckling length of 2.9 mm is predicted, not inconsistent with observations of detached bundles.

Above 150 MNm^{-2} pressure splitting was no longer observed, consistent with its being more difficult than kinking and the first split resulting in catastrophic failure. Accordingly the plot labelled $\sigma_{c(bb)}$ CFRP on Fig.10 can be tentatively identified with the bundle buckling mechanism and that labelled $\sigma_{c(my)}$ with matrix yielding process in this CFRP. The pressure dependence of $\sigma_{c(bb)}$ is low; this could be related to that of the composite modulus in relation (8). $\sigma_{c(my)}$, however, is expected to vary with pressure, to the first approximation, as does the matrix tensile yield stress. The data correspond to ∿0.33 per 100 MNm^{-2}, somewhat higher than the epoxide strength dependence. We have

assumed so far, however, pressure independence of R, the bundle radius of curvature at failure. Transverse compression can only be expected to increase R, thus increasing $\sigma_{c(my)}(H)$. We would therefore postulate that both σ_t and R are pressure dependent, though we have no measurements to support the latter hypothesis. $\sigma_{c(my)}$ will be further discussed when considering GRP data.

(f) GRP in compression

Pressure experiments on 60% V_f GRP pultruded rod were similar to those conducted on CFRP[7]. The samples were also fitted with aluminium end rings to aid alignment within the pressure testing rig. The atmospheric compressive strength was $\sim$1.15 GNm^{-2} and strongly linearly pressure dependent, rising to 2.2 GNm^{-2} at 300 MNm^{-2}, ie by $\sim$0.35 per 100 MNm^{-2} superposed pressure, as did CFRP above 150 MNm^{-2} (Fig.10). The corresponding figure is 0.22 if maximum shear stress and not the maximum principal compressive stress is considered and thus again matrix modulus and fibre shear stress models of failure should be discounted. Additionally data could not be satisfactroily interpreted in terms of microbuckling of individual fibres.

It is to be noted (Fig.10) that for the same type of matrix (epoxide) but fibres of different strengths and moduli the compressive strengths of CFRP and GRP are the same above 150 MNm^{-2} superposed pressure. Failure then has been associated with matrix yielding at $\sigma_{c(my)}$ being the critical stage of the process, and it is now suggested that this is the critical stage in this GRP in all our tests. This implies that bundle buckling at $\sigma_{c(bb)}$ is easier and once a debond of sufficient length has been formed, catastrophic failure ensues. Thus kink bands were observed, but not detached bundles in our microscopic investigations of failed samples. Examination of relation (8) implies that, if all microstructural parameters are the same for CFRP and GRP, $\sigma_{cc(bb)}$ should vary directly with the composite modulus. Accordingly $\sigma_{cc(bb)}$ GRP has been plotted in Fig.10 at $^{48}/_{110}$ (the E_c ratio) of the $\sigma_{cc(bb)}$ CFRP line and it is seen that it can not intersect the $\sigma_{c(my)}$ plot. In weak matrix composites, however, $\sigma_{cc(my)}$ would be lower and then a transition is possible.

DISCUSSION

The subject of the conference being Failure Analysis Techniques for Fibre-Reinforced Composites, the technique of testing under superposed pressure needs to be critically assessed in the context of design data and identifying mecha-

nisms. We would like to concentrate our discussion on the latter point and refer first to discounting mechanisms.

We would recall that independence of σ_1 on pressure can generally be associated with tensile stress-operated mechanisms and a slope of ±1 in σ-H linear plots with shear stress-operated mechanisms in crystalline solids. Whenever we observed the former (in tension) this has been our conclusion: cracking of brittle fibres has been the mechanism postulated. Increasing compressive strength and decreasing tensile strength with increasing pressure have been observed for both CFRP and GRP, certainly at pressures below 150 MNm^{-2}. This is the type of pressure dependence required by fibre shear-stress operated mechanisms. Nevertheless we have discounted them.

The reasons for this are two-fold and illustrate the dangers and advantages of using pressure data. Caution must be exercised and complementary evidence is essential: in our experiments this has been gathered by optical as well as scanning electron microscopy. If the pressure dependences of all the variables in the strength relation are known, exact pressure dependences of composite strength can be predicted. Thus the required tensile strength-H dependence is -1 for a fibre shear strength-operated mechanism, whereas approximately double that has been observed (Figs.5 and 7). For compressive strength it would be +1, whereas it was observed to be always over 3 for GRP and CFRP above 150 MNm^{-2} and approximately, but less than, 1 only for the CFRP data below 150 MNm^{-2} pressure (Fig.10). These data, together with microscopic evidence, appear to us sufficiently strong not to consider critical fibre shear stresses as relevant to failure analysis of unidirectional CFRP and GRP tested in axial tension and compression.

The data on pressure dependences of the tensile and compressive strengths of resin, and unidirectionally aligned GRP and CFRP, with supporting optical and scanning electron microscopic observations of pre-failure "damage" and failure surfaces, have enabled us to consider the relative difficulties of these four processes:

1. Tensile fracture of fibres at σ_{ff} composite stress.
2. Debonding of (curved) fibre bundles at σ_d.
3. Delamination (growth of transverse cracks leading to bundle detachment) at σ_{my}.
4. Kinking or fibre bundle buckling at σ_{bb}.

The debonding/delamination processes were different in the two types of composite we studied, occurring at the fibre/resin interfaces in GRP, but within the resin in CFRP (Fig.9). The mechanisms are thus postulated as being controlled by fibre adhesion and fibre/resin frictional properties in GRP and resin yielding and failure in CFRP. Before a (surface) bundle can kink (buckle), however, the transverse support must be overcome and this will be controlled by the resin yield strength. Thus $\sigma_{c(my)}$ can be the same for the same matrix composite if bundle geometry, size, straightness and V_f are the same for composites with fibres of quite different properties, as are carbon and glass.

The bundle detachment at σ_{my} should mark the end of Hookean behaviour in tension and compression. With increasing stress (and time) the transverse cracks can continue to grow[8] and this process can be impeded or suppressed by transverse (part of the hydrostatic) compression.

In tension the partially detached bundles can continue to be loaded and thus contribute to the increasing load-carrying capacity of the component. One would argue, however, for increased matrix strength, which should increase σ_{my}. For our CFRP there is reasonable scope: from $\sim$1.2 GNm^{-2} to $\sim$2.0 GNm^{-2}, composite strength determined by σ_{ff}. In general thus stronger matrices should be considered whenever $\sigma_{my} < V_f \sigma_{ff}$.

The σ_{my} mechanism appears to operate in compression in GRP and CRFP, the other necessary process is bundle buckling, at σ_{bb}. The latter is relatively easy in GRP, unless fibre alignment is near perfect, because of the low Young's modulus. If our model is correct, increasing σ_{my}, by increasing matrix strength, would be more effective for GRP, although if σ_t were raised in the 2.0/1.2 ratio theoretically worthwhile for CFRP tensile properties, it would also correspondingly raise σ_c to $\sim$1.9 GNm^{-2} at atmospheric pressure. We would add that, if this near equality of atmospheric tensile and compression properties is achieved by a matrix strengthening mechanism, it should not be cited as evidence of fibre-shear operated mechanisms controlling failure in tension and compression.

In many composite applications bending stresses are more important than simply tensile or compressive and the problem of interlaminar shearing arises; accordingly we have also tested CFRP beams of differing span/depth ratios in three-point bending under superposed pressures[5]. A complicating feature, not restricted to our test specimens, is the initiation of "kinking" damage by the "com-

pression" rollers, particularly in three-point bending, especially of short span specimens. At atmospheric pressure kink growth during the non-linear part of the load-deflection curve was followed by kink propagation for span-to-depth ratios of 5, 15 and 40 in 60% V_f CFRP. Kink growth with decreasing load, increasing deflection and accompanying redistribution of stresses led to two types of failure: normally referred to as "flexural" and "interlaminar".

In the former, in specimens with the longer spans, tensile failure was concurrently initiated at peak stress of $\sim$1.6 GNm^{-2} to give the characteristic tensile and compressive zones on the failure surface (Fig.11(a)). The catastrophic failures were preceded by 4-15% non-linear deformation (measured as proportion of peak load). Not only had the failure specimens two zones, tensile and compressive, so had individual fibres, which some[28] have associated with compressive failure in buckling. At pressures up to 170 MNm^{-2} kinking failure was initiated at approximately constant compressive stress (at the limit of proportionality) of 1.6 GNm^{-2} (Fig.12). Failure propagation and accompanying tensile fracture were also similar to the process observed at atmospheric pressure (Fig.11(b)). At higher pressures, however, although failure initiation was similar, kinking was suppressed and tensile/compressive failure boundary moved towards the tensile surface and at 300 MNm^{-2} pressure no evidence of compressive failure was found (Fig.11(c)). In the tensile zone pull-out lengths decreased with increasing pressure (as in axial tensile tests).

Fig.11. The failure surfaces of flexural CFRP specimens tested at (a) atmospheric pressure and (b) and (c) superposed pressures of 150 and 300 MNm^{-2}. Note the movement of the tensile/compressive failure boundary towards the tensile surface as pressure is increased such that no compressive failure is visible in (c) and reduced fibre pull-out lengths.

Tests on beams with span-to-depth ratio of 5 gave a value of 88±1 MNm^{-2} at peak load for the so-called "interlaminar shear strength", the value being 62±2 MNm^{-2} at the limit of proportionality at atmospheric pressure. Then the growing kink initiated interlaminar cracks in resin-rich zones as it propagated, with decreasing load, towards the tensile surface. As pressure was increased to 150 MNm^{-2} the behaviour was not substantially altered, but the peak load for failure in-

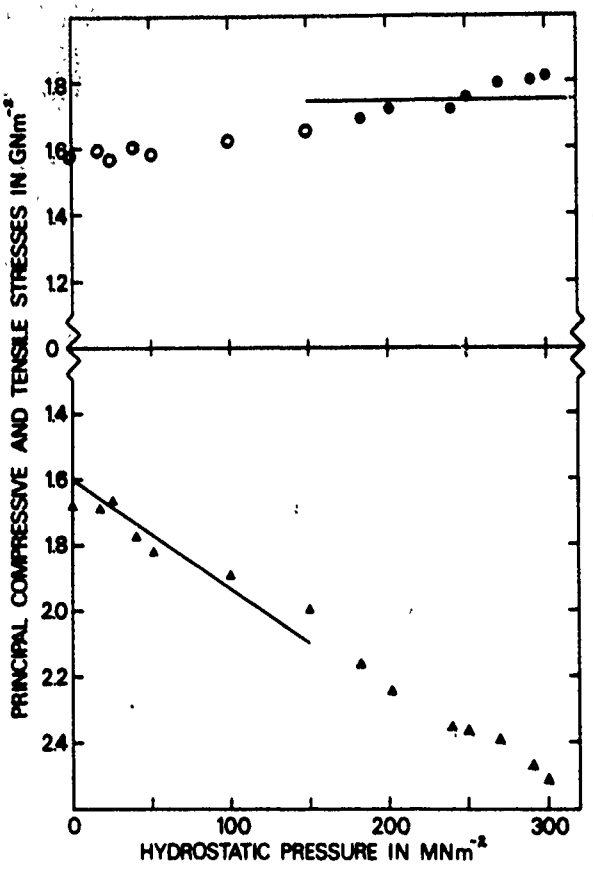

Fig.12

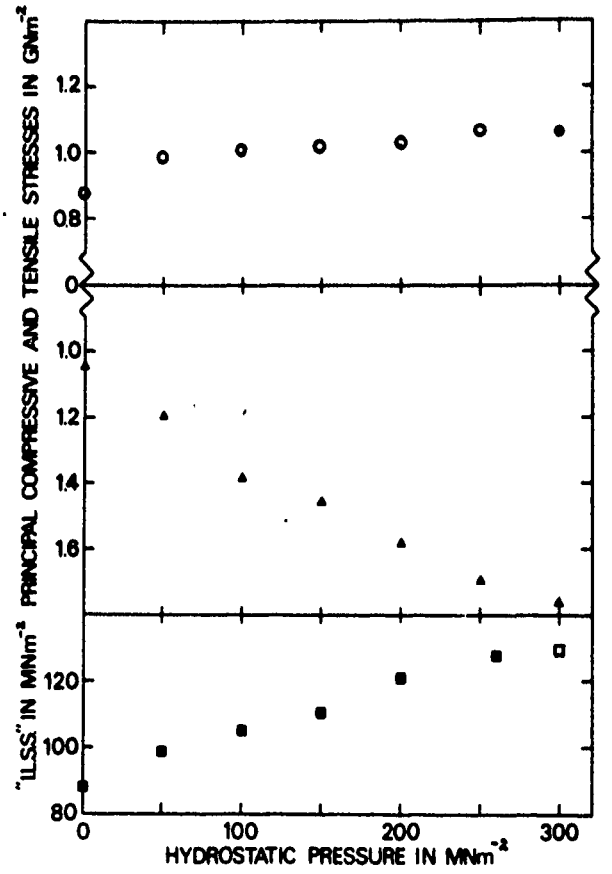

Fig.13

The pressure dependences of (Fig.12) maximum principal tensile and compressive stresses and (Fig.13) also interlaminar shear strength of flexural specimens tested under superposed pressure. Note full symbols refer to modes of failure.

creased somewhat (Fig.13). At higher pressures kinking was not suppressed, but interlaminar cracking was. Failure surface had tensile and compressive failure zones, as the other flexural specimens (Fig.11) and, with increasing pressure, the tensile/compressive boundary moved towards the compressive surface. Maximum principal tensile and compressive, as well as shear, stresses are plotted in Fig.13 and it is seen that the maximum principal compressive stress at peak load for the short beam specimens tested under pressure was $\sim$1.1 GNm^{-2}.

Let us now apply the models of failure involving matrix yielding, fibre fracture and bundle buckling, noting that specimen curvatures are now imposed by the loading fixture. Failure initiation was localised to the rollers and can be regarded as a specimen geometry dependent process, as is debonding in tension.

Let us first consider the longer span specimens: examination of Fig.12 shows

they failed by a "compressive" mechanism at atmospheric and superposed pressures extending to 150 MNm^{-2}. We have a reasonable correlation with uniaxial compressive strength, 1.5 with 1.7 GNm^{-2}, the higher figure being partly due to applying the "strength of materials" formula when the load-deflection response was no longer linear. The pressure dependence is small, less than 0.1 per 100 MNm^{-2}, not markedly different to that for $\sigma_{c(bb)}$ CFRP of Fig.10. It is therefore postulated that bundle buckling controls flexural strength in this pressure region, including atmospheric tests.

At higher pressures failure took place at an approximately constant tensile stress of $\sim$1.8 GNm^{-2}, approximately equal to the tensile strength directly determined at atmospheric pressure. It is to be noted, however, that it is somewhat higher than the directly determined tensile strength at these pressures in specimens of similar material, $\sim$1.5 GNm^{-2}. The discrepancy may well be again partly due to applying the linear "strength of materials" analysis to calculate flexural strength.

Turning now to the short span specimens, we note that failure took place at $\sim$1.1 GNm^{-2} compressive stress and the pressure dependence was approximately 0.25 per 100 MNm^{-2} superposed pressure (Fig.13). The data thus correlate well with the $\sigma_{cc(my)}$-H plot of Fig.10, which has only GRP points below 150 MNm^{-2} pressure. Accordingly we would postulate that the effect of imposed bending and concentrated load was to initiate kinking/buckling at compressive surface stresses much lower than needed in axial compression. Thus there was no longer any need to satisfy the uniaxial compressive σ_{bb} condition. Though kinked, the surface bundles are still able to transmit compressive stresses. This process is thought to continue until matrix yielding and either delamination (at lower stresses) or tensile and compressive failure take place (above 150 MNm^{-2} superposed pressure). The actual surface tensile stresses in a beam which has kinked up to one-third way across the thickness can not be accurately calculated using "strength of materials" theory, procedure adopted for data points on Fig.13. It is suggested that the critical stage, whether delamination or flexural failure ensues, is controlled by matrix yielding to account for the compressive stress dependence, approximately 0.25 per 100 MNm^{-2} superposed pressure (Fig.13). It is to be noted that moreover our compressive stress plot in Fig.13 corresponds fairly well with the matrix yielding plot of Fig.10. At this stage we would suggest that the near equality of atmospheric strengths at $\sim$1.1 GNm^{-2} is fortuitous (unlike the pressure dependence), as the absolute level of "interlaminar" shear strength (and therefore proportionately

maximum compressive stress) can be influenced by loading roller diameter[29] (affecting the concentrated load) and strategic surface reinforcement[30] (affecting difficulty of kinking/buckling).

CONCLUSION

The application of hydrostatic pressure, well able to discriminate between shear and tensile stress-operated mechanisms, has enabled us to obtain composite mechanical properties data susceptible to more rigorous interpretation. Thus for unidirectionally aligned fibrous composites of glass and carbon in epoxide tested in axial tension and compression we were able to demonstrate the roles of matrix yielding (in tension and compression), bundle buckling (in compression), as well as tensile fibre failure mechanisms. Data obtained in flexure can be consistently interpreted.

We appreciate that the composites we considered, as well as the loading system, are simple. We intend to stay with the latter, they are more complex than used for the majority of strength tests, but intend to extend the former to woven fabrics. It is to be noted that our data demonstrate the importance of a structural entity, a bundle, and its curvature. These are more noticeably present in woven fabrics. Application of our analysis for atmospheric pressure tests to two types of satin weave cloth has yielded encouraging correlations with bundle and Euler buckling models of compressive strengths. We hope to substantiate these with pressure testing.

ACKNOWLEDGEMENTS

The work has been supported by the SERC; assistance of Dr M M Rebbeck with scanning electron microscopy is appreciated, as is the preparation of the MS by Mrs B Franks.

REFERENCES

1. P. W. BRIDGMAN, "The Physics of High Pressure. (G. Bell, London, 1949).

2. C. H. ROBBINS and A. S. WRONSKI, Acta Metall., 26 (1978) 1061.

3. C. H. ROBBINS and A. S. WRONSKI, High Temperatures-High Pressures, 6 (1974) 217.

4. T. V. PARRY and A. S. WRONSKI, J. Mater. Sci., 17 (1982) 893.

5. T. V. PARRY and A. S. WRONSKI, J. Mater. Sci., 16 (1981) 439.

6. P. D. EWINS in Composites, Standards, Testing and Design, (IPC Science and Technology Press, Guildford, 1974) p144.

7. A. S. WRONSKI and T. V. PARRY, J. Mater. Sci., 17 (1982) 3656.

8. A. S. WRONSKI and T. V. PARRY, J. Mater. Sci., 19 (1984) 3421.

9. T. V. PARRY and A. S. WRONSKI, J. Mater. Sci., 20 (1985), in the press.

10. T. V. PARRY, Ph.D. thesis, University of Bradford (1980).

11. M. FUWA, A. R. BUNSELL and B. HARRIS, J. Mater. Sci., 10 (1975) 2062.

12. M. FUWA, B. HARRIS and A. R. BUNSELL, J. Phys. D., 8 (1975) 1460.

13. A. R. BUNSELL and D. VALENTIN, Composite Structures, 1 (1983) 67.

14. C. ZWEBEN and B. W. ROSEN, J. Mech. Phys. Solids, 18 (1970) 189.

15. D. G. HARLOW and S. L. PHOENIX, J. Comp. Mater., 12 (1978) 195.

16. B. W. ROSEN, American Institute of Aeronautics and Astronautics Journal, 2 (1964) 1985.

17. M. R. PIGGOTT in Developments in Reinforced Plastics-4, G. Pritchard, Ed. (Elsevier Applied Science, London, 1984) p131.

18. C. R. WEAVER and J. G. WILLIAMS, J. Mater. Sci., 10 (1975) 1323.

19. P. D. EWINS and R. T. POTTER, Phil. Trans. Roy. Soc., A294 (1980) 507.

20. B. W. ROSEN in Mechanics of Composite Strengthening, (ASM Seminar, Philadelphia, Pa., October 1964).

21. J. HAYASHI and K. KOYAMA, Soc. Mater. Sci., Japan, 5 (1974) 104.

22. M. R. PIGGOTT, J. Mater. Sci., 16 (1981) 2837.

23. D. G. SWIFT, J. Phys. D., 8 (1975) 223.

24. B. R. WATSON-ADAMS, J. J. DIBB and A. S. WRONSKI in Metal Matrix Composite Materials (1972 Liverpool Symposium, R. W. Jones, Ed.) paper 4.

25. A. S. WRONSKI, Proc. Third International Conference on Fracture (Munich 1973) II - 332.

26. A. S. WRONSKI and M. PICK, J. Mater. Sci., 12 (1977) 28.

27. P. BOWDEN, J. Mater. Sci., 5 (1970) 517.

28. P. D. EWINS and A. C. HAM, RAE Tech. Rpt. No.73057 (August 1973).

29. T. V. PARRY and A. S. WRONSKI, in High Pressure Science and Technology (B. Vodar and Ph. Marteau, Eds., Pergamon Press, Oxford, 1980) p299.

30. P. D. BRADLEY and S. J. HARRIS, J. Mater. Sci., 12 (1977) 2410.

POST FAILURE ANALYSIS OF SELECTED THERMOPLASTIC AND THERMOSET COMPOSITE TEST COUPONS

Gordon Bourland and John Iaconis
LTV Aerospace and Defense
Vought Aero Products Division

Post Failure Analysis of Selected Thermoplastic and Thermoset Composite Test Coupons

Introduction

Post failure analysis usually involves investigations to determine the failure origin, failure mode and sequence of failure. Failure mode and sequence can usually be determined by a knowledge of the type of test article and load conditions. The origin, however, is frequently difficult to determine because the failure sequence and fracture debris obscures or destroys the initiation site.

Although information on the failure origin is frequently lacking, it is possible to deduce the conditions by microscopic examination of the surrounding areas. Optical and scanning electron microscopy reveal a large amount of information concerning fiber and matrix properties, matrix porosity and fiber/matrix interface conditions. Other physical property tests for fiber volume, per ply thickness, ply orientation and percent of unreacted resin provide insight into material condition when combined with microscopic examinations.

A representative post failure examination is discussed in this paper to illustrate the investigation procedures and the value of the results. The investigation concerned graphite/polyphenylenesulfide, AS4/PPS, thermoplastic test coupons which exhibited lower than expected test values for compression, flexure, and short beam shear properties.

This work was part of an on-going in-house evaluation of new composite materials which also included graphite/polyetheretherketone, AS4/PEEK, graphite/K-II polymer, AS4/KII, and graphite/epoxy, AS4/3502. Vendor data for these materials is shown in Table I.

Material Evaluations

An initial evaluation was made of AS4/PPS and AS4/3502 composites to determine tensile, compression, flexure and short beam shear properties. Results of these tests, along with vendor supplied data, are shown in Table II. It may be observed that the LTV test results for AS4/PPS for flexure and short beam shear strength were well below the values reported by the vendor. Lower than expected values were also found for 0° compression strength.

Subsequent evaluations on the effect of processing variables on thermoplastic composites produced much higher flexure and short beam shear strength for AS4/PPS specimens. Results of these tests on AS4/PPS, AS4/KII and AS4/PEEK are shown in Table III. These tests were performed on a different batch of AS4/PPS.

Because of the wide variations in test values reported in Table III and the low strengths found for one batch of AS4/PPS, it was decided to look at the microstructure of selected thermoplastic specimens and compare them with typical AS4/3502 epoxy specimens as a baseline material. Small samples were taken from failed specimens for examination by scanning electron microscope. Scanning examinations were made on a Cambridge Stereo Scan Electron Microscope, Model 200, at magnifications from 18x to 5000x.

Failure Analysis

Figures 1 and 2 show the fracture surfaces of one of the AS4/PPS and AS4/3502 flexure specimens reported in Table II. Figures 3 and 4 show fractographs of the tension and compression fracture surfaces of the AS4/PPS specimen. Flexure specimens are subjected to compression and tension loads above and below the neutral axis of the specimen which are at a maximum at the point of load application. Tear fractures typical of ductile plastic failure are shown in Figure 3 on the compression surface of the AS4/PPS specimen. The tension side fracture surface for AS4/PPS shown in Figure 4 reveals relatively long fiber lengths with almost no matrix resin adhering to the fiber surfaces, indicative of poor adhesion between the resin and fiber. Fracture of the fiber ends indicates a tensile mode failure. Similar views of the AS4/3502

specimen are shown in Figures 5 and 6. The compression side fracture surface shown in Figure 5 shows a relatively featureless surface characteristic of fracture of a brittle material like the 3502 epoxy resin. The tension side fracture surface shows much shorter exposed fiber lengths with a large amount of resin adhering to the fiber surfaces.

In order to better understand the cause of the poor adhesion between the fiber and matrix it was decided to examine the fracture surface of one ply of AS4/PPS tape "as received" from the manufacturer. This sample was compared with the fracture surface on an "as received" one ply sample of AS4/PEEK (ICI APC-2). The one ply specimens were made by cutting a 1/2" x 3" piece of prepreg from the rolls of prepreg tape and breaking the pieces in a vise in the laboratory. The AS4/PPS sample was from the same batch as the coupons used for the tests reported in Table II. Evidence of poor adhesion on these samples would indicate a supplier manufacturing problem and not a user processing problem.

Figure 7 shows the fracture surface of the AS4/PPS one ply specimen at 1000x magnification. This specimen also showed an appearance of poor adhesion between the fiber and resin as evidenced by relatively long fibers with only a small amount of resin remaining on the fiber surfaces. Figure 8 shows a similar view of the AS4/PEEK one ply specimen at 1000x magnification. This sample appeared to have better adhesion between the fiber and resin as evidenced by the resin material remaining on the fiber surfaces. Figures 9 and 10 show the fracture surfaces of the two samples at 5000x. The AS4/PPS sample had areas where no resin was adhering to the fiber surfaces. However, the AS4/PEEK sample had resin residue remaining on all fiber surfaces. As stated above, these samples were never processed by LTV, but were taken "as received" from the rolls of prepreg tape. The appearance of poor adhesion on the "as received" AS4/PPS material indicated the poor test values reported in Table II were the result of fiber "wet out" problems at the prepreg supplier and not the result of user processing.

A second batch of AS4/PPS was used in making panels 2, 3, and 4 reported in Table III. Specimens made from these panels all had higher flexure and short beam shear strengths than the samples made from the earlier batch of AS4/PPS prepreg. Scanning electron micrographs for a typical flexure specimen made from AS4/PPS panel 3 are shown in Figures 11, 12, 13 and 14.

The compression surface morphology in Figures 12 and 13 shows similarity with the morphology in Figure 3 for a ductile plastic surface. However, the tension side surface in Figure 14 shows much better adhesion of the resin to the fibers than evidenced in Figure 4 for the earlier sample. The improved adhesion apparently was the reason for the better mechanical properties of the second batch of AS4/PPS.

Scanning electron micrographs were also made on selected specimens from the AS4/KII and AS4/PEEK panels reported in Table III. Fracture surfaces for a typical AS4/KII specimen are shown in Figures 15, 16 and 17. Similar fracture surfaces for a typical AS4/PEEK specimen are shown in Figures 18, 19 and 20.

Conclusions

It was concluded from this work that post-failure analysis of test coupons is an aid to materials evaluations and that the scanning electron microscope is a useful tool in this application. Evaluation of fracture surface morphology indicated that poor resin/fiber adhesion, in one batch of thermoplastic composite, was a contributing factor to low values obtained from mechanical strength tests. Subsequent tests on another batch of the material revealed improved resin/fiber adhesion and improved mechanical strength values.

During these investigations it was also shown that valuable information could be gained concerning resin ductile/brittle characteristics, fiber fracture modes, resin/fiber adhesion characteristics and overall fracture surface appearance.

TABLE I

VENDOR DATA ON THERMOPLASTIC AND EPOXY UNIDIRECTIONAL COMPOSITES

	AS4 – PPS	AS4 – KII	AS4 – PEEK	AS4 – 3502
RESIN MATRIX	Polyphenylene-sulfide	Polyimide	Polyetherether-ketone	Epoxy
SUPPLIER	Phillip Chem	DuPONT	ICI	Hercules
RESIN CONTENT, w/o	40	33	32	33
RESIN DENSITY, gm/cc	1.36	1.31	1.32	1.26
FIBER VOLUME, v/o	53	60	61	59
COMPOSITE DENSITY, gm/cc	1.58	1.60	1.60	1.59
PER PLY THICKNESS, IN.	0.0065	0.0053	0.0050	0.0055
0° TENSILE STRENGTH, KSI (60% FV)	192	NA	309	310
0° TENSILE MODULUS, MSI (60% FV)	20.3	NA	19.4	21.5
0° COMPRESSION STRENGTH, KSI	NA	175	160	204
0° COMPRESSION MODULUS, MSI	NA	NA	NA	17.5
0° FLEXURE STRENGTH, KSI	198	222	273	260
0° FLEXURE MODULUS, MSI	15.3	18.0	17.5	18.5
SHORT BEAM SHEAR, KSI	10.5	13.6	15.2	17.5

NOTE: (1) NA Denotes Data Not Available

MP5-1900-24

TABLE II

RESULTS OF VOUGHT TESTS TO VERIFY VENDOR DATA FOR AS4/PPS AND AS4/3502

	AS4/PPS		AS4/3502	
	VENDOR DATA	LTV TESTS (1)	VENDOR DATA	LTV TESTS (1)
FIBER VOLUME, v/o	53	53.8	59	59.1
PER PLY THICKNESS, IN.	0.0060	0.0058	0.0055	0.0057
0° TENSILE STRENGTH, KSI	192	204	310	285
0° TENSILE MODULUS, MSI	20.3	19.0	21.5	23.4
0° COMPRESSION STRENGTH, KSI	NA	101	204	195
0° COMPRESSION MODULUS, MSI	NA	14.9	17.5	20.6
0° FLEXURE STRENGTH, KSI	198	149	260	237
0° FLEXURE MODULUS, MSI	15.3	16.2	18.5	20.2
SHORT BEAM SHEAR, KSI	10.5	6.4	17.5	16.9

NOTE: (1) Results of mechanical property tests are the average of six specimens
(2) NA denotes data not available

TABLE III

MATERIAL	PANEL NO.	NO. OF SPECIMENS	PER PLY THICKNESS	FLEXURE STRENGTH KSI	MODULUS MSI	SHORT BEAM SHEAR, KSI	FIBER VOLUME v/o
AS4/PPS	1 (PREV TBL)	6	0.0058	149	16.2	6.4	53.8
	2	4	0.0058	183	12.6	11.9	
	3	4	0.0058	195	14.1	11.4	52.4
	4	4	0.0059	202	12.9	11.2	
AS4/KII	1	4	0.0051	261	23.9	16.5	
	2	4	0.0051	303	26.2	15.4	
	3	4	0.0051	287	27.5	17.9	
	4	4	0.0050	304	26.5	13.7	59.9
AS4/PEEK	1	4	0.0052	318	28.7	16.5	
	2	4	0.0053	285	25.8	16.4	
	3	4	0.0052	262	23.7	12.2	
	4	4	0.0049	298	23.2	19.7	
	5	4	0.0049	307	25.3	20.0	58.5

AP5-1900-1A

Figure 1. Fracture surface of flexural coupon from AS4/PPS panel 1. Tension side on the bottom.

18X

AP5-1900-2A

Figure 2. Fracture surface of flexural coupon from AS4/3502 panel. Tension side on the bottom.

18X

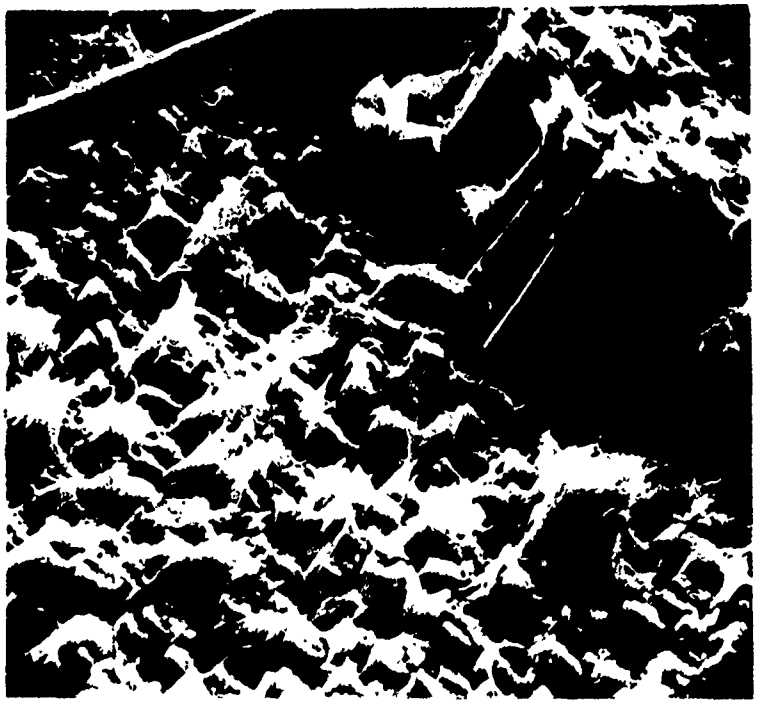

AP5-1900-3

Figure 3. Compression side fracture surface of flexure coupon from AS4/PPS, panel 1.

1000X

AP5-1900-4

Figure 4. Tension side fracture surface of flexure coupon from AS4/PPS, panel 1.

1000X

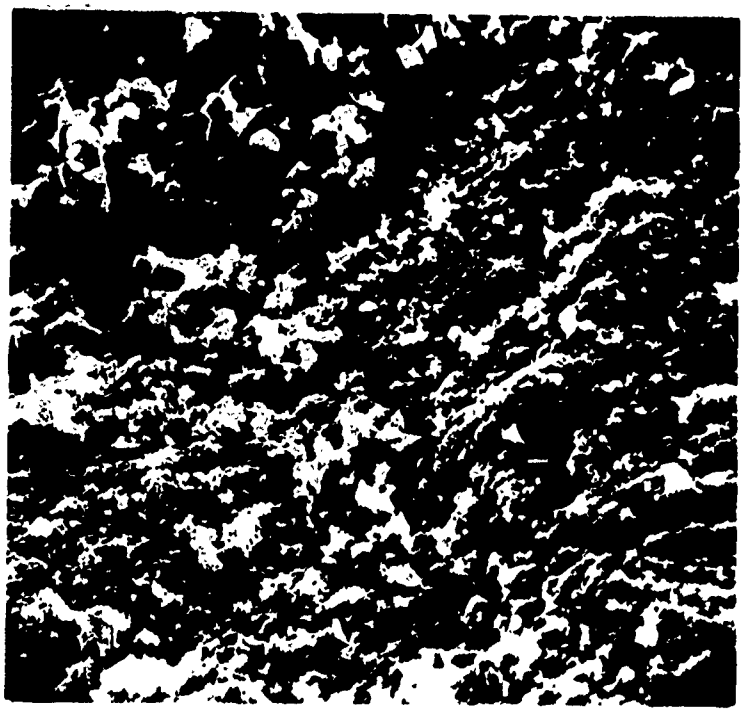

APS-1900-5

Figure 5. Compression side fracture surface of flexure coupon from AS4/3502 Panel.

1000X

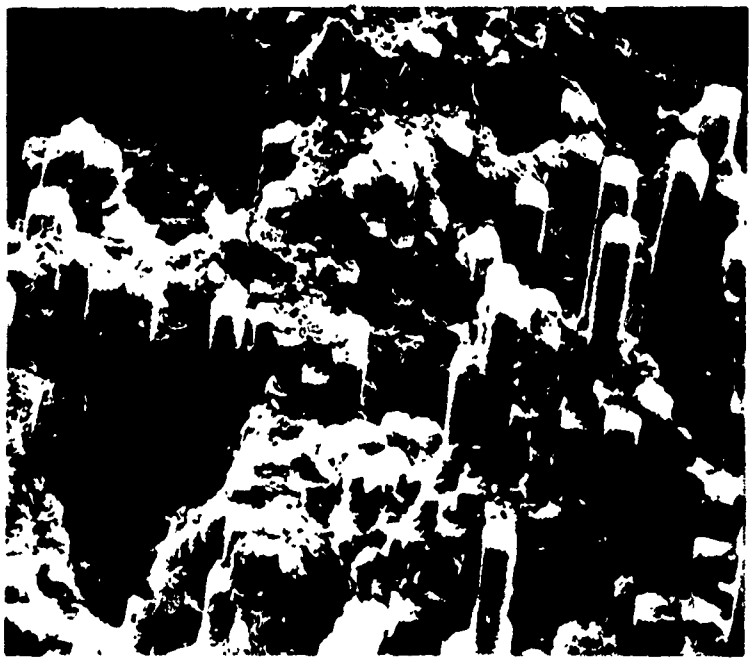

APS-1900-6

Figure 6. Tension side fracture surface of flexure coupon from AS4/3502 Panel.

1000X

AP5-1900-7

Figure 7. Fracture surface of single ply of AS4/PPS.

1000X

AP5-1900-8

Figure 8. Fracture surface of single ply of AS4/PEEK.

1000X

Figure 9. Fiber surfaces of single ply AS4/PPS.

5000X

Figure 10. Fiber surfaces of single ply AS4/PEEK.

5000X

APS-1906-11A

Figure 11. Fracture surface of an AS4/PPS flexure specimen from panel 3. Tension side at the bottom.

19X

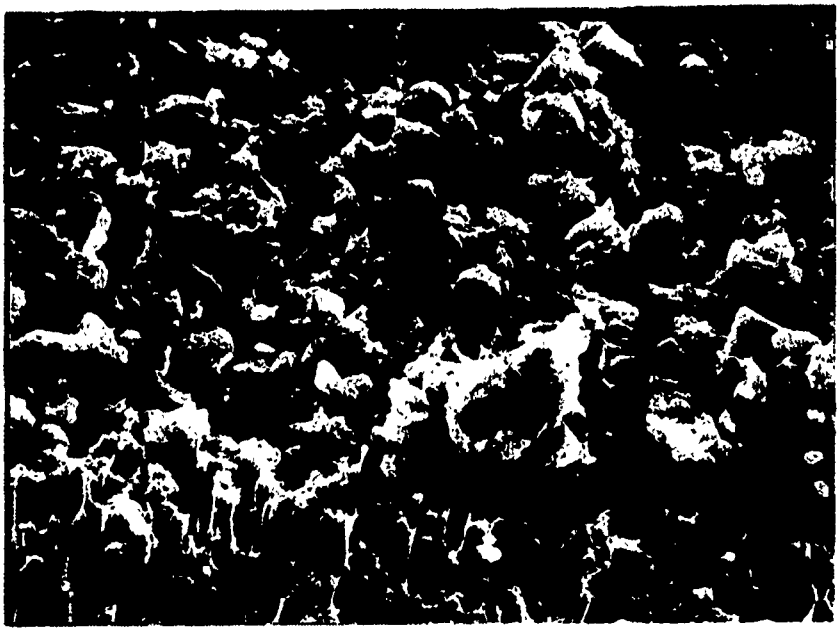

APS-1900-12

Figure 12. Compression side fracture surface of flexure coupon from AS4/PPS, panel 3. 1000X

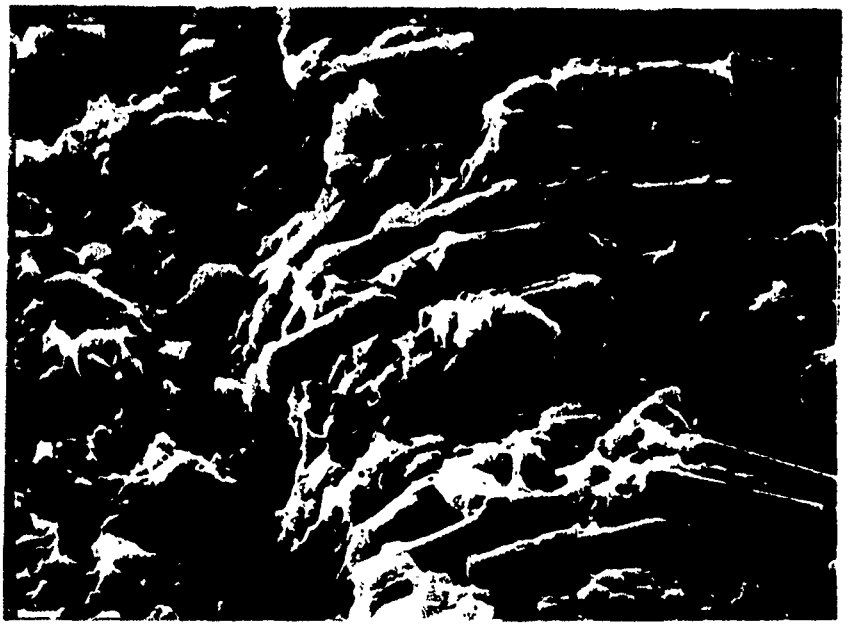

AP5-1800-13

Figure 13. Compression side fracture surface of flexure coupon from AS4/PPS, panel 3. Area in fracture surface where fibers failed in bending.

APS-1900-14

Figure 14. Tension side fracture surface of flexure coupon from AS4/PPS, panel 3. Compare with Figure 4 for resin adhesion to fibers. 1000X

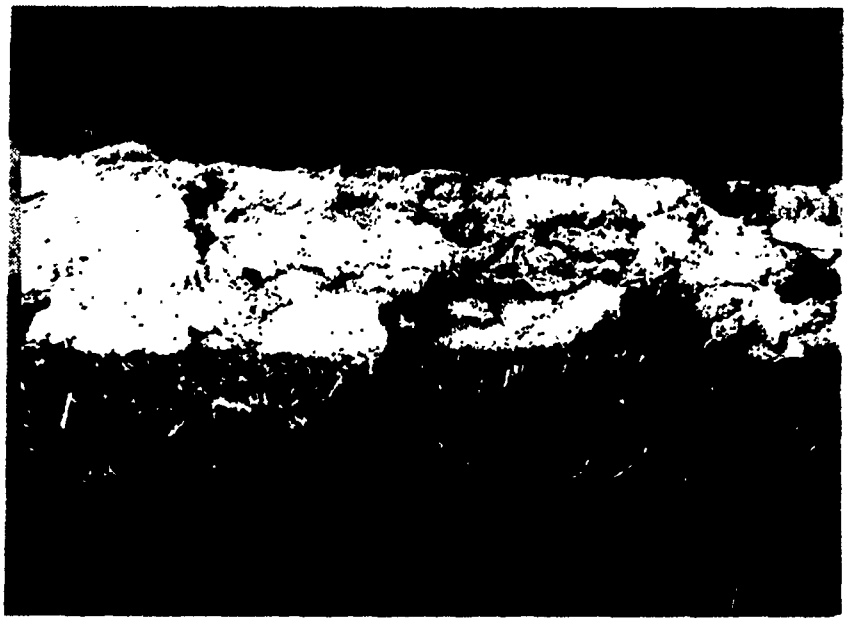

APS-1900-15A

Figure 15. Fracture surface of a flexure specimen from AS4/K-II panel 2. Tension side is shown on the bottom.

20X

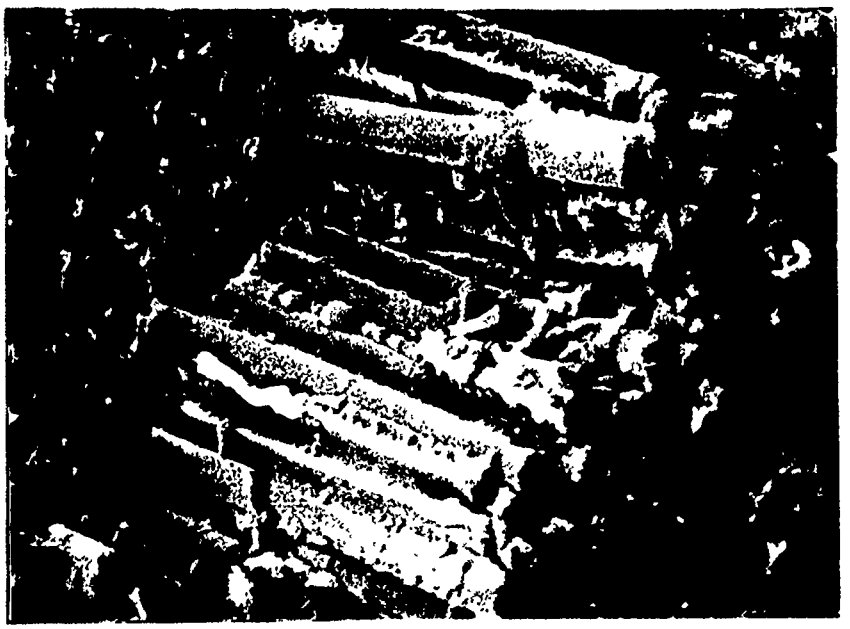

AP5-1900-16A

Figure 16. Compression side fracture surface of flexure specimen made from AS4/K-II panel 2.

700X

AP5-1900-17A

Figure 17. Tension side fracture surface of flexure specimen from AS4-K-II panel 2.

1000X

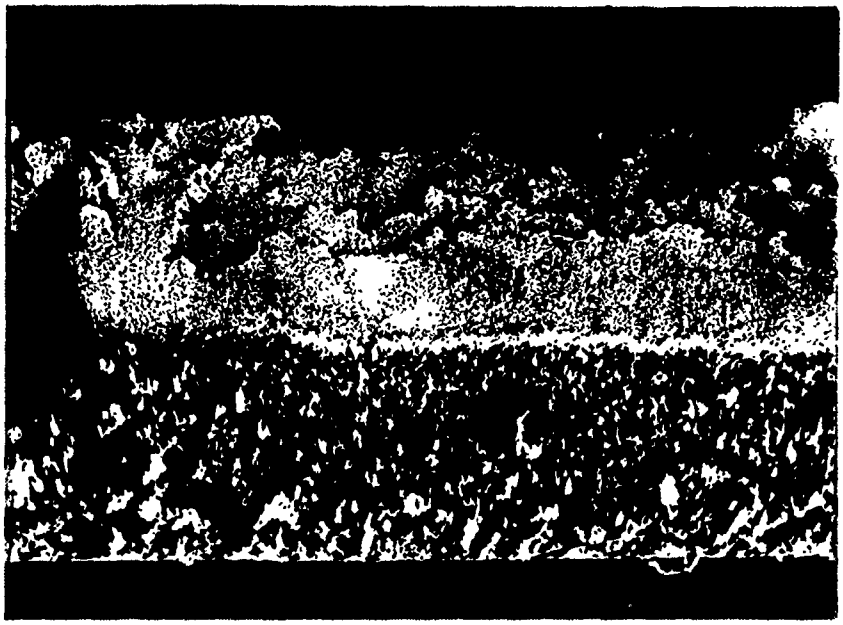

APS-1900-18

Figure 18. Fracture surface of a flexure specimen made from AS4/PEEK, panel 12. Tension side surface is shown on bottom.

30X

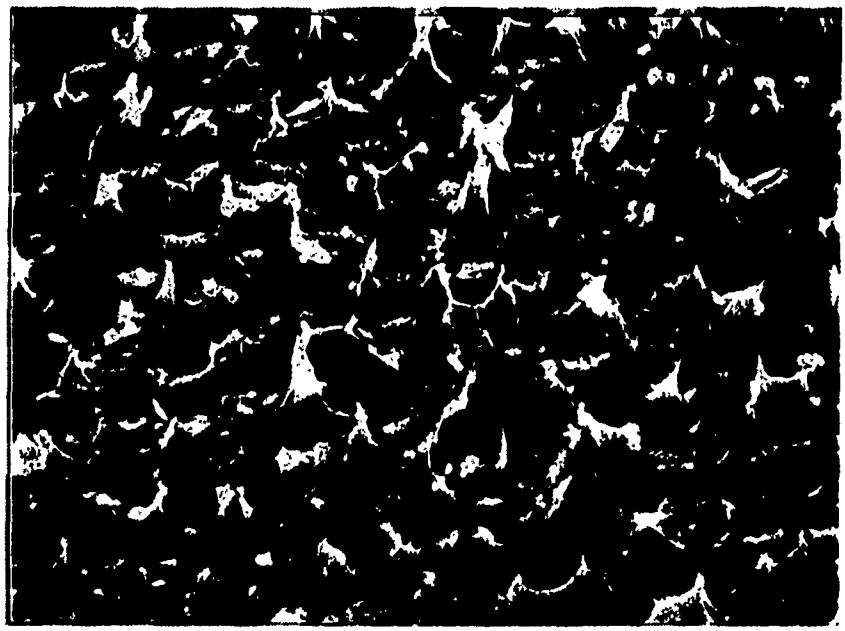

APS-1900-19

Figure 19. Compression side fracture surface of specimen made from AS4/PEEK, panel 12. Resin tear structure indicative of ductile plaster material.

1200X

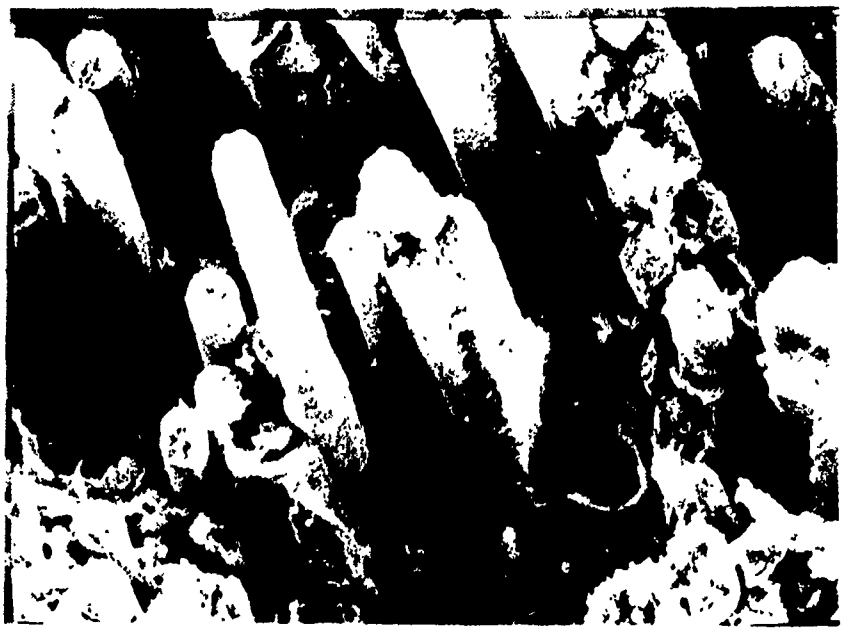

AP5-1900-20

Figure 20. Tension side fracture surface of specimen made from AS4/PEEK, Panel 5. Good adhesion evidenced by resin residue on all fiber surfaces.

1000X

DELAMINATION INHIBITION AND PROMOTION IN FIBER-EPOXY COMPOSITES

B.Z. Jang, W.C. Chung, Y.K. Lieu and L.R. Hwang
Materials Engineering
Auburn University, Alabama

ABSTRACT

Research was initiated to study the delamination mechanisms in continuous fiber reinforced composites. The concept of controlled interlaminar bonding (CIB) was proposed and followed in preparing fiber-epoxy composite laminates with enhanced fracture toughness, without significantly degrading the strengh properties. The interlaminar bonding was manipulated by several techniques including inserting delamination promotors, surface modification of laminae, and incorporating third-direction fibers. Preliminary results indicated that the plane-strain fracture toughness of E-glass-epoxy laminates can be improved by inserting perforated interlaminar films of aluminum foil, paper, fabrics, polyester, and polyimide. Such interlayers were used to promote delamination that will dissipate strain energy as well as diverting and blunting the Griffith crack. The fracture resistance of a laminate was found to depend on the degree of delamination in competetion with the propagation of a main crack, which is in turn controlled by the relative magnitude between the interlaminar strength and lamina cohesive strength. The former is determined by the degree of interlayer perforation, bonding betweaen the interlayer and the laminae, and the concentration of third-direction fibers. Although the third-directional fibers tend to inhibit delamination they compensate for this effect by increasing the interlaminar surface energy, resulting in respectable toughness without excessive delamination. The loading direction is also found very important in dictating the failure processes. The results of a study on several composite systems are presented and discussed along with post-failure observation data.

INTRODUCTION

High strength and high toughness are usually considered to be mutually exclusive in conventionally made high-modulus fiber composites. Composites with a strong fiber-matrix interfacial bond tend to have a high strenth but low toughness. A crack in such materials usually breaks through all the filaments in the path of the crack and complete fracture ensues with very little amount of energy dissipated. Composites with a weak interfacial bond, although may be fracture resistant due to extensive debonding and great fiber pull-out friction, is often of low strength.

To alleviate this problem several attempts have been made to impart high toughness to the composites without sacrificing the strength properties [1-9]. This subject has been reviewed by Mai et al.[10]. They all rely on suitably modifying the interface either between fiber and matrix or between two laminae. In one method [1,2] the fibers are intermittently coated with an appropriate viscous fluid such as polyurethane varnish. The varnish-coated zones would mask the effects of surface finish originally applied to improve the interfacial bonding. The uncoated, and therefore strongly bonded, zones ensure that the fiber strength is picked up while the weak areas serve to blunt the running cracks by the Cook/Gordon mechanism as well as to produce large fiber pull-out lengths, resulting in a large fracture toughness.

Instead of intermittent fiber coating, the method of controlling the bonding between prepreg layers may be used to improve the fracture toughness of composite laminates. Favre [11] used full films of either metallic or orgarnic material as delamination promotors in composite laminates. These films were stacked between prepreg layers to induce an extensive delamination of the test pieces which would absorb a great amount of energy. The main crack propagats in a plane perpendicular to these films while the multiple spliting between layers may impart additional toughness to the laminate by diverting and blunting the main crack. However, the composite is often subject to a loss in strength. Jea et al. [12] have used a technigue for producing intermittent bonding between laminae which consists of interspersing layers of thin Mylar films between adjacent prepreg layers. Each Mylar film consists of a matrix of holes that would allow epoxy resin to flow between laminae. Through these holes a strong bonding can be achieved after cure that would help maintain the strength properties. The remaining solid Mylar film leads to a relatively weak interlaminar bonding and acts as a delamination promotor. Both the strength and the toughness of a laminate can therefore be achieved simultaneously. Similar concept has been explored by Mai et al.[13] and by Elber [14].

In the present report a generalized concept of controlled interlaminar bonding is proposed and discussed. It is suggested that, besides perforated Mylar films, many other materials in several different forms may be used, some of which may be of lower cost, easier to fabricate, and more effective in controlling the composite strength and fracture resistance. A research project has been initiated to attempt to understand the fracture mechanisms of composite laminates prepared according to the concept of controlled interlaminar bonding (CIB). Preliminary results are herein presented that demonstrate the general validity of the CIB concopt. The perforated films used include Mylar, Kapton (polyimide), paper, aluminum, and textile fabrics. Another possible way of practicing the CIB concept is to introduce the fiber reinforcement in the third direction to form a multidimensional (or 3-D) composites. Although certain degree of delamination may imparts fracture toughness to a material, an extensive delamination resulting in a loss of strength is not desirable. Bradshaw et al [15] suggested that a third direction fiber reinforcement may increase the interlaminar strength and fracture energy of composites. Novak [16] also recognized the potential of 3rd direction reinforcement when he stitched plies of boron/glass together with Kevlar-49 fibers and obtained increased resistance to delamination. Herrick [17] showed that multidimensional composites possess superior impact resistance to comparative 2-D laminates. These suggest that an appropriate placement of 3rd direction fibers may lead to a maximum fracture energy with a minimum degree of delamination or fracture damage. The delamination conditions for various configurations of laminate are identified and discussed.

EXPERIMENTAL

Materials

The materials used in the present investigation are listed in Table 1. Prepreg tapes of E-glass-epoxy with commercial name 'Scotchply 1003' were received from 3M. These include unidirectional, crossplied, and quasi-isotropic ($0^{\circ}/+60^{\circ}/-60^{\circ}$) tapes. The delamination promotor (DP) films inserted are Mylar, Kapton, bleached paper, aluminum, or textile fabrics, each containing a uniform distribution of holes. Both film thickness and area fraction of holes are controlled as material parameters. Unless otherwise specified, the stacking sequence of prepreg layer(p) and delamination promotor(d) is pdpdpd...pdp,i.e. the outer layers are prepreg tapes and there is one and only one promotor film sandwiched between two tapes. Since each isotropic tape as received consists of five layers by itself, the total volume of the delamination promotor films only represents a small fraction of the composite laminate.

Sample Preparation

A. Delamination Promotion

The first step in the sample preparation involved the design of a method to perforate the DP films. The first design consisted of a 6"x 8"x 1/2" piece of balsa wood with pins inserted through the wood and glued in place. The films to be perforated were placed and punched on the plateform made of foamed plastic. This design only permits the perforation of a few layers at a time. A second technique of perforation was to stack a number of DP films together and sandwiched these films inbetween two sheets of graph papers. A uniform distribution of holes were then created by drilling through the lattice points of the graph paper. The hole size and the total area fraction of holes may be varied by changing the lattice constant (the grid size) of the graph paper and the drill bit size. Both techniques appear to give satisfactory results. The perforation area was measured by light microscopy followed by a computerized image analysis.

The prepreg tapes with alternating layers of DP film were then placed in a stainless steel mould with cavity dimensions of 6"x 8". The thickness of a sample is determined by the requirement of test piece geometry. For instance, the plane strain fracture toughness test (ASTM E-399) requires a thick specimen. Each isotropic composite laminate used in this test consists of 8 layers of prepreg tapes and 7 layers of DP films, while the corresponding tensile bars consists of 4 and 3 layers, respectively. The material was then cured in a compression molding press according to the temperature and pressure programme suggested by the material supplier.

B. Delamination Inhibition

The laminates prepared in this phase of study are divided into five groups as listed in Table 2. Each group of samples were designed for a specific purpose. Type A samples include unidirectional glass fiber-expoxy laminates (1-D) and their 2-D counterparts. The 2-D materials were constructed by laying up small strips cut from a unidirectional prepreg tape in the second direction on the surface of a first directional tape (Fig. 1). The strips were arranged intermittently with empty space that was later filled with epoxy resin during curing. Such second-dir. fibers were introduced to act as delamination inhibitor in the otherwise 1-D material. They were also used to strengthen the weak planes when loaded in the 2nd or 3rd direction. Volume fraction of the 2nd-dir. fibers were controlled as a material variable.

In type B, the third directional Kevlar fibers (TDKF) were stitched through the 2-D COFAB Kevlar fabrics to produce a 3-D preform which was then impregnated with epoxy resin before

compression-molding. This group of samples were designed to determine if a 3-D composite would possess a greater damage resistance than a corresponding 2-D material.

Type C samples are basically 3-D laminates composed of 2-D graphite fabrics stitched with TDKF. The TDKF were so arranged that in each 3-point bending or impact loading specimen there exists a center zone free of TDKF. The dimension of this 2-D zone was varied to allow possibly varying degree of delamination upon loading of specimen at the center. We were interested in learning how the TDKF would act to affect the delamination process of 2-D laminates. A special 3-D sample with fibers coated with a thin layer of polybutadiene rubber before epoxy impregnation was prepared to see whether delamination promotor (rubber layer) and delamination inhibitor (TDKF) can be concurrently manipulated to achieve an optimum fracture toughness.

Type D materials were prepared from crossply prepreg tapes of E-glass epoxy. They include both 2-D and 3-D laminates, the latter containing TDKF penetrating through the 2-D laminate. Each TDKF yarn consists of 1, 2, 3, or 4 strands of filaments. The yarn was inserted through each lattice point of a graph paper glued on the top prepreg layer to ensure a uniform arrangement of TDKF. The symbol "4+4-*" was used to represent the case where TDKF penetrates through the corner points as well as the face centered points of the square lattice, implying a double implantation of TDKF.

Type E materials also combine the concepts of delamination promotion and inhibition. The 2-D samples include a control group of specimens which are essentially crossplied (or bidirectional). The second and third groups have different stacking sequences comprising alternate layers of Kapton film and prepreg tape. The TDKF was stitched through these 2-D layers to form 3-D laminates.

In order to measure the fracture toughness of a material, the laminate was machined into compact tension test specimens as shown in Figure 2. The chevron notch in the compact tension specimen of an isotropic laminate was positioned so that the loading direction was parallel to the fiber direction of the 0 degree tapes. In the unidirectional laminates the notch is oriented perpendicular to the fiber direction. The chevron notch was further sharpened by a razor blade and used as a starting crack. Standard rectangular bars were used for both impact loading and three-point bending test. The tensile testing bars were obtained by grinding and polishing the thin and rectangular specimens fixed in a dumbell-shaped templet.

Mechanical Testing

In order to determine if incorporation of DP films would degrade the tensile strength of a laminate an ASTM standard test

was conducted on each type of composites prepared. The tensile test was performed in a screw-driven Instron testing machine with a cross-head rate of .1 in./min.. Any specimen that did not fail in the gauge section was considered to be invalid and therefore rejected. The tensile strength presented here represents an average out of several valid tests.

Both unnotched and notched specimens were loaded in a flexural mode along two different loading directions. Both slow three-point bending and high-rate impcact testing were conducted to study the loading rate effects on the failure mechanisms. One loading direction (hereafter referred to as y-direction) was designed to be normal to the original laminar plane (Fig.3a) so as to create natural delamination (between original prereg layers). A second loading direction (z-direction) was oriented to be parallel to the original laminar plane (Fig.3b). These two directions represent the extremes of possible real loading directions. The delamination phenomenon in each case was carefully studied with naked eyes during flexural loading and by light microscopy and scanning electron microscopy (SEM) after flexural or impact loading. The notched specimens in each case were used to study the interaction between the main crack and the perpendicular cracks, as an attempt to understand the criteria of delamination. The slow flexural loading was performed using a fully computerized MTS mechanical testing machine while the impact test was conducted in a Tinius Olsen impact tester.

The ASTM E-399 plane strain fracture toughness test for metallic materials was adapted to measure the fracture resistance of composite laminates. The same MTS machine was used for this test throughout the investigation.

Microscopy

Well-polished specimens were examined by optical and SEM methods before and after mechanical testing to observe the microcracking and macro-delamination phenomena. A few specimens were loaded and unloaded before a complete failure ensued and their crack propagation modes observed intermittently by optical microscopy. Final delaminated or fractured surfaces were also examined by TEM. The instruments used were Zeiss optical microscope, and AMR Model 1000 and ISI 40 SEMs.

RESULTS AND DISCUSSION

A. Delamination Promotion

The tensile and compact tension test results are listed in Tables 3 and 4, respectively. It is clear that adding only seven perforated Maylar films (each of 12.5 um thick) in an 8-ply isotropic glass fiber-epoxy laminate (total thickness ~ 1/4 in.) has increased the fracture toughness by 27% without sacrificing

the tensile strength. Mylar films only occupy 2% by volume of the total laminate. The specifications of delamination promotor materials are listed in Table 5. The delamination promotor (DP) films in this group of samples are designed to be parallel to the propagation direction of the main crack and perpendicular to the main crack plane. This type of configuration is not expected to be effective in promoting delamination.

Eight different types of fabrics with varying hole concentration were used to "reinforce" the isotropic laminates. It was found that, in general, lower area fraction of holes (areas of stronger interlaminar bonding) results in a greater level of delamination and therefore a larger value of impact energy (or larger area under the load-displacement curve obtained from a 3-point bending test).

The samples were loaded in either Y-direction or Z-direction. The isotropic laminates loaded in Z-dir. generally show a slightly higher impact value than those loaded in Y-direction. The former exhibit a combination of transverse buckling, delamination, and main crack propagation. The delamination in the Z-dir. samples is not as extensive as in the Y-dir. samples. However, the splitting in the former usually took place within the original prepreg tape which each consists of several plies with different fiber orientations. The strain energy dissipated in creating a unit area of delamination is greater in this case than in the case of delamination between the fabric layer and the prepreg layer.

The difference in impact energy between the Z-dir. and Y-dir. loading of unidirectional laminates is considerably higher. The main crack propagation mode ("cut tape") during Z-dir. loading of unidirectional samples has been suppressed with the transverse buckling and delamination dominating, resulting in a great level of energy absorption. The delamination is more extensive in the Z-dir. than in the Y-dir. loading. The load-displacement curves obtained from the 3-point bending tests for all composites studied also exhibit significantly different features. For instance, Fig.4a shows that an isotropic laminate loaded in the Z-dir. exhibits a maximum in the load-displacement curve followed by a rapid drop in load, corresponding to the initiation and propagation of a catastrophic crack. Only a very small extent of delamination was observed in this specimen. The considerably higher degree of delamination observed in the corresponding specimen loaded in the Y-dir. was reflected by the numerous steps in the curve of Fig.4b. A careful study of the macroscopic failure modes lead to the following observations.

General Discussion on Delamination

1. Loading In Y-direction

When applying the load in a direction normal to the laminae the unidirectional laminate may exhibit several macroscopic failure modes, the relative importance of each mode depending on loading conditions, specimen geometry, and material parameters. If the beam supported at two ends has a long span than a tension failure mode on the tension side of the beam will occur at the midpoint where the stress is maximum or near it, at the weakest point. As the fibers in the first layer were broken a high shear stress will exist in the matrix between these two layers which may initiate cracks running toward both sides parallel to the layers (delamination). If the tension mode dominates the main crack will cut through the laminate thickness, resulting in very little delamination and dissipating only a small amount of strain energy. This would happen when the interlaminar strength (τ_i) is relatively strong.

If τ_i is moderate, the delamination mode would compete with the tension mode. Consider the interfacial crack (delamination) that initiated near the root of the tensile crack (main crack or Griffith crack). Since the stress is decreasing toward the supports, the interfacial cracks will be arrested after some distance. In the case of a short beam, the interfacial crack may grow all the way to one or both ends. If the loading is continued and when the stress in the second layer is high, the fibers will be broken and the main crack will propagate up to the third layer. Again, delamination may occur and propagate to certain extent. The resulted sample shows delamination as well as main crack failure, leading to a great level of energy dissipation.

If the τ_i is relatively weak, delamination will occur first, preferrably along the neutral axis where the shear stress is high. When this happens to a great extent the beam is essentially split up into two beams each having a neutral axis and tending to undergo separate delamination processes. This extensive delamination mechanism may continue to operate until the beam is bent to the extent that it simply slips through between two supports. In general, the main crack mode is essestially suppressed when such an extensive delamination takes place. However, when main crack does grow through these separate laminae assemblies each assembly (a few layers) tends to show both tensile and compressive failure on both sides of the neutral axis of each assembly. This can be clearly differentiated using SEM.

If the material is cross-ply or isotropic laminate the same mechanism is valid here, except that there are less layers to arrest the propagating crack. Further, in the case of isotropic laminate damage zone may extend at an angle different from 90° or 0°.

2. Loading In Z-direction

When unidirectional glass fiber/epoxy specimens were loaded the specimen often delaminated laterally and high energy absorption resulted. The failure mechanism in this case is transverse buckling and delamination as shown in Figure 5(b). This failure initiates on the compression side of the beam and results from the fact that weak planes are created in the vertical direction and there is no restraint preventing these planes from delaminating. In other words, there is no compressive stress normal to the planes as there would be in the case of Y-dir. loading. When a crossply or isotropic laminate is loaded along the Z-direction the main crack propagation ("cut" type) is always a dominant mode of failure. The energy needed to propagate a crack through the crosssection is much lower than the energy need to form a great deal of delamination between the layers as the crack advances or pushes through the crosssection [18]. In the case of crossply laminate, the crack front is not straight as there are weak layers in the thickness where it can propagate easily. These weak layers let the crack surround the other layers and fracture the fibers without arresting the crack propagation. This explains why crossply and isotropic laminates, when loaded in Z-direction, did not show a high level of energy absorption. All samples loaded in Y-direction do show varying degree of delamination. Sometimes delamination does take place at the compression side but it is restricted to a few layers while in the case of Z-direction loading of unidirectional laminates it starts with many layers and propagate downward, thus absorbing a large amount of energy.

3. Transition of Failure Mode

Aveston [19] considered one longitudinal crack extending the whole length of the test bar in three-point bending. The maximum energy was found to be three times the fracture energy in the brittle mode (Griffith cracking only). Aveston further notes that if the sample repeatedly delaminates according to the successive neutral axes of the bar, more energy can be absorbed. Similarly, Hancox and Wells [20] observed that, for carbon-glass sandwich composites, the work of fracture as measured by the Izod test or the slow bend test was greater than the calculated work from the flexural strain energy stored in the bars.

Bader and Ellis [21] showed that when various carbon fiber-reinforced plastics are compared on the basis of the standard Charpy test, there is a transition from one mode to the other. This transition takes place when:

$$\frac{\sigma_c}{\tau_i} = \frac{2L}{D-d} \qquad (1)$$

where σ_c and τ_i are the flexural strengths and the shear strength, i.e. material parameters, respectively, while L, D, and d are the test parameters, i.e. span and depth of beam and notch length, respectively. This equation may be derived on the assumption that the subcracking (delamination) will take place if the shear stress Fs exceeds the shear strength τ_i of the composite before the flexural stress Ff exceeds the flexural strength σ_c of the composite. Or if:

$$\frac{Fs}{\tau_i} > \frac{Ff}{\sigma_c} \quad \text{or} \quad \frac{Fs}{Ff} > \frac{\tau_i}{\sigma_c} \qquad (2)$$

For a beam loaded in three-point bending at the center (also Charpy testing) :

$$Fs = \frac{3W}{4b(D-d)} \qquad (3)$$

$$Ff = \frac{3WL}{2b(D-d)} \qquad (4)$$

where W is the load at failure and b is the breadth of the specimen. Therefore Eq. (2) reduces to

$$\frac{\tau_i}{\sigma_c} < \frac{D-d}{2L} \quad \text{or} \quad \frac{\sigma_c}{\tau_i} > \frac{2L}{D-d} \qquad (5)$$

and transition between Griffith cracking mode and subcracking mode occurs if Eq. (1) holds. Our data indicates that Eq. (5) is a useful guideline for predicting failure modes in composite laminates subjected to flextural loading.

B. Delamination Inhibition

Type A:

The top curve shown in Fig. 6 indicates that, when loaded in the axial direction of the second directional fibers, the impact resistance of the composite laminate with the 1st-dir. fibers parallel to its length decreases with increasing volume fraction of the 2nd-dir. fibers. Post-failure examination of the specimens shows a decreased degree of delamination when the volume fraction of the 2nd-dir.fibers is increased. In-situ observation of macroscopic failure mechanisms during a three-point bending test confirms this trend. These observations suggest that introduction of a controlled amount of 3rd-dir. fibers should help inhibit the delamination of an otherwise 2-D laminate if so desired.

The bottom curve of Fig. 6 describes the impact resistance of a composite laminate as a function 2nd-dir. fibers when the loading direction is parallel to the 1st-dir. fibers. In this case the 2nd-dir. fibers help to carry an increasing level of load, leading to a higher fracture resistance. Without the 2nd-dir. fibers in the present case the load would be essentially carried by the matrix alone. Corresponding compact tension tests showed that the stress intensity factor (Kq) increased from 1.07, 10.7, 22.9, 23.3, to 28.6 (Ksi-in**.5) when the 2nd-dir. volume ratio (V2/V1) increased from 0, 0.3, 0.5, 0.75, to 1.0. These observations, although appear to be trivial, do have important implications in controlling the failure processes of composites. They can be extrapolated to the case of the 3-D composites which should either show superior fracture resistance over the 2-D materials when loaded in the weak direction or assist in resisting the delamination of the 2-D laminate when loaded in the strong directions.

Type B:

Limited data (Table 6) show that the 3-D all-Kevlar composites exhibit only slightly higher impact energies than the corresponding 2-D materials. However, 3-D materials show a much lower degree of delamination damage when loaded in either Y- or Z- direction.

Type C:

Rubber coating on the fiber surface, if with a relatively weak rubber-fiber bond, should tend to promote microdelamination while the 3rd-dir. fibers tend to inhibit delamination. These two effects seem to be conflicting to each other. However, it is expected that the propagation of the delaminating crack should absorb a greater amount of energy in 3-D than in 2-D (on the basis of per unit area of new surface created). A combination of both effects surprisingly results in a 3-D material with a superior impact strength (Table 7).

Type C and D:

Based on the limited data obtained thus far, the size of a central 2-D zone in an otherwise 3-D laminate did slightly affect the resulted degree of delamination; the higher the size, the greater the delamination. However, no apparent improvement in the impact strength was recorded (fig. 7). The 3rd-dir. fibers, although make it difficult to delaminate (therefore result in a smaller area of delamination), did require a higher energy absorption per unit crack area. These two effects seem to compensate for each other in the present case.

Type D:

The impact strength of 2-D and 3-D composites is plotted against the measured delamination area as shown in Fig. 8. It is clear that greater delamination is generally associated with a higher impact energy. However, given the same resulted delamination area the 3-D material exhibits a superior impact energy. This example vividly indicates the great potential of the 3rd-dir. fiber reinforcement in controlling the damage resistance of composites.

Type E:

Table 8 also reveals that a combination of delamination promotion concept (using Kapton films) and delamination inhibition concept (using 3rd-dir. fibers) could provide an effective method in tailoring the fracture resistance of composite laminates.

CONCLUSION

A new concept of controlled interlaminar bonding (CIB) has been introduced to optimize the damage resistance of composite materials. The interlaminar strength can be controlled by inserting extra layers of delamination promotor films and/or introducing third directional fibers. The macroscopic failure modes have been identified and discussed. The general superiority of 3-D over 2-D composites in failure resistance is also demonstrated. An approprite manipulation of the delamination promotion (DP) and delamination inhibition (DI) agents could lead to a composite with a superior damage resistance.

ACKNOWLEDGMENT

Financial support for this project is provided by the Alabama Research Institute. We deeply appreciate this support.

REFERENCES

1. T. U. Marston, A. G. Atkins, and D. K. Felbeck, J. Material Sci. (1974) 447.
2. A. G. Atkins, J. Material Sci. 10 (1975) 819.
3. J. Cook and J. E. Gordon, Proc. Roy. Soc. A282 (1964) 508.
4. N. L. Hancox and H. Wells, Fiber Sci. Technol. 10 (1977) 9.
5. N. H. Sung,T. J. Jones and N. P. Suh, J. Mater. Sci. 12 (1977) 239.
6. J. G. Morley and R. S. Millman, J. Mater. Sci. 9 (1974) 1171
7. J. G. Morley and J. R. McCall, J. Phys. , D: Appl. Phys. 8 (1975) 15.
8. G. A. Cooper and M. R. Piggott, "Cracking and Fracture in Composits", in Fracture 1977, vol. 1 (ICF4, 1977) p 557.
9. A. G. Atkins and Y. W. Mai, J. Mater. Sci. 11 (1976) 2297.
10. Y. W. Mai and F. Castino, J Mater. Sci. 19 (1984) 1638.
11. J. P. Favre, J. Mater. Sci. 12 (1977) 43.
12. L. C. Jea and D. K. Felbck, J. Composite Mater. 14 (1980) 245.
13. Y. W. Mai, B. Cotterell and R. Lord, in "Progress in Sci. and Eng. of Composits",Vol. 1, ed. by T. Hayashi et al. (ICCM-IV, Tykyo, 1982) pp. 271-277.
14. Wolf Elber, "Toughening of Graphite-Epoxy Composites by interlaminar Perforated Mylar films", NASA TM-78643,1978.
15. F. J. Bradshaw, G. Dorey,and G. R. Sidey, "Impact Resistance of Carbon-Fiber Reinforced Plastics", Royal Aircraft Establishment Technical Report 72240, January, 1973.
16. R. C. Novak, "Materials Variables Affecting the Impact Resistace of Graphite and Boron Composites II", AFML TR-74-196, Part II, June, 1975.
17. J. W. Herrick, "Multidimensional Advanced Composites For Improved Impact Strength", Fiber Materials ,Inc. Tech. Report, 1979.
18. L. J. Broutman and A. Rotem, in "Foreign Object Damage to Composites", ASTM 568, ASTM, 1975 PP 114-133.
19. J. Averston, Conference Proceedings on the Properties of Fiber Composites, NPL (I. P. Guilford, 1971) p. 63.
20. N. L. Hancox and H. Wells, Composites (1973) 26.
21. M. G. Bader and R. M. Ellis, Composites (1974) 253.

Table 1. Materials listing.

Material Used	Commercial Name	Manufactured by
1. Unidirectional E-glass/epoxy prepreg tapes	Scotchply Type 1003	3M Company
2. Crossply E-glass/epoxy prepreg tapes	Scotchply Type 1003	3M Company
3. Two dimensional nonwoven Kevlar fabrics	COFAB Kevlar biaxial A2208	Composite Reinforcements Business
4. Two dimensional nonwoven graphite fabrics	COFAB Carbon biaxial A3313	Composite Reinforcements Business
5. Kevlar yarns	Kevlar-49	E.I.duPont de Nemours&Co.,Inc.
6. Kapton films	Kapton (polyimide)	E.I.duPont de Nemours&Co.,Inc.
7. Epoxy resin	EPON Resin 1001-A-80	Shell Company
8. Epoxy curing agent	ACME-"Z"	Distributors,Inc
9.Rubber toughening agent	CTBN 1300X13	BFGoodrich Co.

Table 2. A summary of samples preparation.

Note: * represents strand

Sample Categories	Variation in preparation	Materials Used
TYPE A	1. Standard (40 layers) (only 1D model) 2. Volume fractions of second direc. E-glass fibers; 0.3, 0.5, 0.75, 1.0 (2D model)	E-glass/epoxy, unidirectional. 30 layers of unidirectional prepreg tapes plus small strips of tapes.
TYPE B	1. Standard (15 layers) (2D model) 2. 2D model + TDKF (3D model)	Kevlar biaxial cloth Shell epoxy added. Kevlar fibers Shell epoxy added.
TYPE C	1. Standard (15 layers) (3D model) 2. Varying volume fractions of TDKF (3D model) 3. Varying the center spacing i.e. 1/4",7/16",9/16",3/4" 4. Surface treatment of fiber with butadiene rubber.(3D model)	carbon biaxial cloth Shell epoxy added. Kevlar fibers added in the third dir. Kevlar fibers added in the third dir. Kevlar fibers in 3rd dir. All fibers treated with polybutadiene.
TYPE D	1. Standard (13 layers) (2D model) 2. Varying the volume fraction of TDKF,i.e. 1-*,2-*,3-*,4-*,4+4-*. 3. Varying the center spacing, i.e. 3/16",7/16", 5/8", 1" (3D model)	E-glass/epoxy, crossply. Same crossply + 3rd dir. Kevlar fibers. Same crossply + 3rd dir. Kevlar fibers.
TYPE E	1. Standard $(0/90)_{13}$ (2D model) 2. $[(0/K/90/K)_{13}0]$ (2D model) 3. $[(0/90/K)_{13}0]$ (2D model) 4. $[(0/K/90/k)_{13}0]$+TDKF (3D model) 5. $[(0/90/K)_{13}0]$+TDKF (3D model)	E-glass/epoxy, bidirectional. bidirectional & Kapton films bidirectional & Kapton films bidirectional & Kapton & Kevlar bidirectional & Kapton & Kevlar

Table 3. Results of tensile tests

Type of Laminate	Type of DP Material	UTS (KSI)	Young's modulus E (KSI)	Fracture strain ε_f (%)
Isotropic* E-glass-Epoxy	None	37.1	752.3	4.6
	Aluminum Foil	37.7	631.8	5.6
	Kapton(50H)	27.6	631.8	6.8
	Mylar(25S)	36.8	821.8	4.3
	Paper	40.7	734.9	5.1

* Loading rate = 0.005 in./ min.

Table 4. Results of compact tension test for isotropic laminates

Type of DP Material	P (lbs)	Pmax (lbs)	K (ksi-$in^{1/2}$)	Rsc
None	717.9	749.7	22.32	1.064
ALUMINUM FOIL	789.8	843.38	23.61	1.049
Kapton	693.3	736.7	20.38	1.31
Mylar	837.0	877.5	27.55	1.30
Paper	656.3	719.3	19.64	0.874

Table 5. Specifications of delamination promotor materials

DP Material	Thickness (μm)	% Perforation
Aluminum Foil	50	30
Mylar 25S	6.4	30
Mylar 48S	12	28
Kapton 50H	12.7	20
Paper	25	25

Table 6. Comparision of 2D and 3D models of Kevlar/epoxy composites in Charpy impact test.

	IMPACT ENERGY-Y		IMPACT ENERGY-Z	
	FT-LBS	Standard Deviation	FT-LBS	Standard Deviation
2D MODEL	10.75	1.06	13.15	0.92
3D MODEL	11.25	0.35	14.0	0.71

Table 7. Comparison of Charpy impact energies of standard, wide spacing, and rubber treated samples loaded in different directions.

	IMPACT ENERGY-Y		IMPACT ENERGY-Z	
	FT-LBS	Standard Deviation	FT-LBS	Standard Deviation
Standard (3D model)	14.5	2.4	12.9	0.7
Wide spac.	14.3	1.1	12.6	0.3
Rubber treated	22.7	3.1	14.5	0.8

Table 8. Comparison of Charpy impact test data of samples with varying stacking sequence and amount of Kapton films.

	IMPACT ENERGY-Y		IMPACT ENERGY-Z	
	FT-LBS	Standard Deviation	FT-LBS	Standard Deviation
$(0/90)_{13}$	28.0	---	24.0	---
$[(0/K/90/K)_{13}0]$	27.5	0.5	24.5	0.5
$[(0/K/90/K)_{13}0]$ + TDKF	40.0	4.4	28.3	4.2
$[(0/90/K)_{13}0]$	25.0	---	20.0	3.6
$[(0/90/K)_{13}0]$ + TDKF	33.9	3.2	23.4	1.8

FIGURE CAPTIONS

Fig.1 Schematic of the procedure used in preparing model 2-D composite from the unidirectional prepreg tapes and the small strips cut therefrom.

Fig.2 Specifications of a compact tension specimen.

Fig.3 (a) Y-direction loading: loading direction perpendicular to the lamina plane. (b) Z-dir. loading: parallel to the lamina plane.

Fig.4 (a) The load-displacement curve of a fabric-reinforced isotropic laminate loaded in the Z-dir.. (b) Loaded in the Y-dir..

Fig.5 (a) Unidirectional laminate loaded in the Y-dir.. (b) in the Z-dir..

Fig.6 The impact energy of a model 2-D composite as a function of volume fraction of 2nd-dir. fibers.

Fig.7 The impact energy of 3-D composites as a function of the dimension of a center 2-D zone.

Fig.8 Impact energy as a function of delamination area and concentration of 3rd-dir. fibers.

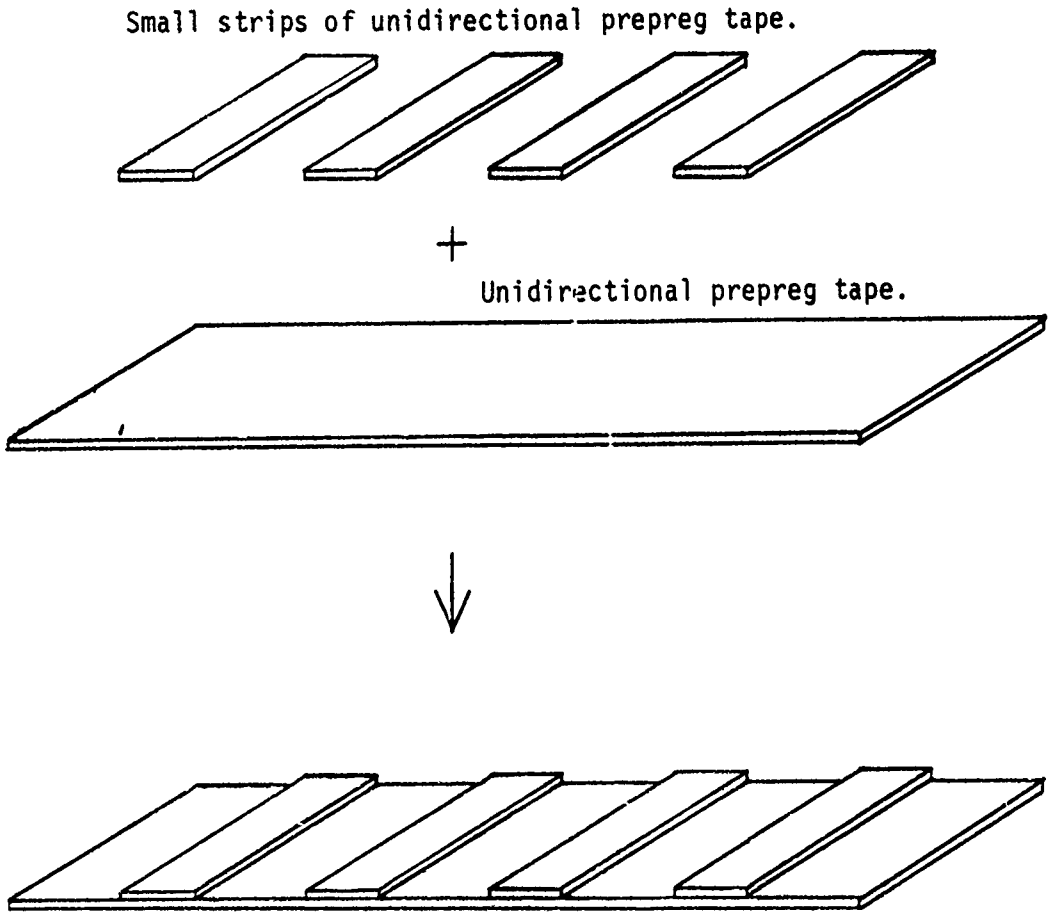

Fig. 1. Model of 2-D composite.

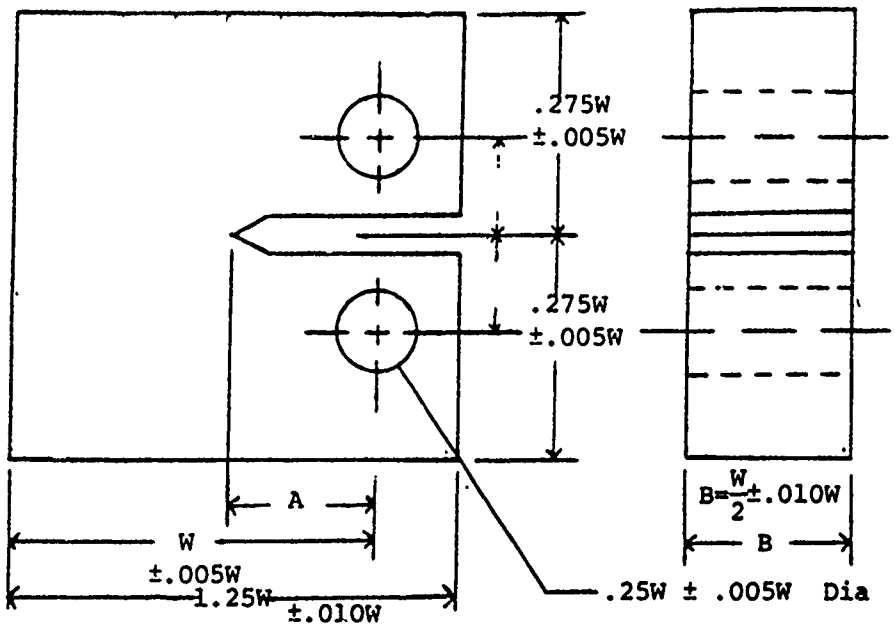

Fig 2.

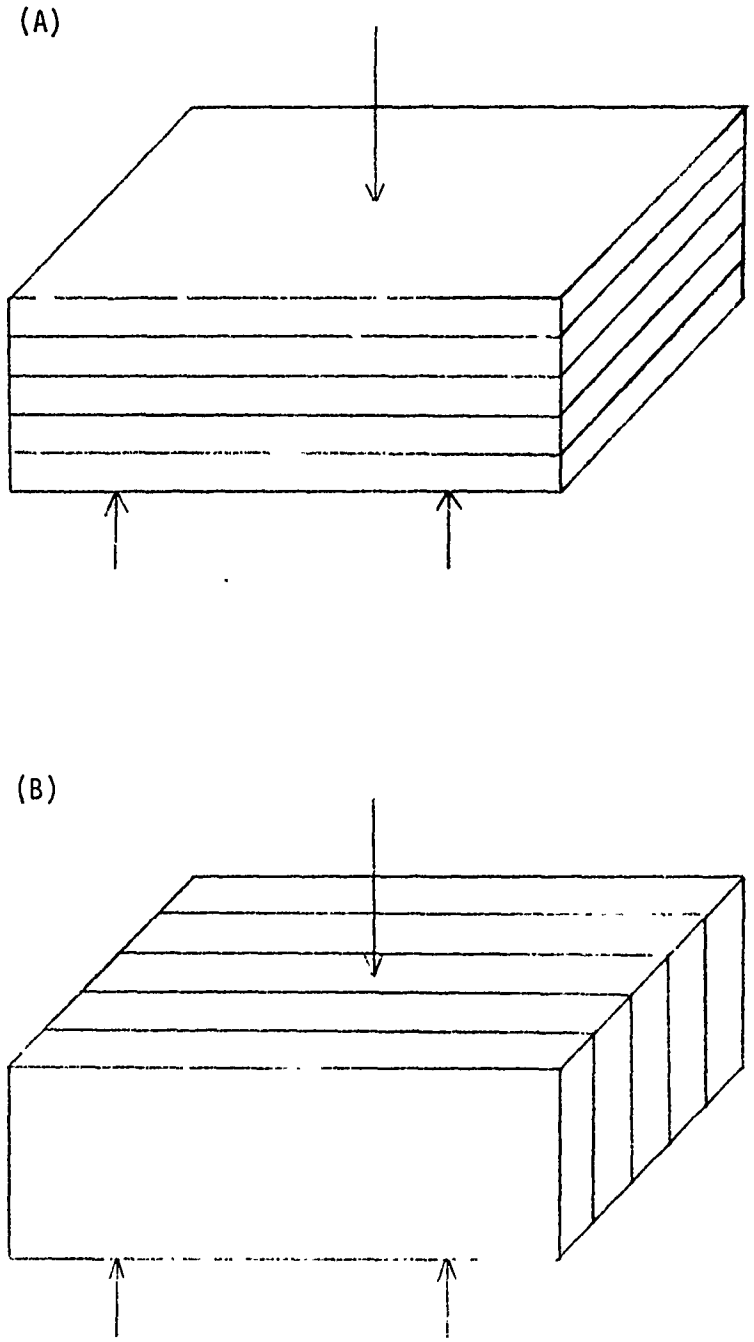

Fig. 3. (A) y-direction loading.
(B) z-direction loading.

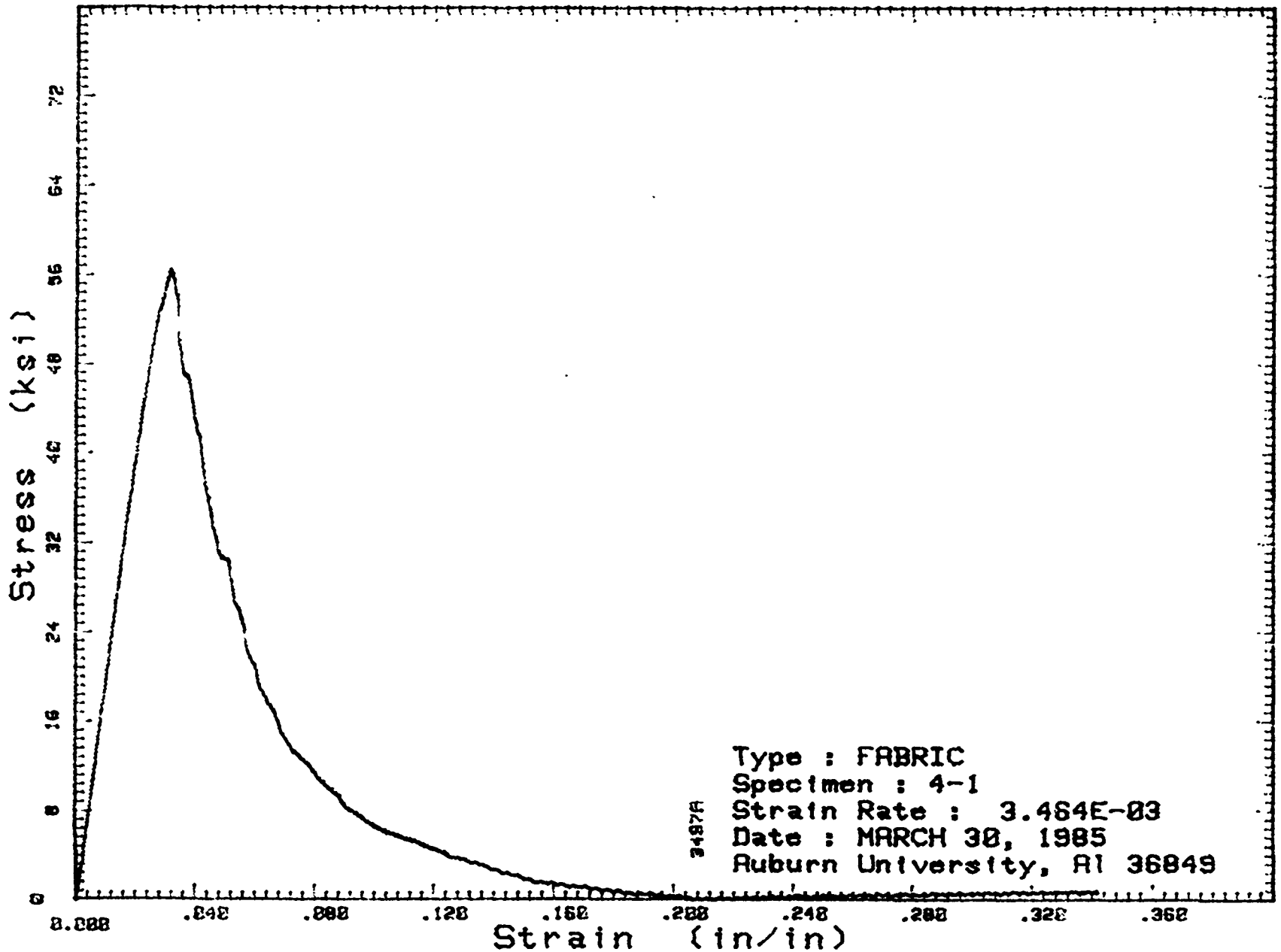
Stress (ksi)
0
8
16
24
32
40
48
56
64
72
0.000
.040
.080
.120
.160
.200
.240
.280
.320
.360
Strain (in/in)
Type : FABRIC
Specimen : 4-1
Strain Rate : 3.484E-03
Date : MARCH 30, 1985
Auburn University, Al 36849
3187A

Type : FABRIC
Specimen : 4-2
Strain Rate : 1.984E-03
Date : MARCH 30, 1985
Auburn University, Al 36849
34878
Stress (ksi)
Strain (in/in)
0
8
16
24
32
40
48
56
64
72
.000
.040
.080
.120
.160
.200
.240
.280
.320
.360

Fig 4

(A)

(B)

Fig. 5. (A) y-direction loading.
(B) z-direction loading.

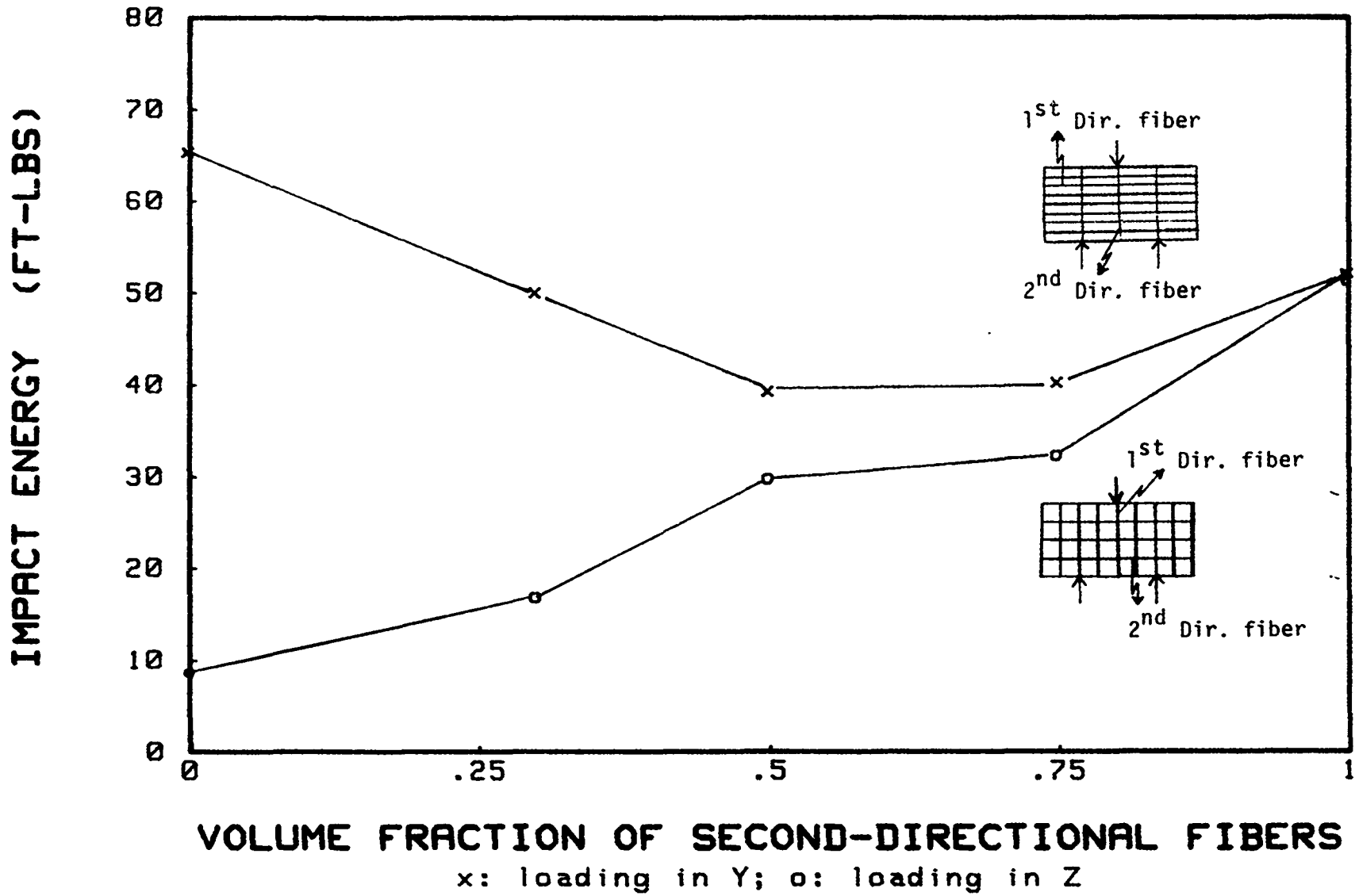
IMPACT ENERGY (FT-LBS)
80
70
60
50
40
30
20
10
0
0
.25
.5
.75
1
1st Dir. fiber
2nd Dir. fiber
1st Dir. fiber
2nd Dir. fiber
VOLUME FRACTION OF SECOND-DIRECTIONAL FIBERS
x: loading in Y; o: loading in Z

Fig. 6.

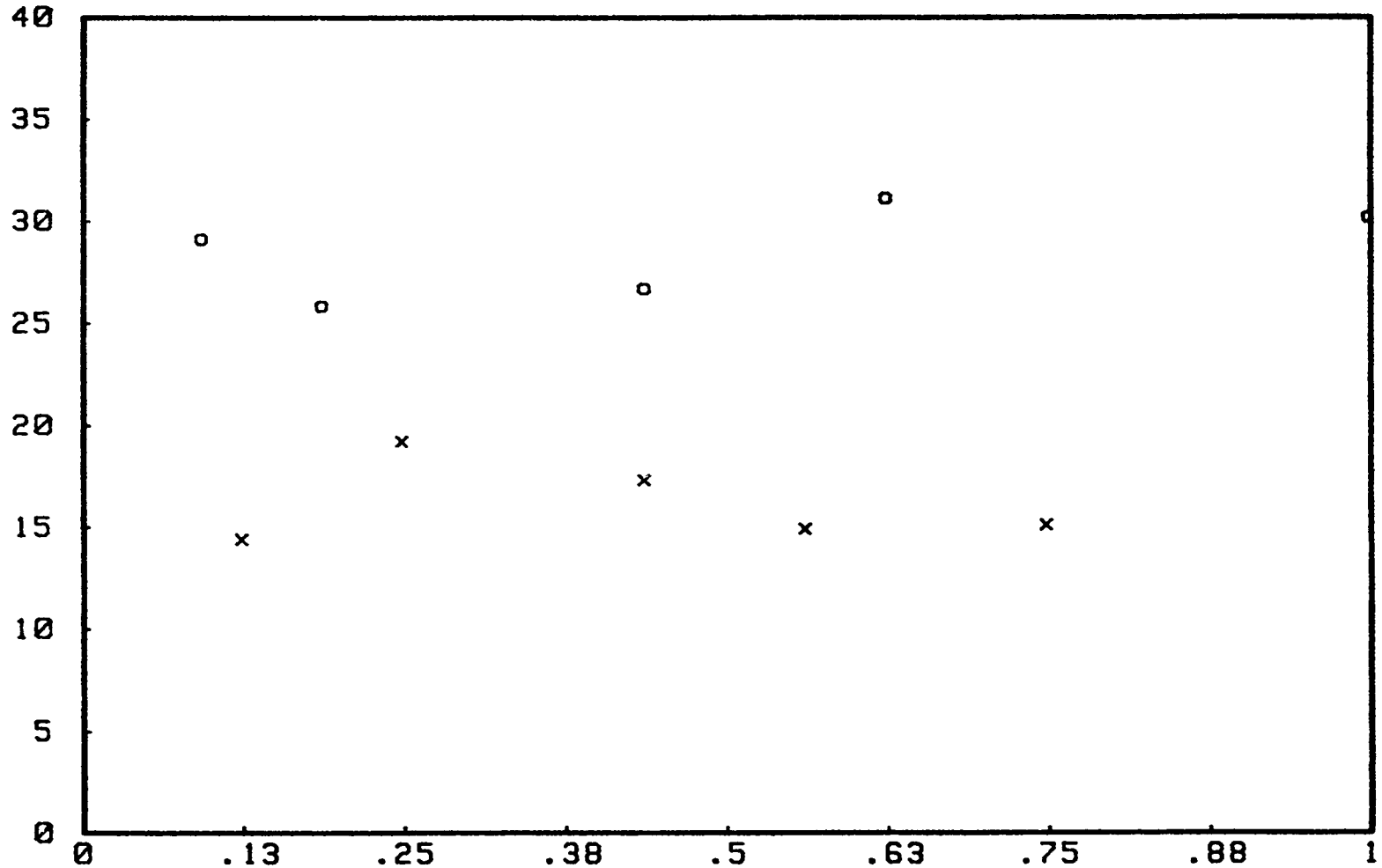
IMPACT ENERGY-Y (FT-LBS)
40
35
30
25
20
15
10
5
0
0
.13
.25
.38
.5
.63
.75
.88
1
CENTER SPACING OF TDKF (INCH)
x: graphite fabrics; o: crossply prepreg tapes

Fig. 7.

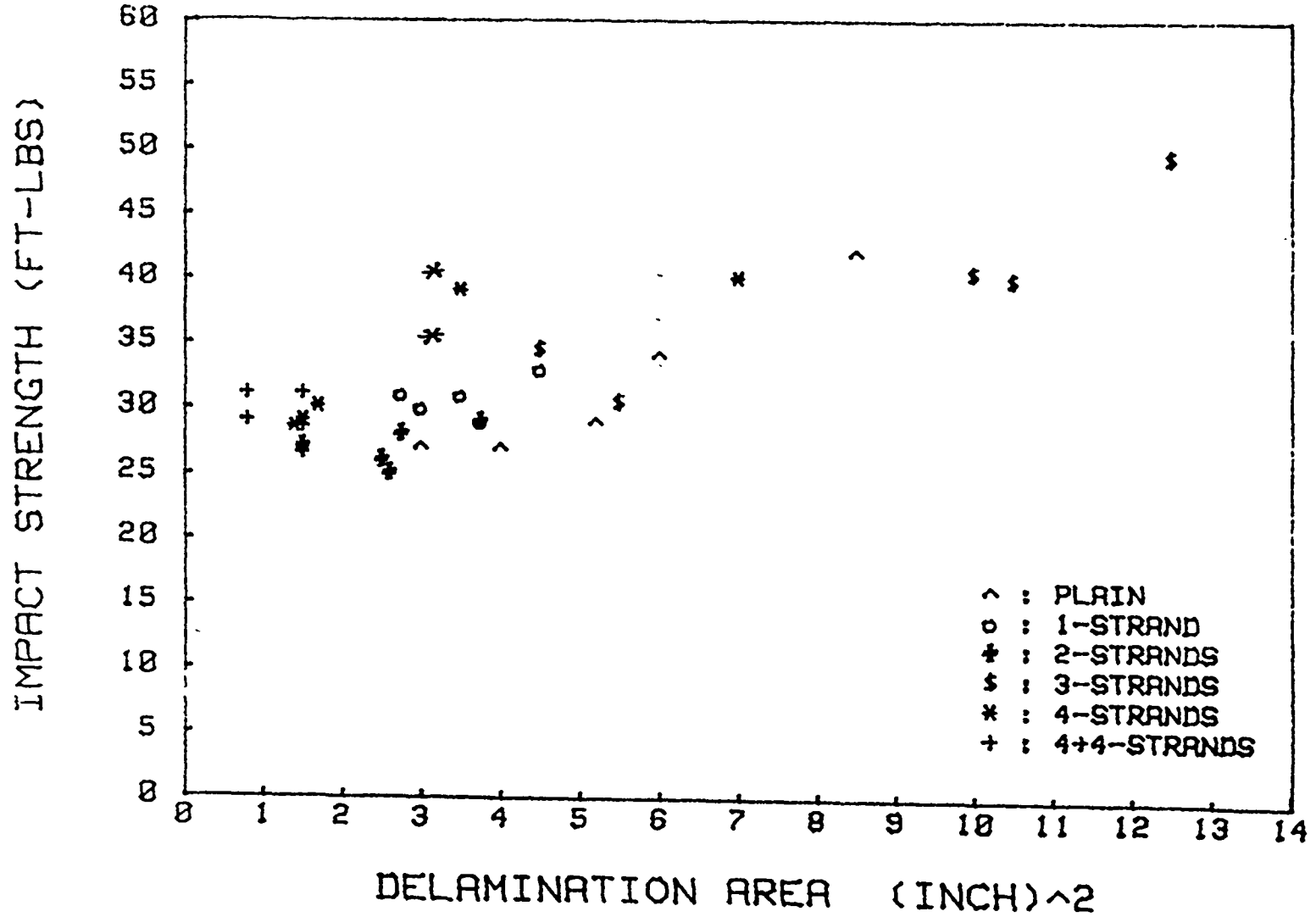

Fig. 8 Impact energy as a function of delamination area and concentration of 3rd direction fibers.

Session II

FAILURE BEHAVIOR;
PREDICTION AND VERIFICATION

RESIDUAL STRENGTH ASSESSMENT OF IMPACT DAMAGED CFRP LAMINATES

W.J. Cantwell and J. Morton
Department of Aeronautics
Imperial College of Science and Technology
London, England

Residual Strength Assessment of Impact Damaged CFRP laminates.

by

W.J. Cantwell and J. Morton.

Department of Aeronautics,

Imperial College,

London.

Abstract

A series of carbon fibre composites were subjected to low velocity impact loading. Damage initiation and propagation was assessed using optical microscopy and thermal deplying. The effect of impact damage on residual tensile strength was then examined.

It was found that impact resistance was strongly dependent upon the flexural stiffness of the composite target. The thin, flexible laminates failed in flexure whereas the stiff target failed at the top surface as a result of the contact stress field.

A simple fracture mechanics model was then successfully applied to predict the variation of residual tensile strength with impact energy.

Introduction

Advanced carbon fibre reinforced composite materials are finding increasing application in aerospace structures. The high specific strength and stiffness of these materials enable considerable savings in structural weight to be achieved at little extra cost. Indeed, carbon fibre composites are now used extensively in the

primary and secondary structures of many modern day aircraft.

One area of particular concern to the designer of aircraft structures is response of composite materials under localised impact loading. Previous studies have shown that impact loading generates large regions of delamination, matrix cracking and fibre fracture, the relative amount of each depending upon parameters such as the impactor geometry, support conditions, material properties and laminate stacking configuration (1-5).

Subsequent loading of impact damaged composites frequently results in significant reductions in residual strength. Previous work (6,7) has shown that impact damage, although invisible to the naked eye, can result in strength reductions of up to forty per cent.

This report details the findings of an experimental programme aimed at understanding the processes by which damage initiates and propagates in a composite structure when subjected to drop-weight impact loading. The effect of this damage on the tensile strength is also considered. A simple fracture mechanics approach is then employed in order to predict the variation of residual tensile strength with incident energy.

Experimental Procedure

The laminates studied in this program were manufactured from preimpregnated sheets of Courtaulds high strength, surface treated XAS fibres in Ciba-Geigy BSL 914C epoxy resin. Details of the laminate stacking configurations are given below.

Lay-up	No. of Plies	Thickness (mm)
$((+45^\circ,-45^\circ)_2)_S$	8	1.0
$(0^\circ,+45^\circ,-45^\circ,0^\circ)_S$	8	1.0
$((0^\circ,+45^\circ,-45^\circ)_2)_S$	16	2.0

After laying up the panels were cured in an autoclave following the manufacturers recommendations. This process yielded panels with a nominal fibre volume fraction of sixty per cent. After post curing the quality of the panels was assessed using an ultrasonic scanning facility.

Test specimens with dimensions 150mm x 25 mm x thickness were cut from the panels using a high speed diamond slitting wheel.

Impact testing was conducted on a drop-weight impact rig. Here a loaded carriage with a six millimetre diameter nose was raised to a predetermined height and released. The falling carriage was guided by two parallel rails to ensure a normal impact at the desired location. In this programme the composite targets were supported between two 12.7mm diameter roller supports positioned 50mm apart.

Impact damage was assessed using optical microscopy and thermal deplying. Thermal deplying was performed by placing the damaged coupons in a furnace preheated to a temperature of 420°C. After one hour the composites were removed and allowed to cool to room temperature. Complete deplying was then achieved with the aid of sticky tape and a sharp knife.

In preparation for static tensile testing aluminium end plates with dimensions 40mm x 25mm x 2mm were bonded to the ends of the damaged coupons. All tests were then conducted on an Instron universal

testing machine at a crosshead rate of 2mm/minute.

Results

Low velocity impact loading generated large regions of damage spreading well away from the point of impact. This damage comprised of delamination, matrix shear cracking and fibre fracture. The initiation and propagation of the damage was assessed using optical microscopy and thermal deplying. The former is now a well established technique yielding a clear two dimensional view of the damage zone. Thermal deplying, however, has not been widely used. This process can be of immense use since it yields a three dimensional view of the damage zone and allows the regions of fibre fracture and delamination to be readily identified. Shown in figure 1 is a deplied layer taken from a perforated sixteen ply (0°,+/-45°) laminate. In the figure the region of fibre fracture is clearly evident. Closer examination of the deply also highlights the presence of a region of delamination around the perforated region. The following section deals with the propagation of damage in the composite targets and the effect of such damage on the residual tensile strength.

It was found that impact resistance and subsequent residual properties were strongly dependent upon the composite stacking configuration. Consequently, the impact and post-impact behaviour of the laminates will be discussed seperately.

Eight ply (+/-45°) composite

The initiaton and propagation of damage in this laminate is detailed in the micrographs shown in figure 2. First damage was

detected in the matrix between the lower surface fibres after an incident energy of 0.63 Joules, figure 2a. This lower surface damage appears to be a result of a flexural failure, that is, the tensile component of the flexural stresses has exceeded the local fibre-matrix interfacial strength. The effect of this damage on tensile strength is shown in figure 3. It appears that this localised matrix fracture has little or no effect on tensile strength of the coupon. With increasing impact energy this lower surface matrix crack propagted upwards through the lowest ply to the neighbouring ply interface where it was deflected to form a plane of delamination. By 1.2 Joules damage has extended upwards through the thickness of the composite via a complex network of delaminations and matrix cracks. Closer examination of the micrographs suggests that two types of translaminar matrix cracks are present those that extend away from the location of lower surface fracture and those that are focussed towards the point of impact on the top surface. In previous work (8), it has been suggested that these two fracture mechanisms are a result of the contact and flexural stresses induced within the target respectively.

Reductions in residual tensile strength were first noted after 1.25 Joules. Examination of the deplies at this impact energy identified the presence of a small region of fibre fracture near the rear surface of the target.

In previous studies (4,9), workers have attempted to quantify the growth of impact damage by monitoring the variation of delaminated area with impact energy. Since this study is principally concerned

with understanding the effect of impact damage on tensile strength the transverse length of fibre fracture was chosen to characterise the growth of damage. The resulting curve for this eight ply laminate is shown in figure 4. Clearly the growth of fibre fracture with incident energy is rapid for energies between the threshold for fibre fracture and the perforation limit. Because this trend in damage growth appears to be approximately linear over this range of energies a least squares fit has been applied to the data and is shown in the figure.

Target perforation occurred after an incident energy of 3.22 Joules. Examination of the resulting micrographs and deplies indicated that the projectile had generated extensive damage extending well away from the location of impact. It was noted that the hemispherical nose of the drop-weight carriage had removed a frustrum shaped shear plug from the impact region, figure 2d. In removing this shear plug a large volume of fibres have been fractured indicating that considerable energy has been dissipated in this shear out process. Examination of the residual strength curve in figure 3 indicates that it is at this energy where the reduction in tensile strength is greatest. At energies above this threshold damage is slightly more localised and the reduction in strength not quite as severe.

Eight ply (0,+/-45°) composite

Although of similar thickness to the previous target the orientation of the fibres in this (0,+/-45°) composite renders it approximately three times stiffer and therefore alters its impact

resistance.

The treshold for first damage in this laminate was 1.0 joules, this being greater than the value of 0.63 Joules observed in the coresponding (+/-45°) target. The deplies and micrograph, figure 5a clearly identified the presence of fractured fibres in the lowest ply of the composite. Since these are the principal load-bearing fibres this damage although small and localised resulted in a twenty percent reduction in tensile strength, figure 6. Therefore, although the (0°,+/-45°) composite had a higher threshold for first damage than that of the (+/-45°) laminate, its threshold for fibre fracture was lower. Consequently the (0°,+/-45°) targets suffered reductuions in residual strength at lower incident energies than the (+/-45°) composites.

The subsequent progression of fracture is detailed in the micrographs shown in figure 5. At energies just above the damage threshold the lower surface fibre fracture generated a region of delamination and matrix cracking between the lower surface plies, figure 5b. This form of interlaminar fracture may be beneficial from a strength viewpoint since it serves to isolate the rear surface fibre fracture thus reducing any local stress concentrations.

With increasing incident energy the propagation of damage is essentially similar to that observed in the previous laminate. Here again fracture extends through the thickness of the composite via a network of matrix cracks and delaminations. Such damage will reduce the flexural stiffness of the target quite considerably, thus precipitating further fibre fracture in the lower surface plies.

The growth of damage with incident energy is shown in figure 7. Here again fibre fracture appears to vary in a linear fashion with impact energy. Damage was most severe at 2.9 Joules, again this being coincident with the threshold for target perforation. The perforation energy of this target is clearly below that of the corresponding (+/-45°) laminate. This disparity in perforation energies is primarily due to the energy dissipated in delamination, the area of interlaminar fracture in the (+/-45) laminate was approximately twice that incurred in the (0°,+/-45) composite. This is discussed in greater detail in reference 8.

Sixteen ply (0°,+/-45°) composite

This two millimetre thick composite represented the thickest and stiffest target considered. The initiation and propagation of damage in this composite is shown in figures 8 and 9.

Damage, in the form of localised matrix cracking, was first detected in the top surface layer after 1.6 Joules, figure 8a. This initial fracture appears to be a consequence of the impactor-induced stress field exceeding the local strength of the composite. Closer examination of the impact region suggested that this top surface matrix damage had initiated at the edge of the area of contact. In considering the contact problem (8), it has been shown that the tensile stresses are a maximum at the periphery of the area of contact. It therefore seems likely that this top surface failure incurred in this laminate is a result of these tensile stresses exceeding the tensile strength of the local fibre-matrix interface. This substantiates the findings of Dorey

(9) who reported a sizeable increase in the damage threshold energy in surface treated composites.

With increasing energy this crack propagated downwards forming a plane of delamination between the uppermost plies. The residual strength curve in figure 10 indicates that this damage has no effect on the tensile strength of the coupon. With increasing incident energy damage propagates through the thickness as shown in figure 8c. In this figure the presence of a number of translaminar matrix cracks are clear. These cracks appear to radiate downwards and away from the point of impact resulting in a conical shaped fracture. This suggests that this damage is principally a result of the contact stress field, flexural effects are not apparent at this stage.

Fibre fracture was first detected after an incident energy of 1.7 Joules. Here a top surface crack was clearly visible extending from the impact location. Examination of the fracture surface under a scanning electron microscope showed that the fracture surface was smooth, indicative of a compression failure, probably as a result of the compression component of the flexural stress field. The resulting growth of fibre fracture with incident energy is detailed in figure 9. Although a greater level of scatter is apparent the trends apparent are similar to those observed in the two eight ply composites.

Target perforation occurred after an incident energy of 6.6 Joules. The micrograph of the perforated composite, figure 8d, clearly shows the characteristic frustrum-shaped shear zone.

Discussion

When subjected to localised transverse impact loading a composite structure will respond with out-of-plane flexural deformations. The mode of response induced by the impinging projectile will depend upon the mass and velocity of the impactor and the target geometry. Under low velocity impact loading, where the mass of the projectile is considerably greater than that of the target, a primary mode of response is excited enabling considerable energy to be accommodated in elastic flexure. This ability to absorb energy in elastic flexure will depend upon such parameters as the support conditions, material properties of the target, structural geometry and fibre stacking configuration. In previous work (7,8) the authors have examined the influence of material properties and target geometry on impact response. In this study both the target thickness and the fibre stacking configuration have been varied. From the experimental evidence it is clear that both of these parameters play an important role in determining the impact response of a composite structure. The two eight ply laminates possessed relatively low flexural stiffnesses and failed in a flexural mode at the lower surface. Fracture in the eight ply (+/-45°) composite occurred when the tensile component of the flexural stresses exceeded the local strength of the fibre-matrix interface. This suggests that the incident energy for first damage can be increased by surface treating the fibre-matrix interface. Indeed, limited testing by Dorey (9) has shown this to be the case. In the eight ply (0°,+/-45°) laminate failure initiated in the lower surface zero

degree fibres, again as a result of the flexural stress system. In these laminates the threshold for first damage could therefore be enhanced by employing fibres with a higher strain to failure (7).

In both of the eight ply laminates fibre damage was localised to the rear surface of the target. Only at energies approaching the perforation threshold the damage become visible in the top surface ply. If such laminates were to be used in aeronautical structures the detection of such damage might prove difficult. However, recent advances in non-destructive inspection techniques have resulted in the introduction of several portable NDI devices which may alleviate the problem.

First damage in the sixteen ply (0°,+/-45°) composite initiated in the top surface ply at the periphery of the area of projectile contact. This change in location of first damage was attributed to the increased flexural stiffness of this target, it being approximately twenty times stiffer than the eight ply (+/-45°) laminate. As a result of this increased flexural stiffness a very large impact force would be required to precipitate flexural failure in the lowest ply. However, at impact loads below this critical value the impacting projectile has induced a contact stress field sufficiently large to initiate failure between the top surface fibres. This damage appears to result from the local tensile stresses exceeding the fibre-matrix interfacial strength. Such localised matrix damage did not, however, affect the residual tensile strength, although it may reduce the compressive strength. It was only at the threshold for fibre fracture that reductions in tensile strength were incurred. Detecting fibre fracture at low

incident energies would not be difficult in stiff laminates of this type since damage initiated in the top surface ply and would therefore be clearly visible.

At incident energies above the damage threshold fracture, often spreading weel away from the point of impact, was observed in all of the laminates. This damage consisted of delamination, matrix shear cracking and fibre fracture. The presence of such extensive damage indicates that a large proportion of the incident energy has been dissipated in initiating and propagating fracture. In Attempting to quantify the energy expended in fracture it is usual to consider the fracture energies of the various damage mechanisms. The fracture energies for matrix cracking and delamination in this XAS-914C system have been determined by conducting dynamic burst tests on a series of circular diaphragms (10). These tests yielded values for the fracture energy that varied between 600 and 700 KJ/M^2.

Transverse fracture tests have been conducted on this composite system and yielded a value for the transverse fracture energy of approximately 38 KJ/M^2 (8). This variation in fracture energies suggests that composite can be designed to absorb incident energies in extensive regions of matrix fracture or localised areas of fibre damage, the choice depending upon the service environment in which the composite will operate.

It is now clear that the tensile strength of composite material is very sensitive to the presence of regions of fibre fracture. By idealizing the region of fibre fracture as a simple notch with similar dimensions it should therefore be possible to estimate the residual strength of the damaged coupons using fracture mechanics

principles.

Experimental programs attempting to examine the effect of a sharp notch on the residual strength of carbon fibre composite have been carried out by several workers (11,12). These tests have identified the formation of a damage zone in the regions of high stress concentration at the notch tip. Closer examination of these damage zones has shown that they consist of regions of matrix cracking and delamination. The effect of this zone is to absorb strain energy and reduce stress concentrations yielding composites with higher than expected residual strengths.

Previous tests on angle ply +/-45° composites have shown that these composites exhibit a notch insensitive behaviour, that is, failure results when the net section stress equals the unnotched strength of the composite (13). In such circumstances the residual tensile strength can be predicted using the net section relationship,

$$\sigma_n = \sigma_o \left[1 - \frac{2a}{w} \right] \qquad (1)$$

where "a" is the semi crack length, the undamaged strength and "w" is the specimen width. This approach was therefore applied to the eight ply (+/-45°) composites. In the analysis the crack length "2a" was taken to be equal to the maximum transverse length of fibre fracture. Equation (1) was then used to estimate the variation of residual strength with crack length. The results of this analysis are shown in figure 11, here the residual tensile

strength has been normalised with respect to the undamaged strength. Included in the figure are the values determined with the aid of the deplies. From the figure is clear that there is a good degree of correlation between the theoretical and experimental values. This was rather surprising since the region of fibre fracture was not a smooth notch nor was it length constant through the thickness of the laminate. This approach was then extended to predict the variation of residual tensile strength with incident impact energy. For a given projectile incident energy, the dimensions of the transverse fibre fracture were obtained from the damage growth curve shown previously in figure 4. By assuming this dimension to be the length of the notch, equation (1) was employed to predict the post-impact residual strength. The findings of this procedure are compared with the experimental evidence in figure 12. It is clear that this simple notch insensitive model provides a simple but successful procedure for predicting the residual strength of this damaged (+/-45°) composite.

A similar approach was used to estimate the post-impact behaviour of the (0°,+/-45°) composites. Previous work by Kellas et al (11) on the XAS-914C system has shown that (0°,+/-45°) composites of this type display a distinct notch sensitive behaviour when tested in tension. They found that by using a simple linear elastic fracture mechanics approach it was possible to predict the residual tensile strength of their notched CFRP laminates. This states the the notched strength is given by the equation

$$\sigma_n = \frac{K_{ic}}{\sqrt{\pi(A + Rp)}} \qquad (2)$$

where "K_{ic}" is the fracture toughness of the composite, "a" the semi crack length, "Y" the width correction factor and "R_p" a dimension accounting for the effective increase in notch length. During their tests, Kellas et al (11) determined values for K_{ic} and R_p of 51MPa$\sqrt{M}$ and $9x10^{-4}$M respectively. This values were applied to the laminates considered here. The variation of normalised residual strength with crack length was then determined for both the eight and sixteen ply (0°,+/-45°) composites, the results of which are compared with the experimental data in figures 13 and 14. Although experimental scatter is quite considerable the predicted curves do describe the trends in the experimental data reasonably well. It is evident that many of the experimental points fall between the noth sensitive and insensitive curves. This behaviour appears to be a consequence of the extensive delamination incurred during impact. This damage has clearly isolated the impact damage and reduced the notch sensitivity of the composite.

This fracture mechanics technique was then used to predict the post-impact variation of residual tensile strength with projectile incident energy. The results of this analysis are detailed in figures 15 and 16. Once again the simple fracture model appears to be in very good agreement with the experimental results.

Conclusions

The impact resistance of carbon fibre reinforced composite has been shown to be strongly dependent upon its flexural stiffness, which

in turn is a function of the fibre stacking sequence. Damage in the flexible targets initiated at the lower surface of the composite as a result of the local flexural stresses. In the stiffer sixteen ply laminate fracture was first detected in the top surface ply having been initiated by the contact stress field.

By treating the region of fibre fracture as a simple notch the variation of residual tensile strength with impact energy was successfully predicted using fracture mechanics principles.

References

1. Cantwell W.J., Curtis P.T. and Morton J., Impact and subsequent fatigue damage growth in carbon fibre laminates, Int. J. Fatigue,6, 1984, 113-113.

2. Rogers K.F., Sidey G.R. and Kingston-Lee D.M., Ballistic impact resistance of carbon fibre laminates. Composites,2, 1971, 237-241.

3. Takeda N., Sierakowski R.L., and Malvern L.E., Transverse cracks in glass/epoxy cross ply laminates impacted by projectiles. J. Mat. Sci., 16,1981, 2008-2011.

4. Cantwell W.J. and Morton J., Low velocity impact damage in carbon fibre reinforced plastic laminates. V. Int. Congress on Experimental Mechanics, Montreal, 1984.

5. Stellbrink K.K. and Aoki R.M., The effect of defects on the behaviour of composites. Proc. ICCM IV, 853-860.

6. Cantwell W.J., Curtis P.T. and Morton J., Post impact fatigue performance of carbon fibre laminates with non-woven and mixed-woven layers, Composites,14,1983,301-305.

7. Cantwell W.J., Curtis P.T. and Morton J., An assessment of the impact performance of CFRP reinforced with high-strain carbon fibres. To be published in Composites Science and Technology.

8. Cantwell W.J. Impact damage in carbon fibre composites. Ph.D. Thesis, University of London, August 1985.

9. Dorey G., Fracture behaviour and residual strength of carbon fibre composites subjected to impact loads. Agard CP163, 1974, Paper B3.

10. Austin C.D., Johnson W. and Walters B.J., Bursting and bulging of carbon fibre composite discs. Composites,13, 1982, 383-388.

11. Kellas S., Morton J. and Bishop S.M., Fatigue damage in a notched carbon fibre composite. To be published.

12. Caprino G., Halpin J.C. and Nicolais L., Fracture mecanics in composite materials. Composites, 10, 1979, 223-227.

13. Lee R.J. and Phillips D.C., The damage tolerance of high performance composites. Composite Structures 1, Ed. I.H. Marshall, 536-554.

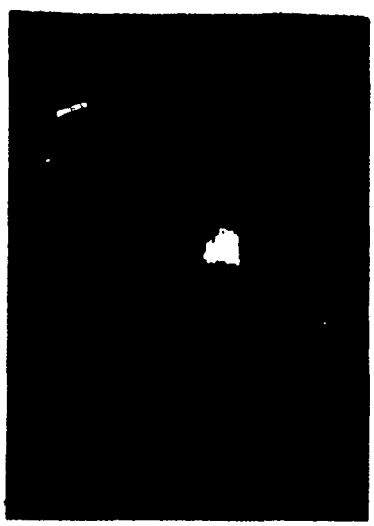

DEPLIED LAYER OF A SIXTEEN PLY (0, +/-45)

COMPOSITE

FIG. 1

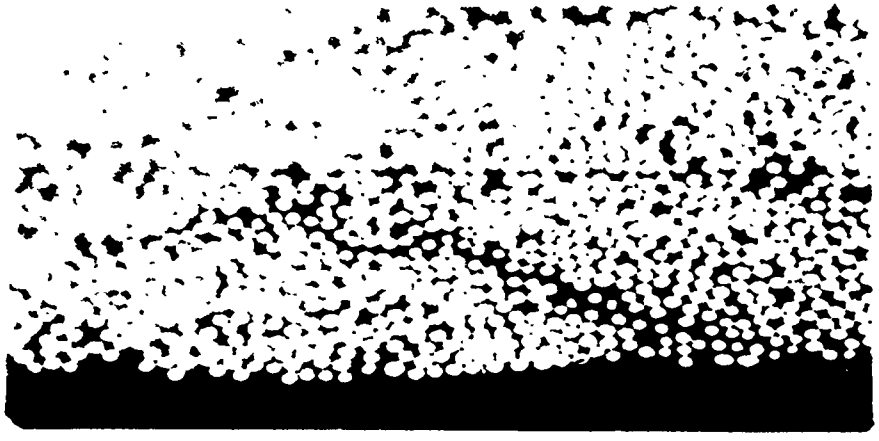

(a) 0.63 JOULES

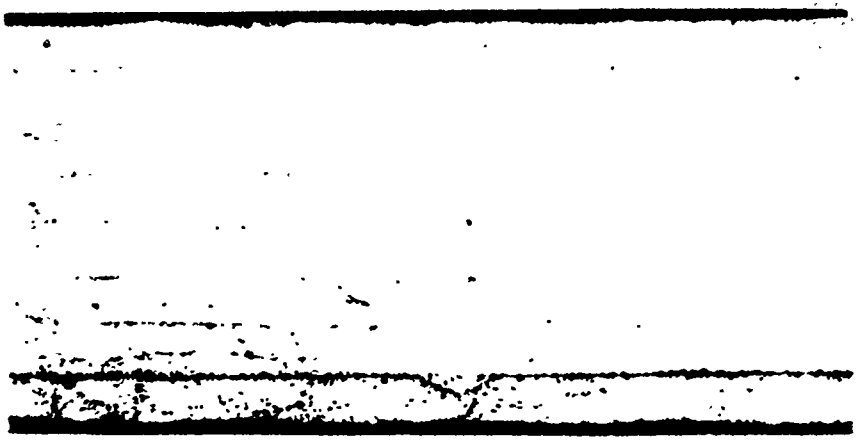

(b) 0.81 JOULES

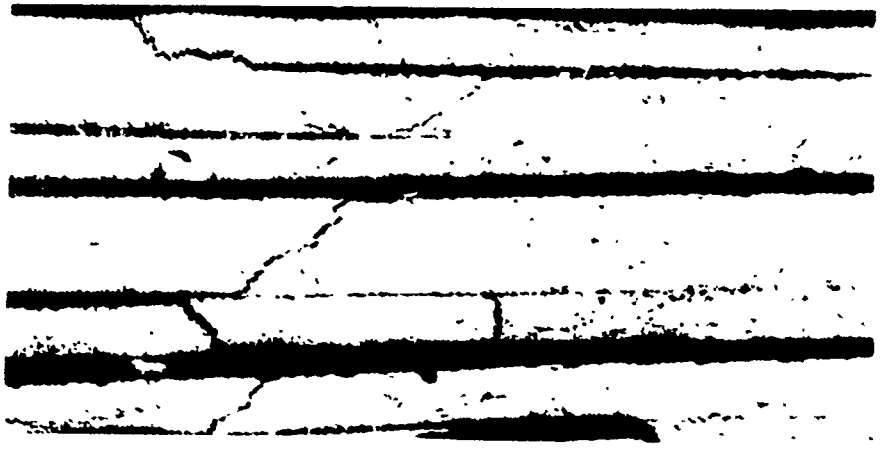

(c) 1.2 JOULES

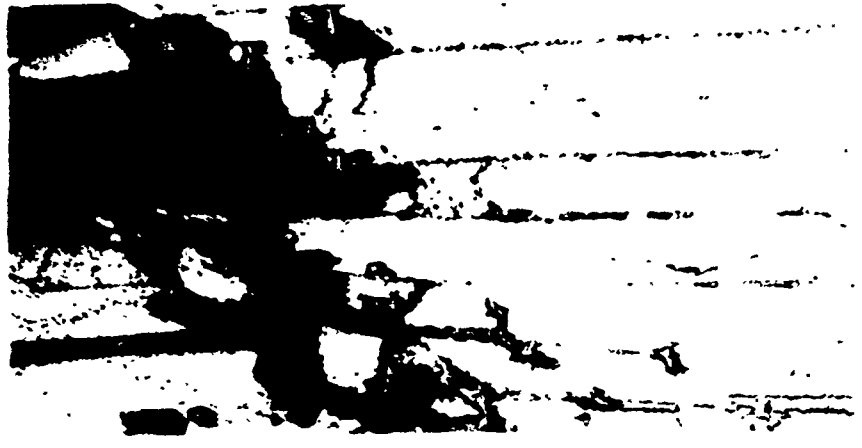

(d) 3.3 JOULES

DAMAGE GROWTH IN EIGHT PLY (+/- 45) COMPOSITES

FIGURE 2

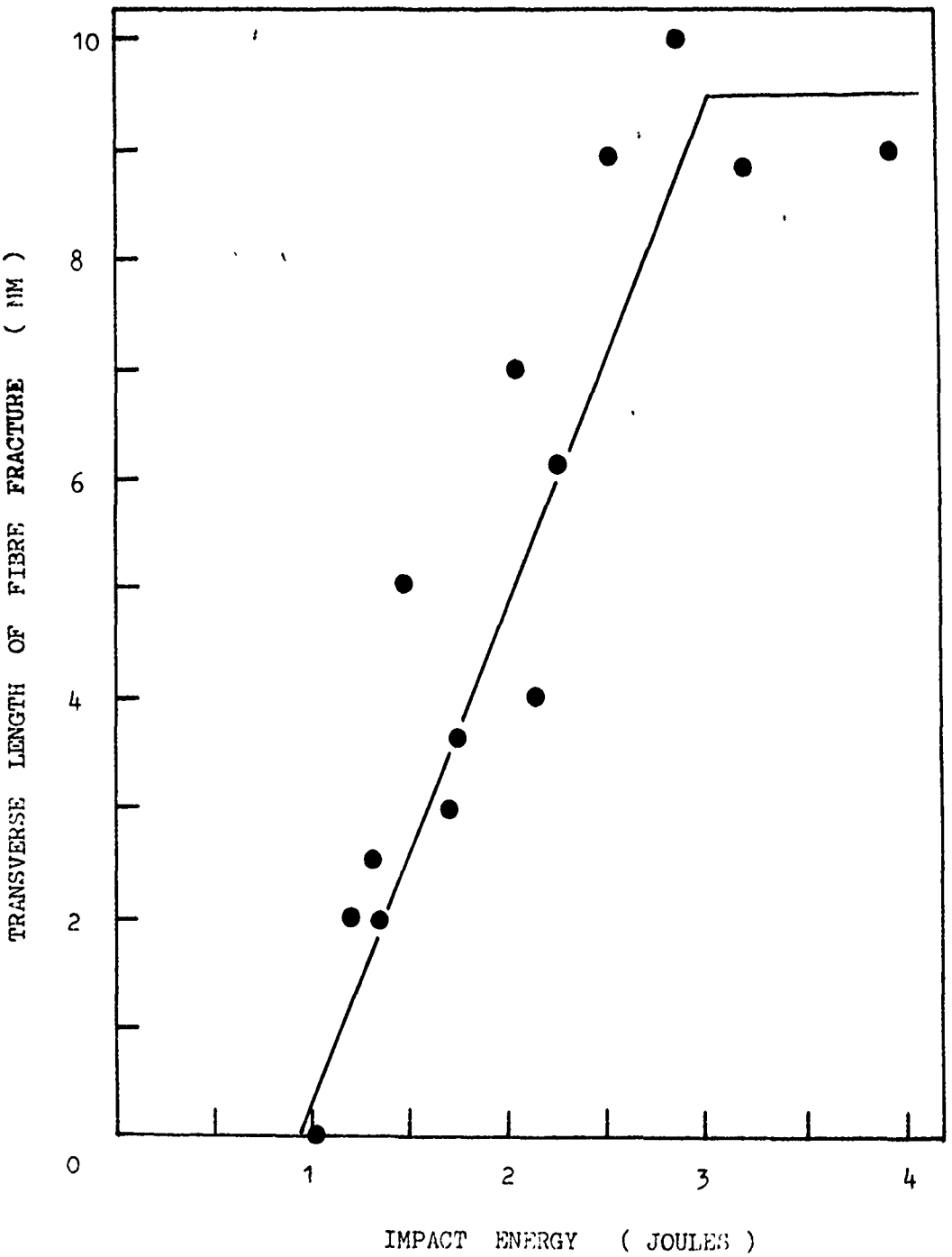

EIGHT PLY (+/- 45)

FIGURE 3

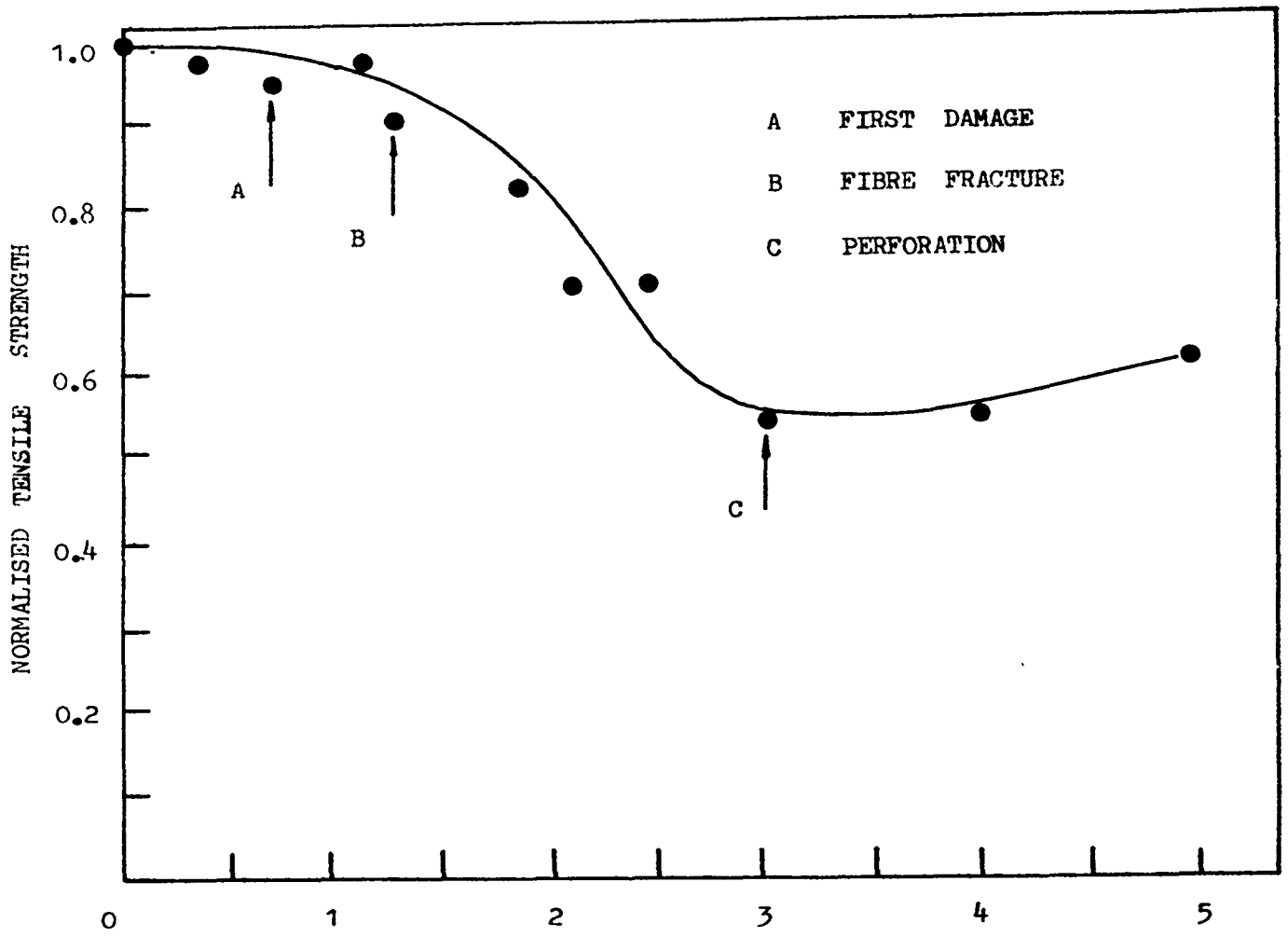

EIGHT PLY (+/- 45)

FIGURE 4

(a) 1.04 JOULES

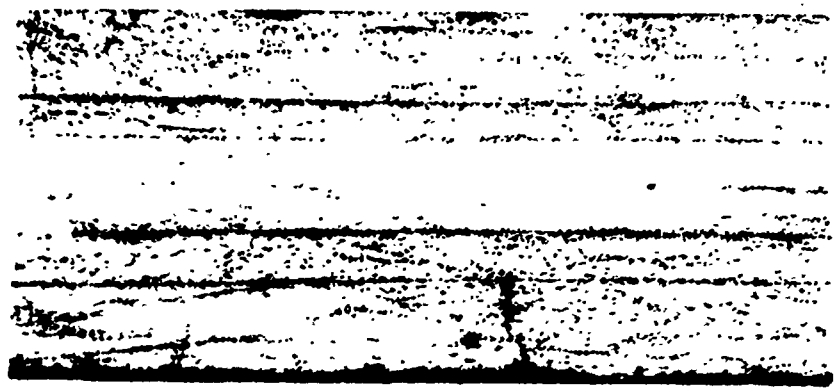

(b) 1.2 JOULES

(c) 1.6 JOULES

(d) 2.75 JOULES

DAMAGE DEVELOPMENT IN EIGHT PLY (0, +/-45) COMPOSITES

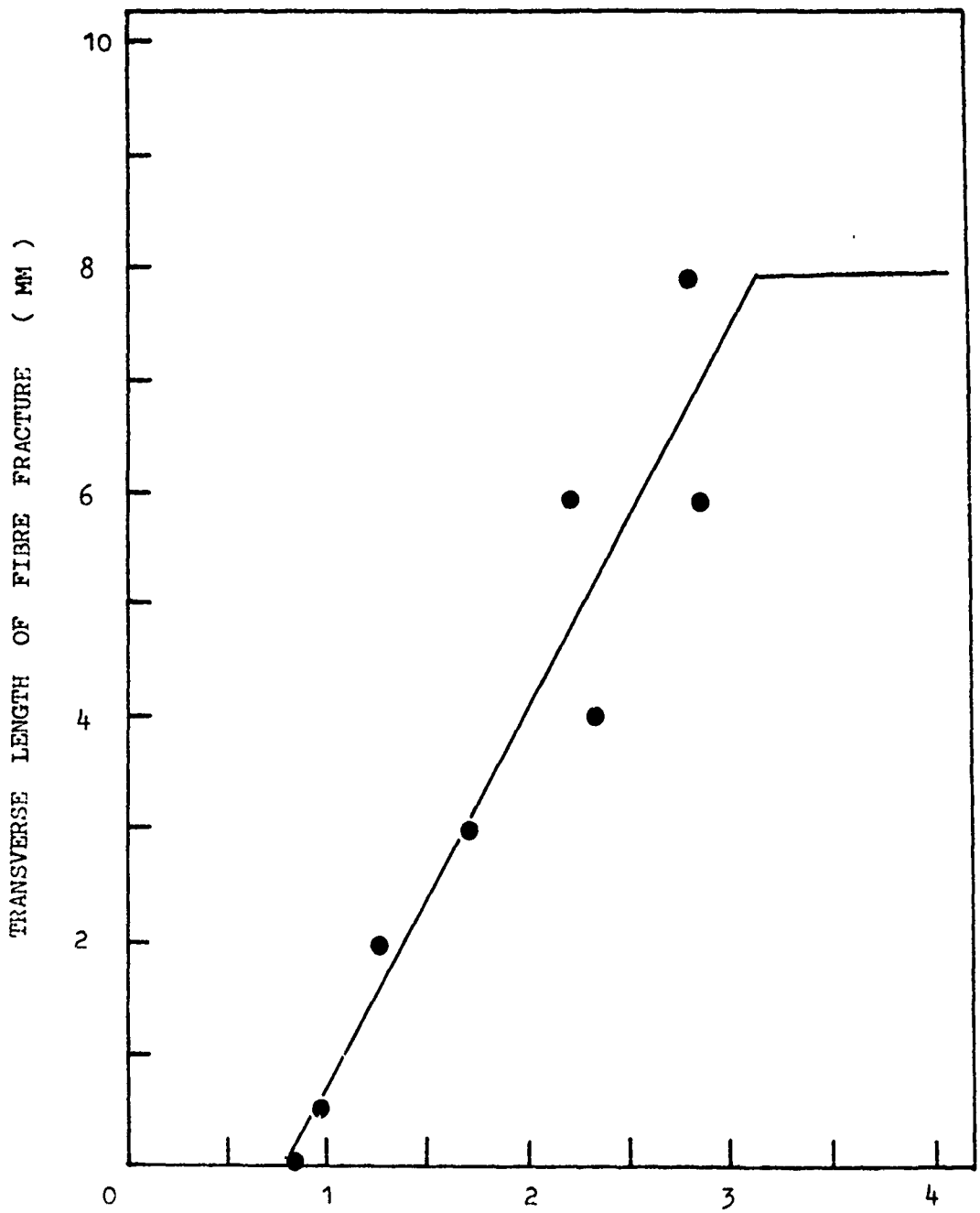

EIGHT PLY (0,+/-45)

FIGURE 6

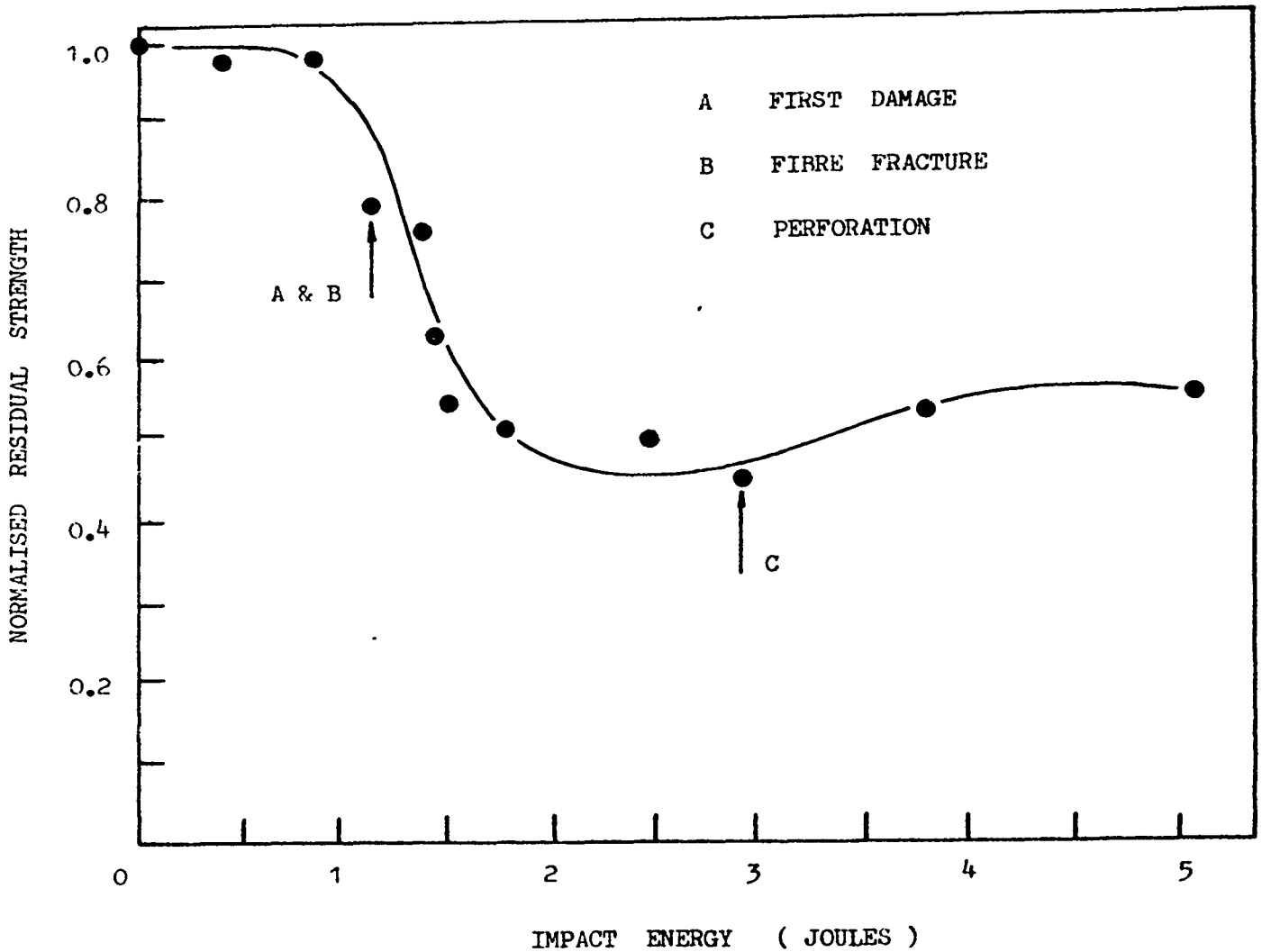

EIGHT PLY (0, +/- 45)

FIGURE 7

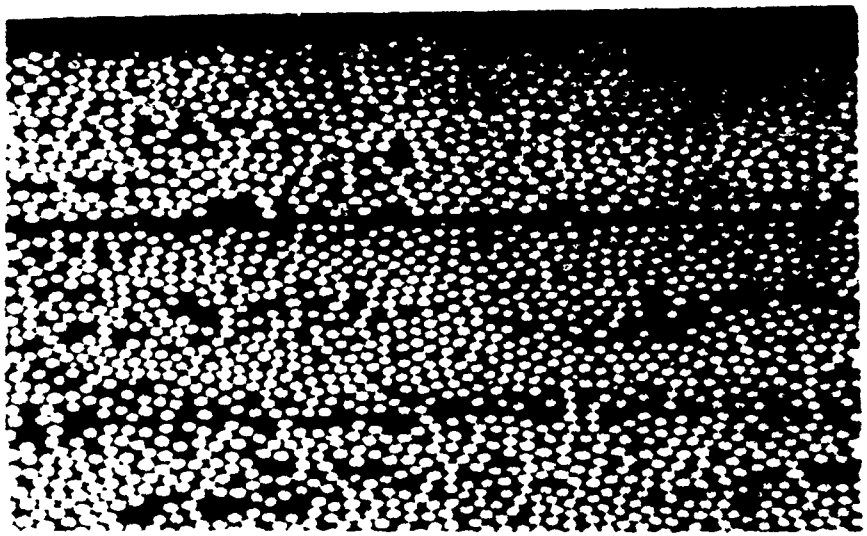

(a) 1.6 JOULES

(b) 2.4 JOULES

(c) 5.2 JOULES

(d) 6.6 JOULES

FIGURE 8

MICROGRAPHS OF DAMAGED SIXTEEN PLY (0, +/-45) COMPOSITES

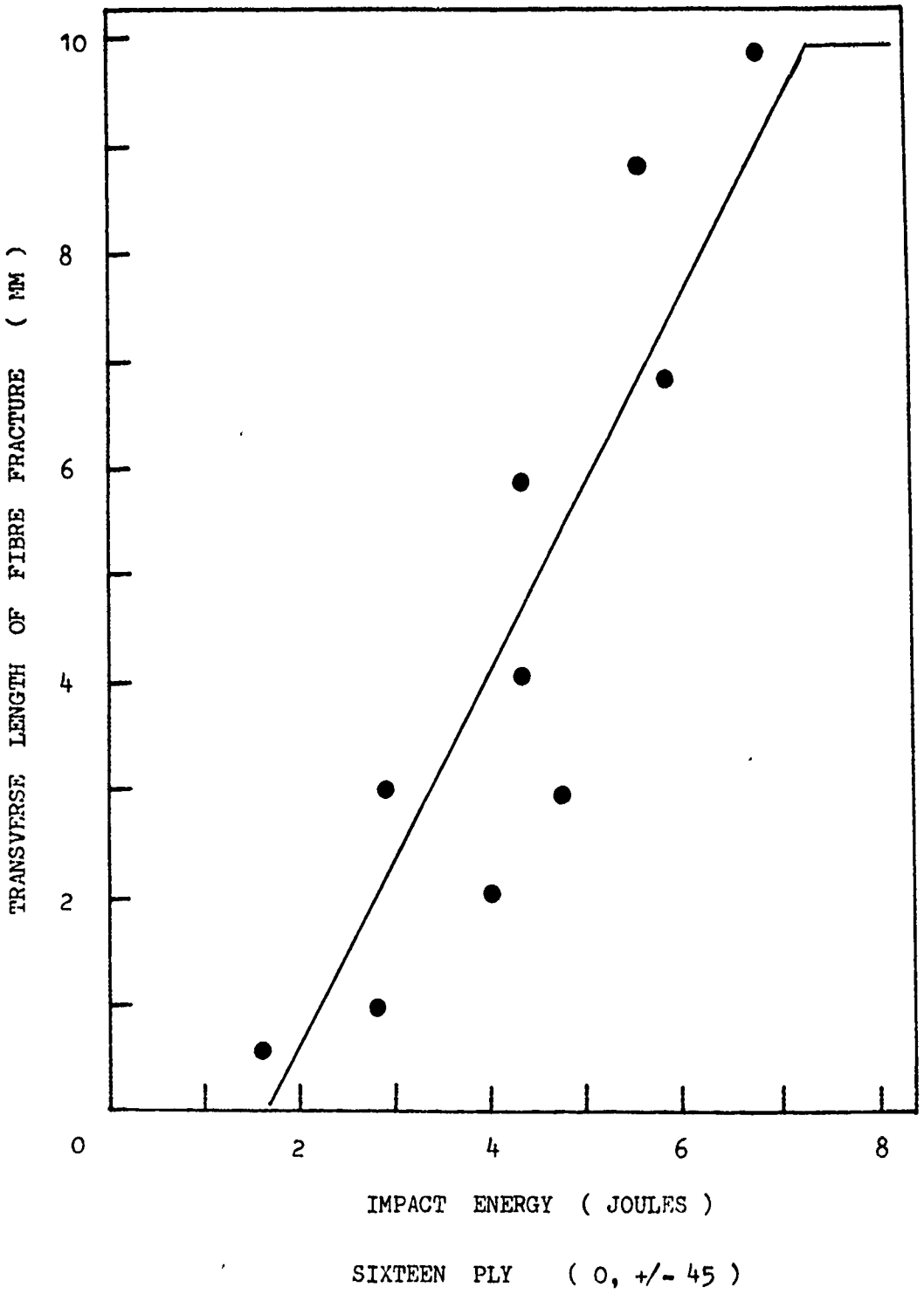
TRANSVERSE LENGTH OF FIBRE FRACTURE (MM)
10
8
6
4
2
0
2
4
6
8
IMPACT ENERGY (JOULES)
SIXTEEN PLY (0, +/- 45)

FIGURE 9

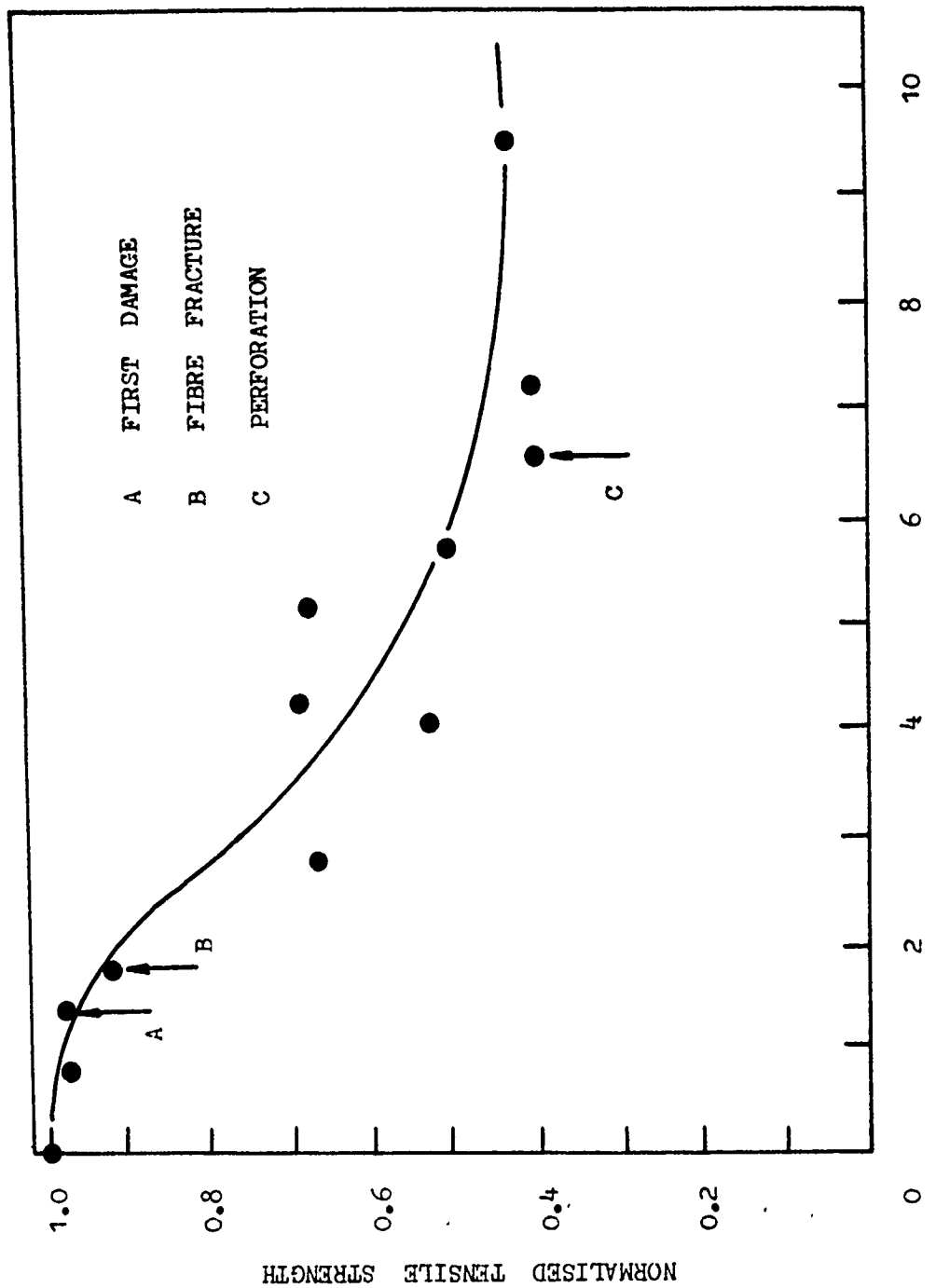

SIXTEEN PLY (0, + / - 45)

FIGURE 10

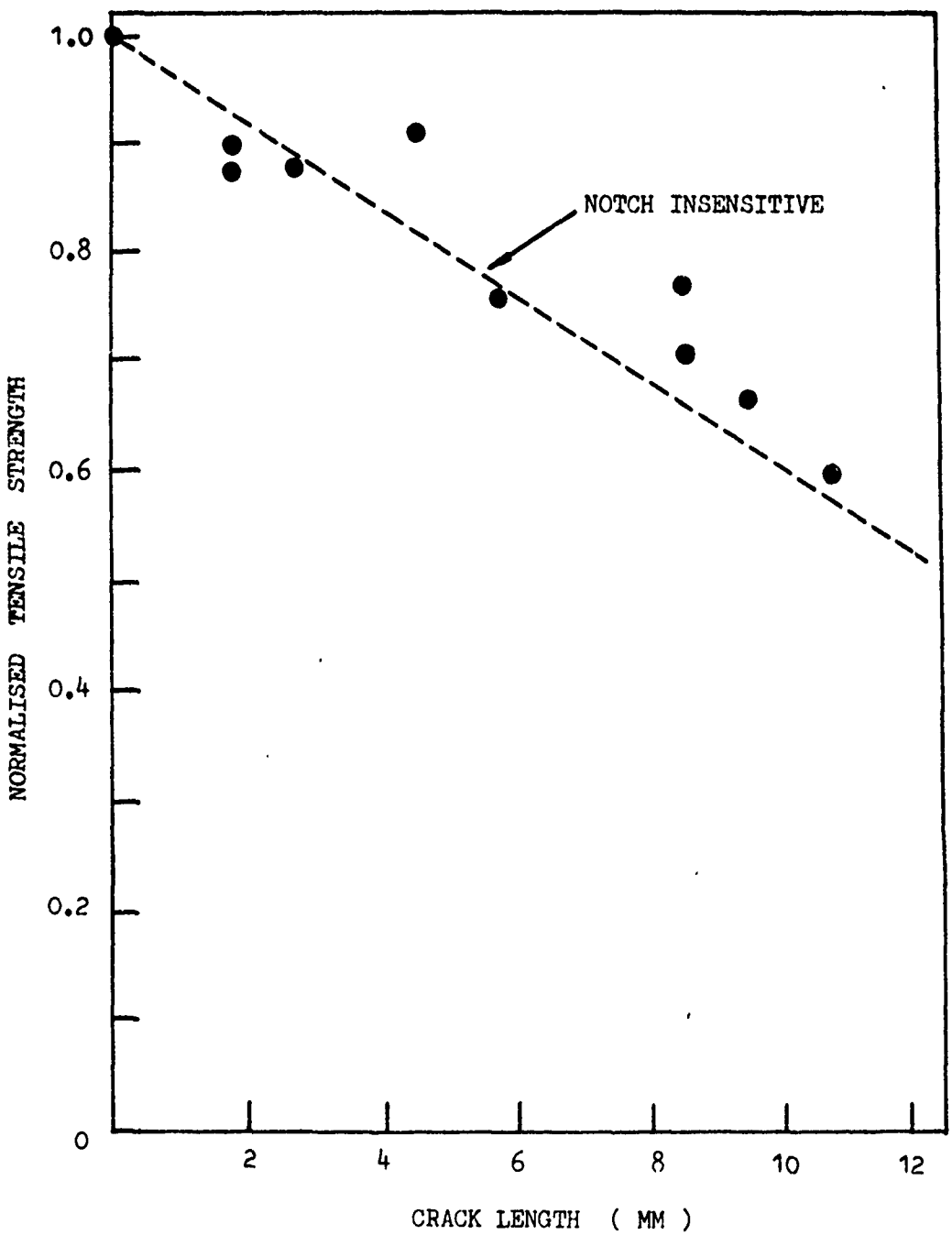

EIGHT PLY (+ / - 45)

FIGURE 11

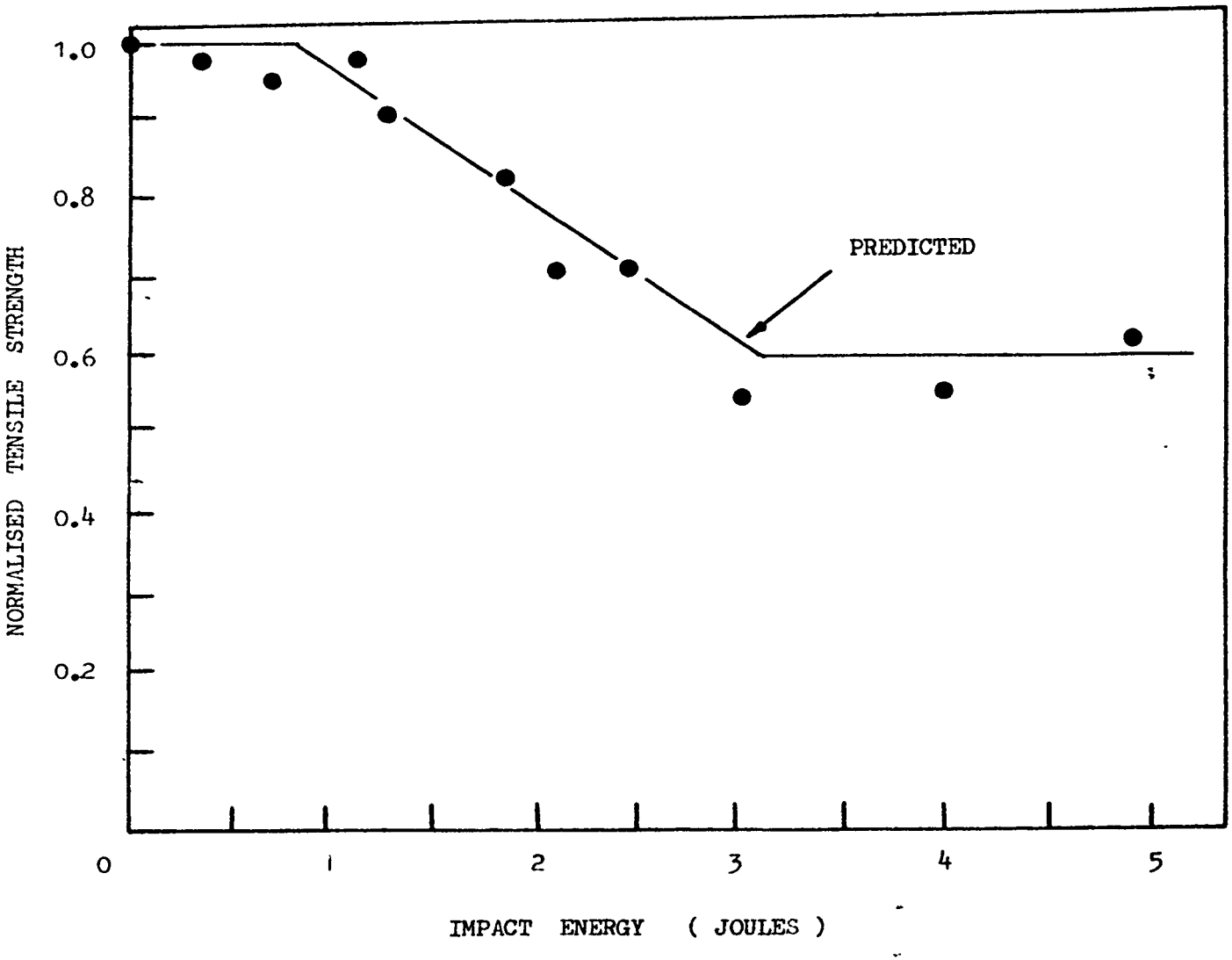

EIGHT PLY (+/-45)

FIGURE 12

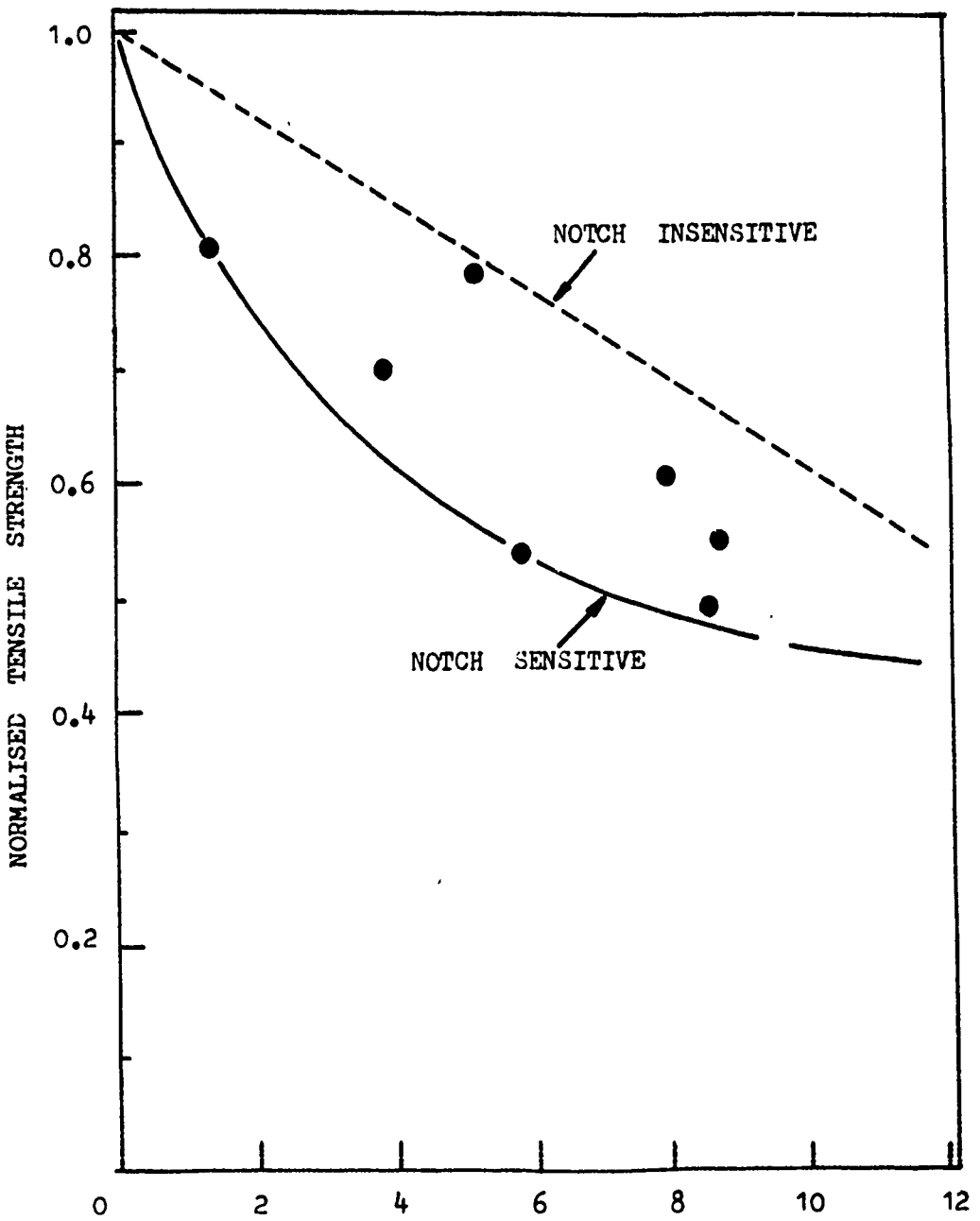

EIGHT PLY (0, +/-45)

FIGURE 13

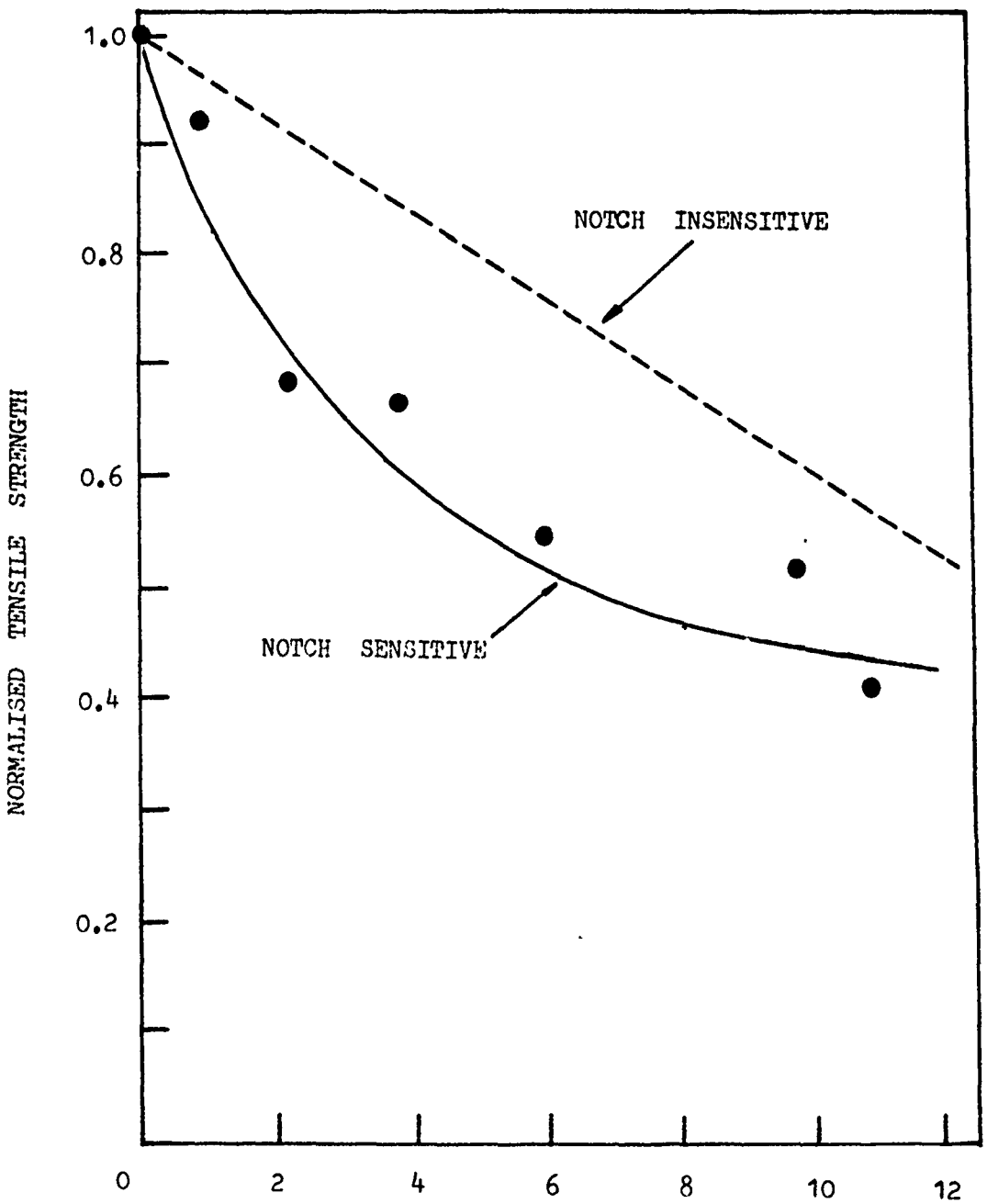

SIXTEEN PLY (0, + / - 45)

FIGURE 14

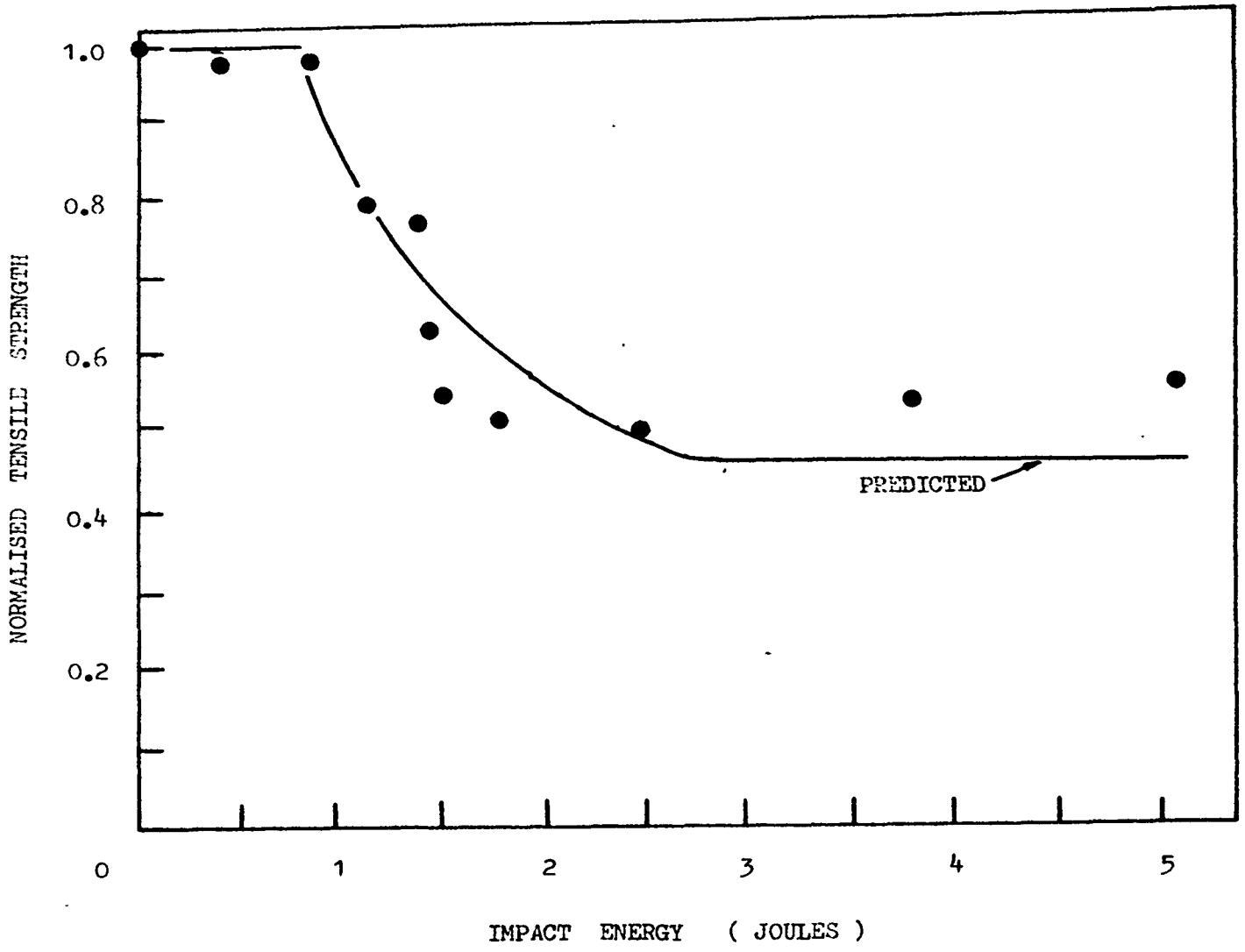

EIGHT PLY (0, +/-45)

FIGURE 15

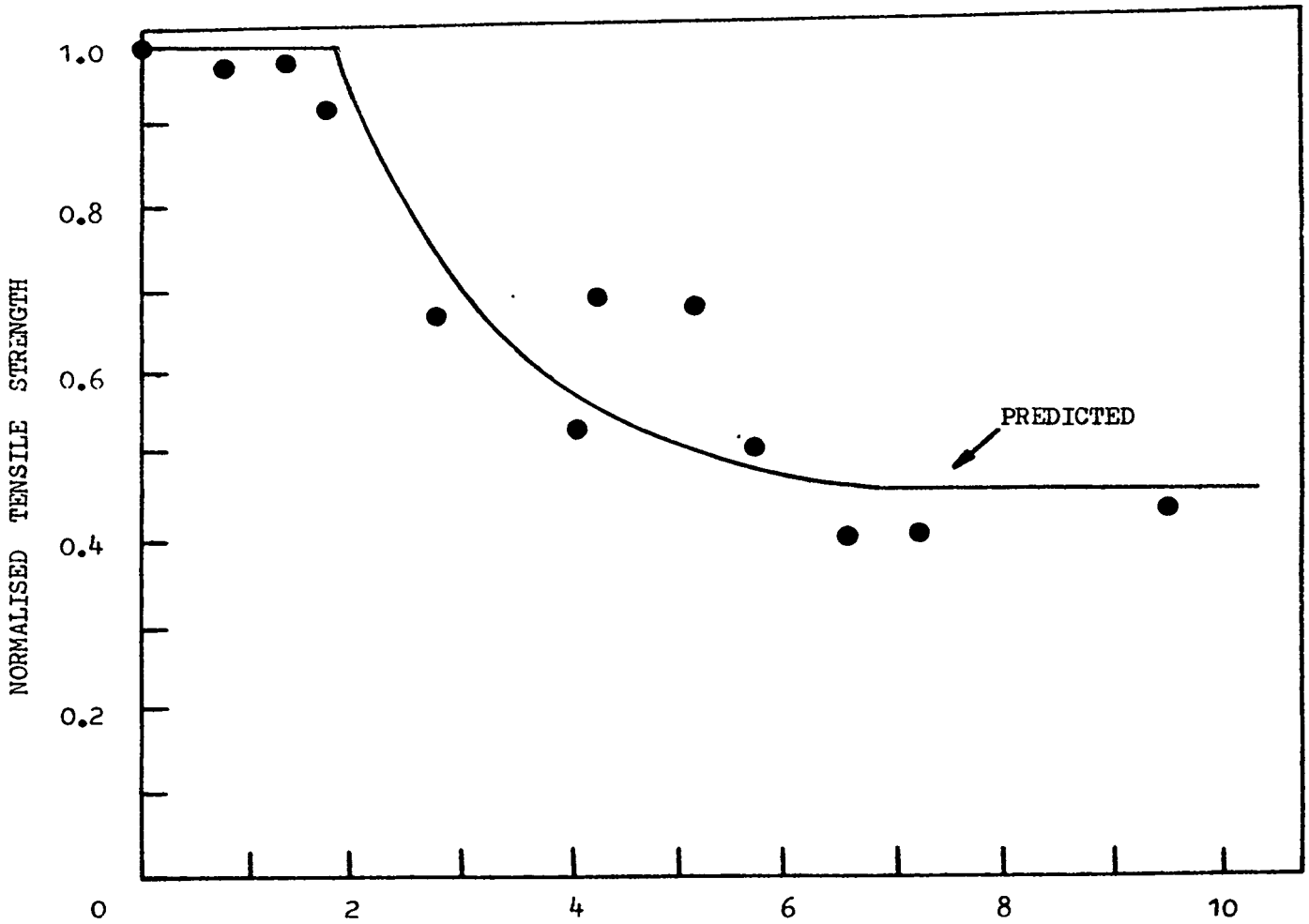

SIXTEEN PLY (0, +/- 45)

FIGURE 16

FAILURE MODE PREDICTION OF BONDED CFRP-STEEL JOINTS

R.D. Adams and J.A. Harris
Department of Mechanical Engineering
University of Bristol, Bristol, England

1. INTRODUCTION

The strength of any adhesively-bonded joint is dependent on the strength of its weakest component. This critical lowest strength may occur in many different parts of the joint and depends on the strength of the adherend, the adhesive or any intermediate zone between them, which may also contain an oxide layer or a primer. In a properly made joint, failure rarely occurs in this intermediate layer, but in the adhesive or, though rather less ofetn, in the adherends.

The low transverse tensile strength of carbon fibre reinforced plastics (CFRP) is well known. Because of this, attention must be paid to the design of bonded joints with CFRP so that premature failure, resulting from excessive transverse tensile stress is avoided. Recently, Cushman et al (1) stated that "although numerous researchers have investigated the state of stress within a bonded composite joint, few have made an attempt to predict actual failure loads. Also most of these prediction techniques assume a failure of the adhesive, and do not address the problem of interlaminar composite adherend failures".

Here finite element methods (FEM) have been used so that joint failure may be based on the conditions in either the adherends or the adhesive layer. The use of FEM also enables more complex geometries to be analysed than is possible with closed form methods.

The basic joint considered was a double lap joint with a unidirectional CFRP central adherend and steel outer adherends, the dimensions being as indicated in design 1 of Fig. 1. The remaining designs shown in Fig. 1 are modifications of the basic design aimed at improving joint strength. In designs 2 and 3 the outer adherends have been modified by tapering; this has been shown by Thamm (2) to reduce the maximum adhesive shear stress in a joint, providing the taper is continued to a fine edge. In design 4, the original joint has been modified to include an adhesive fillet at the critical end of the joint, which has been shown by Crocombe and Adams (3) to reduce the peak maximum principal adhesive stress. Finally, in design 5 the combination of tapering and filleting has been considered.

The adhesive modelled throughout was a toughened epoxy (Ciba-Giegy XD911) which has a Young's modulus of 3.05 GPa, a failure stress of 84 MPa and failure strain of 4.6 per cent when tested in bulk uniaxial tension.

2. ANALYSIS

In a lap joint, the shear deformation of the adhesive is concentrated at the edges of the overlap as a consequence of the well-known shear lag effect caused by differential straining in the adherends, first analysed by Volkersen(4). Also, internal bending moments are set up in the joint, which Volkersen accounted for in his later work (5) so that a distribution of transverse normal stresses exist. The maximum tensile value of the transverse stress occurs in the adhesive layer at the edges where the outer adherends terminate. The so-called "peel" stresses in this region have a significant influence on the failure of the joint, since both the adhesive and the CFRP are weak under this mode of loading.

Many analytical solutions for the state of stress in adhesive joints have been published (6), which, whilst giving a qualitative assessment of the effects of various parameters, do not enable joint strengths to be quantified. There are several reasons for this. A complete analysis of the various components of stress is required, including variations through the thickness of both the adherends and the adhesive. The non-linear properties of the adhesive must be included if realistic materials are to be modelled. In practice, joint strength may be significantly influenced by the local geometry in the critical regions of the joint, so it may be necessary, for instance, to account theoretically for the existence of a fillet of adhesive at the edges of the overlap.

Joint failure is a local phenomenon, so it is necessary to include the above conditions in a model of the joint. In order to achieve this, the finite element method has been employed. Using this method, it has been shown by Adams and Peppiatt (7), that lap joint failure is initiated by tensile failure of the adhesive within the fillet close to the adherend corner. They showed that a crack runs through the fillet at approximately 45° to the adherend surface, perpendicular to the predicted directions of the maximum principal tensile stresses in the adhesive. For double lap joints with aluminium adherends, reasonable predictions of joint strength have been obtained (8) and by also modelling large displacement deformations, reasonable predictions of the strength of single lap joints have been obtained with a range of epoxy adhesives (9).

The adhesive fillet at the edge of the adhesive layer has been shown, using finite element techniques, to reduce the maximum stresses in the adhesive(3). This, together with Thamm's prediction by closed form analysis that, by tapering the adherends to an almost "razor edge", the peak stresses in the adhesive may be reduced (2), was utilised in various attempts to improve joint strength as

shown in the series of joint designs illustrated in Fig. 1. The modifications to the basic design 1 fall into three categories: in designs 2 and 3 the outer steel adherends are tapered with a 10:1 gradient and the edge of the adhesive layer is square; in design 4 the adherends are unmodified, but adhesive fillets, whose size is defined by the angle "α", are included; finally, in design 5, both the tapered adherends and adhesive fillets are included together.

In many cases, it is found that the most highly stressed region in the adhesive often occurs around one corner, the geometry of which results in a singularity. In designs 1-3 the points designated as "A" in Fig. 1 are such points as well as points "C" and "D" in designs 4 and 5 respectively. A fracture mechanics analysis may be applied to the stresses in these critical regions. However, the authors know of no successful fracture mechanics method in which the strength of bonded lap joints has been predicted. An alternative approach has been used here (10) in which a small degree of local rounding is introduced into the finite element model in the critical region, so that the singularity is removed. In this way, the problems of dealing with singularities are avoided and failure criteria applied to the maximum conditions occurring within the predicted stress field may be employed. In practice, the corner geometries are unlikely to be "perfect" anyway, so that the modified geometries are much more likely to be realistic.

For the analysis, both the steel and CFRP adherends were modelled as linearly elastic materials while, for the adhesive, yield and plastic deformation were accounted for. The yield criterion for the adhesive is a function of the hydrostatic as well as the deviatoric stress component and is of the form (11):

$$\left[J_1(S - 1) + (J_1^2(S - 1)^2 + 12\, J_2 S)^{\frac{1}{2}}\right]/2S = Y_T \qquad (1)$$

where J_1 and J_2 are the first and second stress invariants respectively and

$$S = Y_C/Y_T$$

where Y_C and Y_T are the yield stresses in uniaxial compression and tension respectively.

The material constants used for the adherends are given in Table 1. The steel and CFRP properties were taken from the literature, and the adhesive properties determined experimentally by the authors.

Typical stress-strain curves for the adhesive in both uniaxial tension and pure shear are shown in Fig. 2.

3. RESULTS AND DISCUSSION

3.1 CFRP stresses

For all of the joint designs considered, the maximum transverse stresses, $\hat{\sigma}_T$, in the CFRP occurred in the region adjacent to the edges of the outer steel adherends. The values of $\hat{\sigma}_T$ for each joint when subject to a load of 1 MN m^{-1} width derived from the finite element results, are given in Table 2. For designs 1-3, it would appear that tapering the outer adherends has an insignificant effect on reducing $\hat{\sigma}_T$. In Fig. 3, a contour plot based on the interpolation of Gauss point values of the transverse stresses is shown in the critical region of design 1. For this case, as with designs 2 and 3, there is a large stress concentration adjacent to the very edge of the adhesive layer. Because of the abrupt edge to the adhesive layer, the transfer of the load from the inner CFRP adherend to the outer steel adherends is focused in this local edge region; the transverse stresses in the CFRP decay rapidly away from the edge region towards the centre-line of the joint and longitudinally away from the overlap. This pattern of load transfer and concentration of stress is affected very little by including either the outside or inside taper of designs 2 and 3. Note that prediction of the magnitude of the concentration of transverse stress would be very difficult by closed form analytical methods.

The introduction of an adhesive fillet in design 4 leads to an appreciable reduction in the maximum transverse stress in the CFRP. The relatively small modification of a 45° fillet results in a two-fold reduction in the stress. The fillet reduces the focus for the transfer of load at the edge of the overlap, resulting in a more even distribution of transverse stress. Figure 4 shows the stress distribution in the CFRP for a full depth 30° fillet. Compared with the distribution for design 1 in Fig. 3, the stress concentration at the corner has clearly been avoided and there is little variation in stress through the thickness of the CFRP. With a fillet angle of just under 35°, the maximum transverse stress in the CFRP is reduced to almost one-third of that of the basic design. The position at which the maximum stress occurs also depends on the angle of the fillet.

For angles less than 35°, $\hat{\sigma}_T$ is at point B in Fig. 1, inside the adhesive fillet but approximately 0.5 mm outside the overlap. The relative magnitude of the stresses at the two points depends on the relative stiffnesses of the paths by which load is transferred from inner to outer adherends, i.e. the transverse stiffness of the paths through points A and B. The former depends on the angle of the fillet and becomes less as the fillet angle is reduced.

The latter is relatively insensitive to the fillet angle, so that when the fillet angle becomes less than 35^{o}, the value and location of the maximum stress varies little.

In design 5, the combination of the tapered steel adherend with an adhesive fillet results in further reductions in the transverse stress concentration. This is because the transverse stiffness at the edge of the overlap is reduced and, with an adhesive fillet present, the effect of the taper is significant.

3.2 Adhesive stresses

The results of the finite element analyses also give the values of the stress components at the various locations in the adhesive. From these, the direction and magnitude of the principal stresses (and hence strains) are derived. When joint failure is initiated by a cohesive failure of the adhesive, it has been found that failure initiates in regions of maximum stress or strain concentration in the adhesive and cracks propagate at right angles to the direction of these maxima. Thus, by examination of the principal stress distributions, the locations and directions of cohesive failure in the adhesive may be predicted.

For the adhesive layer of design 1 in Fig. 5, the maximum stress occurs close to the interface with the central CFRP adherend and any crack initiating in this region will be driven towards the interface. With an adhesive fillet as in Fig. 6, failure is expected to initiate in the vicinity of the corner of the outer steel adherend and a crack will propagate through the fillet and again down to the interface with the CFRP. With the tapered joint, removing the corner of the steel adherend leads to a relieving of the stress concentration at the corner and now the maximum occurs at the outer surface of the adhesive fillet close to the outer steel adherend corner. Again, cracks initiated in this region would be expected to propagate through the fillet to the interface with the CFRP as indicated.

4. CONCLUSIONS

There are two possible mechanisms of failure for the double lap joints considered here. Either excessive transverse tensile stresses at the edge of the joint close to the interface result in interlaminar failure of the CFRP, or concentrations of the principal stresses in the adhesive result in yielding and straining to failure in tension. Since the latter will result in cracks

running through the adhesive to the interface, so that thereafter interlaminar failure of the CFRP may occur, it may not be clear in the first instance which mechanism is responsible for failure from the fractured surfaces of the joint.

By applying suitable failure criteria to the finite element results, it is possible to predict the load required for failure to occur by each mechanism. For interlaminar failure of the composite, a maximum tensile transverse stress of 40 ± 6 MPa has been found experimentally. For the cohesive failure of the adhesive, a maximum principal tensile strain criterion has been found to predict joint strength reasonably. Here, the limiting value of 0.0475 has been used equal to the strain at failure in bulk uniaxial tension, which closely resembles the state of stress in the critical regions of the adhesive.

Thus, by using finite element techniques, it is possible not only to predict the strength of joints from fundamentals, but also to predict the mode of failure. This greatly assists the post-failure analysis of joints as it otherwise is difficult, if not impossible, to decide where the failure initiated.

REFERENCES

1. Cushman, J.B., McCleskey, S.F. and Ward, S.H.,(1983), "Design, Fabrication and Test of Graphite/Polyimide Composite Joints and Attachments". NASA CR3601.
2. Thamm, F., J. Adhesion, 7, (1976), 301.
3. Crocombe, A.D. and Adams, R.D., J. Adhesion, 13, (1981), 141.
4. Volkersen, O., Luftfahrforsch, 15, (1938), 41.
5. Volkerson, O., Construction Metallique, 4, (1965), 3.
6. Adams, R.D. and Wake, W.C., "Structural Adhesive Joints in Engineering", Applied Science, 1984.
7. Adams, R.D. and Peppiatt, N.A., J. Strain Anal., 9, (1974), 185.
8. Adams, R.D., Coppendale, J. and Peppiatt, N.A. in "Adhesion-2", K.W. Allen (Appl. Sci. Pub., London, 1978), 105.
9. Harris, J.A. and Adams, R.D., Int. J. Adhesion & Adhesives, 4, (1984), 65.
10. Harris, J.A. and Adams, R.D., to be published.
11. Raghava, R., Caddell, R.M. and Yeh, G.S.Y., J. Mats. Sci., 8, (1973), 225.

TABLE 1

Material Properties used in the Finite Element Analysis

(a) Steel: (elastic)

Young's Modulus	210 GPa
Poisson's ratio	0.29

(b) Adhesive: (elasto-plastic)

Young's Modulus	3.05 GPa
Poisson's ratio	0.35
S (constant in eqn. 1)	1.24

(c) Unidirectional CFRP: (elastic)

Longitudinal modulus	140 GPa
Transverse modulus	7 GPa
Interlaminar shear modulus	4.5 GPa
Longitudinal and transverse Poisson's ratio	0.3

TABLE 2

Predictions of the Maximum Transverse Stresses in the CFRP from Elastic Finite Element Analyses with 1 MN m^{-1} with Applied Load

Design	Fillet angle	$\hat{\sigma}_T$ in CFRP / MPa
1	-	38
2	-	37
3	-	36.5
4	45	16
4	30	10
4	17	10
5	45	13
5	30	6.5
5	17	5

1 Basic design

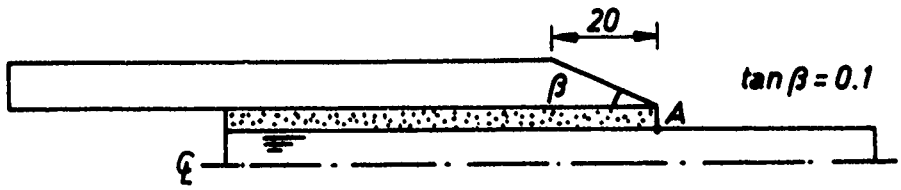

2 Outside taper

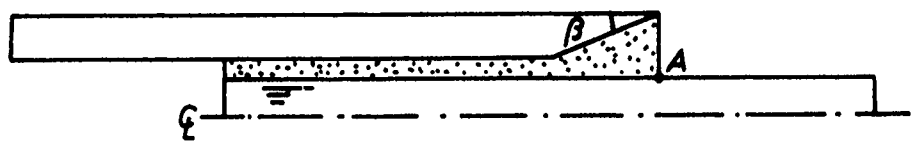

3 Inside taper

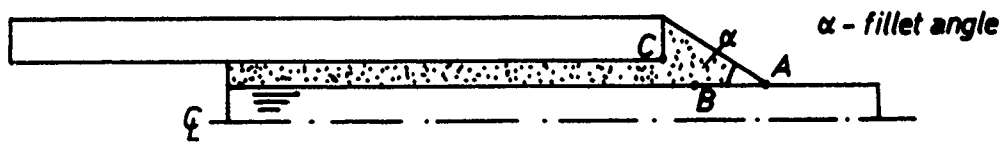

4 Adhesive fillet

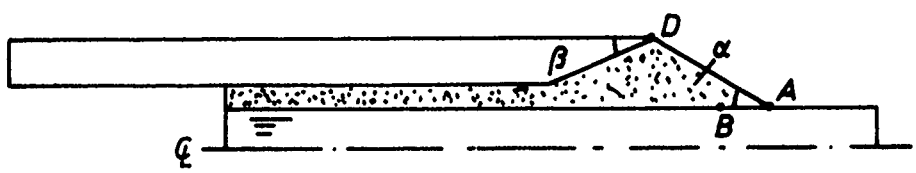

5 Inside taper and adhesive fillet

FIG. 1 VARIOUS DOUBLE LAP JOINT DESIGNS

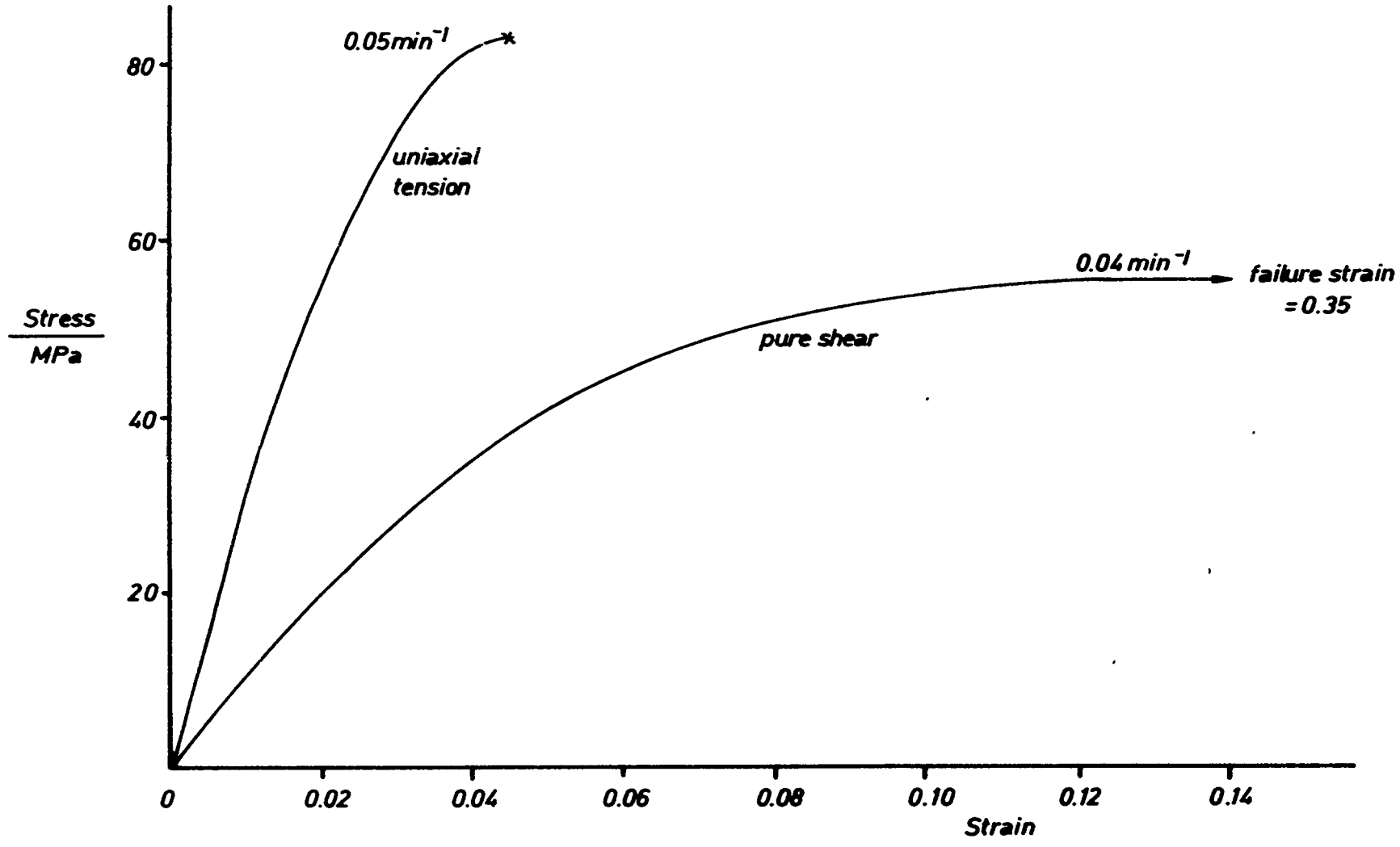

FIG.2 STRESS-STRAIN CURVES FOR ADHESIVE XD911

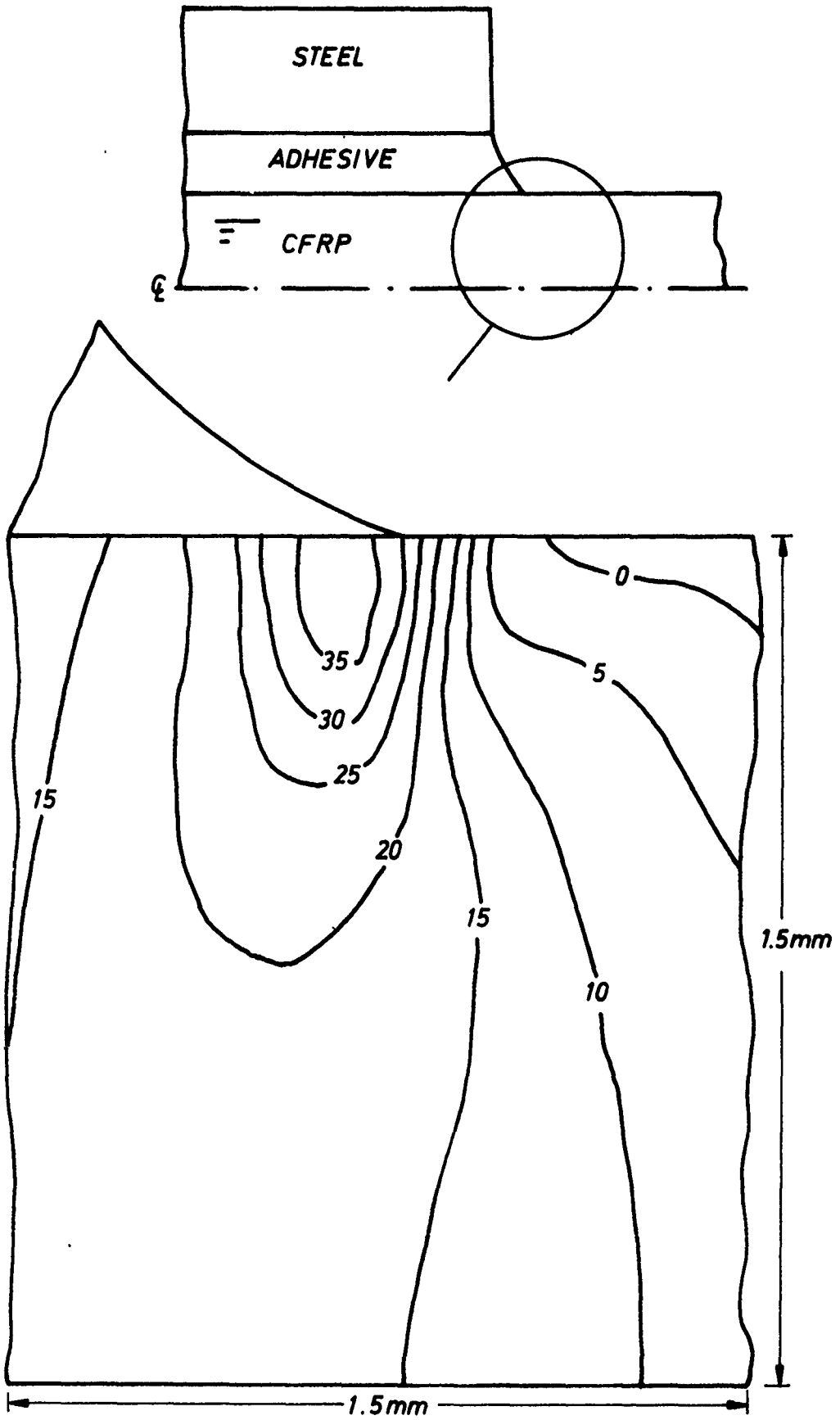

FIG. 3 DESIGN 1. TRANSVERSE STRESSES IN THE CFRP (MPa), FOR A 1 MN m^{-1} WIDTH APPLIED LOAD

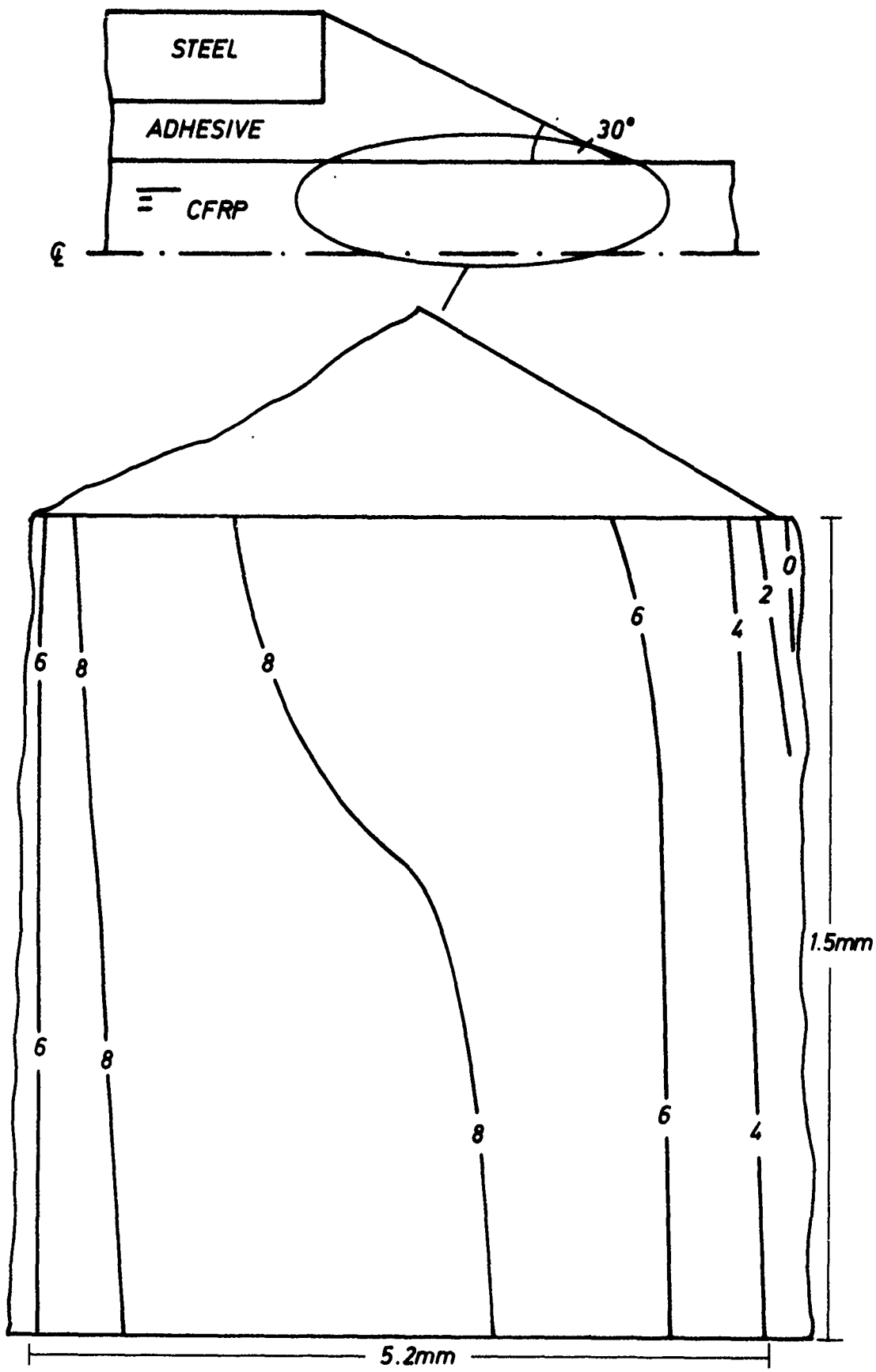

FIG.4 DESIGN 4. TRANSVERSE STRESSES IN THE CFRP (MP a) FOR A 1 MN m^{-1} WIDTH APPLIED LOAD

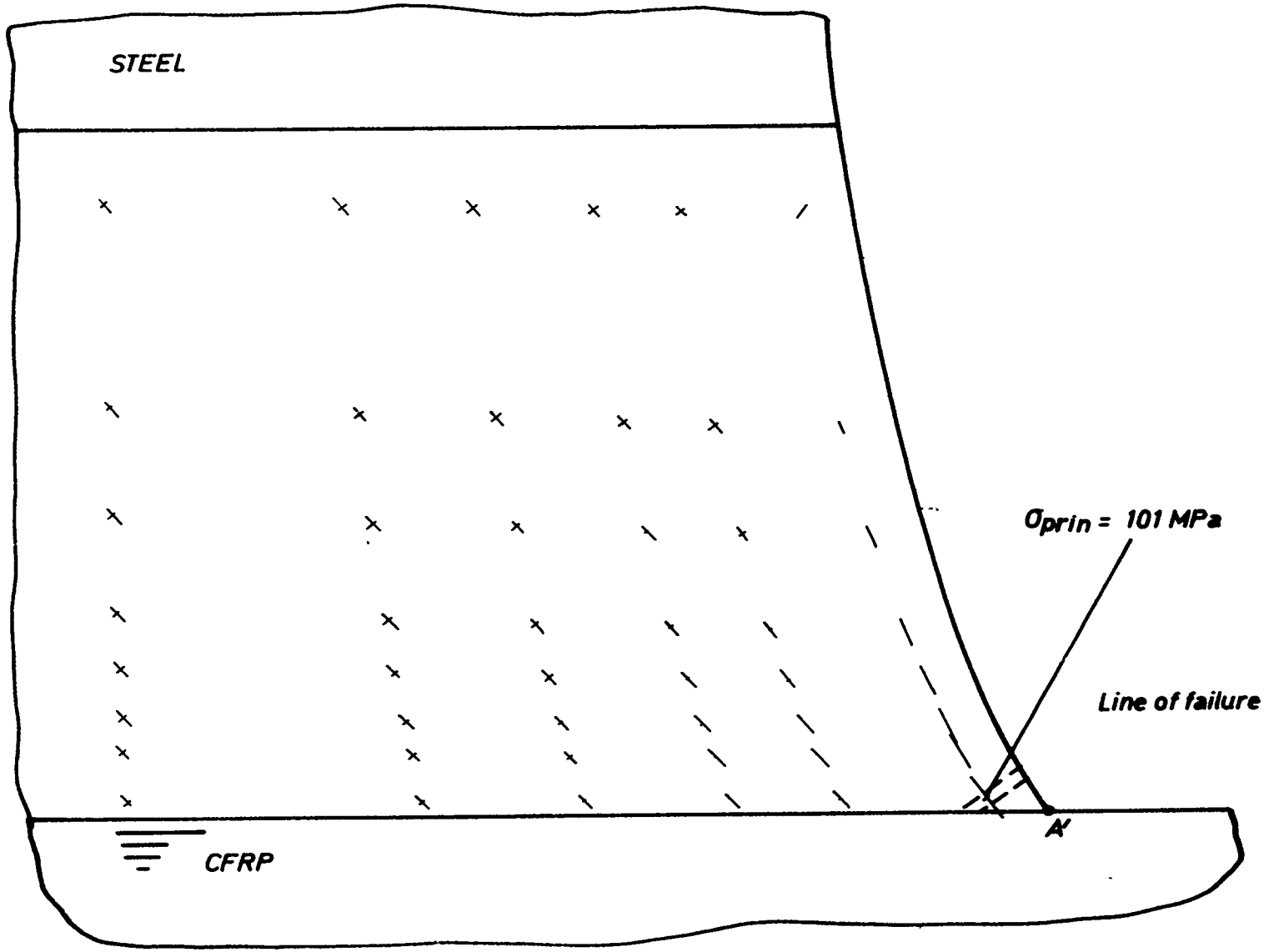

FIG. 5 PRINCIPAL STRESS DISTRIBUTION IN AN ELASTIC ADHESIVE AT THE EDGE OF THE OVERLAP FOR DESIGN 1, WITH A 1MN m^{-1} WIDTH APPLIED LOAD

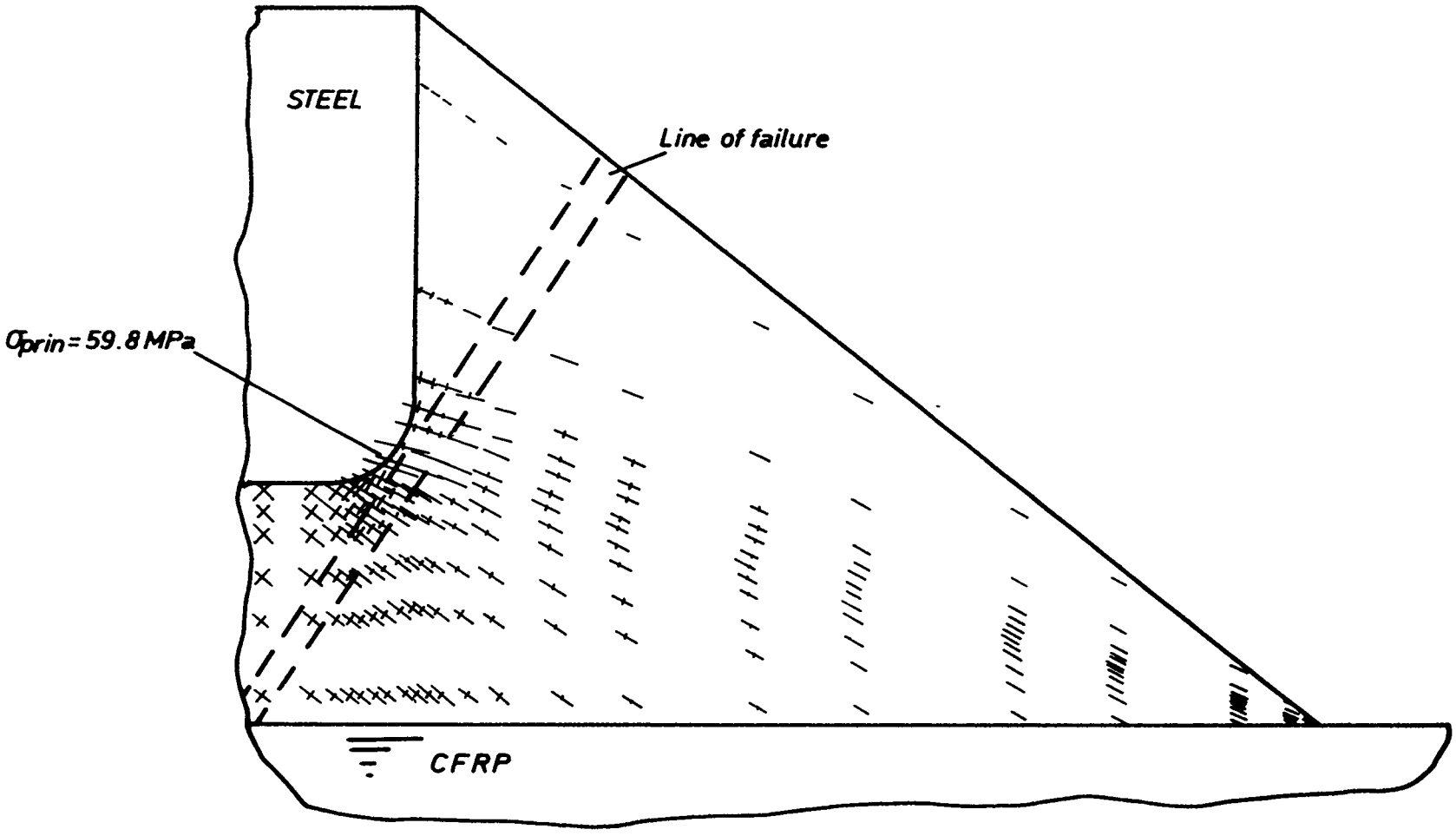

FIG. 6 PRINCIPAL STRESS DISTRIBUTION IN AN ELASTIC ADHESIVE AT THE EDGE OF THE OVERLAP FOR DESIGN 4, WITH A 1MN m^{-1} WIDTH APPLIED LOAD ($\alpha = 30°$)

POSTMORTEM DETERMINATION OF DELAMINATION FAILURES

Paul A. Legace
Department of Aeronautics and Astronautics
Massachusetts Institute of Technology
Cambridge, Massachusetts

POSTMORTEM DETERMINATION OF DELAMINATION FAILURES

Paul A. Lagace
Assistant Professor of Aeronautics and Astronautics
TECHNOLOGY LABORATORY FOR ADVANCED COMPOSITES
Massachusetts Institute of Technology
Cambridge, MA, 02139

ABSTRACT

In using any material in a structure, it is first necessary to characterize the failure of the basic material in order to make predictions as to the strength of the structure. Such procedures are well-established for metals but are still under development for composites. Efforts in this area are complicated by the multiplicity of failure modes which occur in composites, especially the out-of-plane failure mode known as delamination. Failure criteria which are developed often deal only with in-plane phenomena. It is thus important to use experimental results controlled by in-plane phenomena in correlating data via such criteria. Not recognizing the difference between in-plane and out-of-plane failure modes can cause very erroneous conclusions to be drawn from the initial data resulting in poor predictions for failure strength. The effect of ignoring this basic difference in the origin of failure will be discussed in the context of several examples which show that both gross underestimations and overestimations of the actual strength of a structure can be made when extrapolating coupon-type data. In addition, several rules of thumb, which have been established through experience, will be discussed concerning the classification of failure surfaces via macroscopic inspection as due to in-plane or out-of-plane sources. Often, "secondary" effects can cloud the actual fracture areas possibly leading to incorrect conclusions. It is especially important to obtain a physical understanding of the types of failures which can and cannot occur in specific instances.

1. INTRODUCTION

The failure characterization of composite materials is complicated by the fact that there are a number of possible failure modes in composite materials [1] including fiber fracture, matrix cracking, and fiber/matrix debonding. Although these failure modes are all quite different, they do share one common point in that they are all "in-plane" phenomena.

However, out-of-plane phenomena are also important in composite laminates. It has been recognized for a number of years that interlaminar stresses arise in composite materials at free edges [2] or, more generally, in gradient stress fields. These interlaminar stresses often result in an out-of-plane failure mode, known as delamination, which can significantly alter the strength of a composite laminate from its expected "in-plane" value [3-5]. Delamination is a common phenomenon which occurs at the matrix interlayer between plies. This matrix interlayer is the weak link in a composite laminate and thus is susceptible to failure.

It is of the utmost importance to realize these two major different modes of failure in composite materials do exist: in-plane failure, that is failure due to in-plane stresses (σ_{11},σ_{22}, and σ_{12}); and out-of-plane failure, or delamination, prompted by out-of-plane, or interlaminar stresses (σ_{zz}, σ_{1z}, and σ_{2z}). In practice, data from coupon specimens is often used to obtain parameters in semi-empirical formulae to predict the behavior of composite laminates. The applicability of these criteria and the data used in obtaining their parameters must be established and must be compatible. That is to say that criteria which are formulated for in-plane phenomena can only be applied to in-plane phenomena and can only be correlated with data which is due to in-plane phenomena. The same is true for out-of-plane formulations.

The best example of this is failure criteria for composites. A number of semi-empirical formulae have been devised to correlate the failure of composite materials in both the notched and unnotched condition. These, however, generally deal only with in-plane failure. Thus, in using experimental data to determine the parameters in the equations, it is essential that data be used only from specimens which failed via an in-plane mechanism. If this is not done, a valid correlation cannot be attained.

A quick perusal of the literature indicates that generally the failure mode is not taken into account when applying typical failure criteria. A possible explanation is that there are no easy techniques to determine the failure mode of a typical failed laboratory specimen in a postmortem inspection. It is thus necessary to develop such abilities so that failures can be quickly and correctly classified.

In this paper, the failure of typical composite specimens via delamination is discussed and compared to in-plane failure of similar specimens. The possible downfalls of not properly classifying failure modes are pointed out and discussed and several "rules of thumb" are offered in an effort to establish an easy method to perform postmortem determination of composite failure modes. These rules of thumb have been developed over the years from the experience gained in the Technology

Laboratory for Advanced Composites at the Massachusetts Institute of Technology.

2. MOTIVATION

The establishment of such semi-empirical failure criteria are important not only in laboratory research but in the design process for composite structures. Laboratory scale specimens (e.g. coupons) are generally tested in large quantities to characterize the behavior of composite materials and various stacking sequences. This data is then used in the various failure criteria to set the parameters. The criteria are then extrapolated to obtain predictions for larger component behavior. It is essential, as noted previously, that only specimens which fail in a mode consistent with the pertinent failure criterion be used in establishing the applicable parameters. Errors at the coupon level will result in extrapolation errors and possible improper design. Investigators thus need simple and quick techniques to classify specimen failures as either in-plane or out-of-plane.

3. EXAMPLES OF FAILURES VIA DELAMINATION

The discussion herein is centered upon whether the failure of a composite is promoted by in-plane or out-of-plane effects when the composite is loaded by in-plane forces. There is no doubt that there is interaction between in-plane failure mechanisms and out-of-plane failure mechanisms, but as a first approach, it is proposed that these two modes can be separated. It is thus proposed that there is a "competition" between in-plane and out-of-plane mechanisms to cause failure. The first mechanism which becomes critical will prompt failure.

It is important to note that it is the cause of the initiation of failure that is of interest. As will be discussed later, out-of-plane failure cannot cause final failure of a typical coupon specimen, that is breaking the specimen into two pieces. In-plane mechanisms must ultimately cause fiber and matrix failure in the plane of loading for this to occur. Thus, in-plane and out-of-plane failure refer to the mechanism which prompted failure. In the context of this working definition, it would appear that the assumption that these two modes are independent is a good one.

Delaminations occur under a wide variety of conditions and situations in composite laminates. Three specific areas are discussed here which illustrate the basic phenomena and the difference between in-plane and out-of-plane failure.

3.1 Unnotched Tensile Failure

The typical coupon specimen shown in Figure 1, or some variation of that basic form, is generally used in conducting tensile tests. It is data from such experiments which are used to obtain parameters for in-plane failure criteria or to assess the applicability of these failure criteria once the parameters are established.

A typical in-plane failure criterion is the stress interaction criterion (in the quadratic form) proposed by Tsai and Wu [6]:

$$F_{1111}\sigma_{11}^2 + 2F_{1122}\sigma_{11}\sigma_{22} + F_{2222}\sigma_{22}^2 + 4F_{1212}\sigma_{12}^2 + F_{11}\sigma_{11} + F_{22}\sigma_{22} = 1 \qquad (1)$$

The strength parameters, $F_{\alpha\beta\gamma}$, are determined by experimentally measuring the basic ultimate strength values. The interaction term, F_{1122}, can be set either by experimentally measuring biaxial strength or by using the method which likens this term to that in a von Mises formulation [7].

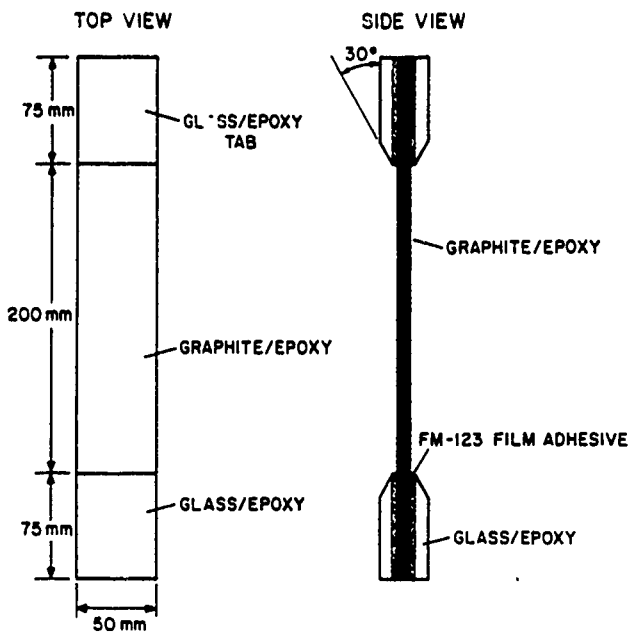

Figure 1. Tensile coupon specimen.

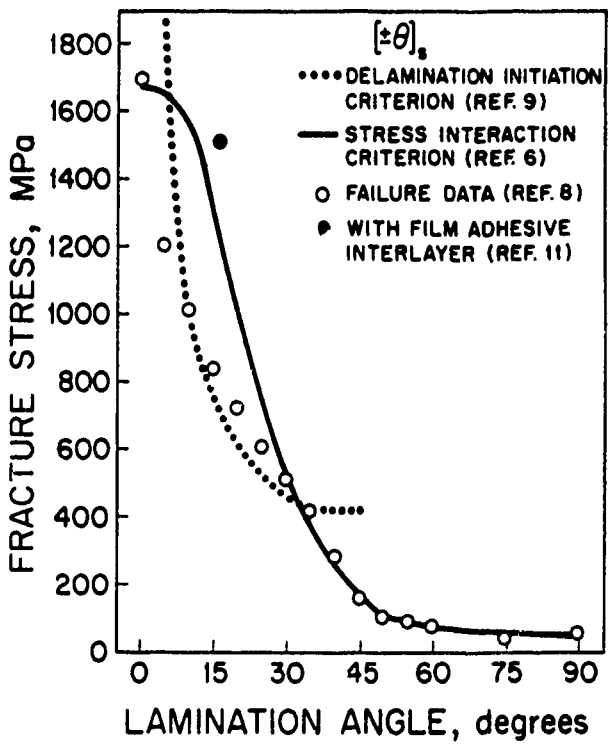

Figure 2. Uniaxial tensile failure stresses of $[\pm\theta]_s$ graphite/epoxy laminates along with in-plane and out-of-plane failure predictions.

Previous authors [3,4] have shown that in many cases the measured unnotched tensile strengths of multidirectional laminates fall short of the predicted values. There are a number of possible explanations for this including improper testing and inappropriateness of the failure criterion. The more likely explanation is that the specimens which had a failure strength below the predicted values failed via a delamination mechanism. This is illustrated in Figure 2 where the failure stresses of $[\pm\theta]_s$ laminates (made of Hercules AS1/3501-6 graphite/epoxy) $[8]^s$ loaded in uniaxial tension are plotted along with the Tsai-Wu prediction (based on first ply failure). For a value of θ less than 30°, the experimental values fall below the predicted values (except, of course, for θ equal to 0°).

Close examination of the failure modes of these laminates indicate that this is due to the fact that failure is originated by delamination. An edge view of a $[\pm 15]_s$ specimen after failure, shown on the left hand side of Figure 3, indicates that there was delamination at failure. Work by Brewer [9] in determining when damage initiates shows that delamination initiates in this case as can be seen on the edge replication of a $[\pm 15]_s$ specimen shown on the right hand side of Figure 3. The edge replication technique [10] is used to highlight the delamination. If a delamination initiation criterion [9] is used, the failure stresses for the laminates which delaminate (θ less than 30°) fall right along this prediction as can be seen in Figure 2.

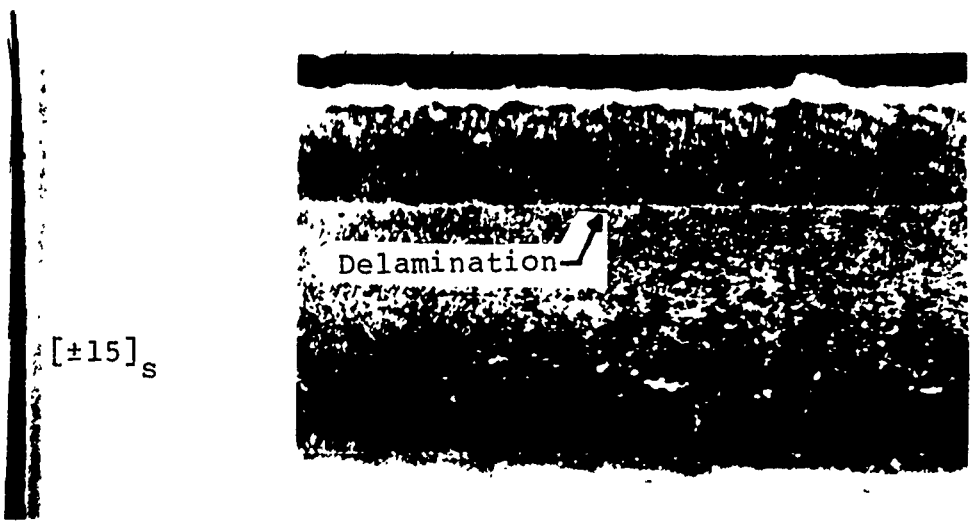

Figure 3. Photographs of (left) edge of failed $[\pm 15]_s$ graphite/epoxy specimen showing extensive delamination; and (right) edge replication of a similar $[\pm 15]_s$ specimen showing initiation of delamination (the white line) before final failure.

A further proof of the fact that the difference in the data is due to the competition between in-plane and out-of-plane failure mechanisms is indicated by the data shown as a solid circle in Figure 2. This is the data for several $[\pm 15]_s$ specimens [11] which have a layer of FM-300 film adhesive (manufactured by American Cyanamid) at the interface between plies of different ply angles. It has been shown [12] that such a layer has the potential of preventing delamination. The results of these experiments indeed show that delamination does not occur and that the failure stress is brought up to, and in fact slightly above, the prediction via the Tsai-Wu criterion.

These results indicate that for these cases, it is essential to classify the failure as due to in-plane or out-of-plane mechanisms or improper conclusions concerning failure criteria would be made.

3.2 Notched Tensile Fracture

A large amount of work has been conducted on the notched tensile fracture of composite laminates [e.g. 13,14]. Much of this work, and the proposed correlations/criteria, are summarized by Awerbuch [15]. The common point linking all these notched failure criteria are that they deal only with in-plane mechanisms. In many cases, the proposed criteria do an excellent job in correlating the data as can be seen in Figure 4. This data was obtained on typical tensile coupons, as shown in Figure 1, made of AS1/3501-6 graphite/epoxy [16] and the two

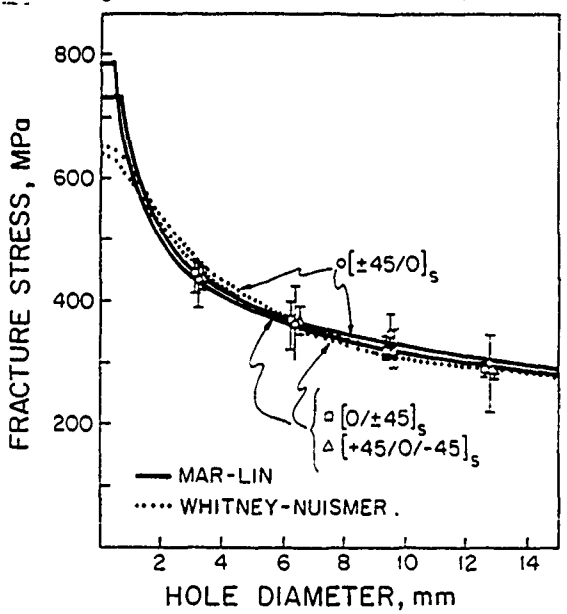

Figure 4. Notched tensile strength for graphite/epoxy laminates and two in-plane correlations (Reference 16).

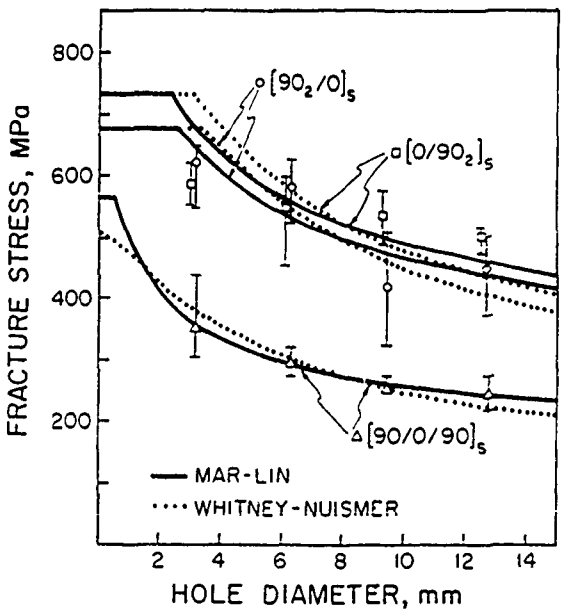

Figure 5. Notched tensile strength for graphite/epoxy laminates and two in-plane correlations (Reference 16).

correlations used are those proposed by Whitney and Nuismer [17] and by Mar and Lin [18].

Much of the data which has been obtained over the years is well-correlated by these various criteria [15]. However, there are many instances where the correlations apparently do not work. One such case is illustrated in Figure 5, again taken from Reference 16, where the failure data for notched $[0/90_2]_s$ coupons do not fall along the correlations from either the Whitney-Nuismer or the Mar-Lin formulation. Many authors, upon seeing such data, have concluded that the proposed correlations are incorrect or that the parameters in the correlation have to be adjusted to fit the data.

A closer look at the failure of the $[0/90_2]_s$ specimens reveals that there is no problem with the proposed correlations but that some of the specimens fail by an out-of-plane mechanism and thus cannot be correlated with an in-plane criterion. Closeup side views of two $[0/90_2]_s$ specimens, one with a 3.175 mm diameter hole, the other with a 12.7 mm diameter hole, are shown in Figure 6. It can clearly be seen that the specimen with the smaller hole fails via extensive delamination whereas virtually no delamination is seen for the specimen with the 12.7 mm diameter hole. This can be explained by looking at the failure as a competition between the two modes: in-plane and out-of-plane. For small holes for this particular laminate, the interlaminar stresses become more critical and cause out-of-plane failure. For larger hole sizes, the in-plane notch sensitivity becomes more critical and an in-plane failure mechanism results.

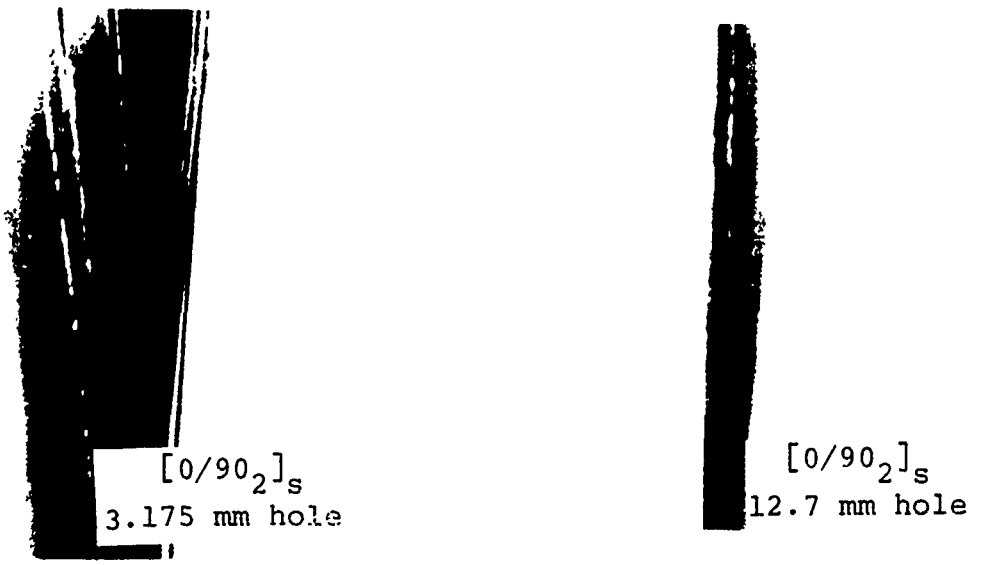

Figure 6. Closeup side views of failed $[0/90_2]_s$ graphite/epoxy specimens: (left) with a 3.175 mm diameter hole showing delamination; and (right) with a 12.7 mm diameter hole showing no delamination (Reference 16).

This is better illustrated in Figure 7 where the $[0/90_2]_s$ notched tensile failure data is replotted on a log-log scale. This is done to better illustrate the "competition" aspect of the failure process using the Mar-Lin equation which is of the form:

$$\sigma_f = H_c(2r)^{-m} \tag{2}$$

where H_c is known as the composite fracture parameter and m is a parameter determined from fiber and matrix properties. Due to the form of the equation, it is very convenient to use a log-log plot which corresponds to the following form of the equation:

$$\log \sigma_f = \log H_c - m \log 2r \tag{3}$$

In this case, a linear regression can be used on the data points and both parameters, m and H_c, can be determined from the data. In Figure 7, the data has been fit using equation (3) first with all four points and then with only the two points which showed failure via in-plane mechanisms. There is a significant difference in the parameters obtained. In the case where the data from the out-of-plane failures is excluded, a linear regression yields a value of 0.28 for m which is equal to the theoretical value obtained for the model [16].

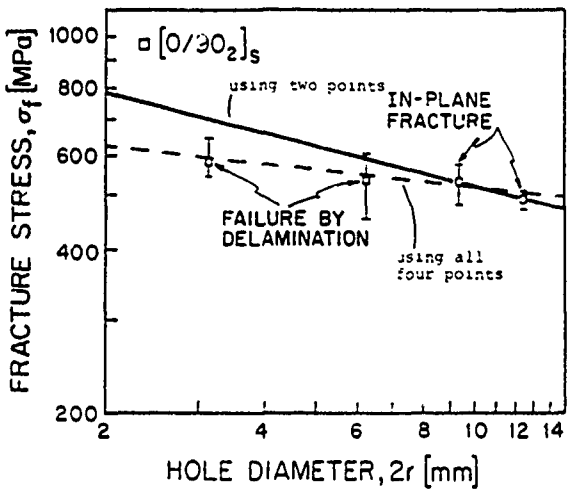

Figure 7. Log-log plot of $[0/90_2]_s$ notched tensile failure stresses as compared to Mar-Lin correlation using two and all four data points (Reference 16).

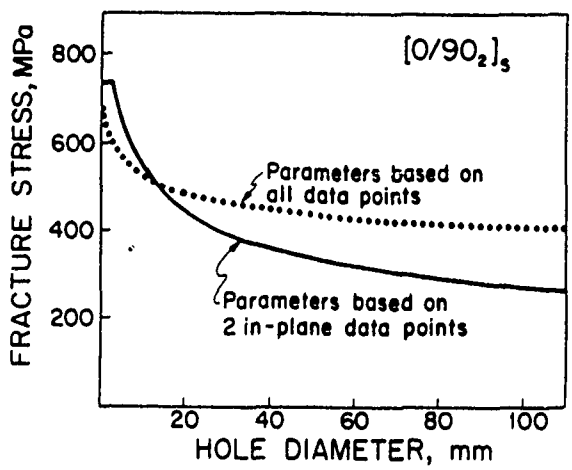

Figure 8. Extrapolated predictions for tensile notched failure stress of $[0/90_2]_s$ laminates using Mar-Lin parameters from Figure 7.

The error which can result by not considering the type of failure and blindly using failure data to obtain values for the parameters in a correlation is illustrated in Figure 8. The parameters determined from the linear regression on all the data

and then on only the data from in-plane failure is used to predict failure for larger holes than that used in the experimental program. It can clearly be seen that there is a difference between the two curves even in the interpolated region (for hole diameters less than 12.5 mm), but that the difference becomes quite significant as that correlation is extrapolated. If all the data is used for the extrapolation, the predicted failure stress at a hole diameter of 100 mm is nearly 50% greater than that using only the in-plane failure data to determine the parameters. This would result in a severely nonconservative design.

This example clearly illustrates the necessity to classify notched failures as due to in-plane or out-of-plane sources and the problems which may arise when extrapolating in-plane failure correlations when using data which includes out-of-plane failures.

3.3 Compressive Failure

Most of the work to date has concentrated on delamination under tensile loads. Recently, however, delamination in composites under compressive loads has bcome of interest. This is due to the phenomenon known as ply or sublaminate buckling which occurs locally when there is a delamination in a composite. This is of special significance in impact related problems where delamination is caused by the impact event and the specimen is later subjected to compressive loads. However, this phenomenon can also occur in seemingly undamaged specimens [19].

A laminate can be thought of as a number of plates (individual plies) each on an elastic foundation (the matrix material between plies). Each plate can then buckle on this elastic foundation. This buckling is promoted by any defect from the manufacturing process. Thus, failure of an unnotched compressive specimen may result from out-of-plane mechanisms even if the failure does not originate from a free edge or a macroflaw.

Experiments were conducted by Vizzini and Lagace [19] on cylindrical specimens of graphite/epoxy illustrated in Figure 9. The laminates tested were of the $[\pm\theta/0]_s$ and $[0/\pm\theta]_s$ configurations. The failure data for the $[0/\pm\theta]_s$ laminates is shown in Figure 10. The data falls well below theoretical predictions of in-plane failure, via the Tsai-Wu criterion, and of shell buckling. Close examination of the specimens showed that the outer ply, in this case the 0° ply, was delaminated and buckled away prior to final failure. A failure of this type is shown in Figure 11 which is a picture of a $[0/\pm60]_s$ specimen after failure. The specimen pictured there is an axial sandwich column, but it exhibits the same failure mode as the cylinder

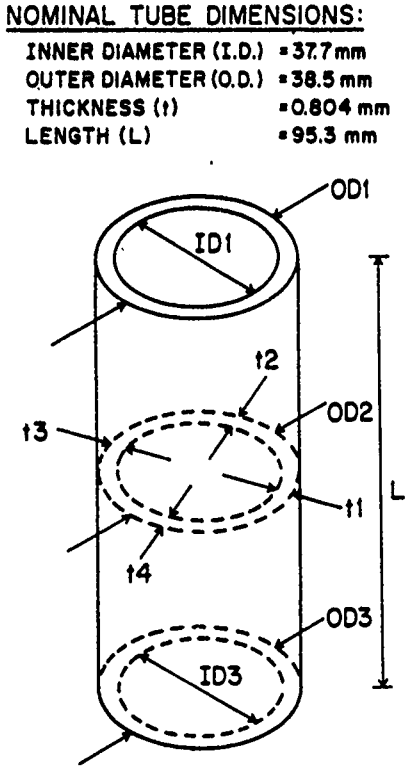

Figure 9. Cylinder specimen for uniaxial compressive tests (Reference 19).

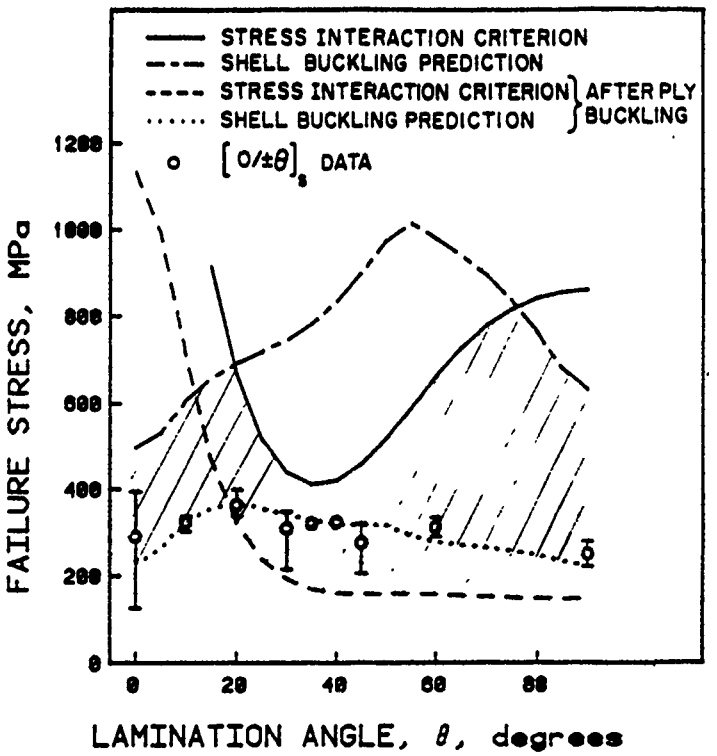

Figure 10. Compressive failure stresses for $[0/\pm\theta]_s$ graphite/epoxy cylinders and several predictions.

specimen of the same laminate. The failure mode can be seen more clearly in the sandwich specimen. This out-of-plane failure mechanism reduces the total load-carrying capability of the cylinder. When this is taken into account (by assuming the buckled ply cannot carry load), a feasible region for failure, shown as the shaded region in Figure 10, results. The experimental data falls within this feasible region.

Once again, this example illustrates the importance of classifying the failure mechanism. The experimental data falls well below the in-plane prediction. Failure to properly observe the out-of-plane failure mode may result in erroneous conclusions concerning the applicability of in-plane failure criteria to compressive failure of composite materials.

Figure 11. Photograph of failure mode of $[0/\pm60]_s$ graphite/epoxy laminate subjected to uniaxial compressive load illustrating ply buckling.

4. POSTMORTEM MACROSCOPIC EVALUATION GUIDELINES

At first glance it would seem obvious how to proceed in characterizing the failure mechanism as in-plane or out-of-plane via a macroscopic evaluation of the postmortem failure: simply observe whether or not significant delamination has occurred. If it has then the mechanism was out-of-plane; if not, then the mechanism was in-plane. Such a simple approach, although attractive, is not valid since it is necessary to identify the mechanism by which failure originates. During the fracture process, the stored energy in the specimen must be released. "Secondary" failure modes often occur to release this energy. Thus, delamination may occur after in-plane mechanisms have prompted failure and vice versa. In fact, as previously discussed, it is necessary that some in-plane modes eventually occur in order for a coupon specimen to end up in two pieces even if delamination was the primary failure mechanism. It thus becomes a problem in terms of classifying "primary" versus "secondary" failure. The following example illustrates this problem.

Uniaxial tensile failure of a $[+45/0/-45]_s$ graphite/epoxy laminate is compared between tests conducted in 1981 [5] and those recently conducted [20]. The conditions are identical except the earlier tests were conducted on AS1/3501-6 while the later tests were conducted on AS4/3501-6. (It should be noted that the former tests were conducted on coupons which are 50 mm in width and the latter on coupons which are 70 mm in width. However, this has no effect on the fracture mechanism.) Typical failures of the two types are shown in Figure 12. The AS1/3501-6 material shows a relatively clean fracture area while the AS4/3501-6 material exhibits significant fiber bridging at the main fracture area. In both cases, however, the ultimate failure strength is virtually the same (approximately 750 MPa).

The actual mode which causes failure in both cases is splitting in the matrix of the 45° plies via shear. The two modes look very different due to the secondary occurrences after

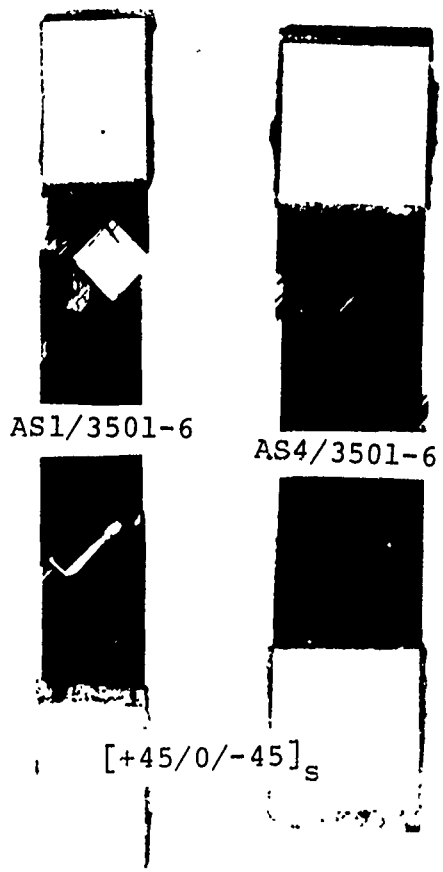

Figure 12. Photographs of uniaxial tensile failure modes of unnotched $[+45/0/-45]_s$ graphite epoxy laminates made from (left) AS1/3501-6; and (right) AS4/3501-6.

failure originates. The AS1 fibers have a mean ultimate tensile strain of 1.2% while the AS4 fibers fail at 1.4%. This difference in ultimate strain is enough to keep the fibers in the 45° plies from failing in the AS4/3501-6 $[+45/0/-45]_s$ laminate while these same fibers fail in the AS1/3501-6 material. Thus, despite their very different final appearence, the basic mode which originates failure is the same.

The five rules of thumb, which are presented, are geared towards aiding in this problem of classifying in-plane versus out-of-plane modes as the primary mechanism in originating failure.

RULE OF THUMB #1: Propagation of "primary" delamination is from a likely initiation site while "secondary" delamination propagates away from the main fracture area.

Both experimental experience and analytical techniques (i.e. calculation of interlaminar stresses and application of out-of-plane failure critria) can be used to identify areas where out-of-plane failure is likely to occur. Locations such as free edges, including holes, ply drops, and bonded or bolted joints, are likely places for delamination to occur. This can be summarized by saying that interlaminar stresses arise, and

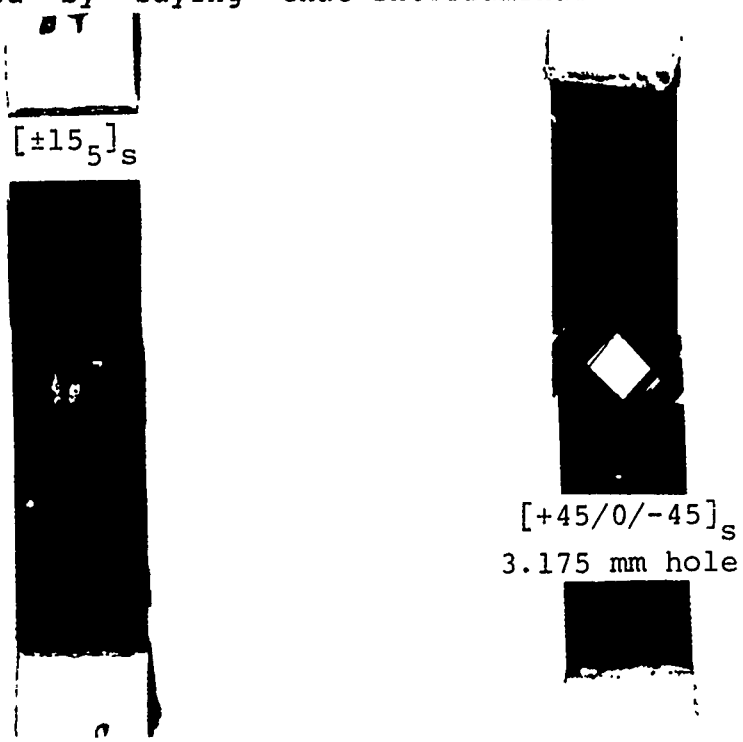

Figure 13. Photographs of uniaxial tensile failure modes of graphite/epoxy specimens: (left) unnotched $[\pm 15_5]_s$; and (right) notched $[+45/0/-45]_s$.

thus delamination is a possiblity, in any gradient stress fields in composites. Additionally, an understanding of the factors which affect delamination is necessary. If delamination then occurs in such a likely place, it is probably the cause of failure. In contrast, if delamination occurs in some other place, for example, leading away from the fracture surface, it is probably due to "secondary" effects.

This is illustrated in Figure 13 where two failed graphite/epoxy specimens are pictured. The left hand specimen is an unnotched $[\pm 15_5]_s$ specimen which shows delamination leading away from the free edge, a likely place for delamination to originate. The other specimen is a $[+45/0/-45]_s$ specimen with a hole. In this case the delamination, which is rather extensive, propagates away from the failure area. Close examination reveals that it does not originate at the hole but is a result of in-plane failure which leads away from the hole and is thus a "secondary" mechanism.

There is one qualification which must be made for this rule. Under compressive loading, delamination may result anywhere due to local defects prompting a ply/sublaminate buckling. Greater care must thus be exercised in looking at compressive specimens.

Figure 14. Photograph of a $[\pm 15]_s$ graphite/epoxy laminate loaded under uniaxial tension, but not to failure, showing initiation of delamination.

RULE OF THUMB #2: "Primary" delamination initiates before final failure and affects the macroscopic stress-strain behavior.

As has been stated, delamination cannot cause final failure in terms of a specimen breaking into two or more pieces. Thus, in-plane failure will always be present in a postmortem examination. Generally, delamination is not catastrophic in that it initiates before the final failure. This can be seen in Figure 14 where a $[\pm 15]_s$ specimen has been tested beyond delamination initiation but before final failure. The delamination can be seen since the label identifying the specimen has been placed between the plies.

In the laboratory, a technique known as edge replication [10] can be used to obtain images of specimen edges before failure and these can be examined under a microscope to see if delamination occurred. An example of such was shown in Figure 3. It is not always possible to perform an edge replication. There are other signs which indicate that delamination has initiated, however. Generally, the stress-strain behavior is affected since delamination causes a compliance change. The stress-strain plot of a $[\pm 15/0]_s$ specimen [5] is shown in Figure 15. A sharp drop in compliance is seen before final failure via a drop in stress without any change in the strain. It is important to differentiate this from the discontinuities in the stress-strain curve caused by transverse cracking as shown in Figure 16 [16]. In this case, the 90° plies in the $[90_2/0]_s$ laminates begin to crack and this causes jumps in the strain of a specimen for constant load. It should also be noted that these aspects will change if tests are conducted in load control rather than stroke control.

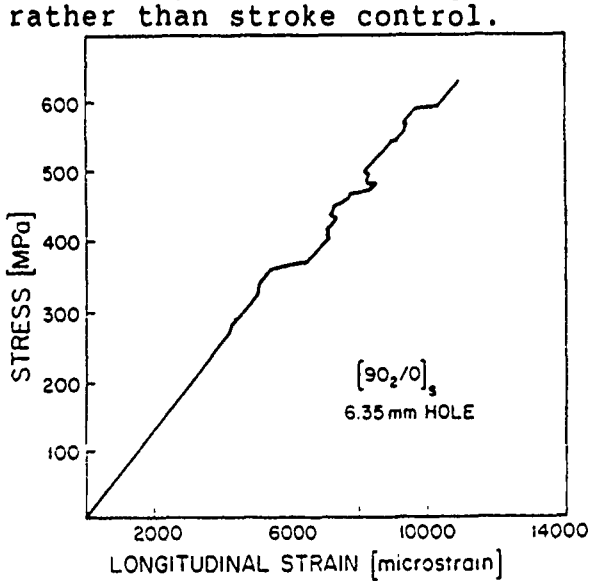

Figure 15. Stress-strain plot for $[\pm 15/0]_s$ graphite/epoxy specimen (Reference 5).

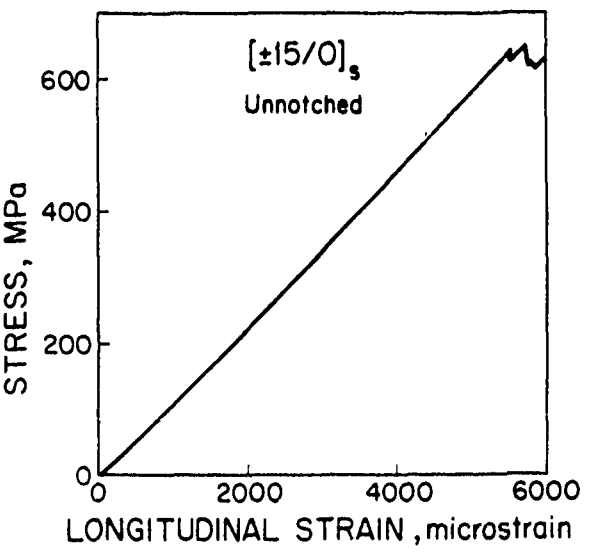

Figure 16. Stress-strain plot for $[90_2/0]_s$ graphite/epoxy specimen (Reference 16).

RULE OF THUMB #3: Calculations before tests are not foolproof in identifying "hot spots" for delamination. This is due to "unknown unknowns".

All the important phenomena which contribute to composite behavior and failure are still not understood nor is it likely that all the phenomena have been identified. These are what are termed "unknown unknowns". An example of such a case concerns delamination. Only two or three years ago the general consensus was that delamination was caused by tensile interlaminar normal stresses [21]. However, the case of a $[0/\pm 15]_s$ composite laminate shows that this is not true. Such a laminate has only compressive values of interlaminar normal stress at the free edge during a uniaxial tensile load. Nevertheless, delamination initiates at the free edge. This is due to the high values of interlaminar shear stress in the region near the free edge. This phenomenon was previously an "unknown unknown". Further proof is that a $[\pm 15]_s$ graphite/epoxy laminate which has no interlaminar normal stress also delaminates via interlaminar shear stress (see Figure 3).

Therefore, although calculations and experience may guide investigators to look for delamination in certain locales (as was suggested in rule of thumb #1), the investigator must stay openminded and question delaminations which occur in other locations. If the failure cannot be explained by an in-plane mechanism, then another explanation must be sought.

RULE OF THUMB #4: Failure data which represents failure promoted by delamination generally have larger scatter than those for in-plane failures.

This rule of thumb comes from observations of a large amount of failure data. It can be seen, for a limited case, in Figure 7 where the specimens with the two smaller hole sizes have larger scatter bars than the other specimens. The former fail via an out-of-plane mechanism and the latter by an in-plane mechanism.

A qualitative argument can be advanced for this larger scatter. The failure promoted by delamination originates in the interply matrix layer. There is less control over the variables involved in this case. The size of the interply layer varies within a specimen by a factor as much as, or greater than, two. This layer is also wavy. Finally, voids and inclusions can be introduced, during the manufacturing process, in this region which will promote delamination. Thus, there is likely to be very large scatter for specimens which fail via delamination.

RULE OF THUMB #5: Failure promoted by delamination always has some "in-plane" failure mechanisms. The opposite is not always true.

This has been referred to several times within this paper and is merely a statement of the fact that in order for a specimen to break into more than one piece (so that no further in-plane load can be carried), the specimen must finally come apart in some in-plane fashion. Thus, delamination failures will always have some in-plane failures associated with them when a postmortem examination is undertaken. However, in-plane failures do not need to have delamination associated with them. Thus, if no signs of delamination are present, the failure mode is definitely in-plane. However, there will be no instances upon inspecting a fully failed specimen where only delamination will be detected.

SUMMARY

It has been demonstrated that it is necessary to classify failure as due to either an in-plane or an out-of-plane mode, especially when using experimental results for correlative equations which will later be used in design. The suppositions that failure can be regarded as a competition between in-plane and out-of-plane mechanisms and that the two mechanisms are separable in terms of failure origin are important and must be remembered when failure criteria are used. In-plane failure correlations can only be used with data from specimens which fail in an in-plane manner while out-of-plane correlations can only be used with data from specimens where failure originates from an out-of-plane mechanism.

The rules of thumb, which have been offered as guidelines, can be used to quickly inspect specimens after failure on a macroscopic basis. These techniques can never substitute for the more intricate and typical methods using optical and electron microscopy, but are essential when a large number of specimens are involved. Such techniques should go hand in hand with the more intricate techniques which can be used to verify the conclusions reached via close examination of a few specimens from a large batch.

No matter what the application, however, the art of identifying failure by delamination is essential.

ACKNOWLEDGEMENTS

The author wishes to acknowledge the support of a number of organizations and the associated contract monitors over the past

several years who have supported the research in the fracture of composites at TELAC. These are the Air Force Office of Scientific Research, the Air Force Materials Laboratory, the Boeing Military Airplane Company, the Naval Air Systems Command, and the Federal Aviation Administration. The author would also like to acknowledge, in a general manner, the students who have worked on this research over the years, but especially John Brewer and Anthony Vizzini who helped organize the material herein and provided useful comments and suggestions concerning the proposed "rules of thumb".

REFERENCES

1. Mullin, J.W., Berry, J.M., and Gatti, A., "Some Fundamental Fracture Mechanisms Applicable to Advanced Filament Reinforced Composites", Journal of Composite Materials, Vol. 2, 1968, pp. 82-103.
2. Pipes, R.B. and Pagano, N.J., "Interlaminar Stresses in Composite Materials under Uniform Axial Extension", Journal of Composite Materials, Vol. 4, 1970, pp. 538-548.
3. Kim, R.Y., "A Technique for Prevention of Delamination", Proceedings of the Seventh Annual Mechanics of Composites Review, Air Force Materials Laboratory, April, 1982, pp. 218-230.
4. Pipes, R.B., Kaminski, B.E., and Pagano, N.J., "Influence of the Free Edge upon the Strength of Angle-Ply Laminates", Analysis of the Test Methods for High Modulus Fibers and Composites, ASTM STP 521, American Society for Testing and Materials, 1973, pp. 218-228.
5. Lagace, P.A., "Delamination Fracture under Tensile Loading", Proceedings of the Sixth Conference on Fibrous Composites, AMMRC MS 83-2, Army Materials and Mechanics Research Center, November, 1983, pp. IX-53-70.
6. Tsai, S.W. and Wu, E.M., "A Generalized Theory of Strength for Anisotropic Materials", Journal of Composite Materials, Vol. 5, 1971, pp. 58-80.
7. Tsai, S.W. and Hahn, H.T., Introduction to Composite Materials, Technomic, Westport, CT, 1980.
8. Lagace, P.A., "Nonlinear Stress-Strain Behavior of Graphite/Epoxy Laminates", to appear in AIAA Journal, November, 1985.
9. Brewer, J.C., "The Effect of Ply Thickness on the Free Edge Delamination of Graphite/Epoxy Laminates", Technology Laboratory for Advanced Composites Report 85-9, S.M. Thesis, Massachusetts Institute of Technology, May, 1985.
10. Klang, E.C. and Hyer, M.W., "Damage Initiation at Curved Free Edges: Application to Uniaxially Loaded Plates Containing Holes and Notches", Recent Advances in Composites in the United States and Japan, ASTM STP 864, American Society for Testing and Materials, 1985, pp. 62-90.

11. Barkey, D.A. and Leistensnider, J., "Suppression of Shear Delamination using Film Adhesive", Technology Laboratory for Advanced Composites Report 85-8, Massachusetts Institute of Technology, May, 1985.
12. Chan, W.S., Rogers, C., and Aker, S., "Improvement of Edge Delamination Strength of Composite Laminates using Adhesive Layers", presented at the Symposium on Composite Materials: Testing and Design, American Society for Testing and Materials, Philadelphia, PA, April, 1984.
13. Waddoups, M.E., Eisenmann, J.R., and Kaminski, B.E., "Macroscopic Fracture Mechanics of Advanced Composite Materials", Journal of Composite Materials, Vol. 5, 1971, pp. 446-454.
14. Nuismer, R.J. and Whitney, J.M., "Uniaxial Failure of Composite Laminates Containing Stress Concentrations", Fracture Mechanics of Composites, ASTM STP 593, American Society for Testing and Mateials, 1975, pp. 117-142.
15. Awerbuch, J. and Madhukar, M.S., "Notched Strength of Composite Laminates: Predictions and Experiments - A Review", Journal of Reinforced Plastics and Composites, Vol. 4, 1985, pp. 3-159.
16. Lagace, P.A., "Notch Sensitivity and Stacking Sequence", to appear in Composite Materials: Testing and Design (Seventh Conference), ASTM STP 893, 1986.
17. Whitney, J.M. and Nuismer, R.J., "Stress Fracture Criteria for Laminated Composites Containing Stress Concentrations", Journal of Composite Materials, Vol. 8, 1974, pp. 253-265.
18. Mar, J.W. and Lin, K.Y., "Fracture Mechanics Correlation for Tensile Failure of Filamentary Composites with Holes", Journal of Aircraft, Vol. 14, 1977, pp. 703-704.
19. Vizzini, A.J. and Lagace, P.A., "The Role of Ply Buckling in the Compressive Failure of Graphite/Epoxy Tubes", to appear to AIAA Journal, 1986.
20. Grapes, T.F., "Sensitivity of Graphite/Epoxy to Implanted Delaminations under Tensile Load: Initial Study", Technology Laboratory for Advanced Composites report under preparation, Massachusetts Institute of Technology.
21. Kim, R.Y. and Soni, S.R., "Experimental and Analytical Studies On the Onset of Delamination in Laminated Composites", Journal of Composite Materials, Vol. 18, 1984, pp. 70-80.

A MICROSCOPY STUDY OF IMPACT DAMAGE ON EPOXY-MATRIX CARBON FIBER COMPOSITES

D.J. Boll, W.D. Bascom and J.C. Weidner
Hercules Aerospace
Magna, Utah

A Microscopy Study of Impact Damage on Epoxy-Matrix Carbon Fiber Composites

D. J. Boll, W. D. Bascom, J. C. Weidner and W. J. Murri

Hercules Aerospace
Magna, Utah

Abstract

The damage associated with the impact of quasi-isotropic epoxy-matrix carbon fiber composites was studied by sectioning through the impact area and photographing the polished sections. Composites with a SOTA low fracture energy matrix resin (Hercules 3501-6) and a new high fracture energy resin (Hercules X8551) were compared. Damage in the low toughness matrix laminate was characterized by a network of interlaminar and transverse cracking that extended some distance beyond the center of impact. A similar network of transverse and interlaminar cracking developed in the impacted tough matrix laminate but was largely confined to a region immediately below the impact center. This difference in the volume of impact damage could be easily attributed to the high interlaminar fracture energy of the X8551 resin compared to the 3501-6 resin.

The type and distribution of impact damage are discussed in terms of energy dissipative mechanisms and the stress patterns that develop during impact due to mechanical deflection and stress wave interaction. Also, the results of the sectioning study are compared with damage assessment by ultrasonic back-scattering.

Introduction

Much of the evidence of a loss in strength of organic-matrix, carbon fiber composites due to relatively low impact forces is the result of work by Starnes, Rhodes, Williams and others (1) at the Langley Research Center (NASA). They demonstrated that the compressive and tensile strength of carbon fiber reinforced laminates are seriously reduced by impact damage. In some instances the compressive strength was reduced by 50% or more after impact by metal projectiles at low energy levels (20-45N) that produced no visible external damage. They also demonstrated that by increasing the matrix resin fracture energy the effect of impact loading was significantly reduced.

The loss in laminate mechanical properties due to impact damage has since been confirmed by a number of workers (2,3,4). Efforts to improve the "damage tolerance" of composites have been directed primarily at developing high fracture energy resins with a minimum trade-off in other resin controlled laminate properties. Other approaches have included variations in fiber orientation and structural design, e.g., stringers or ribs to restrict the growth of delaminations.

Various methods have been devised to determine the effect of impact on laminate strength. In the development of tough resins, where it is necessary to screen numerous formulations, relatively small panels or coupons are fabricated with specific multidirectional fiber orientations, impacted over a short range of energies, and tested for residual strength. This procedure has been very useful in developing damage tolerant matrix resins and in evaluating the effect of different fibers. It is problematical as to how this data translates into the response of larger structures to impact loads.

In the work described here, small (10cm X 15cm X 0.5cm) plates were impacted and then sectioned through the damage zone and the sections examined using reflected light microscopy to determine the type and extent of damage. Two matrix resins were used, Hercules 3501-6 and Hercules X8551, where the latter has an 8X higher fracture energy and a post impact compressive strength 2X greater at 109N impact load than the 3501-6. The study revealed major differences in the extent, type and location of the damage for the two matrix materials.

Experimental

Panels of Hercules 3501-6/IM7XG and Hercules X8551/IM7XG were fabricated into 4in. (10.2cm) X 6in. (15.2cm) and 32 ply (0.5cm) panels. The fiber orientation was $(+45/90/-45/0)_{4S}$. The pertinent properties of the resins, including cure conditions, are given in Table I. The pertinent fiber properties are given in Table II.

The plates were impacted using an ETI 630 impact drop tower test system at an impact load of 24.6 ft-lbs (109N). The impactor was a 0.625in. (1.59cm) diameter steel ball. The plate was held against an open frame as shown in Figure 1. Note that this arrangement allows some limited flexure of the plate and also that the unsupported backside constitutes a low impedance stress wave boundary.

A set of six plates were cut from a 14in. (35.6cm) X 14in. (35.6cm) panel. All plates except one were impacted and then tested for residual compressive strength (post impact compressive strength, PIC, Table I). The plate that had not been compression tested was examined by an acoustic backscatter technique (5) originally described by Bar-Cohen and Crane (6) to locate the region of greatest internal damage. A schematic of the experimental arrangement is shown in Figure 2. The transducer, which serves as both transmitter and receiver, is positioned at a small angle ($\gamma = 11°$) from the normal to the plate front surface and at a selected azimuthal angle β. Positioning the transducer at a small angle off normal incidence directs the strong front and back surface reflections away from the backscattered signal. The backscattered signals have a maximum amplitude when β is such that fibers or discontinuities (i.e. broken fibers, cracks, etc.) are normal to the incident ultrasonic beam. Backscatter C-scans were performed at several azimuthal angles ($\beta = 0°$, $\pm 45°$, and $90°$) on the impacted plates to produce two-dimensional maps of the damaged area.

For both the 3501-6 and the X8551 matrix materials the damage area was largely contained within a 2in. X 2in. (5.1cm X 5.1cm) area centered on the point of impact which could be readily seen on the plates. The plates were then cut and sectioned as shown in Figure 3. It was subsequently found from the sectioning study that the damage in the 3501-6 plate extended well beyond the 2in. X 2in. area. The square around the damage zone was cut with a diamond cut-off saw (Micromech Precision Slicing and Dicing Machine, Model WMSA 1018, Micromech Mfg. Co.). A cut was then made through the center of the damage zone using a diamond wafering saw (Buehler Isomet Low Speed Saw) with a 0.015in. (0.038cm) thick blade as shown in Figure 3. One of the halves was potted in an amine (Jeffamine 230) cured diglycidylether Bisphenol A (Dow 332) epoxy with an amine accelerator (399, Texaco Chem. Co.) and a fluorescein dye (0.3 wt% Dayglo Fire Orange). The sample was covered with the liquid embedding resin, degassed at 0.25mm Hg and then cured at ambient temperature and pressure. Excess potting resin was polished off (see below) to the cut laminate surface.

Slices were cut from the potted section at 0.075 in (0.190cm) intervals. One face of each slice was polished (Buehler Econonet polisher) sequentially with No. 320, No. 400 and No. 600 SiC grit papers followed by a 6μ diamond paper and wet polishing with 1μ CeO paste on a velvet cloth.

The polished surfaces were examined using reflected light microscopy for the type and extent of damage in each ply.

Results

3501-6/IM7XG: The damage observed within the 3501-6 laminates was dominated by delamination between plys connected by transverse cracks through 90° and 45° plys. This network of delamination and transverse cracking is illustrated in Figure 4. This photograph was taken from the LHS of a laminate slice immediately below the center of impact. Although it shows extensive damage, the major damage in this plate occurred below the mid-plane and away from the impact center as shown in Figure 5. The isometric drawing in Figure 5 presents the outer bounds of damage in each ply without any attempt to distinguish the type of damage. However, the most predominate type of damage throughout all of the indicated areas was a network of interconnecting delaminations and transverse cracks (Figure 4). To find the outer bounds of delamination it was necessary to slice and polish sections beyond the initial 2in. square (Figure 2).

The development of the interlaminar and transverse crack network appears to involve the propagation of a delamination with the coincident formation of transverse cracks which frequently, but not always, diverted the delamination through an adjacent 45° or 90° ply; but rarely through a 0° ply. In Figure 4 it is possible to find transverse cracks that terminated without redirecting or initiating a delamination.

There was a strong tendency for the delamination to propagate in the resin rich areas between plys but near the fiber-resin boundary as shown in Figures 6 and 7. It is reasonable that residual stresses in the resin near the fibers provided a low energy path for propagation. Indeed, in propagating along this boundary the delamination in Figure 7 was almost diverted into a transverse crack.

It was not always clear what caused a delamination to divert into a transverse crack. Sometimes a resin rich pocket (as in Figure 7) could be identified with crack redirection. From a fracture energy point of view, opening mode ($\mathcal{G}_I$) for transverse cracking is greater than for delamination based on laminate tests (7). However, the difference is small and could easily be reversed by local variations in fiber volume, resin heterogeneities, etc. Moreover, these considerations are complicated by the effects of reflected stress waves and plate deflections as discussed below.

Although the delamination tended to propagate along fiber-resin boundaries the associated deformation did extend into the interply resin as shown in Figure 8. In these photomicrographs there are tear markings in the resin reminiscent of the hackle or chevron markings reported in fractography studies of carbon fiber composite delaminations (8,9).

X8551/IM7X: The characteristic damage of the X8551 matrix laminate included transverse cracking, delamination and fiber breakage. These features are shown in the photomicrographs in Figures 9A and 9B taken from a section just below the point of impact (Figure 9A is the LHS and Figure 9B is the RHS of the impact center line). The top surface indentation had a

diameter of about 0.5 in (1.3cm) compared to 0.08 in (0.2cm) for 3501-6. Moreover, there was plastic deformation of the top ply of the X8551 matrix laminate. At the top of Figures 9A and 9B the 45° ply disappears near the center of the impact zone. Visual inspection of the impact area indicated the material had been radially moved from the impact, "epicenter."

The internal damage was dominated by transverse cracking with limited delamination (Figure 10). In many instances the transverse crack propagated through adjacent plys including fiber fracture of 0° fibers (Figure 11). Note in Figure 11 that fiber breakage in the 0° ply included some intra-ply delamination. Also, fracture through a 0° ply often involved wide delaminations above and below the ply fracture which terminated a short distance from the break.

The most striking characteristic of the X8551/IM7XG laminate was that the extent of damage was much reduced compared to the 3501-6 matrix laminate. This difference is easily seen by comparing Figure 6 and Figure 12, and also in the plot of impact areas in Figure 13. These charts indicate that the lateral extent of damage in the 3501-6 laminate was 2-3X greater than in the X8551 material. Most of the damage in the latter near the center of impact was transverse cracking. However, the propagation of damage away from the center shown in Figures 12 and 13 was primarily delamination.

Occasionally, an air void was observed in a cut section. There was no evidence that damage initiated from these voids. In fact, Figure 14 shows that the void had no influence on delamination propagation.

Ultrasonic Backscattering: Microsectioning, polishing and microscopy is a destructive and very laborious method of determining impact damage. However, there are no nondestructive methods of characterizing this damage in as much detail as can be obtained by sectioning. An acoustic backscattering technique (5,6) is capable of determining variations in the extent of damage within a laminate both indepth and radially from the impact center. This technique for producing backscatter C-scans is being developed at Hercules (5) and was used here to supplement the sectioning study and to indicate directions to improve the acoustic technique to better characterize internal damage.

The C-scan results are presented in two formats in Figures 15 and 16 for the 3501-6 matrix laminate and the X8551 laminate respectively. The shaded dot-patterns indicate the damage within the 2in. (5.1cm) square area denoted in Figure 2. The shading intensity is proportional to the amount of total damage through the laminate thickness. The shaded maps were replotted as three-dimensional maps of backscatter energy as shown in Figures 15 and 16. The cut made through the 2in. square is indicated on the 3-dimensional plots and sections were sliced from the back portion of the cut.

The C-scan plots indicate a number of features also revealed by microsectioning. The much larger diameter of damaged area in the 3501-6 matrix laminate compared to the X8551 matrix laminate is evident in

comparing Figures 15 and 16. The damage was most severe directly under the point of impact for the X8551 resin. The damage was more widely spread for the 3501-6 resin laminate. The maximum damage on the 3501-6 matrix plate is slightly off-center in Figure 15 suggesting the impact load was not precisely normal to the plane of the laminate. Microsectioning confirmed that the damage through the laminate was not symmetrically distributed. Figure 15 indicates that all of the damage in the 3501-6 matrix laminate did not radiate from the impact center. Areas of damage, some of which extended beyond the 2in. square area, developed without any apparent initiation from the region of maximum damage. Similar isolated damage areas can be found on the map (Figure 5) developed from the sectioning study. In some instances these isolated damage areas resulted from delamination being redirected by transverse cracking which went undetected by the C-scan. Nonetheless, compared to conventional (normal incidence) C-scan the backscatter technique used here is more sensitive and yields significantly more information about damage distribution.

The principle deficiency of the backscatter C-scan technique in its present state of development is that the signal gives a summation of damage through the laminate thickness. Work is in progress here to process this signal for changes in intensity as a function of penetration depth.

Discussion

Impact damage in the 3501-6 matrix laminate was dominated by delamination and transverse cracking that extended well beyond the center of impact; out to ~4cm (1.7in.). In sharp contrast, the X8551 damage was dominated by transverse cracking, local delamination and fiber breakage within 1.8cm (0.7in.) of the impact center. These differences are attributed to the higher fracture energy of the X8551 resin compared to the 3501-6 resin (Table I).

The damage in the 3501-6 laminate was characterized by a network of interconnecting delaminations and transverse cracks. It appears that this network forms by the growth of delaminations away from the impact center that are redirected into transverse cracks due to local conditions that cause transverse propagation to be energetically favored. Rarely did a transverse crack continue into the next ply. To do so would require a reorientation of the crack front; e.g., from a path parallel to the 45° fibers to a path parallel to 90° fibers, which would require more energy than to initiate a new delamination. In some cases the delamination branched into a transverse direction rather than being totally diverted. This branching may occur when the delamination growth rate exceeds the materials capacity to dissipate strain energy, i.e., Yoffe Effect (10).

Interlaminar cracking was further favored by an apparent low energy path along the boundary between the fibers and resin. Presumably, residual thermal stresses near the fibers reduces the local fracture energy below that of the resin itself.

In the higher fracture energy X8551 laminate the bulk of the damage was concentrated near the impact center. This damage, like that in 3501-6, was predominately a network of interconnecting delaminations and transverse cracks. However, the high resin toughness prevented the propagation of the delaminations away from the impact center. Instead, the impact energy was consumed by cross-ply transverse cracking which, as already mentioned requires a reorientation, or twisting of the crack front. This reorientation of the crack is a high energy process and reflects the high level of strain energy available which, because of the resin toughness, cannot be dissipated by delamination.

The high energy density near the center of impact also caused fiber breakage and cracking through the 0° plys in the X8551 matrix laminate. It is not obvious why fiber fracture, which generally involves fracture energies 2-3X greater than interlaminar fracture (11,12) should be favored over delamination. Fiber breakage was usually accompanied by local interply separation (Figure 11) which suggests some competition between fiber fracture and interlaminar fracture.

These rationalizations of impact damage in terms of quasi-static fracture energies (primarily $\mathcal{G}_{Ic}$) are compelling in their simplicity but must be tempered by the actual complexity of impact dynamics. One obvious reservation is that by sectioning in only one plane--parallel to the plys designated as 0° in the lay-up sequence--we are presuming that damage is symmetrical about the point of impact and that a similar damage pattern would be observed at any other sectioning angle. Where damage is primarily delamination and transverse cracking the mapping of damage areas from successive sectioning in one plane (Figures 5 and 12) is probably representative of radial damage. However, narrow delaminations within 0° plys would be difficult to detect. Also, transverse cracks parallel to the cutting direction would be missed. The latter could be important in the case of the X8551 matrix laminate.

The dynamic stresses that develop during impact are complex, especially in an organic matrix composite. Greszczuk (13,14) has reviewed this subject and analyzed the compressive stress (Z, θ, r,) and shear stresses (τ_{rZ}) as defined in Figure 17. We would not expect the compressive stresses to induce the type of damage observed here (except as reflected normal stresses discussed later). On the other hand, shear stress, as shown in Figure 17 taken from reference 13, could easily induce transverse cracking. Note in Figure 17 that the maximum shear stresses are displaced below and away from the impact center; at about r/a = 1.0 and Z/a = 0.4 where "a" is the radius of the area of contact. Inspection of Figure 4 and Figures 9A and 9B suggests a concentration of transverse damage below the top surface and radially displaced from the impact center. These concentrations of damage are not displaced as far from the impact center as predicted by the analysis. None the less, it is reasonable to assume that crack initiation begins in this high shear stress region as transverse cracks. Subsequent damage occurs along paths of least resistance by the high strain energy density available for crack propagation.

Other important features of impact dynamics are the reflected tensile stress wave and the bending displacement of the laminate which would produce tensile stresses (σ_z) below the laminate midplane. These tensile stresses may initiate delaminations, especially in the 3501-6 matrix. In Figures 5 and 12 the maximum extent of damage, primarily delamination, is below the mid plane (ply 16). Moreover, a simple calculation of stress wave reflections indicates a maximum tensile stress development beginning at about ply 25. This estimate is consistent with the plots of impact damage area for both 3501-6 and X8551 matrix laminates (Figures 5, 12 and 13).

In the absence of preexisting flaws, it seems doubtful that tensile stress waves or bending stresses are large enough to initiate cracking. More likely, these stresses reinforce the propagation of delamination or transverse cracks already formed by shear stresses. Two possible examples are crack branching in the 3501-6 laminate and multiple ply transverse cracking in the X8551 laminate.

It is clearly evident why the post impact compressive strength of the 3501-6 laminate is significantly lower than the X8551 system. Due to the extensive delamination the plys are loaded independently and the laminate literally fails like a deck of cards. A similar failure mode may occur in the X8551 laminate but the stresses for ply buckling (and delamination growth) would be much higher. One aspect of post impact compressive failure brought out by this study is that in toughening the matrix to reduce delamination there is a concentration of strain energy under the impact area which causes fiber fracture in the 0° plys. Fiber fracture in the 0° plys as well as multiple ply transverse cracking will seriously reduce the laminate resistance to compressive loads.

This comparison of the different types of impact damage in high fracture energy vs low fracture energy matrix composites suggests two important conclusions. First, that the fiber strength becomes increasingly important as the matrix resin toughness is increased. Second, that there may be a limit to which PIC strength can be increased by increasing the toughness of the matrix resin (for a given impact energy). When the matrix has a sufficiently high fracture energy to prevent delamination, then the post impact strength is determined by transverse cracking and fiber fracture. There is some evidence (2) for a limit in matrix $\mathcal{G}_{Ic}$ above which the increase in post impact compressive strength is minimal. The issue is complicated by the fact that resin shear strength and mode I fracture energy are not independent. It is quite possible that increasing $\mathcal{G}_I$ beyond the level necessary to essentially eliminate delamination would also increase resin shear strength and improve the laminate resistance to transverse cracking.

Conclusions

The results of this study comparing impact damage in a low fracture energy matrix carbon fiber composite with the damage in a high fracture energy matrix composite indicate that:

a. The area of damage through the entire thickness of the laminate was much greater (4-5X) for the low fracture energy matrix resin.

b. The internal damage in the low fracture energy composite was characterized by an extensive network of delaminations and transverse cracks.

c. The internal damage in the high fracture energy composite was characterized by multiple-ply transverse cracks, fiber breakage, and localized delaminations.

d. Much of the damage characteristics can be explained in terms of quasi-static fracture mechanics.

e. Crack initiation appears to result from shear stresses developed during the early stages of impact.

f. The principle effect of normal stress wave reflection and laminate bending is the propagation of cracks already formed by shear failure.

g. As the fracture energy of the matrix resin is increased, the fiber strength will play an increasing role in impact damage and post impact residual strength.

h. There may be an upper limit in matrix fracture energy beyond which the post impact compression strength is only marginally improved (for a given impact loading).

i. As the upper limit in matrix fracture energy is increased, the shear strength of the resin may become the controlling factor in impact damage.

Acknowledgements

This work was fully supported by Hercules Inc., IR&D funding. We wish to thank Dr. L. H. Pearson for his very helpful discussions during the course of this work.

4805d/p23

TABLE I

Properties of Hercules 3501-6 and X8551 Resins

Resin	Fracture Energy (J/m^2) Resin	Interlaminar	Glass Transition Temp., T_g, °C	Post Impact Compression, k
3501-6	95	180*	210	25
X8551	780	740**	178	45

Cure Schedule: Vacuum bag/autoclave, 2 hrs at 350°F (177°C)

TABLE II

Properties of Hercules IM7XG Carbon Fiber

0° Tensile Laminate Properties			
Strength (MPa)	Modulus (GPa)	Elongation (%)	Diameter, μm
5.52	276	1.9	5.2

* Tested in AS4 fiber
** Tested in AS6G fiber

References

1. Starnes, J.H., Rhodes, M.D., and Williams, J.G., ASTM STP 696, Nondestructive Evaluation of Flaw Criticality for Composite Materials, Ed., R.B. Pipes, Amer. Soc. Testing Materials Philadelphia, 1979, p 145.

2. Jonas, T.F., Siegmund, R.F., SAMPE, 5th Technology Conference, Montreux, Switz. 1985, Paper 5.

3. Cantwell, W.J. and Morton, J., Composite Structures 3 241 (1985).

4. Bishop, S.M., Composite Structures, 3 295 (1985).

5. Murri, W.J., Sermon, B.W., and Pearson, L.H., 15th Symposium on Nondestructive Evaluation, Proceedings, San Antonio, TX, April 1985.

6. Bar-Cohen, Y., and Crane, R.L., Mat. Eval., 40 970 (1982).

7. Bradley, W.L. and Cohen, R.N., ASTM Symp. on Delamination and Debonding of Materials, Pittsburg 1983.

8. Bascom, W.D., Boll, D.J., Fuller, B., and Phillips, P.J., J. Mat. Sci., in press.

9. Sinclair, J.M., and Chamis, C.C., Mechanical Behavior and Fracture Characteristics of Off-Ancis Fiber Composites I, Experimental Investigation, NASA Tech. Paper 1081, NASA Washington, D.C., December 1977.

10. Yoffe, E.H., Phil. Mag. 42 739 (1951).

11. Konish, H.J., Swedlow, J.L., and Cruse, T.A., J. Composite Mat. 6 114 (1972).

12. Bascom, W.D., Bitner, J.L., Moulton, R.J., and Siebert, A.R., Composites, January 1980, p 9.

13. Greszczuk, L.B., in ASTM STP 568, Foreign Object Impact Damage in Composites, L. B. Greszczuk, Ed., Amer. Soc. for Testing and Materials, Philadelphia, 1975, p 183.

14. Greszczuk, L.B., in Impact Dynamics, J. A. Zukas, T. Nicholas, H.F. Swift, L.B., Greszczuk, and D.R. Currin, Eds., Wiley, N.Y., 1982 Chap. 3, p 55.

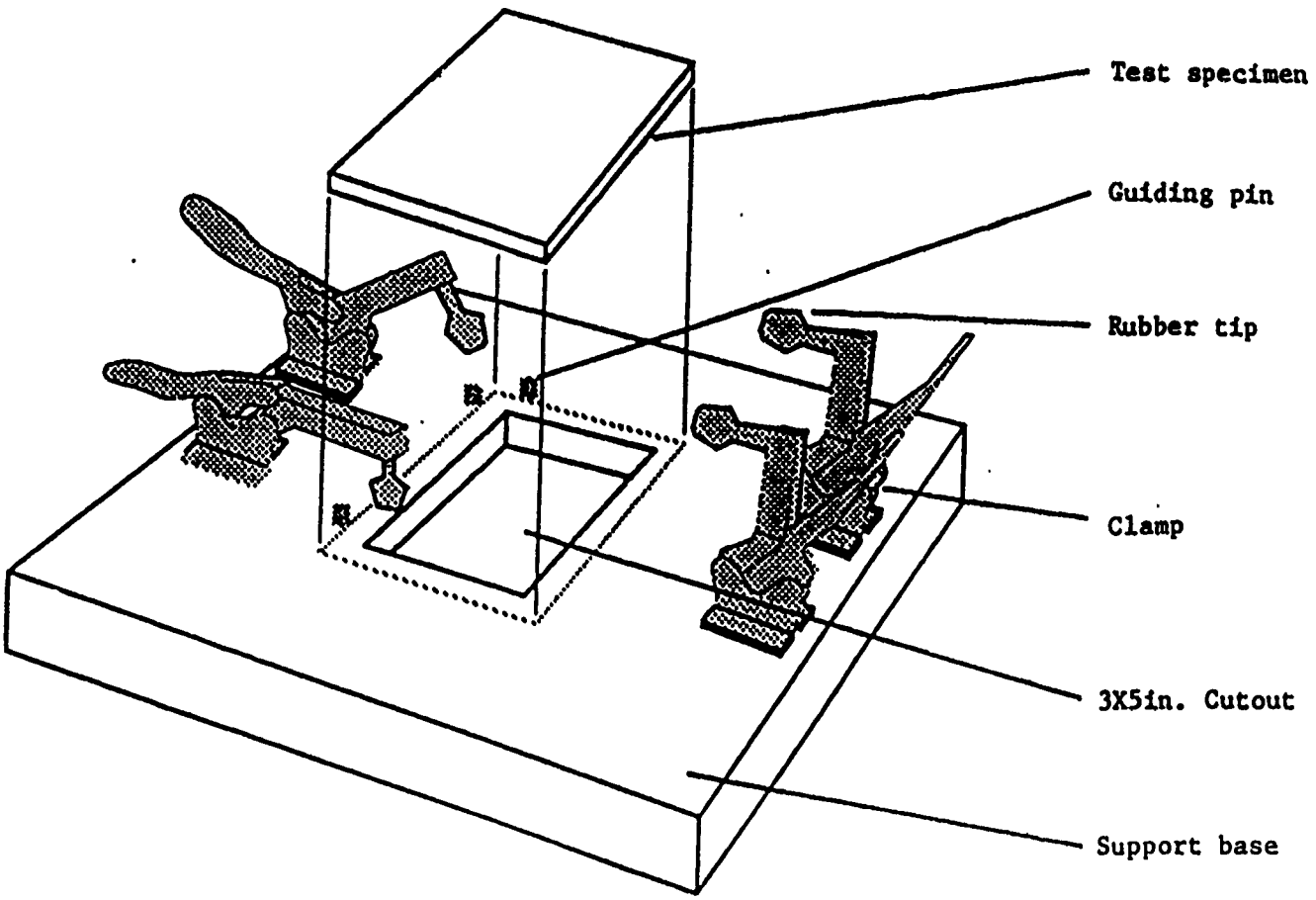

Figure 1: Impact test fixture

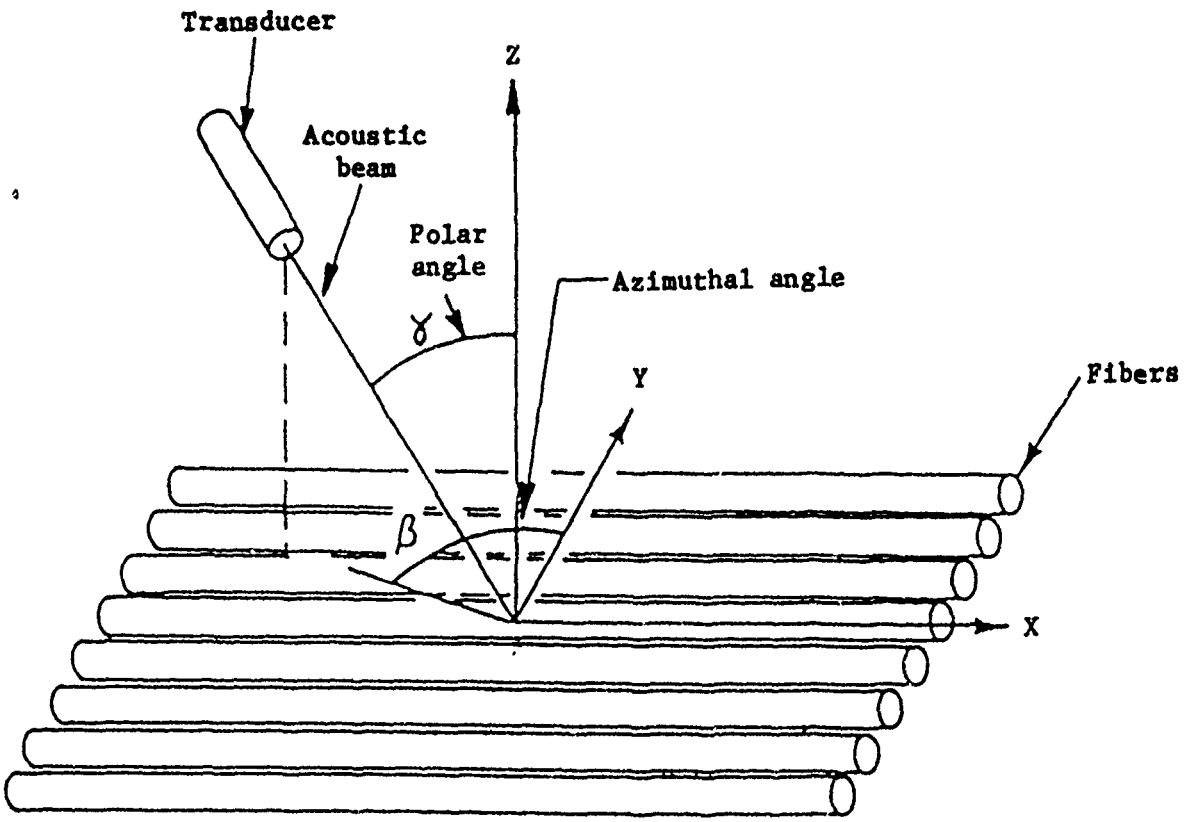

Fig 2: Diagram of experimental arrangement for acoustic backscattering from composite panels

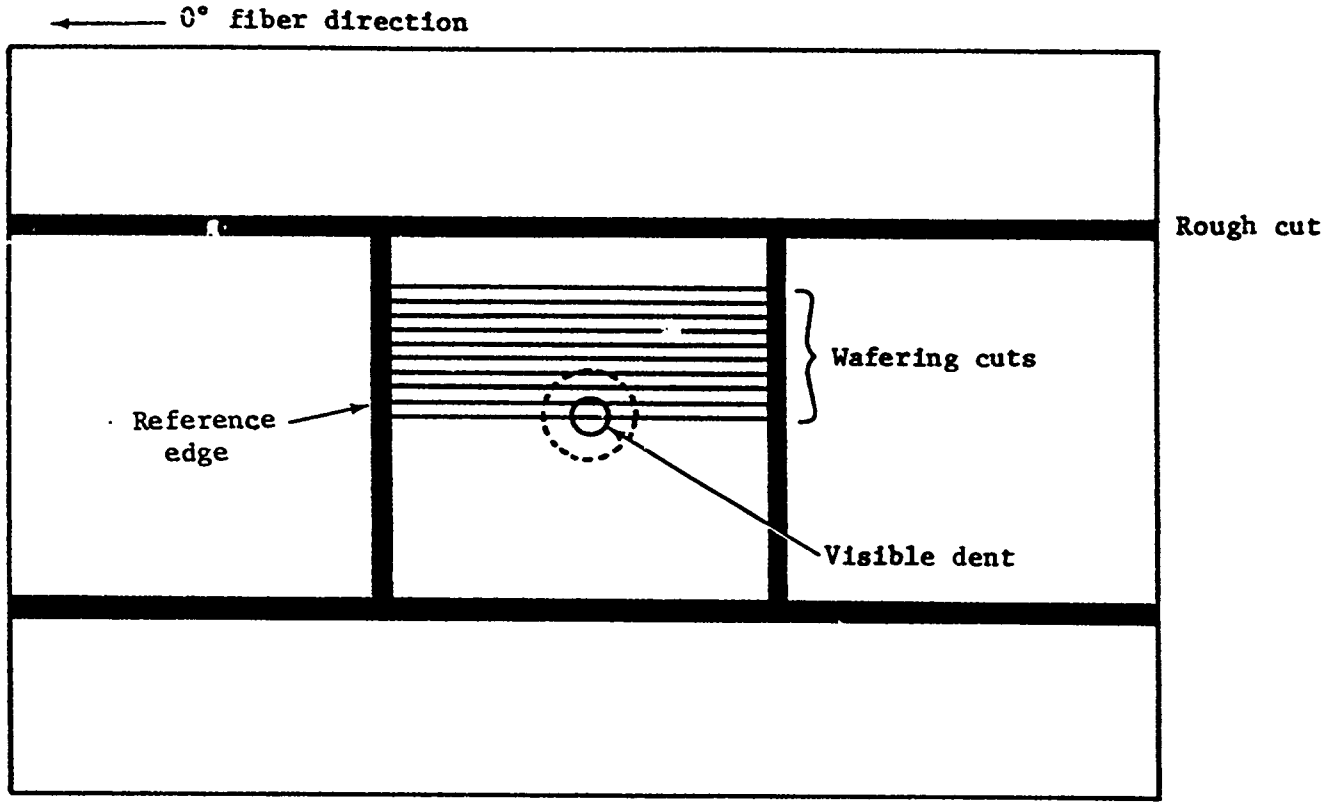

Figure 3: Sectioning digram (impact side)

(location of damage was measured from reference edge, Figures 5 and 12)

HERCULES

Impact damage 3501-6/IM7XG

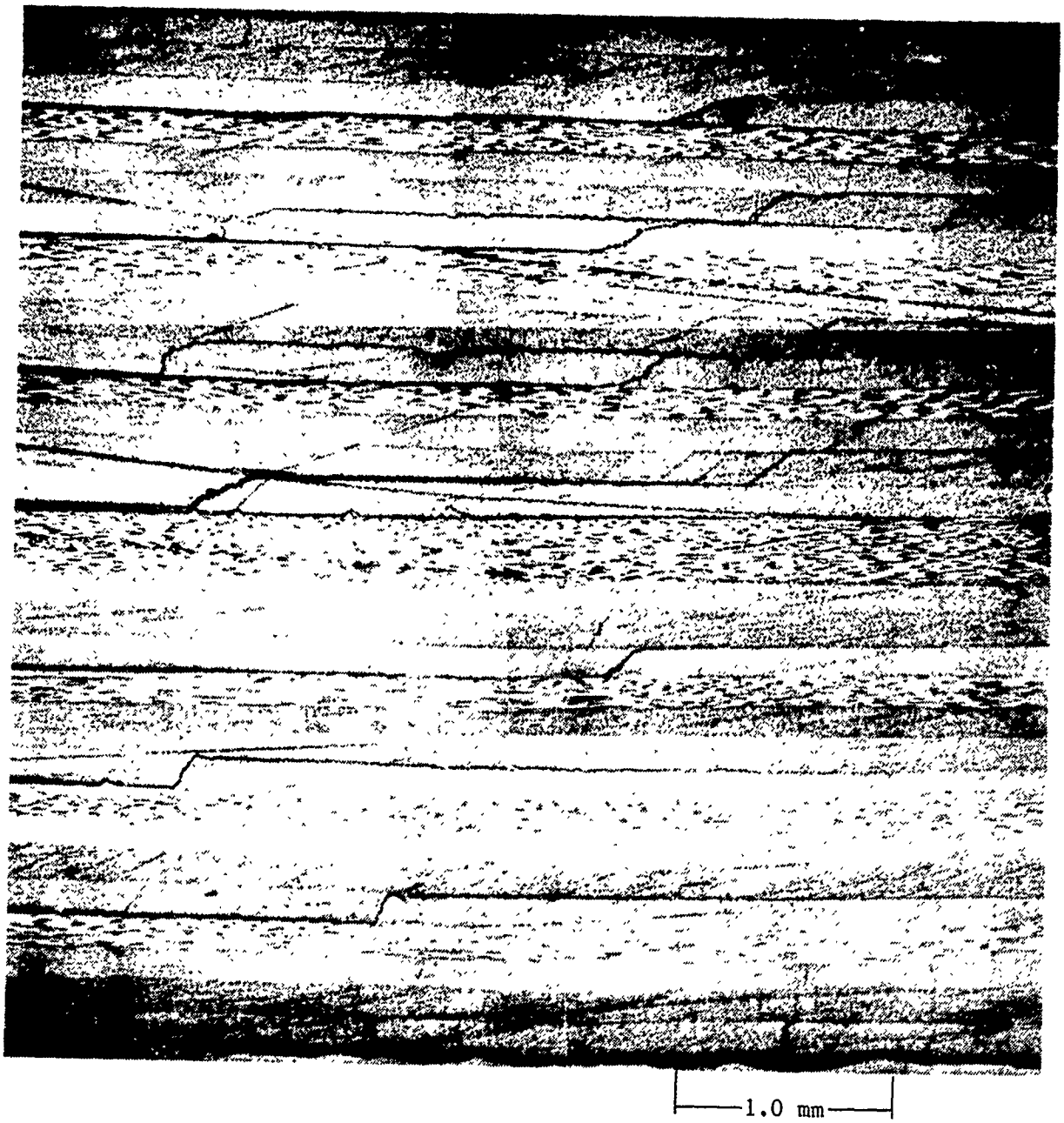

Figure 4

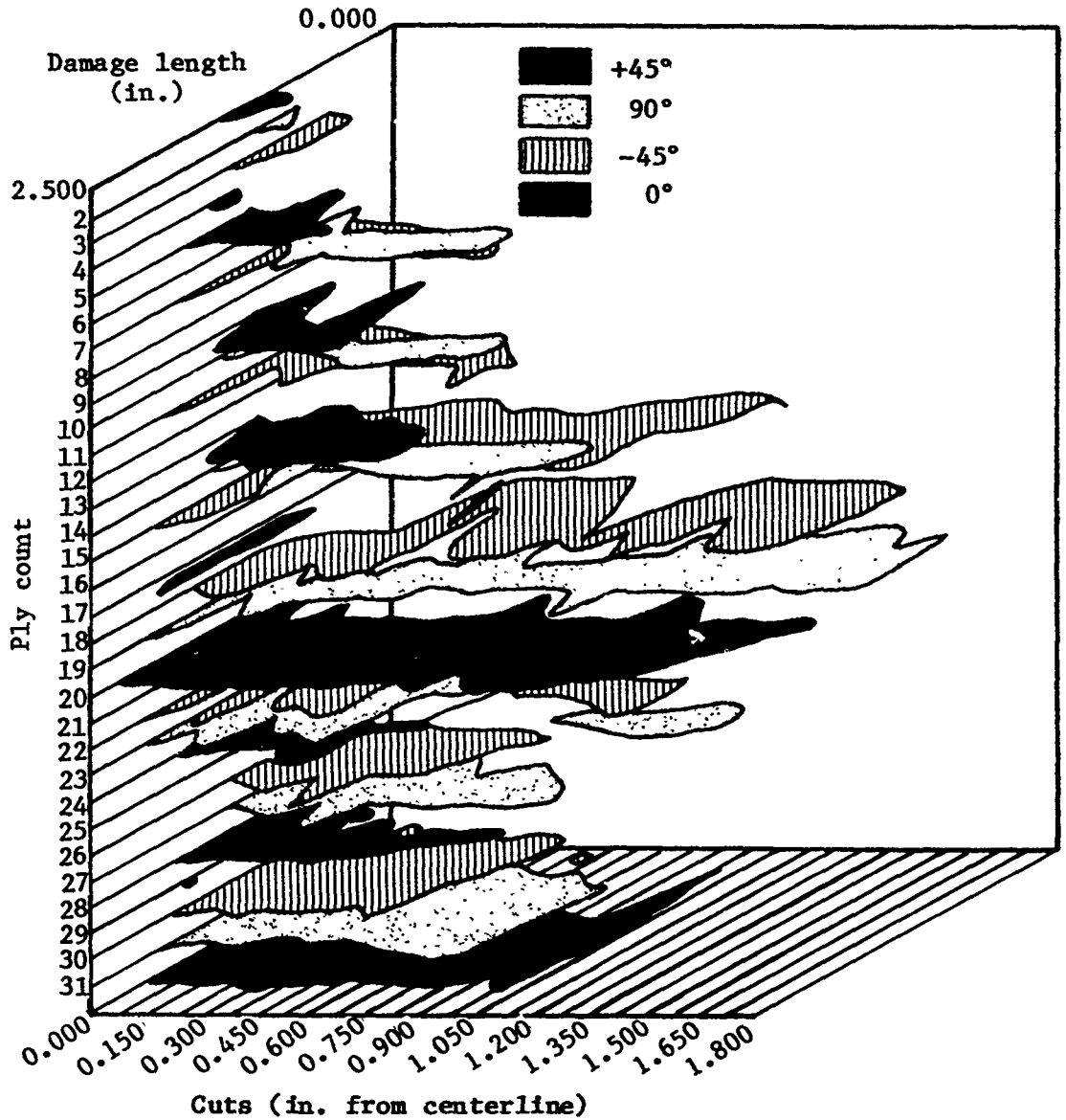

Damage area 3501-6-IM7XG (half section)

Figure 5

Multiple ply transverse cracking
3501-6/IM7XG

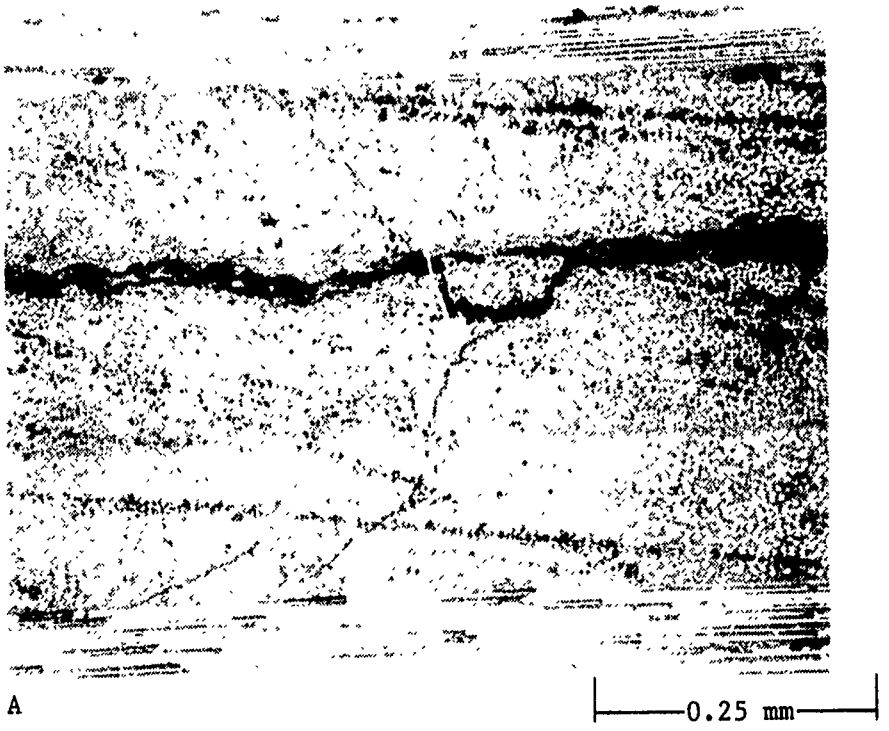

Figure 6

Propagation of a delamination at the fiber-resin boundry
3501-6/IM7XG

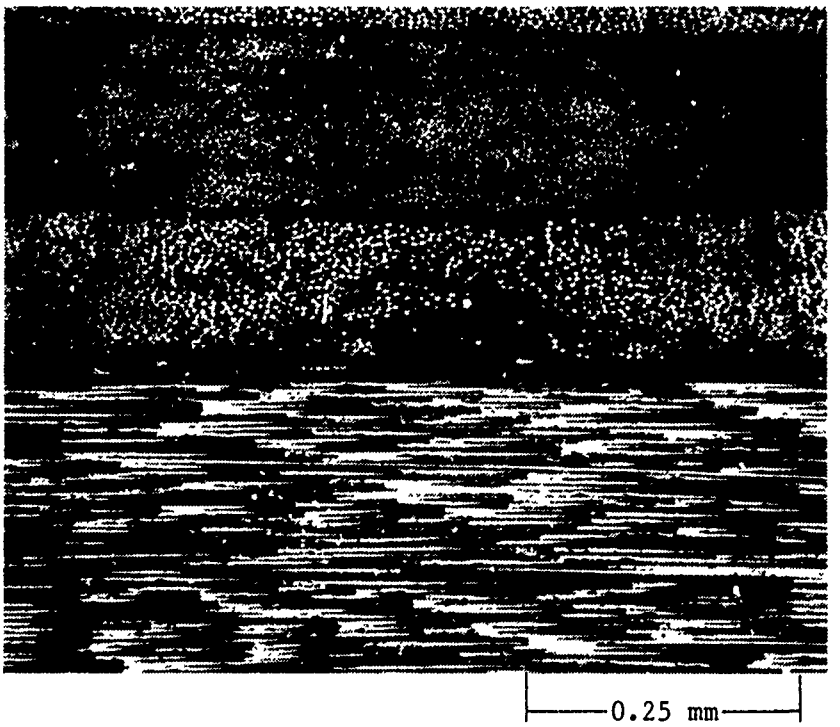

Figure 7

Resin tearing associated with delamination
3501-6/IM7XG

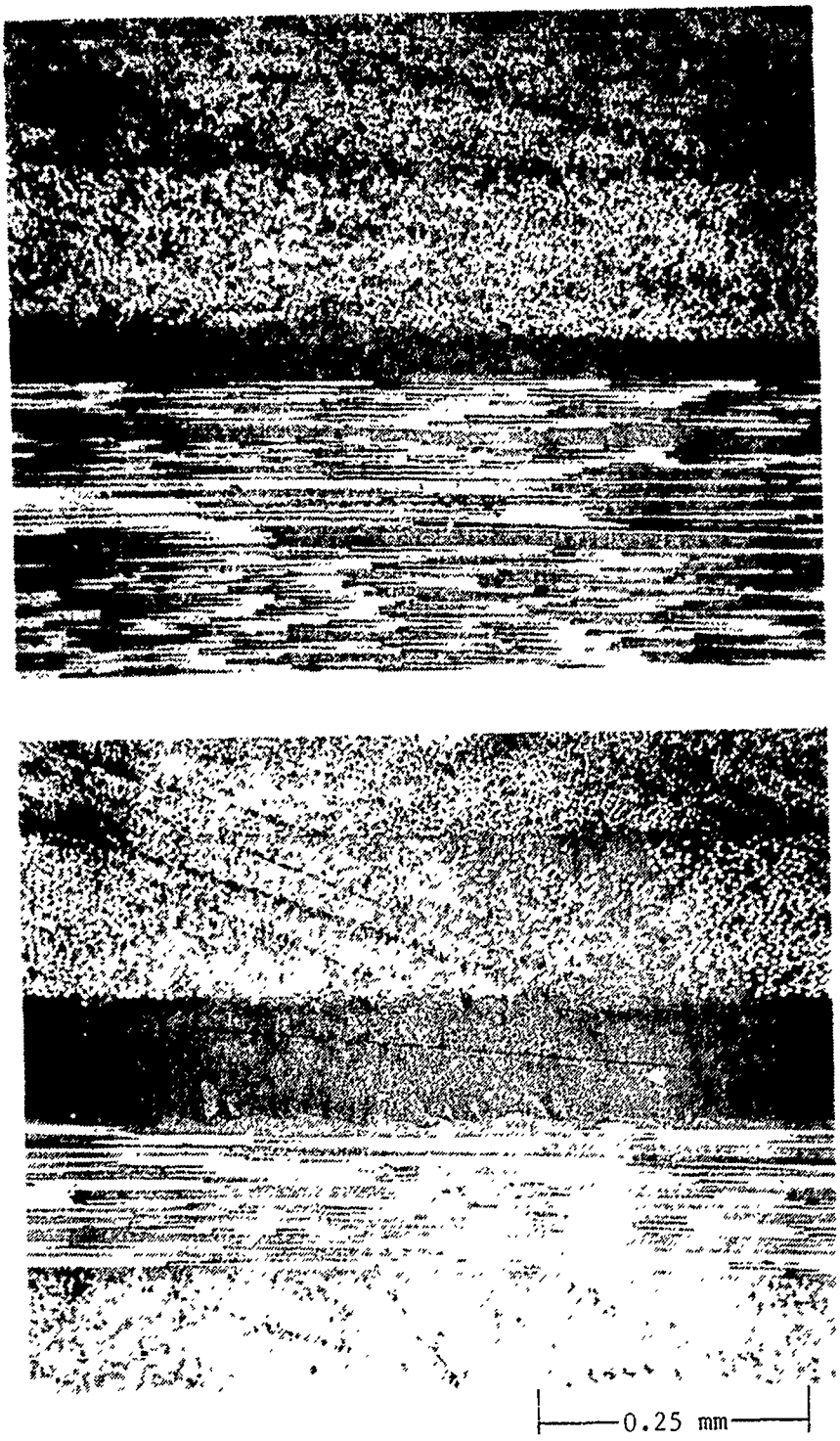

Figure 8

Left side damage 8551/IM7XG

Figure 9A

Right side damage 8551/IM7XG

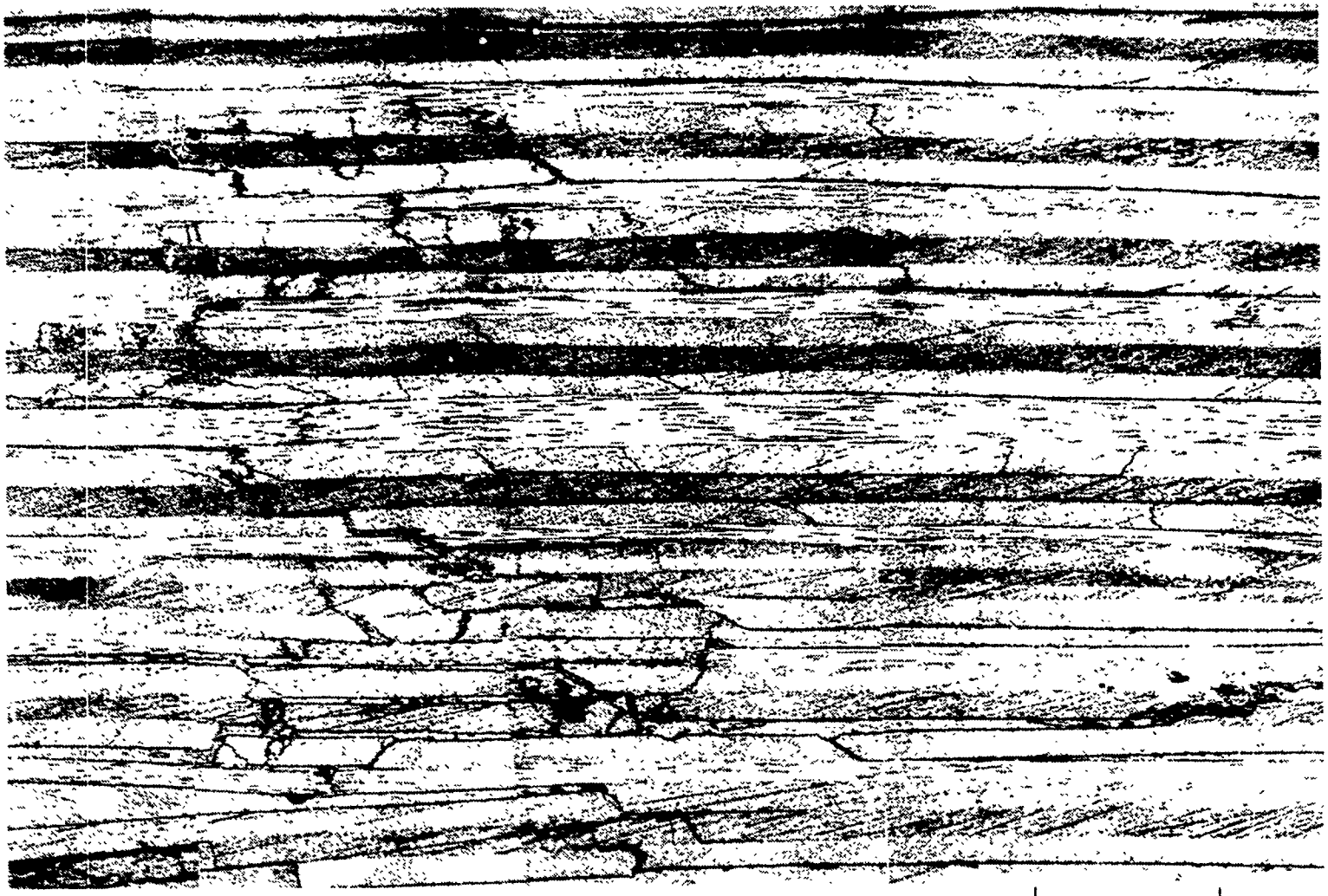

Figure 9B

Transverse cracking 8551/IM7XG

Figure 10

Transverse cracking in 0° plys
8551/IM7XG

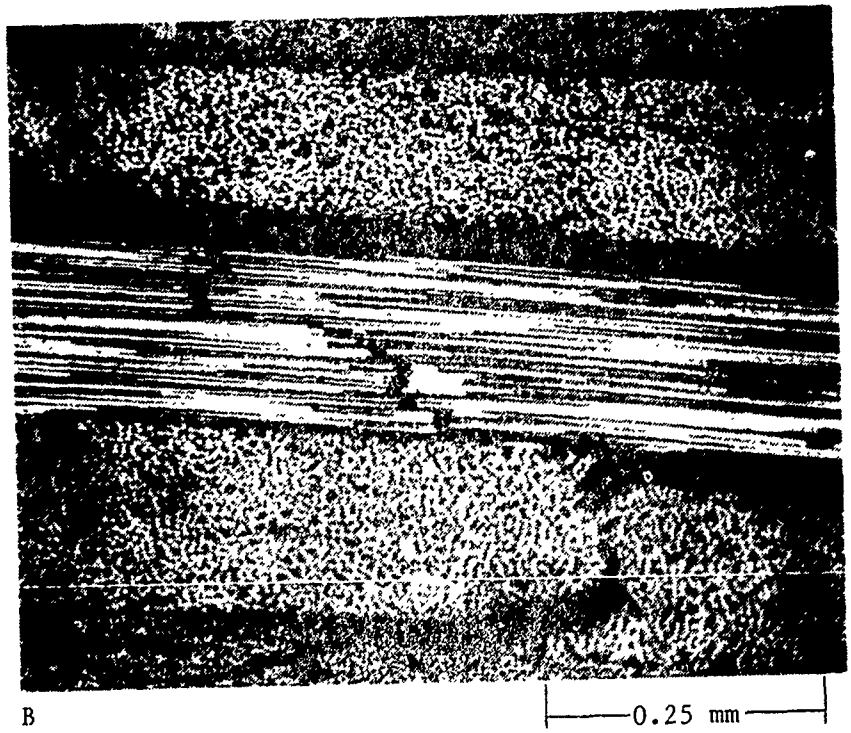

Figure 11

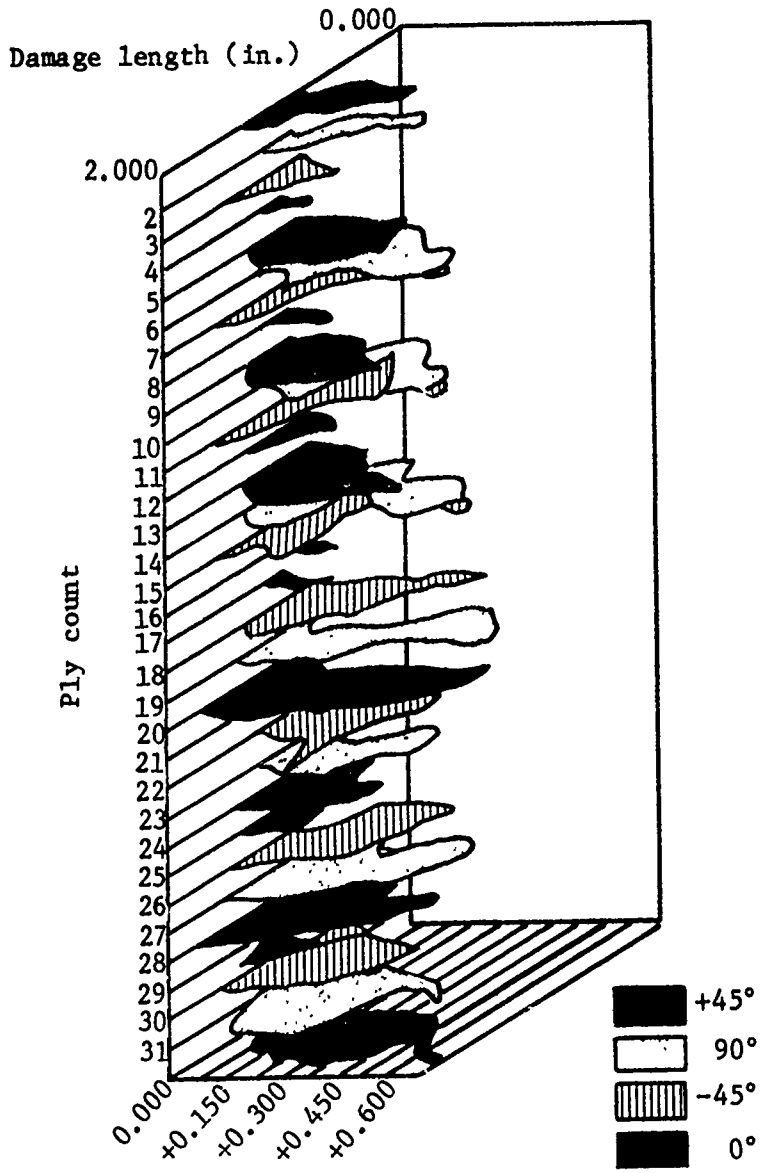

Damage area 8551/IM7XG

Figure 12

Impact damage area

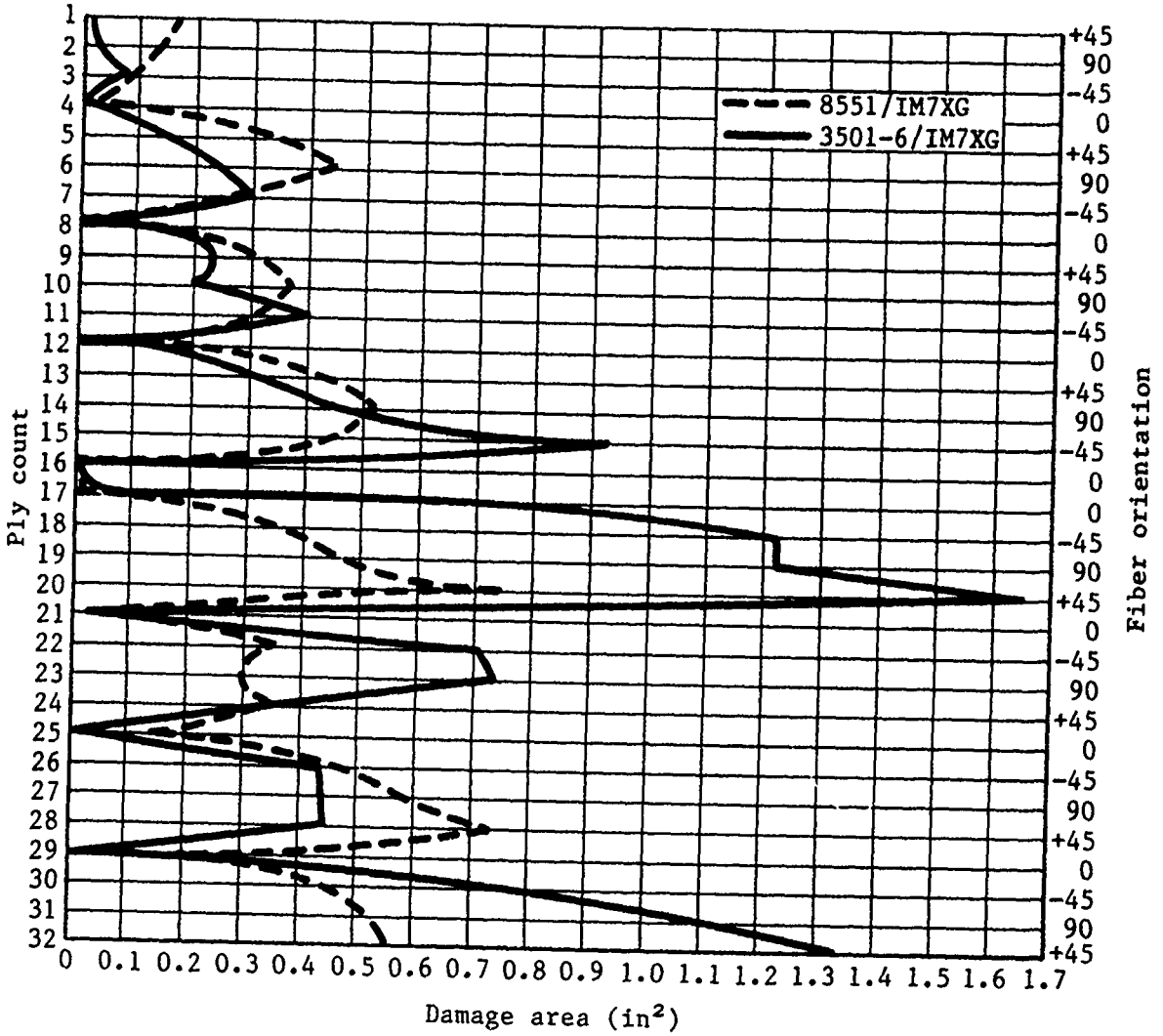

Figure 13

Influence of voids on impact damage
3501-6/IM7XG

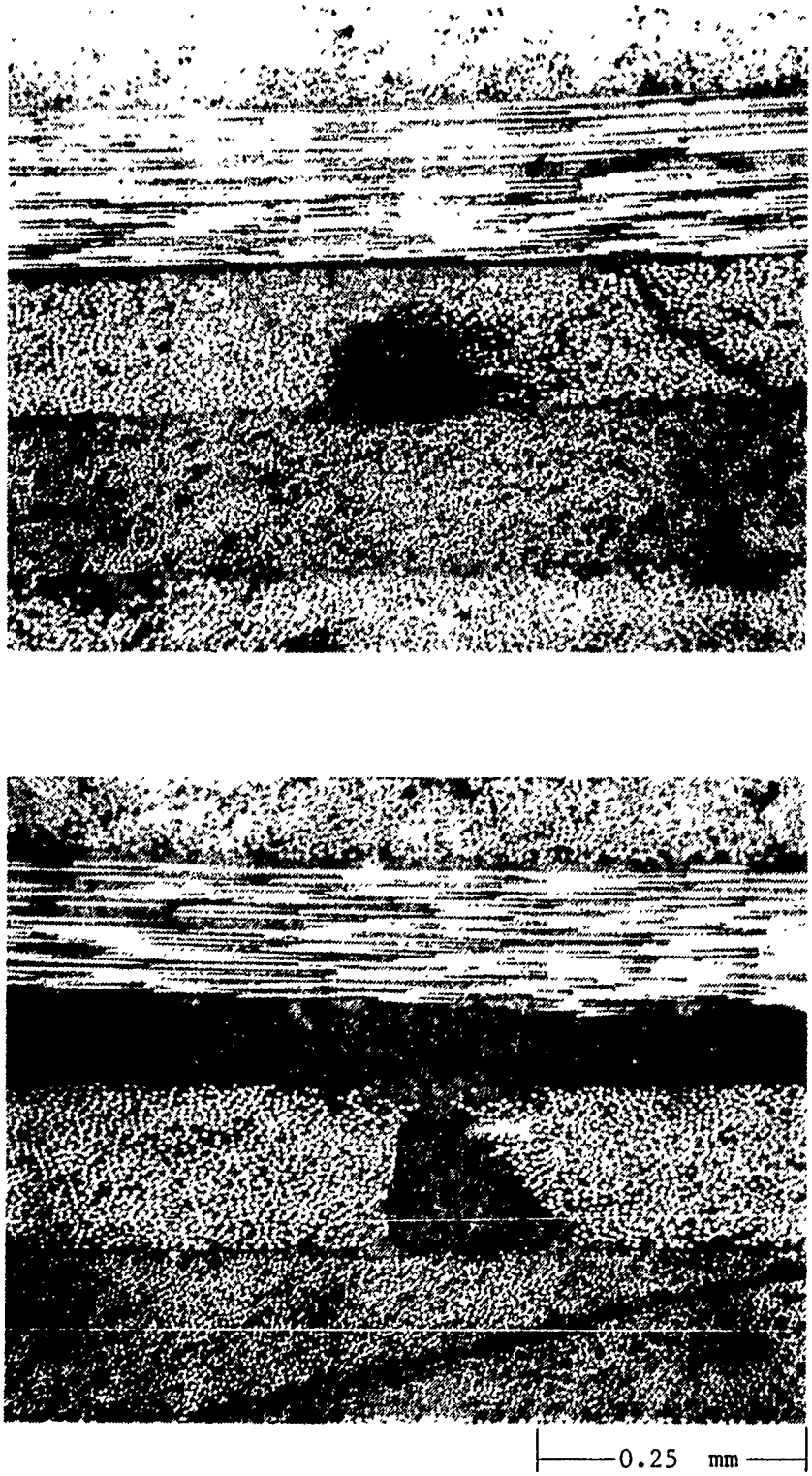

Figure 14

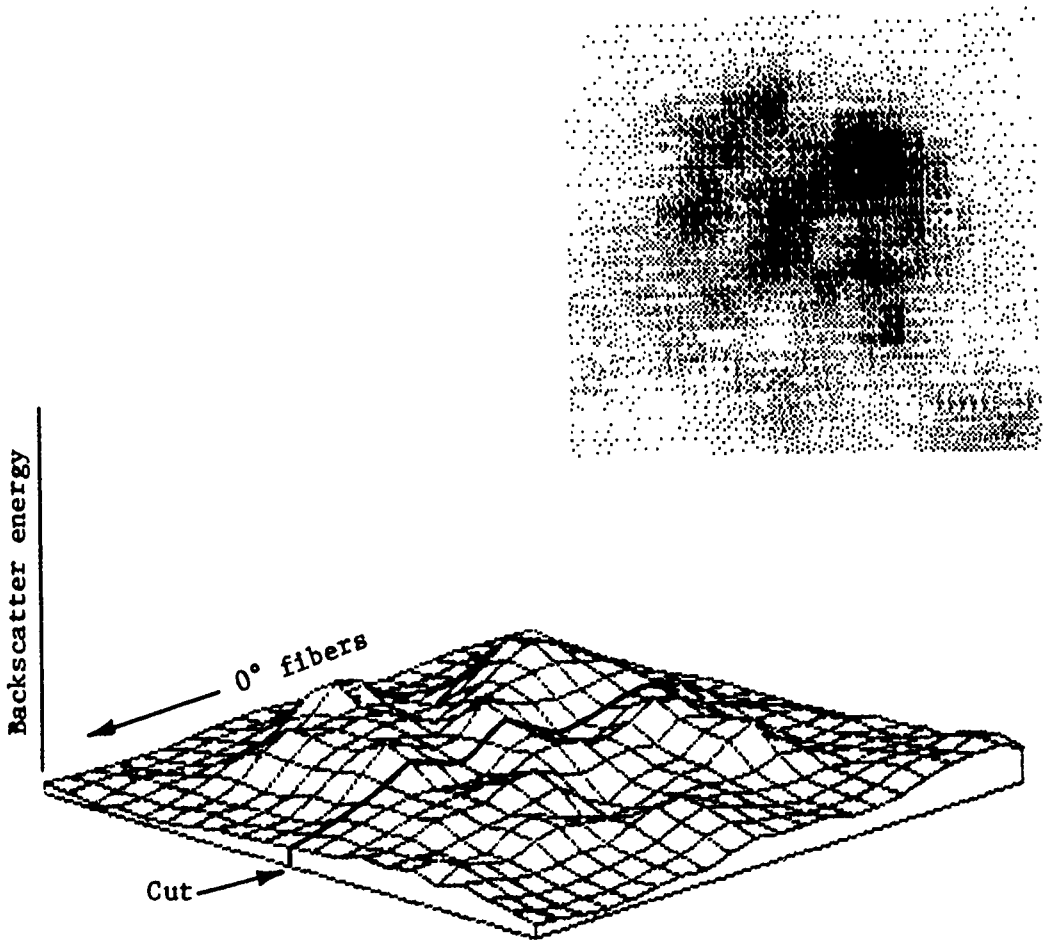

Acoustic backscatter C-scan
3501-6/IM7XG

Figure 15

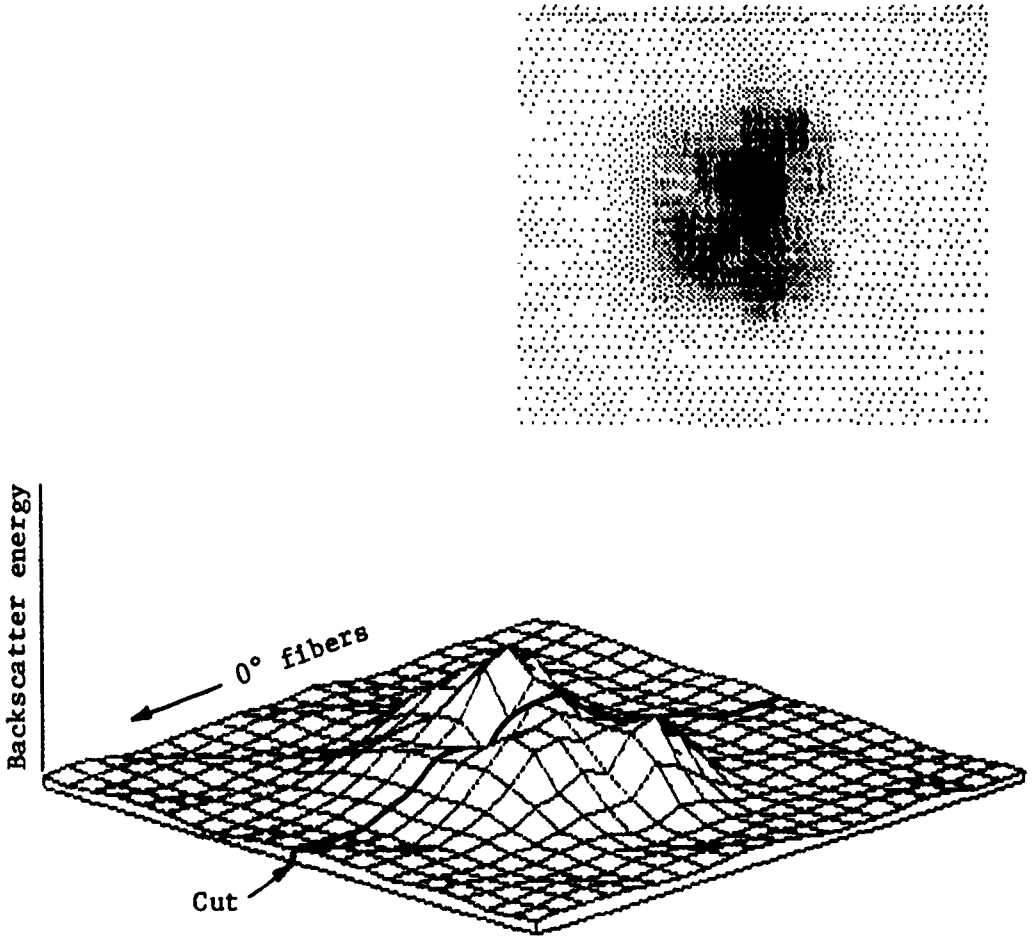

Acoustic backscatter C-scan
8551/IM7XG

Figure 16

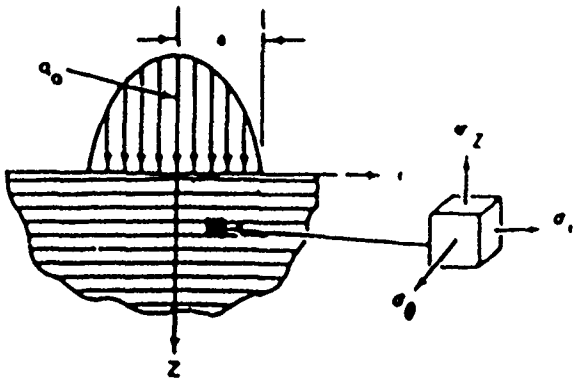

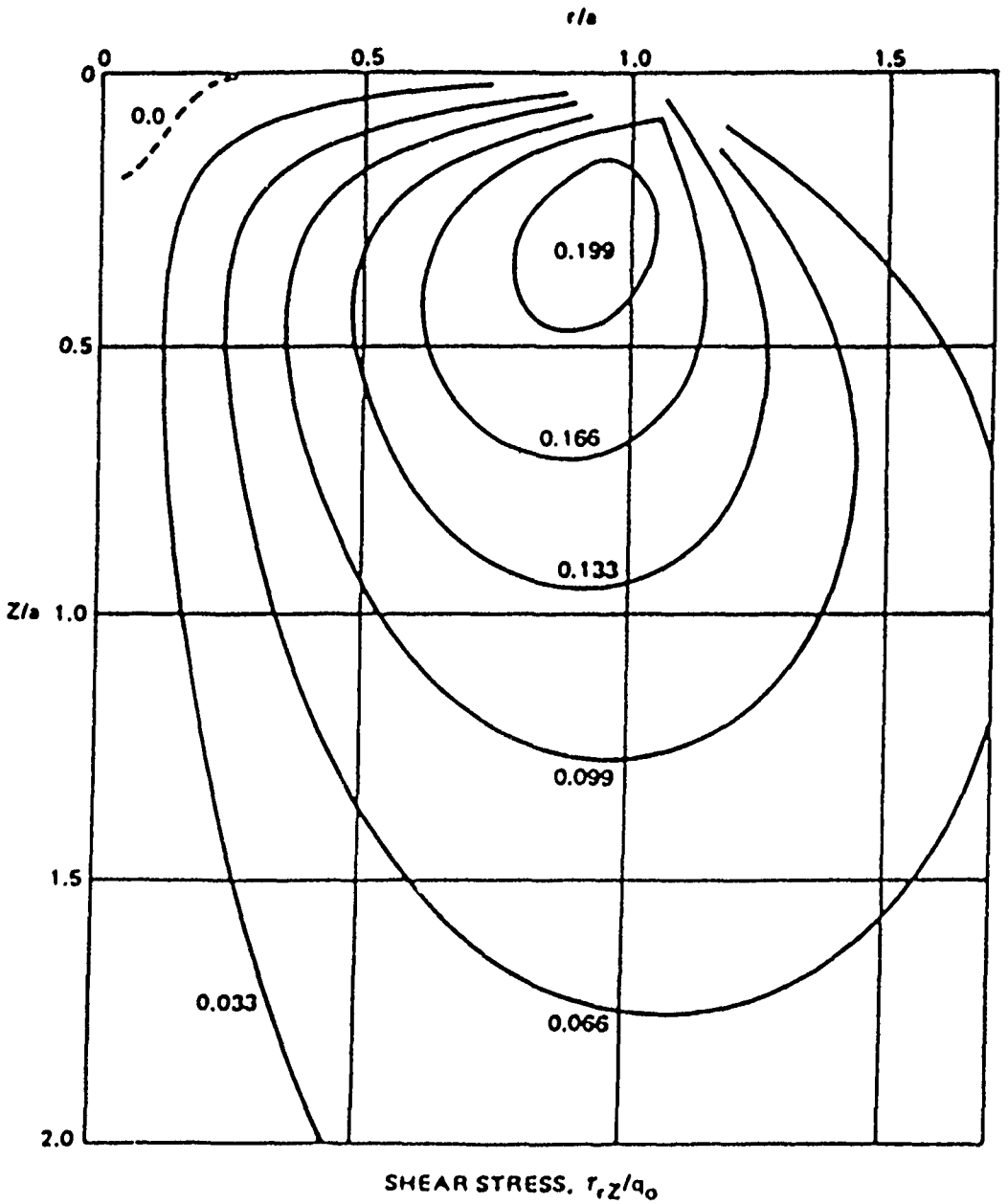

Figure 17: Stress coordinates and shear stress distribution at impact of a metal sphere on a pseudo-isotropic glass-epoxy laminate (Reference 17)

FRACTOGRAPHIC ANALYSIS OF INTERLAMINAR FRACTURES IN GRAPHITE-EPOXY MATERIAL STRUCTURES

B.W. Smith, R. Grove and T. Munns
Boeing Materials Technology
Boeing Commercial Airplane Company
Seattle, Washington

FRACTOGRAPHIC ANALYSIS OF INTERLAMINAR FRACTURES IN GRAPHITE-EPOXY MATERIAL STRUCTURES

Presented by Brian W. Smith, Ray A. Grove and Thomas E. Munns

1.0 Introduction

When material failure occurs, the fracture surfaces produced generally contain a physical record of the events and conditions leading to fracture. The science of understanding and interpreting this physical record, "fractography", has been a relatively well established science since about the mid-1950's. However, modern fractographic analyses have only recently been applied to composite material structures. In general, fractographic studies on other materials (metals and unreinforced polymers) have made significant impacts in a) understanding the microscopic mechanisms of cracking and b) identifying the causes of component failure. Of these two areas, the latter is perhaps the most significant. Through fracture examinations, the origin, direction of crack growth and load conditions involved in premature component fractures can generally be identified. In many cases, the definition of defects, damage conditions or anomalous fracture modes by such studies may be sufficient to identify the cause of fracture. In those cases where such causes are not apparent, understanding the sequence of events leading to fracture on a microscopic scale is often crucial to accurately direct stress or materials characterization analyses. With the recent influx of graphite/epoxy materials into aircraft use, there is a particular need to be able to examine and interpret the fracture features of composite materials. Through an understanding of these features, the cause(s) of premature fractures occurring either in-service, or during component test, can be identified to provide valuable feedback to designers and engineers.

In this investigation the microscopic characteristics of interlaminar fractures in graphite/epoxy laminates were examined. This work was conducted as part of an Air Force funded composites failure analysis program (ref. 1). Long-term efforts within this Air Force program are aimed at developing an overall post-failure analysis capability for composite materials. In the current investigation, the principal objectives were to develop a fractographic capability to identify 1) the direction of crack propagation and 2) the relative load state (shear or tension) involved in interlaminar fractures. These two objectives were selected with the post-mortem analysis of failed components specifically in mind. In general, experience with composite

materials has shown delaminations to be one of the more dominant fracture modes commonly observed. As with most material systems in which several failure modes exist, delaminations may in some instances comprise the principal failure mode. In other cases delaminations may represent secondary fractures formed due to the extremely low interlaminar toughness of most composite materials. In either case, the ability to identify the origin, direction and load states of such fractures is crucial to understanding their significance and in reconstructing the sequence of events leading to failure.

In this study, these objectives were addressed by generating interlaminar fractures under controlled load and crack propagation conditions. Two interlaminar load states were examined, pure mode 1 tension and pure mode 2 shear. In real structures, fractures are likely to occur by neither pure interlaminar shear or tension. However, these two load states provide a logical framework for understanding the characteristics of interlaminar fractures under model conditions. Because of the interest in this study in identifying the direction of crack growth, fracture toughness test geometries were utilized to provide controlled initiation and crack growth conditions. The use of such toughness coupons loaded under singular load states represents a relatively standard approach commonly utilized in metals fractography. However, in composite materials, the cross-ply interface and the orientation of fibers with respect to the direction of crack propagation must also be considered. In this study, fractures were produced between 0/0, 0/90, and +45/-45 degree ply interfaces such that the effects of differing interfacial fiber orientations could be investigated.

2.0 Materials and Test Procedures

A wide variety of resin systems and fiber combinations exist for use in current graphite/epoxy composite applications. However, due to the high performance demands of aircraft structures, the number of materials commonly used is limited to those systems which exhibit good environmental behavior and ultimate strengths. These matrix systems are typically 350 F curing tetraglycidyl diaminodiphenyl methane (TGDDM)-diaminodiphenyl sulphone (DDS) epoxies with BF3 amine catalysts. For the following investigation Hercules 3501-6 with AS-4 fibers was selected for examination as a material representative of such systems. A resin content of 35% by weight on 145 grams/sq. meter unidirectional tape was selected for examination because of its extensive use in commercial and military aircraft structures.

In this study, delaminations were produced in which both the direction of cracking and load state at fracture were well controlled. As discussed previously, fractures were produced under pure mode 1 tension and pure mode 2 shear. Mode 1 tension fractures were generated utilizing a double cantilever beam geometry. Whereas, mode 2 shear fractures were produced using an end notch flexure geometry. Both of these specimen geometries have seen extensive use by several investigators (ref. 2-7) in the measurement of the interlaminar toughness of composite materials. Figure 1 illustrates the double

cantilever beam geometry. In this specimen, two beam halves are formed at one end by an implanted FEP insert. Interlaminar tension conditions are produced by deflecting these two beam halves in opposite directions. The end notch flexural specimen geometry used to generate mode 2 shear fractures is illustrated in Figure 2. Similar to the DCB specimen, two beam halves are formed at one end by an implanted FEP insert. In this case, conditions of interlaminar shear are imposed at the specimen midplane by cantilever deflection of both beam halves in the same direction. Fracture along the desired ply interfaces (0/0, 0/90 and +45/-45) was produced by fabricating (0)24, (0/90)12s and (+45/-45)12s laminates. In each case the FEP insert was located at the approximate specimen mid-plane between the cross-plies of interest. Each laminate was cured in accordance with standard Boeing procedures at 350F and 85 psi.

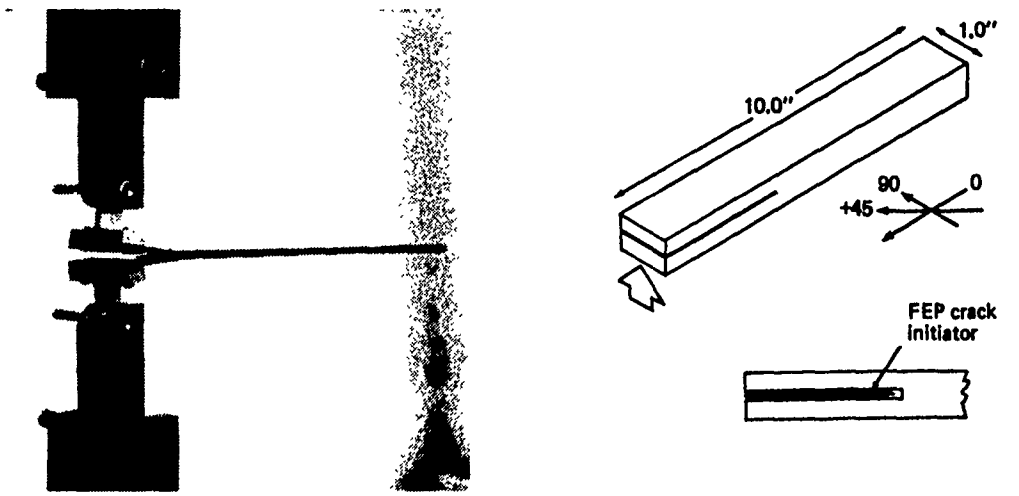

Figure 1. Double Cantilever Beam (DCB) Specimen Geometry and Test Configuration Used to Generate Mode 1 Delaminations

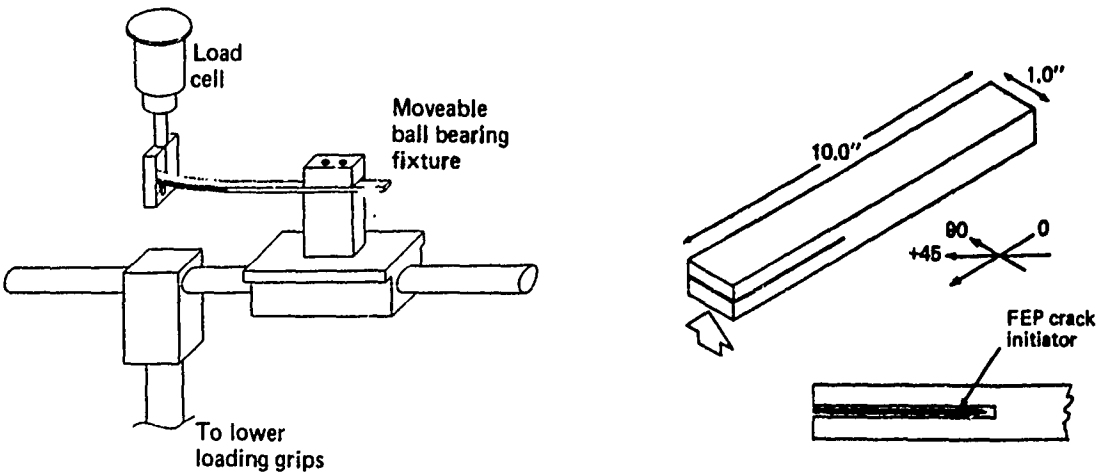

Figure 2. End Notch Flexure (ENF) Geometry and Test Configuration Utilized to Generate Mode 2 Delaminations

Testing was performed on a MTS servo-hydraulic load frame under deflection controlled loading. For both the mode 1 and mode 2 specimen geometries, increasing cross-head speeds were required to provide a relatively uniform rate of crack propagation. Mode 1 crack growth generally occurred in small stable increments, while mode 2 crack growth exhibited a mixture of both rapid and slower, more stable growth. During all of the subject tests, macroscopic crack growth was visually observed to proceed from the implanted FEP initiator toward the opposite specimen end along the 0 degree direction. Following test, fracture surfaces from five specimens of each type (mode 1 and mode 2) were examined using optical microscopy to verify that fracture had occurred between the intended ply interfaces. Based on these preliminary optical examinations, representative areas were selected for detailed scanning electron microscopy (SEM). In order to prevent charging, these areas were sputter coated with approximately 200 angstroms of gold-palladium prior to SEM examination.

3.0 Results

The following sections describe the fracture surface features characteristic of delaminations generated under mode 1 tensile and mode 2 shear loading conditions. The first section presented considers those fractures generated under mode 1 tension, while the second section presents mode 2 shear fracture features. In both sections the results are sequentially organized based on the three different ply orientations (0/0, 0/90 and +45/-45 degrees) between which fractures were generated.

3.1 Mode 1 Tension Fractures

Typically, interlaminar fractures in fiber reinforced composite materials involve a combination of fiber/matrix separation and cohesive fracture of the surrounding matrix material. The extent to which either of these two features occur depends upon both the volume percent of reinforcing fibers and proximity of the fracture plane to these fibers. In this study, delaminations produced under interlaminar tension typically exhibited a mixture of both fiber/matrix separation and cohesive resin fracture. In general, areas of fiber/matrix separation were found to be relatively smooth and featureless. For the most part, conditions of cohesive resin fracture dominated the overall fracture surface topography. As discussed below, such areas of fracture typically appeared flat and exhibited pronounced river markings and resin microflow features. The combination of these later features generally appeared unique to interlaminar tension and was found to provide a means for identifying the direction of fracture.

0 Degree/0 Degree Interface Fracture Surface

The fracture surface characteristic of delaminations produced under tension between adjacent 0 degree plies are illustrated in Figures 3 and 4. As visible in Figure 3, one of the most distinctive features of this fracture is its relatively smooth, flat, planar topography. As illustrated at 400X, the overall fracture surface is microstructurally composed of areas of cohesive resin fracture, fiber/matrix separation,

and partially buried fibers. Of these three, regions of cohesive resin fracture constitute the predominant feature in terms of exposed area. These areas are roughly divided into longitudinal segments by locations of fiber/matrix separation and partially buried fibers. As illustrated at higher magnification, partially buried fibers occur when the fracture plane intersects underlying fibers at a shallow angle. In such cases, a general progression from cohesive matrix fracture to interfacial fiber/matrix separation occurs. In this transition region residual resin can generally be seen adhering to the fiber surface. However, as illustrated in Figure 4, once the fiber intersects the surface the cleanly replicated impression of the AS-4 fiber becomes apparent. This condition indicates that fiber separation under interlaminar tension occurs adhesively, except where the fiber just intersects the fracture surface. Because of this adhesive characteristic, areas of fiber/matrix separation were generally found to be devoid of any specific morphological features related to the direction of crack propagation.

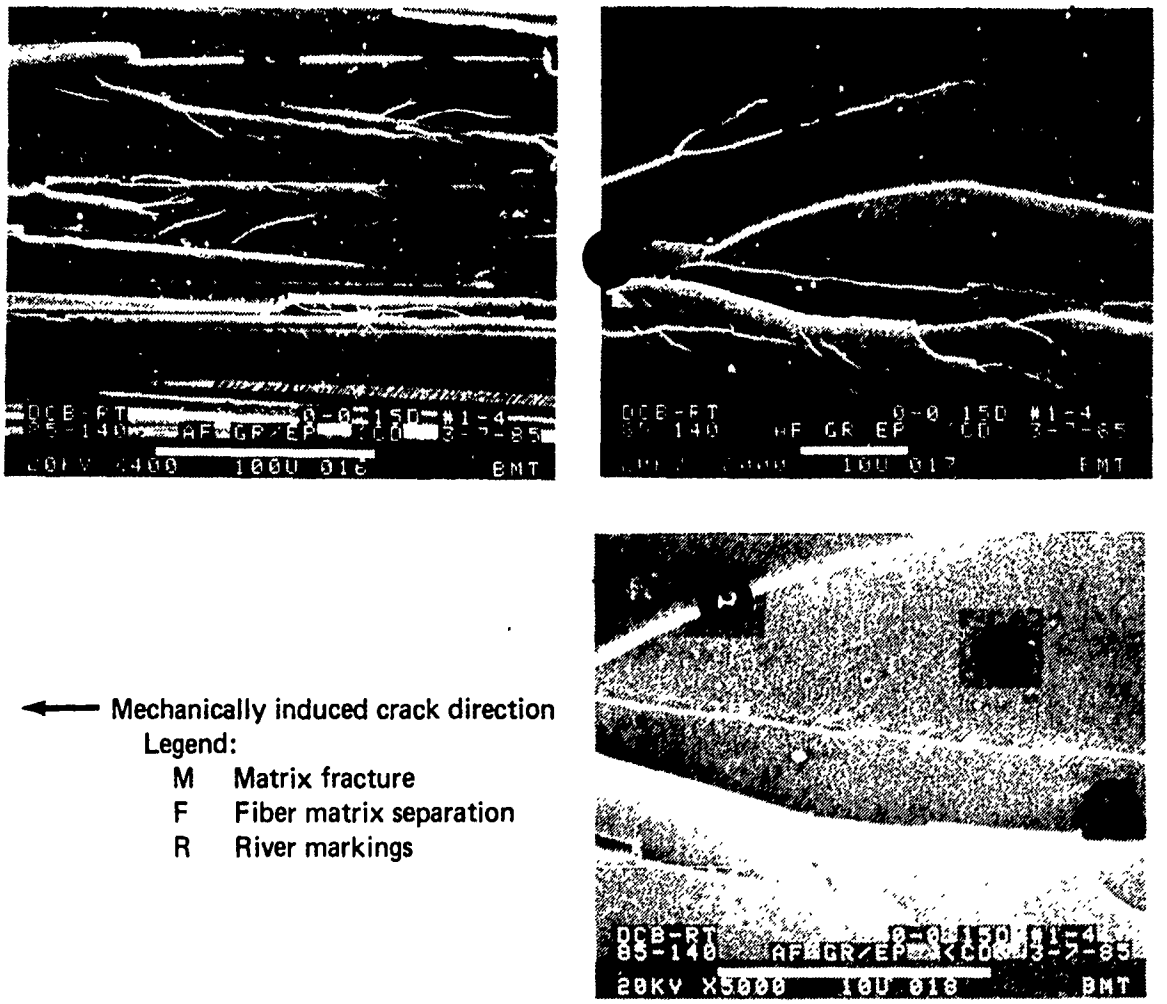

Figure 3. SEM Fractographs of Mode 1 Delamination Between Adjacent 0 Degree Plies.

As discussed above, areas of flat resin fracture represent one of the more dominant features of mode 1 tension delaminations. Detailed inspection of these cohesive matrix fracture regions reveals several distinctive morphological features. The most easily distinguishable of these features are a series of longitudinal branching lines which form a riverlike pattern, Figure 3 (400X and 2000X). These river markings are analagous to the cleavage fracture features commonly recognized in brittle metals, ceramics and polymeric materials (ref. 8). In these materials, such features have been determined to occur as a result of the progressive joining of adjacent microscopic fracture planes during crack growth. More specifically, each line segment represents a local step formed when the thin ligament separating these displaced planes is fractured during crack growth. As presented by Griffith (ref. 9), the amount of strain energy involved in fracture is proportional to the area of created fracture surface and amount of material plastic deformation. As a result, a large number of locally displaced fracture planes represents a higher energy condition than a single continuous fracture surface. Consequently, there is a large driving force for the number of planes involved in fracture to decrease during fracture. In metals and other material systems, the joining up of these planes is generally recognized to produce coalescence of each of the ligaments resulting in a riverlike pattern. As a result, the direction of coalescence of these ligaments indicates the local direction of crack growth. This argument appears to be valid for the river markings visible in Figure 3, since the general direction of macroscopic cracking agrees well with the average direction of river mark coalescence.

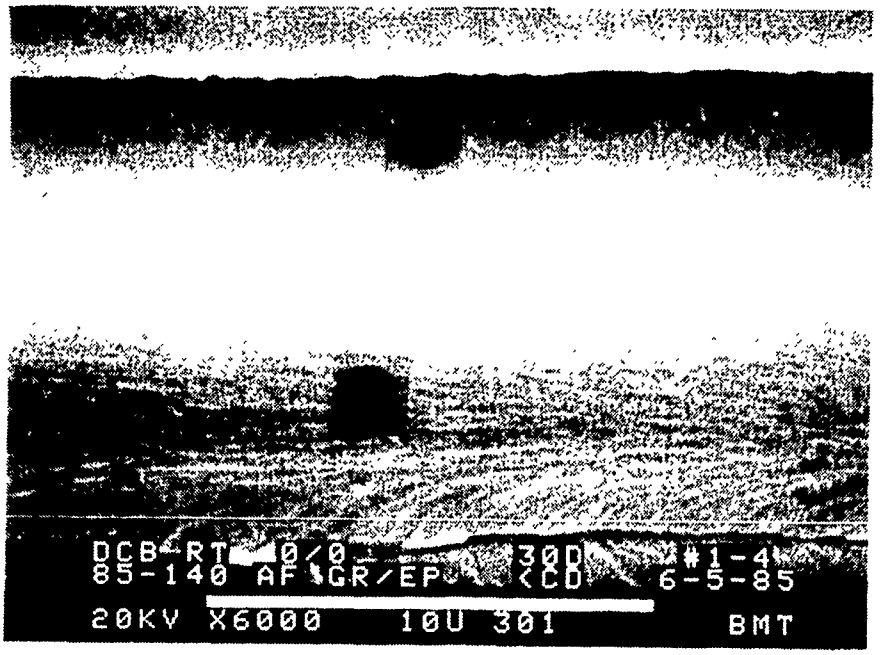

Figure 4. Micrograph Illustrating Adhesive Areas of (F) Fiber/Matrix Separation and (T) Textured Microflow

The second distinctive feature visible in areas of cohesive matrix fracture are microflow lines. These microflow lines are visible at high magnifications as a fine grained structure or texture on the fractured resin surface, Figure 4. Detailed inspection of the overall flow of this grained structure reveals a herringbone shaped pattern oriented in the direction of induced crack propagation. This pattern is similar in appearance to chevron patterns commonly encountered in the fracture of metallic structures. The appearance of chevrons in metals is associated with microscopic deformation in the direction of local crack propagation. The herringbone pattern arises from the inherent tendency of a propagating crack to take the shortest path to a free surface. As such, chevrons tend to rotate from the direction of overall crack growth towards adjacent cracks of free surfaces. Based on this interpretation, the localized direction of crack propagation can be determined by examining the direction and orientation of herringbone shaped patterns. As illustrated in Figure 4, the induced crack propagation direction coincides with the direction of expanding and radiating microflow texture.

Cross-Ply Interfaces (0/90 and +45/-45) Fracture Surfaces

The fracture topography typical of delaminations produced between cross-plied orientations under tension are illustrated in Figures 5 and 6. For both cross-ply orientations examined (0/90 and +45/-45), matrix fracture and regions of fiber/matrix separation remained the dominant fracture features. In general, cross-ply orientations produced significant differences in the extent of fiber/matrix separation and size and shape of these fractured matrix areas. As illustrated in Figure 5, fracture between 0 and 90 degree ply orientations produced considerably more exposed resin fracture than in the adjacent 0 degree ply case discussed above. Once again, the overall flatness of these areas appears to be characteristic of mode 1 tension. In general, examination of exposed fiber areas reveals both partially buried fibers as well as regions of adhesive fiber/matrix separation. As before, the degree of adhesive separation appears to depend upon the amount of fiber exposure, with more exposure favoring adhesive separation.

As illustrated at 400X, locations of 0 and 90 degree fiber/matrix separation tend to divide the overall fracture surface into roughly rectangular areas of matrix fracture. Examination of these areas reveals both distinct river markings as well as subtle conditions of resin microflow. In this fracture it is particularly interesting to note that river mark branching appears to be associated with areas of partially buried or exposed fibers. This suggests that local disruption of the plane of fracture result in crack plane divergence and initiation of multiple crack microplanes. As visible at high magnification, the direction of coalescence of these microplanes and the general texture of microflow coincides with the direction of crack propagation. These findings indicate that these features can be used to fractographically identify the direction of crack propagation.

Fractures produced between +45 and -45 degree ply orientations generally exhibited a rougher overall topography with larger amounts of fiber/matrix separation than either of the two fracture conditions

discussed above. As illustrated in Figure 6, the fracture surface is composed of longitudinally oriented rows of fan shaped matrix fracture bounded by areas of 45 degree fiber/matrix separation. In general, these fan shaped areas appear to be oriented with a slight tilt to the overall fracture surface. Further detailed examination of these areas reveals river markings associated with areas of fiber/matrix separation as well as subtle conditions of resin microflow. As illustrated, the direction of river mark coalescence and microflow progression often deviates from the direction of induced crack propagation. This condition can be attributed to local rotation of the direction of crack propagation towards adjacent microscopic fracture zones. These local variations average together so that the overall direction of river mark branching and resin microflow correspond well with the direction of induced fracture. This finding indicates that the overall behavior of the fracture surface must be considered when utilizing microsopic features to identify the direction of crack propagation.

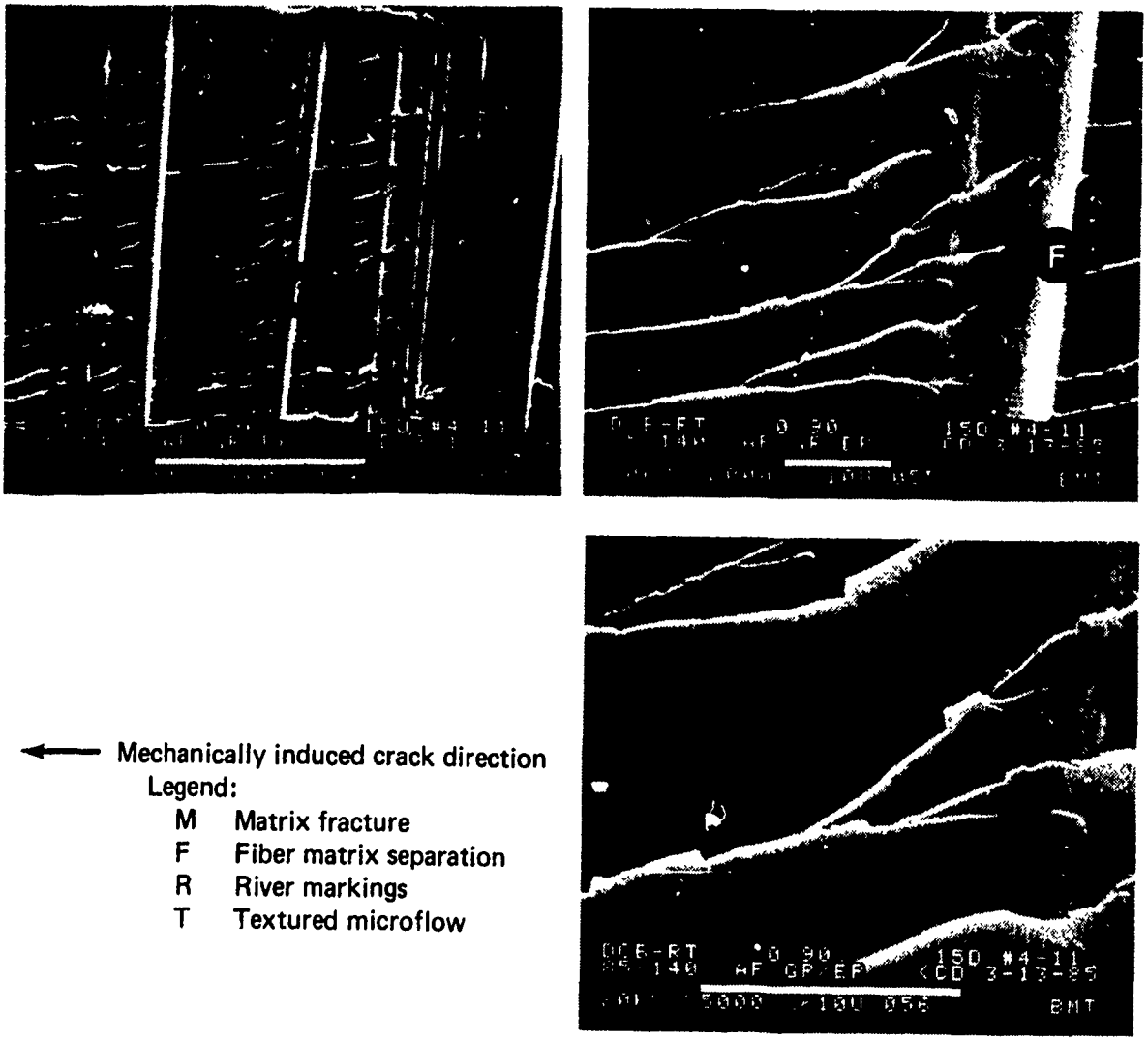

Figure 5. Fracture Topography Typical of Mode 1 Delamination Between 0 and 90 Degree Plies.

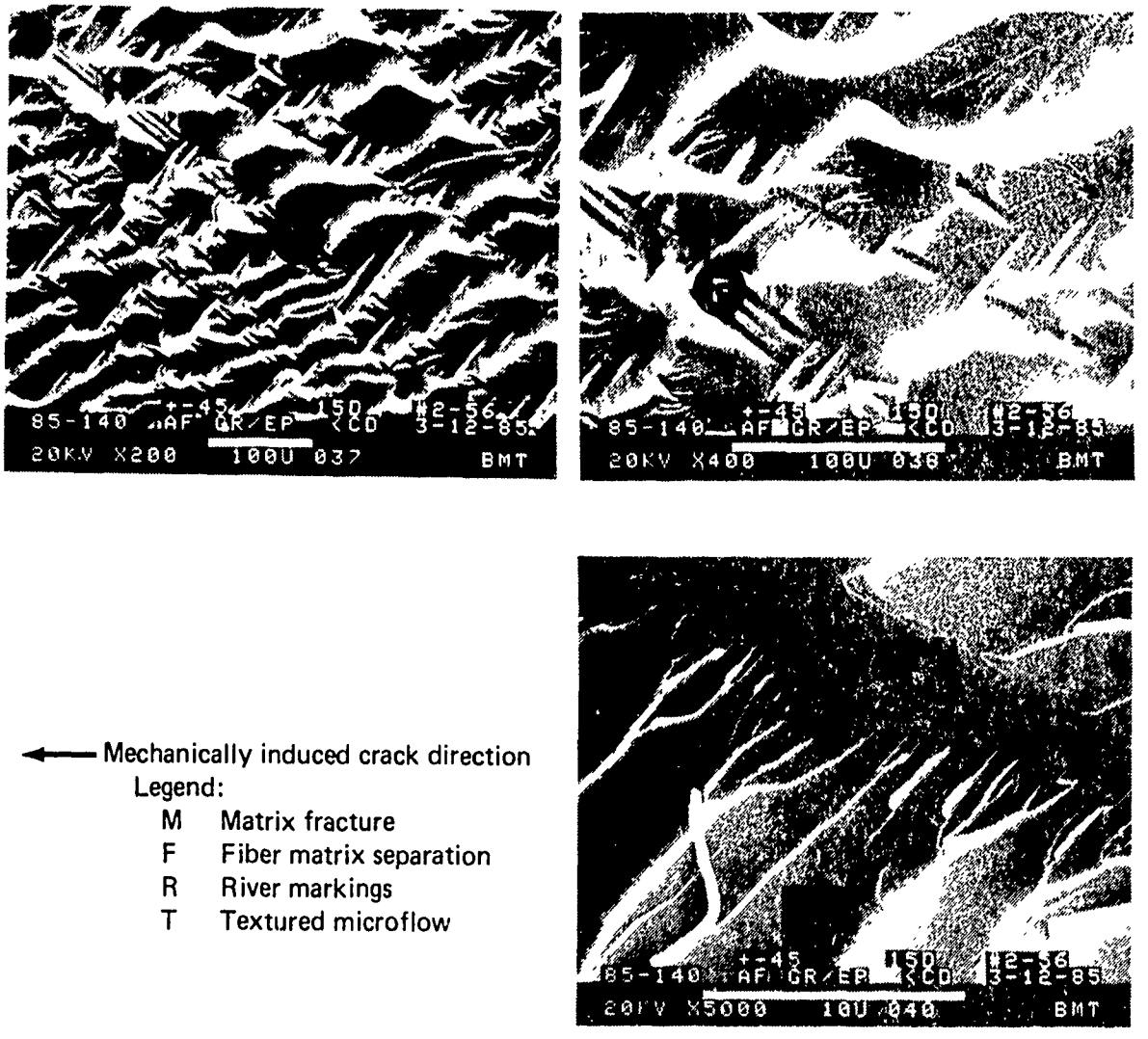

Figure 6. Fractographs of Mode 1 Delamination Between +45 and -45 Degree Plies.

3.2 Mode 2 Shear Fractures

Interlaminar fractures produced under mode 2 shear appeared distinctly different from delaminations produced under mode 1 tension. In both cases, two principal zones of fracture were observed; 1) areas of resin matrix fracture and 2) regions of fiber/matrix separation. However, fractures produced under interlaminar shear were found to exhibit larger amounts of fiber/matrix separation and smaller, finely spaced areas of cohesive matrix fracture. In contrast to mode 1, these finely spaced areas of matrix fracture exhibited a relatively rough topography. Detailed inspection of these areas revealed numerous inclined platelets (hackles) of fractured epoxy oriented normal to the direction of resolved tension. Under certain instances, the orientation of these hackles were found to positively correlate with the direction of induced cracking.

0 Degree/0 Degree Interface Fracture Surface

The fracture characteristics of delaminations produced between adjacent 0 degree plies under interlaminar shear are illustrated in Figure 7. At low magnification (400X), the overall fracture surface topography is noticably rougher than that typical of mode 1 tension (see fig. 3). At this magnification, regions of fiber/matrix separation interspersed with narrow rows of cohesive resin fracture are visible. In general, a larger degree of fiber/matrix separation appears evident under mode 2 shear as compared to mode 1 tension. Under mode 2, the shear couple is formed at the crack tip by transferring flexural loads, carried by the fiber, into the interlaminar matrix region. As a result, increased conditions of fiber/matrix separation appear reasonable under mode 2 conditions inasmuch as higher interfacial stresses exist. Because of this higher level of interfacial separation, significantly less exposed matrix fracture is apparent under mode 2 conditions. As illustrated in Figure 7, this condition is reflected in the existance of relatively small zones of cohesive resin fracture confined to small narrow rows by areas of fiber separation. In general, detailed inspection of these areas of fiber separation revealed the lightly crenulated impression of the AS-4 fiber indicating adhesive interfacial separation.

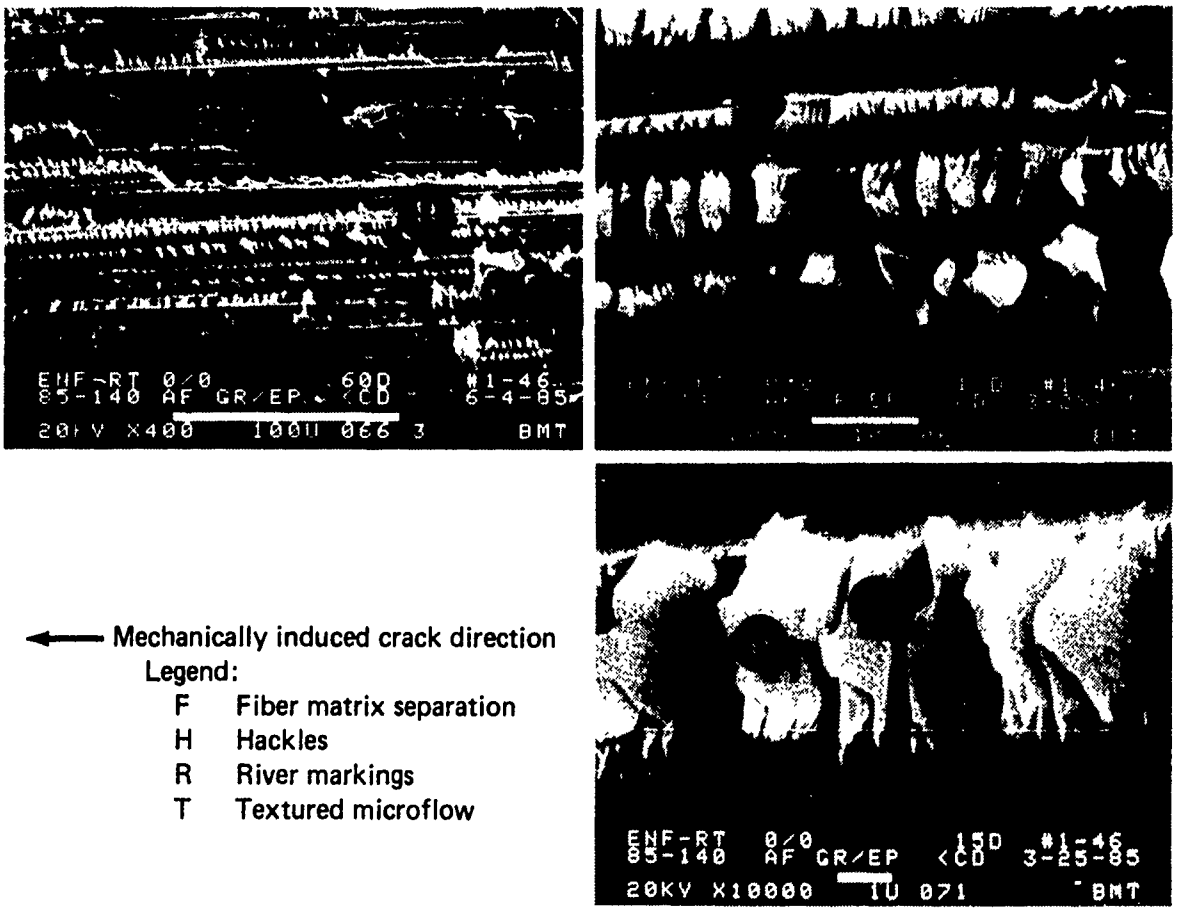

Figure 7. Fracture Topography Typical of Mode II Delamination Between Adjacent 0 Degree Plies.

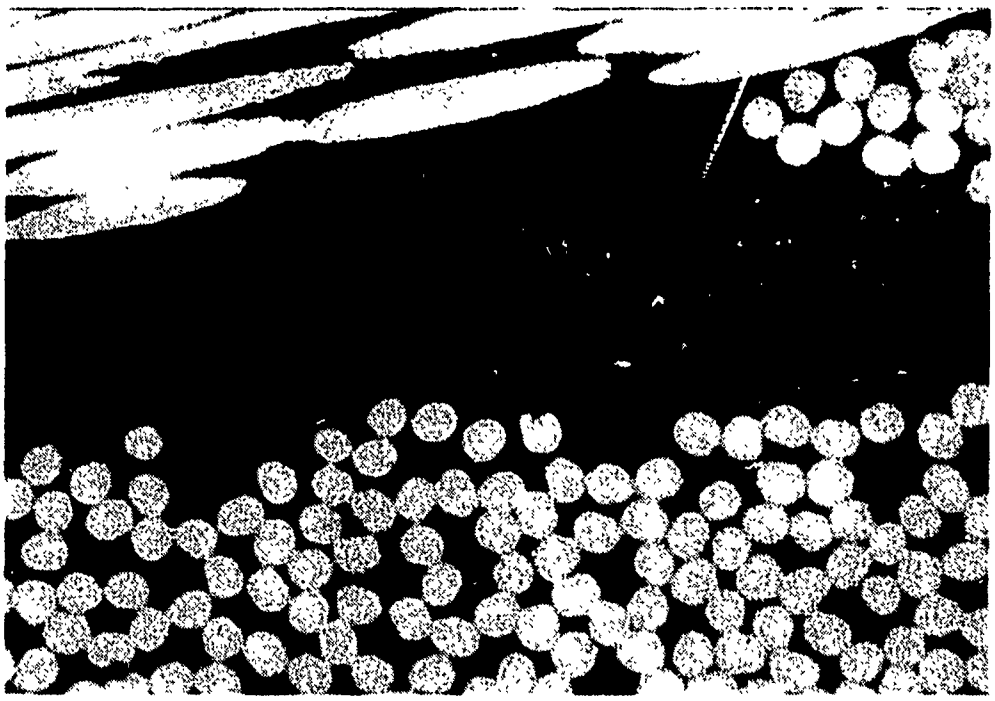

Figure 8. Microstructure of Cracks Found in Short Beam Shear Specimen Tested at 132 C (Ref. 11) Mag. 775X.

Upon detailed examination, the narrow rows of cohesive resin fracture located between areas of fiber separation, were found to exhibit numerous inclined platelets oriented cross-wise to the 0 degree fiber orientation. In a variety of other investigations, these platelets have often been referred to as hackles. Other investigators (ref. 10), have suggested that hackles are a result of flexural loading associated with local bending of the fracture surface just behind the crack tip. However, the presence of hackles exclusively under conditions of mode 2 shear, rather than mode 1, suggests interlaminar shear as the primary load source for their formation. The overall appearance of these hackles suggests that their formation may occur by coalesence of numerous microcracks inclined at an angle to the plane of applied shear. This model was supported by the observation of S-shaped cracks located at the midplane (highest shear loading) of short beam shear specimens in previous Boeing studies (ref. 11) as illustrated in Figure 8. In general, the hackles structures visible in Figure 7, and those microcracks visible in Figure 8, were oriented at an angles of approximately 40 to 60 degrees to the plane of applied shear. This orientation is approximately normal to the resolved tension component of applied shear. This finding suggests that hackle and microcrack formations occur under locally resolved tension conditions. Based on these observations, the sign of of applied interlaminar shear (clockwise or counterclockwise, i.e. + or -) can be determined from examining the tilt of hackles with respect to the plane of fracture.

Further inspection of the fracture surface discussed above revealed areas of scalloped, or concave shaped, resin fracture (Figure 9). Detailed examination of the size and shape of these scalloped features suggests that their formation results from the separation of hackles from the fracture surface. This conclusion appears substantiated by the existance of nearly separated hackles and the formation of underlying scalloped areas as shown in Figure 9. Separation of hackles can produce two possible relationships between hackle tilt and the direction of crack propagation, dependent upon which side of the shear plane hackles are retained (Figure 10). In mechanism A, separation occurs such that hackles are retained on the side in which the direction of crack propagation coincides with the local shear component direction. This first condition produces hackles tilted in the direction of crack propagation, as well as normal to the direction of resolved tension. Conversely, in mechanism B, separation occurs such that hackles are retained on the side in which the direction of crack propagation opposes the local shear component direction. In this later condition, the tilt of hackles oppose the direction of crack propagation.

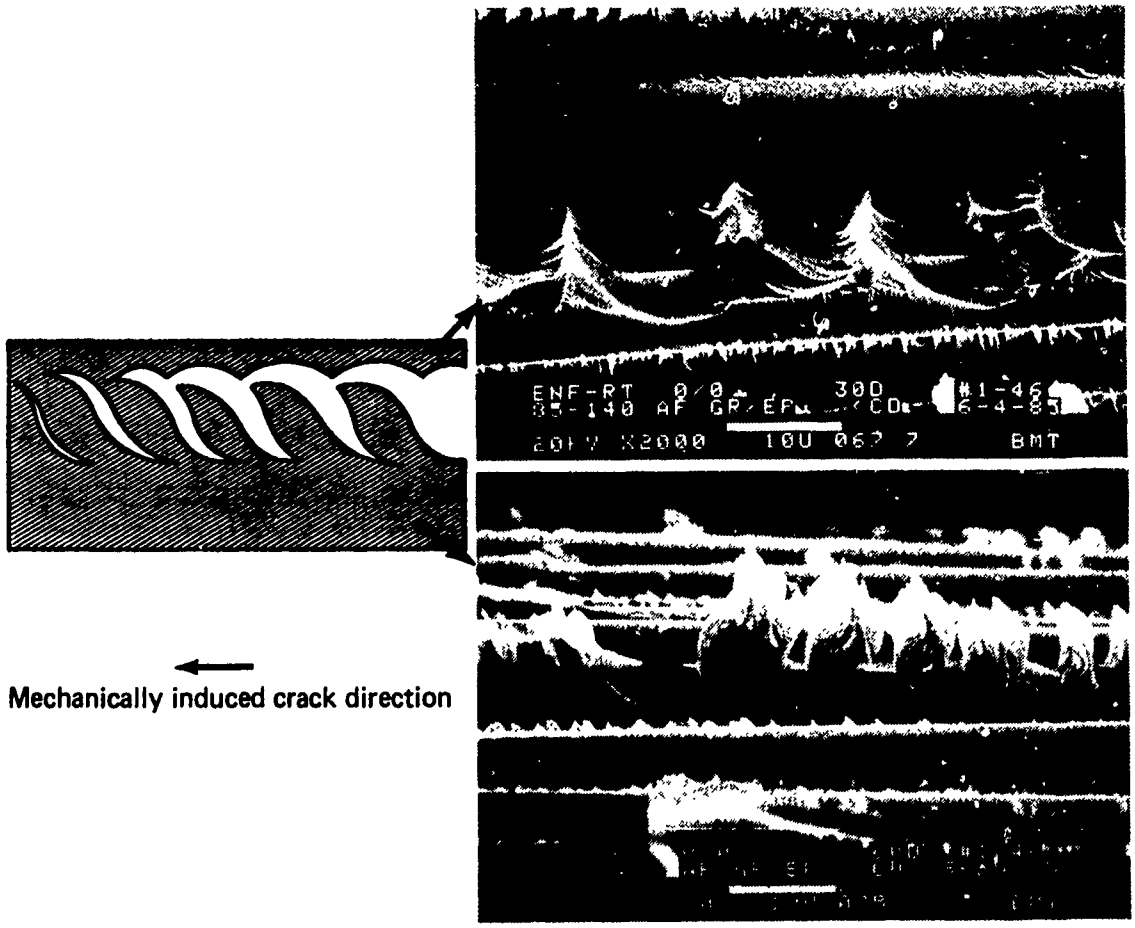

Figure 9. SEM Micrographs Illustrating Scalloped Resin Fracture Areas and Their Development. The Upper Micrograph Illustrates (S) Scallops, and (R) River Markings While The Lower Micrograph Illustrates (H) Hackle Separation and Underlying (S) Scallop Formation.

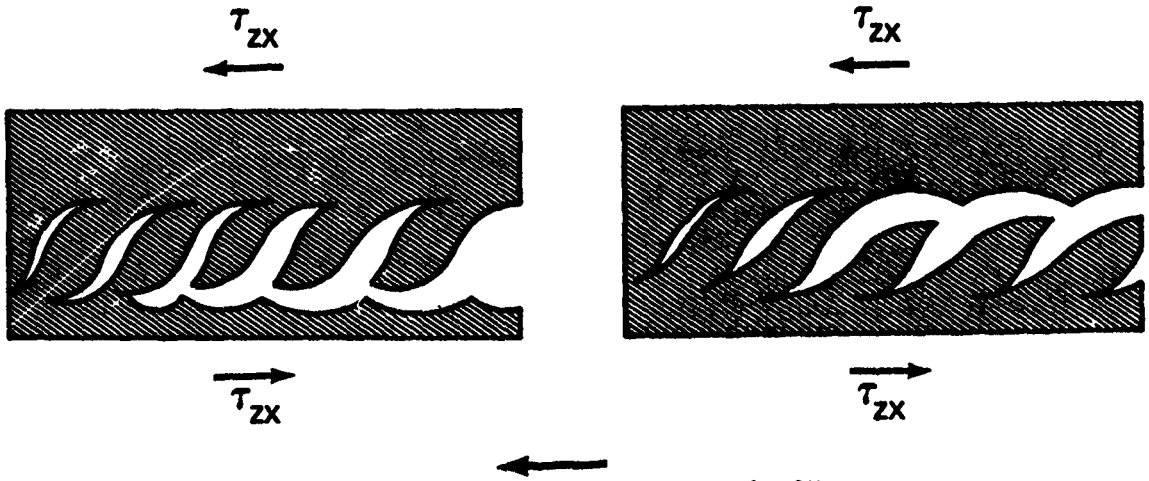

Figure 10. Schematic Illustration of Possible Hackle Separation Mechanisms. Mechanism A Illustrates Hackle Formation Coincident With the Direction of Crack Propagation, Whereas Mechanism B Illustrates the Formation of Hackles Opposite to the Direction of Crack Propagation.

Inorder to identify the dominant mechanism of hackle separation, both sides of each fracture surface were examined. As shown in Figure 11, both sides of fracture between adjacent 0 degree plies exhibit pronounced hackle formations. The existance of hackles on both surfaces indicates that hackle separation occurred by both mechanisms A and B. This finding indicates that hackle tilt is not a viable means of fractographically determining the direction of crack propagation for shear fractures between adjacent 0 degree plies. While the above discussion has been concerned with the overall structure of hackles, several finer morphological features are apparent on both hackle and scalloped areas. As illustrated in Figures 7 and 9, both hackle and scalloped areas exhibit textured resin microflow and branched river markings analogous to those identified under mode 1. For the most part, these features appear to eminate from areas of fiber/matrix separation and rotate to align with the direction of hackle tilting, either coincident with or opposite to the direction of imposed crack propagation (mechanism A or B). Based on their microscale, these features probably reflect the local direction of crack propagation involved in hackle formation and separation. The emination of these features from areas of fiber/matrix separation suggests that hackle formation initiates along the fiber interface and progresses either coincident with or opposite to the direction of overall propagation.

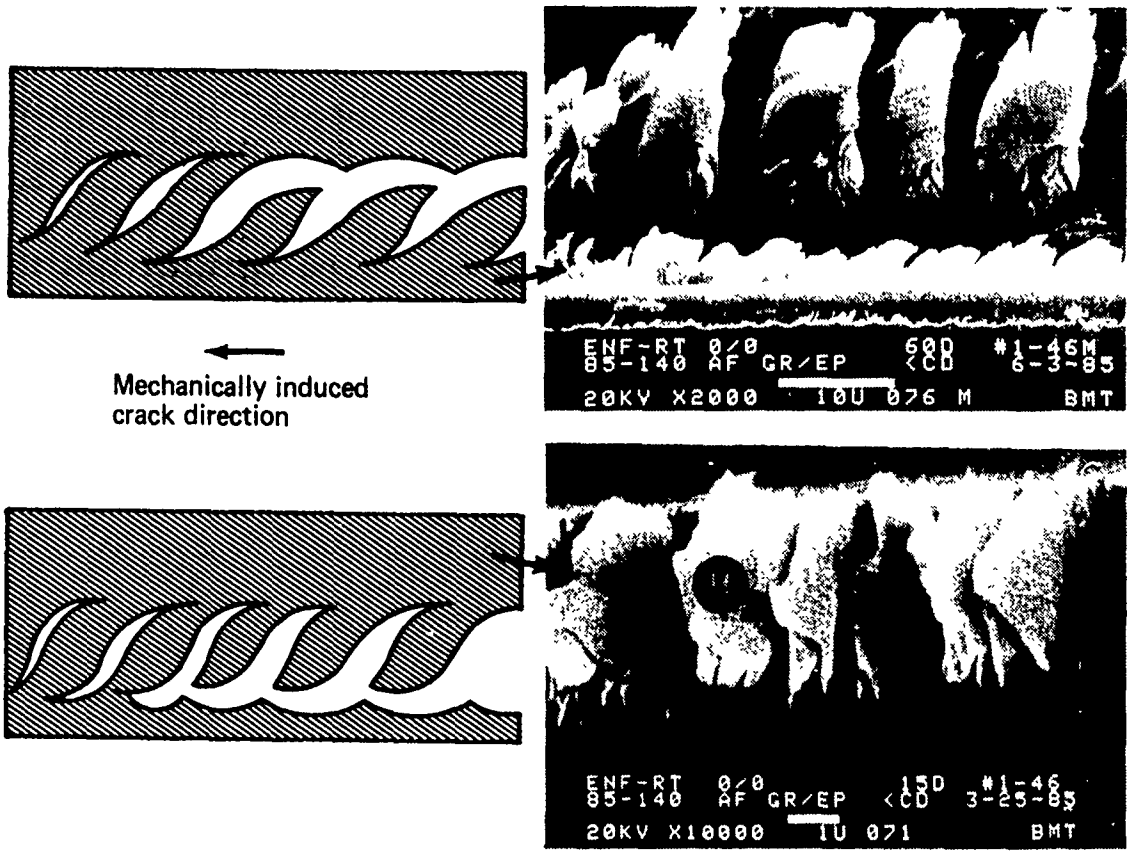

Figure 11. Illustration of Opposing (H) Hackle Tilts on Mating Sides of Mode 2 Delamination Between Adjacent 0 Degree Plies

Cross-Ply Interfaces (0/90 and +45/-45) Fracture Surface

The fracture surface features characteristic of mode 2 induced shear delaminations between 0/90 and +45/-45 degree oriented plies are illustrated in Figures 12 through 15. Consistent with the above findings, delaminations produced between cross-ply orientations exhibited more fiber/matrix separation and smaller, narrower rows of cohesive resin fracture than mode 1 delaminations. As illustrated in Figures 12 and 14, areas of cohesive resin fracture exhibited inclined hackles independent of the cross-ply orientation examined. In comparison to adjacent 0 degree plies, however, cross-plying produced some slight alteration in the amount of exposed fiber separation and in the size and shape of hackles. Figure 12 illustrates the topography typical of that produced between 0 and 90 degree ply orientations. As shown, the overall topography appears somewhat similar to the morphology characteristic of adjacent 0 degree ply delaminations. However, as shown in comparing Figures 7 and 12, some slight reduction in the size of hackles is apparent. In contrast, delamination between +45/-45 ply interfaces exhibited some distinct differences in fracture morphology. As illustrated in Figure 14, the overall fracture surface exhibited more cohesive matrix fracture as well as larger, triangular shaped hackle structures.

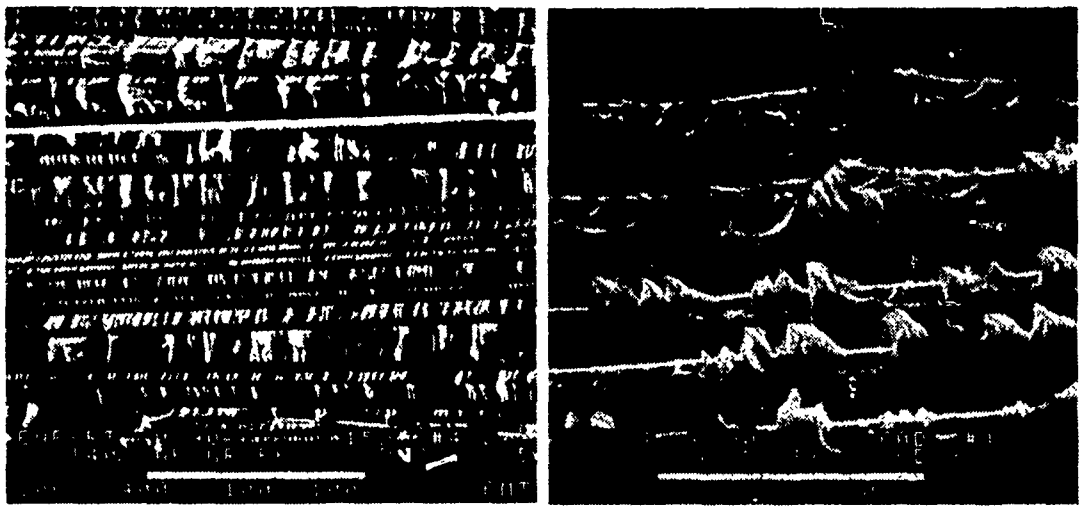

Mechanically induced crack direction

Figure 12. Fracture Morphology of Mode 2 Delamination Between 0 and 90 Degree Plies Illustrating Areas of (F) Fiber/Matrix Separation and (H) Hackles

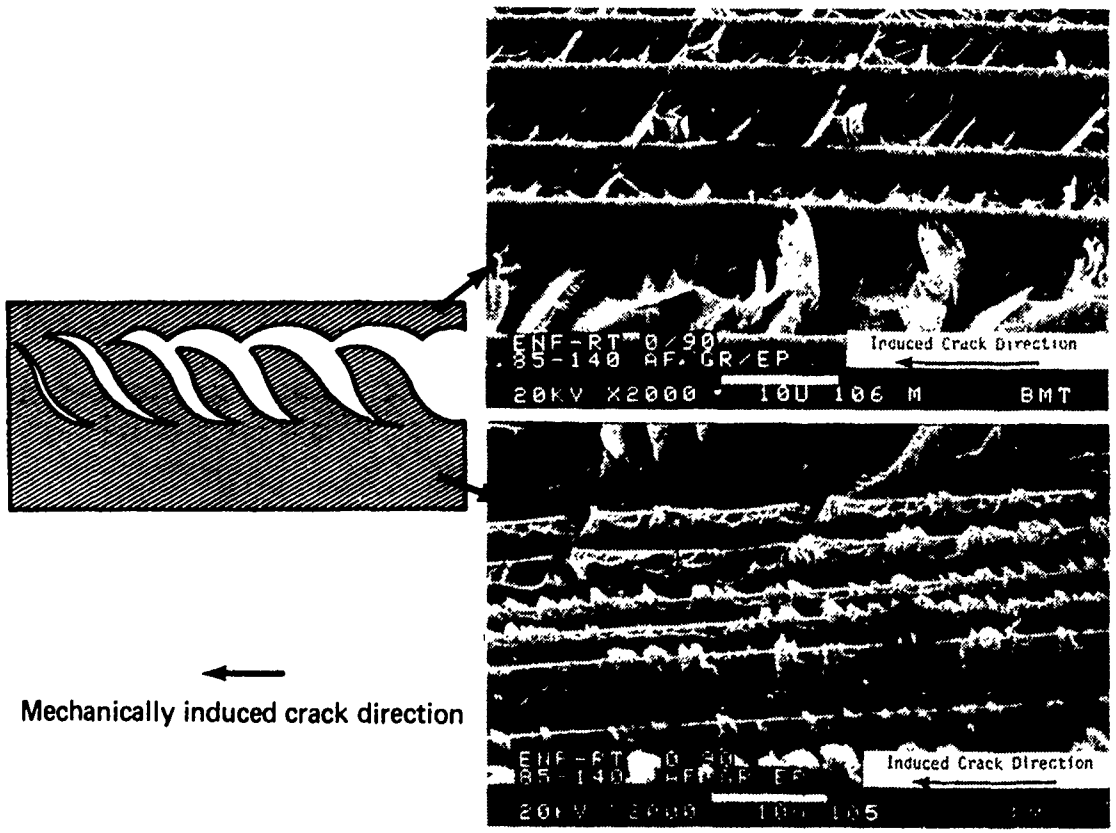

Figure 13. Topography of Mating Fracture Surfaces Produced Under Mode 2 Between 0 and 90 Degree Ply Orientations. (H) Hackle Separation Occurs by Mechanism A with Hackles Tilted in the Direction of Crack Propagation.

With respect to both of the above cross-ply orientations, hackles were found tilted normal to the local direction of resolved tension. As illustrated by examining Figures 13 and 15, these hackles were found to occur almost exclusively on one side of the fracture surface, with scallops on the adjoining side. With respect to Figure 10, these hackles are tilted coincident with the direction of crack propagation indicating separation by mechanism A. In contrast to the adjacent 0 degree ply condition, this observation indicates that a positive correlation exists between hackle tilt and the direction of crack propagation for cross-ply interfacial conditions. However, further studies need to be performed to determine if the mechanism of hackle separation is dependent upon conditions such as specimen geometry, lay-up, and degree of mixed mode loading.

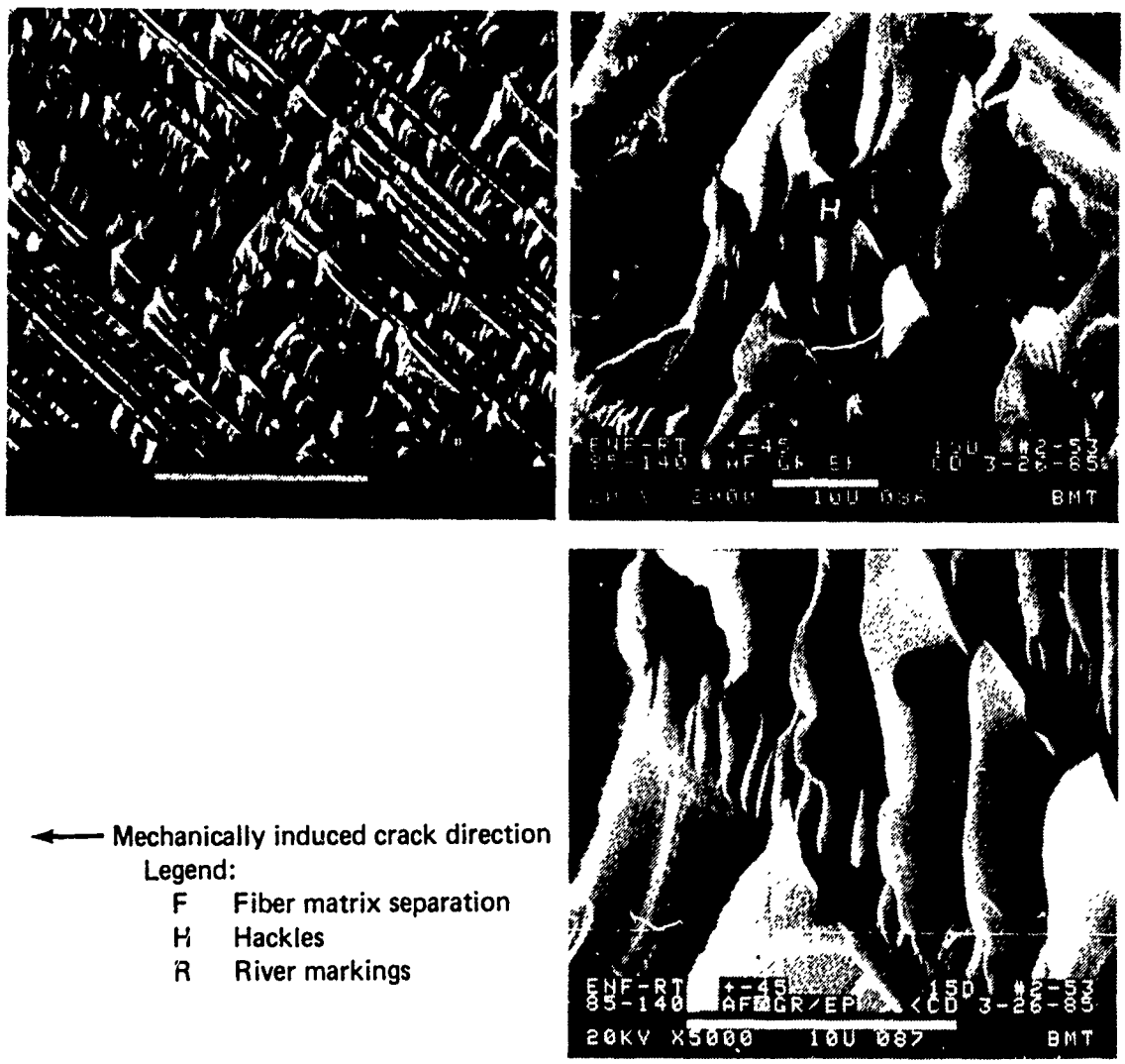

Figure 14. Fractographs of Mode 2 Shear Delamination Between +45 and -45 Degree Plies.

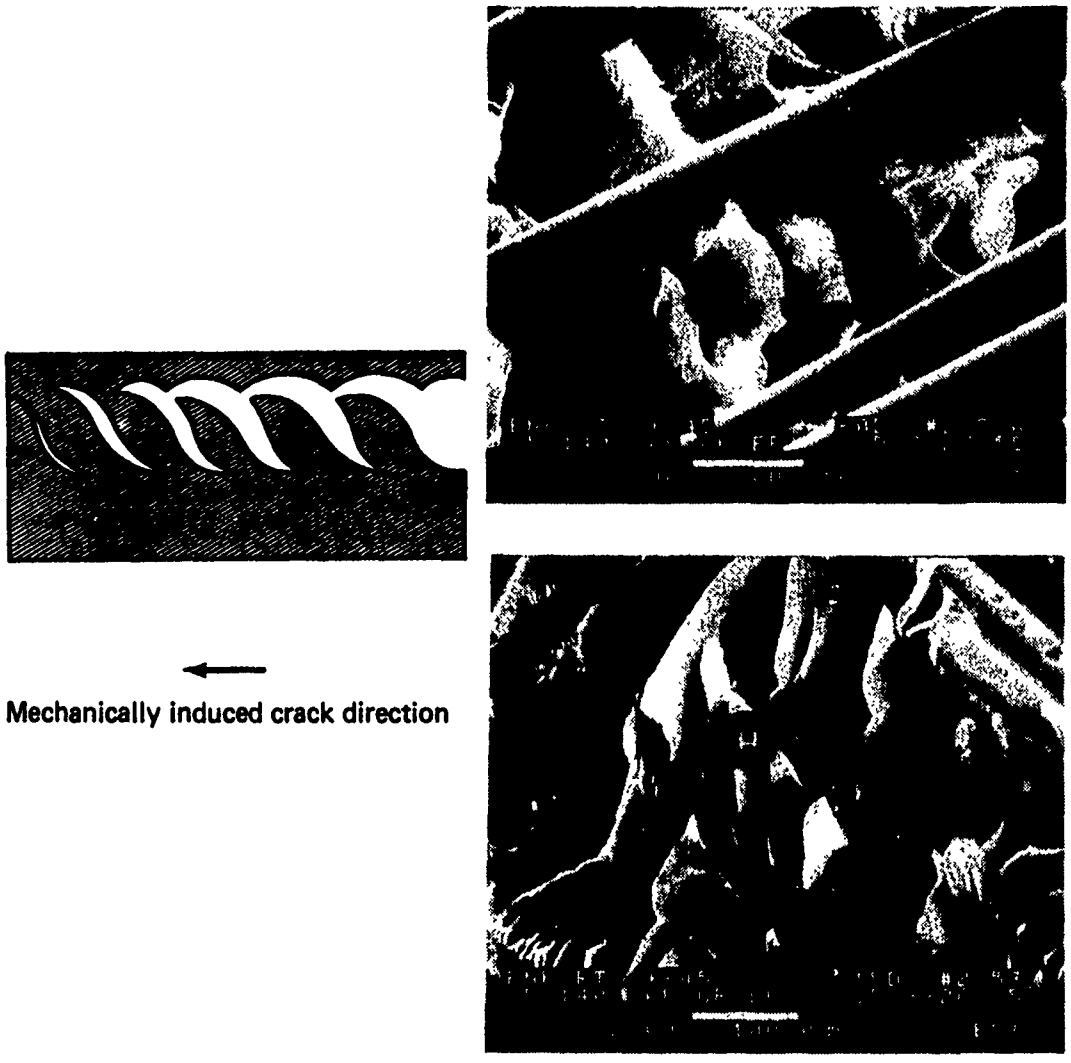

Figure 15. Fractographs of Mating Fracture Surfaces Produced Under Mode 2 Between +45 and -45 Degree Plies. Coincident with Mechanism A (H) Hackles are Retained on One Side, Tilted in the Direction of Crack Growth.

Further inspection of both hackles and scalloped fracture areas reveals several finer morphological features in addition to the gross topography discussed above. As illustrated at 5000X, detailed examination of hackles and scalloped areas revealed conditions of both textured resin microflow as well as branched river mark features. Both of these river marks and resin microflow features appear for the most part to eminate from regions of fiber/matrix separation. In the case of delamination between adjacent 0 degree plies discussed previously, these features were found to progress both towards and away from the macroscopic direction of crack propagation. However, in contrast to this case, microflow and river markings for both cross-ply orientations were found to progress only in the direction of crack propagation. Because of their microscopic nature, these features probably reflect the microsopic direction of cracking involved in

fracture. Consequently, hackle formation between cross-ply orientations appears to occur by the initation and growth of s-shaped microcracks in the direction of macrosopic crack growth. This situation supports the interpretation of hackle separation by mechanism A (see Figure 10).

4.0 Conclusions

In the study above, the fracture surface characteristics of delaminations produced under mode 1 tension and mode 2 shear were investigated for a variety of interfacial ply orientations (0/0, 0/90 and +45/-45). Conclusions of this investigation were:

1. Mode 1 tension fractures could be differentiated from mode 2 shear fractures based upon their relative fracture surface topographies. Fractures produced under mode 1 tension were characterized by the existance of relatively large areas of flat cohesive matrix fracture interspersed with areas of fiber/matrix adhesive separation. Conversely, fractures produced under mode 2 shear exhibited relatively narrow rows of hackled resin fracture separated by exstensive amounts of fiber/matrix separation.

2. The direction of crack propagation could be determined for mode 1 tension fractures by the examination of river markings and resin microflow features present on flat areas of cohesive matrix fracture. Examination of these features with respect to the direction of imposed fracture revealed that river mark branch coalescence and microflow progression coincide with the direction of crack propagation in the same manner as for metallic and polymeric materials.

3. Detailed examination of cohesive resin fracture areas generated under mode 2 shear revealed epoxy platelets inclined approximately normal to the resolved tensile component of applied shear. Separation of these hackles from the fracture surface was shown to occur by one of two mechanisms, yielding hackles aligned either coincident with (mechanism A), or opposite to (mechanism B), the direction of crack propagation.

4. The direction of crack propagation and tilt of observed hackles was found to correlate positively for 0/90 and +45/-45 interfacial mode 2 fractures, which occurred predominantly by mechanism A. In this case, the tilt of observed hackles may provide an identifiable feature by which local crack propagation can be determined. However, further work will be required to verify this capability.

5. Fractures produced between adjacent 0 degree plies typically occurred by a mixture of both mechanisms A and B. Therefore, the direction of crack propagation could not be determined via the examination of hackle tilt orientation for this interface condition. However, further studies should be performed to determine if the mechanism of hackle separation is dependent upon specimen test geometry.

6. In general, both hackles and their regions of separation (scallops) exhibited both river markings and resin microflow conditions similar to that noted under mode 1 fracture. These features were found to initiate at regions of fiber/matrix separation and progress in the direction of hackle tilt.

Acknowledgements

The authors wish to acknowledge the contributions of R. E. Smith, S. D. Pannell, and Dr. A. G. Miller for their assistance in these investigations.

References

1. "Failure Analysis For Composite Structure Materials", contract F33615-84-C-5010; Air Force Systems Command, Aeronautical Systems Division/PMR RC, Wright Patterson AFB, 1984.

2. Miller, A.G., Hertzberg, P.E., and Rantala V.W., Proceedings of the Twelfth National Society for the Advancement of Material and Process Engineering (SAMPE) Technical Conference, Seattle, WA, October 1980, p. 279.

3. Devitt, D.F., Schapery, R.A. and Bradely, W.L., "A Method for Determining the Mode I Delamination Fracture Toughness of Elastic and Viscoelastic Composite Materials", Vol. 14, 1980 pp. 270-285.

4. Jurf, R.A. and Pipes, R.B., "Interlaminar Fracture of Composite Materials", J. Composite Materials, Vol. 16. 1982, pp 386-394.

5. Vanderkley, P.S., "Mode I - Mode II Delamination Fracture Toughness of Unidirectional Graphite/Epoxy Composite", Texas A & M University Report MM 3724-81-15, December 1981.

6. Wilkins, D.J., Eisenmann, J.R., Camin, R.A., Margolis, W.S. and Bemson, R.A., "Characterizing Delamination Growth in Graphite-Epoxy", in Damage in Composite Materials, ASTM STP 775, 1982, pp. 168-183.

7. Ramkumar, R.L., "Performance of a Quantitative Study of Instability-Related Delamination Growth", Nasa CR 166046, March 1983.

8. "Failure Analysis And Prevention", American Society for Metals Handbook, Vol. 10, 1975.

9. A. A. Griffith, Transactions, Royal Society of London, Vol. 221, 1920.

10. Morris, G.E., "Determining Fracture Directions and Fracture Origins on Failed Graphite/Epoxy Surfaces", Nondestructive Evaluation and Flaw Criticality for Composite Materials, ASTM STP 696, 1979, pp. 274-297.

11. Miller, A.G., Wingert, L.E., "Fracture Surface Characterization of Commercial Graphite/Epoxy Systems", Nondestructive Evaluation and Flaw Criticality for Composite Materials, ASTM STP 696, pp 223-273.

Session III

A NEW METHOD FOR NONDESTRUCTIVELY EXAMINING BONDED STRUCTURES

FRACTURE CHARACTERISTICS: LOADING MODES, INVESTIGATIVE TECHNIQUES AND NDE METHODS

R.D. Adams and A.M. Allen
Department of Mechanical Engineering
University of Bristol
Bristol, England

and

P. Cawley
Department of Mechanical Engineering
Imperial College
London, England

INTERPRETATION OF FRACTURE SURFACES

H.N. Chou
McDonnell Douglas Astronautics Company
St. Louis, Missouri

ABSTRACT

Specimens of woven glass/polybenzimidazole composites were subjected to flexural and interlaminar shear tests. The profiles and the fracture surfaces of failed specimens were examined using a scanning electron microscope to identify the surface morphology and the microstructure of the composites. The findings were related to the applied loading conditions. The dominant failure surface features were found to be fiber breaks, fiber pull-out, fiber/matrix debonding, matrix debris, cross-ply cracks, ply delamination and microbuckling of fibers. No indications of matrix hackles were observed in the composites. The post failure examinations found the crack locations in the specimens were in agreement with the flexural and shearing stress distribution theories.

INTRODUCTION

Advanced composites are rapidly emerging as a major material for use in next-generation missile structure because in many areas they provide greater structural efficiency. A serious drawback of polymers as engineering materials is their relatively poor heat resistance and low thermal stability. Aromatic polymers are stiffer and more resistant to deformation than their aliphatic counterparts. The presence of aromatic rings improves thermal stability of a polymer, since aromatic rings are thermally very stable. The application of these principles in creating new polymers has brought remarkable improvement in heat and oxidation resistances. Polybenzimidazole (PBI) is one of these specific polymeric materials and shows heat resistance for a short time up to a temperature of about 600°C.

Successful application of these materials requires an improved understanding of their failure mechanisms. At present, there is insufficient knowledge to interpret the nature of these failures in glass/PBI composites through fractographic methods. A systematic approach is necessary to develop the analytical techniques for understanding the modes and mechanisms of the glass/PBI failures. The purpose of this paper is to present the progress on an in-house study at MDAC-St. Louis to obtain an understanding of the failure modes and mechanism of woven glass/PBI composites.

PANEL FABRICATION

The panel was composed of 16 woven prepreg plies of S2 glass fiber in a matrix of PBI resin and was laid up in sequences of $(0,90,90,0)_4$. In the woven prepreg, the warp was in 0° direction and the fill was in the 90° direction; each prepreg ply was 0.0074 inch thick. The laid up 16 ply material was placed between heated platens of a laboratory press and loads were applied on the platens to generate a maximum pressure of 2000 psi. The panel was cured in three holds (Figure 1). The first hold is designed tc have resin wetout and to have a balanced resin content. In the second hold at higher temperature and pressure, polymerization reactions take place and off-gassing starts. In the third hold at the highest temperature and pressure, crosslinking of the matrix material and diffusion of the volatiles are completed. The pressure, temperature and time in the three holds were different for the curing processes of each panel. The cured panel was 5.5 by 5 by 0.12 inch thick.

SAMPLE PREPARATION AND TESTING

Samples for the testings were removed from the cured panels using a diamond cut-off wheel. The dimensions of the flexure test samples and the short beam shear test samples were 3.5 by 0.5 by 0.12 inch thick and 0.7 by 0.25 by 0.12 inch, respectively. The samples were placed on a three-point loading system utilizing a center loading of 0.5 inch radius of loading nose, and were tested to fracture at room temperature in a hydraulically actuated universal testing machine. The flexure test was performed in accordance with ASTM standard D790-81 using a 2.0 inch span length and a loading rate of 150 pounds/minute. The short beam shear test was performed in accordance with ASTM standard D2344-76 using a 0.4 inch span length and a loading rate of 200 pounds/minute.

EXPERIMENTAL RESULTS

Using equations specified in ASTM D790 and ASTM D2344, the maximum fiber stresses in the flexural test and the maximum interlaminar shear stresses in the short beam shear test were calculated for a total of 31 specimens (Table 1). The calculated stresses for specimens in the same panel scattered in a very wide range which reflected the variations of the curing processes for the panel. The stress-strain curves were plotted from the incremental loads and the corresponding specimen deflections. The stress-strain curves are essentially linear which indicates Hooke's law is applicable in this range.

SCANNING ELECTRON MICROSCOPE (SEM) EXAMINATION RESULTS

Fractured samples were submitted for examination using a scanning electron microscope (SEM). The microscopes used for the analysis were a AMRAY 1000A SEM and a Jeol JSM P15 SEM. Prior to the examination, the surfaces of the samples were made electrically conductive by coating them with a gold film. The film was approximately 300Å thick and was applied by vapor deposition in a vacuum evaporator. SEM photomicrographs taken of five specimens from the flexural test are presented in Figures 2 through 6.

In the compressive surfaces of the flexure tested specimens, shallow cracks in zig-zag paths were observed in the applied load areas through the width of the specimens and were exhibited in a light color band. Fiber microbuckling and fiber fracture were presented in the light band areas of the specimens; the majority of the fibers in the microbuckling areas were bent and only a few fibers were broken. In areas away from the microbuckling locations, the fibers in the specimens were still mechanically interlocked. Cracks in individual fiber were detected in the microbuckling areas of Specimen 9. Adhesion between fiber and matrix was evident as indicated by the matrix debris on the surfaces of the buckled fibers.

No cracks were detected in the tension surfaces of the specimens.

The specimens were re-oriented in the SEM by rotating the side surfaces of the specimens toward the electron beam of the SEM; SEM photomicrographs taken of the side surfaces of the specimens are shown in Figures 7 through 11.

In Specimen 5, fiber debonding and cross-ply cracks in the transverse plies developed into delaminations at the interfaces between the transverse and longitudinal plies (Figure 7). In plies close to the compression surface of the specimen, fiber debonding in the longitudinal ply developed into a delamination at the interface. No cracks were observed in the outermost fibers adjacent to the tension surface. The side surface of Specimen 9 revealed multiple cracks in plies close to the compression surface, Figure 8. In the longitudinal plies underneath the microbuckled fibers of the compressive surface, delaminations resulted in debonding in the transverse plies

and developed into more delaminations. In the transverse plies adjacent to the compressive surface, cross-ply cracks also developed into many delaminations at the interfaces. In the outermost plies close to the tension surface of the specimen, no cracks were detected. The side surface of Specimen 15 revealed multiple cracks in the vicinities of the microbuckled fibers and in areas close to the tension side of the specimen (Figure 9). Fibers in the longitudinal ply underneath the compressive surface were buckled and resulted in debonding in the adjacent transverse plies; delamination and cross-ply crack consequently were developed. In areas close to the tension side, a delamination in the fiber/matrix interface resulted in a cross-ply crack and the formation of more delaminations. The side surface of Specimen 22 revealed few cracks at the center of the specimen below the compressive surface, Figure 10. Fiber microbuckling in the compressive surface extended into the long and transverse plies; fiber debonding and cross-ply cracks were developed in the adjacent plies. The side surface of Specimen 30 is presented in Figure 11 and exhibited similar topographic features as that of Specimen 22. Fiber microbuckling in the compressive surface developed into debonding and cross-ply cracks. In the outermost fibers close to the tension sides of Sepcimen 22 and 30, no delaminations or cracks were observed.

SEM photomicrographs taken of two specimens from interlaminar shear tests are presented in Figure 12. The side surfaces of Specimen 15 revealed a large delamination in the midplane extending from the end of the specimen to the center. Multiple small cracks were exhibited in plies close to the center position of the specimen. The side surface of Specimen 30 showed a large delamination in the midplane and many parallel delaminations in the areas between the midplane and the compressive surface. These delaminations extended from the end of the specimen to the center and were confined at the interfaces between the longitudinal and transverse plies. Fiber debonding and cross-ply cracks were revealed in the transverse plies in areas between the midplane and the tension side of the specimen.

When the SEM examination of the outside surfaces of the specimens were completed, the defects at locations close to the compression and tension surfaces of the flexure test specimens were exposed and the resulting fracture surfaces were coated with a gold film. The prepared specimens were examined using a SEM. SEM studies were carried out to define the microstructure details and the dominant mechanism during testing of the specimens. The topographic features of Specimens 5, 9, 15, 22 and 30 were similar; parts a through g in Figure 13 show the representative photomicrographs of the specimens. In the outer fiber region at the compression side of a specimen (part a), fibers in the longitudinal plies were deformed and fractured; debris of matrix fracture was present adjacent to fibers. In the transverse plies (part b), shear failure took place; the surface appearances of the fractured matrix and fibers were flat and brittle.

Ridges on the surfaces of the fractured fibers pointed to the same direction as the compression loading direction (part c). Cracks in fibers and in the fiber-to-matrix interfaces were evident. Fiber pull-out and fiber debonding were exhibited (part d). In the outer fiber region at the tension side of the specimen, (part e), fib detachment and fractures of fibers and matrix were observed in the longitudinal ply region. Fiber pull-out and fiber debonding were present in the transverse ply region; cracks in the fibers were also observed (part f). The appearance of fracture surface in this region was brittle. Ridges on the surfaces of the fractured fibers were subtle and the ridge directions could not be associated with the loading direction (part g).

The midplane delaminations in Specimens 15 and 30 were exposed and the resulting fracture surfaces were coated with a gold film and were examined in a SEM. The topographic features of the specimens were similar; Figure 14 shows the representative photomicrographs of the specimens. Voids and microcracks were observed in the resin rich areas of the exposed delamination region. The delamination failure was observed to be a matrix failure and most of the fibers were still mechanically interlocked. Matrix debris and fiber imprints were observed. Hackles, characteristic

feature of epoxy matrix fracture, were not observed in the fracture of PBI matrix. The smooth feature of the fiber surfaces indicated wetting between the matrix and fiber surfaces were insufficient and adherence of matrix to fibers was poor.

DISCUSSION

When a beam of homogeneous elastic material is tested in flexure as a simple beam supported at two points and loaded at the midpoint, the maximum stress in the outer fibers occurs at the midspan. Strains in its fibers vary linearly as their respective distances from the neutral surface. Normal stresses resulting from bending also vary linearly as their respective distances from the neutral axis. The stress is (y/c) (σ_{max}), where y is the distance and c is measured from the neutral axis to the most remote fiber of the beam. The normal stresses resulting from three-point bending are maximum at the outermost center plies. Therefore, cracks in the flexure test specimens should be located at the outermost ply location in the center of the specimen. The SEM examination of the side surfaces of the specimens found the crack locations were in agreement with the predication.

Cracks of microbuckling initiate in the compressive surface, propagate into plies underneath and result in cross-ply cracks and delaminations. The stresses decrease linearly toward the midplane and diminish to zero at the neutral axis of the specimen and no cracks are present in the center areas. The stresses increase linearly from the neutral axis toward the tension surface of the specimen and reach another maximum on the surface. Large wide cracks appear in the vicinities of the outermost plies.

From the theory of shearing-stress distribution in a beam of solid rectangular cross-section transmitting a vertical shear V, the horizontal shearing stress varies parabolically and is $V/2I[(h/2)^2 - y^2]$, where h is the thickness of the beam. The maximum shearing stress occurs at the neutral axis where y is zero.

In the short beam shear test specimens, the interlaminar shear stresses vary parabolically and reach a maximum value at the center neutral axis of the specimen. At increasing distances from the neutral axis, the stresses gradually diminish and cease to exist at both the compressive and tension surfaces. The SEM examination of the specimens found the largest delaminations initiated at the midplanes of the specimens and were in general agreement with the predication. Since the material system is not homogeneous elastic, the behavior of the specimens under loading deviates somewhat from the predication and multiple cracks take place at the locations away from the midplanes of the specimens.

CONCLUSIONS

The post failure analyses of the woven glass/PBI specimens from the flexure and short beam shear tests find that the failure locations are in general agreement with the theoretical predictions. The SEM examinations reveal flat and brittle appearances in the fracture surfaces of the composites. In the material systems, fiber pull-out and interface debonding are common features and no hackles are observed in the fracture surfaces. Most fibers are still mechanically interlocked which is not unusual for high fiber content glass/PBI composites. There is considerable room for improvement in crack exposure techniques without disturbing the microstructure of the composites. This paper should be considered as a preliminary study or point of departure for subsequent study of post failure analysis for high temperature composites.

ACKNOWLEDGEMENTS

The author wishes to express his appreciation to Dr. Roger Fountain and Mr. R. E. Bohlmann of MDAC-STL for their helpful discussions and to Mr. R. R. Wilcox of MDAC-STL for his assistance in SEM operations.

REFERENCES

1. Zbigniew D. Jastrzebski, The Nature And Properties of Engineering Materials, John Wiley & Sons, Inc., New York, 1976.
2. E. P. Popov, Mechanics of Materials, Prentice-Hall, Inc., Englewood Cliffs, N.J., 1952.
3. G. E. Morris, Fractographic Analysis Of Failed Graphite/ Epoxy Composites, MDC A5505, 1978.
4. R. C. Sanders, E. C. Edge and P. Grant, Basic Failure Mechanisms of Laminated Composites And Related Aircraft Design Implications, Composite Structures 2(1983), 467-485.
5. B. D. Agarwal and Lawrence J. Broutman, Analysis and Performance of Fiber Composites, John Wiley & Sons, Inc., New York, 1980.

Table 1 - Flexure and Interlaminar Shear Stresses

PANEL	Flexural Stress (KSI)			Shear Stress (KSI)		
	Mean	Low	High	Mean	Low	High
1	17.46	14.14	20.27	1.91	1.32	2.48
2	89.20	86.35	91.70	8.51	7.99	9.31
3	60.03	31.29	66.62	5.25	2.78	5.43
4	76.57	72.86	83.14	5.84	5.21	6.32
5	64.25	37.48	127.60	4.11	2.89	16.13
6	26.97	20.74	32.11	1.36	1.19	1.56
7	65.86	57.04	114.40	5.23	4.95	12.95
8	81.98	76.69	86.71	7.62	6.35	7.93
9	32.90	30.53	34.61	2.89	2.37	3.34
10	84.23	70.00	89.57	7.42	6.80	8.06
11	80.01	74.92	86.80	7.21	5.94	9.40
12	55.46	82.70	87.08	3.39	2.14	6.98
13	98.35	86.47	100.97	5.20	3.69	8.89
14	39.22	35.75	42.09	6.20	2.29	7.77
15	53.48	49.50	59.00	8.69	7.63	9.98
16	32.15	27.92	36.35	2.07	1.90	3.63
17	33.95	29.04	38.21	2.32	2.29	2.76
18	51.73	49.29	56.22	3.46	3.18	4.67
19	40.44	30.68	54.25	2.34	2.17	2.60
20	35.02	29.12	41.00	1.43	0.87	2.59
21	99.20	94.05	104.43	8.27	7.70	9.99
22	91.32	84.48	98.55	6.41	5.91	8.77
23	33.23	32.56	36.67	2.56	2.32	2.71
24	48.19	43.68	66.00	4.35	2.43	4.92
25	33.20	25.26	39.08	2.64	2.57	2.69
26	48.62	44.00	51.53	3.25	1.94	5.68
27	87.30	75.71	92.96	7.26	6.99	9.51
28	95.14	87.91	112.75	8.36	7.61	9.17
29	41.47	33.85	57.97	3.68	3.12	4.68
30	80.23	73.33	86.60	6.34	5.43	7.73
31	69.47	55.36	80.90	6.03	3.61	7.92

FIGURE 2. SEM PHOTOMICROGRAPHS SHOWING THE COMPRESSIVE SURFACE OF SPECIMEN 5.
σ_{FLEX} = 127.60 KSI

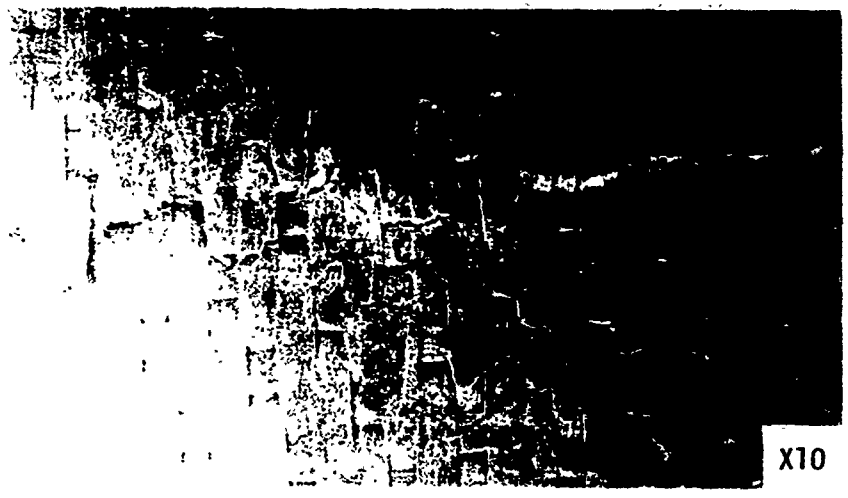

FIGURE 3. SEM PHOTOMICROGRAPHS SHOWING THE COMPRESSIVE SURFACE OF SPECIMEN 9. σ_{FLEX} = 34.61 KSI (Cont'd)

(Figure 3 cont'd)

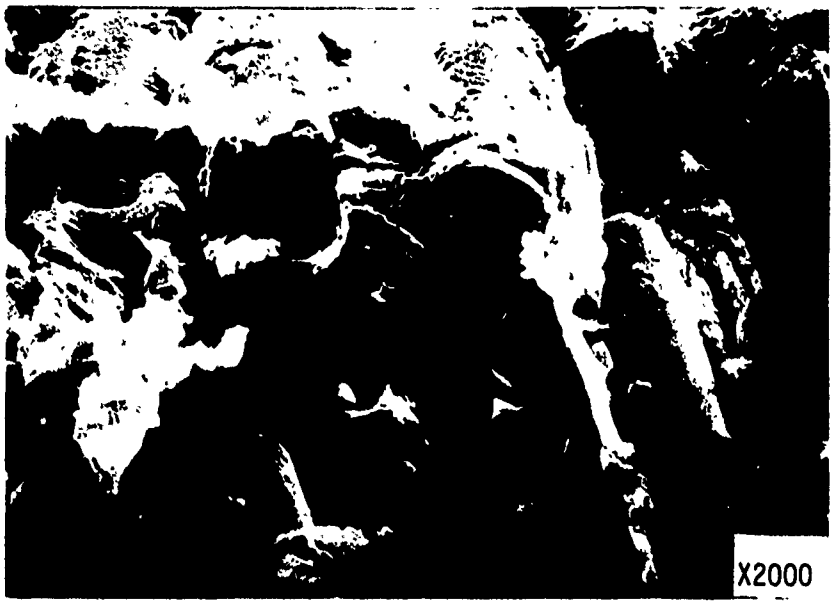

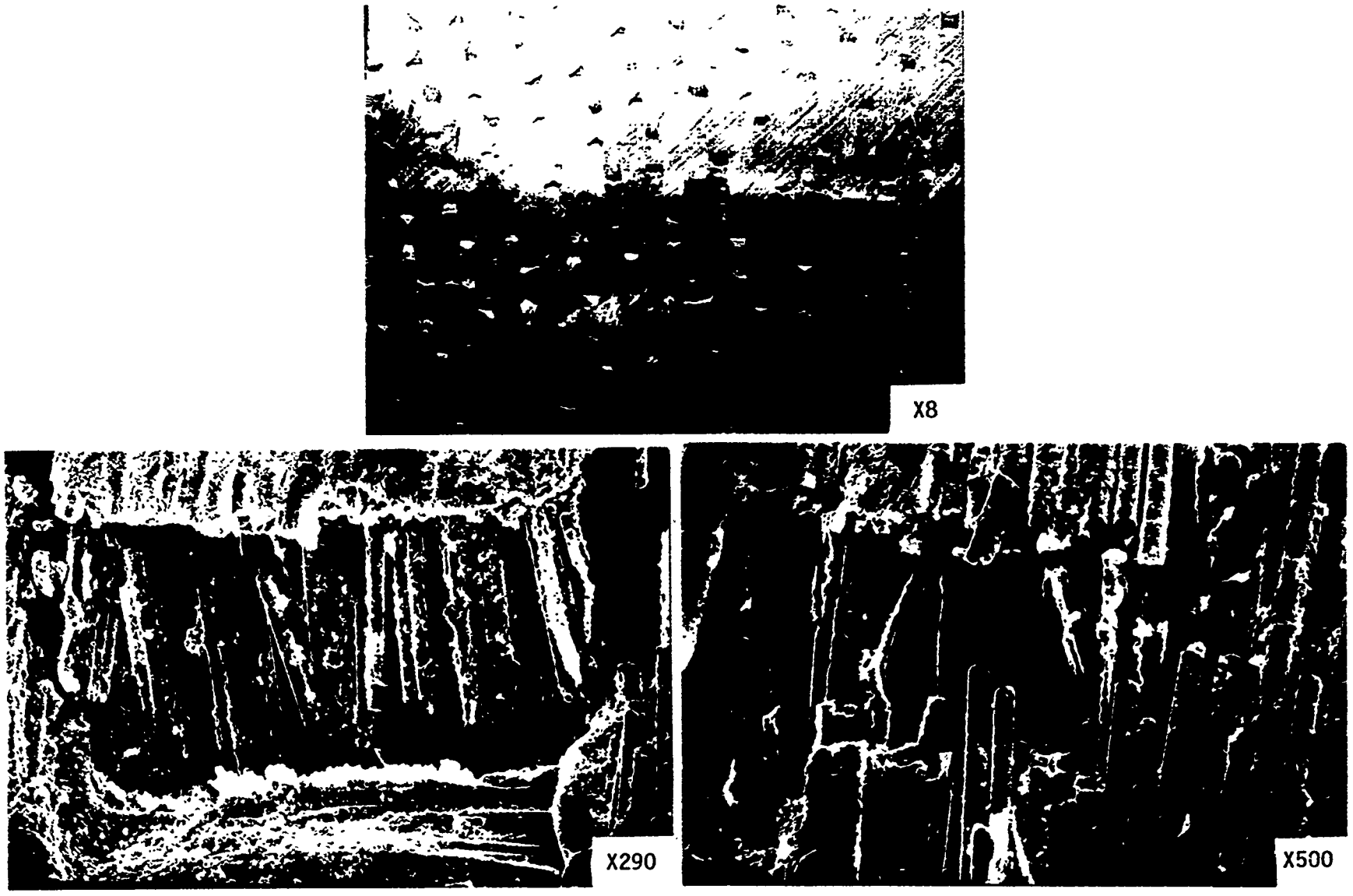

FIGURE 4. SEM PHOTOMICROGRAPHS SHOWING THE COMPRESSIVE SURFACE OF SPECIMEN 15.
σ_{FLEX} = 59.00 KSI

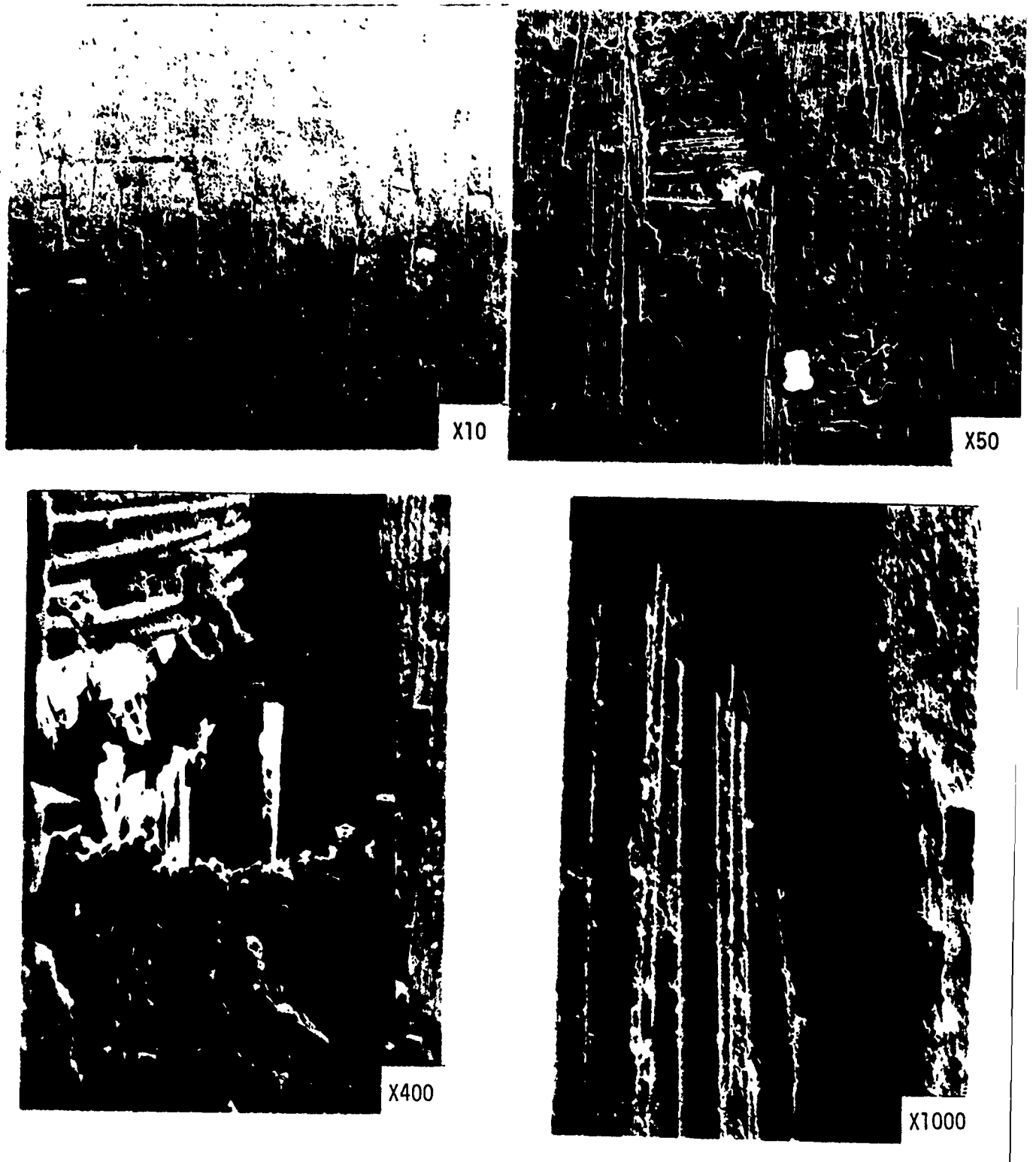

FIGURE 5. SEM PHOTOMICROGRAPHS SHOWING THE COMPRESSIVE SURFACE OF SPECIMEN 22
σ_{FLEX} = 98.55 KSI

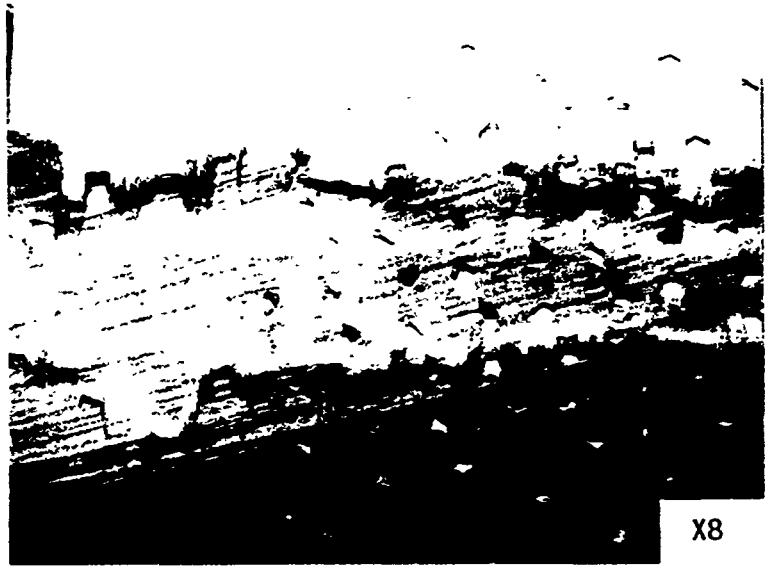

FIGURE 6. SEM PHOTOMICROGRAPHS SHOWING THE COMPRESSIVE SURFACE OF SPECIMEN 30.
σ_{FLEX} = 86.60 KSI

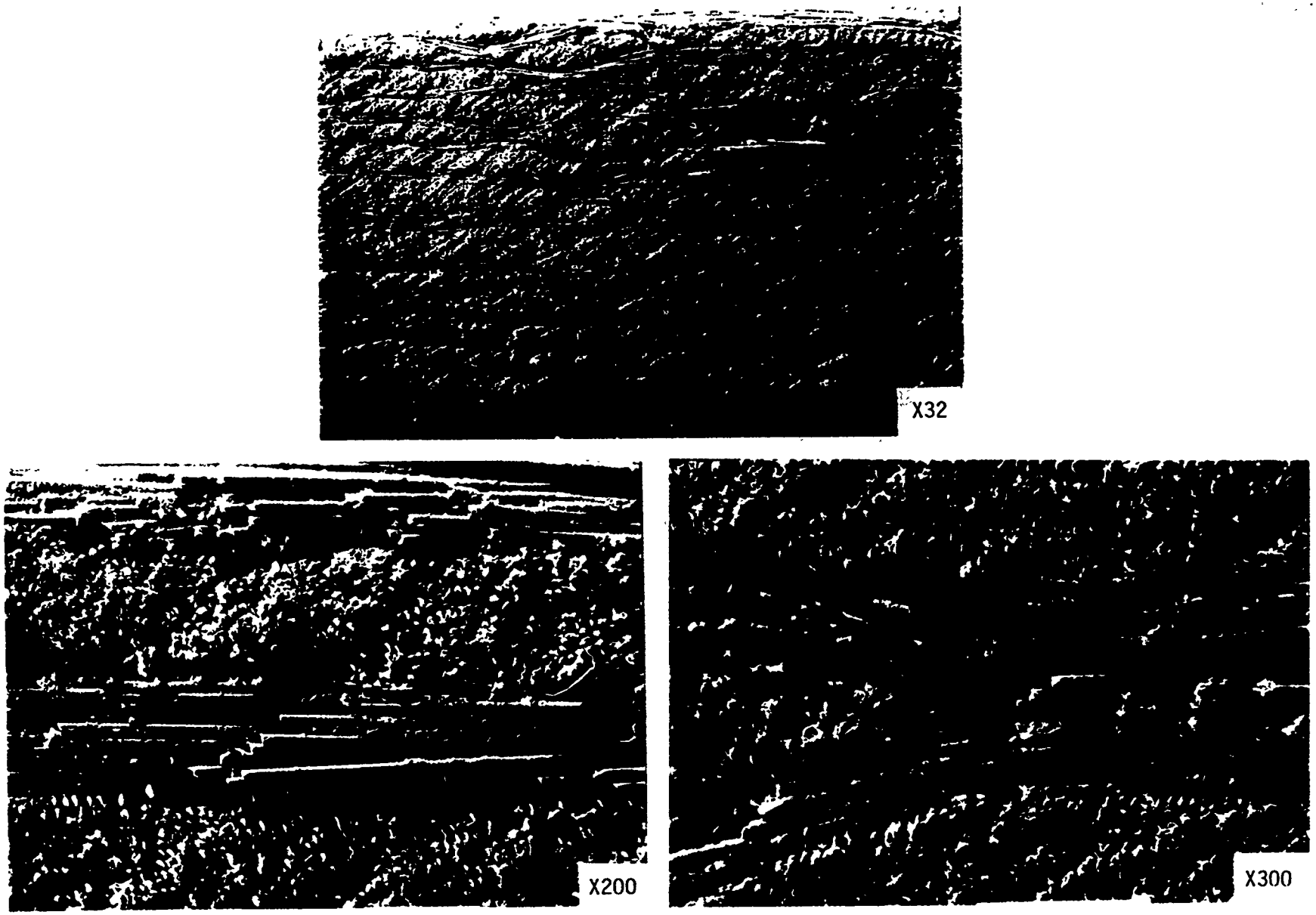

FIGURE 7. SEM PHOTOMICROGRAPHS SHOWING THE SIDE SURFACE OF SPECIMEN 5.
σ_{FLEX} = 127.60 KSI

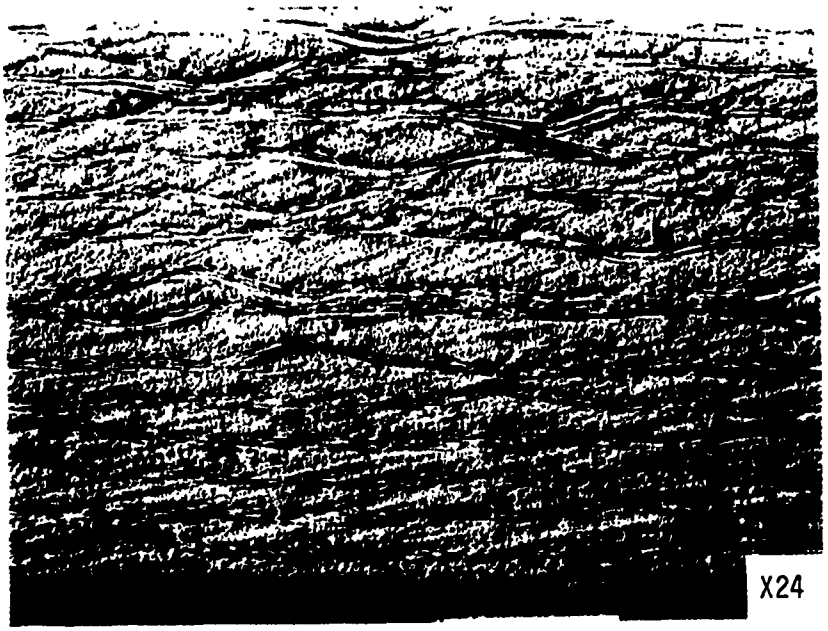

FIGURE 8. SEM PHOTOMICROGRAPHS SHOWING THE SIDE SURFACE OF SPECIMEN 9. σ_{FLEX} = 34.61 KSI

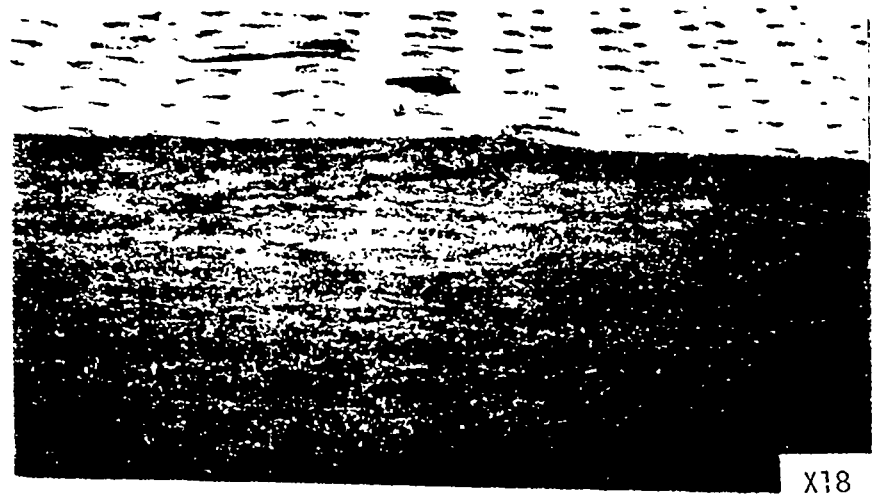

FIGURE 9. SEM PHOTOMICROGRAPHS SHOWING THE SIDE SURFACE OF SPECIMEN 15.
σ_{FLEX} = 59.00 KSI

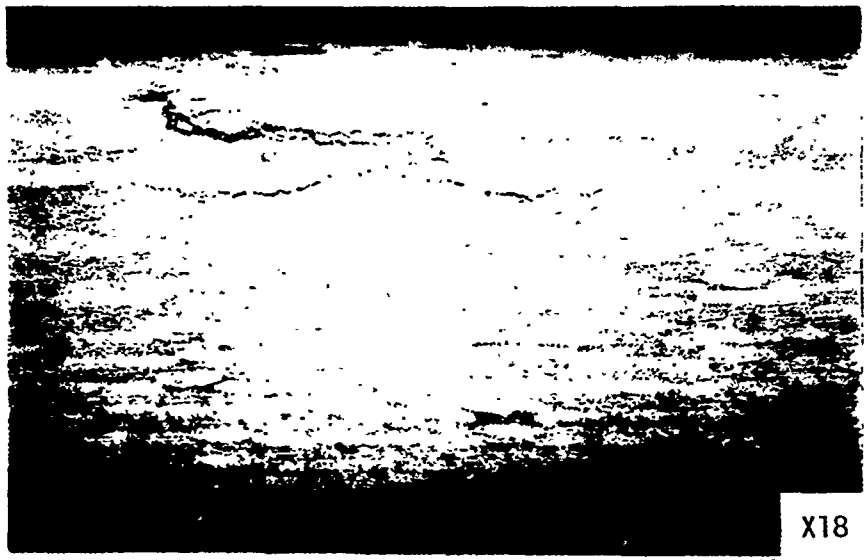

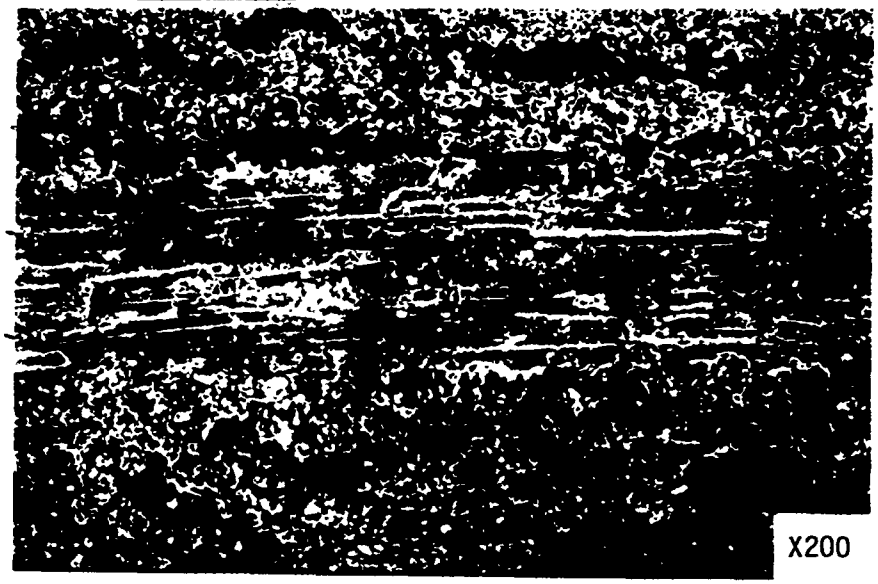

FIGURE 10. SEM PHOTOMICROGRAPHS SHOWING THE SIDE SURFACE OF SPECIMEN 22.
σ_{FLEX} = 98.55 KSI

FIGURE 11. SEM PHOTOMICROGRAPHS SHOWING THE SIDE SURFACE OF SPECIMEN 30.
σ_{FLEX} = 86.60 KSI

Specimen 15

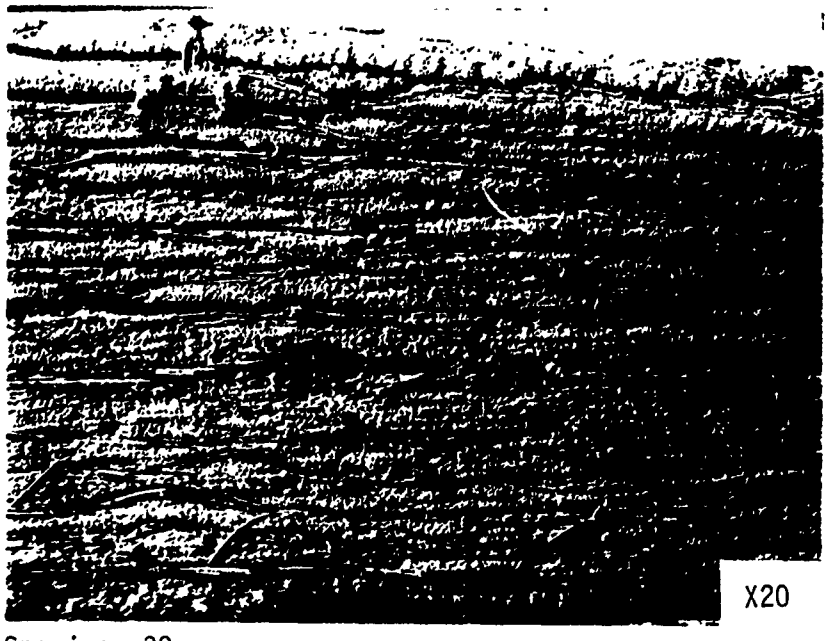

Specimen 30

FIGURE 12. SEM PHOTOMICROGRAPHS SHOWING THE SIDE SURFACES OF SHEAR TEST SPECIMENS 15 & 30
$\tau_{f,15}$ = 9.98 KSI $\tau_{f,30}$ = 7.73 KSI

(Figure 13 cont'd)

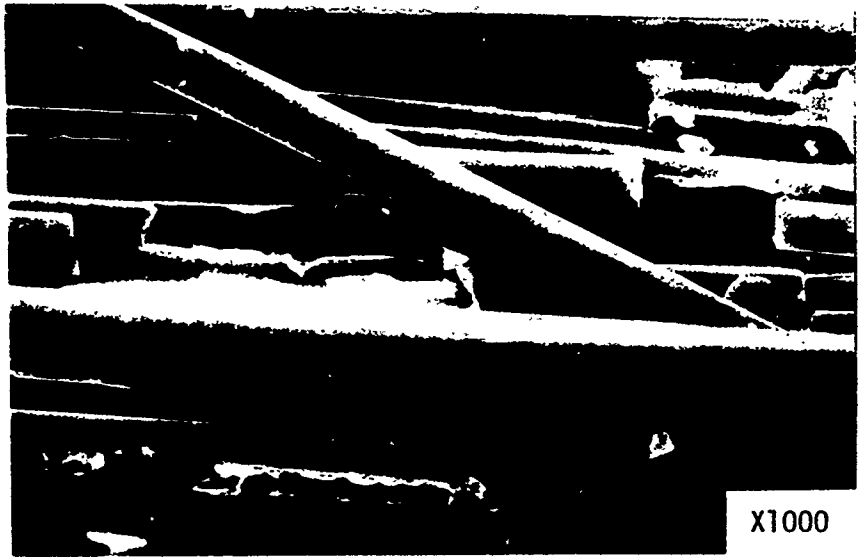

Part e

Part f

Part g

FIGURE 13. SEM PHOTOMICROGRAPHS SHOWING THE FRACTURE SURFACE FEATURES OF A FLEXURE TEST SPECIMEN.

Part a

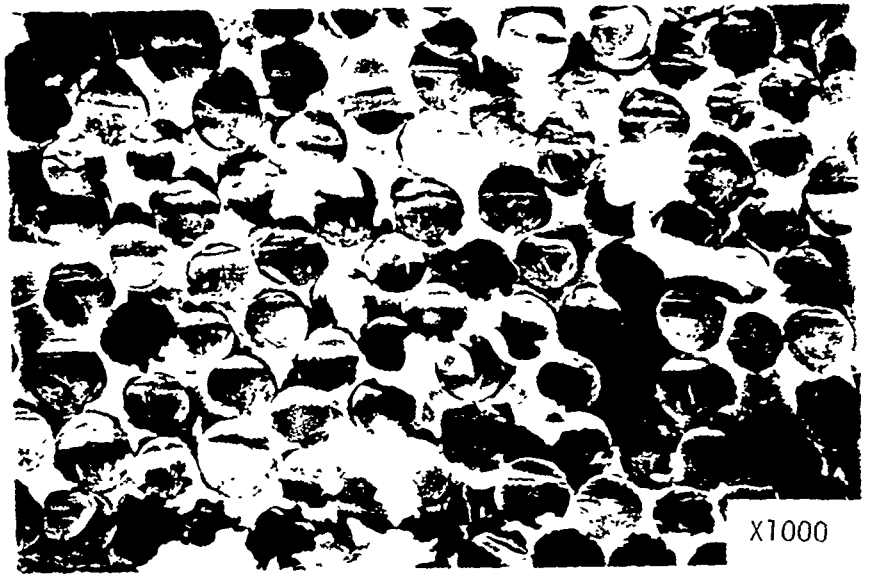

Part b

Part c

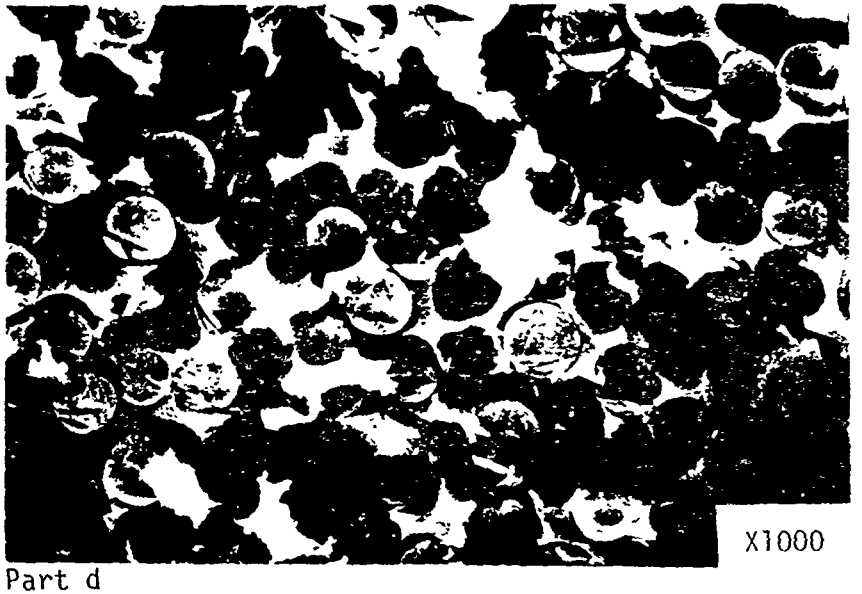

Part d

FIGURE 13. SEM PHOTOMICROGRAPHS SHOWING THE FRACTURE SURFACE FEATURES OF A FLEXURE TEST SPECIMEN. (Cont'd)

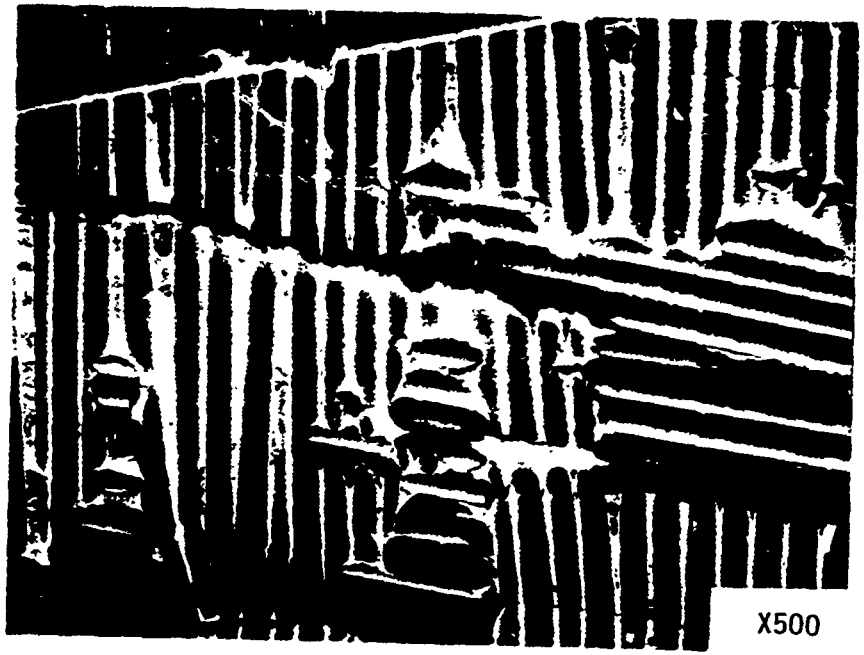

FIGURE 14. SEM PHOTOMICROGRAPHS SHOWING THE FRACTURE SURFACE FEATURES OF A INTERLAMINAR SHEAR TEST SPECIMEN. (Cont'd)

(Figure 14 cont'd)

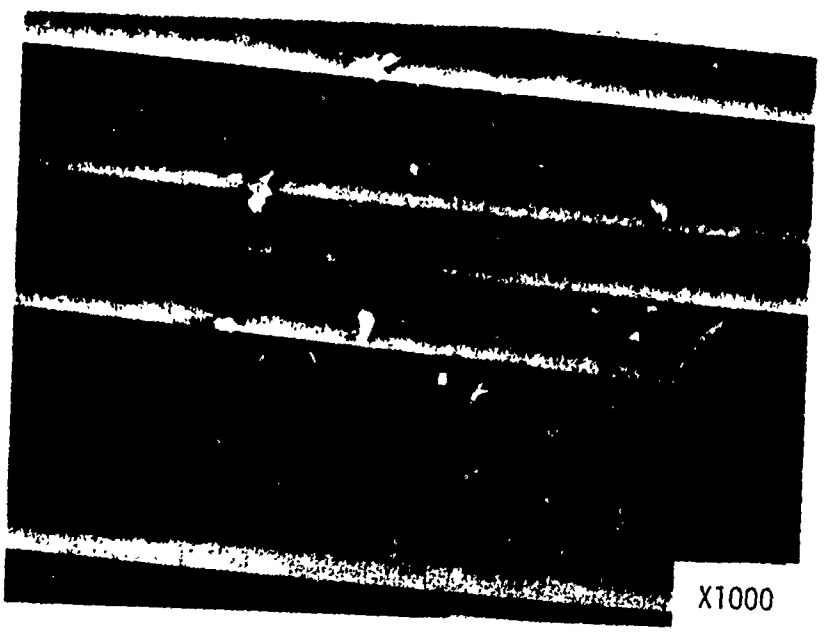

METALLOGRAPHIC ANALYSIS OF COMPOSITE MATERIALS BY FLUORESCENCE MICROSCOPY

G. Hopple
Lockheed Missiles & Space Company
Sunnyvale, California

Metallographic Analysis of Composite Materials by Fluorescence Microscopy

by George Hopple

ABSTRACT

A metallographic technique has been developed to delineate cracks and voids in organic composite materials while preserving good edge sharpness. A metallographic mount containing a composite specimen is made using standard techniques but that a fluorescing dye is added to the mounting material. When the mount is viewed in a metallograph that incorporates the proper filters, the mounting material will fluoresce brightly, thus permitting easy delineation of defects in the composite matrix. This paper presents an overview of reflected light fluorescence microscopy, a detailed description of the specific equipment and chemicals necessary to perform fluorescence microscopy, and actual applications of the technique to graphite-epoxy and glass-epoxy systems.

INTRODUCTION

Metallography of polymer matrix composite materials has been difficult to interpret in the past because of the low level of brightness and the lack of contrast between the composite matrix material and the metallographic mounting material. Generally, both materials are epoxies, and epoxies cannot be distinguished in a metallograph. The need to preserve edge sharpness and improve adhesion requires that the metallographic mount be vacuum degassed before curing. Degassing also eliminates voids (bubbles) that form during mount curing, which subsequently can entrap polishing debris and scratch the mount surface. This degassing procedure frequently fills voids and cracks and makes delineation and identification of these defects within the composite very difficult.

The most common method of preserving and delineating the edges of a metallographic specimen is by plating them with a hard metal, usually electroless nickel. This technique has been applied to the study of fractures within composites (ref. 1), however, metal deposition tends to be limited by the throwing power of the plating solution. In this respect, the metal does not plate readily in cracks or small intersticies. Moreover, it requires an additional sample preparation step. Therefore, an analysis procedure that incorporates a fluorescent dye was developed to facilitate differentiation between the mounting medium and the composite matrix material without adding an additional preparation step.

THEORY

Fluorescence microscopy techniques were originaly developed and implemented by biologists for analysis of antigens from immune reactions (ref. 2). Use of recently developed interference filters has expanded this field greatly. In the engineering disciplines, fluorescence techniques are most widely used in nondestructive testing on a macroscopic scale. The most notable example is dye penetrant testing of metals to detect surface flaws.

The physics of fluorescence is well known and a short description of the theory is useful in understanding practical applications of the technique. Fluorescence is defined as the luminescence of a substance excited by

radiation. This process is governed by Stokes law which states that the wavelength of the emitted light (luminescence) is longer than that of the excitation radiation. In other words, part of the incident energy is absorbed by the substance, while energy not absorbed is emitted again in a process known as fluorescence. One of the most potent fluorescing substances (and hence most widely used) is fluorescein. This compound absorbs light wavelengths from 450 nm to 500 nm (maximum at 490 nm) which is in the violet region of of the visible color range. Fluorescein then fluoresces at higher wavelength levels (lower energies) extending from 500 nm to 550 nm (maximum at 515 nm) which yield a yellow green color (Fig. 1). The energy efficiency for fluorescence is poor. The ratio of the intensity of excitation light to emitted light generally is no better than 100 to 1. This is the most difficult factor encountered in fluorescence microscopy and requires that the small amount of emitted light be conserved.

To observe fluorescence in a microscope, three pieces of hardware are necessary. The first is a light source that emits radiation in the blue-violet range. Most light sources (tungsten, mercury, zenon, etc.) provide this to some degree, however, the intensity varies depending on the source. The second is a filter that eliminates all light except that required to induce fluorescence; this is known as an exciter filter. The third essential piece of hardware is a barrier filter. This filter is required to suppress the original excitation light that is reflected, thereby permitting only emitted light to be transmitted. The exciter filter is positioned in the light path ahead of the specimen, while the barrier filter is positioned in the light path after the speciman (Fig. 2).

EQUIPMENT AND PROCEDURE

Based on the previous discussion, all that is needed to perform fluorescence microscopy is a fluorescing compound, a pair of filters, and a microscope or metallograph. However, to obtain high-quality images, the proper optical components must be coupled with a procedure that optimizes light efficiency.

The choice of fluorescein as the fluorescing compound was based upon its inherent high brightness of emitted light when compared to other fluorescing compounds and its wide availability. Fluorescein is available in two forms, regular or practical grade and as a sodium derivative known as uranine. Uranine originally was developed to be soluble in water, but it is also soluble in the hardening component of epoxy. In this case, 0.5 weight per cent uranine appears to be soluble in the epoxy hardening component (diethanolamine), which comprises 0.05 per cent of the total mixture when combined with the resin (Dow Epoxy Resin 332). The fluorescein is probably soluble in most epoxy compounds, and no doubt some experimentation is necessary to find the optimum solution. For convenience, the fluorescein can be mixed with a large quantity of epoxy hardener and the resulting mixture can be used when needed. The metallurgical mount containing a composite specimen is made by standard epoxy casting technique except that the fluorescein is added to the hardener.

After curing, grinding and polishing are also performed using standard metallographic techniques and the details of these procedures are presented elsewhere (refs. 3,4). It should be emphasized, however, that several problems can occur while polishing organic composites. Since the graphite fibers are brittle, they tend to chip during grinding. This is especially true for fibers normal to the polishing surface. Careful polishing using a diamond paste with

a particle size less than than that of the graphite fiber diameter on a low-nap silk or nylon cloth will normally eliminate this problem. Similarly, over-polishing with an extremely fine compound will cause rounding of the composite edges. Another problem that can occur, especially with undercured resin (composite matrix or mount), is the deposition of polishing debris on the graphite fiber surfaces. These deposits appear to be promoted by an overabundance of polishing compound on the cloth and from use of "paper" cloths. The existence of these artifacts can be verified by examining the mount in a scanning electron microscope.

It should be noted that, once the mount is ground to an area of interest on the composite specimen, a small amount of epoxy containing fluorescein can be placed on the ground surface, and the mount vacuum degassed and cured again. This procedure (known as backfilling) fills internal voids and cracks, although, subsequent grinding and polishing will uncover small, micron-sized defects. Another technique capable of filling small defects with fluorescent dye involves the use of a traditional dye-penetrant nondestructive method. With this approach, the polished mount is ultrasonically vibrated in a dye penetrant (for example, Zyglo) and subsequently cleaned and examined in the microscope. This technique detects small cracks in metals, but results in only limited success with organic composite materials. The dye-penetrant in this case tends to migrate down interfaces making interpretation difficult. Suitable modification of the dye-penetrant viscosity might eliminate this effect. In any event, this method of filling small cracks and voids is attractive and will receive further consideration as more potent and a greater variety of dye penetrants are developed.

Illumination of the mount does not require any special light, since almost every light source used on a metallograph is color balanced and will provide some radiation in the required blue-violet color range. However, for reasons discussed previously, the brighter the source, the better. The work described subsequently in this paper was carried out with a xenon source.

The best filters for fluorescence microscopy are the interference type that only recently have become available (ref. 5). Ten years ago, only colored glass or gelatin filters were available. Unfortunately, these materials had low light intensity transmittance and wide wavelength bandpass characteristics. Interference filters have much better properties although they are more expensive. They are produced by vacuum depositing thin layers of metallic salts. The thickness and refractive index of the layers can be selected to transmit or reflect specific wavelengths. Hence, there is little loss of excitation light intensity.

For fluorescein, the excitation wavelength should lie between 450 and 490 nm. This can be accomplished by using a shortwave pass filter that has a steep cut-off at 490 nm. This allows 50% of the 490 nm light and all light of a shorter wavelength to be transmitted. Since the light below 450 nm is not needed for fluorescein excitation, its elimination will reduce background light and, as a result, increase contrast. A longwave pass filter with a steep 450 nm cut-off that allows 50% of the 450 nm and all of the longer wavelength light to be transmitted can be combined with the shortwave pass filter. This combination of filters is sometimes referred to as a bandpass filter. To prevent the excitation light from reaching the observer, a longwave pass filter with a 520 nm cut-off is needed. This barrier filter would 50% of the 520 nm light and all light of longer wavelength to be transmitted.

Collectively, these exciter and barrier filters provide only the light necessary for fluorescence and prevent any overlap of exciting and fluorescing radiation (Fig. 3). Microscope manufacturers generally offer custom-designed fluorescein filter sets consisting of exciter-barrier filter combinations. Most manufacturers, in fact, offer a number of different exciter-barrier sets for fluorescein alone. The standard set incorporating the filters described above will facilitate satisfactory examination of organic composites.

A fluorescent image also can be enhanced by use of a chromatic beam splitter (ref. 6). Metallographs incorporate a semi-transparent beam splitter (mirror) that is needed to illuminate the specimen and to provide an image for viewing. This mirror reduces the light to the observer by 50%. For fluorescence microscopy, this loss of light intensity is unnecessary. The standard mirror can be replaced by an interference mirror, which, like the filters, selectively splits the beam according to wavelength. With fluorescein, light wavelengths below 510 nm would reach the specimen for excitation, while light above 510 nm would be transmitted through the mirror. For emitted light, the opposite effect would occur (Fig. 4). This not only provides a brighter image to the observer, but also enhances contrast. In practice though, the chromatic beam splitters are not particularly efficient devices and cannot be used alone.

Unfortunately, the beam splitter cannot be removed without considerable effort from most metallographs. Good results still can be obtained with just exciter and barrier filters. The exciter or bandpass filter can easily replace the removeable green filter or diffusion filters near the light source. Placement of the barrier filter, however, can be more difficult. Since practically all metallographs have removeable binoculars, the barrier filter can be placed in the light path at this location. In any event, the microscope manufacturer can and should be consulted as to selection and placement of filters. When using a Zeiss Axiomat metallograph, the entire assembly consisting of interference filters and mirror can be conveniently housed in a replaceable module. This allows a quick change from standard to fluorescent microscopy.

Fluorescent specimen mounts can also be observed and photographed at low magnifications using a graphics camera. Oblique lighting with an ultraviolet (UV) source provides sufficient illumination. Although commercial UV mercury sources used in dye-penetrant testing have a spectral output centered on 365 nm (ref. 7), they apparently provide sufficient light in the blue-violet range to excite fluorescein. Thus, only a barrier filter is needed to allow the fluorescent emitted light to be transmitted. This filter is easily inserted in the camera. A glass barrier filter will provides good results since the emitted light from the fluorescent dye is more concentrated at low magnifications.

One of the problems with photographing the fluorescing images is that exposure times are long due to the low intensity of light. The metallographic photographs of the fluorescent images that appear later in this report were about 15 minute exposures; those taken on a graphics camera were 2 minute exposures. Both images were recorded on type 52 Polaroid film (ASA 400). Negatives were taken with either Kodak Extapan (ASA 75) or Royal pan (ASA 400). Higher speed film will provide faster exposures at the expense of resolution. Adequate results could probably be obtained with type 57 Polaroid film (ASA 3000) and Kodak Royal X-Pan (ASA 1000).

APPLICATIONS

The first example is of a glass-epoxy composite that sustained impact damage. Visually, the damage did not appear extensive. However, when the material was cross-sectioned through the impact points, extensive delamination was detected (Fig. 5). Photography using a graphics camera was sufficient to delineate the fracture paths in this sample. This material was manufactured without use of a pressurized autoclave and, hence, had a considerable amount of porosity. Since the strength of the composite is related to the amount of porosity present, an accurate assessment of the amount of porosity (especially with regard to fracture path) was needed. This was accomplished only because the mounting material could easily be differentiated from the composite matrix material after the fractures allowed mounting material to seep into the pores (Fig. 6).

It can be seen that a difference between the resin-rich regions and the pores filled with mounting material also exists in the photograph taken for comparison (Fig 6a). This is because the comparison photograph was taken by removing the exciter filter (which incidently provides a green light similar to that used for black and white photography). Even without the exciter filter, the brightness of the fluorescein can be seen with use of only the barrier filter and chromatic beam splitter. This example also illustrates one of the problems with this system, light smearing. Both the fibers and the epoxy are translucent. At the matrix epoxy-mounting epoxy interface, some of the light emitted by the fluorescein containing epoxy will cause the matrix epoxy to be brighter. This light smearing can make analysis difficult in some cases.

Fluorescence microscopy can delineate fracture paths in graphite epoxy and thus provide valuable failure analysis information. This was demonstrated in an analysis of a graphite-epoxy panel that was failing mechanical properties. Subsequent metallographic analysis indicated that the fracture paths were confined to specific prepreg plys (Fig. 7). These prepreg plys were traced to a lot that was found to be defective.

A common fiber composite failure mode is delamination. Scanning electron microscopic (SEM) photography is useful in characterizing the fracture surface morphology as to the presence of hackles (Fig. 8). However, the SEM photographs rarely can provide information to determine whether the lack of hackles was due to resin starvation or adhesion failure. In this example, fluorescence metallography conclusively showed that the failure was due to a lack of adhesion between the epoxy and the carbon fibers (Fig. 9). Moreover, the adhesion failures could be characterized as to the percent of the average fiber circumference the adhesion failure had propagated. This failure resulted from an improper curing cycle. This adhesion fracture appears much different than that of a typical fracture that has hackles (Fig. 10). Note that the light smear problem described earlier tends to obscure the hackles which makes the hackle direction difficult to assess. (Fig. 10b).

This fluorescence analysis system has many failure analysis applications in addition to those presented in this paper. Metallographic examination of polymer fractures is almost always enhanced when the mounting material can be differentated from the polymer of interest. This technique has been found useful in examination of defects in wire insulation and polmer coatings. Another unique application is the detection and tracking of leak paths in electronic components.

REFERENCES

1. Morris, G. E. "Determining Fracture Directions and Fracture Origins on Failed Graphite/Epoxy Surfaces", ASTM STP 696, R. B. Pipes, ed., 1979, p. 282.

2. Coons, A. H., "The Application of Fluorescent Antibodies to the Study pf Naturally Occurring Antibodies", New York Acad. Sci. Ann. 69, 1957, p. 658-662.

3. T. J. Bertone, Metallographic Specimen Preparation, Optical and Electron Microscopy, J. L. McCall and W. M. Mueller, ed. Plenum Press, 1974, p. 251-273

4. Clements, L. L., "Fiber Composite Materials", to be published in vol. 9 of the 9th edition of Metals Handbook entitled Metallography and Microstructure.

5. Holz, H. M. Worthwhile Facts about Fluorescence Microscopy, Zeiss Publication, Available from Carl Zeiss, Inc., p. 17

6. Ibid. p 25.

7. Betz, C. E., Principles of Penetrants, Magnaflux Corporation, Chicago, Il, 1969, p. 202.

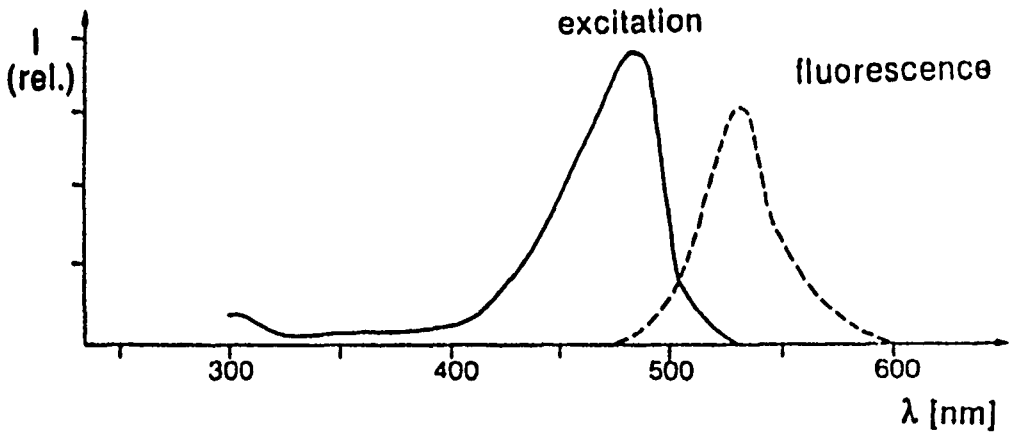

Fig. 1. Absorption and fluorescence spectra for fluorescein. Courtesy of Carl Zeiss, Inc.

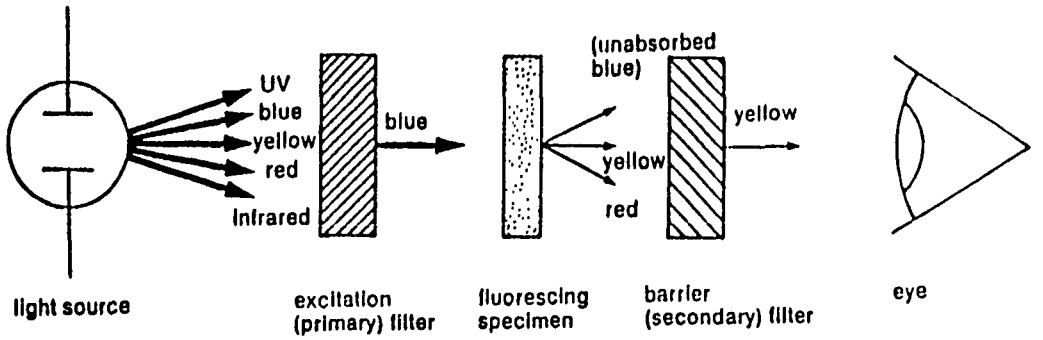

Fig. 2. Diagram of equipment necessary for fluorescein fluorescence microscopy. Courtesy of Carl Zeiss, Inc.

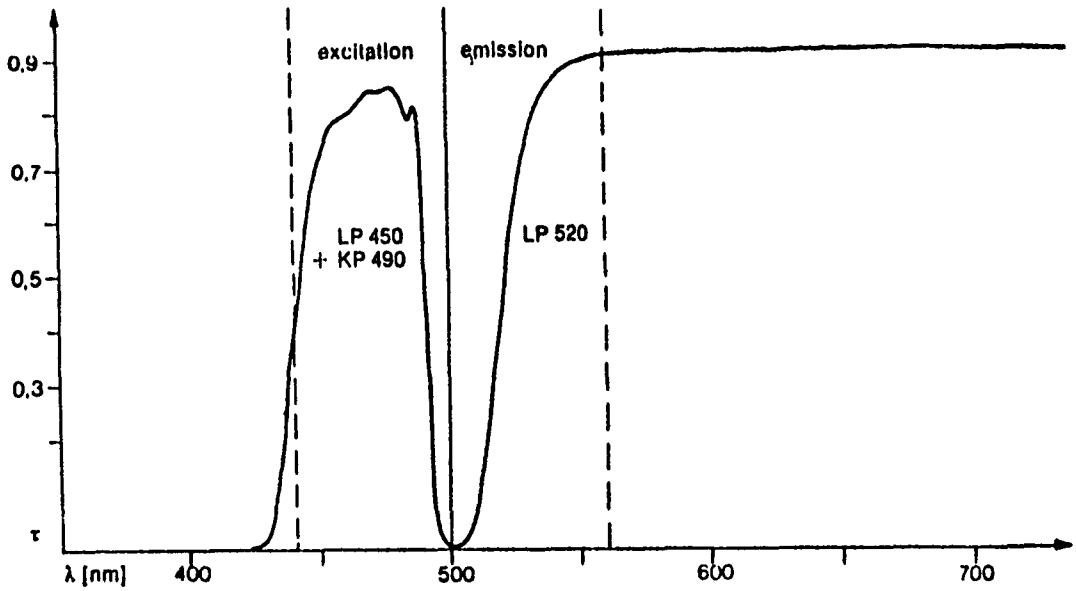

Fig. 3. Filter set charateristics for fluorescein fluorescence microscopy incorporating a set of exciter filters (LP 450 and KP 490) and a barrier filter (LP 520). Courtesy of Carl Zeiss, Inc.

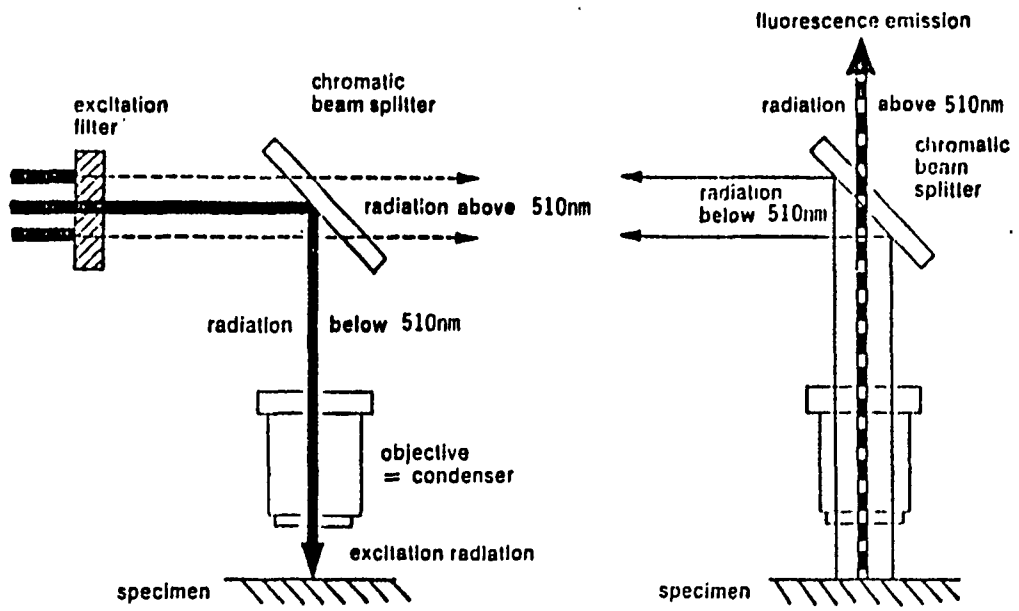

Fig. 4. Fluorescence microscopy using a chromatic beam splitter. Courtesy of Carl Zeiss, Inc.

Fig. 5. Fluorescent photomacrograph of a glass-epoxy composite cross-sectioned through an impact point. Extensive delamination is evident.

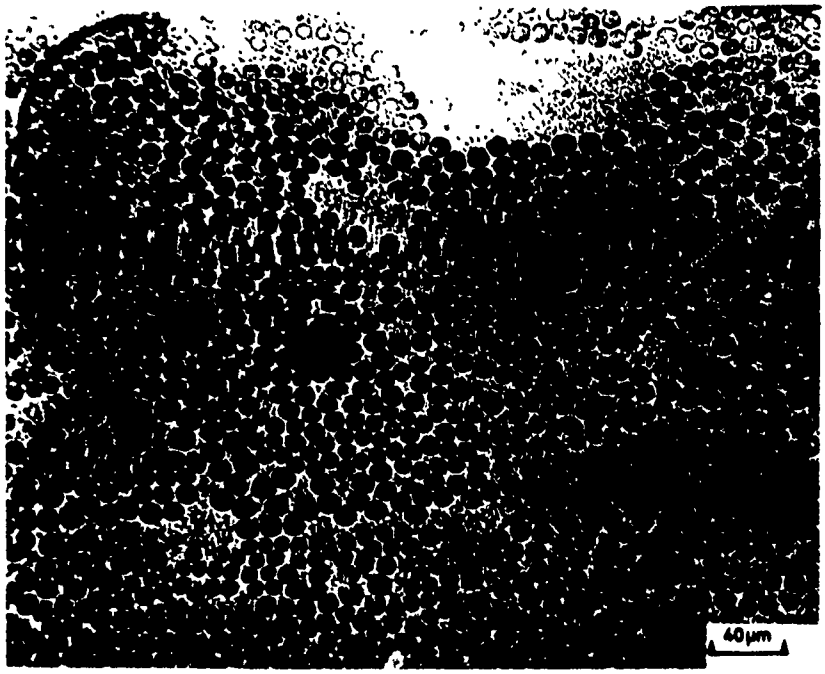

(a)

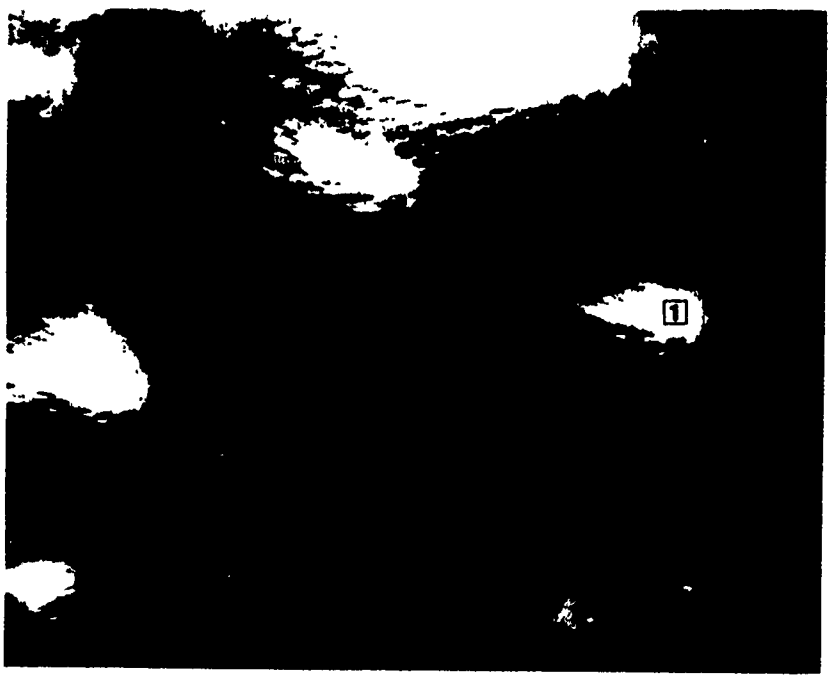

(b)

Fig. 6. Brightfield (a) and fluorescent brightfield (b) optical micrographs of a glass-epoxy composite. A pore filled with fluorescent epoxy (1,b) can be differentiated from a resin rich region (2,b).

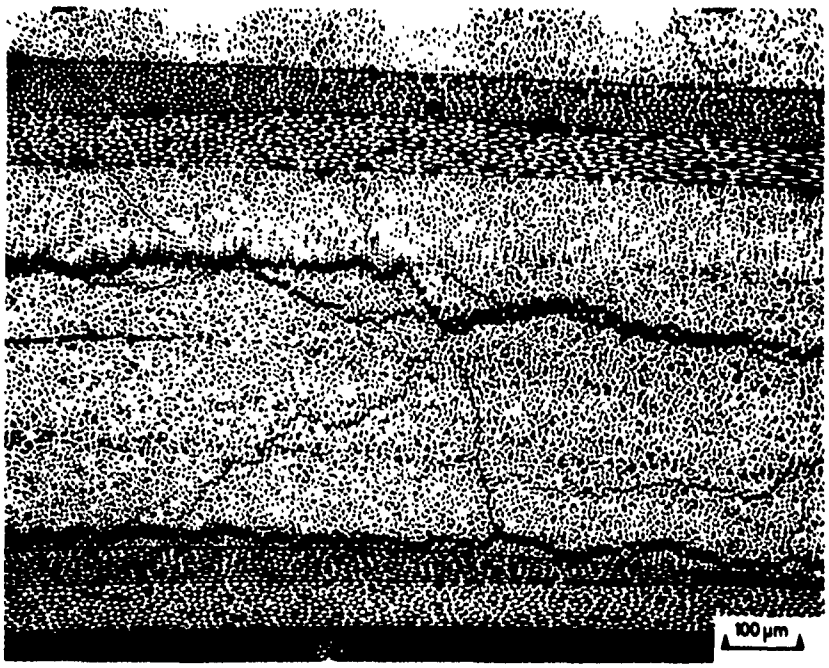

(a)

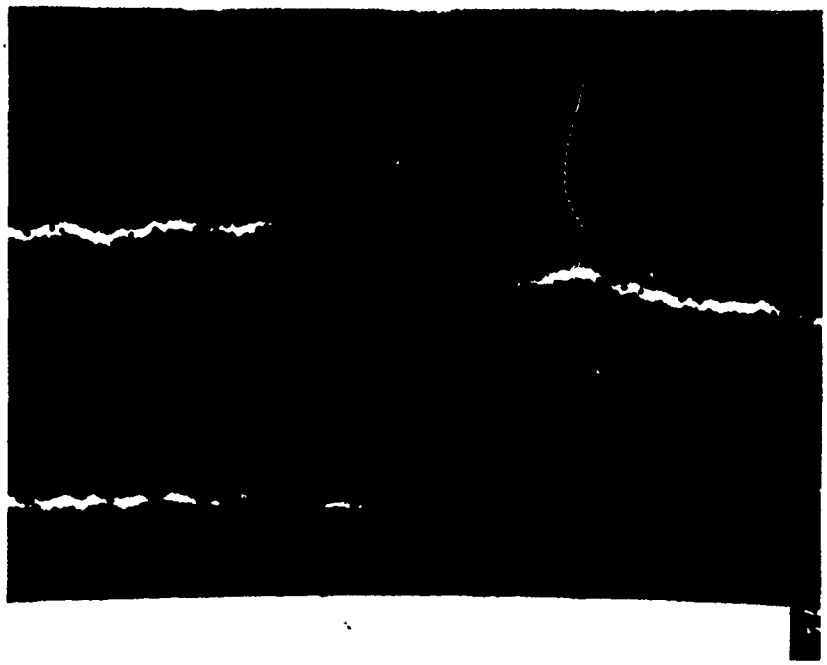

(b)

Fig. 7. Brightfield (a) and fluorescent brightfield (b) optical micrographs of a crackpath in a specific ply of a graphite-epoxy composite.

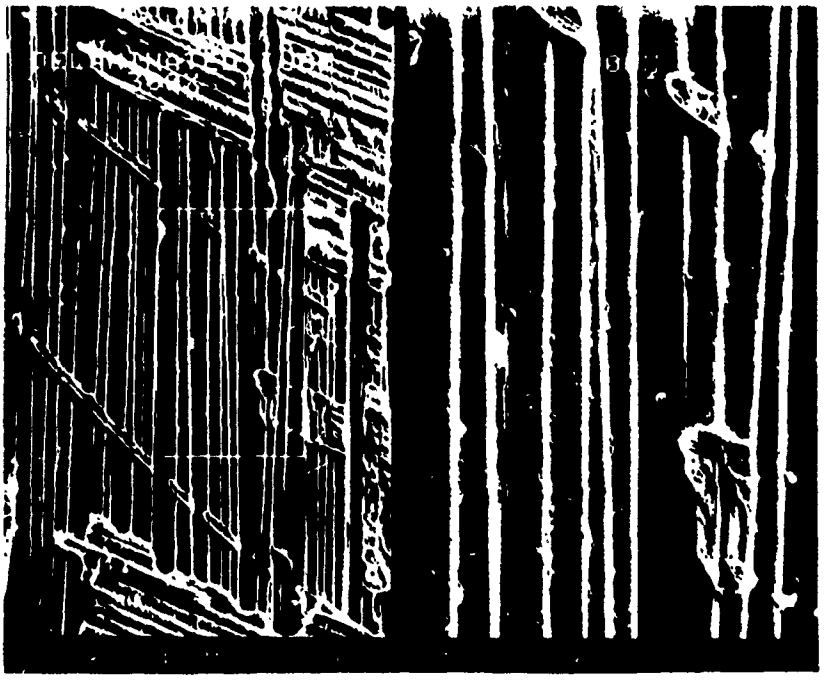

(a)

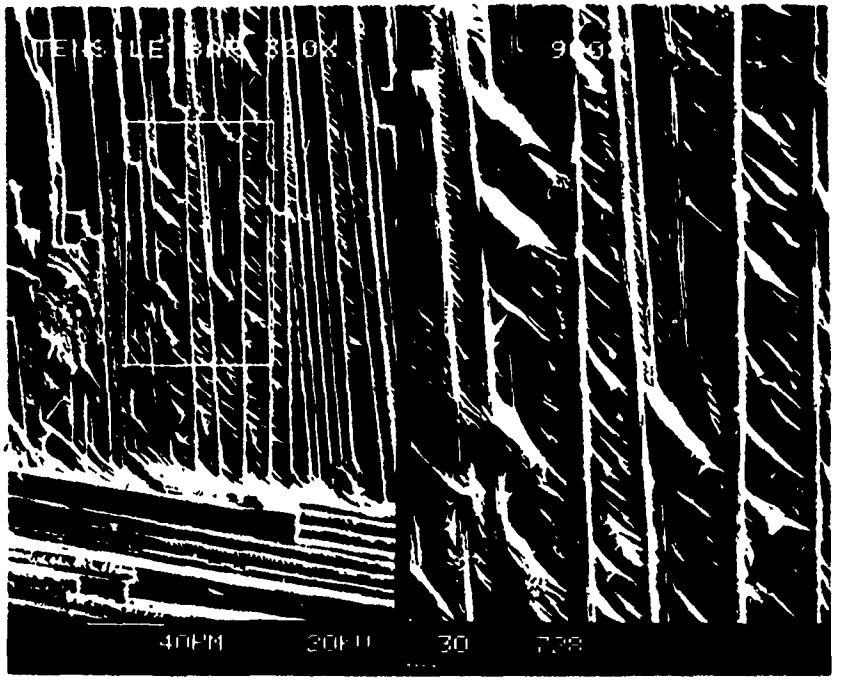

(b)

Fig. 8. Electron micrographs of a smooth fracture surface (a) and a fracture surface with hackles (b) in a graphite-epoxy composite.

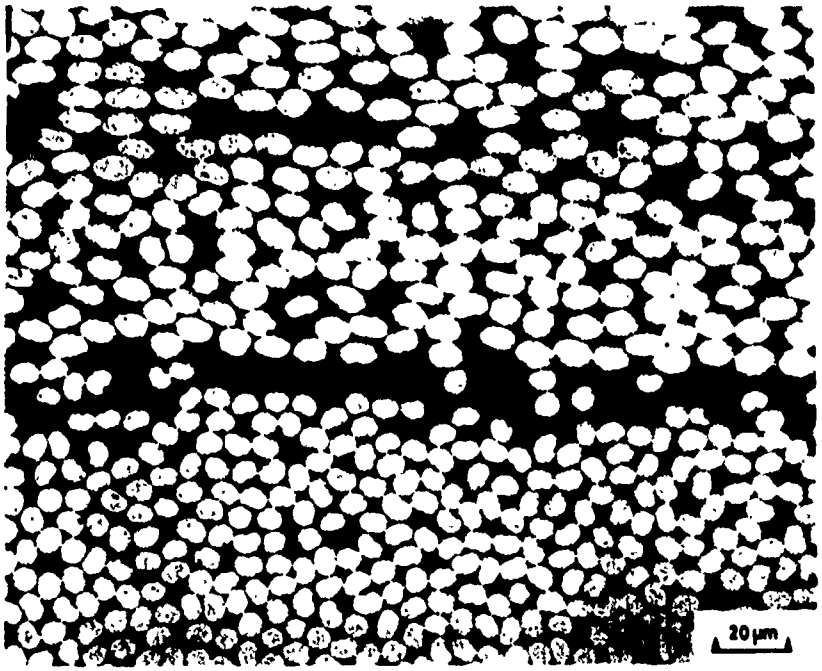

(a)

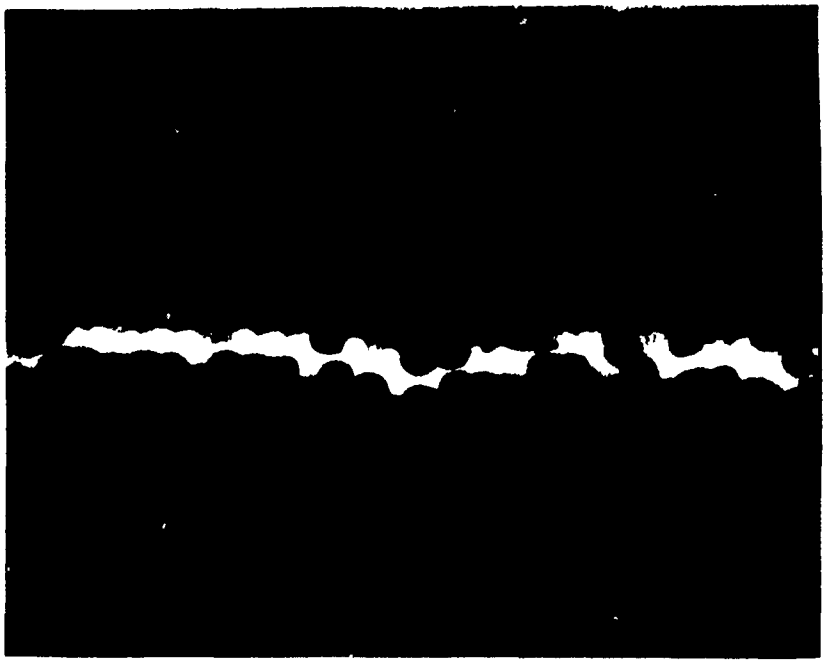

(b)

Fig. 9. Brightfield (a) and fluorescent brightfield (b) optical micrographs of a graphite fiber to epoxy matrix adhesion failure. Compare to Fig. 8a.

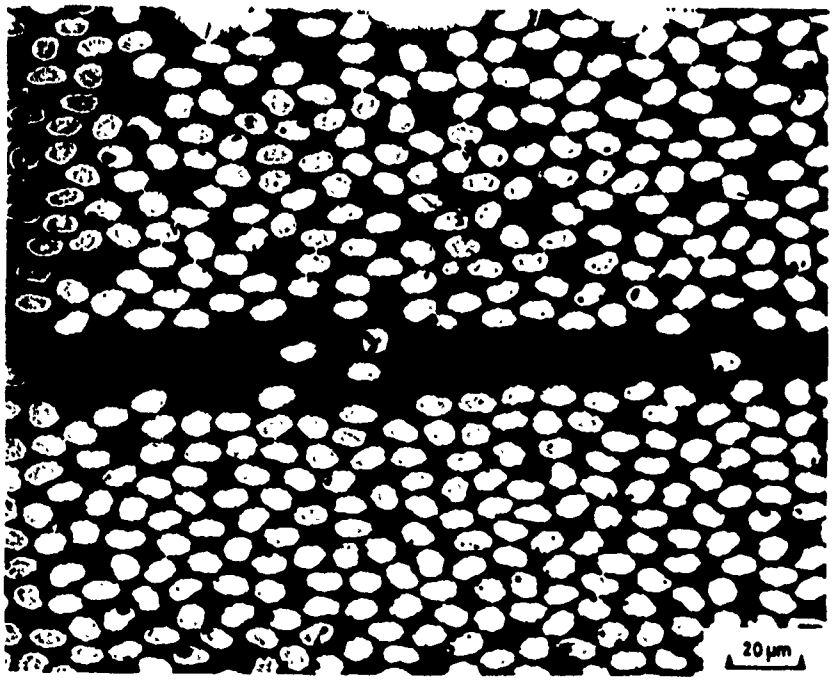

(a)

(b)

Fig. 10. Brightfield (a) and fluorescent brightfield (b) optical micrographs of a fracture with hackles. Compare to Fig. 8b.

A NEW METHOD FOR NONDESTRUCTIVELY EXAMINING BONDED STRUCTURES

R.D. Adams and A.M. Allen
Department of Mechanical Engineering
University of Bristol
Bristol, England

and

P. Cawley
Department of Mechanical Engineering
Imperial College
London, England

A NEW METHOD FOR NONDESTRUCTIVELY EXAMINING BONDED STRUCTURES

by

Robert D. Adams and Anne M. Allen
Department of Mechanical Engineering
University of Bristol
Bristol. BS8 1TR
U.K.

and

Peter Cawley
Department of Mechanical Engineering
Imperial College
London. SW7 2BX
U.K.

Presented at the 'International Conference on Post Failure Analysis Techniques for Reinforced Composites' at Dayton, Ohio, July 1985.

1. INTRODUCTION

It is essential to be able to interrogate bonded structures and composites to establish the existence and extent of fracture surfaces in the investigation of damage propagation. Even though the structure may have experienced initial failure, it may not yet have failed catastrophically. Sometimes, for cost considerations, it is essential to keep a component in service for as long as possible, while monitoring the crack or other damage propagation so as to avoid failure occurring under load - particularly if the structure concerned is class 1 airframe. On the other hand, in laboratory investigations of progressive failure, such as by fatigue loading, it is important to correlate crack growth (or damage area) with load history.

In composites, failure often takes place by interlaminar shear or transverse tensile cracking. It is possible to detect such damage using standard ultrasonic techniques using immersion C-scan or robot-controlled jet probes. For many composites, particularly if woven cloth or honeycomb is used, or if the fibres are absorbent, it is essential to avoid contact with water as this may cause environmental problems in addition to the intentional loading.

One test which is widely used, albeit often covertly, is the coin-tap test. Until recently, this test has been largely subjective and there has been considerable uncertainty about the underlying physical principles. In this test, defects are located by tapping the structure, adjacent good and defective areas being detected by subjective acoustic assessment of the resultant structural response. An instrument has been developed in the U.S.S.R. which quantifies the structural response by indicating the acoustic amplitude at a series of pre-set frequencies. This instrument is, in effect, a quantified ear.

It should be stressed that this test is quite different from the "wheel-tap test" even though the testing technique and subjective interpretation of the sound produced is similar in both cases. The wheel-tap test is a global test which investigates the whole test component from a tap applied at a single point, the difference between good and defective components being determined from acoustically-detected changes in the natural frequencies and damping. The coin-tap test will only find defects in the region of the tap, so it is necessary to tap each part of the structure under investigation.

2. BACKGROUND

When a structure is tapped, the sound produced is mainly at the frequencies of the major structural modes of vibration. The frequencies and modes of vibration are structural properties which are independent of the position of excitation. By applying the same impulse to two adjacent good areas, similar sounds will be produced. The difference in the sound produced when adjacent good and defective areas are tapped must therefore be due to a change in the characteristics of the force input.

When a structure is tapped by a coin or a light hammer, the characteristics of the impact depend on the local impedance of the structure and on the impactor. Damage such as an adhesive disbond results in a local decrease in structural stiffness and hence a change in the nature of the impact. The time history of the force impulse may be measured by a force transducer. Typical force-time histories from taps on sound and de-bonded areas of an adhesively bonded structure are shown in Fig. 1. On the sound structure, the impact is more intense and of shorter duration than that on the damaged area. Typically, an impact duration of about 1 millisecond will be measured on a sound structure.

The force pulse may therefore be used to indicate good or defective local parts of a structure. By establishing a standard value for a pulse on a good area, the rest of the structure, or even similar structures, can be interrogated. The pulse is characterised by its magnitude, P, and its time duration, T. (Fig.1). The time duration can be measured for any value of force, although the zero value is often convenient. The main problem is in providing a consistent means of applying the impulse. If the size of the applied impulse varies, then so will P, even over a sound area. The time period T is only weakly dependent on variations in the impulse, but it is much less easy to measure. However, provided a consistent impulse can be obtained, this method is quite suitable for interrogating structures.

The difference between the two impulses is more readily quantified if the *frequency content* of the force pulses is determined. A Fourier transform is carried out on the force-time records, and corresponding spectra derived from the force-time histories shown in Fig.1 are given in Fig.2. The impulse on the damaged area has more energy at low frequencies but the energy content falls off rapidly with increasing frequency, while that on the sound area has a much lower rate of decrease of energy with frequency. Thus, the impact on the good area excites the higher structural modes more strongly than does the impact on the defective zone. The sound produced at a bad area will therefore be at a lower frequency and the structure will sound "dead".

The frequency spectrum of the impulse contains more identifiable characteristics than does the force-time pulse alone, and it is therefore more amenable to analysis via pattern recognition techniques. Although the height of the spectrum will again be dependent on the magnitude of the impulse, the *shape* of the curve is little unchanged, so the chance of erroneous results being obtained due to variations in the velocity of the tapping head at impact are greatly reduced.

3. THE TAPOMETER

A prototype instrument, called the 'Tapometer', has been produced. This can be used in either the time domain or the frequency domain to compare good and bad areas on a bonded or composite structure.

The unit which produces and measures the impulsive force consists of an electromagnetic relay which is pulsed with an electric current for about 20 msec. This accelerates the tapping head, which incorporates

a piezoelectric force transducer, towards the surface of the test object. The head strikes the surface at some suitable velocity, typically in the region of 0.1 to 0.5 m/sec. One version of the tapping head is shown in Fig. 3.

Force-time characterisation

It is possible to use the unit in the time domain such that a force-time pulse is output to an oscilloscope screen where it can be compared with a standard pulse for a good component which has been stored in the memory. The head can be hand held, or attached to the frame of a C-scan apparatus which is driven to and fro across the specimen and indexed along it in the same way as the conventional ultrasonic C-scan. A signal proportional to the magnitude of the pulse was output to a quantiser and so to a recorder using voltage breakdown on electrosensitive paper. An alternative is to use the digital information to input to a grey or colour monitor, different shades of grey or colours representing different levels of damage. A test on a honeycomb sandwich plate with built-in defects is shown in Fig.4. All the defects were found and it was often possible to see the shape of the honeycomb cells when testing such plates.

Force-frequency characterisation

It is possible to carry out various pattern recognition procedures on the Fourier transform of the pulse, outputting a single number or a series of numbers to give a quantitative measure of what can easily be discerned by eye. Although it is quite easy to use the eye to determine a good section from a defective one, by comparing with a standard "good" spectrum, this is not always convenient, even when doing manual testing. The pattern recognition can be manipulated from the digital force-frequency data so that a pass or fail level is established for a given series of structures, a buzzer or red/green light indicating failure. The tapping head can then be moved by hand over the surface and the operator does not have to make repeated reference to a screen.

Alternatively, a scanning frame can be used to traverse the head over a structure, giving a hard copy of the defect map, or whatever other realisation is required.

4. CONCLUSIONS

A prototype instrument, called a 'Tapometer' has been built which incorporates both time-domain and frequency-domain methods of comparing

mechanical impulses on good and bad areas of a structure. The Tapometer will work wherever "coin-tapping" has been used but, being quantitative and hence more discriminatory than the old subjective test, it can be carried out by relatively unskilled operators and is more sensitive. Being quantitative and recordable, it can be used to "legalise" this age-old method.

The technique has been used successfully on a wide variety of composite and honeycomb structures. It can be used on a point-by-point basis, comparing the pulse with a standard stored in a memory, or it can be connected in a scanning frame to produce a map of a structure in the same way as an ultrasonic C-scan immersion tank. The technique can show any form of defect which causes a local loss of stiffness. Examples are crushed honeycomb, delaminations in sandwich structures, delaminations in solid fibre reinforced plastics, adhesive debonds, and so on. Some of the components tested were so lossy that even in their "good" form, it was virtually impossible to send ultrasound through them for conventional ultrasonic NDT. By using this technique, it is therefore possible to monitor the growth of cracked areas in some structures which often cannot be examined by any other method.

A particular advantage of the Tapometer is that it is used dry and no couplant is necessary between the tapping head and the test structure. This is a great advantage when testing many honeycomb and fibre reinforced composites, especially where woven or porous material is concerned.

A commercial unit should soon be available (late 1985) and it will be similar in size to a conventional ultrasonics set.

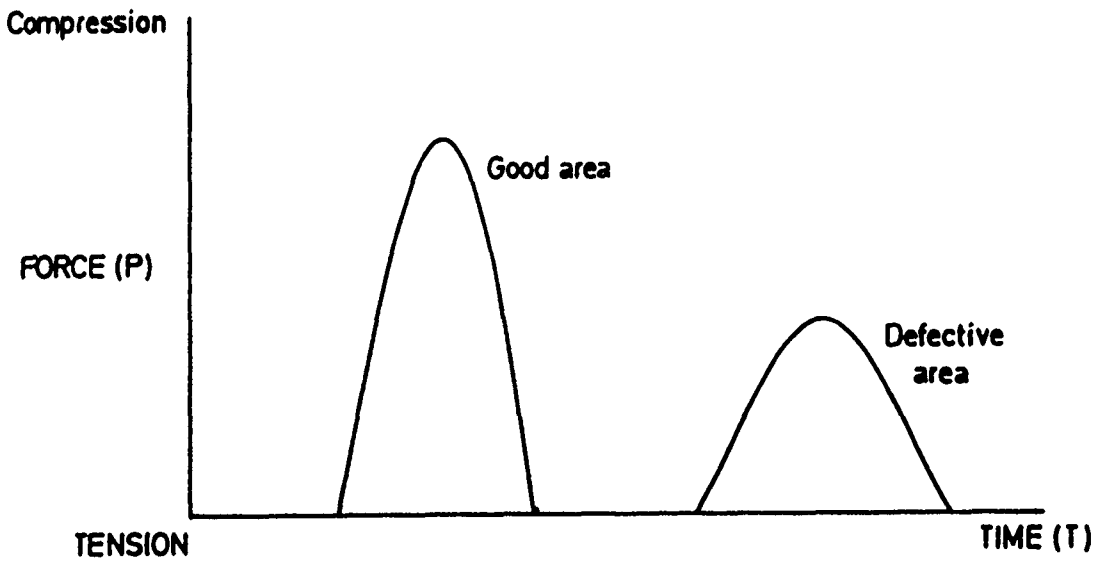

FIG.1. Time domain representation of a force impulse.

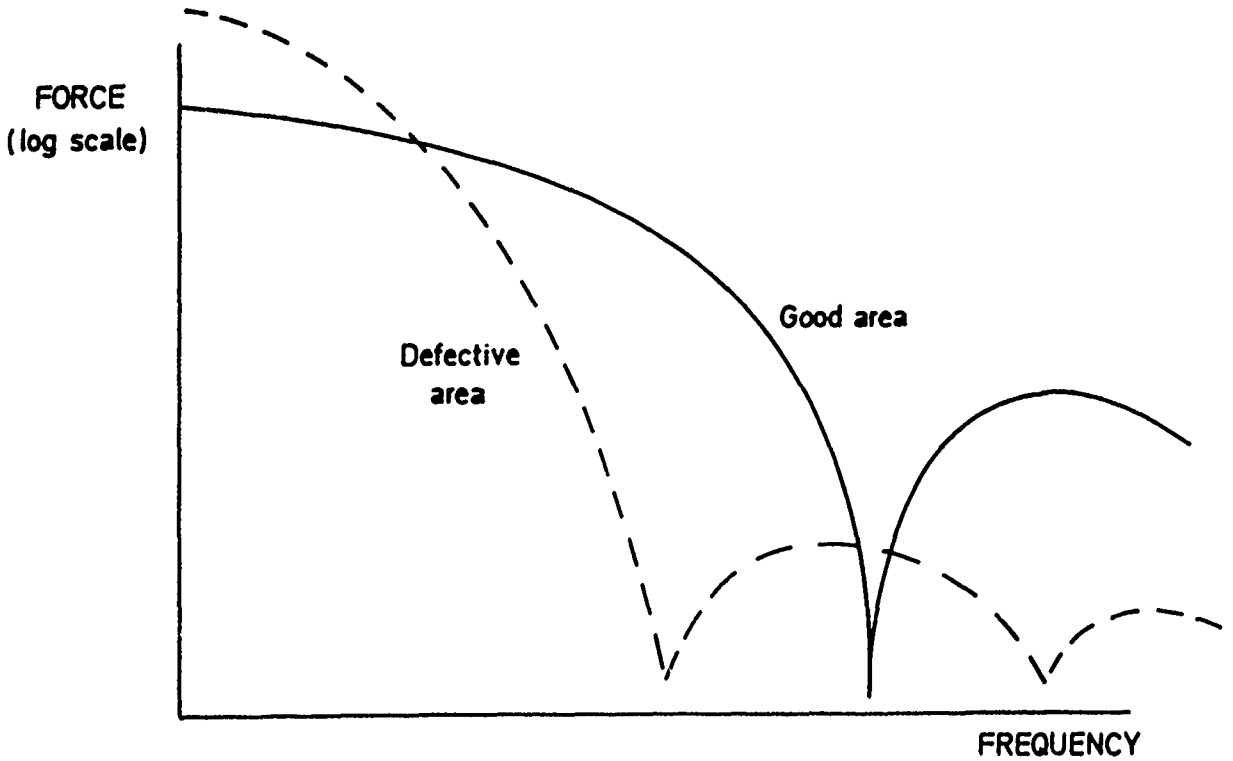

FIG.2. Fourier Transform of the impulse to give frequency-domain information.

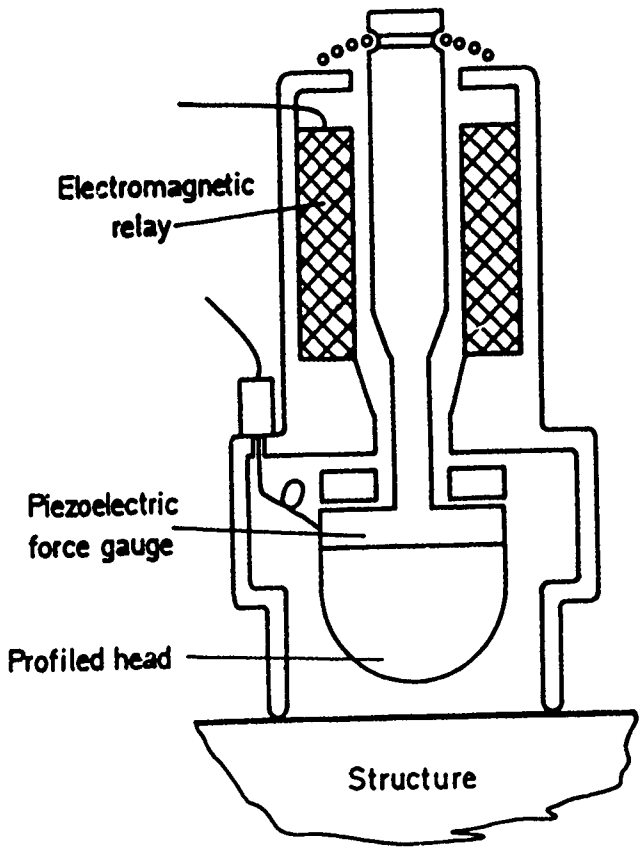

FIG.3. TAPPING HEAD

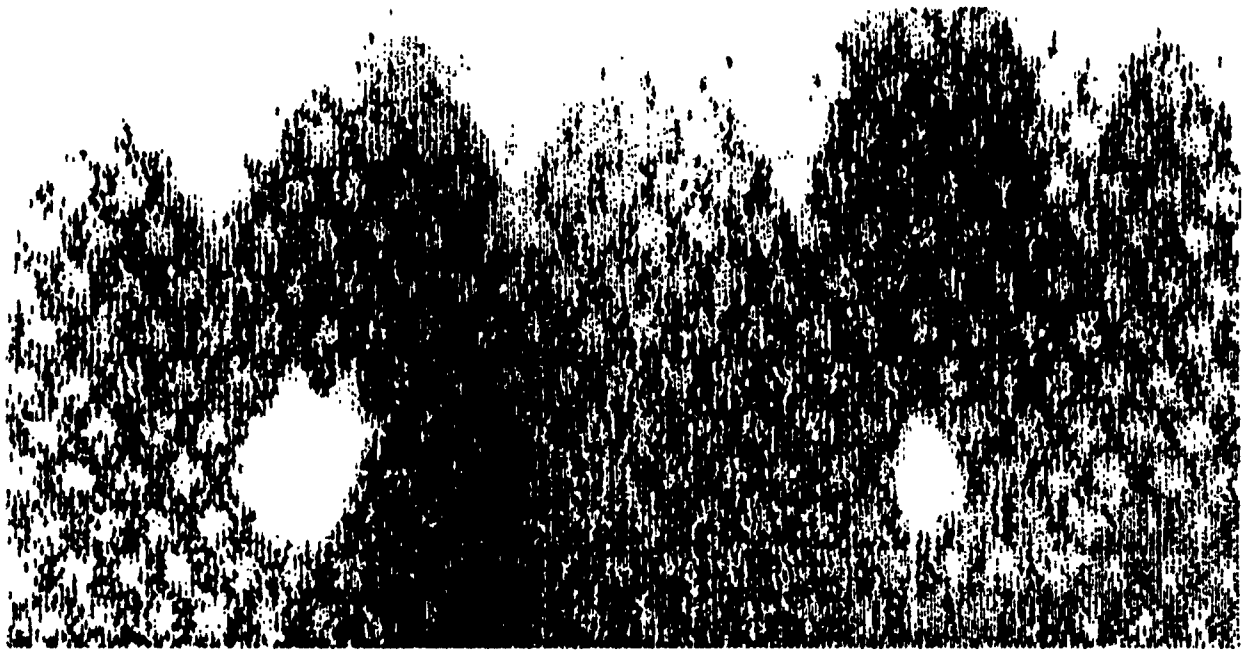

FIG.4. Scan of defective honeycomb laminate containing circular disbonds and edge areas where triangular shims have been pulled out between the skin and the core.

ON-SITE INSPECTION BY COMPACT TV-HALOGRAPHY

O.F. Lokberg
Physics Department
University of Trondheim
Trondheim, Norway

ON-SITE INSPECTION BY COMPACT TV-HOLOGRAPHY.

OLE J. LØKBERG
PHYSICS DEPARTMENT, TECHNICAL UNIVERSITY OF NORWAY
N-7034 NTH, TRONDHEIM, NORWAY

ABSTRACT. In this paper we describe how holographic measuring techniques are combined with the speed and convenience of video recording and display to give a real-time system which can be used to reveal extremely small movements. In this way the behaviour of the test objects can be studied in great detail. By various excitations like heating, pressure and vibrations we are able to observe object defects and structural weaknesses.
We describe briefly the system's construction, its modes of operation and give some examples of its applications.

I. INTRODUCTION

Different holographic techniques has been used for a wide variety of applications in industrial research since modern laser holography was introduced about two decades ago. Of special interest for industrial purposes has been the hologram interferometry technique whereby tiny movements of the test object are revealed as contour lines representing constant movement across the image of the object. A very comprehensive description of the technique and its application area can be found in the book by Vest (1). However, with a few notable exceptions, hologram interferometry has been mainly confined to the laboratory surroundings and has not found much use for on-site inspection. This is mainly due to stability problems which can be solved by use of pulsed lasers, but these lasers are bulky and expensive. In addition the conventional holographic process is based upon the use of photographic film whereby the slow and cumbersome development process prohibits an effective inspection rate.
In this paper we describe how the inspection rate of hologram interferometry can be greatly speeded up by recording the holograms directly on the photosensitive surface of the video-camera and reading out the image by electronic processing. The resulting TV- holography system is usually called ESPI (electro-

nic speckle pattern interferometry) in the optical literature. ESPI provides pictures of lower quality than conventional holography, but this is amply outweighed by the speed and real time operation of the system. In a way we are faced with the same situation as in ordinary pictorial recording in reseach and industry. Although photography undoubtedly gives superior quality pictures and therefore is chosen for documentation purposes, video systems are the logical choice for real-time surveillance, inspection and automation.

II. THE ESPI SYSTEM

We will describe the ESPI-system briefly with reference to the flow chart depicted on fig.1. Readers which are interested in a more complete description of the technique should consult e.g references (2 - 4).

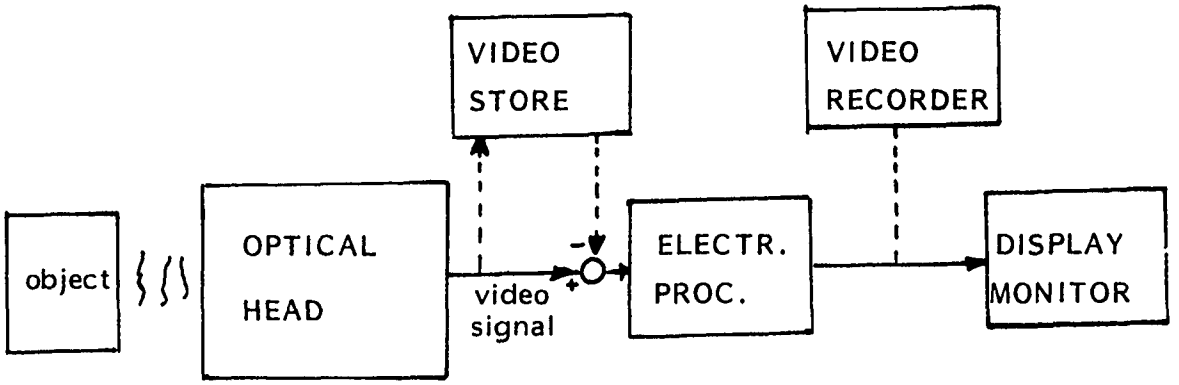

Fig.1
The ESPI system

The optical head on fig.1 is the core of the system and contains the laser, the optical interferometer and the video camera. The laser is usually a 5 mW He-Ne laser which allows us to investigate areas up 1 ft^2 on objects of normal reflectivity. For certain applications, especially when bigger or very unstable objects are to be inspected, more powerful lasers like Ar-laser or even pulsed lasers can be incorporated. The optical interferometer is really a simple holography set-up where the object is imaged on to the photosensitive surface of the video camera. Another wave from the same laser, the so-called reference wave, is also directed towards the recording area from the same

direction as the object wave. The two waves combine by interference to create an image interferogram which is transformed into a corresponding video signal by the scanning action of the camera's read-out beam . This signal is subsequently electronically processed before it is converted into an object image on the video monitor. This image is now highly sensitive to any movements of the object due to the interference priciples involved in the recording. For example lightly tapping the object will make the monitor image go dark wherever the movement during the video exposure is larger than one laser wavelenght. By various techniques we can use this interference sensitivity to study vibrations and slow deformations of an object surface.

For practical use, however, there is no need to understand the physics and construction of the ESPI-system. The optical head is contained in a box sized like a piece of carry-on luggage and weighing between 30 to 40 lbs while the remaing electronics is confined in a case of similar size. Just pointing the illuminating beam at the test area and choosing an appropiate magnification will in most cases ensure that good hologram recordings can be made.

a.Vibrations.

This is the simplest but maybe most powerful application of the system. By placing a harmonically vibrating object in the illumination beam we observe immediately its resonance mode of vibration. The monitor image will be covered with a fringe pattern where each fringe represent a constant value of the vibration amplitude as shown on figs.2a-b.

a) b)

Fig.2

ESPI-recordings of a vibrating propellor

Fig.2a shows a propellor of about one foot diameter vibrating in its first torsional mode at 1028 Hz. The brightest areas represents nodal regions where the center of the areas do not move at all. Each bright fringe thereafter represents an amplitude increment of about 1.5 * 10^{-4} mm. Fig.2b shows only one blade of the same propellor vibrating at a higher resonance frequency - 2443 Hz.

The analysis of vibrating objects can be extended by various means. For example we can show the vibrations in slow motion (5), we can accurately plot the vibration phase values across the surface (6) and measure the sharpness of the resonances or the Q-factors. Measurements have been made on highly unstable objects (7) ranging in sizes from 0.1 mm^2 to over 1 m^2. The measuring range is equally impressive as frequencies from virtually zero to the MHz.-region have been recorded with amplitudes ranging from 10^{-6} to 10^{-2} mm.

We would again like to stress the ease and speed these vibration tests can be performed at. The object is simply put in the illumination and as we change the frequency and excitation, we immediately see how the resonance pattern of the object changes.

b.Deformations.

We should maybe first point out that we here want to look at slow movements of the test object which are either naturally occuring or induced by some external changes like loading or heating. In practise this means that we want to measure the change of the object's surface from one video frame to another. This means that we must be able to store one particular video frame and compare its content to the subsequent frames coming from the video camera. This process is performed by using the digital video store on fig.1, which enables us to store and automatically subtract a reference frame from the camera frames by simply pushing a button. As the object deforms the monitor image will be covered with fringes indicating contours of constant movement. Typical examples of such recordings are shown on fig.3 a-b where a ceramic plate is deformed due to increasing load. As the load is increased from fig.3a to fig .3b the fringe density increases indicating a larger deformation. The contour spacing in

this case represents a movement of about 2.5 * 10^{-4} mm and we can easily measure the absolute deformation of the plate by counting the fringes and multiply by this value. Note that the fringe patterns on fig.3 a and b are discontinued along certain directions, which indicates cracks in the surface. By carefully measurements along these dicontinued fringe patterns we can get information about the lenght and to a certain degree also the depth of the crack.

a) b)

Fig.3

ESPI-recordings of a deforming ceramic plate

When the fringes becomes too closely spaced to be resolved by the video system, a new reference state is recorded in the store and the fringe build up is followed a new as the loading is increased. In this way an object's deformation can be monitored from its initial state until failure. If the experiment is recorded by a video tape recorder, the deformation process can be studied in great detail afterwards in slow motion or by single frames.

***

We have already stressed the ESPI-system's real-time speed of operation, its stability and easy handling. As a holographic system it also represent a non-contact, non-destructive measurement method without any calibration problems as the wavelenght of the laser light is fairly constant around the world. The system can also be used under rather adverse conditions without very special precautions. We may for example use it to study very hot objects so far up to about +2900 °F (8). Consequently the system can also be used in broad daylight.

The recorded holograms are also in one stage of the process available as an electronic signal. In this way the optical head can be placed in locations far away from the test laboratory and the signals relayed back by cable or even wireless. In this way the behaviour of critical components in e.g radio-active areas can be observed and measured.

***

It should be strongly stressed that the ESPI-technique like hologram interferometry and other optical measuring methods only provides information about the behaviour of the object's surface in case of normal,non-transparent objects like composites. In fact, if the laser light penetrates somewhat into the surface , the light scattered from the deeper layers contributes to the fringe patterns only in terms of lower image quality. Therefore if we are looking for abnormalities in the object's interior, we must find excitation mechanisms which transform interior changes into interpretable surface movements. This problem has been extensive studied in holography, see e.g. ref.(1), and to a lesser extent in ESPI (9).

In general we can use mechanical loading, heating, vibration excitation and in some cases magnetic fields.

Appropriate mechanical loading may bring out failures like e.g. debonds by corresponding excessive surface movement's. However, as the loading also may produce quite dense and complicated fringe patterns due to the natural response of the structure it can be very difficult to pick out interior faults in this way. A special and and in some cases very effective case of loading is provided by using air pressure differences. Especially if the object can be internally pressurized like some honeycomb panels the detection of internal flaws can be extremely effective.

Heating acts in a way like pressure loading as the heat make cavities or debonds expand in different way from the rest of the structure. Heating can be very effective on certain materials, but does not work well on e.g. steel or aluminum due their high heat conductivity.

Vibration excitation can make the flaws vibrate strongly compared to the rest of the object at certain resonance frequencies. Due to the speed and simplicity of ESPI-vibration testing this

excitation mechanism is to be preferred whenever feasible. however, to detect very small defects we have to use rather high frequencies and the amplitudes may become too small to be easily observed even by the highly sensitive ESPI-techniques.
All these excitation mechanisms will fail to provide any interpretable surface movement if the defect is too small or if it is located too far away from the surface. It is hard to give any definite values to either parameters as we will get variations due to object construction and material.

III.SOME APPLICATIONS OF ESPI

In principle the ESPI-technique can be used for the same applications as hologram interferometry.
Our group has earlier worked mainly with the vibration testing by ESPI, where quite impressive results have been reached see for example ref.(10). A typical on-site application area in this field is the testing of gas turbine parts. We constructed an ESPI-set up for a Norwegian gas turbine manufacturer 10 years ago to be used on-site to check the resonances of each blade (11). The rather primitive set up has been used by ordinary mechanics full days in critical periods during production and the system was claimed to have repaid its cost within the first two months. Our new compact version of the ESPI-instrument has now been ordered by the manufacturer.
The last four years we have also been working with deformation testing where we found the detection and monitoring of cracks to be especially an especially interesting area. As an example of on-site application we took our prototype instrument to an industrial test laboratory where the strenght of materials for melting electrodes was tested. Looking at the object in the loading rig we was able to predict at very modest load, about 50 kg.,the crack pattern of the surface. The object cracked at about 11000 kg. exactly where we had predicted.
We have also looked at some composite materials and hope to start a more extensive project in this field. We will show two examples of the potentials of the technique for composite evaluation.
Fig.5a on the next page shows an delamination in a honeycomb panel brought to us from Royal Air Force, England. The delamination is seen as the bull's eye pattern while the individual cells

with good bonding are seen around the delamination area. All the introduced flaws could be found in the panels.

a) b) c)

Fig.5

ESPI-recordings of composites

Fig.5b shows experiments with a test panel provided for our group by the Material Labs.,Wright-Patterson. The "flaws" represents a "secret" message ("god jul" which means Merry Christmas in Norwegian) written by paper letters some plies below the surface. By using a special heating mechanism the "message" could be read quite clearly. Note that the surface movement over the letters is only about $5 * 10^{-5}$ mm compared to the movement of the rest of the surface. Fig.5c shows the fringe pattern on the front surface due to a paper clip fastened to the back surface.
Finally we would like to point out that these still pictures shown here are not fully representative for the potentials of the technique as the real-time representation of the holograms allows for manipulation of the fringes which can bring out very fine details in the dynamical monitor image.

IV.CONCLUDING REMARKS

Although rather few examples of composite testing have been cited here, it should be quite obvious that the ESPI-technique is able to provide valuable information within this application area and enable us to do on-site inspection of e.g. impact damages on aircrafts. Preferably the technique should be combined with other

more established techniques like accoustic emission for optimum results.

Future development in this field will include automatic fringe read-out to aid the operator and the construction of very compact optical heads which can be placed directly on the object.

REFERENCES

1. C.V.Vest. Holographic Interferometry. John Wiley & Sons. New York (1979)

2. O.J.Løkberg. Phys. Technol.11, 16 (1980)

3. R.Jones and C.Wykes. Holographic and Speckle Interferometry. Cambridge University Press, Cambridge (1983)

4. O.J.Løkberg and G.A.Slettemoen. Electronic Speckle Pattern Interferometry. To be published in Applied Optics and Optical Engineering

5. K.Høgmoen and O.J.Løkberg. Appl.Opt.16,1869 (1977)

6. O.J.Løkberg and K.Høgmoen. Appl.Opt.15,2701 (1976)

7. O.J.Løkberg. Appl.Opt.18,2377 (1979)

8. O.J.Løkberg,J.T.Malmo and G.A.Slettemoen. To be published in Appl.Opt. Sept.1985

9. B.P.Holownia. Opt.& Lasers in Engr.6,79 (1985)

10. O.J.Løkberg. J.Accost.Soc.Am.75,1783 (1984)

11. O.J.Løkberg and P.Svenke. Opt.& Lasers in Engr.2,1 (1981)

ACOUSTIC EMISSION AND FAILURE ANALYSIS OF KEVLAR COMPOSITES

Itzhak Roman
The Hebrew University of Jerusalem
Jerusalem, Israel

FAILURE ANALYSIS AND ACOUSTIC EMISSION OF KEVLAR COMPOSITES.

I. Roman, A. Mittleman and G. Marom
Graduate School of Applied Science and Technology
The Hebrew University of Jerusalem
Jerusalem 91904, Israel

ABSTRACT

Results obtained in a research program, which employed three point bend and tensile testing of unidirectional Kevlar-Epoxy Composites, to produce different failure modes, are described. The paper exemplifies how the study of fracture surfaces, produced in such research programs, can be utilized to identify the nature of the operating fracture mechanism and provide information about its cause, thus being instrumentil in post failure analysis.

1. INTRODUCTION

One of the inevitable stages of almost any failure analysis involves a careful investigation of fracture surface characteristics. Such a study of the fracture surface is conducted in order to identify the failure mechanism(s), loading mode(s), material properties and environmental conditions that were involved in causing the failure. Extensive fractographic work that correlates the fracture surface of metalic with specific mechanisms has been documented and published in numerous readily available handbooks.

The increasing deployment of advanced composite materials in high performance and demanding applications, makes it essential that similar detailed fractographic references be prepared for the different composite material systems subjected to a variety of loading modes and environmental exposures. Much of the information needed for such important compilations can be made available by the many researchers who have been studing failure machanisms in composites under well documented conditions.

This paper exemplifies, how information gained during the study of acoustic-emmision and mechanical behaviour of unidirectional Kevlar-Epoxy composites, can be used for post failure analysis. First, asummary of results is given which is followed by a section demonstrating the application of some of the results to post failure analysis.

2. RESULTS

Testing was conducted in both three point bend and tensile loading of unidirectional Kevlar-Epoxy composites. Details of the experimental conditions is given in [1 - 2]

2.1. FLEXURAL TESTING

2.1.1. Modes of Failure

The failure of Kevlar-reinforced epoxy composited in 3-point bending occurred by either one of two modes being failure by longitudinal fracture of fibres in the tensile side, or by shear delamination in the neutral plane. Each of these failure modes was preceded by compressive yielding in the compressive side typical of Kevlar composites. The first failure mode was typical of the lower volume fraction composites and the second was typical of the higher, with a distinct transition in the volume fraction range 45-48%. With interlaminar loading the transition occurred at the lower end of the transition range, ∿45%, and with translaminar loading the transition occurred at the higher end, ∿48%.

Figure 1 is a qualitative representation of the load-deflection curves for the respective failure modes. The curve of the fibre fracture mode is characterized by a yielding stage and a longer ultimate deflection. These result from compressive failure occurring in the compressive side of the specimen as discussed below. The curve of the delamination mode is characterzied by a main delamination event followed by a number of secondary delaminations.

The transition from failure by fibre fracture to failure by delaminatic was governed by the fibre volume fraction. It was therefore detectable by monitoring various mechanical properties and plotting them versus the fibre volume fraction. Figure 2 presents the transition as reflected by strength measurements. The results show that the transition occurs around ϕ_f=0.45 - 0.48. Although the ultimate strength values, σ, were calculated for the entire ϕ range, only those below the mode transitin points are appropriate. Hence, in view of the observed transition to a delamination mode controlled by the shear stress at the neutral plane, the ultimate shear strength values, τ, were claculated for ϕ_f values above the transition point. These are shown in Figure 2.

The reason for the mode transition at a critical ϕ_f point lies with the different functions that σ and τ have in ϕ_f. Whereas σ increases linearily with ϕ, τ decreases due to increasingly high proportions of interface at the shear plane. In fact, at high ϕ values τ is governed by fibre-fibre contacts of zero strength and by the fibre-matrix interfacial strength being relatively weak with Kevlar fibres. Hence, the critical ϕ_f point is the value of ϕ_f for which σ and τ attain their ultimate values simultaneously. In the translaminar case τ may be higher due to the action of misaligned fibre, resulting in a somewhat higher critical ϕ_f.

Regarding the actual values of σ up to the transition point, they indeed seem to increase linearily with ϕ_f. However, they are smaller compared with the rule-of-mixtures values calculated with σ_f=2.75 GPa. The lower values derive from a calculation assuming both tensile and compressive elastic behaviour of the Kevlar-reinforced composites. As a matter of fact these composites exhibit non-linear compressive behaviour, resulting in a different stress distribution, as discussed in detail by

Fiscuher and Marm (1984) [3] producing the rule-of-mixture values for σ. Another important outcome of the non-liner compressive behaviour is that stresses above the compressive yield stress shift the neutral axis downward. The marking of this shifting is obtained by the onset of delamination failure, taking place within the neutral plane in its ultimate new location away from the centroidal axis. This is shown in Figure 3 with four specimens representing differnt fibre volume fractions above the critical ϕ_I, which sets the failure mode transition.

2.1.2. Fracture Mechanisms

Fractographic examinations of the fractured specimens revealed typical features of the two observed modes of failure. Figure 4 contains examples of scanning electron fractographs showing the details of a tensile failure mode. The important observation concerns the fracture of the Kevlar fibres and their pull-out from the fractured matrix. It is seen that the fracture of the Kevlar fibres occurs through an axial splitting machanism, followed by a pull-out stage of the two opposing split portions.

Examples of the details of the delamina·ion mode are presented in Figure 5 by scanning eiectron fractrographs showing the final shear damage in the matrix typical of the delaminatin mode, and the typical splitting of the fibre. Although fibre splitting occurs under both tensile and delamination failure modes, fracture proceeds differently in each case. Three typical fibre failure events under the delamination of an individual filament also shown in Figure 5. The other two events are the tearing off in the axial direction of the fibre skin to form a continuous ribbon, and the production of deformation kink bands on the compression side of a sharp bend. For a more comprehensive examination of the fracture mechanisms see Davidovitz et al (1984) [1].

Additional fracture mechanisms studied where those related to compressive failure and to transverse failure (obtained by transverse 3-point bending). Figure 6 and 7 present examples of corresponding micrographs related to these respective failure.

2.1.3. Preliminary AE Results

Figure 8 presents acoustic emission amplitude distributions obtained for 3 different failure modes. It is obvious that the different modes are distinguishable by their typical acoustic responses. Moreover, the tensile delamination mode transition is also detectable through the AE date. This is exemplified in Figure 9 by plotting the ratio of the event count in the amplitude range 10-20 dB to the total event count versus the fibre content. The preliminary AE results aleady indicate that matrix fracture events probably are of lower amplitudes while fibre fracture events are of higher amplitudes.

2.2. RESULTS OF TENSILE TESTING

2.2.1 Fracture Mechanisms

Failure under tensile loading occurred by a combination of fibre fracture and longitudinal matrix and interfacial shear failure.

The first occurred progressiveely with the loading of the specimen, and the latter occurred at the onset of failure. The mechanism of fibre fructure exhibit the typical splitting regardless of the fibre content. The matrix and interfacial shear failure events exhibited dependence on the fibre content, with the longitudinal shear damage increasing as the fibre contect is increased. This is seen in Figure 10, where only one longitudinal shear crack is observed in 4.7% fibre content, while multiple longitudinal shear is observed in 73% fibre content.

Typical details of tensile failure-related fracture mechanisms are shown by the scanning electron micrographs of Figure 11.

2.2.2. AE Data

The AE informatin was analyzed at a number of points during the loading of the specimen. This enabled to establish a correlation between the acoustic signal and the source event. Some of the AE results are presented in Figure 12. The left hand side of this figure showes peak amplitude distributions for the events which occurred up to 95% of the ultimate load. The amplitudes appear in the range 39-65 dB and result from fibre breakage which occurs progressively with the loading. The right hand side of Figure 12 shows the coummlative amplitude distibution at the instant of failure. The high fibre content composites exhibit an addition of events having peak amplitudes in the range 18-38 dB, related to matrix and interfacial failure.

These partial AE results already indicate that amplitude distribtion ranges may be correlated with source events such as fibre or matrix fracture, with a high degree of confidence. Additional information obtained for instance, by tensile testing of transverse specimens strengthens this picture. A fuller account of the AE result is in preparation.

3. APPLICATION OF RESULTS TO POST FAILURE ANALYSIS

Fractographic evaluation can be considered exist on two levels of scale: visual and low magnificaition optical microscopy - macroscopic examination or study using high magnificaition optical and electron beam instruments - microscopic examination.

3.1. Macroscopic examination

The results indicate that in unidirectional Kevlar-Epoxy composites of $\phi_f > 0.5$, failure occurs almost exclusively by fractures parallel to the fibre direction. This is accomplished by longitudinal splits in the matrix, the number of which increases with the volume fraction of fibre and the strength level for a given volume fraction, ϕ_f.

In a few cases transverse fractures were observed; these were associated whith either low ϕ_f's in bending or areas of extremely high ϕ_f's (fibre with almost no matrix) in tensile samples.

Thus, when examinig the fracture surface of a faild aerospace component made of unidirectional Kevlar-Epoxy ($\phi_f \sim 0.6$) composite, multiple longitudinal spliting is indicative of a sound component and failure is most likely due to excessive loading. Conversely, few longitudinal splits or transverse fractures will indcate a deficient material system.

3.2. Miscrosopic examination

Our experience shows that fractographic studies of failed fibres provide little information as to the failure mode. In all cases fibre failure occurs by spliting, however seconday effects described in section 2.1.2. can, in some events, point to the loading mode.

The fracture surface of the macroscopic longitudinal splits of a sound material exhibit features typical of shear damage (hackles) on the microscale. Conversely, it was observed that the fracture surfaces of the few splits in a deficient maerial are typified by plait like features shown in Figure 13.

4. CONCLUSIONS

The major conclusion of this study is that fractographic data obtained as a result of laboratory studies can and should be incorporated in post failure analysis as outlined above.

5. REFERENCES

1) Davidovitz, M., Mittelman, A., Roman, I,. and Marom, G. J. Mater. Sci.,19, 377-384 (1984).
2) SPI (1983), Ist Int. Symp.on AE from RP. San Francisco July 19-21.
3) Fischer, S. and Marom, G., Fibre Sci. Tech., 20,91-98 (1984).

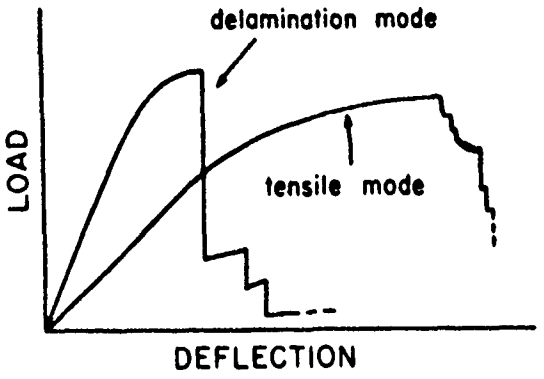

FIGURE 1.
Load-deflection curves for delamination and tensile failures.

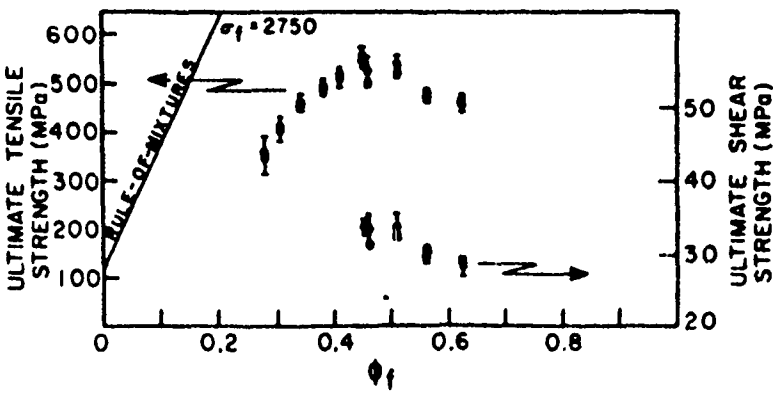

FIGURE 2.
Ultimate tensile and shear strength values.

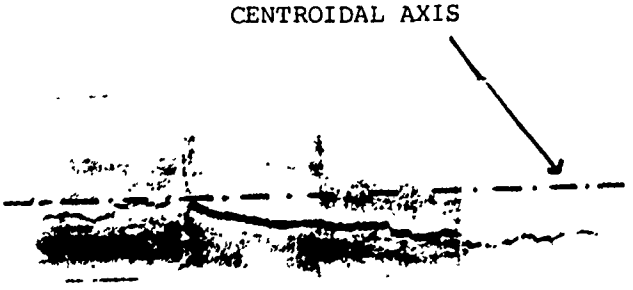

FIGURE 3.
The displacement of the neutral plane (marked by delamination) from the centroidal plane as affected by the fibre volume fraction.

x 100

x 200

FIGURE 4.

Scanning electron fractographs of tensile failure related fracture mechanisms.

x 500

x 1000

FIGURE 5.

Scanning electron fractographs of delamination failure related fracture mechanisms.

X 100

FIGURE 6.

A kink bend formed on the specimen surface in the compression side.

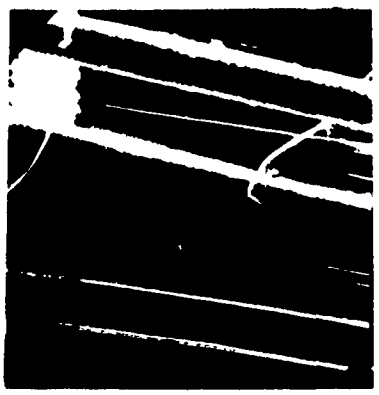

x 500

FIGURE 7.

A typical transverse fracture surface.

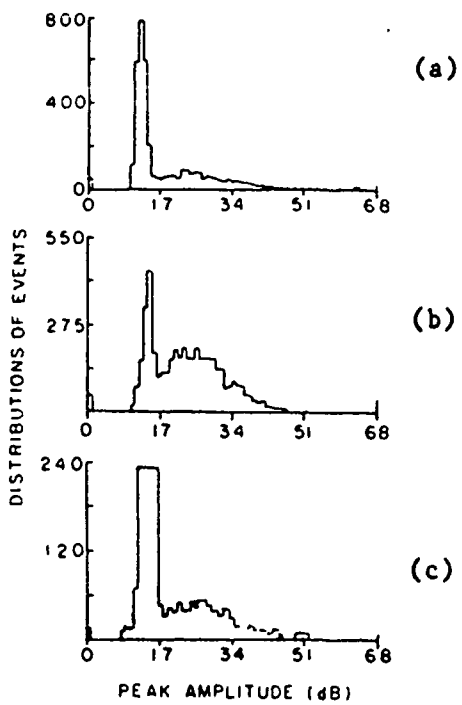

FIGURE 8.

AE amplitude distributions by a 375 kHz sensor: (a) tensile; (b) delamination; (c) transverse failure modes.

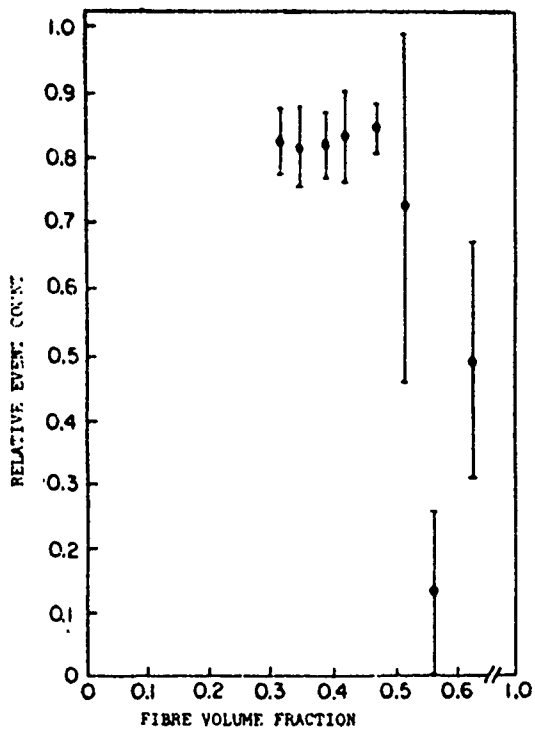

FIGURE 9.

Event count ratio as a function of the fibre content, showing the failure mode transition at ϕ_f=0.50

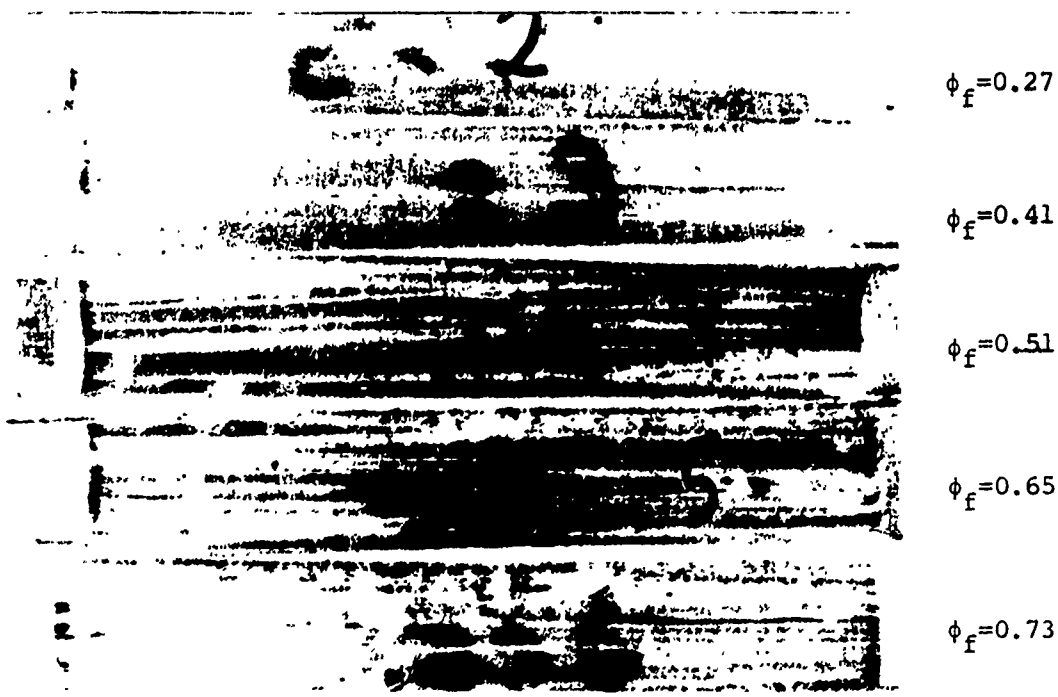

FIGURE 10.

Longitudinal shear damage in fractured tensile specimens as a function of the fibre contect.

(a)

x10

(b)

x75

(c)

x500

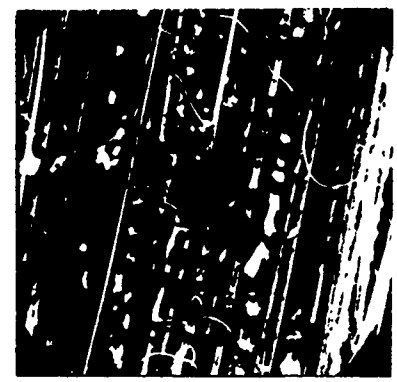

x150

FIGURE 11.
Tensile failure of unidirectional Kevlar-reinforced composite: (a) longitudinal shear damage; (b) fractured fibres; (c) matrix and interfacial shear damage.

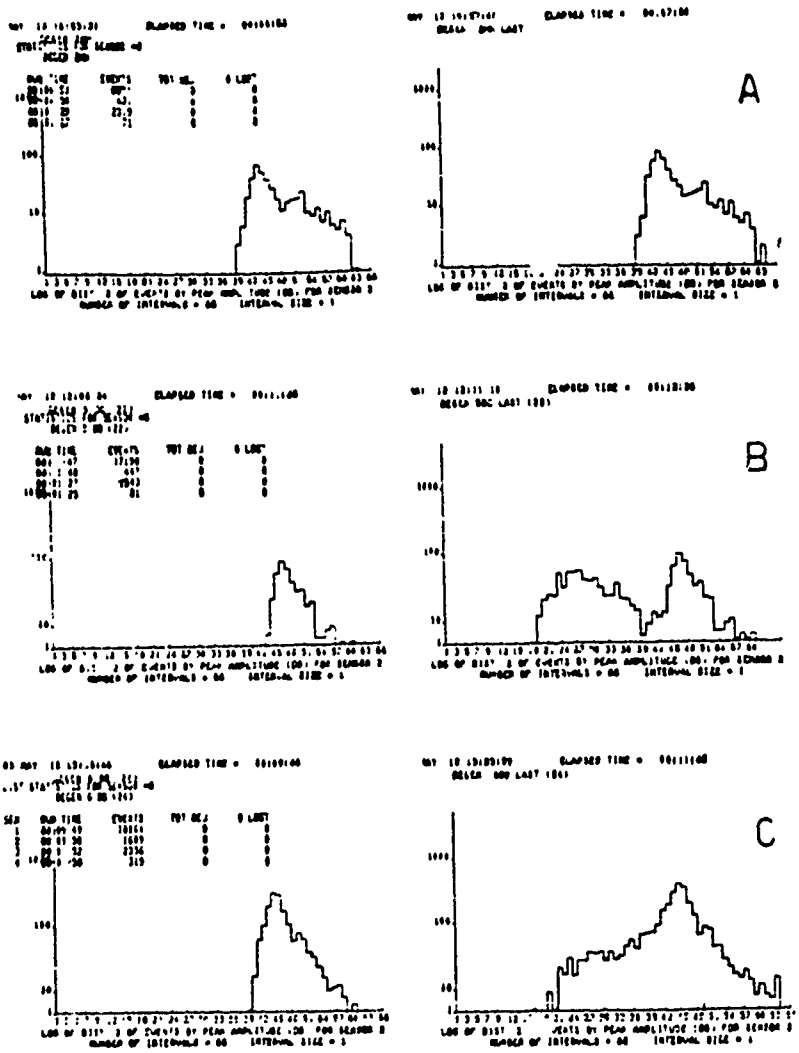

FIGURE 12.

Amplitude distributions for fibre volume fractions 27% (A), 65% (B) and 73% (C); from left to right: distributions at 95% of ultimate load, and the instant of failure, respectively.

x150

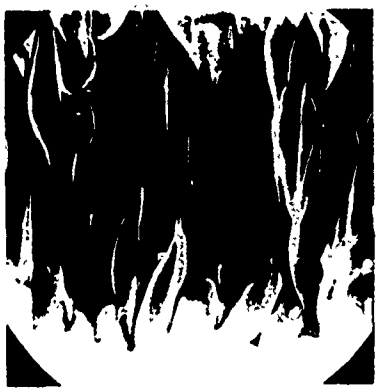

x2000

FIGURE 13.

Plate like matrix fractured surtaces

ADVANCES IN COMPOSITE MATERIAL INSPECTION WITH COMPUTER INTEGRATED ULTRASONIC IMAGING

R.P. Simpson, R.H. Grills and G.A. Andrew
Ultra Image International
Division of Science Application International Corporation
New London, Connecticut

ADVANCES IN COMPOSITE MATERIAL INSPECTION WITH COMPUTER INTEGRATED ULTRASONIC IMAGING*

by Ronald P. Simpson**

ABSTRACT

The ability to inspect composite materials reliably with ultrasonics has improved, with recent technological advances. Systems are now available that will do color imaging with reliability for documentation and analysis capabilities. This paper reviews these advances to understand the tools currently available for examining and evaluating the quality of composite materials, both in the initial manufacturing environment and in the field. Delamination can be detected on a ply-by-ply basis at different depths throughout the thickness of a part. Color graphics and detailed analysis software aid in interpretation of inspection results Careful selection of color distribution provides a descriptive graphic tool for evaluating damage anywhere through the thickness of a composite part. Results presented demonstrate this feature and the ability to quantify details of impact damage in composite materials.

INTRODUCTION

There has been a significant change in the technological capabilities of ultrasonics for inspection of composite materials in the last five years. This has been achieved through the integration of ultrasonics with the microprocessor for data acquisition and storage, with controlled scanners, both manual and automatic, for precise position identification and assurance of full area coverage, and finally with detailed software and color graphics for data analysis. As a result, the ability to inspect composite materials reliably with ultrasonics is entirely different from what it was a few years ago with hand-held manual ultrasonics The technology provides a valuable tool for designers (both structural and materials), inspection, manufacturing and maintenance personnel. There are a few systems on the market now that will do color imaging, each has a little different approach and different degrees of reliability for documentation and analysis capabilities. This paper examines the advances in this technology in an effort to give an understanding of the tools that are available today for examining and evaluating the quality of composite materials, both in the initial manufacturing environment and in the field.

BASIC HARDWARE

To set the stage for understanding how the technology and capabilities of ultrasonic imaging are different, we look at one particular system – the ULTRA IMAGE III™. Understanding the basic hardware and software logic for data acquisition is essential to appreciate the mechanism of data acquisition, the inspection detail and precision it provides, and the variety of applications where this "new" technology can be applied A picture of the system is shown in **Figure 1**. There are four relatively small, portable components The lower left is a microprocessor, it has four boards. the graphics board for the color graphics display; memory board for storage of up to 680 kilobytes of information, the CPU board for managing all of the microprocessor interactions, and an interface board that ties all intercommunications together. Above the microprocessor is a display package which has both a CRT for C-scan and an oscilloscope for A-scan displays The lower right shows two double-density, double-sided disk drives. In the normal operation, one is used to read the main program disk, the other is used for data disk(s) They are interchangeable, adding flexibility and reliability for performance in the field. Finally, the upper right is the ultrasonics package It is the part of the system which most resembles a conventional hand-held ultrasonics unit To the very left is the pulser, just to the right of that a receiver, and on the far right a thickness gate.

* This paper was presented at the International Conference Post Failure Analysis Techniques for Fiber Reinforced Composites Dayton, Ohio, July 1-3 1985

** Dr Ronald P Simpson is Director of Marketing and Business Development, Ultra Image International Division of SAIC New London, CT 06320

One other component that is coupled with an ultrasonic imaging system for data acquisition is a reliable scanner to give precise position identification and control of the information collection. It insures full area coverage and provides an ability to go back and repeat the same examination at any future time. So, for example, one could find a flaw or delamination in a composite that was below critical size but want to reinspect it after a certain number of flight hours to see how it had changed or grown. That can be done now routinely with these highly reliable scanners. The key function of the scanner operation is to provide an accurate means to identify and record position and correlate this position with inspection results. Two approaches have been used:

1. Optical encoders coupled through gears to a mechanical tracking/motion system,
2. High frequency ultrasonic transmission with a triangulation system of receivers.

Most systems use direct tracking; there is only one component to be coupled to the part, and it does not require line-of-sight that an ultrasonic or laser beam triangulation system requires. For applications where this latter requirement is not a limitation, the indirect referencing of triangulation has some advantages in simplicity.

While they look fairly simple, good reliable scanners are relatively sophisticated mechanical devices. Each is also designed for certain objectives. The Ultra Image scanner, for example, shown with a custom modification for through transmission inspection and its flexible track coupled to a horizontal stabilizer in **Figure 2**, was designed for simplicity, flexibility in application, reliability, and ease of use and maintenance. It has 50 percent fewer parts than an earlier scanner designed for flexibility in small spaces. And a newer, low profile scanner design, just completed for accurate position identification in confined space, is 57 percent lighter and has another 25 percent reduction in the number of parts. Each application may require a different scanner or modification of an existing scanner. Some may be automated and some may be manually operated. No matter what the requirement created by the inspection objective and component geometry, it is not a limiting problem, but there is more technology to scanner design than an inexperienced evaluator might suspect. It is best to utilize and build on existing experience. Refinement is an iterative process.

DATA ACQUISITION LOGIC

To understand how ultrasonic imaging works, it is important to know how the data is acquired. It is collected in a grid arrangement. In the case of the ULTRA IMAGE III™ system, the grid is 200 units by 100 units, **Figure 3**. It provides a 200 × 100 rectangular display with 20,000 data points of both depth and signal amplitude. Each grid is a square, the size of which is controllable in software anywhere from .020″ up to .600″. With minor modifications to the scanner calibration, those numbers can be expanded on either end of the scale even further. The area covered by each scan is controlled by the size of the grid, as is the minimum detectable flaw size. Grid size is determined generally by the required inspection productivity, balanced with the critical flaw size. With a .020″ grid size, there is a high reliability in finding a flaw .030″. If finding delamination .300″ to .400″ on a side is all that is required, then a ¼″ grid size is very reasonable. In that case, the area covered would be 25″ × 50″.

The other key factor in data acquisition is determining what signal is recorded. In each grid, the equipment records the first signal in a gate that exceeds a threshold amplitude level. The gate is set electronically by two switches on the ultrasonic part of the system; the threshold is set in software, and can range anywhere from 0 percent to 100 percent full scale voltage of the A-scan. This is shown graphically on **Figure 4**. The A-scan shows one reflected signal in the gate approximately 15 percent to 20 percent above the background level, but does not exceed threshold set at 35 percent to 40 percent full amplitude. It is not recorded. The reflection further to the right exceeds the threshold and is in the gate. At the very bottom, the figure shows timing pulses that continue to count until the first signal in the gate exceeds threshold, at which point both the depth and the amplitude of the returned signal are recorded. This is repeated for each of the 20,000 grid spaces to form one inspection image.

In addition to increased precision and reliability of data acquisition, ultrasonic imaging stores inspection parameters and results together in a permanent record. This allows more in-depth analysis as well as exact test duplication. An example of the inspection parameter permanent record available with the ULTRA IMAGE III™ system is shown in **Figure 5**. There is administrative, scanner set-up, calibration, and ultrasonic data. The administrative information is for identification purposes, and is typed in at the discretion of the

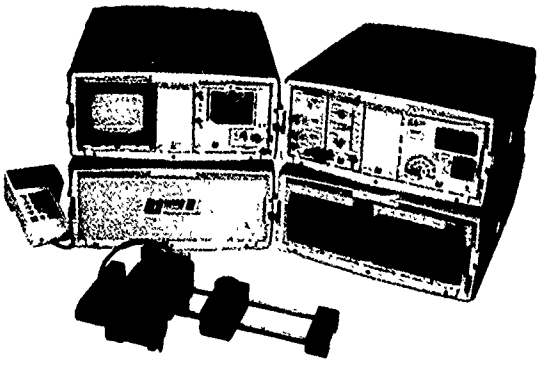

FIGURE 1. ULTRA IMAGE III™ Ultrasonic Imaging System.

FIGURE 2. ULTRA IMAGE III™ scanner, modified for through transmission "Pitch-catch" inspection, mounted on a horizontal stabilizer.

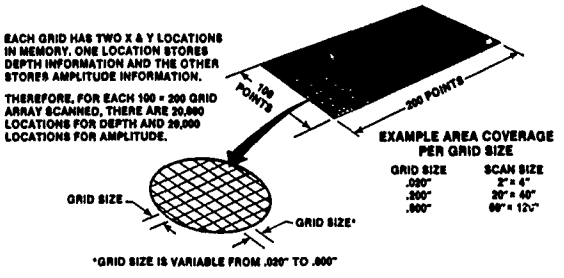

FIGURE 3. Rectangular grid arrangement containing 20,000 data points used for each ultrasonic image recording.

FIGURE 4. A-Scan showing "Threshold" and "Gate" setting with timing pulses (clock) counting until "First signal-in the gate-that exceeds threshold" is reached and recorded.

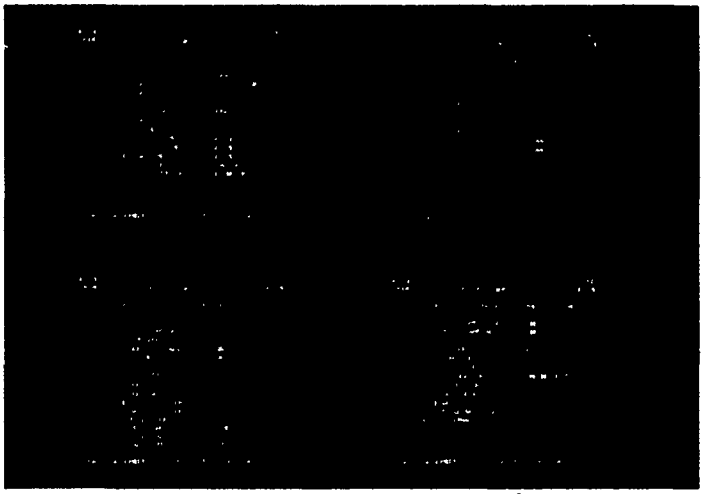

FIGURE 5. Example of permanent record "Header" information.

inspector. The scanner set-up information includes the grid size, the scale factors for the optical encoders along the track and arm of the scanner, the scanning axis which determines whether the track or the arm is the 200 unit or the 100 unit part of the scan, the transducer angle, and the delay time and orientation of the transducer. The calibration data records the material velocity constant, the threshold level, and a number of other factors which are important in calibrating and having a record of how the system was calibrated. Finally, the ultrasonic information records each switch setting on the ultrasonic package. Every switch setting is checked for each of the 20,000 data points, to insure every switch is set as the system is calibrated and as recorded in the header. This insures that whenever a scan is recorded, it was taken, and every data point in that scan was taken, with the equipment set just as the header says it was. If it were not, if any switch were changed, then the system would stop taking information, it would not lose the good information taken to that point, and it would prompt the operator with the value of the switch(es) that needs to be reset. The end result is that information is acquired with a high degree of reliability, very precisely from a controlled area. The scan provides a record of the area, a map that can be superimposed over the part, so when a flaw is found, its exact location can be identified. In addition, the permanent record allows one to go back at any time in the future, reinspect the same area and compare results to see how the part is performing, to see how the flaw might be growing or changing.

APPLICATION SUCCESS RESULTS

There are many areas where ultrasonic imaging can contribute to safety and reliability immediately. To demonstrate this and stimulate ideas on how the technology can best be used, whether it be initial manufacturing or field service inspection, we are going to look at a number of scan results for a variety of applications, all directed toward inspection of composite materials. The first is a graphite epoxy (G/E) horizontal stabilizer section scan from an F-16, as shown in **Figure 6**. The ultrasonic scan is from a tapered section, shown as cross-section in **Figure 7**. The taper is manufactured by reducing the number of graphite epoxy layers, one layer at a time, as it is assembled, so that the thinner areas have fewer and fewer sheets of graphite epoxy. Each G/E layer is .010" thick. The scan result shown in **Figure 8** displays the data with the color distribution selected such that there is a color change in each of the .010" layer taper reductions. Consequently, a different color occurs at each of the reduced sections. Notice in this case the colors are distributed between 0 and 20%. A Y-slice B-scan of the y = 49 curser location shows each taper step just below the color map (C-scan) of the scan. Each step change in the B-scan comes directly under the step location on the C-scan and also aligns with the color bar on the left. There is a sketch of this in **Figure 9**, showing the part is .500" thick, the taper occurs over the outer .100" (20%), and it occurs in ten .010" steps. A 2X enlargment of the upper right quarter of **Figure 8** shows the steps and Y-slice more clearly in **Figure 10**. Notice when the colors are spread between 0 and 20%, there are a number of areas of delamination, all of which appear to be pink. That means the delamination all occurs in the bottom 80% (.400") of the sample. Now by spreading the colors between 0 and 50% instead of 0 and 20%, we can start to show that some of those areas of delamination are in the top 50% and some in the bottom 50% of the material, **Figure 11**. The large area that appeared all in one color now appears in four different colors, which means this area of delamination is not all in one plane. It is a superposition of delamination from at least four planes. Notice that the colors are all in the upper orange, red, and pink area; there are none of the darker colors (green, blue, or even the yellow). That means no delamination occurs in the top 37% of the stabilizer, all indications are from the lower 63% of thickness. To provide more color discrimination of delamination location, the ten colors are again distributed over 20% (.100") of the thickness, as in **Figure 10**, only this time the spread is between 37% and 57%, see **Figure 9**. The results now show in **Figure 12** that the major area of delamination is in at least six different planes. There are six different colors.

The ultrasonic imaging system acquired and stored all this information, with a thickness resolution of .002", although each layer is only .010". The colors can be spread so they reveal each composite ply, layer by layer, and display precisely where any delamination is located. A cursor can also be moved to any of the 20,000 grid areas to measure the exact depth at each point. There is also a Y-slice across the cursor location in each picture. Each shows a B-scan perpendicular to the Y axis at the cursor location.

Another example of composite material inspection application of ultrasonic imaging is the barely visible impact damage (BVID) shown in **Figure 13**. The material is also graphite epoxy. The samples were inspected to evaluate impact damage from three different ball-bearings dropped on the graphite epoxy

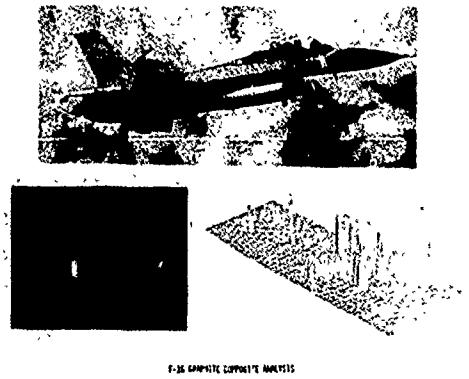

FIGURE 6. F-16 with scan result from tapered stabilizer section.

FIGURE 7. Cut-away section of tapered horizontal stabilizer.

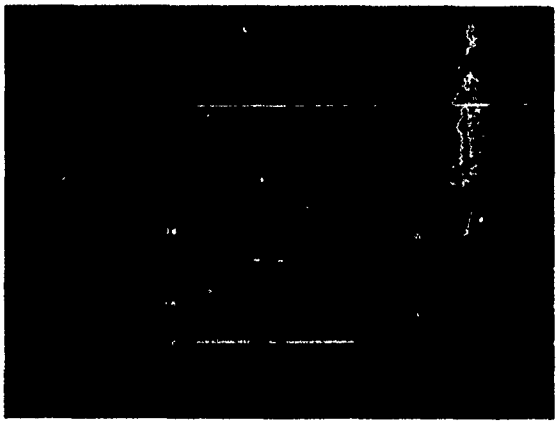

FIGURE 8. ULTRA IMAGE III™ scan result of tapered section with color distribution selected to show a color change at each .010" taper change. All brown areas are full .500" thick, while pink "blotches" show delamination.

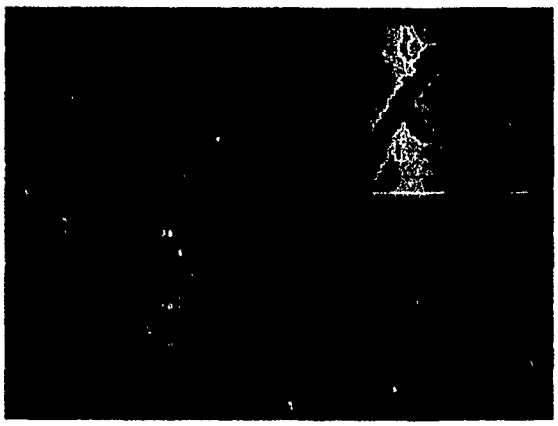

FIGURE 10. Enlargement (2x) of upper right-hand area in Figure 8 showing more detail of each tapered step. Each color change is .010".

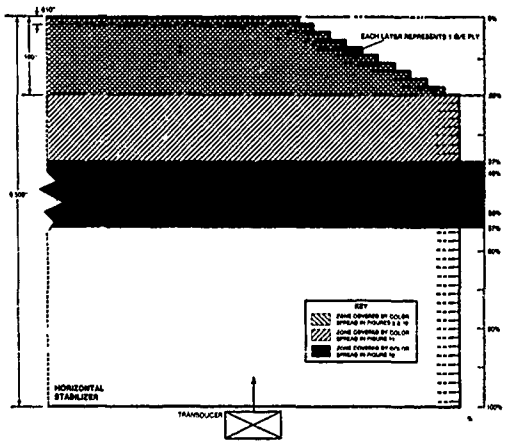

FIGURE 9. Sketch of horizontal stabilizer showing each .010" G/E ply layer, ten-layer tapered zone in outer .100" (20%), transducer surface location for inspection, and each of three zones examined by color distribution shown in Figure 10 (0-20%), Figure 11 (0-50%), and Figure 12 (37%-57%).

surface. Physical examination of this surface shows no apparent damage, but pulse echo examination with the ultrasonic imaging system shows, very graphically, areas of delamination. Each of the different colors shows delamination at different depths. Further examination of the BVID in **Figure 13** and 2X enalrgements of the left and right areas, in **Figures 14** and **15**, respectively, shows that the delamination follows the orientation of the plies. The part is made up by laying plies in cross directions, 0 and 90 degrees, and then at 45 degrees to each of the two perpendicular axes. One can see that the delamination tends to fall in the direction of these plies.

In another case, to establish what precision is achievable for finding flaws in Trident missile graphite epoxy component inspection, a graphite epoxy standard was produced with a series of square flaws of different size at different depths. Each flaw was created by insertion of a .001" thick mylar film. The sample was inspected with a .075" grid size to cover the full area. The inspection results in **Figure 16** show that the flaws started at 1/16" on a side and increased in 1/16" increments, up to 1/2". It also reveals that the test sample is a tapered section. The four background colors are representative of the four different thicknesses of the part. Furthermore, it shows the mylar squares are inserted in one plane for each of the different thicknesses. This is a good example of the precision available for flaw detection with an ultrasonic imaging system. It would not be possible to find flaws of this kind with such precision, clarity, and detail, using conventional, hand-held ultrasonics.

Another application very important to aerospace structures, both composite and metallic, is the inspection of bond soundness between a facesheet and a honeycomb substructure. Development of microprocessor-based, ultrasonic data acquisition imaging sytems, where amplitude as well as distance are recorded, has created a new, reliable way to perform this inspection. Portability of the equipment further allows the inspection to be performed in the field on the aircraft or missile as well as in a maintenance or manufacturing facility. Inspection results showing depth and amplitude for one example of this honeycomb-to-facesheet bond are given in **Figures 17** and **18**, respectively. The sample is a satellite antenna material inspected for British Aerospace with a nomex facesheet and a fibre-core honeycomb cell. The nomex facesheet is only .002" thick. Freon was used as a couplant to prevent wetting the surface. Analysis of this data is best understood from the sketch in **Figure 19**. It shows amplitude variation in three different positions over the honeycomb substrate. As the sound hits the area that has been damaged in the honeycomb (Area 3) it scatters in many directions due to the rough surface, and the amplitude in the return signal (A_3) is lowest, **Figure 18**. In contrast, open areas in the middle of a honeycomb cell (Area 1) are flat, efficient sound reflecting surfaces; there is little scattering loss of the sound. Consequently, the highest amount of energy is returned, so the amplitude (A_1) is highest in this honeycomb cell area. In between these cell centers, there is an area where the sound is centered over the cell walls of the honeycomb (Area 2). A portion of the energy travels down those cell walls, lowering the amplitude of return signal from the honeycomb-facesheet interface (ΔA_2) below what is returned when the sound beam (transducer) is located over the center of the cells, but not lowering it as much as the loss that occurs when the sound hits the rough surface (ΔA_3) where the cells have been damaged. The end result is the image seen in **Figure 18**. What is unique about this figure is that it is the return signal amplitude, not its travel distance (thickness), that reveals the detail The thickness inspection is seen in **Figure 17**. Since all return signals come from the honeycomb-facesheet interface, and even the damaged area returns some signal, albeit low amplitude, there is no discrimination of the cell center, bonded area, or damaged area in the thickness data. All return signals are from the same distance; they all show in one color. Such an inspection was impossible before ultrasonic imaging systems allowed the collection and detailed analysis of amplitude information.

There are numerous other examples. The honeycomb-to-facesheet bond integrity has been examined two other ways. Both involve a go, no-go test; either a signal is returned or it is not. The distance or amplitude is not important In one case an angle beam was used such that a good bond returned a signal and a bad bond had no return signal, as shown in **Figure 20**. It shows when there is a good bond, some of the sound bounces off the portion of the honeycomb cells that extends into the adhesive, and a small signal is returned, thereby giving some return energy. This test was used successfully in the field for examining over 40 aircraft for lack of bonding on the leading edge of the horizontal stabilizer. The advantage to this approach is that the exact position of debonding is identified quite reliably, facilitating direct repair, often right on the spot.

FIGURE 11. Same scan data shown in **Figure 10** with ten colors distributed from 0-50% of distance below back surface. Each color change is .025". Delamination now shows as smaller areas at varying depths.

FIGURE 12. Same scan data shown in **Figure 10** with ten colors distributed from 37-57% of distance below back surface Brown area is all reflections from 320" depth or greater. Each color change is .010" above .320" base. Pink is all reflections above .220" depth. Colors show at least 7 different delamination depths.

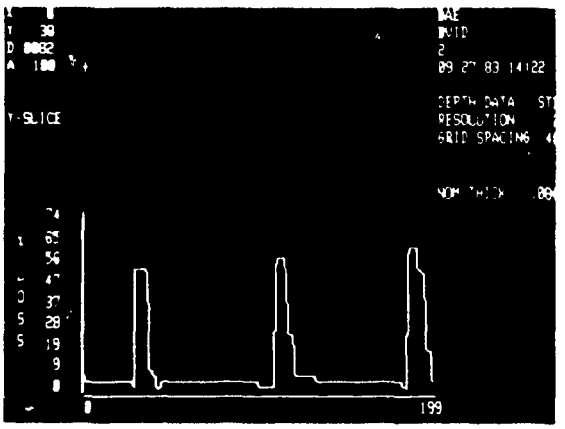

FIGURE 13. Ultrasonic image from straight beam inspection of graphite-epoxy sample with three sites of barely visible impact damage (BVID) caused by impact from three different ball bearings.

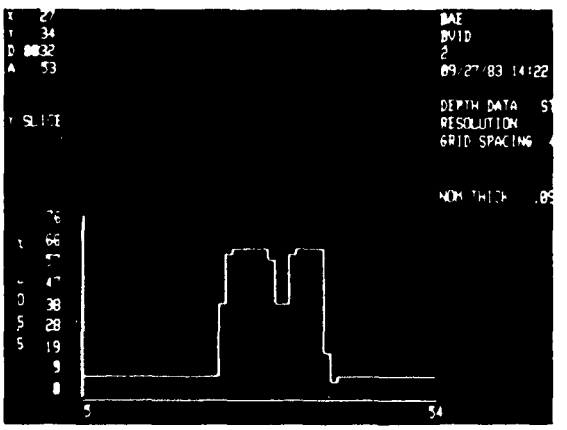

FIGURE 14. Enlargement (2x) of left-hand BVID indication in **Figure 13**. Notice horizonal, vertical, and 45° cross ply indication of delamination.

In the other facesheet-to-honeycomb bond inspection case, through transmission "pitch-catch" was used. For this approach, a return signal also means good bond – the sound went through the part – and no signal indicates lack of bond. Special fixturing was built for both cases, allowing fast inspection on the flightline. **Figure 2** shows the modified scanner in use for this particular application. Both components were horizontal stabilizers from two different aircraft. Custom fixturing is often needed to meet the particular geometrical requirements of in-the-field inspection. It is not a limiting factor in utilization of this ultrasonic imaging technology. It is, however, an opportunity for clever ingenuity.

DISCUSSION AND CONCLUSION

The fundamental principles reviewed and application experience presented demonstrate a technology that is available now for a variety of composite material inspection needs. We have looked at precise identification of delamination from barely visible impact damage, including its position, size, and depth. We have evaluated flaw size detection capability with flaws created by a 1 mil thick mylar layer. We reviewed honeycomb-to-facesheet bond evaluation with three different approaches.

This technology can greatly change the way we deal with composite materials in aerospace structures. It will improve reliability of flaw detection and sizing while giving a permanent record of inspection results. It is now possible to find flaws as small as .030" to .060" with a high degree of reliability and to monitor their growth in time. This allows not only the detection of flaws, but establishing a data base which will give an empirical basis for flaw growth rate for different materials in different structural designs. The technology is well proven. It has been used in many different tests and applications for composite materials around the world. It is something that both designers and testers of composite structures and maintenance people of aircraft systems can use to their advantage. It will change the way we test and evaluate composite materials, and it will change or expand the tools available to the designer and the materials people for application of these materials.

As the technology is applied, experience will lead to continued automation. Systems are already being integrated to robots. It is now possible to communicate inspection results real-time from one location to another via modum. It is only a matter of time before this computer-based ultrasonic data acquisition system is integrated into a CAD/CAM facility. The most significant feature, however, is what it can do already to inspect composite materials with unparalleled flaw detection and analysis capability.

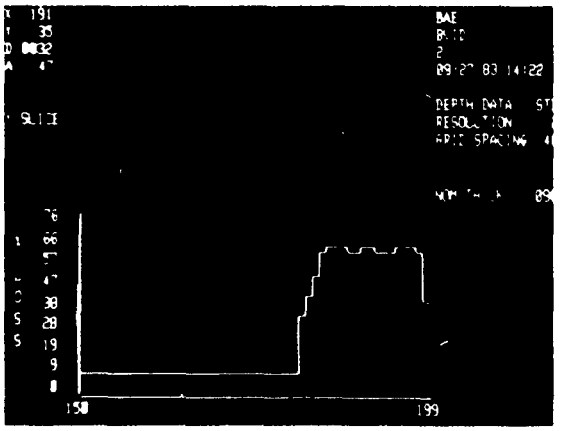

FIGURE 15. Enlargement (2x) of right-hand BVID indication in Figure 13. Notice horizontal, vertical, and 45° cross ply indication of delamination.

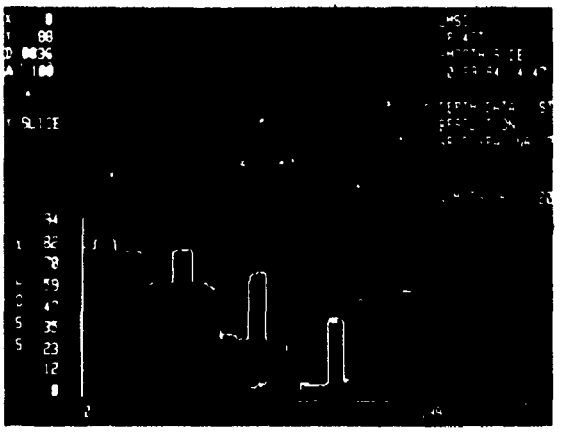

FIGURE 16. Ultrasonic imaging inspection results of graphite-epoxy test standard with flaws created by insertion of square .001" thick mylar patches from 1/16" to 1/2" on a side Test standard contains four thickness layers each with same sequence of flaws, all within same layer.

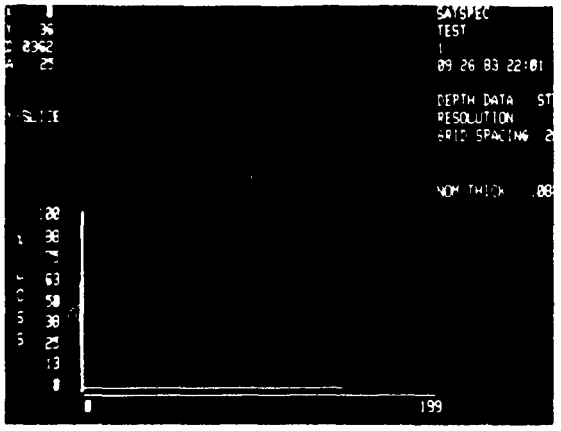

FIGURE 17. Thickness (time of flight) inspection results of a facesheet-to-honeycomb bond integrity analysis.

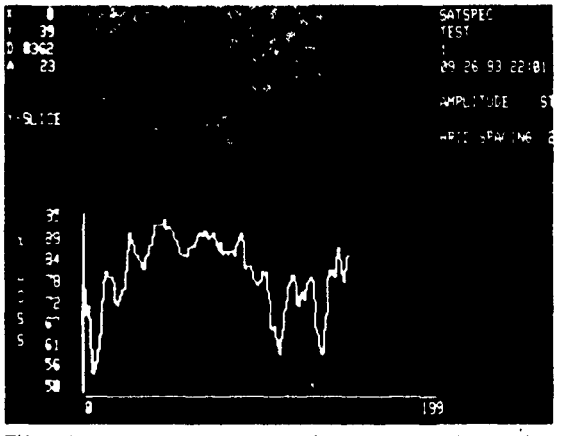

FIGURE 18. Amplitude results from the same inspection data collected during facesheet-to-honeycomb bond integrity analysis shown in Figure 17.

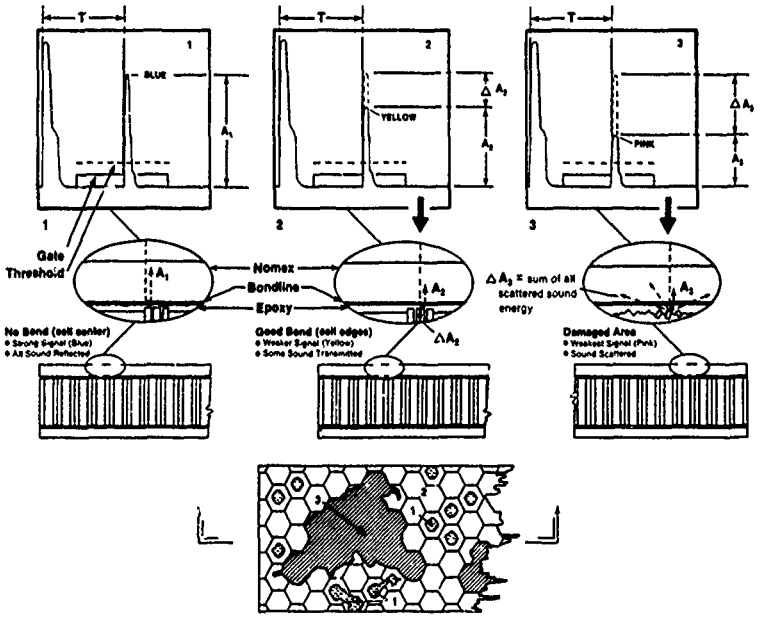

FIGURE 19. Schematic diagram showing analysis of facesheet-to-honeycomb inspection results in Figure 18. Three areas each have different amplitude of return ultrasonic signal. Cell centers, Area 1, have highest return amplitude, A_1, cell walls, Area 2, have lower return signal, A_2 as some of the sound travels down the cell walls, lowering amplitude of return signal by ΔA_2. Area 3 was damaged; the rough area scatters more sound energy, ΔA_3 resulting in lower return signal, A_3.

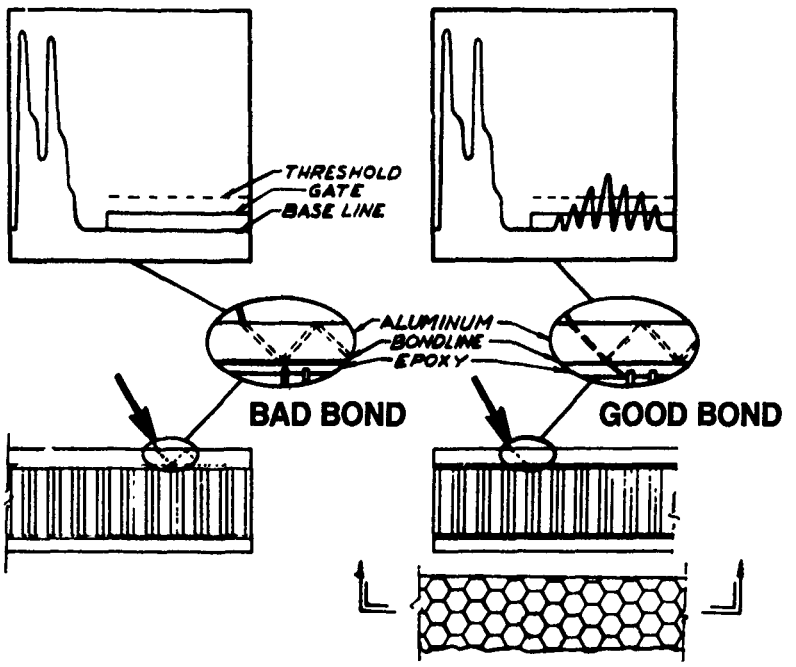

FIGURE 20. Schematic representation of angle beam "go, no-go" test for facesheet-to-honeycomb bond integrity evaluation. Left side of the figure shows an A-scan and cut-away of facesheet/honeycomb interface for a bad bond. There is no return signal. Right side of the figure represents a good bond where some energy is returned and exceeds threshold resulting in a signal detection.

Session IV

FRACTURE SURFACE CHARACTERISTICS ASSOCIATED WITH LOADING MODE AND ENVIRONMENTAL EXPOSURE

FRACTURE SURFACE CHARACTERISTICS IN FIBER COMPOSITE MATRIX RESINS AND THE DIRECTION OF CRACK GROWTH

R.E. Robertson and V.E. Mindroiu
Metallurgy Department
Ford Motor Company
Dearborn, Michigan

FRACTURE SURFACE CHARACTERISTICS IN FIBER COMPOSITE MATRIX RESINS AND THE DIRECTION OF CRACK GROWTH

Richard E. Robertson and Viorica E. Mindroiu

Research Staff
Ford Motor Company
Dearborn, Michigan 48121-2053

Abstract

Three fracture surface characteristics have been found that are indicative of crack-growth direction. Each developed from the "basic longitudinal texture," which in turn is hypothesized to arise from a fingering at the crack front in analogy with the meniscus instability in flowing liquids. Many fracture surface characteristics in crosslinked matrix resins have been found capable of being rationalized by assuming that the fingers are individually affected by the local stress field and composition.

INTRODUCTION

Failure reconstruction usually requires that the conditions at the origin of failure be examined. But the origin must be located first, and this is often difficult with large delamination failures. In many instances, the entire delamination area must be examined microscopically. To reduce the burden of such an exhaustive search, fracture surface characteristics are being sought that can be used to indicate the direction of crack propagation. Rather than having to examine the entire area, then, only regions backwards along the direction of fracture propagation would have to be examined.

FRACTURE CHARACTERISTICS INDICATIVE OF CRACK-GROWTH DIRECTION

Three indicators of crack direction have been found. The first is the gradual development of a "step" and associated "welt" parallel with crack growth on the upstream side, as the crack begins to bifurcate, and the sudden interruption or merging of the step and welt with another step and welt on the downstream side. Examples of this are seen in Fig. 1, which is an SEM micrograph of the cleaved fracture surface of an anhydride-cured epoxy resin. The fracture direction was from right to left. The "welts," so-called because of their similarity to the welts on the edges of upholstered furniture, are the white to light

colored objects attached or associated with each step.[1] The welts are cores of matrix resin that are cut out by pairs of initially parallel cracks that tend to dive toward each other as the fracture pieces are separated.[1-3] The welts are shared between the two fracture pieces. As a result, only about one-half of the steps in Fig. 1 have welts associated with them. The light color of the welts results from their tending to become charged in the SEM.

The second indicator of crack growth direction is the in-plane divergence of the lines of the "basic longitudinal texture." This is also visible in Fig. 1. The "basic longitudinal texture" is the smallest-scale regular marking visible on the fracture surface. The fanning-out results when the crack spreads out from a narrow source. After the crack bifurcates several times, relatively narrow crack segments are left on each of a number of different planes. Although the general crack motion would have been from right to left in Fig. 1, there is a tendency also for the crack to grow laterally until separation causes the crack on different planes to intercept one another, forming the welts.

The third indicator of crack growth direction is the development of rows of reoriented or skewed cracks in the direction of crack growth. Although the reorientation of the cracks is not discontinuous, the entire row tends to develop more or less all at once. The rows of skewed cracks results from a sudden rotation of the principal stress direction about an axis with a component parallel with the propagation direction. Sometimes the rotation is large enough to cause the crack fingers to fall in behind one another and produce a "stacked lamellar texture."[4] This texture is often seen on the fracture surface of the matrix between pairs of fibers. With smaller angles of rotation, a series of gouges may be left on the fracture surface, an example of which is seen in Fig. 2. This is an SEM micrograph of the fracture surface of a highly crosslinked polystyrene, simulating a polyester type of matrix resin. The fracture direction was from top left to bottom right. While all of the cracks were reoriented together along a line, each crack undergoes its own subsequent evolution.

EXPLANATION

All of the indicators of crack-growth direction found so far developed from the "basic longitudinal texture." This texture is shown in Fig. 3 for the anhydride-cured epoxy resin. It is seen to consist of shallow grooves and low ridges running mostly parallel with the crack direction in an otherwise nearly flat field. This texture has been observed on the fracture surfaces of many thermosets, although in published photographs the basic longitudinal texture is sometimes difficult to distinguished from the much grosser steps and welts. (Two steps

and associated welts are visible in Fig. 3.)

The basic longitudinal texture is suggested to arise from an instability of the crack front,[1] in analogy with the instability of the meniscus in a moving liquid.[5] The suggestion of a meniscus instability at the crack front in solids was first described by Argon and Salama[6] and by Fields and Ashby.[7] The instability causes the crack front to consist of a series of fingers. The fundamental periodicity of the fingers in crosslinked matrix resins may be of the order of 10 nm and may depend on the resin. The periodicity of the texture in Fig. 3, however, is 350 nm, which suggests that there is some regrouping of the smallest fingers into larger fingers.

In a homogeneous material with a completely uniform strain field, which appears to have been true for the material in Fig. 3, coherence is maintained between the fingers, and a nearly planar crack results. When either the material composition or the strain field becomes inhomogeneous, however, the coherence between the fingers may be lost and adjacent fingers may move onto different planes.

It is this gradual divergence of adjacent fingers onto different planes that is suggested to be the explanation for the first indicator of crack-growth direction above. Because the strain and compositional gradients are usually small, they result in only a gradual bifurcation of the crack. The stability of the bifurcated crack, with the two halves of the crack on different planes, may seem a little surprising. But an analysis of the stress field shows that for non-overlapping cracks, there is no stress tending to draw the cracks together again.[8] This also explains why the basic longitudinal texture resulting from the bifurcated crack, as seen on the ledges in Fig. 1, is largely parallel with the general crack direction. That is, instead of the narrow front of the multiply bifurcated crack spreading out radially, it is seen to continue growing in the general crack direction and to only slowly begin to diverge laterally.

The third indicator of crack-growth direction, the development of a row of reoriented or skewed cracks, is seen in other contexts. For example, Knauss has described the occurrence of a row of skewed cracks when a homogeneous material is subjected to mode III cleavage.[9] The conditions under which the row of skewed cracks is produced in Knauss's experiments are effectively the same as those under which the row of skewed cracks in Fig. 2 were produced. Beginning with an initial crack in a block specimen, which could have been produced by mode I cleavage, an anti-plane shear was applied in Knauss's experiment. In effect, the principal stress direction was suddenly rotated about an axis with a component parallel with the propagation direction. Somewhat surprising, however, are the complex changes in the stress field that occur in neat matrix resin specimens, or in resin-rich regions away

from any fibers in fiber composites, when subjected to nominally simple stress fields. Such complexity, of course, is the norm when the fibers and their debonding are involved.

Because the front of the initial crack is not linear, at least microscopically, but consists of a series of fingers reaching ahead of the crack, the rotating stress field acts on each finger individually. This allows an immediate response. Moreover, if the rotation is large, the crack fingers may line up behind one another and produce the "stacked lamellar texture." With smaller angles of rotation, the series of gouges seen on the fracture surface in Fig. 2 results.

APPLICATION

The first job in determining the direction of crack growth is to determine the axis of crack growth. For this, one should seek the basic longitudinal texture. (The specimen must sometimes be tilted toward the detector in the SEM, so that the incident beam strikes the surface obliquely, for enough contrast to be developed.) The much more readily visible steps and welts also can be used to indicate the axis, although they are not always exactly parallel with crack growth. In any case, one should remember that the local axis and direction of crack growth are not necessarily the same as the global or nominal axis and direction.

Three specific fracture surface characteristics have been described that can indicate crack direction in crosslinked matrix resins. Unfortunately, however, the typical fracture surface can be so complex that these features are obscured. The features described may have other features superimposed on them. Also, changes in the stress field can be more complex than described. For example, any rotation of the stress is usually about an axis with components both along and perpendicular to the crack-growth direction. Nonetheless, we have found that most, if not all, of the fracture surface features can be disentangled if during the analysis one keeps in mind the fingering at the crack front and the influence of the local stress and composition on these crack fingers.

References

1. R. E. Robertson, V. E. Mindroiu and M. F. Cheung, Fracture in epoxy matrix resins, Composites Sci. Tech., 22 (1985), 197-207.

2. M. Atsuta and D. T. Turner, Fractography of highly crosslinked polymers, J. Mater. Sci. Lett., 1 (1982), 167-9.

3. M. Atsuta and D. T. Turner, Fractography of Polyethylene glycol dimethacrylate doped with poly(methyl methacrylate), Polym. Eng. Sci., 22 (1982), 1199-1204.

4. R. E. Robertson and V. E. Mindroiu, The stacked lamellar texture on the fracture surfaces of fiber composites, J. Mater. Sci., in press.

5. G. I. Taylor, The instability of liquid surfaces when accelerated in a direction perpendicular to their planes, I, Proc. Roy. Soc. (London), A201 (1950), 192-6.

6. A. S. Argon and M. Salama, The mechanism of fracture in glassy materials capable of some inelastic deformation, Mater. Sci. Eng., 23 (1976), 219-30.

7. R. J. Fields and M. F. Ashby, Finger-like crack growth in solids and liquids, Phil. Mag., 33 (1976), 33-48.

8. S. Melin, Why do cracks avoid each other? Int. J. Fracture, 23 (1983), 37-45.

9. W. G. Knauss, An observation of crack propagation in anti-plane shear, Int. J. Fracture Mech., 6 (1970), 183-87.

Figure 1. SEM micrograph of the fracture surface of an anhydride-cured epoxy resin showing terraces or ledges between steps. Associated with the steps are the white to light colored "welts." Visible on the ledges is the "basic longitudinal texture" and continuing crack bifurcation. Fracture propagated from right to left; specimen fractured by mode I cleavage.

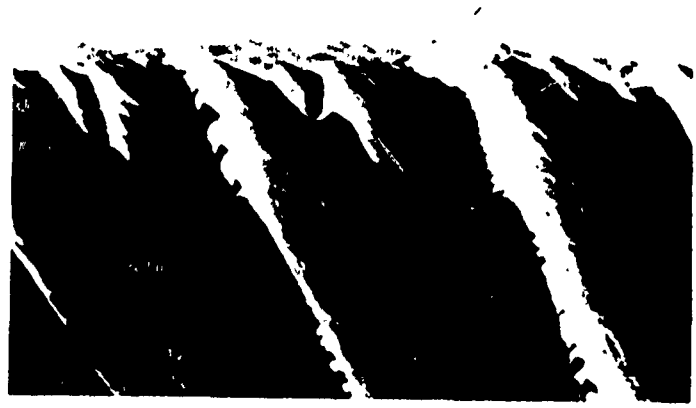

Figure 2. SEM micrograph of the fracture surface of a crosslinked polystyrene showing gouges resulting from the re-orientation of the stress field as the crack propagated from the top left to the bottom right. This specimen had fractured during cure at 75 °C; the reorienting stress resulted from a constraint imposed on the curing resin.

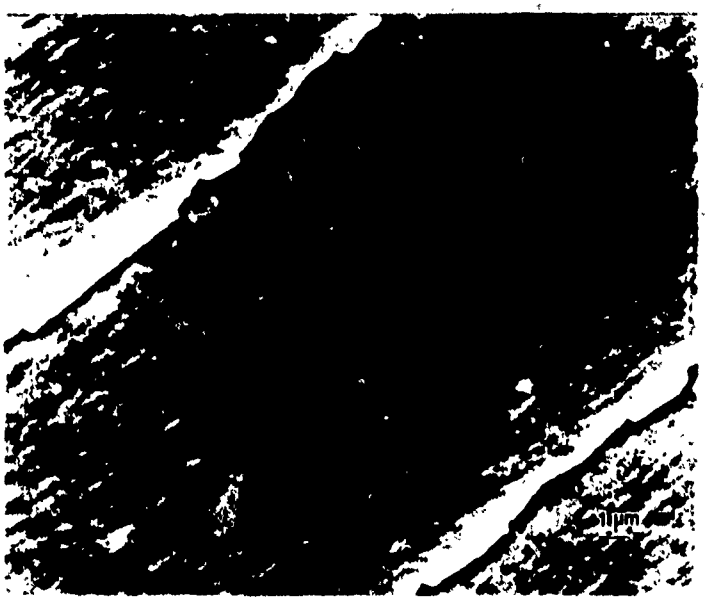

Figure 3. SEM micrograph of the fracture surface of the anhydride-cured epoxy in a different location from Fig. 1 that shows the basic longitudinal texture as well as two steps and associated welts. The axis of crack propagation is from lower left to upper right.

THE MEANING AND SIGNIFICANCE OF HACKLES IN COMPOSITE MATERIALS FAILURE ANALYSIS

W. Jordon
M. Hibbs and W. Bradley
Texas A&M University
College Station, Texas

The Meaning and Significance of Hackles in Composite Materials Failure Analysis

by

William Jordan, Michael Hibbs, and Walter Bradley
Texas A&M University
College Station, Texas 77843

INTRODUCTION

The dramatic increase in use of graphite/epoxy composites in many diverse applications has brought about the need for reliable failure analysis techniques of these materials. For years, fracture surface morphology has been successfully used as means of identifying the fracture origin and direction of crack propagation in metals. There have been recent attempts by Hahn(1,2)and others to apply similar techniques to graphite/epoxy composites. In order to more easily use fracture surface characteristics as a tool in failure analysis, a better understanding of the micromechanical processes involved in failure in these materials is needed.

In the case of delamination of a graphite/epoxy composite, the fracture surface is characterized by the amount of fiber pullout, interfacial debonding, and the extent of the resin deformation or microcracking. One of the most common features of resin deformation have been identified as 'hackles'. These hackles appear as lacerations or scallops in the resin that form regular saw tooth or zipper patterns. The works of these authors and others (Hahn) have shown that, as the shear or mode II component of the state of stress

at the delamination crack front is increased, both the number and angle of the hackle with respect to the ply plane also increase. Several attempts have been made to relate the orientation of the hackles to the direction of crack propagation. Early works indicated that hackles slant towards the direction of crack growth (3,4). A more recent study has indicated that the hackles slant in opposite directions on the top and bottom surfaces of the crack face (5).

In this study, the effects that the state of stress, direction of crack growth, and resin ductility have on the formation of hackles in delamination failure will be explored. Evaluations will be made on the basis of scanning electron microscope (SEM) observations of the post-mortem fracture surfaces of unidirectional split laminate double cantilever beam specimens (DCB). These DCB specimens have been loaded in mode I, mode II, and mixed mode I & II conditions. Also, observations through the SEM of a mixed mode failure provided by unidirectional crack lap shear specimens (CLS), described by Wilkins, et al. (6) were made. These specimen gave approximately 75% mode II and 25% mode I loading.

To better understand the micromechanics involved in the formation of hackles and to help in the interpretation of the post-mortum fractography, in-situ SEM observations of delamination fracture of small DCB specimens loaded in mode I and mode II conditions were made.

Because, in most applications of composites, multidirectional laminates are used, a discussion of the resulting fracture surfaces from multidirectional laminates is also included.

EXPERIMENTAL PROCEDURES

The graphite/epoxy composites used in this study were made from three resins, Hercules 3502, Hexcel 205 and Dow Chemical Q6 (a new experimental resin system). These three resins were chosen because they had very different toughnesses. In the case of the 3502 and Q6, pre-preg tape was obtained from the manufacturer and made into a 30 cm. square unidirectional panel with 24 plies. The panels were cured according to the manufacturers recommendations. A thin 0.03 mm teflon strip was placed between the center two plies to provide a starter crack. Hexcel provided unidirectional laminate made from prepreg of HX205 resin and graphite fibers. Test specimens 2.5 cm. by 25 cm. were cut from each panel. Double cantilevered beam specimens were tested on an MTS system in stroke control. Small specimens (2 cm x 0.4 cm) were cut from the larger panels for testing in the scanning electron microscope.

A schematic of the loading for the various tests is shown in Figure 1. Mixed mode conditions are obtained by superimposing a pure mode II load upon a mode I load. Pulling down only on the lower surface gives 43% mode II conditions if the upper arm is unloaded. Note pure mode II loading is obtained by pulling down on the top surface. To remove as much as possible any rubbing together of the fracture surfaces, a teflon strip about .1 mm thick was placed between the ends of the top and bottom surfaces.

Crack lap shear tests with approximately 75% mode II were conducted using the test specimen shown by Wilkins. The samples were tested on an Instron test machine in stroke control.

Fractographs were obtained by sectioning the fractured coupons with a jeweler's saw. The amount of cutting debris was minimized by cutting the samples before the top and bottom surfaces were separated. Any loose

debris that did occur was blown away by compressed air. The surface was then coated about 200 A thick layer of gold-palladium. The photographs were made on Tri-X film, using a JEOL JSM-25 Scanning Electron Microscope at accelerating voltages of 12.5 and 15 kv.

A limited number of mode I and mode II delamination tests were observed in the scanning electron microscope using a specially designed stage capable of loading specimens in the SEM. These observations were recorded in video tape and on tri-X sheet film. The edge of the specimen to be observed during delamination was carefully polished using standard metallographic techniques and coated with a 200 A gold-palladium alloy.

EXPERIMENTAL RESULTS

Post-mortem Fractographic Examination

In this section post-mortem fractographic results for delamination of three graphite/epoxy composites will be presented.

Brittle resin composite AS4/3502 (G_{1c} = 189 J/m^2) - Fractography of the post-mortem delamination surfaces indicates that the number of hackles increase as the percentage of shear loading is increased, with the most dramatic increase being between 43% and 100% mode II loading (Figure 2). Mode I fracture surfaces were characterized by a flat corrugated roof appearance with a limited number of shallow hackles. The angle or slant between these hackles and the plane of the fracture surface is seen to increase as the percentage of shear loading is increased. At near pure mode II loading, the hackle are observed to be nearly perpendicular to the plane of the plies, and their edges appeared drawn and "tuffed". For the most part, the orientation or slant of the hackles remains constant on a

given fracture surface and point in opposite direction on the matching fracture face.

Because the interfacial bonding is so poor in AS4/3502, almost all fracturing occurred at the interface for pure mode I loading. AS1/3501-6 shown in Figure 3 indicates the more typical corrugated roof appear of pure mode I fracture with fracture occurring primarily through the resin. It should be noted in Figures 2 and 3 that almost no hackles are observed in the brittle system for pure mode I loading.

Moderately ductile resin composite HX205 (G_{1c} = 455 J/m^2) - The fracture surfaces of the more ductile resin composite system HX205 were similar in appearance to those seen in AS4/3502, except for a much greater degree of resin deformation (Figure 4). As the percentage of shear loading was increased both the number and slant of the hackles increased. As the mode II loading is increased the shape of the hackles appeared more pulled or drawn than those seen in the brittle AS4/3502 system.

Ductile resin system Dow Q6 (G_{1c} = 850 J/m^2) - The fracture surfaces of the ductile system Q6 were characterized by considerable resin deformation with good fiber/resin adhesion. Fractography reveals no distinct hackles (Figure 5). Only at near pure mode II loading conditions were some ill defined hackle like features seen. These features seen to be random with no consistent orientation.

In-situ delamination fracture observations in SEM

In-situ observations of fracture in the SEM of the three composite systems are seen in Figure 6. For mode I loading, both the brittle system AS4/3502 and the moderately ductile system HX205, the primary crack is seen to proceed by interfacial debonding. A limited amount of microcracking

is seen to occur in the resin behind the primary crack tip, and is normally associated with fiber bridging and eventual pullout.

In the mode I fracture of the ductile Q6 system, crack propagation occurs primarily by resin deformation and fracture with only occasional interfacial debonding. Considerable resin deformation and microcracking is seen in the regions outside the resin rich area between the plies.

In the mode II delamination of the AS4/3502 system, a series of sigmodial shaped microcracks are seen to develop in the resin rich region between the plies, well ahead of the crack tip. The primary crack extension occurs by the growth and coalescence of these microcracks.

DISCUSSION

Hackle Formation in More Brittle Resin Systems

The fractography for both the brittle system AS4/3502 and the moderately ductile system Hexcel HX205 clearly shows that the number of hackles as well as their orientation, or angle with respect to the ply plane, increase as the percentage of shear loading is increased (Figures 2-4). In mode I failure, the in-situ observations indicate that the primary micromechanism of delamination is by interfacial debonding (Figure 6) or continuous growth of the microcrack through the resin rich region between plies. This brittle fracture as it occurs for debonding or resin cracking occurs perpendicular to the principal normal stress in the region of the crack tip.

As the percentage of mode II loading is increased, the angle which the principal normal stress at the crack tip makes with respect to the ply plane changes from being parallel to the ply plane in mode I to 45° to the ply plane in pure mode II loading. The hackles formed are apparently

the result of the cracking occurring in a brittle fashion on the principal. normal stress plane, giving a whole series of microcracks running through the resin rich region between plies until they are stopped by the fibers. Coalescence of these microcracks, usually by interfacial debonding gives macrocrack advance and leaves a zipper appearance to the fractured surface, as shown in Figure 2.

The above conclusions have important implications to failure analyst. If the state of loading is known, the direction of the principle normal stress can be calculated from the tensile and shear components of the load. By assuming that the hackles are oriented perpendicular to the direction of the principle normal stress, one should be able to estimate the fraction of mode I and mode II loading which caused the delamination. To accomplish this, one must measure the hackle angles by looking at their profiles. This may be done by nickel plating the fracture surface to preserve the hackles, sectioning and polishing one edge.

Bascom (7) has recently indicated that resin flow or yielding may be an important mechanism in the formation of hackles. Indeed, at a high percentage of the shear loading in the moderately ductile system HX205 or near pure mode II loading for the brittle AS4/3502, the shape of the hackles seems to indicate some resin drawing (Figure 4). This is probably due to resin flow before final microcrack coalescences takes place. The amount of resin flow in the development of hackles can be evaluated by annealing the fracture surface near the resin's Tg to see the extent of recovery but, at the time of this writing, annealing tests had not been performed on cur specimens.

Fracture Characteristics of Very Ductile Systems

The large amount of resin deformation and the lack of any distinct hackles indicates that the processes of fracture in the ductile Q6 system are different from those seen in the more brittle systems. This is confirmed by the in-situ mode I delamination observations (Figure 6) that show that failure is by resin cracking and deformation. The good fiber/resin adhesion indicates that the shear loads must be effectively transferred to the resin. Because of the resin's ductility, failure from yielding occurs before the development or coalescence of a regular system of microcracks can take place. Clearly the use of fracture surface topography in the failure analysis of any ductile system is much less instructive.

SUMMARY

Hackles form in graphite/epoxy composite materials when the following requirements are met: (1) relatively brittle epoxy is used; (2) some regions of resin concentration are present (e.g., low fiber density in delamination plane between plies); and (3) some mode II loading must be present locally in the crack tip region. Such conditions are routinely met in laminates with a multiaxial layup since interlaminar shear stresses are always present in such laminates, even when they are loaded with only mode I loading conditions. Furthermore, fiber nesting is not possible in such systems, which means that regions of resin concentration are always present at the interface between adjacent plies. Thus, it is not surprising that hackles are a very dominate feature on the fracture surface of delaminated multi-directional laminates.

In a unidirectional laminate, hackles will be a common feature of the delamination fracture surface only when the macroscopic loading conditions give a significant fracture of mode II loading. Otherwise, hackles will only

be observed occasionally when local heterogeneities in the composite cause the crack tip to experience a significant mode II contribution even though the macroscopic loading conditions are pure mode I. Furthermore, fiber nesting in unidirectional layups give a smaller volume of resin concentrated regions where hackles may form.

Since hackles result from sigmodial shaped microcracks for unidirectional layups, we do not believe that crack growth direction can be deduced from the macroscopic orientation of the hackles, since they will point in the direction of crack growth on one fracture surface and in the opposite direction on the other fracture surface. Sometimes a more detailed examination of individual microcracks may indicate "river patterns", and these may be useful in accertaining crack growth direction. We believe that only the hackles angle of inclination with regard to the plane of delamination gives useful information, and this information has to do more with state of stress than crack growth direction.

Finally, a change in loading conditions during crack growth could give a change in crack growth direction which might be reflected in a change in hackle orientation in a multi-directional laminate. Thus, it might be difficult to determine crack growth direction from hackles for proportional loading; nonproportional loading and subsequent changes in crack growth direction could probably be accertained from changes in hackle orientation.

ACKNOWLEDGEMENT

This work was performed at Texas A&M University through the support of the Air Force Office of Scientific Research under the direction of Major David Glasgow.

REFERENCES

1. Hahn, H. T. and Johannesson, T., "A Correlation Between Fracture Energy and Fracture Morphology in Mixed Mode Fracture of Composites," presented at 4th International Conference on Mechanical Behavior of Materials, Stockholm, Sweden, August 15-19, 1983.

2. Hahn, H. T. and Johanneson, T., "Fracture of Unidirectional Composites: Theory and Applications," presented at Meeting of ASME, Bostom, MA, Nov. 13-18, 1983.

3. Richards-Frandsen, R. and Naerheim, V., "Fracture Morphology of Graphite/Epoxy Composites," J. of Composite Materials, Vol. 17, March 1983, pp. 105-113.

4. Morris, G. E., "Determining Fracture Directions and Fracture Origins on Failed Graphite/Epoxy Surfaces," in Non Destructure Evaluation and Flaw Critically for Composite Materials, ASTM STP 696, 1979, pp. 274-297.

5. Liecht, K. M., Masters, J. E., Ulman, D. A., and Lehman, M. W., "SEM/TEM Fractography of Composite Materials," report no. AWAL-TR-82-4085, report by General Dynamics, Fort Worth, for Materials Laboratory, AFWAL, 1982.

6. Wilkins, D. J., Eisenmann, J. R., Camin, R. A., Margolis, W. S., and Benson, R. R., "Characterizing Delamination Growth in Graphite-Epoxy," in Damage in Composite Materials, ASTM STP 775, 1982, pp. 168-183.

7. Bascom, W. D., personal communication.

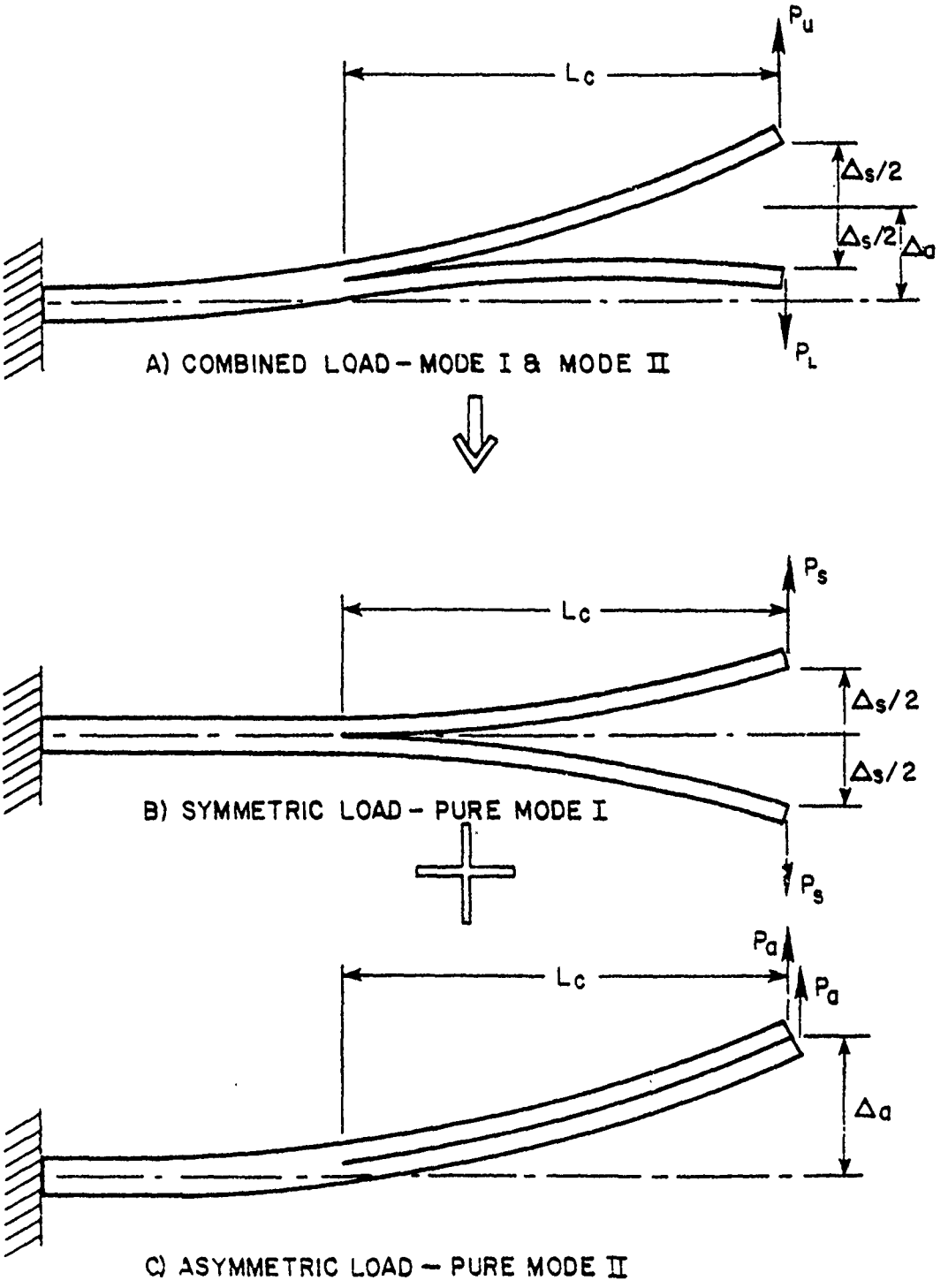

Figure 1. Schematic showing mixed mode test conditions obtained by asymmetric loading of a double cantilevered beam test specimen.

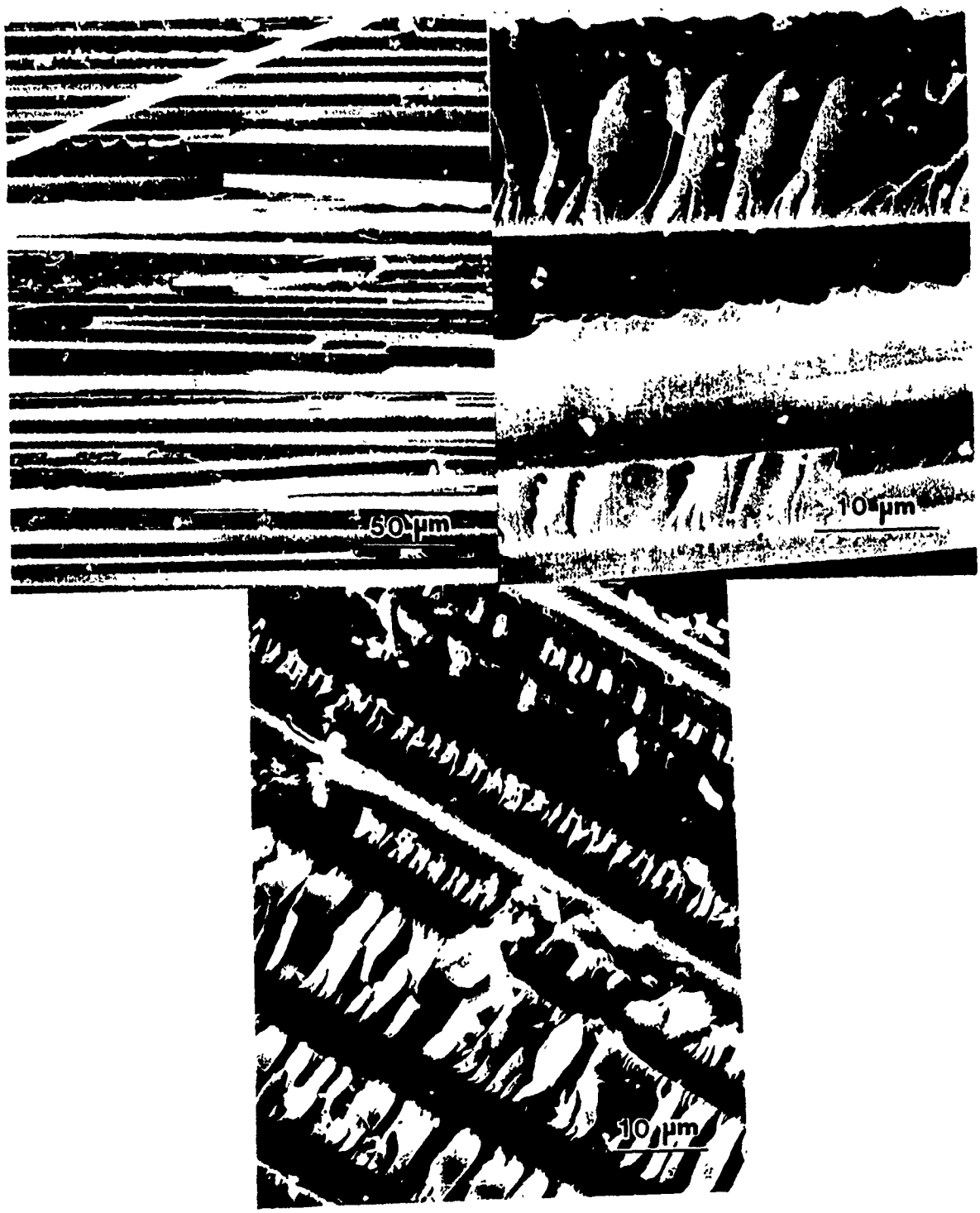

Figure 2a. Fracture surface of AS4/3502 system fractured in mode I conditions (left, 300 x).

Figure 2b. Fracture surface of AS4/3502 system fractured in 43% mode II conditions (right, 4500 x).

Figure 2c. Fracture surface of AS4/3502 system fractured in mode II conditions (bottom, 1500 x).

Figure 2d. Fracture surface of AS4/3502 system fractured in mode II conditions showing how on top surface (top, 1500 x) and bottom surface (bottom, 1000 x) the hackles point in opposite directions.

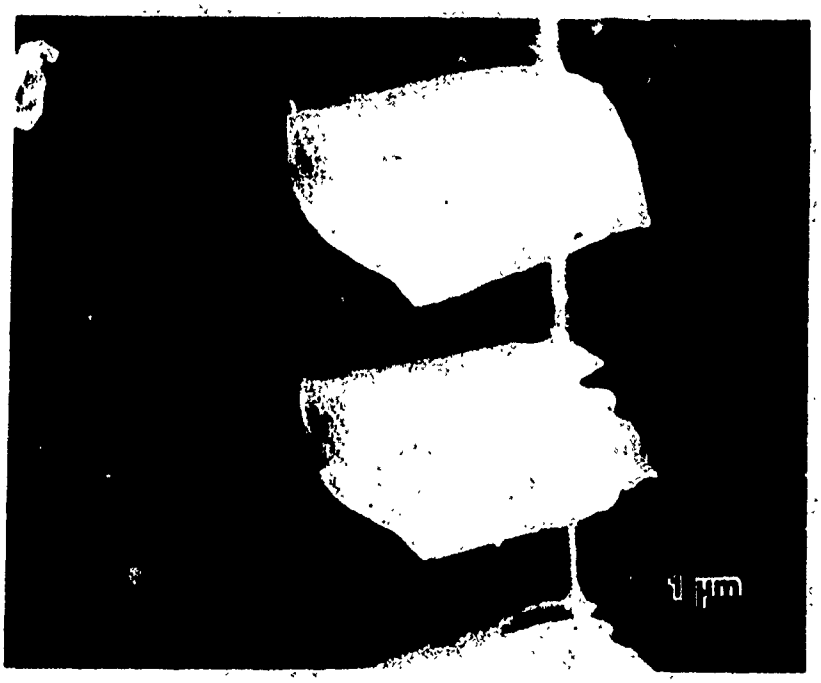

Figure 2e. Enlarged view of hackle in AS4/3502 mode II test showing sigmoidal shape of hackle surface (10,000 x).

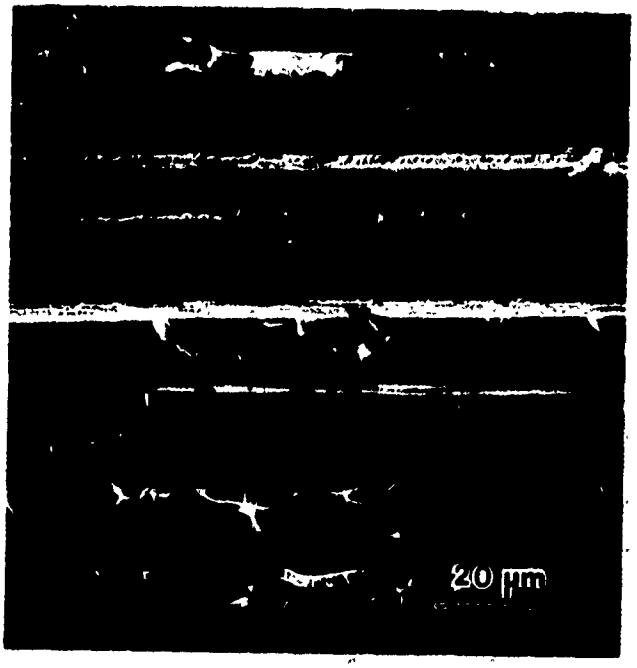

Figure 3. Fracture surface of AS1/3501-6 system fractured in mode I conditions (1000 x).

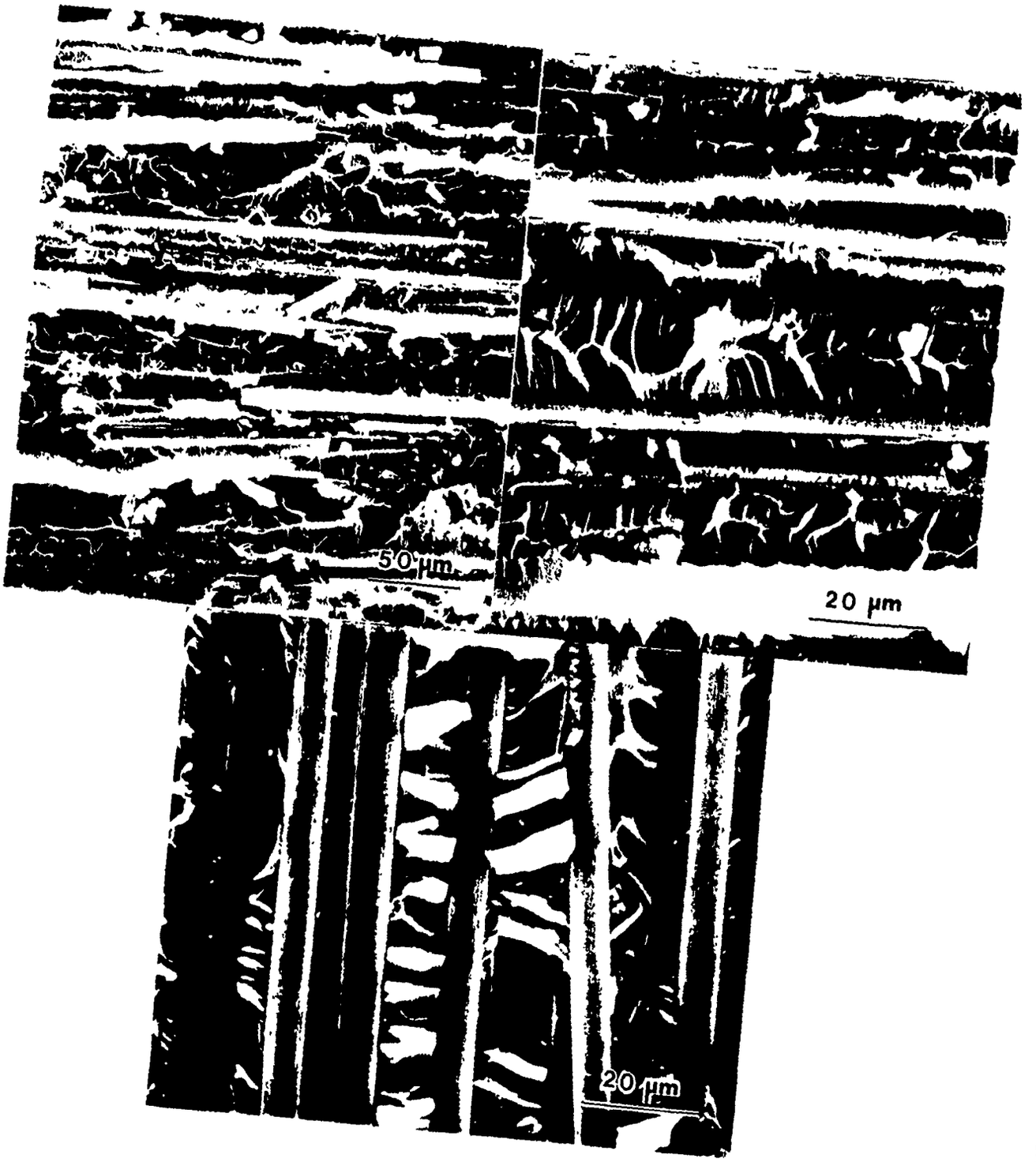

Figure 4a. Fracture surface of Hx205 system fractured in mode I conditions (left, 300 x).

Figure 4b. Fracture surface of Hx205 system fractured in 43% mode II conditions (right, 1000 x).

Figure 4c. Fracture surface of Hx205 system fractured in mode II conditions (bottom, 1000 x).

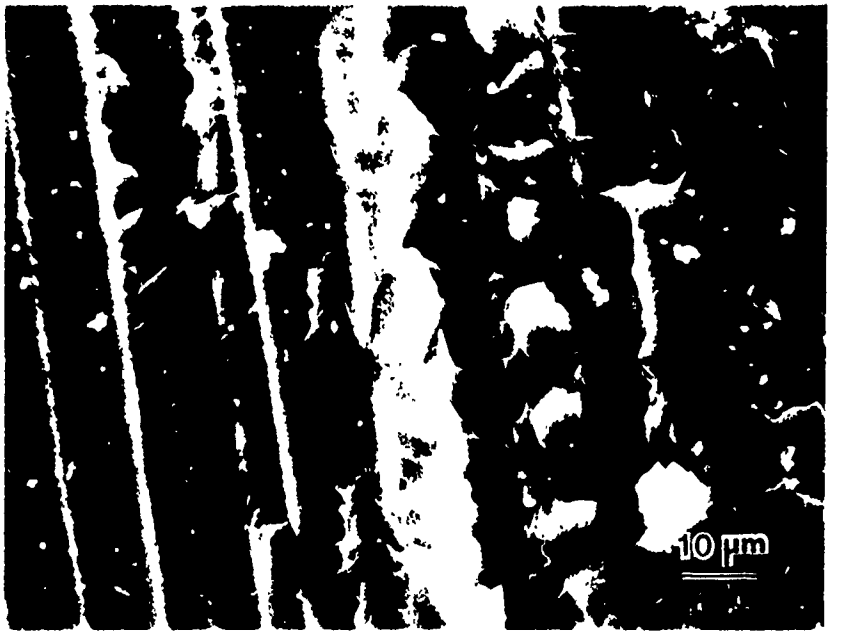

Figure 5a. Fracture surface of Q6 system fractured in mode I conditions (left, 450 x).

Figure 5b. Fracture surface of Q6 system fractured in 43% mode II conditions (right, 1500 x).

Figure 5c. Fracture surface of Q6 system fractured in mode II conditions (bottom, 1000 x).

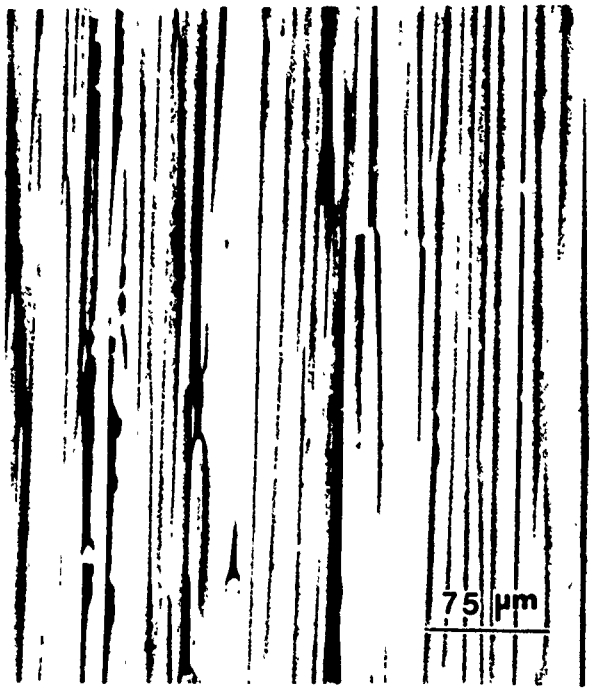

Figure 6a. Insitu delamination of AS4/3502 system (top, 220 x).

Figure 6b. Insitu delamination of Hx205 system (bottom. 1000 x).

SOME FRACTOGRAPHIC INVESTIGATIONS OF COMPRESSIVE FAILURES IN CARBON FIBRE REINFORCED PLASTICS

R.T. Potter
Materials & Structures Department
Royal Aircraft Establishment
Farnborough, Hants, England .

SOME FRACTOGRAPHIC INVESTIGATIONS OF COMPRESSIVE FAILURES IN CARBON FIBRE REINFORCED PLASTICS

by

R T Potter
Materials and Structures Department
Royal Aircraft Establishment
Farnborough
Hants
UK

1 INTRODUCTION

For more than a decade, fractographic analysis has been employed in research programmes at RAE to elucidate the mechanisms of failure in carbon fibre reinforced plastic (CFRP) test specimens and structural elements under a wide range of loading conditions.[1,2] From the extensive study of the fracture surfaces of simple coupon specimens followed by the evaluation of more complex specimens containing structural features, techniques have been developed by which the failure of full-scale structural items may be analysed.

This Paper first describes the general procedure used at RAE for post-failure analysis of CFRP structures. It is shown that the method relies to a considerable extent on fractography, that is, on the ability to interpret the wealth of information yielded by detailed examination of the fracture surfaces. The paper then describes some of the work carried out at RAE which has contributed to the development of fractography as applied to the compressive failure of carbon fibre/epoxy resin composites. The understanding gained from early studies of failure in unidirectional material[3] has been developed and extended in more recent studies of the effects of environment on failure due to notches in multidirectional composites.[4] Another area of considerable significance for aerospace structures which has been studied is that of impact damage and post-impact compressive failures.[5,6] From programmes such as these, a sound understanding of compressive failure mechanisms has been gained so that the characteristic features of fracture surfaces resulting from particular mechanisms may be recognised. This, together with corresponding programmes on failure under tensile and shear loading, forms the 'data base' which is an essential prerequisite to successful post-failure analysis.

2 POST-FAILURE ANALYSIS OF CFRP STRUCTURES

The general procedure adopted at RAE for the post-failure analysis of large structural items is illustrated in Figure 1. Before removing any material for analysis it is important to obtain an adequate photographic record of the failed item showing the relative positions of all fractured sections and any visual evidence of significant events, such as debris from an impacting object for example. The next stage is to select samples from each of the principal fracture surfaces in order to establish the local mode of failure (ie tension, compression or shear) and, where possible, the direction in which failure propagated. From this information it is generally possible to construct a 'movement diagram' indicating the relative movement of the failed segments. Whilst studying the local failure modes it is important to observe and record any microstructural anomalies such as voids, inclusions, fibre kinks, impact-induced delaminations etc, which might have significantly

reduced the strength or stiffness of the composite. Combining this information with that contained in the movement diagram it is generally possible to deduce the sequence of failures and hence determine the origin and primary cause of failure.

The success of the above procedure depends to a large extent on the selection of samples from the fracture surfaces. Clearly, samples taken adjacent to structural features such as fastener holes, cut-outs and changes of section are desirable. Moreover, it is important to select samples in which the fracture surfaces have not been severely damaged by post-failure movement. As indicated in Figure 1 there may be additional information such as design and test data, non-destructive inspection (NDI) records and possibly even strain gauge or stress wave emission (SWE) data to assist in sample selection. Such information may also be required to distinguish between two or more possible failure sequences although, since much of it may be circumstantial in nature, it is preferable to use such information only to confirm the sequence deduced from the direct evidence of the fracture surfaces.

In practice, no two investigations are the same and the procedure must be adapted to suit the evidence available. Nevertheless, it has been found that successful post-failure analysis depends primarily upon the interpretation of the local fracture surfaces. In particular, it is important not only to be able to recognise the general characteristics of fracture surfaces formed under various loading conditions, but also to be able to distinguish between the significant and insignificant anomalous features which inevitably occur. The former capability depends partly on the experience of the investigator, although the need for such experience could be greatly reduced by the generation of a comprehensive catalogue of fracture surfaces. However, the latter capability relies heavily upon a detailed understanding of the mechanisms of damage propagation and failure at a microstructural level. It is fortunate therefore that fractographic analysis of test specimens has been a routine part of many research programmes at RAE and that this has provided a qualitative understanding of the failure processes on which to base the current post-failure analysis capability for CFRP structures.

3 THE COMPRESSIVE FAILURE OF UNIDIRECTIONAL CFRP

The nature of compressive failure in unidirectional (UD) CFRP was studied at RAE by Ewins and Ham[3] in the early seventies. Their work is of particular significance not only because it provided the basis of current understanding of compressive failure in CFRP, but also because it was the first programme in which the detailed observation of fracture surfaces was used to elucidate the failure mechanisms in CFRP and to explain variations in composite strength. It may therefore be regarded as the first application to CFRP of modern methods of fractographic analysis.

Most early attempts to model the compressive failure of CFRP were based on the assumption that strength was governed by fibre instability. Such models imply that composite strength should increase with fibre modulus, but Ewins and Ham observed that composites made from high modulus fibres gave lower compressive strengths than those made from high strength (lower modulus) fibres. A further observation arose from experiments being carried out at RAE in which specimens were subjected to transverse compressive stress whilst Poisson expansion was inhibited. Failure therefore occurred by shear across the fibres and matrix, as shown in Figure 2. For composites containing either high strength or high modulus fibres, it was observed that the transverse compressive strength measured in such a test was similar to the

longitudinal compressive strength in a conventional test. This suggested a common link between the failure mechanisms. Since there was no possibility of fibre buckling in constrained transverse compression, Ewins and Ham postulated that, in both cases, failure occurred by shear across the fibres and matrix and that strength was governed primarily by the shear strength of the fibres. This suggestion was further supported by experiments on composites of varying fibre volume fraction. As illustrated in Figure 3, it was observed that both compressive strength values varied linearly with fibre volume fraction as would be predicted from a rule of mixtures approach based on a constant fibre stress at failure.

Experiments to investigate the effects of temperature on both types of compressive failure showed that the link between the failure mechanisms was maintained for temperatures from -50°C up to about 100°C. Again the variation of strength was consistent with a rule of mixtures approach based on constant fibre stress at failure; the gradual reduction of strength with temperature appeared to be due simply to the reducing matrix stiffness. However, above about 100°C, the longitudinal compressive strength started to fall away quite rapidly whilst the constrained transverse compressive strength continued its more steady decline, as shown in Figure 4. This suggested a change in the longitudinal compressive failure mechanism at about 100°C.

In order to study these phenomena further, the fracture surfaces of a number of specimens were examined in a scanning electron microscope (SEM). In longitudinal compressive specimens tested below about 100°C the broken fibre ends were generally ill-defined and there was considerable matrix debris. The fracture surfaces therefore exhibited a uniformly granular appearance as shown in Figure 5. The fracture surfaces of specimens failed in constrained transverse compression exhibited similar characteristics supporting the hypothesis that both types of failure were governed by the shear strength of the fibres. In longitudinal compressive specimens tested at temperatures above about 100°C the fibre ends were well defined and there was little matrix debris as shown in Figure 6. Many fibres exhibited two different types of fracture surface separated by a well defined line, as illustrated in Figure 7. The rougher surface texture was typical of tensile fibre fractures and suggested that the individual fibres had buckled and failed in flexure. The relative positions of the fracture surfaces and the parallelism of the neutral axes (see, for example Figure 6) indicated that adjacent fibres generally buckled in the same direction. At lower magnification, the fracture surface of the composite exhibited well defined steps, as illustrated in Figure 8. Each step was of similar height, and detailed examination of the fibre ends on either side showed that the relative positions of the two types of fracture surface generally reversed at the step. Evidently the direction of flexure changed at each step.

By correlating fractographic evidence with the measured variations in strength properties, Ewins and Ham had been able to show that, at moderate temperatures, both longitudinal compressive failure and constrained transverse compressive failure occurred by shear across the fibres and matrix. Under both types of loading strength was governed primarily by the shear strength of the fibres and variations in strength due to changes in fibre volume fraction or temperature were due simply to changes in the proportion of load carried by the matrix. Under longitudinal compressive loading at high temperature the reduction of matrix stiffness allowed the fibres to buckle so that composite strength was determined by matrix stiffness rather than by fibre strength.

In recent years the strength of carbon fibres has steadily increased whilst the stiffness properties of the commonly used matrices have changed very little. Current carbon fibre/epoxy resin composites therefore fail by a fibre buckling mode throughout the temperature range. It follows that without improvements in matrix stiffness the high strength of carbon fibres cannot be fully exploited in compression. More importantly, the effects of environment on compressive strength are determined by the relatively strong effects on the matrix and fibre-matrix bond. If matrices of sufficiently high stiffness were to be used the effects of temperature and moisture on composite compressive strength might be greatly reduced.

It should also be noted that whilst the term fibre buckling is used here, there remains some debate about the details of the failure process. The term buckling generally suggests that there is a well-defined load above which stability is lost. But for fibres which may have some initial curvature and which are supported in an elastic matrix it is possible to conceive a mechanism whereby laterial deflection of the fibres increases steadily from zero load up to failure. Moreover, the cause of the final collapse is uncertain since it could be precipitated either by flexural failure of the fibres or by shear failure of the matrix or fibre-matrix bond at the points of inflexion. In early carbon fibre composites there was little evidence of such a shear failure and even with the current higher strength fibres the balance of evidence seems to suggest that fibre flexural failure is the primary cause of the final collapse. Clearly, there is scope for much additional research to elucidate the fine details of this failure mechanism.

4 THE COMPRESSIVE FAILURE OF MULTIDIRECTIONAL CFRP

Early investigations of compressive failure in multidirectional (MD) CFRP were hindered by the lack of a specimen which could be relied upon to give failure in a region of uniform uniaxial stress unaffected by stress concentrations or free edge effects. However, in spite of these reservations, work such as that reported by Port[7] suggested that the compressive stress which could be achieved in the axial plies of MD laminates was sometimes significantly less than that achieved in UD material. This suggested that the mechanism of failure in the axial plies could be affected by adjacent off-axis plies. The first attempts to investigate such phenomena by fractographic methods were greatly hindered by extensive post-failure damage. The release of strain energy from both specimen and test machine tended to cause a substantial amount of delamination making it difficult to study the relationships between failures in different plies at a microstructural level. Nevertheless, it was clear from visual examination of specimens that the line of failure in the axial plies was often influenced by the orientation of the off-axis plies.

To study such failures in greater detail it was clearly necessary to control the amount of post-failure damage. This could be achieved to some extent by testing very small samples in a machine of very high stiffness, but ideally, one would like to detect the initiation of failure and to arrest or control its progress across the specimen. In an attempt to do this, a test system has been developed at RAE in which a mini-computer is used to generate the command signal for a servo-hydraulic test machine. Signals proportional to the current values of load, ram displacement and strain (as measured by a bonded metallic foil strain gauge) are continuously monitored by the computer and used to modify the command signal if any indication of 'failure' is detected. The response rate of the test system is clearly an important factor but it has been found that the control of failure is governed primarily

by the ability to detect the onset of the failure process at a sufficiently early stage. Attempts to do this by monitoring load or ram displacement have been unsuccessful since neither parameter changes by a measurable amount before a considerable amount of damage has occurred. However, measurement of local strain has been found to be very effective if the gauge can be located sufficiently close to the origin of failure. In plain, uniformly stressed specimens this is clearly difficult to achieve but in notched specimens the possible locations at which failure may initiate are predetermined. The system has therefore been used to study failure mechanisms in notched CFRP and in particular to investigate the effects of temperature and moisture on the failure processes.

24-ply laminates having two different stacking sequences have been studied.[4] The first had a stacking sequence $(+45,-45,0,0,+45,-45,0,0,0,+45,-45,0)_s$ whilst the second had a stacking sequence $\{(+45,0,-45,0)_3\}_s$. It may be seen that both laminates contained the same proportion of plies in all three directions and they should therefore exhibit the same in-plane stiffness properties. Moreover, for a notch of given geometry the in-plane elastic stress concentrations should be of equal magnitude so that one might expect to observe the same compressive strengths. Specimens containing a circular notch of 5 mm diameter were tested at room temperature having been stored in a dessicator since laminate manufactu e to ensure a moisture content of virtually zero. For the first laminate, in which the axial plies were grouped in blocks of two or three, the notched strength was found to be 570 MPa. However, the second laminate, in which the axial plies were well-distributed, yielded a notched strength of only 465 MPa.

Taking specimens in which failure had been arrested using the test system described above, the damage within and between the various plies was studied by two techniques. The first involved grinding away each ply by hand so that the damage near the mid-plane of the ply could be observed using a stereo optical microscope. In the second technique the plies were successively removed by peeling them from one edge of the specimen using a sharp modelling knife to initiate failure. In areas of delamination the ply peeled away cleanly to reveal the ply below, but where there was no delamination the failure occurred just within the ply being removed. In practice it was found that this latter technique also revealed fibre fractures and many of the translaminar cracks within the plies and the former technique is now rarely used. A typical example of a peel fracture surface is shown in Figure 9(a).

For both laminate types it was found that translaminar cracks (running parallel to the fibres) formed near the notch in the majority of plies. The cracks were generally tangential to the notch and were frequently associated with delamination as shown in Figure 9(a). Translaminar cracks in the axial plies were seen to induce some fibre failures in adjacent off-axis plies as shown in Figure 9(b). Both tensile and compressive failures were observed depending on the direction of shear in the axial ply.

The translaminar cracking and associated delamination was generally similar to that which constitutes damage zones in notched tensile specimens and presumably had a similar stress relieving effect. However, as for tensile failure, compressive failure will ultimately be governed by failure of the axial fibres which carry most of the applied load. Perhaps the most significant observation therefore was that the location and direction of the fibre buckles in the axial plies was frequently governed by the presence of a translaminar crack in an adjacent off-axis ply, as illustrated for example

in Figure 10. In this Figure the axial fibres buckled in a direction determined by the shear displacement due to a crack which is tangential to the notch in the 45 degree ply immediately below the axial ply. The fact that the fibres buckled in the plane of the laminate was confirmed by examination of the individual fibre ends in an SEM to determine the orientation of the neutral axes resulting from the flexural failure of each fibre. Recent experiments on unnotched specimens have shown that compressive strength may be significantly reduced by a superimposed shear stress.[5] Ply interaction effects are therefore likely to reduce the load carrying capacity of the axial plies, and the magnitude of the effect will depend on the extent to which the plies of different orientation are intimately mixed. The observed difference in the notched compressive strengths for the two laminate types is therefore to be expected.

Specimens were also tested at elevated temperature (120°C) with a moisture content of about 1%. It was found that under these conditions the difference in strengths between the blocked and distributed lay-ups was negligible, values of 340 MPa and 350 MPa being observed respectively. Examination of specimens in which failure had been arrested showed that there was significantly less translaminar cracking in all plies, probably because failure occurred at a substantially lower stress. More importantly however, it was observed that failure of the axial fibres occurred by out-of-plane buckling along a line at right angles to the specimen axis and at the minimum cross section as illustrated in Figure 11. Again, the direction of fibre buckling was confirmed by examination of the fibre ends. There was no evidence of a link between the buckling of the axial fibres and any damage in the off-axis plies. The location of axial ply failure appeared to have been determined simply by the position of maximum axial stress. This would explain the absence of any difference in strength due to ply lay-up. The out-of-plane buckling was necessarily associated with a significantly greater amount of delamination in the region of the notch. As illustrated by the SEM photographs in Figure 12, it appears that the fibre-matrix bond strength was reduced by the hot-wet conditions and that the interlaminar strength was therefore insufficient to prevent the relatively early buckling failure of the axial plies.

Other specimens tested under hot-dry and room temperature-wet conditions exhibited intermediate modes of failure which have been described in detail elsewhere.[4] In each case it appeared that notched strength was dependent upon both the extent of damage zone growth before buckling failure of the axial plies and upon the extent to which that failure was influenced by ply interaction effects.

5 IMPACT DAMAGE AND POST-IMPACT COMPRESSIVE FAILURE

The extent and form of damage due to impact depends upon a wide range of parameters including the shape, hardness and energy of the impactor and the thickness, ply lay-up and support conditions of the laminate. Thick laminates struck by sharp, high energy impactors tend to exhibit damage which is clearly visible at the impact surface. If complete penetration of the laminate occurs the internal damage is often only slightly greater in area than the surface visible damage. Thinner laminates struck by blunt, low energy impactors tend to exhibit larger areas of internal, unseen damage, particularly if the laminate was able to flex locally during the impact event. It it generally accepted that, from a practical viewpoint, the most severe condition which must be accommodated in service is that of barely visible impact damage (BVID) in thin laminates. More severe damage can be readily detected by visual inspection whereas BVID might go unnoticed until detected by, say, ultrasonic inspection.

In general, thin laminates of less than about 24 plies (2 mm) which are subject to significant compressive loads will be stabilised by a honeycomb or foam core. In the present Paper we shall therefore consider the results of studies of BVID in CFRP/aluminium sandwich panels in which the CFRP skins had a pseudo-isotropic lay-up $\{(0,+45,-45,90)_3\}_S$. These panels were tested as part of a programme to study possible interaction effects between impact damage and tapered-thickness sections,[6] but we shall consider only panels of uniform thickness here. Each panel was subjected to an impact from a 6 mm diameter steel ball having an incident energy of 5 Joules. This produced damage on the impacted surface which could be detected quite easily in the laboratory but which could be regarded as barely visible under realistic inspection conditions on a full scale aircraft.

In order to obtain a detailed description of the impact damage, specimens were investigated by successively peeling away the individual plies as described in Section 4 above. In delaminated areas, each ply peeled cleanly away from the ply beneath so that fibre fractures and even some translaminar cracks could be detected in the lower ply using a stereo optical microscope. When illuminated from an oblique angle, the boundary of the impact-induced delamination could be accurately located by a change in reflectivity of the fracture surface, as illustrated in Figure 13. The SEM photograph in Figure 14 shows the boundary between the two types of fracture surface at higher magnification, and it may be seen that whilst the impact-induced delamination exposed the fibres in the lower ply, the peel fracture left a thin layer of matrix on the surface. In some areas this layer contained fibres from the ply which had been removed but, close to the boundary, the layer often contained only the imprints of fibres as shown here. In either case the linear features on the peel fracture surface were at a different angle to those in the region of impact-induced delamination, and this gave rise to the observed difference in reflectivity under oblique illumination. The correlation between this change in surface texture and the area of impact-induced delamination was confirmed by subjecting specimens to penetrant-enhanced X-radiography prior to peeling.

A series of maps of the impact-induced damage observed on the front surface and at each ply interface of the 24 ply pseudo-isotropic laminate has been prepared as shown in Figure 15. Interface 12, which is the laminate mid-plane, is not shown since it was difficult to separate two plies of the same fibre orientation. It may be seen that the delamination at each interface tended to exhibit a double lobe shape reflecting the stiffness properties of the adjacent plies. Fibre fractures were evident only in the plies close to the impacted surface. Although it is often suggested that impact damage occupies an approximately conical volume with the apex at the point of impact, it is evident here that the areas of delamination quite close to the front surface are not much smaller than those near the back surface.

Under static compressive loading the delaminated plies buckled at relatively low strain levels. Close to failure the buckling was quite visible to the naked eye but to detect it at lower strain levels it was necessary to use a shadow moire fringe technique. The fringes were recorded on videotape for subsequent analysis but it was found difficult to identify a true critical strain level since some displacement occurred at very low loads. However, above about 0.2% strain there was quite substantial out-of-plane movement and it was evident that above this strain level there would be significant peel stresses around the perimeter of the delamination due to the induced bending moments. Finite element analysis of a single rectangular delamination[8] has shown that the strain energy density is slightly greater at the transverse

edges, suggesting that the delamination should grow laterally rather than longitudinally. This has been confirmed in tests using laminates containing artificial delaminations and, whilst the situation in impact damaged laminates is much more complex, it seems likely that impact-induced delaminations will also tend to grow laterally. Certainly in the case of the pseudo-isotropic laminates considered here the damage was always found to grow laterally. Also, it has been observed by X-radiography that even after static compressive failure the extent of delamination in the axial direction was no more than that of the initial impact-induced delamination. In examining the fracture surfaces after failure, the prior existence of impact damage was evident from differences in surface texture and the characteristic double lobe shape of the impact-induced delaminations as described above, an observation which could prove particularly important in post-failure analysis of structures.

Under compressive fatigue loading the delaminations also grew laterally as a result of the peel stresses induced by ply buckling. However, it was observed that such growth occurred only when the peak loads were a substantial proportion of the static strength. Typically, failures occurred in constant amplitude tests only after 10 000 to 1000 000 cycles at about 75% of the static strength. It seems likely that if the peak strain level had been insufficient to cause significant ply buckling there would have been no measurable fatigue damage growth within realistic timescales. Figure 16 shows damage maps derived by deplying a laminate which had been subjected to 10 000 cycles at 80% of the static strength (R=10). Comparison with the unloaded specimen illustrated in Figure 15 shows that the damage at each interface retained the characteristic double lobe shape. But, more significantly, it may be seen that substantial delamination growth has occurred at only one of the interfaces near the surface of the laminate. Comparison of the damage growth rate for this specimen as determined from video recordings of the shadow moire fringe patterns, with that in specimens loaded to failure, suggests that this specimen was itself very close to failure when the loading was discontinued. It is assumed therefore that delamination growth deeper within the laminate occurs only at the very end of the fatigue life and might even be regarded as part of the final collapse mechanism. As under static loading, the prior existence of impact damage is evident when examining the fracture surfaces of failed specimens due to differences in surface texture and the characteristic double lobe shape of the impact-induced delaminations. However, the fact that so small a proportion of the total damage occurs during fatigue may partly explain the current lack of success in trying to distinguish between static and fatigue failures from direct observation of the fracture surfaces.

It may be noted that there was little evidence of fibre buckling in any of the impacted specimens, whether tested under static or fatigue loading. It appears that impact-induced failures always occur by progressive delamination, first in the outermost plies and subsequently in plies deeper within the laminate. It is of interest to note, however, that in an impacted +/-45° shear web, buckling due to the compressive component of stress at, say,+45° tends to be inhibited by the tensile component of stress at -45° and, under these conditions, some fibre buckling has been observed.

6 CONCLUDING REMARKS

In the design of CFRP aerospace structures the compressive field strain is generally limited to about 0.4% to allow both for the effects of notches under hot-wet conditions and for the effects of impact damage. It is anticipated therefore that in post-failure analysis of CFRP structures in which

compressive failure has occurred, the ability to interpret fracture surfaces due to notch or impact-induced failures will be of particular importance. From the programmes described briefly herein it has been shown that compression failures in current carbon fibre/epoxy resin composites are generally associated with instability. Those induced by notches appear to involve fibre 'buckling', the direction and location of fibre buckles being dependent upon the ply lay-up and environmental conditions. Impact-induced compressive failures involve buckling of entire plies and subsequent delamination growth. Each type of failure gives rise to characteristic features on the fracture surface which may be used to identify the cause of failure.

Programmes such as those described here, together with similar work on tensile and shear loading, have provided a sound fractographic basis for the post-failure analysis of CFRP structues using the current generation of epoxy resin systems. Considerable work remains to be done, however, to achieve a comparable capability for toughened epoxy or thermoplastic based composites.

REFERENCES

1 D Purslow — Some fundamental aspects of composites fractography. Composites 12, 4, pp 241-247 (1981) RAE Technical Report TR81127 (1981)

2 D Purslow — Fractographic analysis of failures in CFRP. AGARD CP 355, Paper 1 (1983)

3 P D Ewins, A C Ham — The nature of compressive failure in unidirectional CFRP. RAE Technical Report TR73057 (1973) Also presented at the AIAA/ASME/SAE 15th Structures, Structural Dynamics and Materials Conference, Las Vegas, April 1974. AIAA Paper No 74-353 (1974)

4 D Purslow, R T Potter — The effect of environment on the compression strength of notched CFRP - a fractographic investigation. Composites 15, 2, pp 112-120 (1984) RAE Technical Report TR84034 (1984)

5 R T Potter — Unpublished work

6 R T Potter — The interaction of impact damage and tapered-thickness sections in CFRP. Composite Structures 3, 3&4, pp 319-339 (1985)

7 K F Port — The compressive strength of carbon fibre reinforced plastics. RAE Technical Report TR82083 (1983)

8 R Jones, W Broughton, R F Mousley, R T Potter — Compression failures of damaged graphite epoxy laminates. Composite Structures 3, 2, pp 167-186 (1985)

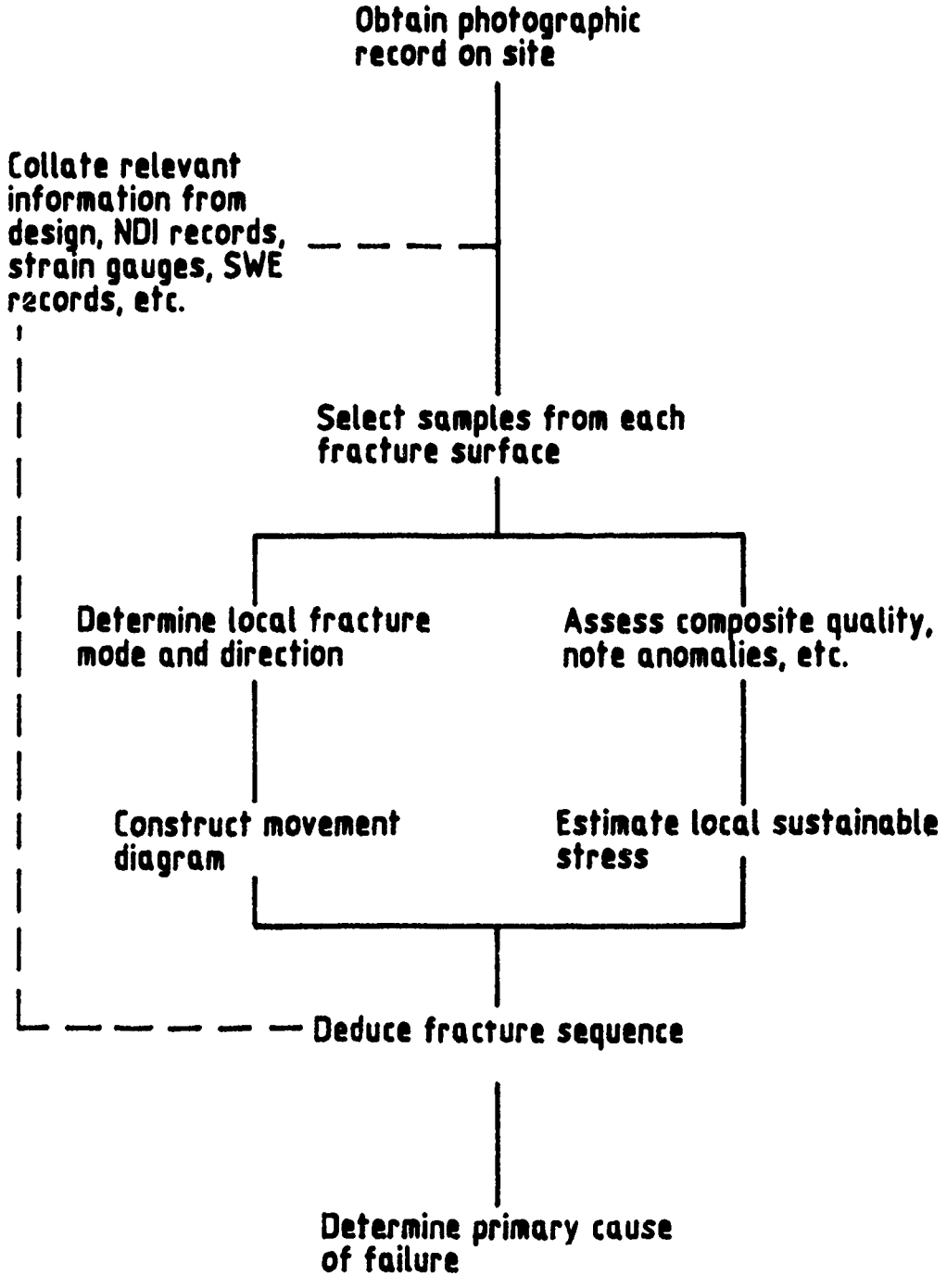

Figure 1. General procedure for post-failure analysis of CFRP structures

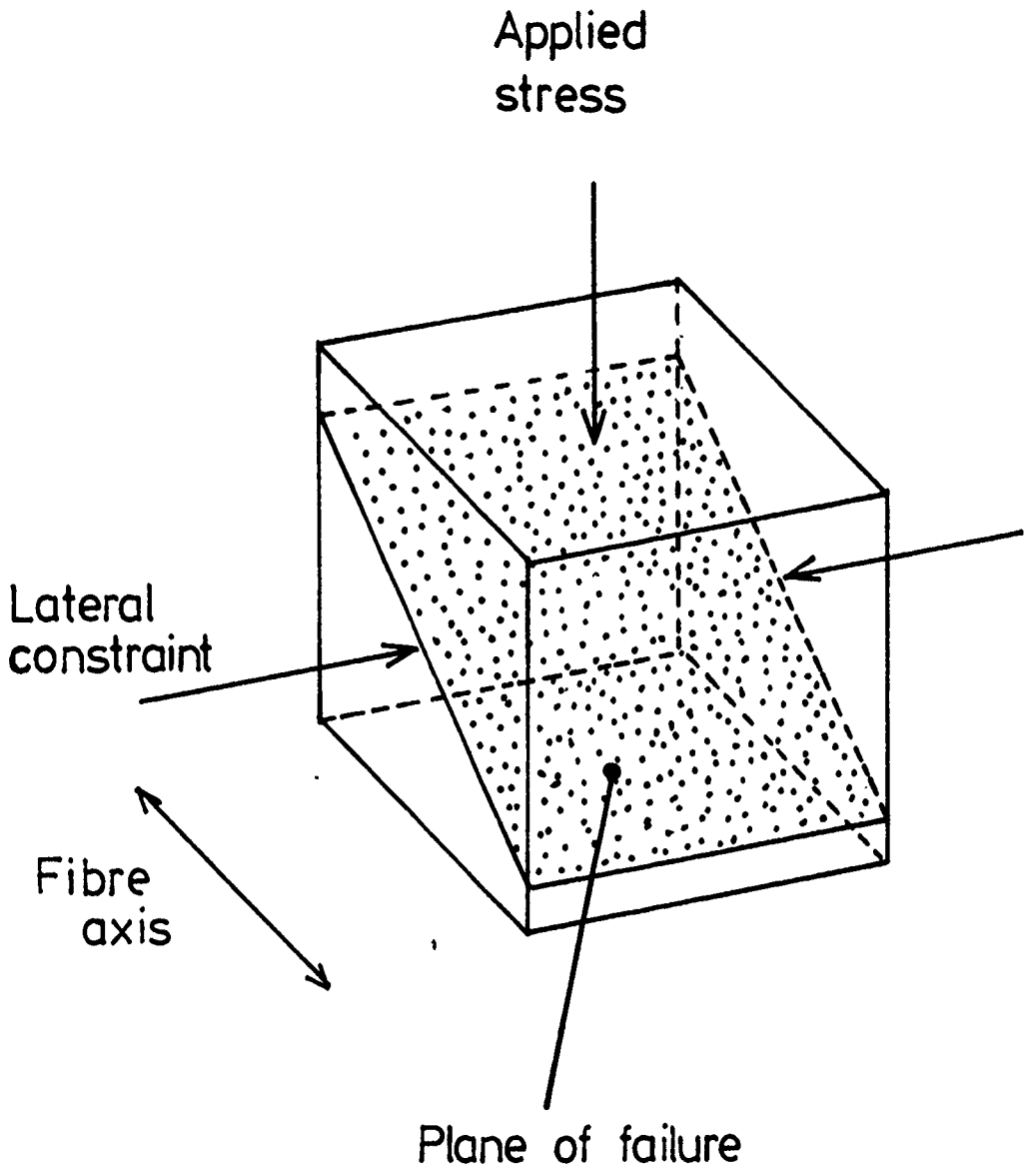

Figure 2 Constrained transverse compressive failure

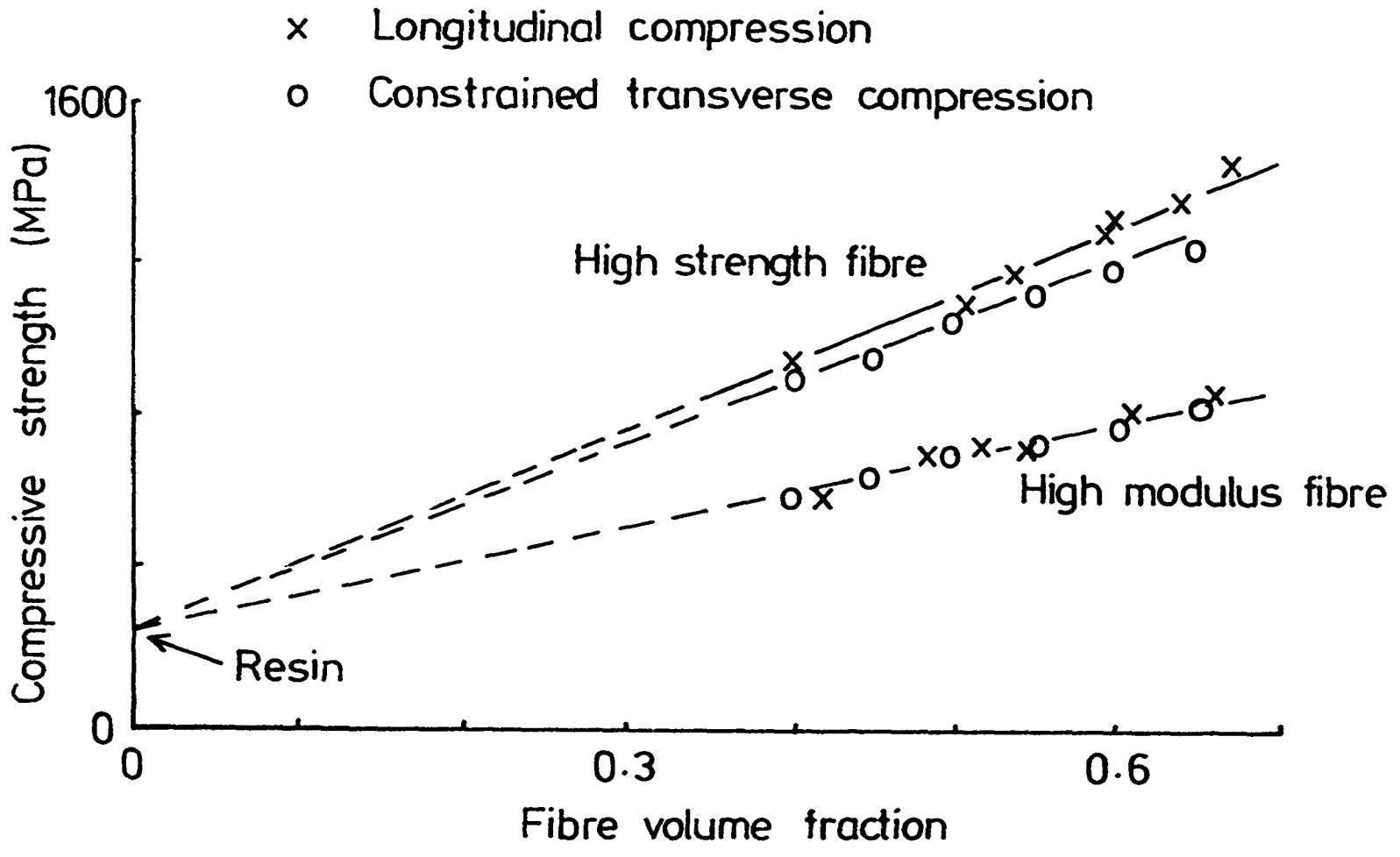

Figure 3. Variation of compressive strength with fibre volume fraction

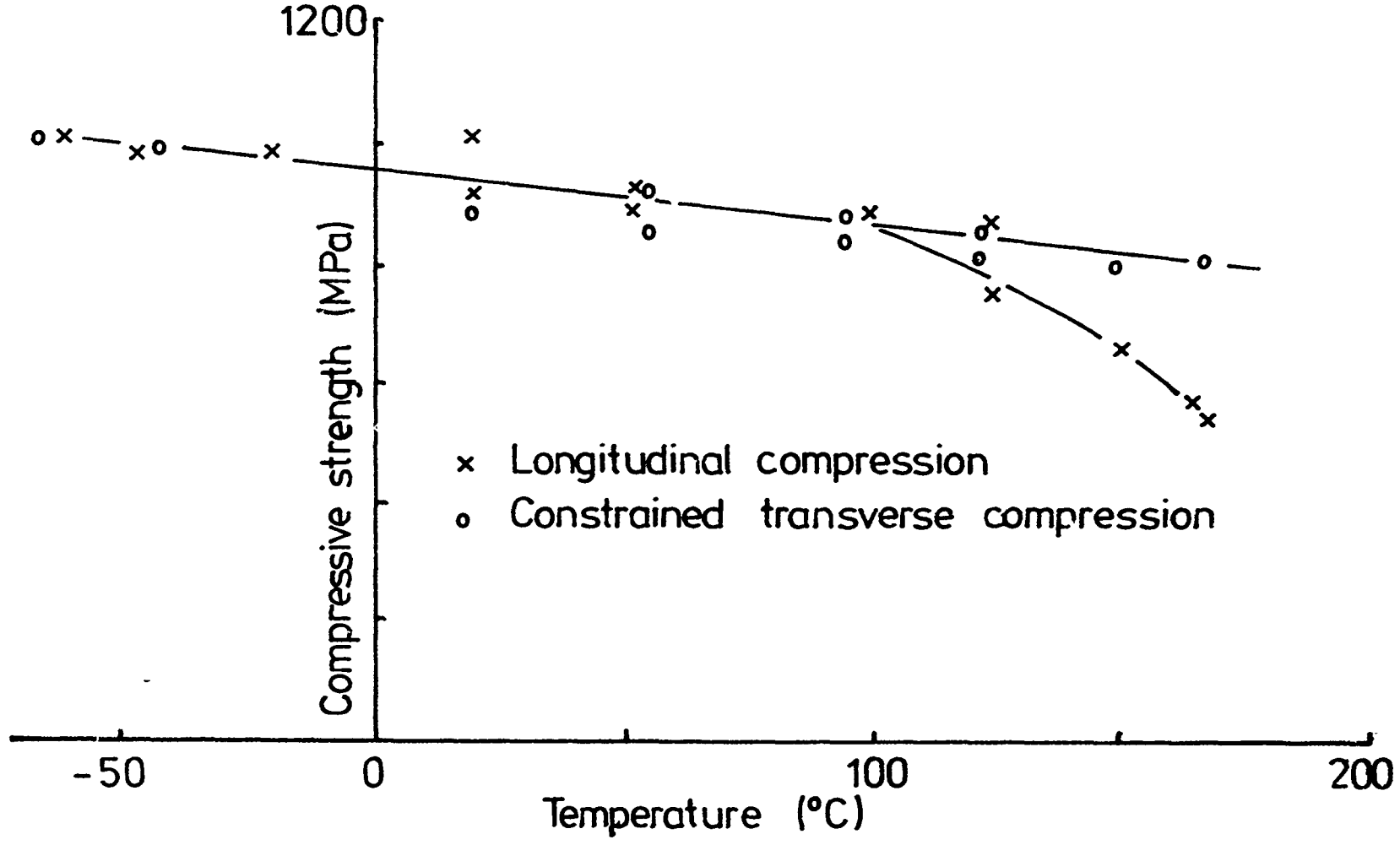

Figure 4. Variation of compressive strength with temperature

Figure 5. Longitudinal compressive fracture at room temperature (X2500)

Figure 6. Longitudinal compressive fracture above 100°C (X2000)

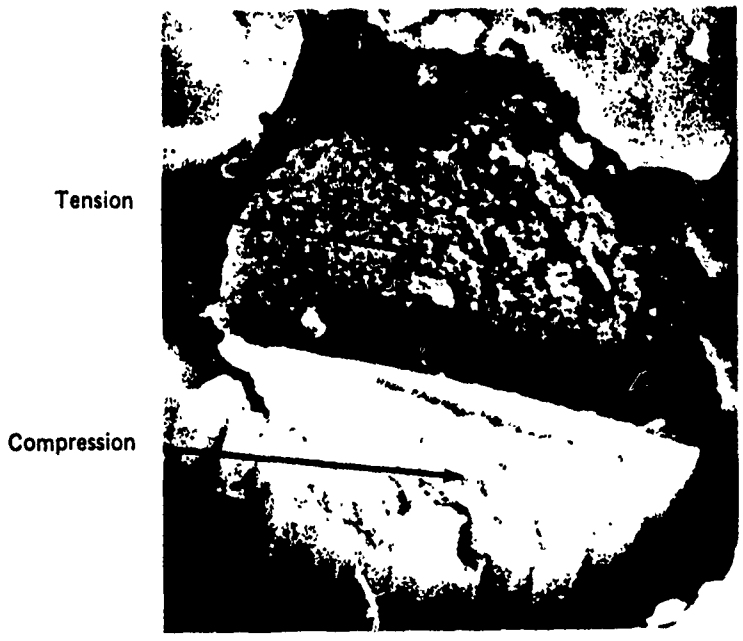

Figure 7. Longitudinal compressive fracture above 100°C (X8000)

Figure 8. Longitudinal compressive fracture above 100°C (X200)

Figure 9(a). Peel fracture surface

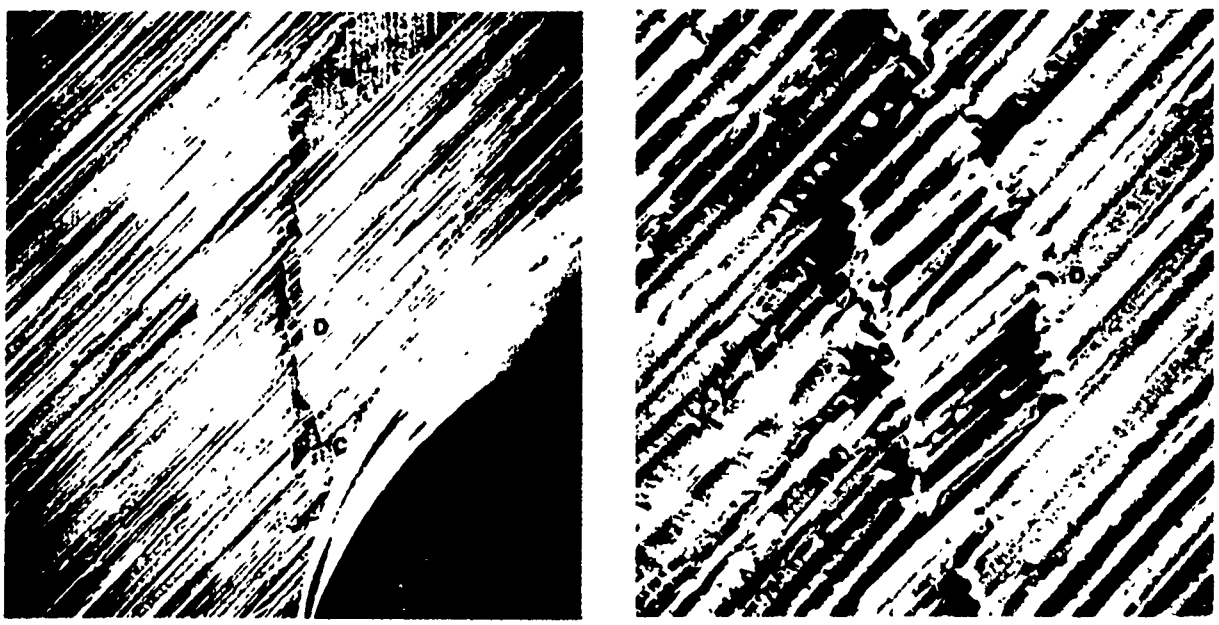

Figure 9(b). Fibre fractures in off-axis ply

Figure 10 Buckling failure in axial ply - RT - dry notched compression

Figure 11 Buckling failure in axial ply - hot-wet notched compression

a. failure of matrix (RT - dry)

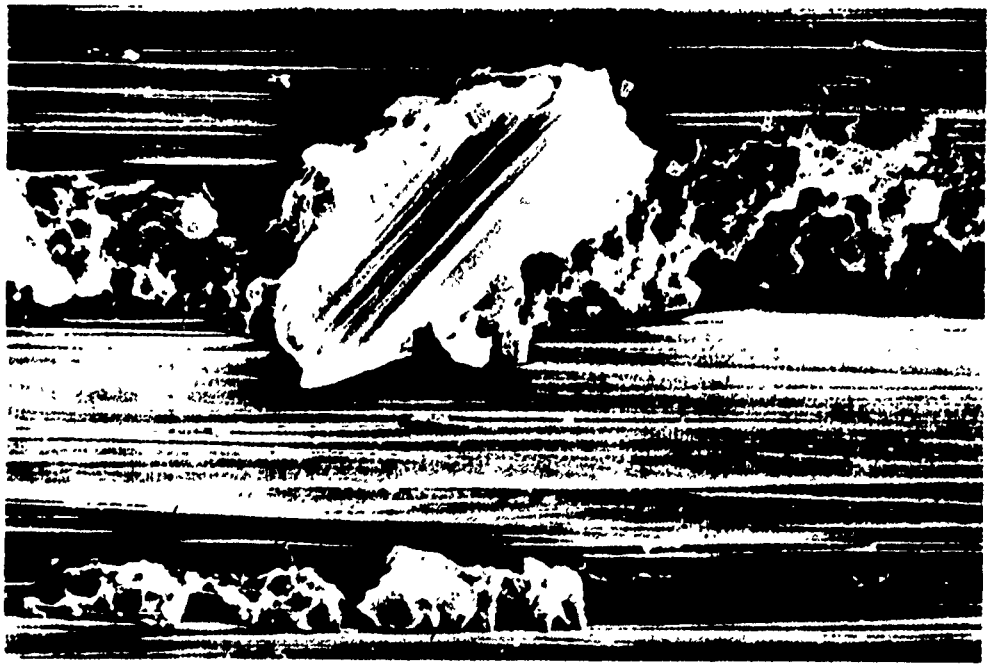

b. failure of bond (hot - wet)

Figure 12. Interlaminar fracture surfaces

Figure 13. Peel fracture surface of impacted laminate

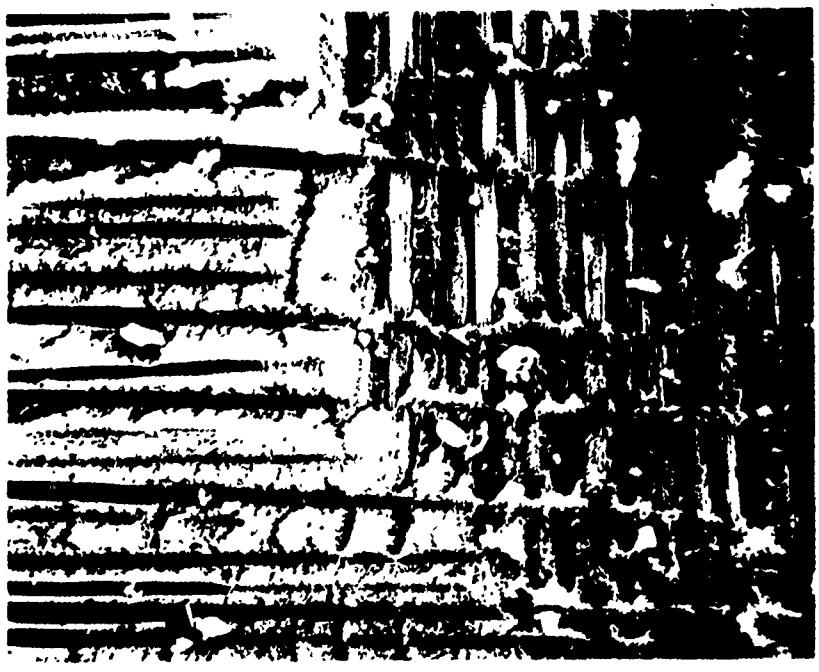

Figure 14. Impact - peel fracture surface boundary

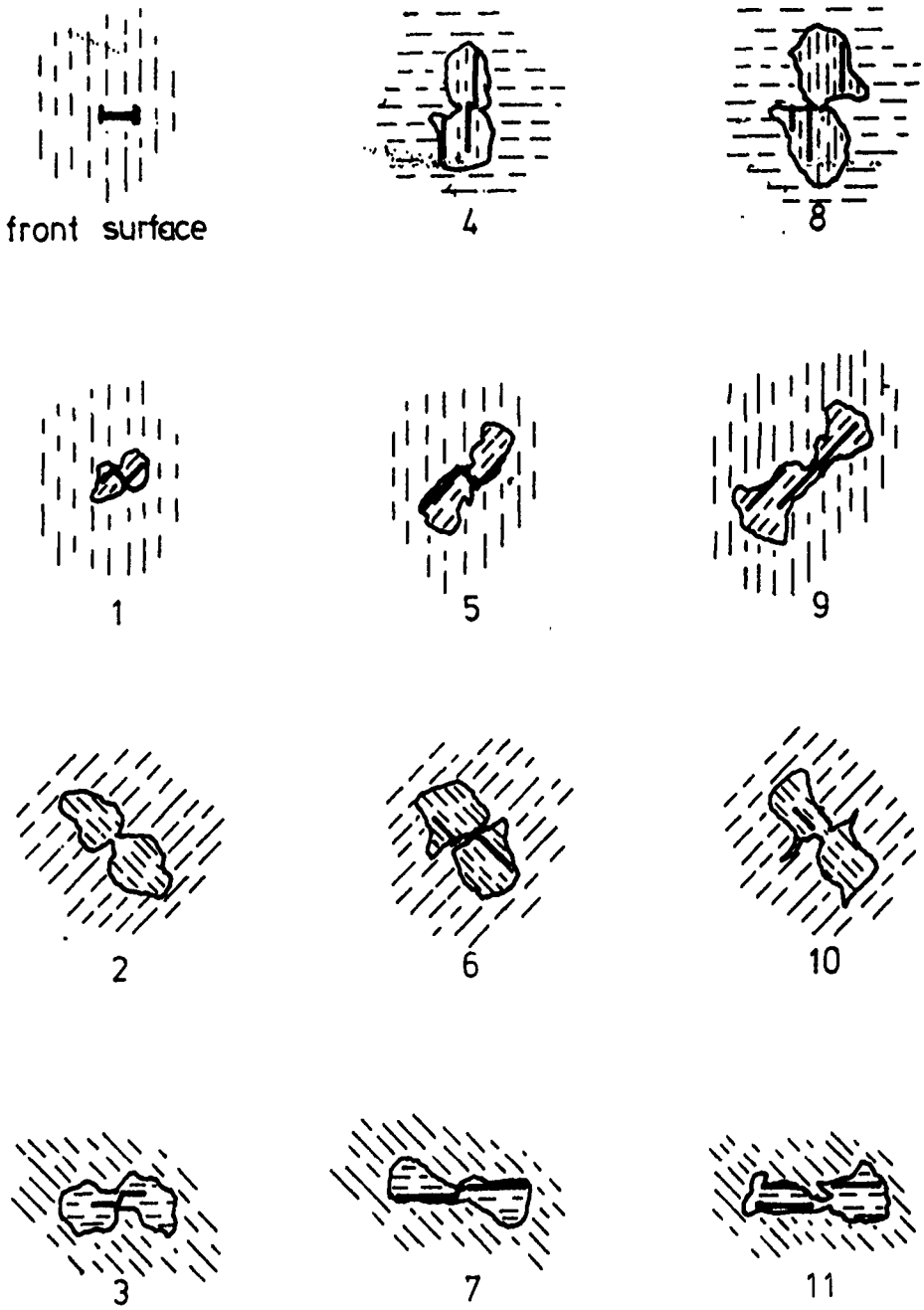

Figure 15(a). Damage due to impact - front surface and interfaces 1-11

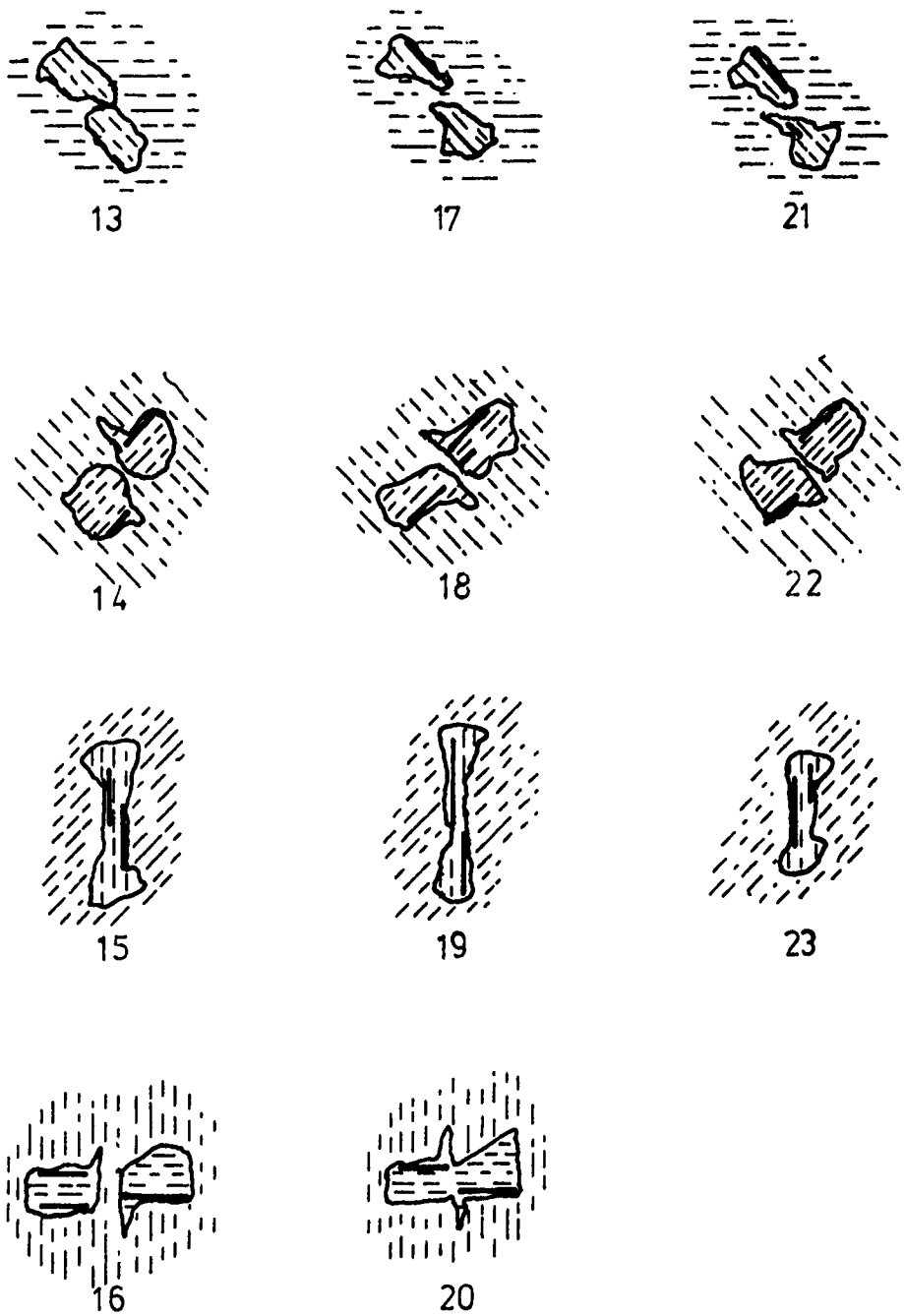

Figure 15(b). Damage due to impact - interfaces 13-23

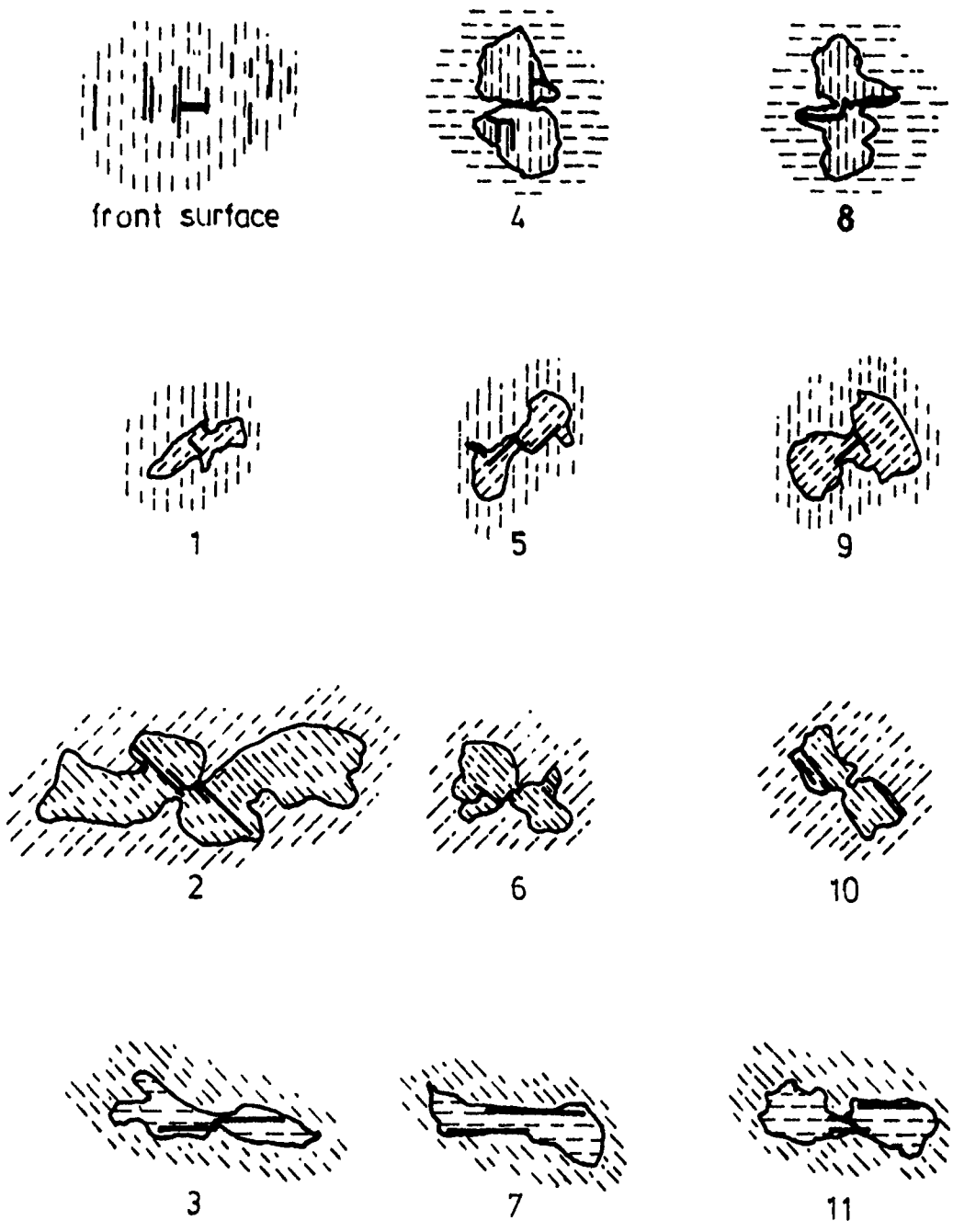

Figure 16(a). Damage due to impact and fatigue - front surface and interfaces 1-11

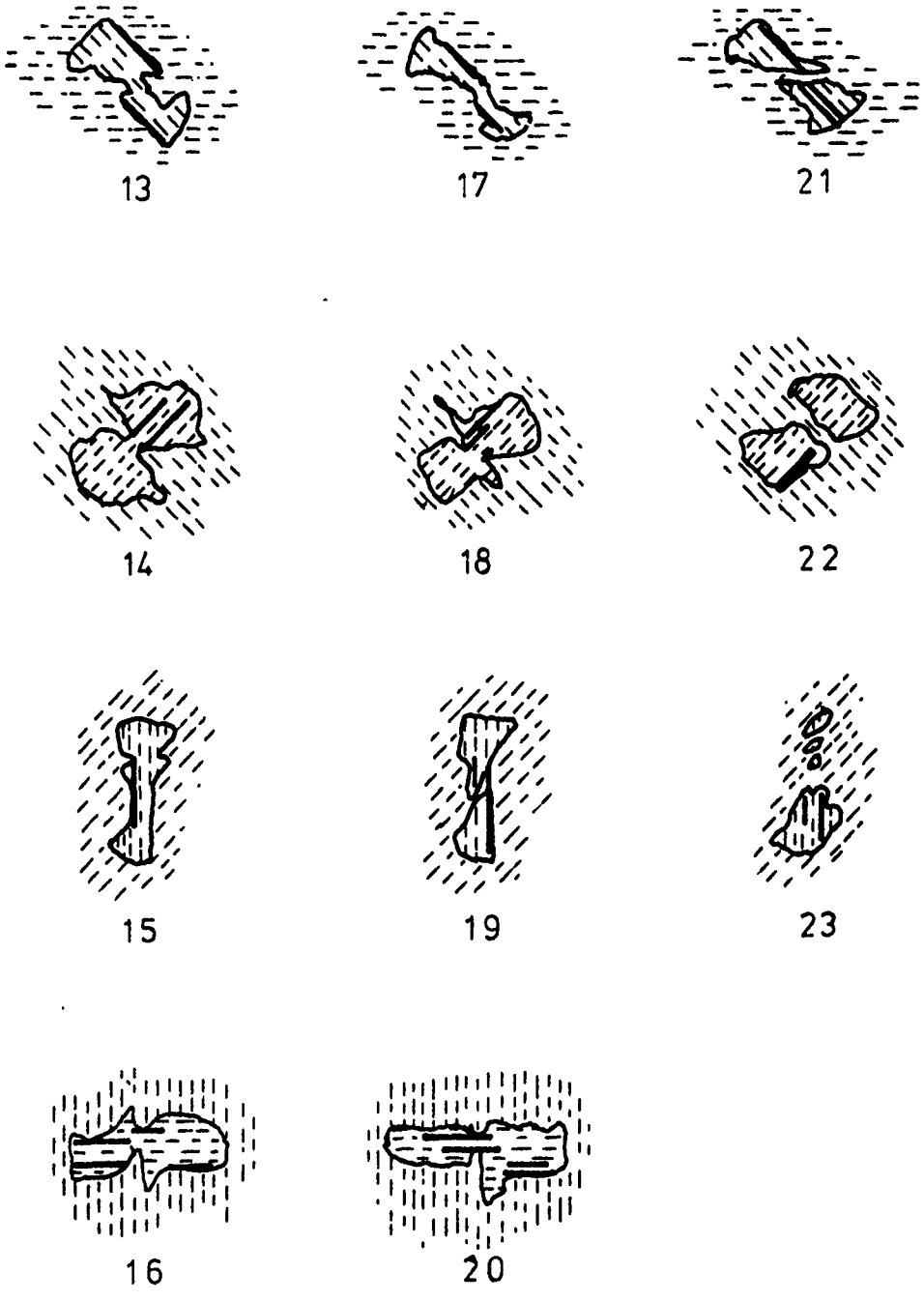

Figure 16(b). Damage due to impact and fatigue - interfaces 13-23

ENVIRONMENTAL EFFECTS ON INTERLAMINAR FRACTURE SURFACE CHARACTERISTICS OF Gr/Ep MATERIAL STRUCTURES

R. Grove, T. Munns and B.W. Smith
Boeing Materials Technology
Boeing Commercial Airplane Company
Seattle, Washington

Environmental Effects on The Interlaminar Fracture Surface Characteristics of Graphite/Epoxy Material Structures

Presented by; Ray A. Grove, Brian W. Smith, Thomas E. Munns

Abstract

The following paper presents the results of an investigation into the effect of environmental exposure on the interlaminar fracture surface characteristics of graphite/epoxy composite materials. This study advances work previously presented in which the room temperature fracture characteristics of interlaminar tension (mode 1) and interlaminar shear (mode 2) were presented. In the current study the effect of various temperature and absorbed moisture states on interlaminar fracture features is explored. Specimens were preconditioned in either ambient lab humidity or 160 F /100% relative humidity and fractures were produced at -65, 70, and 270 F. Interlaminar tension fracture surfaces were generated with a double cantilever beam configuration and the interlaminar shear fractures with an end notch flexural configuration. In both cases, controlled crack initiation and progression was produced between various cross-ply orientations. The correspondence of observed fracture features with imposed load conditions, cross-ply fiber orientations and induced crack propagation directions are presented. These results illustrate pronounced differences in the amounts of fiber/matrix separation and resin matrix fracture with increasing temperature and absorbed moisture conditions. However, characteristic fractographic features were not found to be significantly altered, indicating that the examination of these features remains a viable means of determining the mode and direction of crack propagation for components fractured under extreme environmental conditions.

1.0 INTRODUCTION

Because of their high specific strength and stiffness, laminated graphite/epoxy material systems are seeing substantial levels of use in military and commercial weight-critical aircraft structures. Thus, a wide variety of environmental exposure conditions are encountered. Additionally, the anisotropic strength characteristics of laminated fiber reinforced plastics often lead to component interlaminar fracture at low load conditions. The extremely low interlaminar fracture resistance of composite materials (GIc= 0.5 in.-lb/sq.in., vs. translaminar GIc values of 200 in.-lb/sq.in.) makes interlaminar fracture a particularly significant mode in nearly all composite fractures. Thus, the understanding of environmental effects on interlaminar fracture characteristics of graphite/epoxy laminates is fundamental to the development of the analytical discipline of fracture analysis. The development of this discipline is in turn required for the evolution of a comprehensive post-mortem failure analysis capability for

composite material structures. The following paper presents the intermediate status of an investigation into the effect of environment on the fracture surface characteristics of delaminations generated under mode 1 tension and mode 2 shear. This investigation represents part of an Air Force funded program (ref. 1) aimed at the development of a comprehensive fracture analysis capability for composite materials structures. The specific environmental conditions evaluated in this study include -65F/dry, 70F/dry, 270F/dry, and 270F/wet. The principal objectives were 1) the identification of the characteristic features associated with interlaminar environmental fractures, and 2) verification of the suitability of these characteristic features to identify the direction of crack propagation and load state at fracture. The fundamental approach was to generate closely controlled interlaminar tension (mode I) and shear (mode II) fractures under various environmental conditions, analyze and characterize the observed macro- and microscopic fracture features relative to each environmental condition, and contrast results with well understood and documented room temperature/ambient humidity fracture surface morphologies.

2.0 MATERIALS AND TEST METHODS

For this study, a TGDDM based resin system, Hercules 3501-6/AS4 graphite/epoxy system was chosen due to extensive aerospace utilization, well documented environmental behavior and high ultimate strength. Panels with (0 deg)24 and (+45/-45)12s layups were fabricated, microstructurally inspected to ensure proper ply stacking sequence/orientations, and subjected to Thermo-Mechanical Analysis (TMA) to verify extent of cure and to determine Tg. 1" X 10" specimens were fabricated and each was Through-Transmission Ultrasonically (TTU) inspected for defects. Environmental preconditioning consisted of two states; 1) room temperature/ambient humidity and 2) 160F, 100% relative humidity which resulted in a moisture weight gain of 1.0%. The 1.0% level has been shown by NASA (ref. 2) to be the stable equilibrium value for 3501 epoxy systems following long-term outdoor exposures. Mode I interlaminar tension fractures were produced utilizing a split laminate double cantilever beam (DCB) specimen configuration. An FEP insert was implanted at one end of the specimen to provide controlled mid-plane crack initiation and propagation. Mode II interlaminar shear fractures were generated with an end notch flexural (ENF) test configuration, with identical specimen geometry as the DCB specimen, including the FEP insert. The ENF configuration involves loading of both beam halves in the same direction at the split end, while supporting the opposite end. Specimens were fractured with an MTS 20 Kip load frame, increasing cross-head deflection rates to maintain relatively constant crack extension rates across the specimen length. Observed Mode I crack growth was very stable, exhibiting crack growth rates ranging from 0.5 to 1.0 inch/minute. Mode II crack growth typically involved rapid growth during the first crack extension, followed by several increments of slower, more stable growth. In all cases, observed crack growth was directed away from the FEP crack starter, in the 0 degree direction.

3.0 RESULTS

Interlaminar Tension Fracture Features

As a result of their laminated fibrous construction, interlaminar tension fractures typically exhibit a mixture of flat, cohesive resin fracture and zones of fiber/matrix separation. In general, examinations within this study revealed a pronounced increase in the level of fiber/matrix separation with increasing temperature and absorbed water content. This trend is illustrated in Figures 1 and 2 in which the effect of environment are contrasted at relatively low magnifications for fractures produced between adjacent 0 degree plies. The fracture topographies characteristic of -65F and 70F appeared relatively similar to one another. Both exhibited extensive amounts of flat, planar resin fracture divided into relatively large longitudinal areas

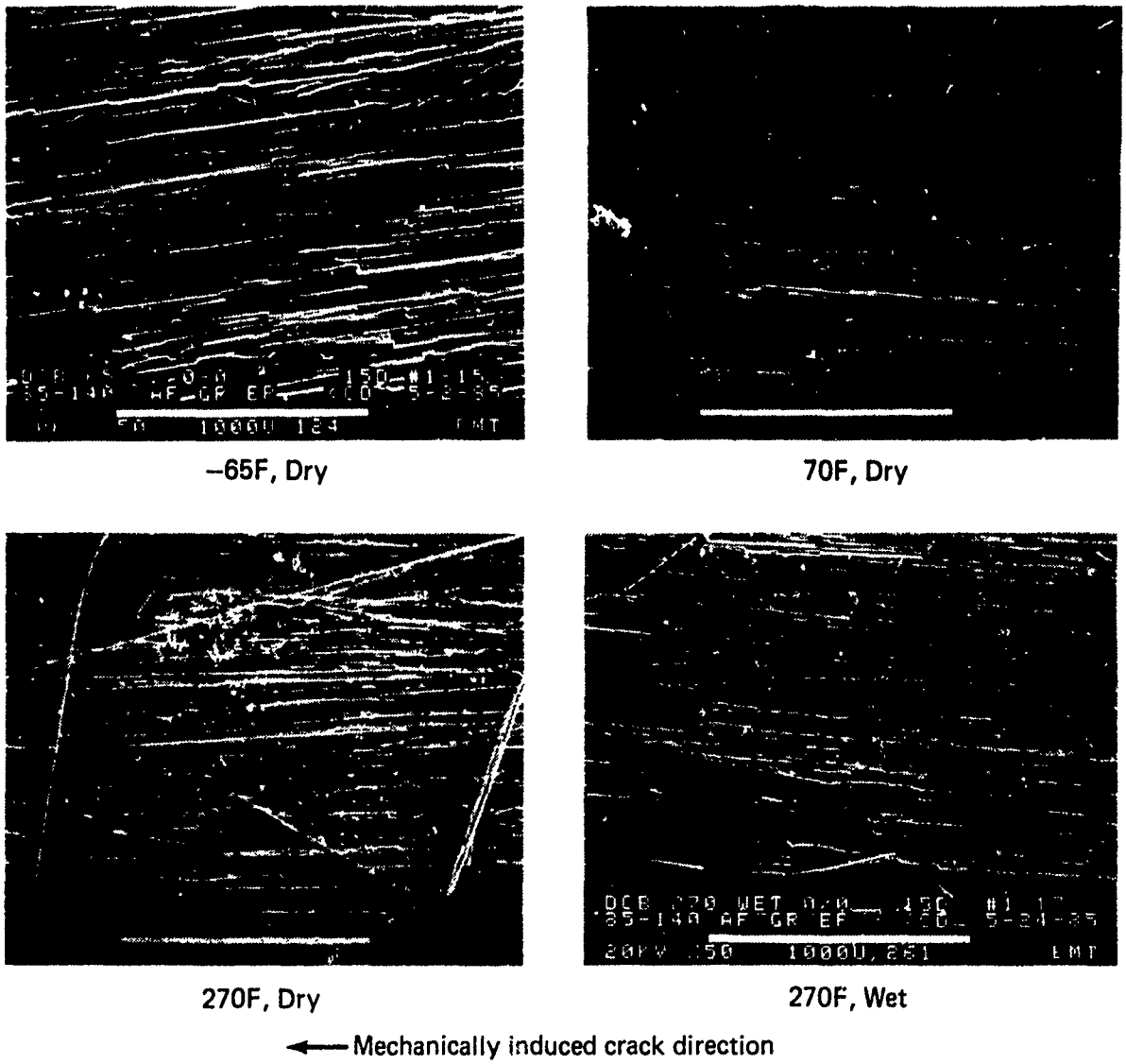

Figure 1. Low Magnification Series of Fracture Surface Topographies Characteristic of 0/0 Interface Mode I Fractures at Each Environmental Condition.

by zones of fiber/matrix separation. Microscopic examinations of 270F dry and wet specimens indicated that each of these elevated temperature fractures were similar to one another, although quite different from the -65F dry and 70F dry fractures. As shown, both fracture topographies are characterized by a significantly larger amount of exposed areas of fiber/matrix separation. Consequently, a corresponding decrease in the individual size and overall amount of flat resin matrix fracture zones was evident. As illustrated in Figure 1, fractures at 270F dry and wet resulted in extensive amounts of randomly orientated fibers scattered over the fracture surface which appear to have been pulled out from the surrounding matrix. Macroscopically, the 270F fracture surfaces appear distinctly different than those generated at -65F and 70F because of these easily visible pulled out fibers.

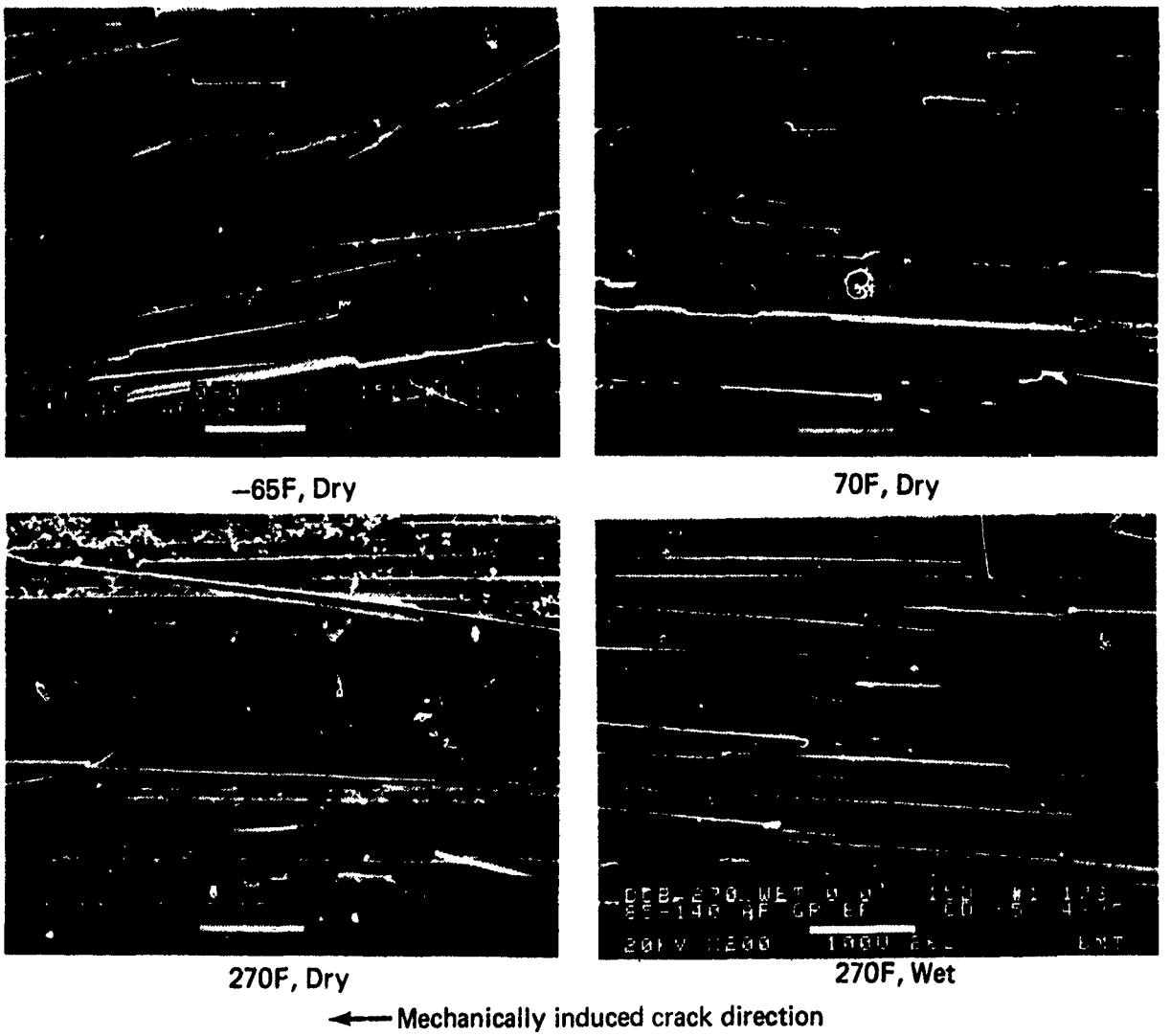

Figure 2. Higher Magnification Series of Same Locations in Figure 1. Note the More Fiber Domi ated Appearance for the 270°F Fractures.

In a similar manner, interlaminar fractures produced between -45 and +45 ply interfaces exhibited increasing amounts of fiber/matrix separation with increasing temperature and absorbed water content. As illustrated in Figures 3 and 4, -65F and 70F fracture conditions appear relatively similar. Generally, for these lower temperature conditions, regions of cohesive resin fracture appear somewhat smaller than those noted for adjacent 0 degree fractures, divided into locally discrete regions by areas of exposed cross-ply fiber/matrix separation. The fracture surfaces generated at both 270F dry and wet fracture conditions for this cross-ply configuration appear distinctively different than those generated under lower temperature conditions. As shown in Figures 3 and 4, the overall fracture surface topography is dominated by extensive amounts of fiber/matrix interfacial fracture with occasional locallized regions of cohesive matrix fracture and randomly pulled out fibers (similar to the 0/0 degree interface fractures noted above).

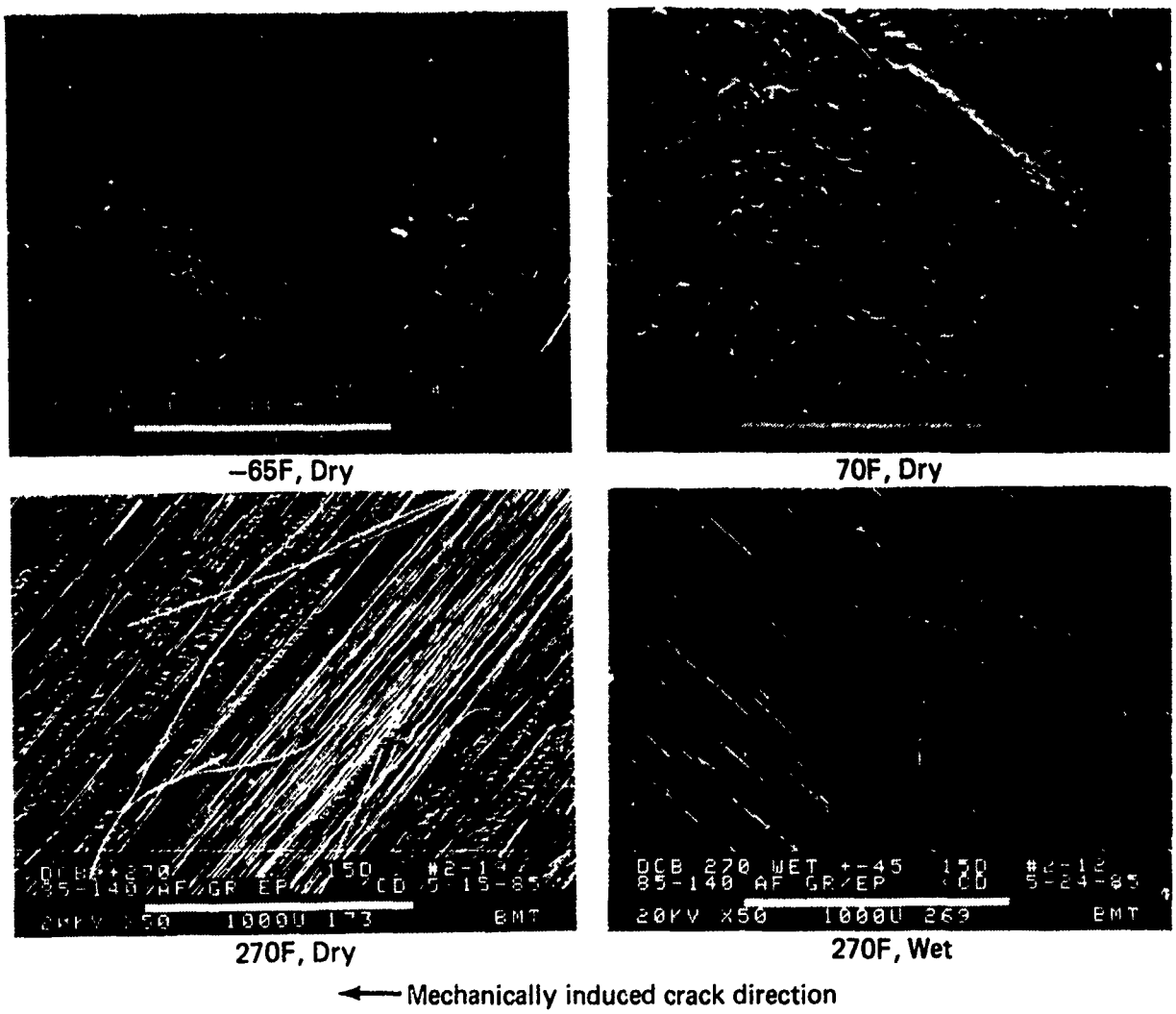

Figure 3. Low Magnification Series of Fracture Topographies Characteristic of +45/-45 Interface Mode I Fractures at Each Environmental Condition.

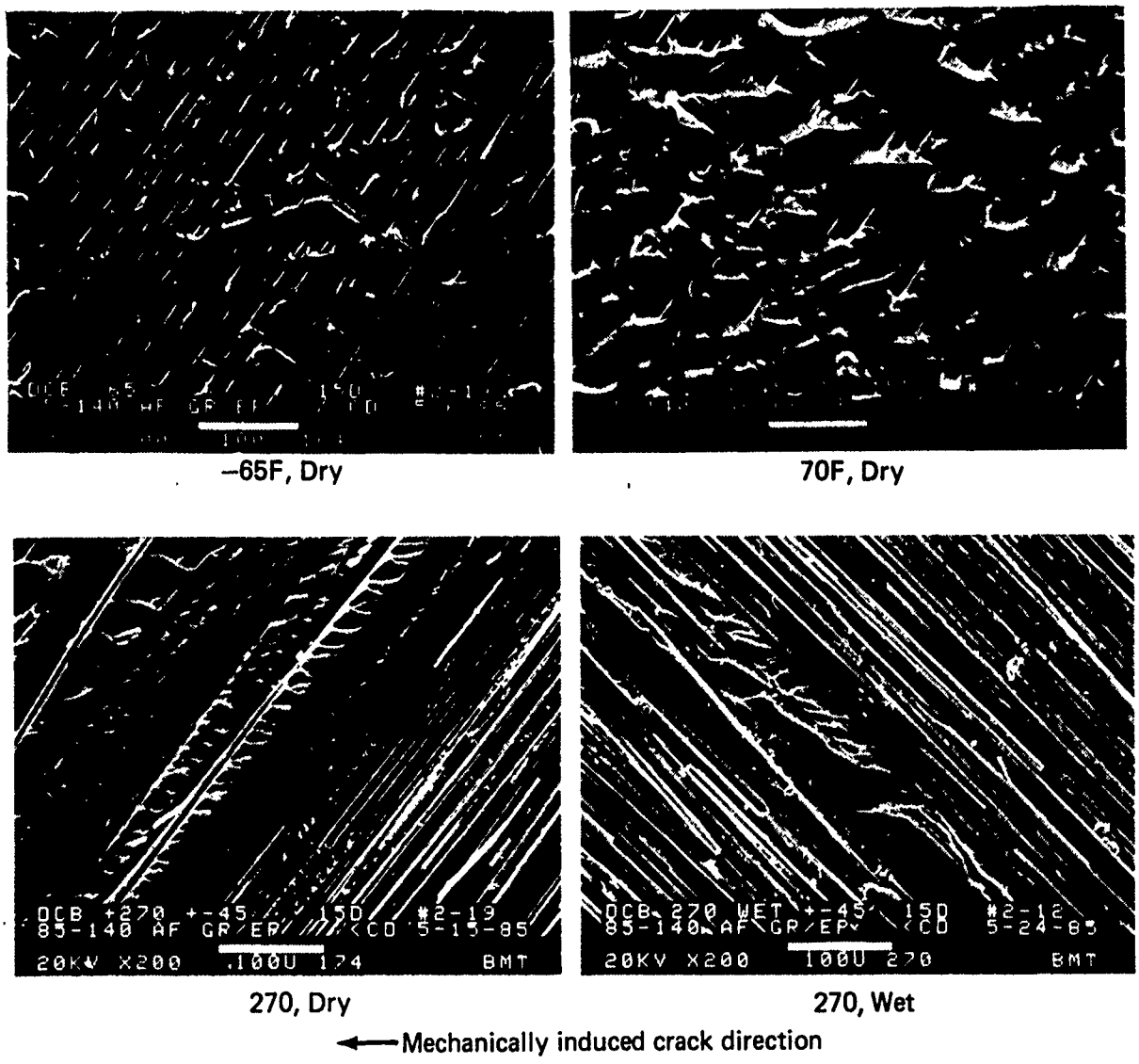

Figure 4. Higher Magnification Series of Same Locations in Figure 3. Note Increased Fiber Dominated Appearance for the 270°F Fractures.

For both 0/0 and +45/-45 degree interface orientations, increasing amounts of fiber/matrix separation is manifested by crack propagation within, or immediately adjacent to, dense-packed areas of fibers within the laminate ply. However, at the lower temperatures, the fracture plane occurs within the thin, resin-rich zones located between plies. In general, the phenomena of increasing fiber/matrix separation is consistent with behavior observed for graphite/epoxy translaminar tension fractures (ref. 3) as illustrated in Figure 5. In this investigation by Miller and Wingert, increasing amounts of fiber pullout and fiber/matrix interfacial fracture were observed with increasing temperature and absorbed moisture. This behavior, observed for both interlaminar and translaminar tension fractures, suggests that a decrease in fiber/matrix interfacial strength occurs with increasing temperatures and moisture content. However, an alternative explanation may be that increased matrix resin toughness and ductility results in an increased resistance to crack propagation within the

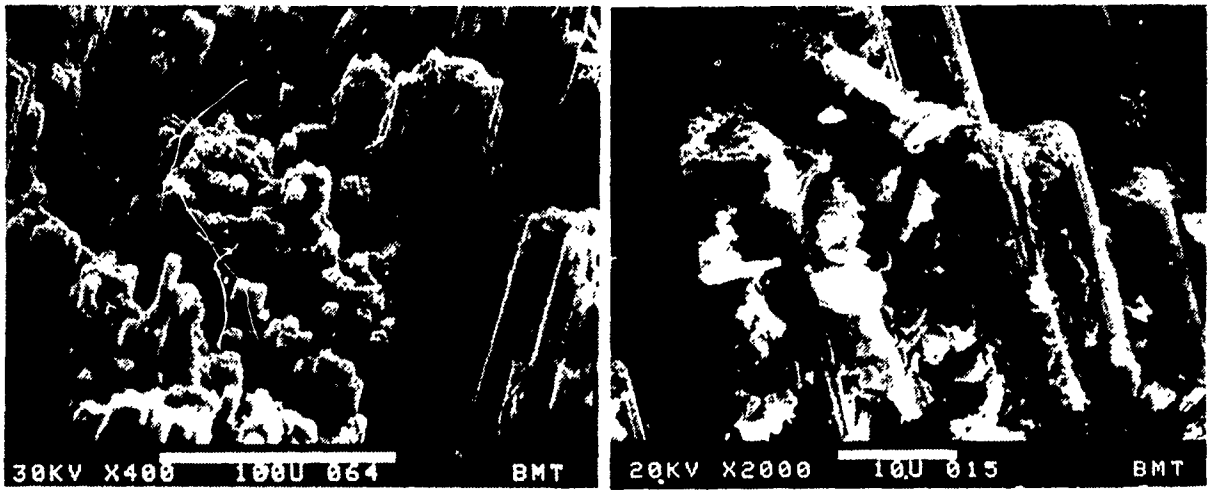

–65F Condition

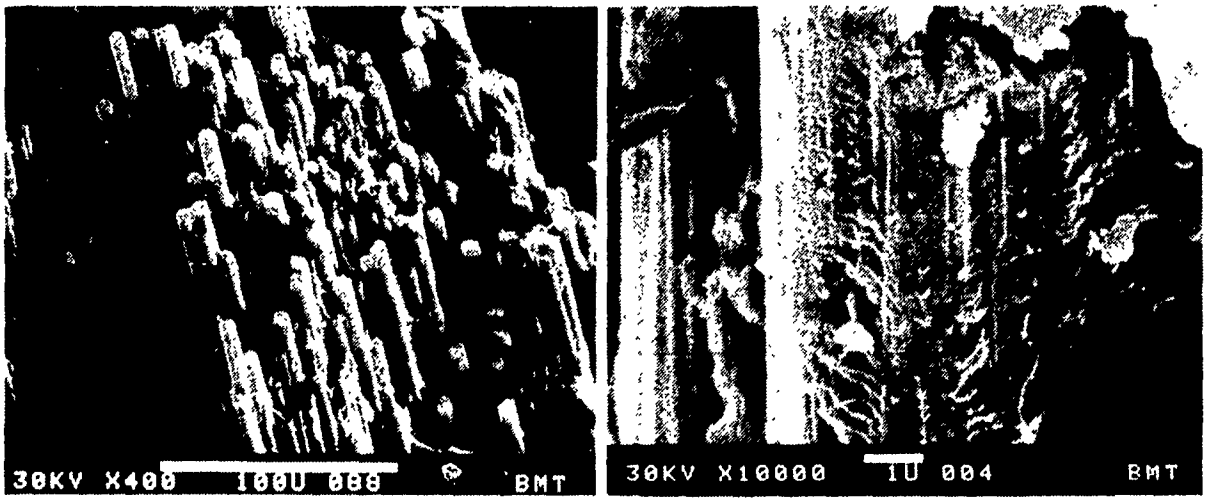

70F Condition

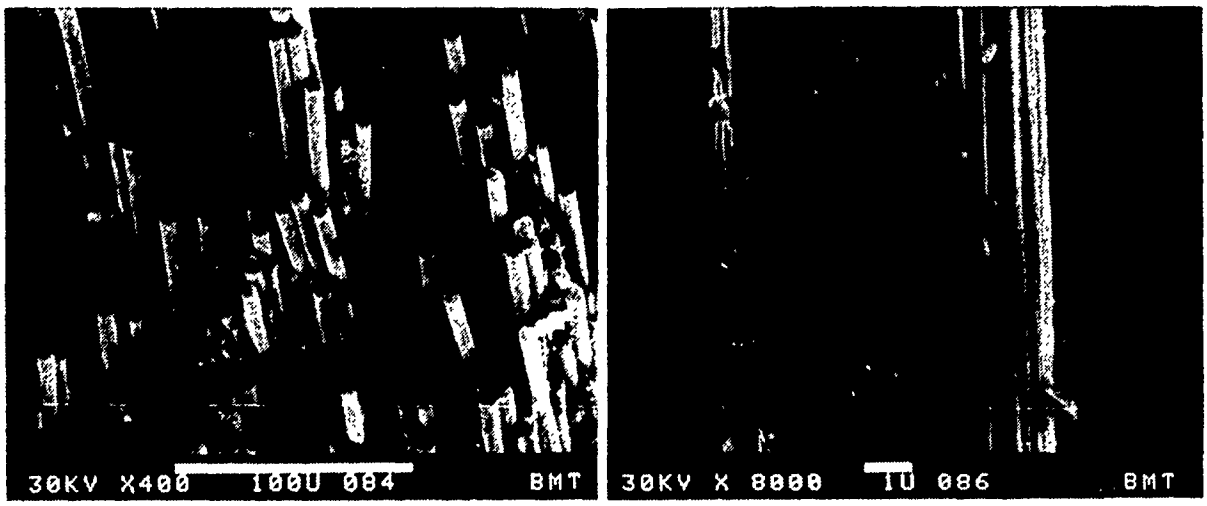

270F Condition

Figure 5. Characteristic Fractographic Features for Translaminar Tension Fractures Generated Under Various Environmental Conditions. Note Tendency at Higher Temperatures for Adhesive Separation at Fiber/Matrix Interface.

resin rich zones. Most likely, a combination of these two factors provide the driving force for crack divergence into the fiber dominated laminae. However, further studies need to be performed to determine the dominant causative factor for this phenomena.

In a previous study (ref. 2) under the current Air Force program, river markings and resin microflow were identified as characteristic features found in the flat cohesive matrix fracture zones. These features were found to provide a means of determining the local crack propagation for interlaminar tension fractures produced under 70F dry conditions, as illustrated in Figures 6b and 7b. Examination of these

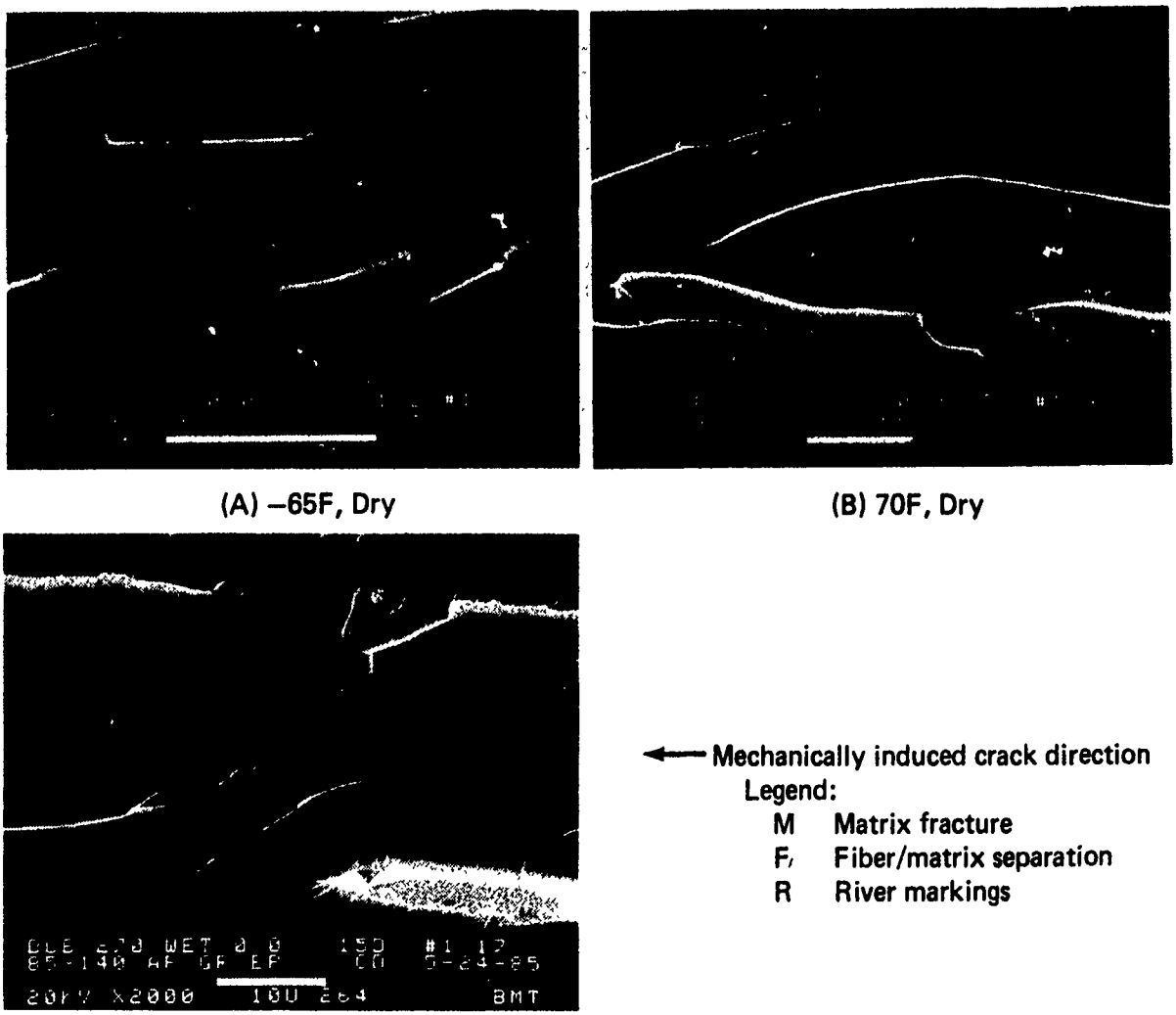

Figure 6. High Magnifications of Typical Matrix Resin Fracture Features For 0/0 Interface Mode I Tension Fractures.

70F fractures revealed that river mark branch coalescence and micro-flow progression coincide with the direction of induced crack propagation. Correspondingly, the conditions of environment for this study were not found to significantly alter these characteristic features, even at environmental extremes of -65F dry or 270F wet, for both the 0/0 and +45/-45 ply orientations (see Figures 6 and 7). Therefore, examination of these features still provides an accurate means of determining the direction of crack propagation for both ply orientations at each environmental condition evaluated in this study.

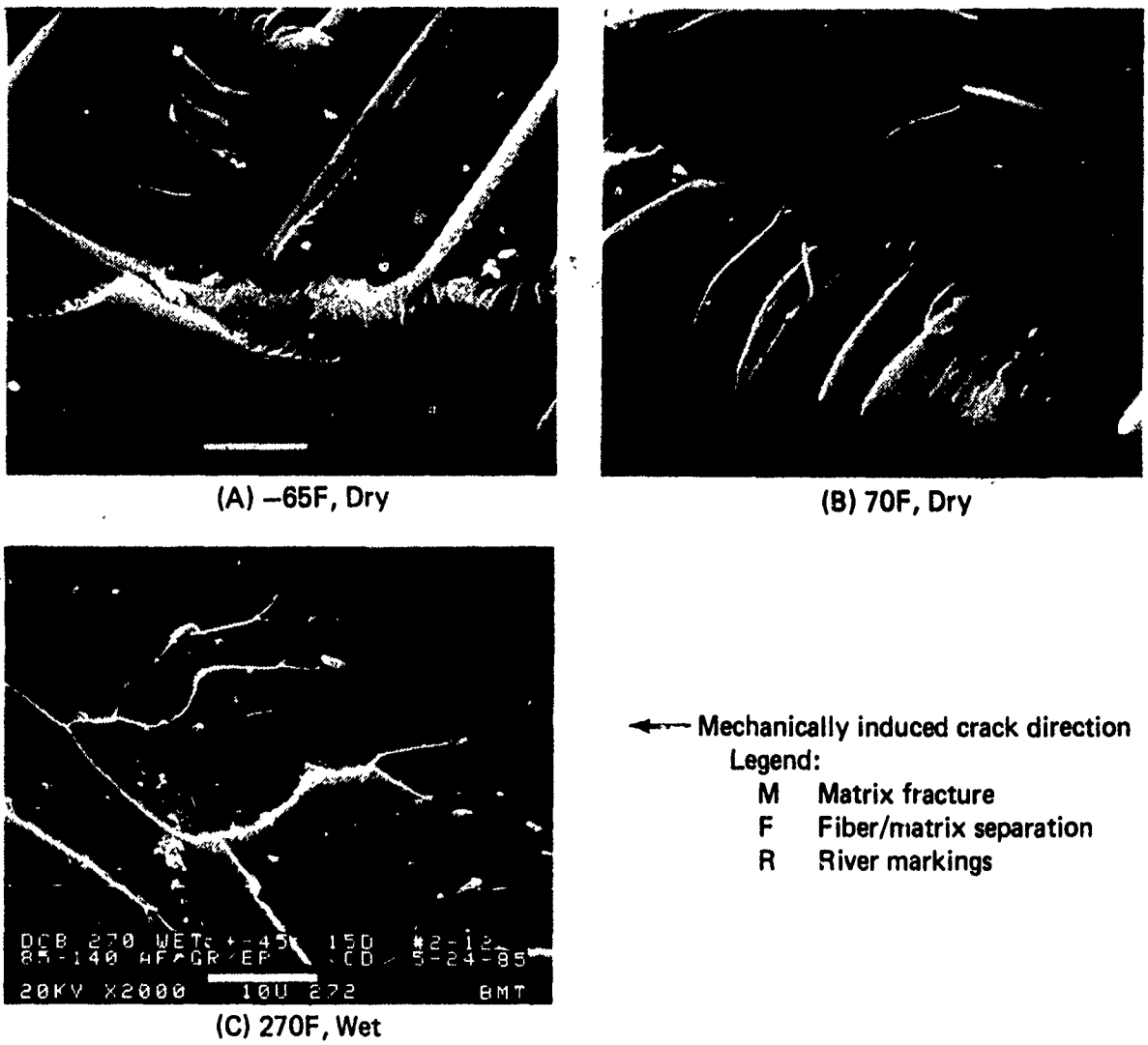

Figure 7. High Magnification of Typical Matrix Resin Fracture Features for +45/-45 Interface Mode I Tension Fractures.

Although significant alterations did not occur, locallized regions exhibited variations in the observed crack propagation direction. This was most evident for both the 270F dry and wet 0/0 interface specimens. For these delaminations, locallized zones exhibited significant alterations in the direction of river mark branching with respect to the known overall direction of induced crack propagation. As illustrated in Figure 8, an approximately 95 degree variation in the locallized crack propagation direction exists for this 270F dry specimen. This condition can likely by attributed to local rotation of the crack front towards the nearest free surface, which in this case was the immediately adjacent fiber/matrix interface. However, by averaging these local variations, the overall direction of river mark branching and resin microflow was found to directly correspond to the direction of macroscopically induced fracture.

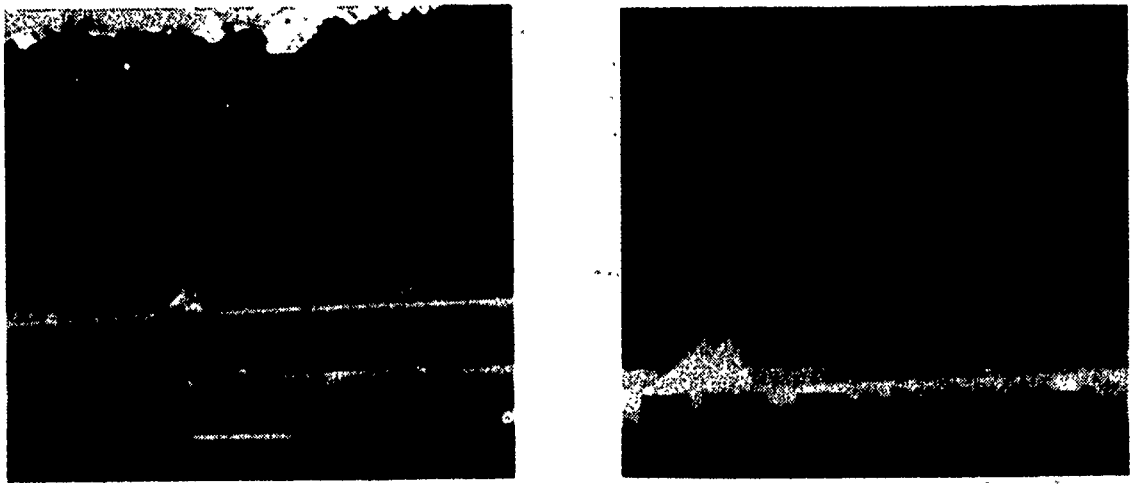

Figure 8. Locally Altered (R) River Mark Branch Directions for the 270°F/Dry, 0/0 Interface Mode I Tension Specimens. Arrows Indicate Locally Divergent Crack Propagation Toward the Adjacent (F) Fiber/Matrix Separation Region.

3.1 Interlaminar Shear Fracture Features

Similar to mode 1 tension, fractures produced under mode 2 shear conditions typically exhibited a mixture of fiber/matrix separation and cohesive resin fracture. However, in the case of mode 2 shear, areas of cohesive matrix fractures typically exhibited numerous rows of inclined resin platelets (hackles), as opposed to a nearly flat matrix topography representative of mode 1. These "hackle" features provided a means to positively differentiate mode 2 fractures from mode 1, for all environmental conditions tested. In general, the overall effect of environment on mode 2 fractures was a pronounced increase in the amount of fiber/matrix separation, as similarly found for mode 1 tension fractures. This effect is illustrated in Figures 9 and 10, in which controlled fractures were produced between adjacent 0 degree plies at -65F/dry, 70F/dry, 270F/dry and 270F/wet. The topographies characteristic of -65F and 70F fractures appeared very similar. Each of these lower temperature conditions exhibited extensive amounts of fractured resin, in which long rows of inclined

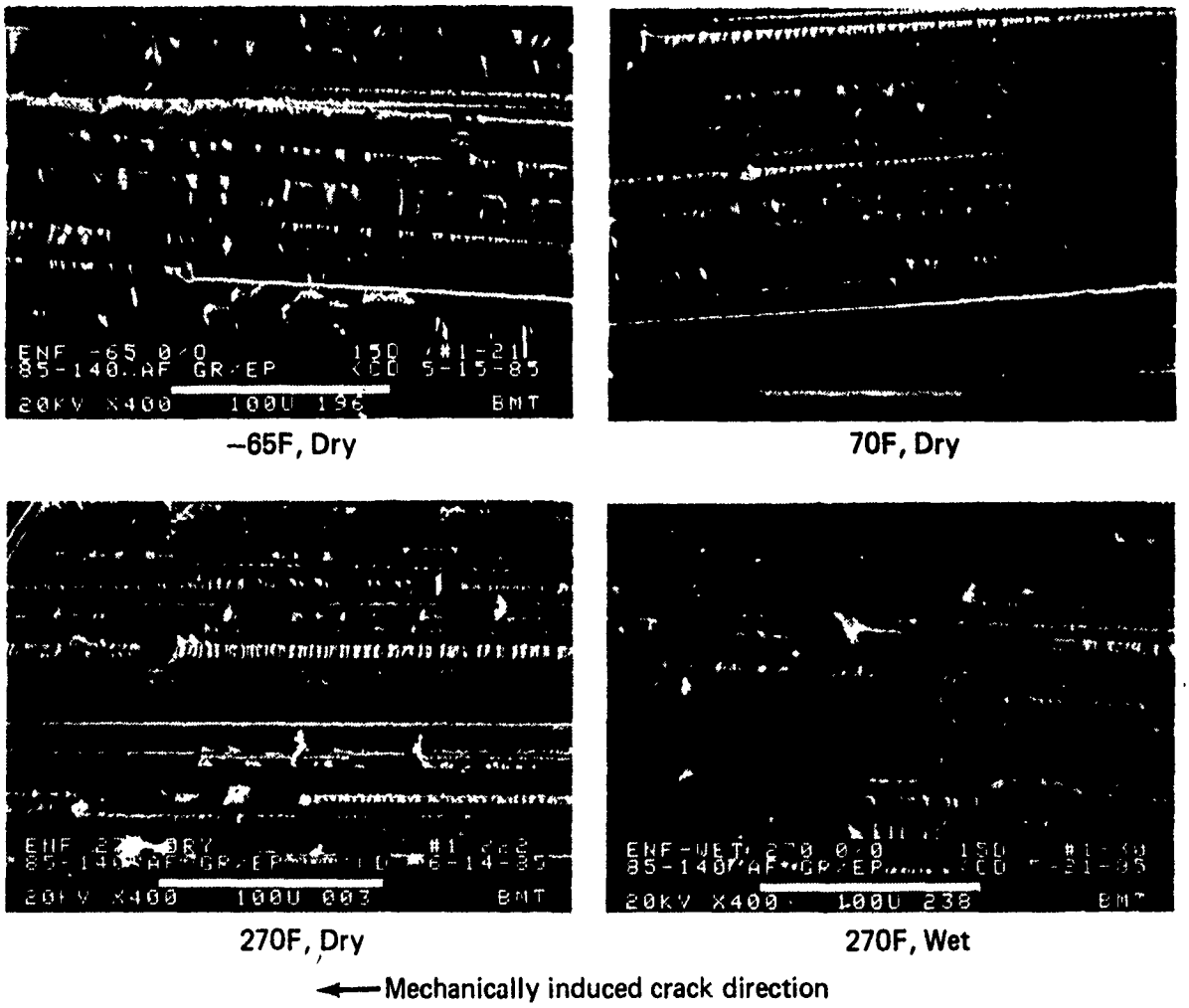

Figure 9. Low Magnification Series of Typical Fracture Topographies Characteristic of 0/0 Interface Mode 2 Shear Fractures at Each Environmental Conditon.

−65F, Dry

70F, Dry

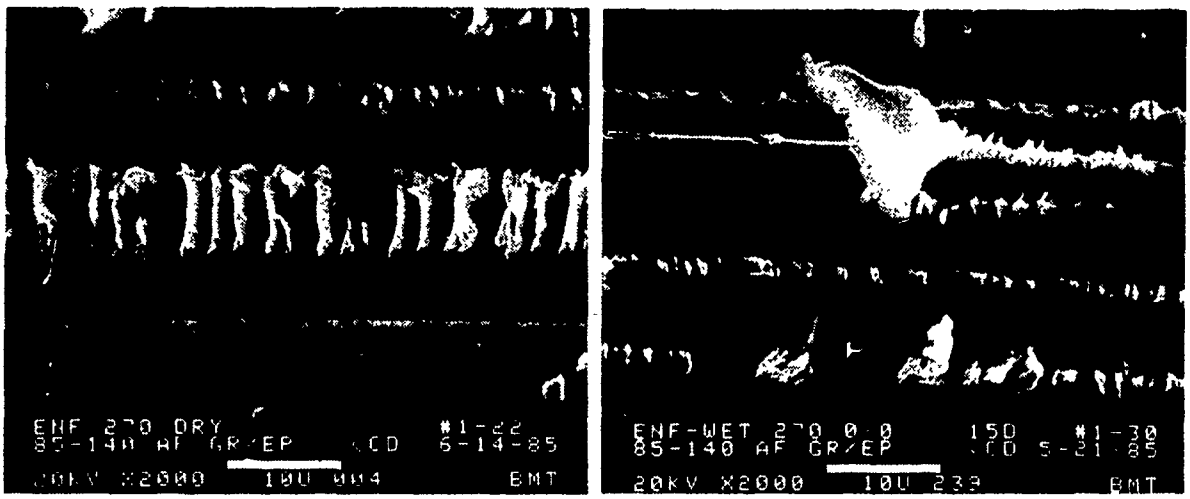

270F, Dry

270F, Wet

← Mechanically induced crack direction

Figure 10. Higher Magnification Series of Same Locations Presented in Figure 9. Shown are Features of (F) Fiber/Matrix Separation and Matrix Resin (H) Hackles.

hackles were bounded by zones of fiber/matrix separation. In contrast, fractures produced under 270F dry and wet conditions were characterized by a significantly larger amount of fiber/matrix separation and a corresponding decrease in the individual size and overall amount of resin hackle features. The hackles were sometimes twisted and deformed, indicative of an increase in matrix ductility at these elevated temperatures (see Figure 10, 270F specimen). As found for interlaminar tension, the 270F conditions resulted in pulled out fibers scattered over the fracture surface. These fibers could be seen at both a macro-and microscopic level. Similar to 0/0 interface fractures, delaminations produce between +45/-45 crossply interfaces exhibited increasing amounts of fiber/matrix separation with increasing temperature and absorbed water content. These features are shown in Figures 11 and 12. This phenomena is particularly evident in the low magnification photomicrographs presented in Figure 11, in which a more overall fracture surface morphology can be seen.

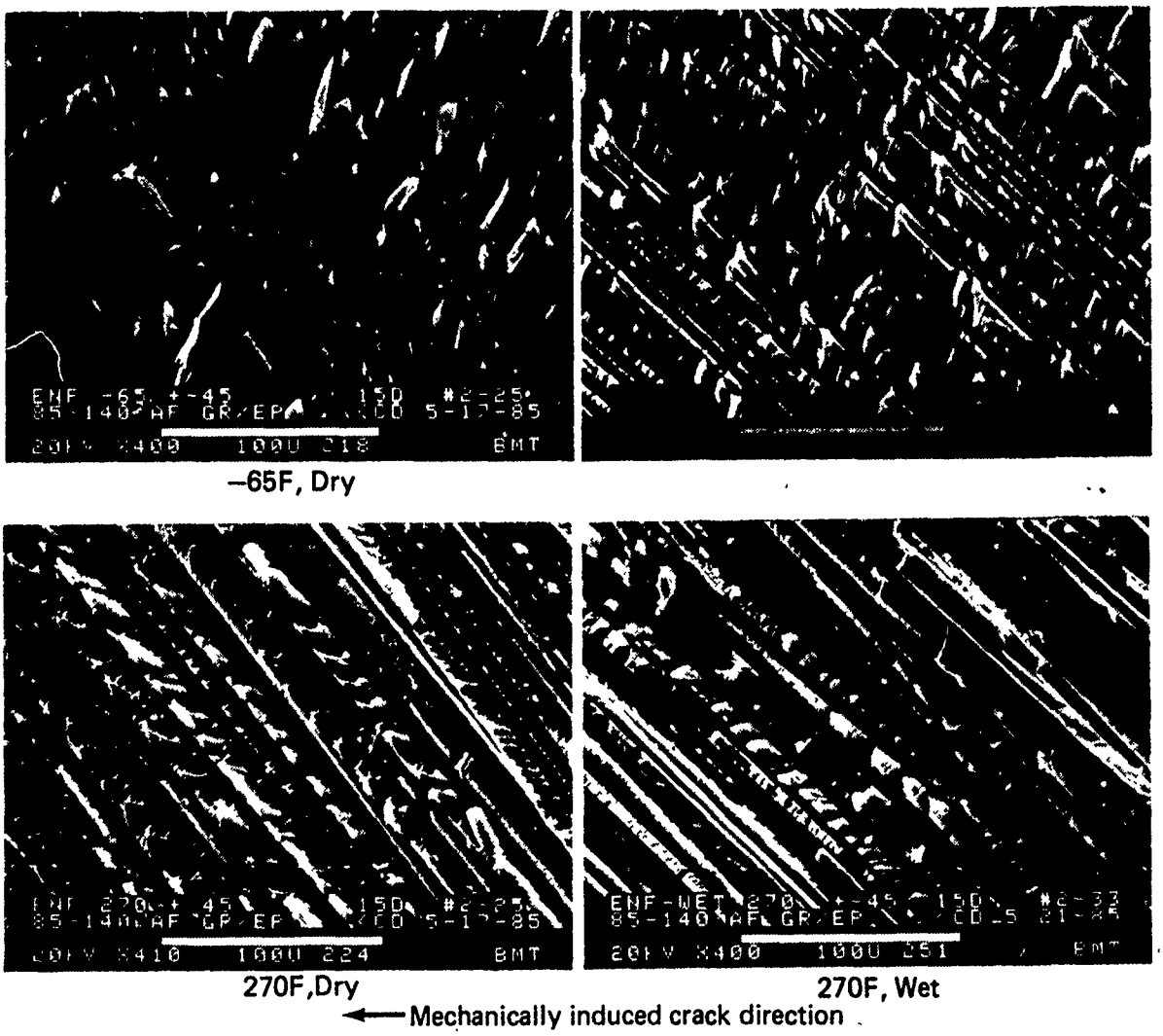

Figure 11. Low Magnification Series of Typical Fracture Topographies Characteristic of +45/-45 Interface Mode 2 Shear Fractures at Each Environmental Condition.

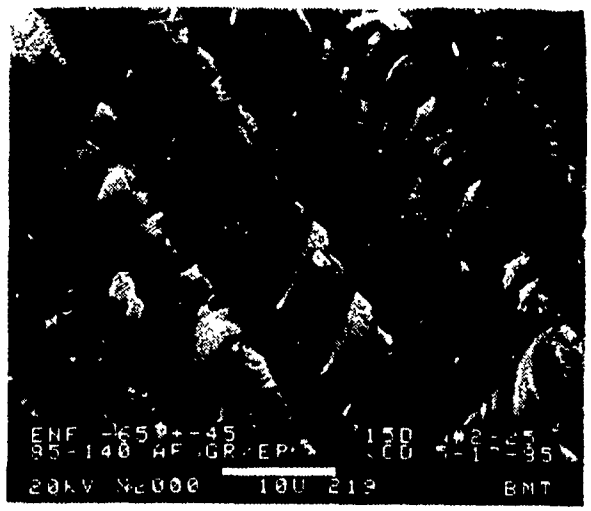

−65F, Dry

70F, Dry

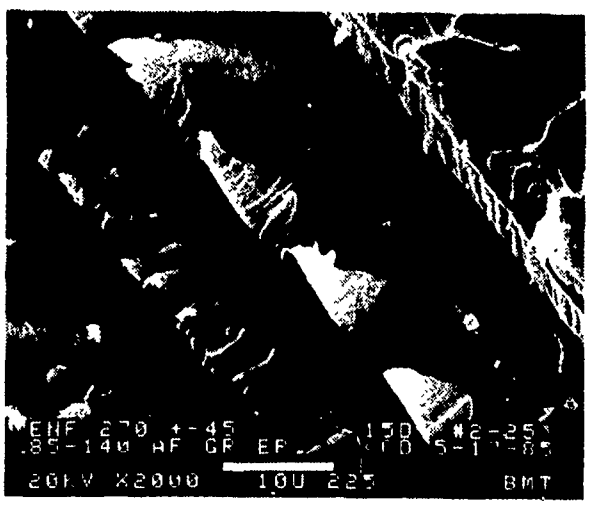

270F, Dry

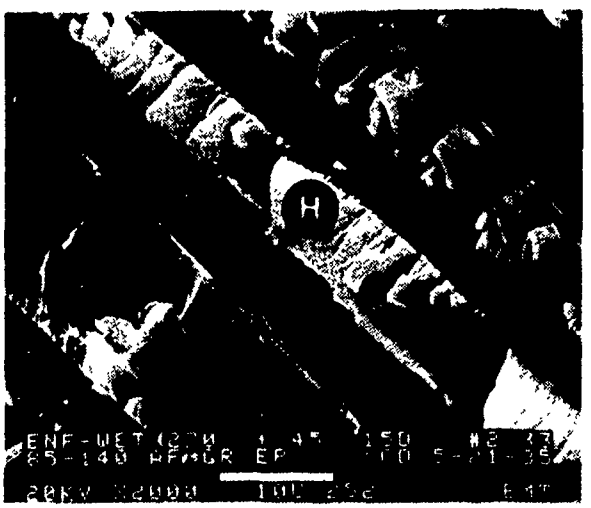

270F, Wet

← Mechanically induced crack direction

Figure 12. Higher Magnification Series of Same Locations Presented in Figure 11, with Conditions of (F) Fiber/Matrix Separation and (H) Hackles.

4.0 CONCLUSIONS

In the study presented above, the intermediate status of an ongoing investigation into the effect of environment on the interlaminar fracture characteristics of mode 1 tension and mode 2 shear are discussed. Evaluated were controlled delaminations produced between two ply orientations (0/0 and +45/-45) at -65F/dry, 70F/dry, 270F/dry and 270F/wet. Conclusions derived as a result of this investigation are:

1) Environmental effects on interlaminar mode 1 tension fractures did not result in significant alterations in the characteristic matrix resin fracture features. As a result, examination of river mark branching and resin microflow remains a viable means of determining the load state and crack propagation direction of fractured components, even for fractures produced at environmental extremes.

2) Similarly, environmental effects on interlaminar mode 2 shear fractures did not result in significant changes in observed resin matrix features. Therefore, examinations of matrix fracture regions for delaminations generated at environmental extremes still remains to be an acceptable means by which to determine the load state at fracture.

3) A significant increase in fiber/matrix separation was observed at elevated temperature and absorbed moisture contents for both mode 1 tension and mode 2 shear fractures.

4) Typically, -65F/dry and 70F/dry fractures appeared similar to one another for each fracture mode and crossply type. Fractures generated at these temperatures tended to occur within the thin, resin rich zones located between laminae, resulting in relatively large cohesive resin fracture zones.

5) In general, 270F/dry and 270F/wet fractures appeared similar for each fracture mode and crossply type. Fractures at these environmental conditions tended to occur within, or adjacent to, dense packed fiber regions within the laminae, resulting in a fiber dominated fracture appearance, with small, localized regions of resin fracture.

Acknowledgements

The authors would like to thank Mr. R. E. Smith of The Boeing Company for his efforts and the Air Force Aeronautical Systems Division for their generous support (contract F33615-84-C-5010).

References:

1. "Failure Analysis For Composite Materials", contract F33615-84-C-5010; Air Force Systems Command, Aeronautical Systems Division/PMR RC, Wright Patterson AFB, 1984.

2. Dexter, H.B., and Baker, D.J., "Worldwide Flight and Ground-Based Exposure of Composite Materials", ACEE Composite Structures Technology Conference, Seattle, WA, August, 1984, p. 40.

3. Miller, A.G., and Wingert, A.L., "Fracture Surface Characterization of Commercial Graphite/Epoxy Systems", Non Destructive Evaluation and Flaw Criticalities for Composite Materials, ASTM STP 696, R.B. Pipes, Ed., American Society for Testing and Materials, 1979, pp. 223-273.

4. Smith, B.W., Grove, R.A., and Munns, T.E., "Fractographic Analysis of Interlaminar Fractures In Graphite-Epoxy Material Structures", Proceedings of the International Conference: Post Failure Analysis Techniques For Fiber Reinforced Composites; AFWAL/MLSE, Dayton, OH, July, 1985.

PROGRESSIVE DAMAGE AND FRACTURE PREDICTIONS AND POST MORTEM CORRELATIONS

C.C. Chamis and C.A. Ginty
NASA Lewis Research Center
Cleveland, Ohio

CONTENTS

Keywords:

Graphite/epoxy, Progressive Damage, Fracture,

RUSCAN, CODSTRAN, Microstructural Characteristics

Star Category: 24

PROGRESSIVE DAMAGE, FRACTURE PREDICTIONS, AND POST MORTEM CORRELATIONS FOR FIBER COMPOSITES

by

C. A. Ginty*

NASA Lewis Research Center

Cleveland, Ohio

SUMMARY

Lewis Research Center is involved in the development of computational mechanics methods for predicting the structural behavior and response of composite structures. In conjunction with the analytical methods development, experimental programs including post failure examination have been conducted to study various factors affecting composite fracture such as laminate thickness effects, ply configuration, and notch sensitivity. Results have indicated that the analytical capabilities incorporated in the CODSTRAN computer code are effective in predicting the progressive damage and fracture of composite structures. In addition, the results being generated are establishing a data base which will aid in the characterization of composite fracture.

*Aerospace Structures Engineer

INTRODUCTION

The ability to design complex composite components and structures for both aeronautical and space applications requires a working knowledge of several disciplines. In an effort to characterize composite fracture, at Lewis Research Center, several disciplines were employed including: (1) an extensive experimental program with a unique RUSCAN (Real-Time Ultrasonic C-Scan) facility, (2) post failure analysis with a scanning electron micorscope (SEM), and (3) analysis methods in the CODSTRAN (COmposite Durability STRuctural ANalysis) computer code (ref. 1). The data provided by RUSCAN AND SEM were used to verify the progressive damage and fracture predictions by CODSTRAN.

CODSTRAN incorporates a constituent material property databank, composite micro- and macromechanics, finitè element analysis, and failure criteria modules to predict progressive damage and fracture loads of fibrous composite structures. In its prediction of progressive fracture, CODSTRAN identifies damage occurring at the microstructural level through the application of an iterative scheme described in detail below. Ultimately, CODSTRAN yields fracture load and mode predictions.

The material system selected for testing and analysis in the composite fracture characterization program was graphite fiber/epoxy resin. Understanding the significant factors affecting composite (graphite/-epoxy) fracture including ply layup, laminate thickness, and notch sensitivity became the impetus for the several experimental programs which will be discussed. These same factors were modeled in the CODSTRAN program and their effects on fracture behavior were documented. Finally, and most importantly, the capability for using the data generated from the post failure analysis of the fracture surfaces in verifying and corroborating the measured and predicted results were demonstrated.

EXPERIMENTAL PROGRAM

The first experimental program that significantly contributed to the data base of the composite fracture characterization study was conducted in 1977. The objective was to study the mechanical behavior and fracture characteristics of unidirectional, high-modulus, graphite fiber composites subjected to off-axis tensile loads (ref. 2). The specimens were fabricated from Modmor I - graphite fibers in a matrix of ERLA-4617 epoxy resin in an eight ply unidirectional configuration. This investigation produced stress-strain data, fracture loads, and fracture modes of the off-axis specimens.

Subsequently, to determine the effects on the fracture process, another series of experiments was conducted with angleplied $[\pm\theta]s$ configured specimens, where θ = 0, 3, 5, 10, 15, 30, 45, 60, 75, and 90 degrees. In addition to smooth specimens, notched samples were also prepared with both 0.25-inch centered through-thickness slits and holes to determine: (1) the notch sensitivity of the composite structure, and (2) the effect, if any, of the notch type.

The 12-inch by 18-inch angleplied panels were fabricated from Fiberite 1034E Prepreg (934 resin matrix with Thornel 300 graphite fibers). For the notch sensitivity analysis, all of the 2-inch specimens were cut from the same panel (Fig. 1) to insure that the fabrication technique, itself, did not become one of the factors affecting the composite fracture.

The specimens were incrementally loaded in unaxial tension until fracture occurred. Progressive fracture of these specimens was recorded by a unique facility developed at the Lewis Research Center known as Real-Time Ultrasonic C-Scan (RUSCAN). Depicted in Figures 2 and 3, the

RUSCAN facility consists of a microprocessor system, a monitor with 16-level gray scale reproduction capability, an ultrasonic signal conditioning system, and ultrasonic transducers in conjunction with a CGS 50 kip load frame (ref. 3).

The facility is unique in that the specimen is scanned while sustaining a load. At each load increment, a scan is taken which records the real-time damage occurring at the microstructural level. When viewed in sequence, the individual scans display the progressive damage in the fibrous composite.

Future experimental efforts include tensile testing of eight-ply unidirectional off-axis laminates. As an extension to the earlier work performed, these specimens will contain machined notches. Again, both slits and holes will be used to determine the notch sensitivity of these thicker laminates.

ANALYTICAL METHODS

As previously mentioned, the analytical methods used in modeling the progressive fracture of composites are incorporated into the CODSTRAN finite element computer code. The major elements comprising CODSTRAN are shown in the flow chart in Figure 4 and include: (1) Executive Module, (2) Input/Output Modules; (3) Analysis Module (ref. 4); (4) Composite Mechanics Module (ref. 5), and (5) Fracture Criteria Module (ref. 6).

CODSTRAN assesses composite durability in terms of defect growth/-progressive damage. Using one of two available combined-stress failure criteria, damage is determined on a ply-by-ply level for each finite element comprising a particular model. The iterative scheme employed is initiated with the application of a load to the finite element model.

If intraply damage has occurred in any of the plies of an element, the stiffness coefficient for that element is reduced in the direction affected by the damage. When all plies in that element suffer damage (due to increased incremental loading) such that the element can no longer sustain a load, the element is considered destroyed and is purged from the finite element mesh. Thus damage is being predicted in a progressive manner until the iterations cease with the destruction of a sufficient number of elements which result in fracture.

In addition to determining the damage, CODSTRAN predicts the mode of fracture by registering the direction (longitudinal, transverse, or shear) of damage that occurred. CODSTRAN therefore provides a complete history of the failure process by predicting the progressive damage, the fracture load, and fracture mode.

CODSTRAN analyses were conducted in conjunction with the experimental investigations involving the angleplied ($[\pm\theta]s$) laminates. Three finite element models were generated to represent the solid and notched (centered through-slit and centered through-hole) specimens. The mechanical, thermal, and hygral material properties of the prepreg are entered into the data bank. Environmental conditions such as the thermal and moisture conditions are also input parameters; thereby, demonstrating the versatility of the program and its capability to adequately model the physical composite specimen/structure.

Similarly, CODSTRAN will be used to analyze the off-axis laminates. One major difference in this study lies in the orientation of the 0.25 inch through-slit. Since the plies are unidirectional it is desirable to orient the slit parallel to the fiber direction. This requires a generic-type model which can be rotated for the series of laminates involved. This model is currently being generated for the off-axis laminate studies.

FRACTURE SURFACE ANALYSIS

Thus far, in our attempt to characterize fracture, experimental data and predictive results have been generated. Another source of valuable information exists on the surfaces of the fractured graphite/-epoxy specimens. The microstructural characteristics observed on the surfaces will be used in conjunction with the results, previously mentioned, to explain the failure process of graphite/epoxy laminates.

The majority of specimens fractured into two distinct puzzle-like pieces (Fig. 5). Areas of particular interest exist on either side of the machined defects. To further investigate these areas, 0.75-inch wide specimens were cut for the microscopic analysis using a diamond wheel, while carefully preserving the fractured surfaces from additional debris.

The specimens were mounted onto aluminum seats in preparation for the microscopic analysis. Using a vapor deposition process, the entire configuration was coated with a gold film approximately 200-Å thick to enhance the conductivity of the specimen and hence improve the transmission of the microscope.

Using the Amray 1200 Scanning Electron Microscope (SEM), at least one section from each fractured surface was observed at varying angles and magnifications. Particular attention was directed toward sections possessing extensive damage indicated by RUSCAN and/or CODSTRAN. Microstructural damage such as fiber fracture, matrix cracking, matrix hackling, and delaminations was observed and permanently recorded on Polaroid Type 52 film.

RESULTS AND DISCUSSION

This section summarizes the efforts from each discipline previously discussed. The outcome of the research including experimental data (RUSCAN), analytical solutions (CODSTRAN), photomicrographs (SEM), and the conclusions derived therefrom on the characteristics of composite fracture will be presented.

Photomicrographs were taken of the fractured surfaces of the off-axis Modmor I graphite/ERLA-4617 epoxy off-axis specimens in an effort to fulfill the objective of the project: to establish criteria that can be used to characterize fracture surfaces with respect to a predominant "single-stress" fracture mode (ref. 7). Thorough examination of the photomicrographs revealed that each fracture surface did indeed exhibit distinct morphological characteristics (Figs. 6 and 7) which could be associated with a dominant fracture mode.

The angleplied ($[\pm\theta]s$) Fiberite graphite/epoxy laminates were studied to determine the effect of ply orientation. It was observed that as the angle of the ply orientation increased with respect to the "X" axis, (which is coincident with a vertical axis and where $+\theta$ is measured clockwise and $-\theta$ is taken counter clockwise from this axis) the fracture load decreased. This result is evident from the data shown in Tables I and II, which contain the experimentally determined fracture loads and the CODSTRAN predicted fracture loads, respectively. Note, that for the unnotched specimens, the experimental and CODSTRAN fracture loads are in good agreement.

When considering the notch sensitivity of the composite, the experimental results indicate that in terms of ultimate strength, the presence of a notch had little effect. CODSTRAN fracture load predictions, however, were conservative in comparison, indicating notch sensitivity.

This disparity is in part due to the excessive predicted stress concentrations at the defect (slit/hole) edge. Though not completely determined at this time, it appears that the stress concentration does not occur. Currently, modifications are being incorporated into the CODSTRAN code to determine the exact nature of the problem.

In addition, both the experimental and CODSTRAN fracture loads indicate that the type of notch is not a factor affecting the composite fracture. The microstructural characteristics on the surfaces of select specimens support this conclusion because the damage observed on the surface of the unnotched specimen is similar to that observed on the notched fracture surfaces. Figure 8 depicts the microstructural damage in four ply unidirectional specimens, including fiber pull-out and a tiered fracture surface. In Figure 9, the damage observed on all the surfaces of the $[\pm 45]s$ specimens is identical and consists of a combination of tiered and flat morphology along with fiber pull-out and extensive matrix hackles. These observations demonstrate the use of post failure analysis in corroborating the experimental (RUSCAN) results for both unidirectional and angleplied laminates.

As discussed earlier, CODSTRAN also has the capability of predicting fracture modes based on progressive damage and the direction in which damage occurs. Figures 10, 11, and 12 depict the progressive damage of $[\pm 15]s$ graphite/epoxy specimens including unnotched, notch/-slit, and notch/hole respectively. In comparing the meshes for the notched specimens, note that the damage patterns are almost identical, indicating insensitivity to notch type.

The entire set of angleplied specimens was tested using the RUSCAN facility which monitors and records progressive damage. Output is a 16-level full Gray scale image of the digitized ultrasonic signal.

A typical RUSCAN output is shown in Figure 13. These real-time damage images were then compared with CODSTRAN results. Figure 14 shows the excellent correlation which exists not only for this particular [±45]s specimen, but for the majority of the specimens tested.

Having established confidence in CODSTRAN's predictive capability, analyses were performed to establish the fracture mode of the angleplied laminates. Four predominant fracture modes -- longitudinal tensile, intraply shear, interply delamination, and transverse tensile -- were predicted and are shown in Table III. One obvious characteristic observed from the table is that the mode of fracture is a function of the ply configuration.

It was at this time that a section from each fracture surface was examined to document the microstructural characteristics and establish criteria relating these characteristics to a dominant fracture mode. The type of behavior indicated by CODSTRAN was verified with the microscopic analysis: that the predominant fracture mode is a function of ply orientation. Specifically, for lower angleply laminates ($[0]_4$ - [±15]s) fracture is the result of a longitudinal tensile mode characterized by a tiered surface, fiber pull-out and fiber breakage. Laminates with a lay-up of [±30]s - [±45]s fracture from the combined effect of longitudinal tensile and intralaminar shear modes characterized by both tiered and level surfaces, fiber pull-out and breakage, and an abundant amount of matrix hackles. The cause of fracture in laminates with a higher angleply orientation ([±60]s - $[90]_4$) is the transverse tensile mode characterized by level surfaces, matrix cleavage, and matrix cracking. The typical microstructural characteristics observed are shown in Figure 15.

The complete documentation of the microscopic analysis is included in Reference 8. From the analysis, Table IV was derived. The observed fracture modes are in good agreement with the CODSTRAN predicted modes. Note, that due to the violent actions occurring in the fracture region at the time of failure, it is difficult to discern interply delamination as a failure mode. Nonetheless, the data provided from the post-failure analysis are a valuable source of information in both the verification of analytical results and in the development of a data base for post-fracture analysis.

CONCLUSIONS

In characterizing the fracture of graphite/epoxy composites, several methods of analysis were utilized. The experimental and RUSCAN facilities, the CODSTRAN computer code, and the post fracture microscopic investigation are independently effective techniques to study composite fracture. In combination, however, the ability to study progressive fracture and all the many factors which affect it is synergistically enhanced. Use of the fractographic results in verifying previously established experimental and analytical results is of particular importance in that it has enhanced the level of confidence in the predictive capabilities of CODSTRAN which is proving to be a valuable tool in the determination of composite durability.

REFERENCES

1. Chamis, C. C. and Smith, G. T.: CODSTRAN: Composite Durability Structural Analysis, NASA TM 79070, 1978.
2. Sinclair, J. H. and Chamis, C. C.: Mechanical Behavior and Fracture Characteristics of Off-Axis Fiber Composites. I - Experimental Investigation, NASA TP 1081, 1977.
3. Irvine, T. B. and Ginty, C. A.: Progressive Fracture of Fiber Composites, NASA TM 83701, 1983.
4. McCormick, C. W. (ed.): NASTRAN User's Manual (level 15). NASA SP-222(01), 1972.
5. Chamis, C. C.: Computer Code for the Analysis of Multilayered Fiber Composites - User's Manual, NASA TN D-7013, 1971.
6. Chamis, C. C. Failure Criteria for Filamentary Composites. Composite Materials: Testing and Design, ASTM STP460, 1969, pp. 336-351.
7. Sinclair, J. H. and Chamis C. C.: Fracture Surface Characteristics of Off-Axis Composites, NASA TM 73700, 1977.
8. Ginty, C. A. and Irvine, T. B.: Fracture Surface Characteristics of Notched Angleplied Graphite/Epoxy Composites, NASA TM 83786, 1984.

TABLE I

FRACTURE LOADS (LB) OF $[\pm\theta]_s$ G/E LAMINATES (DETERMINED EXPERIMENTALLY)

Notch type	Ply configuration: $[\pm\theta]_s$; θ in degrees									
	0	3	5	10	15	30	45	60	75	90
Unnotched--solid	8060	6500	5200	4500	3700	2620	900	420	220	260
Notched--thru slit	7820	5500	4940	4160	2750	2150	880	320	180	180
Notched--thru hole	6000	5720	4700	4240	3300	1750	950	360	220	120

TABLE II

FRACTURE LOADS (LB) OF $[\pm\theta]_s$ G/E LAMINATES (PREDICTED BY CODSTRAN)

Notch type	Ply configuration: $[\pm\theta]_s$; θ in degrees									
	0	3	5	10	15	30	45	60	75	90
Unnotched--solid	8300	7400	6950	5000	4400	2150	900	400	200	200
Notched--thru slit	4500	3950	3600	2850	2250	1000	425	300	175	150
Notched--thru hole	4700	3850	3500	2700	2150	1100	425	200	150	100

TABLE III

FRACTURE MODES[a] OF $[\pm\theta]_s$ G/E LAMINATES (PREDICTED BY CODSTRAN)

Notch type	Ply configuration: $[\pm\theta]_s$; θ in degrees									
	0	3	5	10	15	30	45	60	75	90
Unnotched--solid	LT	LT S[3]	LT S[3]	LT S[3]	I S	S	I S	TT	TT	TT
Notched--thru slit	LT S[1]	LT S	LT S	S	S	I S	I S	I TT S[2]	TT	TT
Notched--thru hole	LT S	LT S	LT S	S	S LT	I S	I S TT	I TT	TT	TT

[a]LT = Longitudinal tension
TT = Transverse tension
S = Intraply shear:
1) Intraply shear occurring around notch tip during progressive fracture
2) Minimal intraply shearing during fracture
3) Some intraply shear occuring near constraints (grips)
I = Interply delamination

TABLE IV

FRACTURE MODES[a] OF $[\pm\theta]_s$ G/E LAMINATES (DETERMINED BY SEM ANALYSIS)

Notch type	Ply configuration: $[\pm\theta]_s$; θ in degrees									
	0	3	5	10	15	30	45	60	75	90
Unnotched--solid	LT	LT S	LT S	LT S	LT S	LT S	S LT	TT S	TT	TT
Notched--thru slit	LT S	LT S	LT S	LT S	LT S	LT S	S LT	TT S	TT	TT
Notched--thru hole	LT S	LT S	LT S	LT S	LT S	LT S	S LT	TT S	TT	TT

[a]LT = Longitudinal tension
TT = Transverse tension
S = Intraply shear

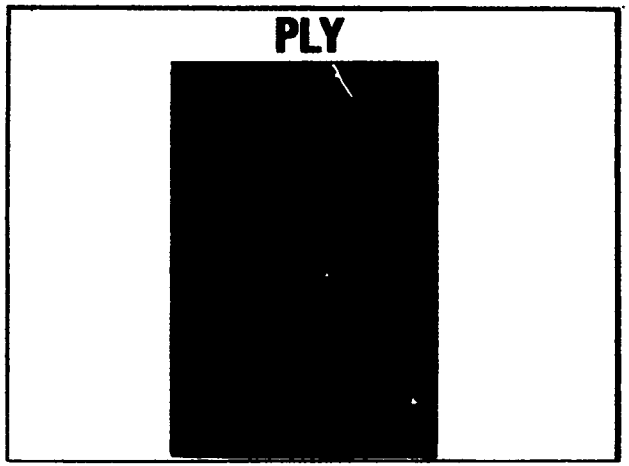

Step 1; Fiberite 934 prepreg; T 300 graphite fiber.

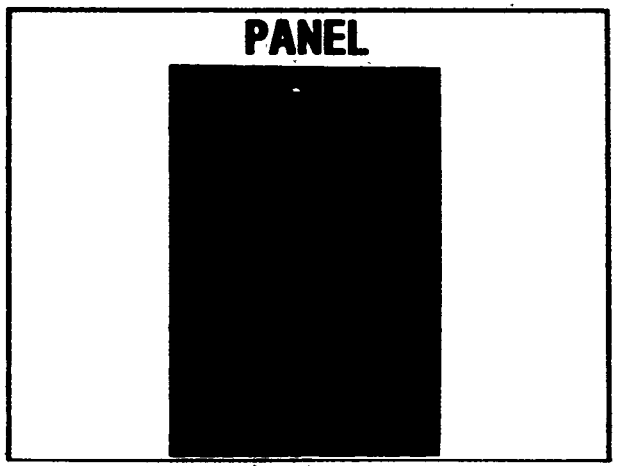

Step 2; 4 plies cured at 350^{0} for 2.5 hours.

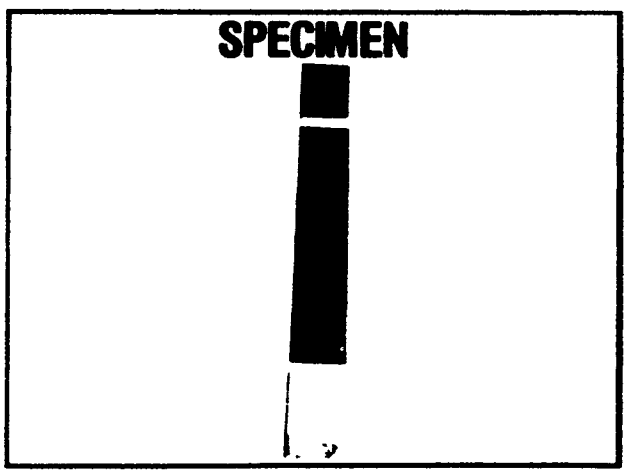

Step 3; specimen dimensions: 18. X 2. X .02 inches; machined with diamond tipped cutting wheel; beveled aluminum tabs.

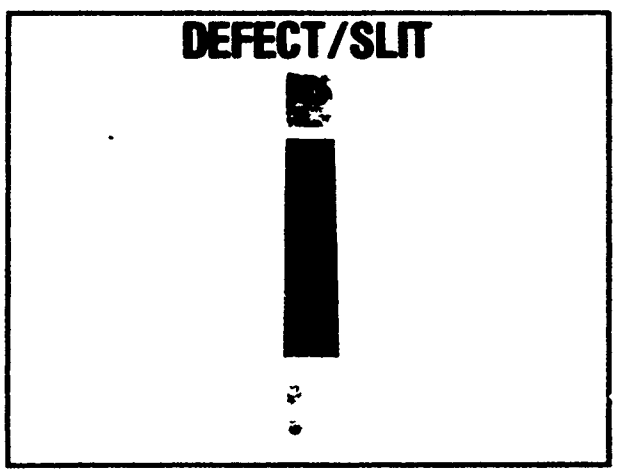

Step 4; slit dimensions: 0.25 X 0.05 inches; notching by ultrasonic abrasive slurry.

Figure 1. - Specimen fabrication procedure for graphite/epoxy angleplied laminates with a centered notch (slit).

Figure 2. - Load frame used for testing of uniaxial composite tension specimens with ultrasonic transducers mounted on the frame.

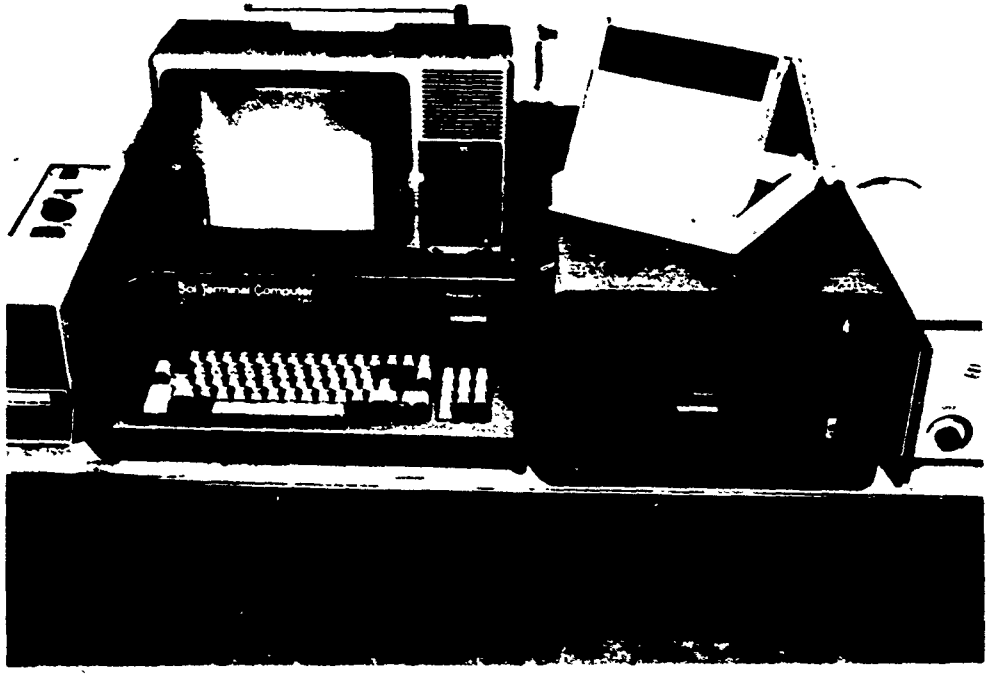

Figure 3. - The Real-Time Ultrasonic C-Scan (RUSCAN) facility. From left, the disk based microcomputer test rig control and data acquisiti system, the ultrasonic transducers in the water bucket with a notched composite specimen in grips on the load frame.

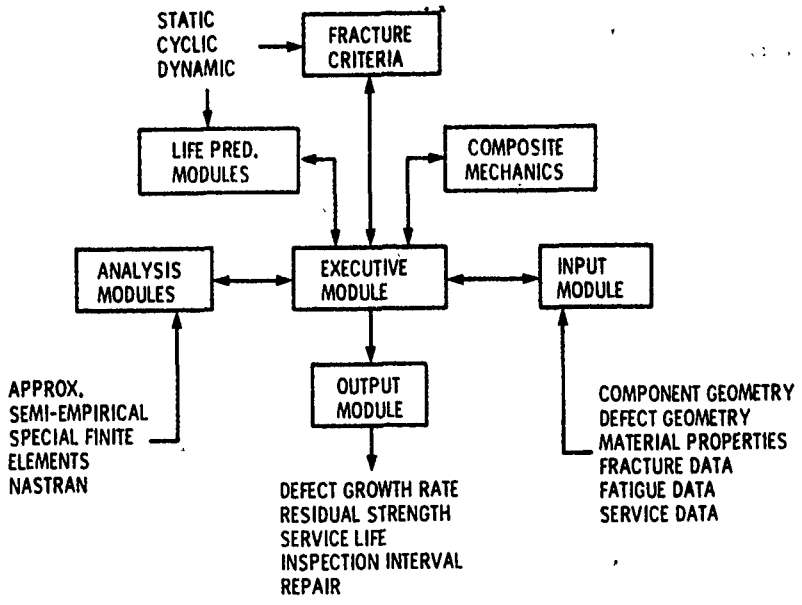

Figure 4. - CODSTRAN flow-chart.

(a) unidirectional.

(b) [±45]s.

Figure 5. - Fractured G/E specimens from left to right -- solid, notch/slit and notch/hole.

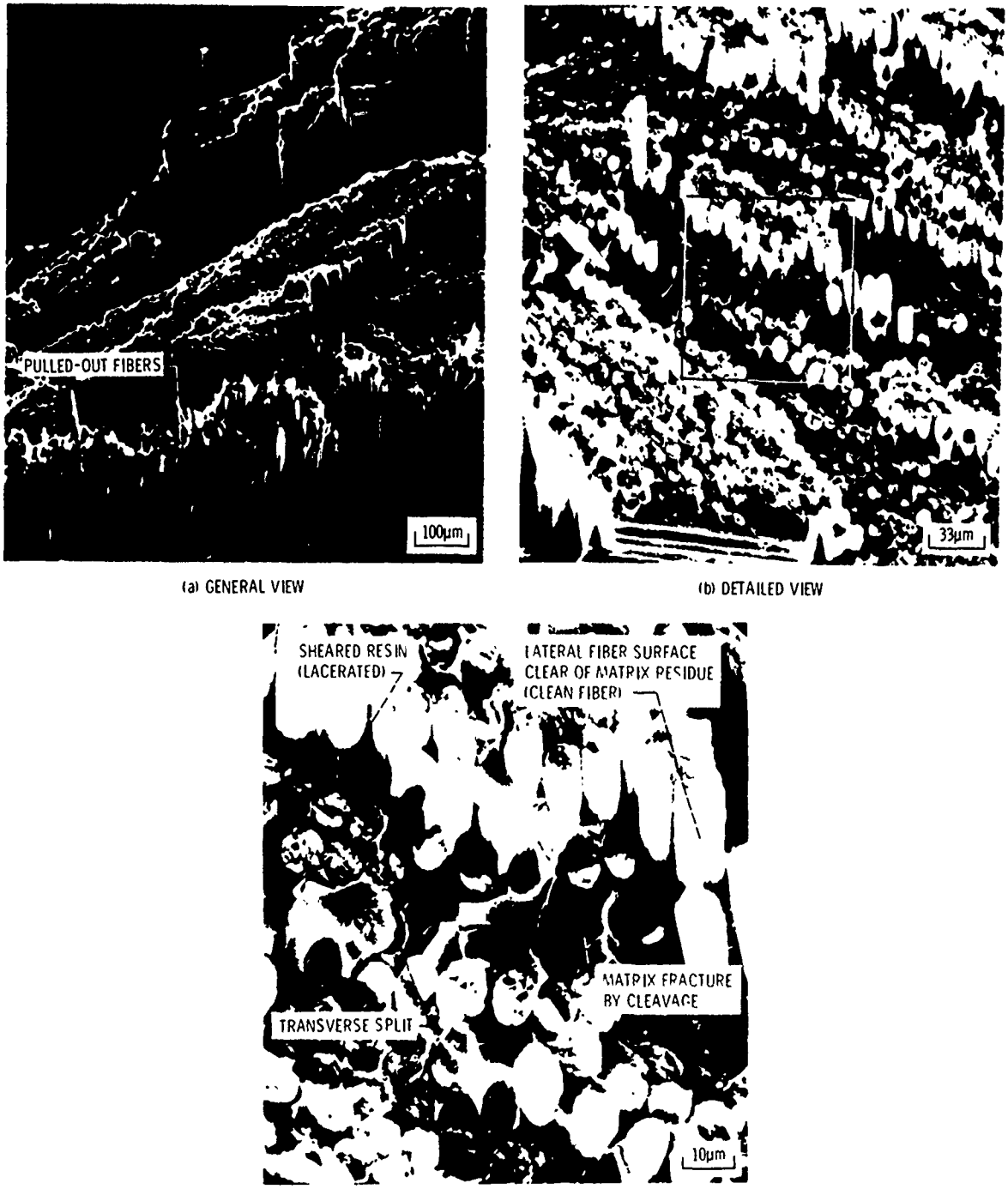

(a) GENERAL VIEW

(b) DETAILED VIEW

(c) ENLARGEMENT OF DETAIL IN (b) TO SHOW FRACTURE MODE

Figure 6. - Microstructural characteristics of fractured surface of MOD I/Epoxy unidirectional composite associated with a longitudinal tensile fracture mode.

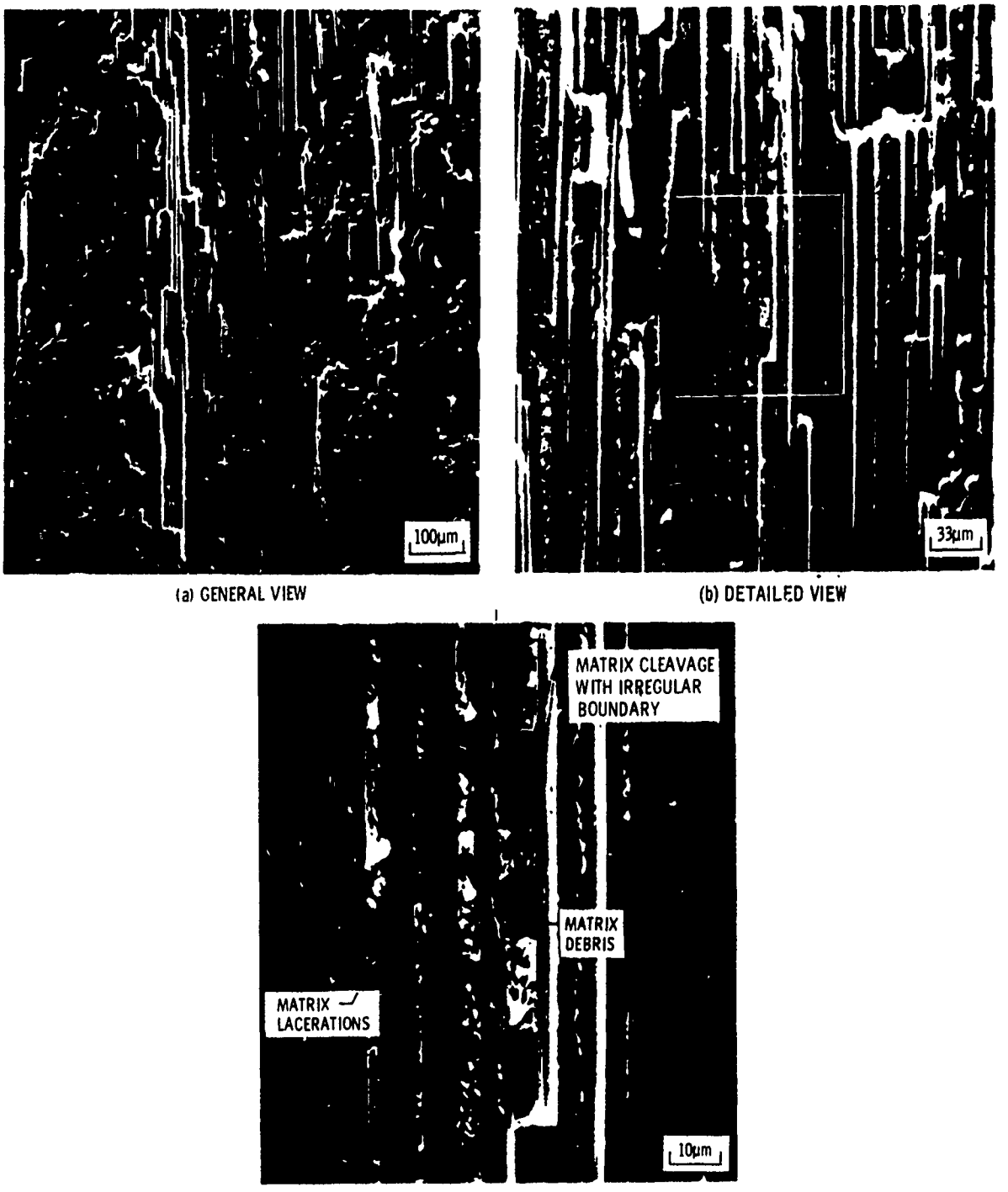

(a) GENERAL VIEW

(b) DETAILED VIEW

(c) ENLARGEMENT OF DETAIL IN (b) TO SHOW FRACTURE MODE

Figure 7. - Microstructural characteristics of fractured surface of MOD I/Epoxy unidirectional composite tested at 45 degrees associated with a mixed mode fracture.

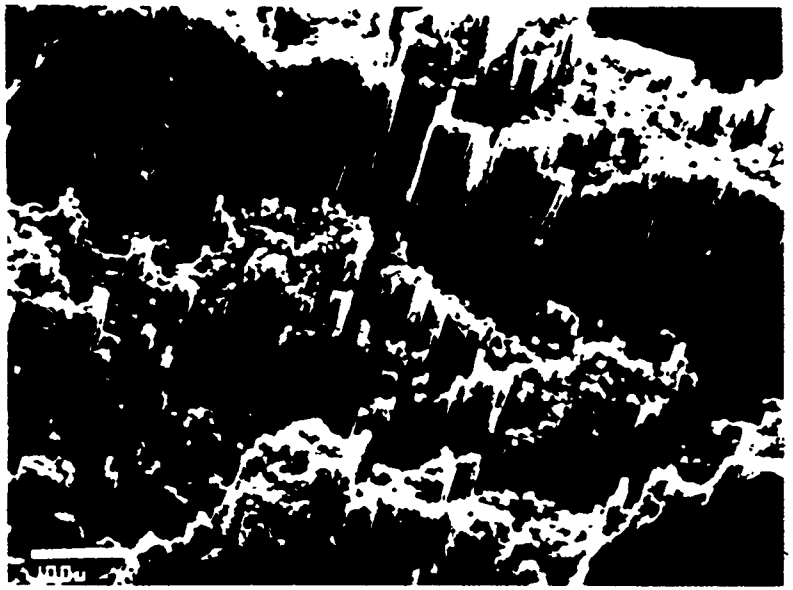

(a) Solid at 140X.

(b) Notch/slit at 240X.

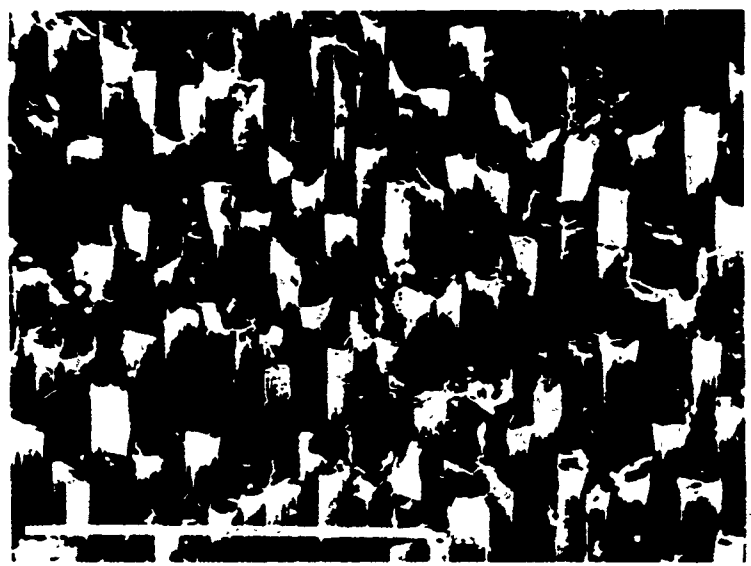

(c) Notch/hole at 250X.

Figure 8. - The microstructural fracture surface characteristics of the unidirectional G/E laminate.

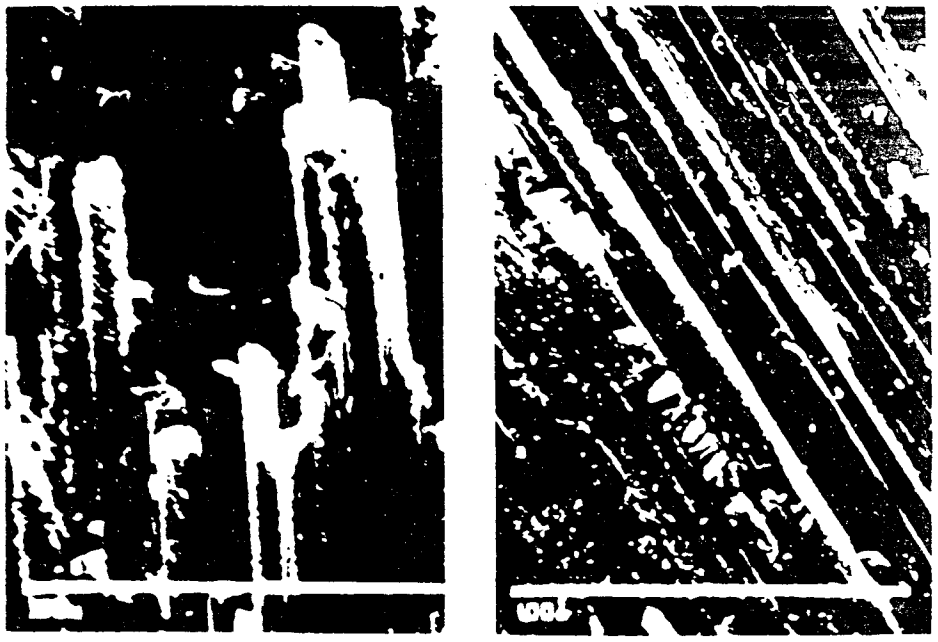

(a) Solid specimen at 710X / 560X.

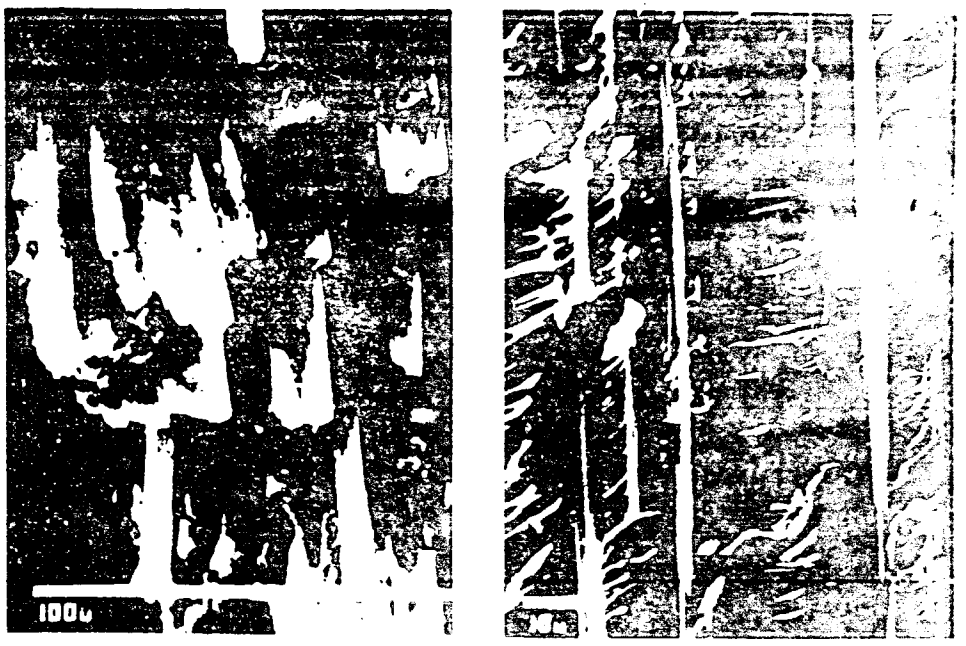

(b) Notch/slit specimen at 600 X / 1200X.

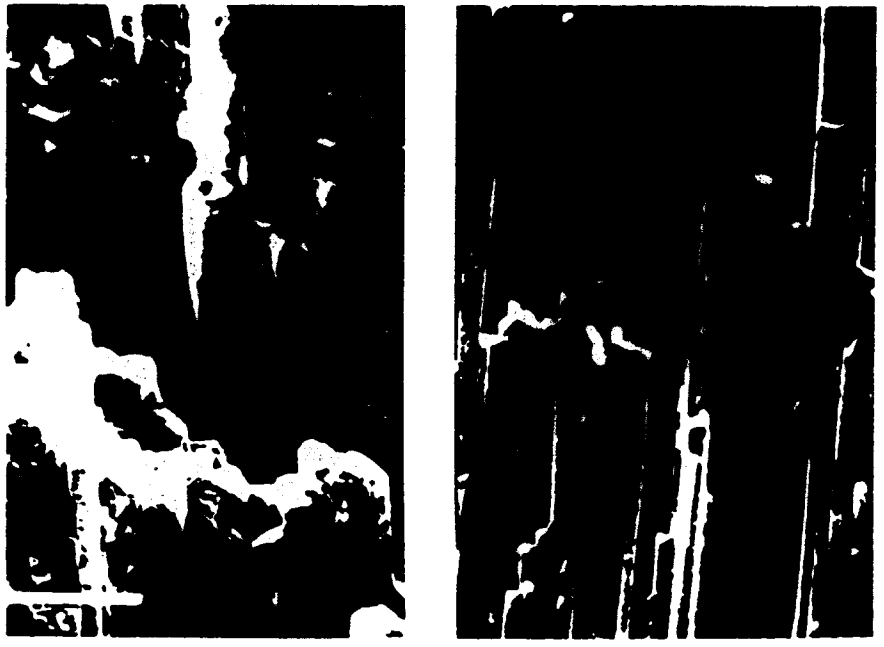

(c) Notch/hole specimen at 730X / 200X.

Figure 9 - Fracture surface charateristics of the [±45]s G/E laminate.

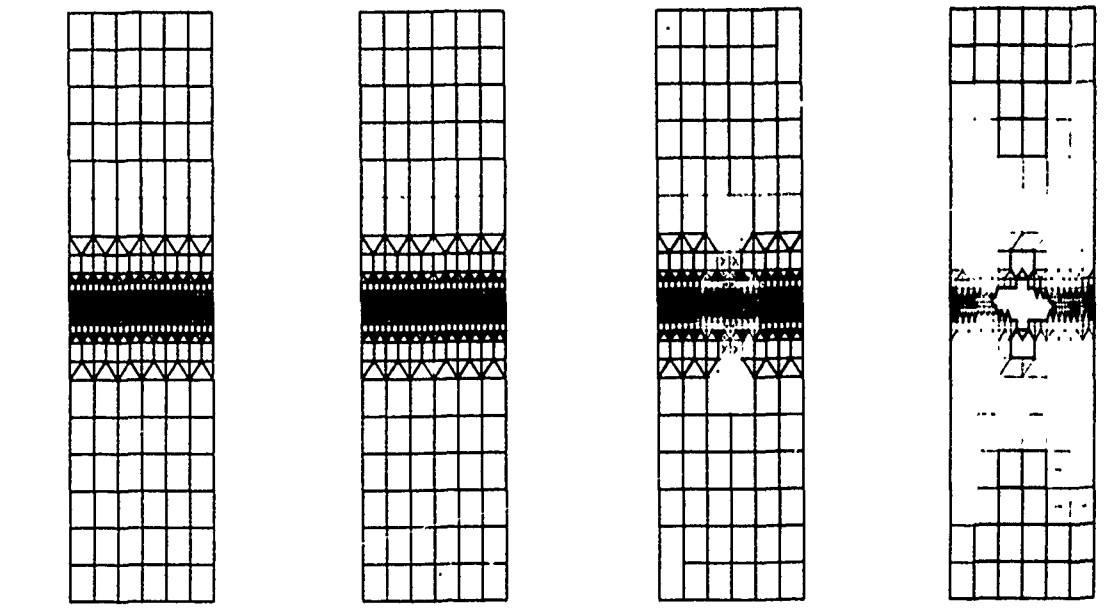

Figure 10. - CODSTRAN determined successive damage extent and defect growth as a result of progressive fracture in a $[\pm 15]_S$ graphite/epoxy solid laminate. Finite elements marked with a '+' denote damaged elements and those marked with an 'X' denote destroyed elements.

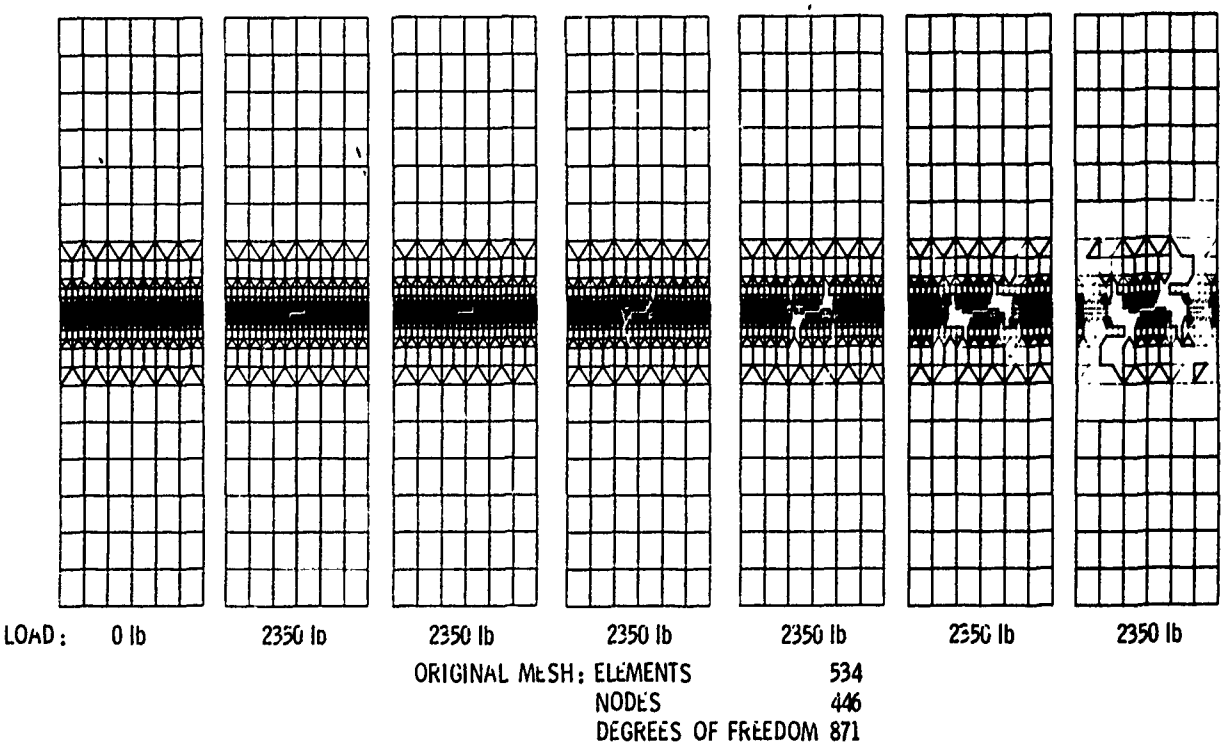

Figure 11. - CODSTRAN determined successive damage extent and defect growth as a result of progressive fracture in a $[\pm 15]_S$ graphite/epoxy laminate with a 0.25 in. by 0.05 in. centered through-slit. Finite elements marked with a '+' denote damaged elements and those marked with an 'X' denote destroyed elements.

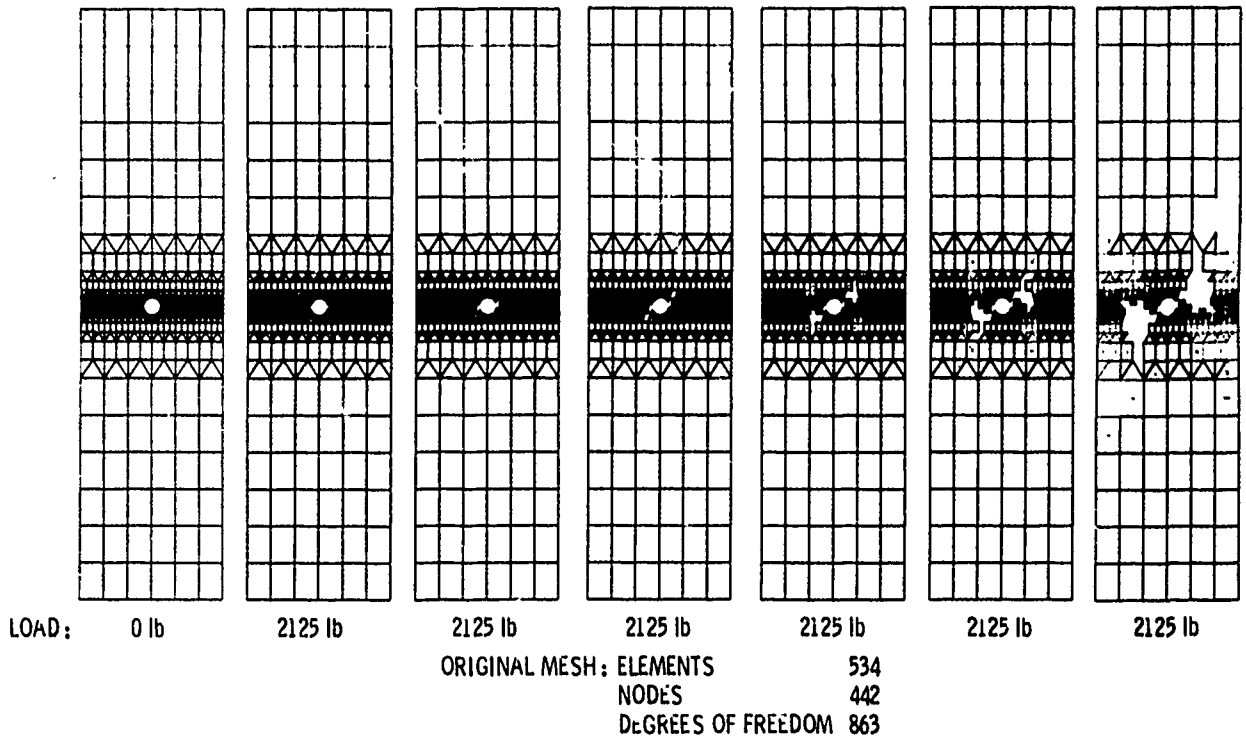

Figure 12.- CODSTRAN determined successive damage extent and defect growth as a result of progressive fracture in a $[\pm 15]_s$ graphite/epoxy laminate with a 0.25 in. diameter centered through-hole. Finite elements marked with a '+' denote damaged elements and those marked with an 'X' denote destroyed elements.

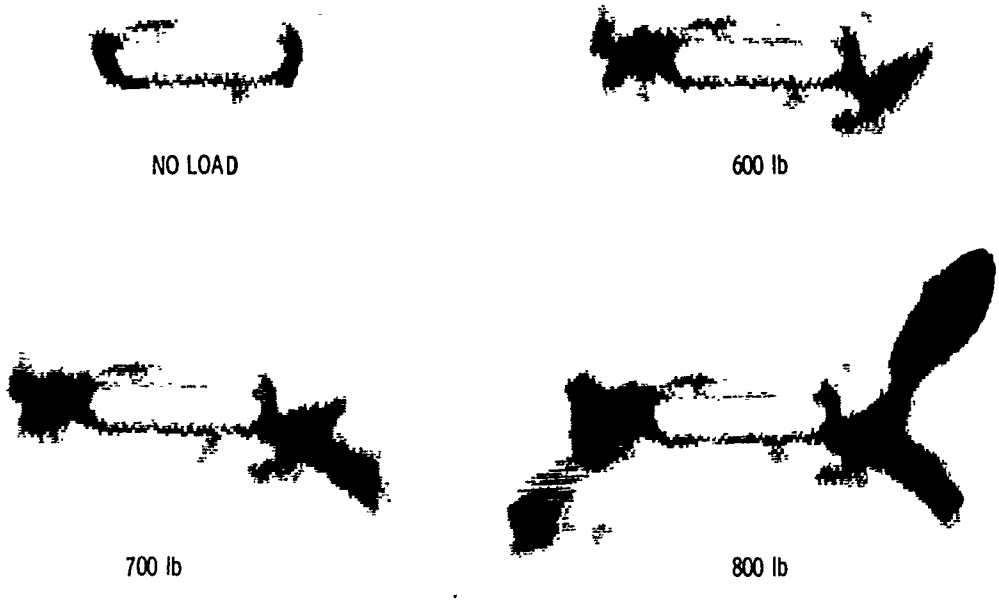

Figure 13. - C-Scan images of the $[\pm 45]_s$ laminate reveal an increase in delaminations at the tip of the notch/slit as the load increment increases until final fracture occurs at 880 lb.

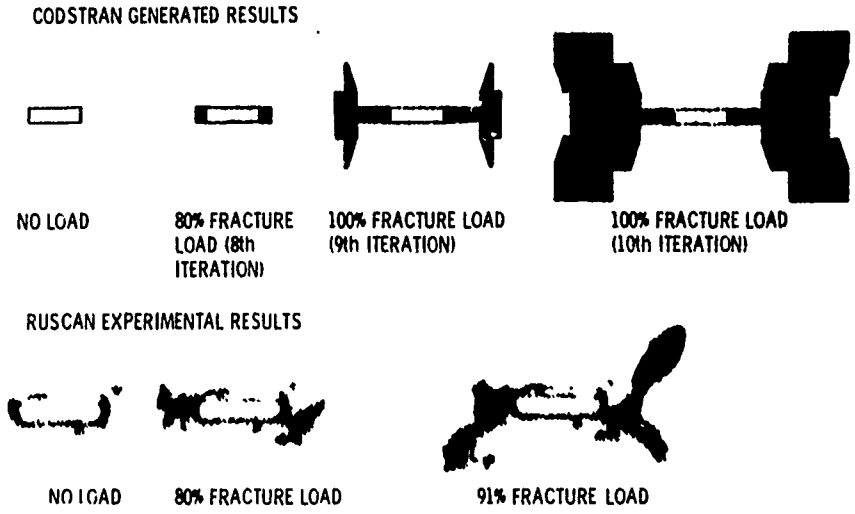

Figure 14. - Progressive fracture of a $[\pm 45]_s$ laminate. Results shown are for a 2 in. wide tension specimen with a 0.25 x 0.05 in. centered slit.

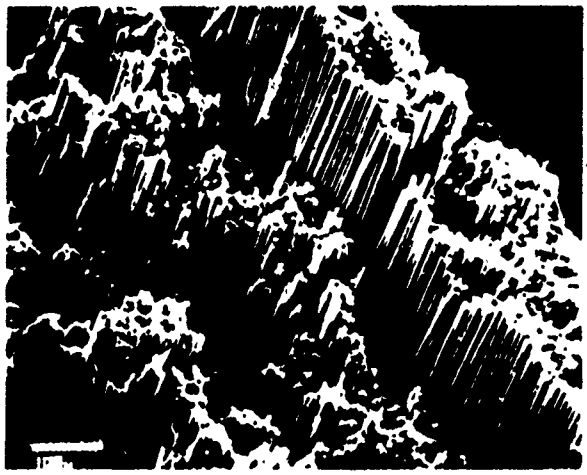

(a) Longitudinal tensile fracture characterized by a tiered surface caused by fiber fracture.

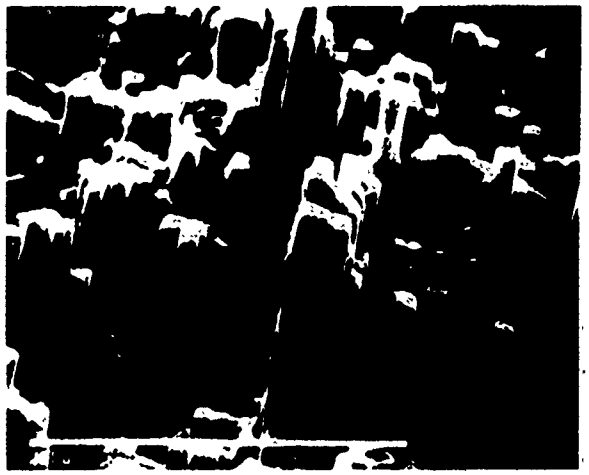

(b) Intralaminar shear fracture characterized by a surface with extensive matrix hackling.

(c) Transverse tensile fracture characterized by smooth fiber surfaces with some apparent matrix cleavage.

Figure 15. - Typical fracture surfaces from unidirectional and angleplied graphite/epoxy composite laminates.

A FRACTOGRAPHIC INVESTIGATION OF THE MATERIAL BEHAVIOR OF GRAPHITE FIBER REINFORCED COMPOSITES UNDER VARIOUS LOAD AND ENVIRONMENTAL CONDITIONS

P. Stumpff
Structural and Electronic Failure Analysis Group
Systems Support Division
AFWAL/Materials Laboratory
Wright-Patterson AFB, Ohio

A FRACTOGRAPHIC INVESTIGATION OF THE MATERIAL BEHAVIOR OF GRAPHITE/FIBER REINFORCED COMPOSITES UNDER VARIOUS LOAD AND ENVIRONMENTAL CONDITIONS

P. L. Stumpff
Air Force Wright Aeronautical Laboratories, WPAFB, Ohio

ABSTRACT

This paper will present fractographs taken from a number of graphite/epoxy specimens tested under various orientation, load and environmental conditions. The load conditions consist mainly of 0° and 90° unidirectional layups. The load conditions consist of tension, compression, flexure, fatigue, interlaminar shear, Mode I and Mode II crack growth behavior. The main portion of the data is for room temperature ambient conditions with some results reported for temperature and moisture variations. This paper is intended to give a general overview of composites fractography by identifying the types of features found on the fracture surfaces and relating those features to the specific conditions at the time of failure.

INTRODUCTION

Failure analysis is used to determine the cause of failure so that a successful redesign of a component can be accomplished if necessary. Failure analysis entails three major aspects; the first is the determination of the failure initiation site, the second is the determination of the failure mechanism and the third is the determination of the cause of failure. The work to be presented will focus only on the first two aspects; the third aspect - the determination of the cause follows from the first two and is specific to the failure and will not be discussed here.

Specimens with known initiation sites and failure modes were examined for fracture features which were thought to be either indicative of the crack initiation and propagation direction or specific to the failure mode. The first portion this work deals with initiation sites and crack growth direction; the second portion focuses on the surface features as related to failure modes.

INITIATION SITES

River patterns are often found in brittle materials failing in an overload mode and can be used to determine crack propagation direction even in metals. As can be seen in Figures 1a to 1e, taken from a double cantilever beam specimen, macroscopic river patterns are found on the surface and may be able to be used to determine crack propagation direction. These photo's, taken with a Zeiss optical microscope, show river patterns pointing in the basic direction of crack propagation as indicated by the arrows. However, the river patterns do not directly indicate the macroscopic crack propagation direction in all instances. While the macroscopic crack direction is in the horizontal direction, the river patterns show a semi-circular type pattern across the width of the specimen. As can be seen in Figure 1f, the river patterns show a microscopic crack growth pattern in which the river patterns point horizontally in the center of the specimen, but tend to point toward the specimen edges as the crack moves away from the center toward the sides of the specimen. Additionally, it was noted that these river patterns get closer together and more numerous as the crack gets closer to the edge of

the specimen. The reason for this is unknown. However, it should be noted that if using the river patterns to predict crack propagation direction, examination of the entire width of the specimen surface must be made so the proper macroscopic crack direction can be determined.

FAILURE MODES

The work on failure modes will be broken up by layup, i.e., fiber orientation and then by load condition. Differences in surface features due to material and environmental conditions will be presented last. The orientations examined were the 0° and 90° unidirectional specimens. The loading conditions consisted of tension, compression, flexure, interlaminar shear, fatigue, Mode I and Mode II type loadings. The material under consideration for most of the specimens was graphite/epoxy with some data for graphite/PEEK. The environmental work focuses on the differences in the surface morphology due to variations in the temperature and moisture levels of the sample at the time of failure.

0° ORIENTATION - TENSION

A graphite/epoxy 0° oriented tension specimen is one with the load applied parallel to the fiber orientation. Failure in this type of specimen in a ductile mode has a rather rugged brushlike failure surface with some splitting along the 0° fibers as seen in Figure 2a. The broken fibers are arranged in bundles which have a steplike nature similar to spires as shown in Figure 2b. The spires are thought to be created by the means shown in Figure 2e in which the fiber breaks releasing some of the intrinsic energy upon load application; this, however, may not be enough to stop the crack. As the crack continues to grow it breaks additional fibers near it and on the same level until it either comes to a disbond or has only enough energy to break a fiber/matrix interface. As additional load is applied, the crack may begin to grow where it left off breaking fibers around it or it may begin to break new fibers so that the final appearance is similar to spires as shown. Some fibers have been pulled out onto the opposite fracture surface leaving holes in the fracture surface being examined. These are known as fiber pullouts. Higher magnification of the broken fiber ends show the feature known as fiber radials; this feature is shown in Figure 2c. These line markings usually emanate from the edge of a fiber or at an inclusion within the fiber and radiate outwards. These radials often end on one fiber and begin on an adjacent fiber at the same point; this feature is identified in Figure 2d. In addition to the radials on the fibers and the spired nature of the surface, the matrix also shows features indicative of a tensile failure. These features consist of cleavage steps which are also known as river patterns and are similar to those found on the macroscopic scale. These however, are smaller and emanate through the matrix between the fibers.

A tension specimen broken in a brittle mode has features similar to the ductile mode fracture, however, this surface is relatively flat since it may take only one initial break sequence to fracture the entire component.

0° ORIENTATION - COMPRESSION

The failed compression specimen shows broken 0° fibers, fiber splitting, some delamination and possibly some buckling of the outer plys. See Figure 3a. Scanning electron microscopic examination reveals a layered appearance

with secondary cracking perpendicular to the surface as seen in Figure 3b. This layered appearance is thought to be due to fiber kinking as shown in Figure 3c. Fiber kinking is the breaking of fibers at an angle to the applied load at two points on the fiber. The kinked layer which often exists on both fracture surfaces is often found lying at an angle to the lower surface with cracking on that layer exactly at the point of the lower layer.

The chop marks as seen on the next photo of Figure 3d are thought to be indicative of fiber buckling shown in Figure 3e. Half the fiber contains fiber radials and the other half a line type marking with a flat surface. This appears to indicate that the fiber buckled with one half failing in tension and the other in compression. When arranged in a row pattern as these are, they are thought to be indicative of macrobuckling with the tensile radial side pointing in the direction of the outer plys, which in this case, buckled first.

Another type of compressive failure surface shows the individual fibers broken in compression revealing an angular fiber breakage type surface as shown in Figure 3f or some post failure damage (though not actually a compression failure, it is often seen on compression surfaces and so is shown here for completeness) in Figure 3g.

0° ORIENTATION - INTERLAMINAR SHEAR

The fracture surfaces found on interlaminar shear specimens as determined using the thin short beam shear specimens have the following fractographic features as noted and shown in Figure 4a. This surface feature consists of broken bits of matrix covering the fibers over the entire fracture surface. Other shear type specimens however, such as the edge notched flexure, tested in the Mode II condition, have "hackles" over the entire surface. The reason for this difference is thought to be due to the nature of the loading condition for thin short beam shear specimen. Various stress analysts do not believe that this specimen gives a pure shear mode failure but a failure due to combination of loading modes. This is because the specimen often breaks near the top of the specimen near the loading points and not at the midplane as predicted by theory. Hence this feature is not thought to be indicative of shear, but a complex loading combination including compression and shear.

0° ORIENTATION - FLEXURE

The 0° orientation specimen tested in 4 point bending that was examined broke only on the lower plys under tensile loading with splitting along the fibers between the two points of loading. See Figure 4b. On examination, the fracture surface was nearly identical to the specimen failed in tension so that the two can not necessarily be distinguished.

0° ORIENTATION - FATIGUE

The 0° fatigue specimens are similar in fracture surface appearance to the 0° unidirectional tension specimens. Indeed, both macroscopically and microscopically, similar features are observed. Macroscopically, the features consist mainly of broken 0° fibers and 0° fiber splitting. Microscopically, the features consist of river patterns in the matrix and fiber radials on the fibers across the main transversly cracked surface. Hackles are found on the split surfaces. There may be a slight difference in the two

types of specimens in their microscopic fracture appearances with the fatigue surfaces exhibiting slightly more rounded fiber edges on the main fracture surface and possibly more damage on the fracture surfaces (see Figure 4c).

0° ORIENTATION - MODE I

The 0° unidirectional Mode I Double Cantilever Beam (DCB) specimens are characterized by matrix covered fibers on a rather smooth surface with relatively few broken fibers, river patterns throughout and some matrix wedges, i.e., pieces of matrix pulled up and away from the surface. The surface, when viewed optically, is often seen to have areas of dark and light bands as shown in Figure 5a. These bands have been thought to be caused by different rates of crack growth. Further magnification of these areas are shown in Figures 5b and 5c where the dark areas are seen to be relatively flat with the fibers and matrix on the same plane, whereas the light regions appear to have fibers protruding from the main fracture surface. Though the typical surface of this specimen is rather flat and featureless except for the river patterns, some areas have a "curtained" type matrix structure as seen in Figure 5d and some hackle formation may be found.

0° ORIENTATION - MODE II

The 0° unidirectional Mode II Edge Notched Flexure (ENF) specimens show the following features. "Hackles" can be seen covering most of the surface and lie between the fibers and fiber imprints. No river patterns are found. As most authors have indicated, the hackles, which appear to overlap one another as shingles on a roof, appear on both sides of the separating surfaces. Additionally, the hackles appear to overlap in opposite directions on mating fracture surfaces. The hackles appear to alternate sides, but in no particular pattern - usually an area of hackles followed by some hollowed out areas. See Figures 6a and 6b. These hollowed out areas, magnified in Figure 6c, appear to correlate with the hackles found on the opposite fracture face. Scallops, the feature shown in Figure 6d are also found on the Mode II fracture surfaces but their formation is not yet understood. The fracture surface may be somewhat debris covered.

90° ORIENTATION - TENSION, COMPRESSION, FLEXURE AND FATIGUE

The 90° orientation specimens also have differences in surface topography depending on load and environmental conditions though not as pronounced. In order to better illustrate the differences seen in the 90° fiber oriented samples, the next set of figures, Figures 7a to 7d, illustrate the major features of the 90° tension, compression, flexure and fatigue samples.

The failure surface of the tension specimen is usually perpendicular to the principal load direction and as seen in Figure 7a, is characterized by fibers that are not only broken but are pulled away from the surface below. Basically, as the load is applied, the crack front is thought to move across the fibers so that they are pulled away from the separating surfaces. This is known as fiber bridging. As additional load is applied, the fibers are broken in tension or flexure. However, except for being pulled away from the surface at the broken fiber edges, the fibers remain intact with the rest of the surface.

The 90° compression sample, shown in Figure 7b, shows fibers which are often broken in more than one place; however, these broken fibers appear to

remain totally intact with the surface below. Additionally, the surface is more debris covered than is the tension specimen.

The 90° flexure specimen, shown in Figure 7c, shows both features - one side seemingly indicative of a specimen loaded in tension and one side indicative of a specimen loaded in compression.

The 90° tension-tension fatigue specimen, Figure 7d, is rather rugged in appearance with some features from both the compression and tension specimens. There do appear to be some, although fewer, fibers being pulled out from the surface. However, more of the fiber breaks appear slanted and more intact with the surface thaN seen in the tension sample.

EPOXY VERSUS PEEK MATRICES

Some work was done on the graphite/PEEK material, and some of the differences in the surface morphologies between the thermosetting epoxy resin and the thermoplastic PEEK resin are noted here.

The PEEK matrix shows much more ductility than the epoxy matrix with no river patterns apparent on the Mode I tension samples taken from a [±30°/±30°/90°] 2s specimen. They are probably not formed because the matrix is not brittle enough for a cleavage type fracture to occur. See Figure 8a where the ductile matrix can be seen adhering to the fibers. Additionally, there appears to be a "star" pattern covering some of the fibers. See Figure 8b. These "stars" appear to correlate in size to the crystallites which are found to form in the semi-crystalline PEEK material. Additionally, these crystallites have been found to attach themselves in an orderly arrangement to the graphite fibers. It is this semi-crystalline attachment that is thought to be seen here and thought to be the reason for the success of the adhesion of the PEEK to the graphite fibers as compared to other amorphous type thermoplastic materials. Some hackles are also found on the mode I type surface and are similar in appearance to the hackles seen on the graphite/epoxy mode I type specimens. See Figure 8c.

The typical fracture surface of a Mode II PEEK matrix specimen is shown in Figure 8d. Here the matrix forms a "peak" like area over the fiber surfaces - which also appear to be lying on top of one another similar to shingles on a roof. These "peaks" are also formed on both mating fracture surfaces and appear to be leaning in opposite directions similar to the hackles found earlier.

ENVIRONMENTAL EFFECTS

As for the environmental effects on the graphite/epoxy materials, the following features are noted. In 0° tension samples, significantly more fiber splitting was noted for increasing temperatures. See Figure 9. This phenomenon is thought to be due to increasing fiber/matrix failure. However, most of the mechanical properties are only slightly degraded and apart from the additional fiber/matrix debonding, no other microstructural differences due to temperature variations were found.

As for increasing moisture content, samples with 50% and 100% saturation levels show more matrix plasticity than the room temperature samples. Again, there is only a slight drop in most of the mechanical properties and no other differences in surface fractures were found.

As for specimens tested under both increasing temperature and moisture conditions, i.e., for hot/wet samples, both an increase in fiber/matrix debonding as well as an increase in matrix plasticity can be seen. The

mechanical properties in this instance are severely degraded. Figures 10a and 10b illustrate the differences in the room temperature dry versus the 260°F saturated interlaminar shear samples.

CONCLUSION

If river patterns can be found on the fracture surfaces, they may be helpful in locating the failure initiation site and determining the direction of crack propagation. Surface morphology does appear to be indicative of load and environmental conditions at the time of failure indicating that fractography will be a useful tool in the failure analysis of composite components.

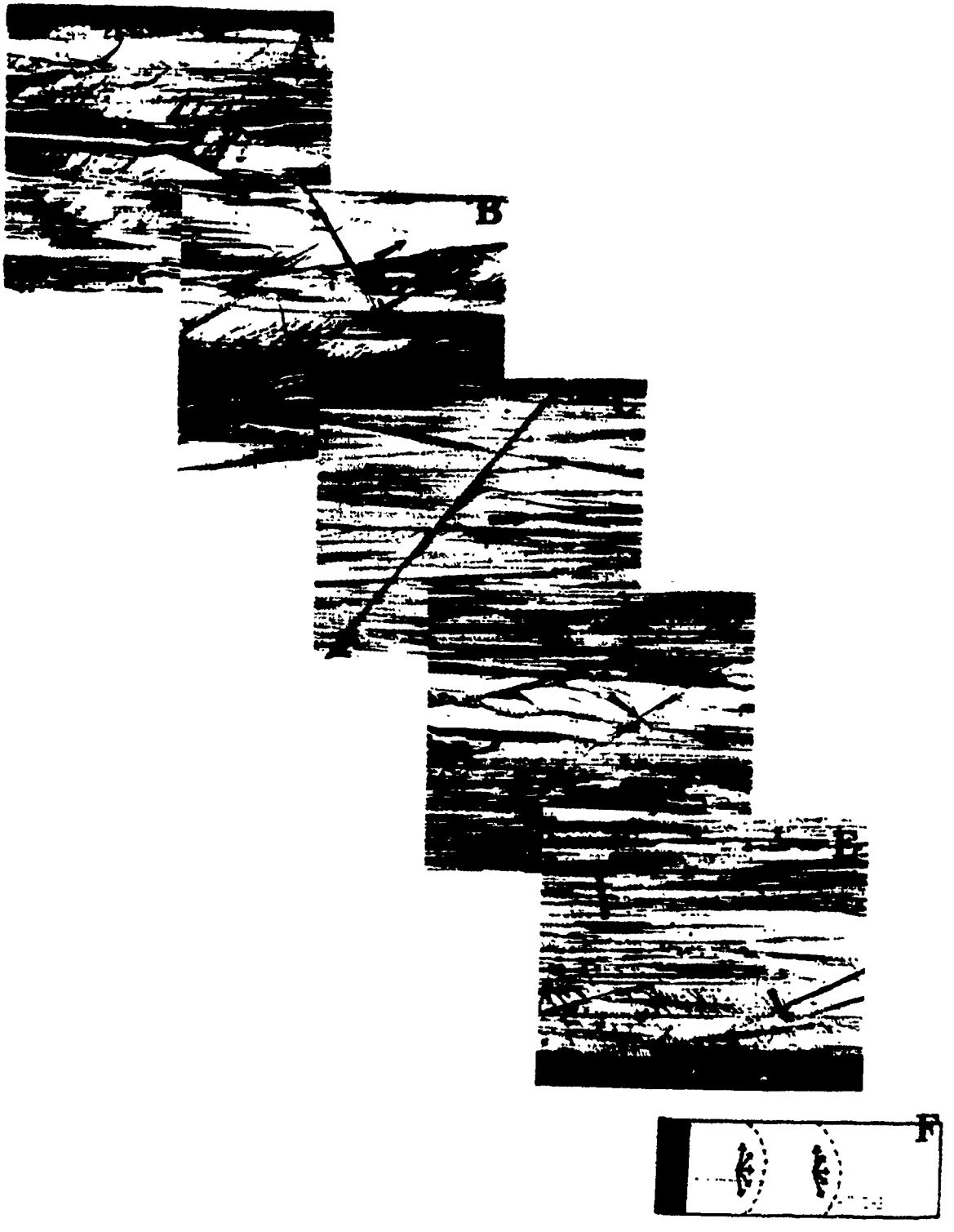

FIGURES 1A - 1F MACROSCOPIC CRACK GROWTH DIRECTION AS DETERMINED USING RIVER PATTERNS FROM A 0° UNIDIRECTIONAL DCB GRAPHITE/EPOXY SPECIMEN 200X

A

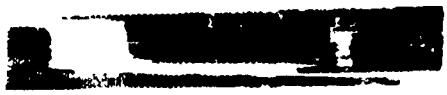

0·5X

200X

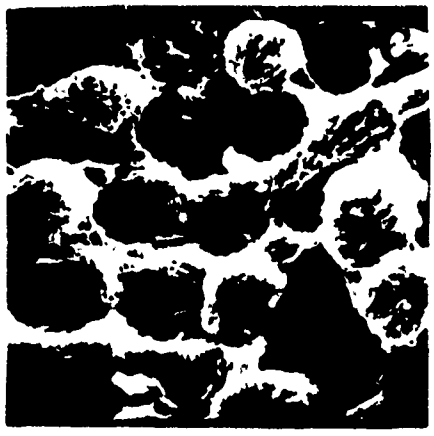

2500X

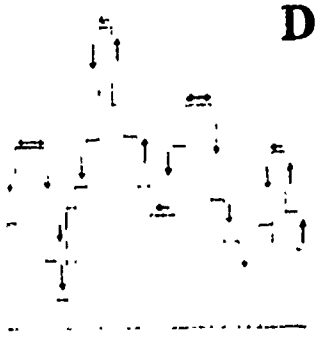

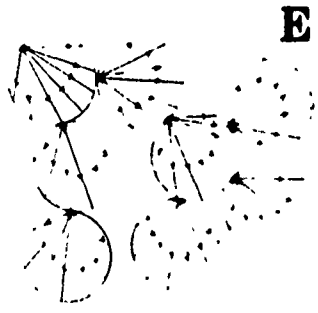

FIGURES 2A - 2E FRACTURE CHARACTERISTICS OF A 0° UNIDIRECTIONAL SPECIMEN FAILED IN TENSION

4X

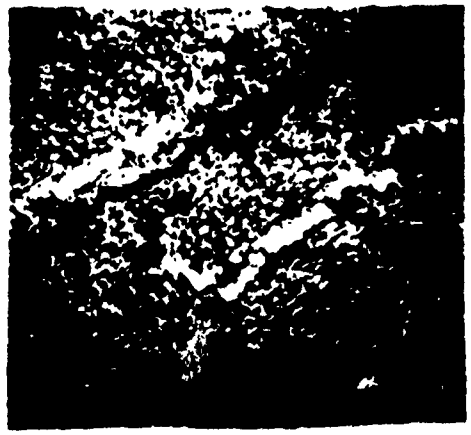

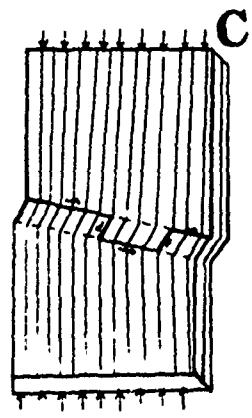

300X

3500X

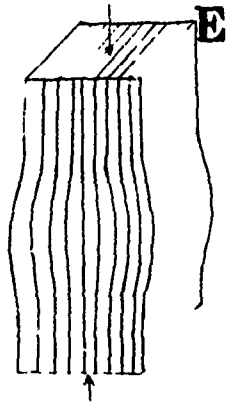

2000X

2000X

FIGURES 3A - 3G FRACTURE CHARACTERISTICS OF A 0° UNIDIRECTIONAL SPECIMEN FAILED IN COMPRESSION

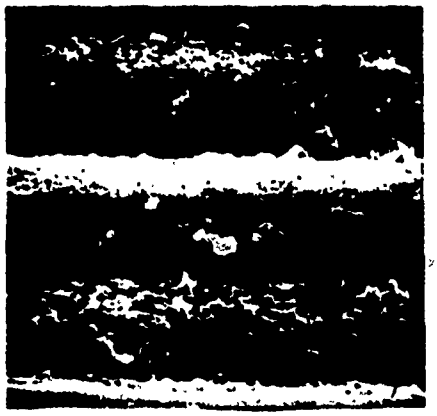

4000X

B

4X

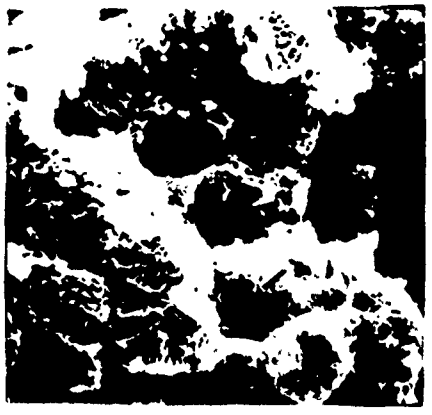

3000X

FIGURES 4A - 4C FRACTURE CHARACTERISTICS OF 0° UNIDIRECTIONAL SPECIMENS BROKEN IN SHEAR, FLEXURE AND FATIGUE

A

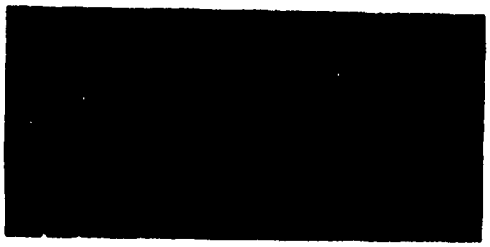

1X

500X

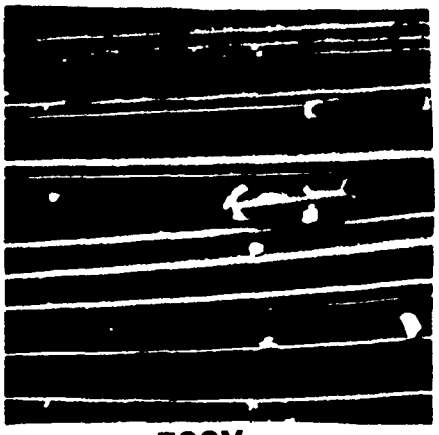

500X

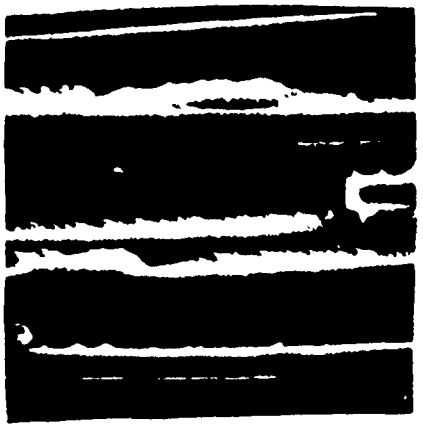

1000X

FIGURES 5A - 5D SURFACE CHARACTERISTICS OF A 0° UNIDIRECTIONAL DCB SPECIMEN

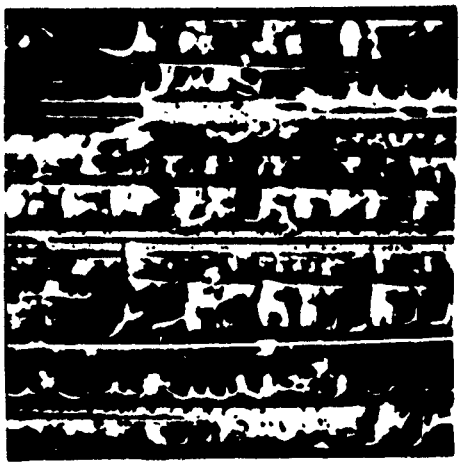

500X

2000X

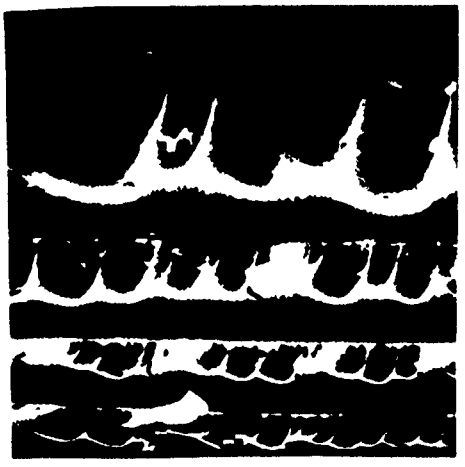

3000X

2500X

FIGURES 6A - 6D SURFACE CHARACTERISTICS OF A 0° UNIDIRECTIONAL MODE II ENF SPECIMEN

150X

150X

150X

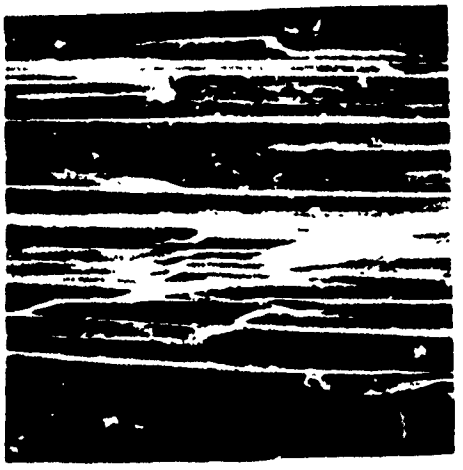

500X

FIGURES 7A - 7D SURFACE CHARACTERISTICS OF 90° UNIDIRECTIONAL SPECIMENS FAILED IN TENSION, COMPRESSION, FLEXURE AND FATIGUE

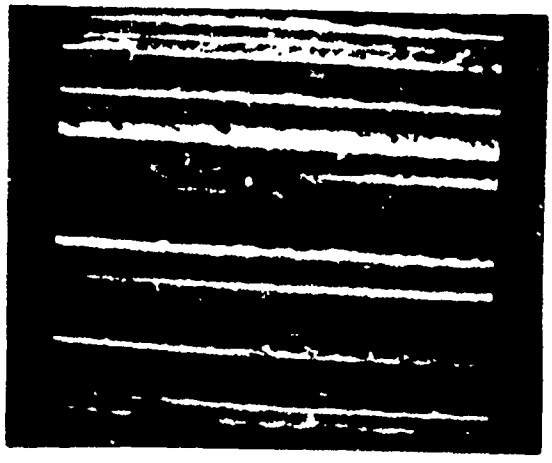

500X

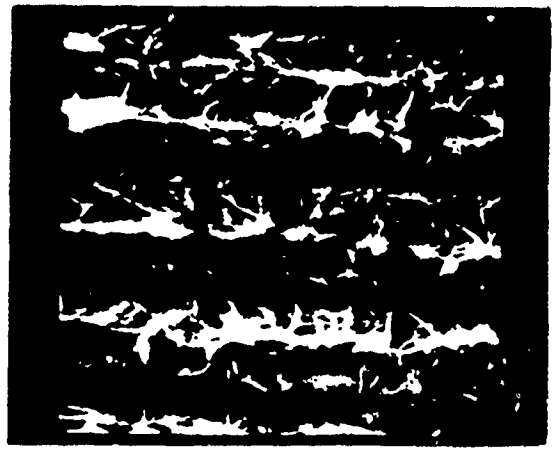

1500X

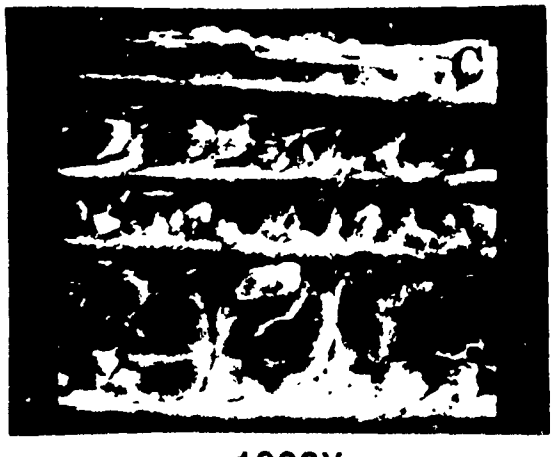

1000X

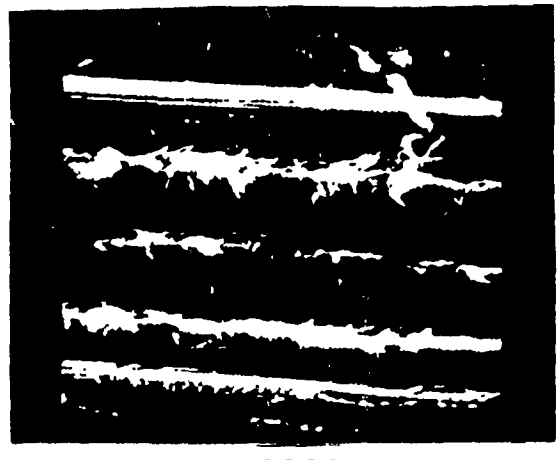

2000X

FIGURES 8A - 8D GRAPHITE/PEEK MODE I AND MODE II SURFACE CHARACTERISTICS

A

-67°F

B

70°F

C

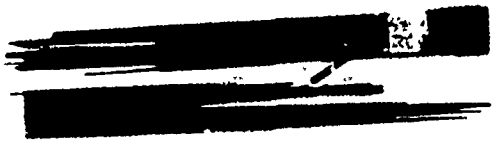

260°F

FIGURES 9A - 9B TEMPERATURE EFFECTS OF GRAPHITE/EPOXY 0° UNIDIRECTIONAL SPECIMENS

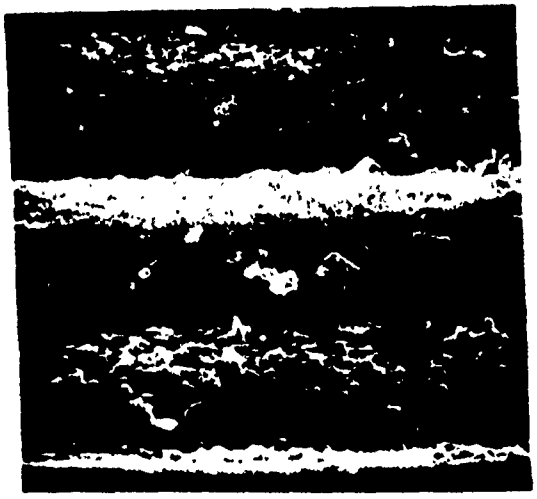

4000X

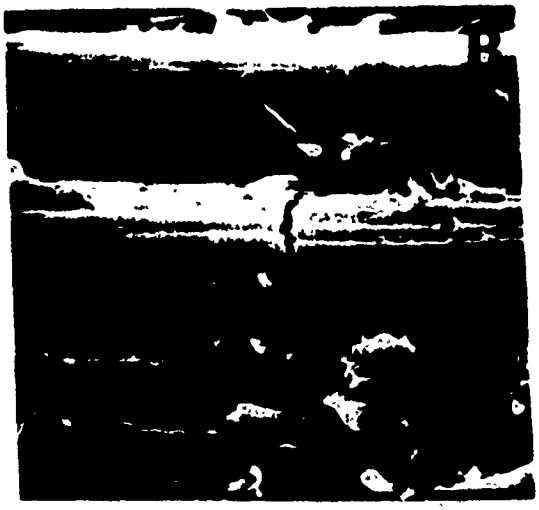

5000X

FIGURES 10A - 10B ROOM TEMPERATURE AND HOT/WET CHARACTERISTICS OF 0° UNIDIRECTIONAL INTERLAMINAR SHEAR SPECIMENS

CRYOGENIC FAILURE MECHANISMS OF FIBER-EPOXY COMPOSITES FOR ENERGY APPLICATIONS

B.Z. Jang, Y.K. Lieu and Y.S. Chang
Materials Engineering
Auburn University, Alabama

ABSTRACT

Fiber-reinforced composites used in the production, storage, and transport of energy are often exposed to extreme environments such as cryogenic temperatures and/or radiation. The fracture resistance of composites subjected to these conditions are also of fundamental interest. A study was therefore undertaken to examine the effects of γ-radiation on the structure and properties of fibers, matrix and their interfacial bonding in terms of their influence on composite failure mechnisms. Thermomechanical analysis was conducted to estimate the residual thermal stresses due to differential thermal expansion coefficients both between fiber and matrix and between two laminae. Results indicate that the impact energy of a composite laminate could be increased by 100% by immersing the specimen in liquid nitrogen for only five minutes. Samples impact-tested at cryogenic temperatures were found to possess a great degree of delamination and crack bifurcation. Thermomechanical analysis and SEM investigation both agree that microcrack and small-scale delamination are promoted because of differential thermal expansion coefficients. Such effects could be responsible for the observed crack branching and delamination phenomena during impact loading. Although under certain circumstance the γ-radiation may yield a small increase in fracture resistance it generally degrades the cohesive strength of the matrix as well as reduces the interfacial bonding between fiber and matrix. Detailed results of a mechanical and microscopic analysis are presented and discussed.

INTRODUCTION

Because of their low density, high specific strength, and high specific stiffness fiber reinforced composites have been widely used in many critical applications such as national defense and space technology. Polymer-composite materials have also been playing an important role in many phases of energy production, transport, use, and conservation. Composites are used as electrical and thermal insulator in fusion reactor power systems. Composites are also used in the construction of liquefied natural gas (LNG) tanks and pipelines [1,2].

Composites for energy applications have to satisfy three basic requirements: (a) They should be readily processable into large-dimensional load-bearing structures, (b) They should be of high strength and high toughness at both room and low temperatures, and (c) They have to be radiation-resistant if used in the radiation environment such as for insulation of the nuclear power superconducting magnets [1].

The materials currently in use as superconducting magnet insulation are polyester, epoxy, and polyimide reinforced with glass, graphite, boron, or aromatic fibers [1,2]. There are two serious problems with this group of insulation materials: a very limited data base [3-9], particularly on the machanical properties of composite laminates, and the lack of knowledge of their behavior under irradiation at low temperatures. Even without radiation, the cryogenic mechanical behavior of composites in relation to the material structure is largely unexplored. One important subject, which was often overlooked in the previous studies of cryogenic mechanical properties [3-9], is the effects of thermal stresses due to the difference in thermal expansion coefficients between the matrix and fiber and between two laminae. The differential thermal contraction may have a major effect on the residual stresses within a composite material that are additional to the stresses produced by external loads. The residual stresses may be sufficient to produce microcracking even in the absence of external loads [10, 12,44-47].

Both experimental and analytical methods [11-35] have been advanced to investigate the microresidual stresses in a multiphase system. Experimental methods usually involved the technique of photoelasticity [17-19,23]. Classical elasticity analytical methods [eq. 13] were usually based on the assumption that the fibers were arranged in a regular array (eg., hexagonal). The results of both experimental and theoretical investigations indicate that (1) The radial stress at the fiber-matrix interface can be either tensile or compressive; its value depends on the stiffness of the constituents as well as the fiber volume fraction, (2) Shear stress exists along the fiber circumference and may locally debond the fiber within the matrix, and (3) The hoop stress near the interface in the matrix or interfacial bond is generally tensile and of relatively high magnitude [10,22].

Earlier studies on the differential thermal stresses have been reviewed by Chamis [22] and by Hull [10]. Recent attempts to estimate the residual thermal stresses in high performance composites have also been reviewed [35]. As pointed out by Nairn [35], limited work has been done to characterize the effect of residual thermal stresses on properties of high performance composites. One exceptional case was the contribution of Bailey and coworkers [25-28] who suggested that the residual thermal strains affect microcracking and stress-corrosion in crossply laminates. In all the previous studies the

end-use temperature was taken to be the room temperature and therefore a temperature differential ΔT of @ 154°C was assumed in estimating the thermal stresses induced on cooling from a cure temperature T_c of 177°C. The thermal residual stresses are expected to be aggravated when considering the cryogenic mechanical behavior of composites. A cure temperature differential of approximately 373°C (with end use temperature T_2 =-196°C) could easily double the residual stresses previously calculated.

We have analyzed the thermal stresses in composites on the micromechanic level and estimated these stresses at both room temperature and liquid nitrogen temperature for epoxy composite systems consisting of glass-, graphite-, or organic fibers. The effects of such thermal stresses on the mechanical behavior of composites were assessed and discussed. Also presented in this paper are the failure mechanisms in these composites and the observed effects of moisture and radiation on the impact resistance of these materials.

ANALYSIS

The residual thermal stresses in a fibrous composite may be analyzed at different levels of complexity. First, the differential thermal stresses established between a single fiber and the matrix may be estimated either analytically or numerically. Second, the residual stress fields developed within a group of regularly arrayed fibers may also be determined either theoretically or experimentally. Third, the thermal stresses that occur between two laminae with different effective thermal expansion coefficients (eg. due to different fiber orientations) may also be calculated using, for example, the classical lamination theory. In each level of study certain assumptions have to be made to render the problem more tractable.

In the present report the results of a simple elasticity analysis of the residual stresses in a single fiber-polymer matrix system are first given. The analysis, which is detailed in the Appendix, is based on a thick cylinder model (TCM). The materials studied include single glass-, graphite-, and Kevlar-fiber embedded in an epoxy matrix. It is the objective of this analysis to obtain a first order approximation to the residual stresses and to determine if these stresses are sufficient to cause microcracking.

There are several possible sources to the development of residual stresses in a single fiber-matrix system. For a thermosetting resin, curing (or crosslinking) of the resin may cause the resin to shrink, leading to a compression exerted by the matrix on the fiber. If curing takes place at high temperatures the shrinkage stresses may be relieved or reduced (annealing effect). Curing shrinkage stresses that occur at low temperature will unlikely be totally relieved. For a crystalline thermoplastic matrix, solidification stresses will develop due to polymer crystallization; the magnitudes of these stresses being dependent upon the degree of crystallinity (d_c) which is in turn dictated by the crystallization temperature (T_c). The higher the T_c, the higher the value of d_c, implying a greater extent of volume shrinkage. However, crystallization/annealing at a higher T may relieve or reduce the solidification stresses. The solidification stresses induced on cooling through the glass transition temperature (T_g) of an amorphous thermoplastic matrix are expected to be relatively small and negligible. Two competing factors therefore exist: the solidification/curing shrinkage and the annealing effect.

A second source of residual stresses is the compression or tension exerted by the matrix on the fiber as a result of thermal mismatch during cool-down from the high curing solidification temperature. For instance, when a graphite fiber (α_f=18 x 10^{-6} /°C) embedded in an annulus of cured resin (α= 40 x 10^{-6} /°C) cools down, the fiber diameter will reduce to a lesser extent than the epoxy shrinkage. Thus, the resin would exert a radial compression on the fiber at room temperature. This compression would produce better contact at the interface and would also hold the fiber tighter during a fiber pull-out test. Based on the thick cylinder model (TCM) the equation for pressure at the interface of a cylindrical fiber in an infinite medium is given by modifying Eq. (20) in the Appendix to include the effects of curing or solidification shrinkage:

$$P = \frac{(\alpha_m - \alpha_f)\Delta T + \varepsilon_c}{\frac{(1+\nu_m)}{E_m} + \frac{(1-\nu_f)}{E_f}} \qquad (20B)$$

where α, ν, and E are thermal expansion coefficient, Poisson's ratio, and Young's modulus, respectively, m and f are the subscripts denoting matrix and fiber, and ε_c is the linear shrinkage in matrix due to curing or crystallization.

Both the first and the second term in the numerator of Eq. (20B) depend on the temperature T_c where cure or crystallization is effected. If the interface pressure P is obtained as a function of T_c the results may be used to verify whether the previous arguments are valid or not. Several model material systems each containing single monofilament were examined. Specimens were prepared so that a single filament passed perpendicularly through a film of resin. The materials used were carefully chosen so that little or no chemical bonding will occur between fiber and matrix. To further assure minimal chemical bonding the fiber surface was coated with a thin layer of silicone oil before resin impregnation. The interfacial adhesion would therefore come solely from the mechanical interaction between fiber and matrix. A significant lock and key configuration does not seem to exist since the fibers involved appear relatively smooth under SEM. Therefore, the bond strength at the interface as evaluated by the fiber pull-out test should reflect indirectly the magnitude of the residual thermal stress.

The stresses within a group of fibers should be different than those near a single fiber. Marloff and Daniel [17] indicated that the maximum hoop stress in a model multifiber inclusion system could be two times greater than that near a single fiber. The hoop stress is tensile and is maximum at the point midway between the fibers. The longitudinal stress is also tensile and remains almost constant between fibers [17]. The tensile hoop stress should have the tendency to crack the matrix. The actual fiber distribution in a typical advanced composite should have some fibers more or less isolated from the others as well as fibers regularly arrayed. Both can be considered as the extreme cases and the actual stress fields should be more complex. Fortunately, only the maximum tensile stresses and the interfacial shear stresses that will promote microcracking and therefore affect the composite failure mechanisms need be considered here.

EXPERIMENTAL

Fiber Pull-out Test

In order to assess the mechanical interaction between a fiber and matrix resin due to differential thermal contraction a monofilament pull-out test, as described elsewhere [48,49], was conducted on several model material systems: nylon monofilament, and polypropylene (PP) monofilament embedded in either epoxy or polyethylene (PE) matrix. In this experiment graphite, Kevlar, and glass fibers were not used due to the difficulty in handling such fine fibers. Our experience of working with these fibers indicates that extreme thin discs are required to facilitate pull-out test.

The composite systems each consisting of a single fiber embedded in a resin disc were cured (for epoxy) or crystallized (for crystalline PE) at several different temperatures to permit the formation of different residual stresses. All specimens after cure or crystallization were ground to a desired dimension for testing. Tensile loading was performed using an Instron universal testing machine (Model 1122) with the crosshead speed set at 0.1 in./min. The "debonding" load was assigned to be the maximum load in the force-displacement curve which is a measurement of the pressure exerted on the fiber by the matrix.

The Irradiation of Composites with Gamma-ray

Composite laminates prepared from E-glass fiber/epoxy prepreg tapes (3M Scotchply 1003) were exposed to γ-radiation in the Nuclear Science Center of Auburn University for various priods of time. Unidirectional, crossply, and isotropic laminates, all symmetrical with respect to the midplane of a laminate, were each subjected to varying level of dosage up to 150 Megarad. One group of samples (Group A) were stored in the laboratory for one year after γ-radiation exposure. A corresponding second group (Group B) of samples were tested immediately after radiation exposure. Both groups were impact loaded at room temperature (23°C) and the liquid nitrogen temperature (-196° C).

The Effects of Temperature and Nitrogen Environment

The last phase study of the γ-irradiated materials indicated that, regardless of the dosage, a composite loaded at -196 C consistently exhibit a higher impact energy than if tested at 23°C. Fracture surface examination indicates a pronounced what appears to be a microcracking phenomenon in samples tested at low T. The same samples also show a great deal of delamination or splitting. We suspected that this difference in impact response was possibly due to the thermal residual stresses. To verify this possibility an extensive study was carried out to understand the low temperature behavior of several types of composites including glass fiber-epoxy, graphite fiber-epoxy, and Kevlar fiber-epoxy. In the case of glass fiber composites unidirectional, crossply, and isotropic laminates were moulded from Scotchply 1003 prepreg tapes. The graphite- and Kevlar-composites were prepared by impreganating the biaxial Cofab fabrics with epoxy resin and curing the system in a specially prepared compression mould. The Cofab biaxials are bidirectional reinforcement fabrics constructed by a precision knitting process by the Composite Reinforcements Business (Tuscaloosa, AL). The warp and weft reinforcements are locked by a knit stitch untwisted and uncrimped into a stable form. The Cofab biaxials may be considered to be similar to the crossply configuration in a conventional prepreg tape.

To facilitate low temperature impact testing the samples were immersed in the liquid nitrogen contained in a dewar. To check if the liquid nitrogen gas is an effective environmental stress cracking agent two groups of specimens were prepared: one with specimen wrapped and sealed by a thin layer of Scotch tape to prevent direct nitrogen (N_2) contact while the other open to N_2 attack. Most specimens were given 10 minutes to reach thermal equilibrium before they were removed from the dewar and quickly impact loaded. A few specimens were allowed to stay in the dewar for as long as one hour to ensure a reasonable amount of N_2 absorption. We were also interested in learning if the rapid cooling process induced any structural change.

The Effects of Moisture and Temperature

The charpy impact bars were moulded from unidirectional, crossply, and isotropic prepreg tapes (Scotchply 1003). Each of these three types are separated into two groups: those to be examined by the light microscope and those to be impact tested. Each group is further separated into three subgroups according to moisture level: the control samples (exposed to the lab air), the dry samples (placed in a dessicator containing cupric sulfate as a water absorbant; a state of low vacuum was maintained), and the wet samples (immersed in a water bath for two weeks). After each sample has been metallographically polished and subjected to its appropriate environment the cross sections are viewed under the optical microscope. Samples which have not been altered by environmental conditions are compared to those samples in which moisture attack and thermal stressing (cooled to -196°C and warmed up to 23°C) has occurred. In each case the samples are visually scanned for possible defects and microcracks. A Tinius-Olsen impact testing machine was used to determine the toughness of the composite samples. The samples to be tested at 100°C are placed in an oven and allowed 20 minutes to reach thermal equilibrium. Both room and liquid nitrogen temperature testing were performed following a similar procedure described above. It is expected that the lower the test temperature the higher the residual thermal stresses.

Fracture Behavior of Continuous Fiber Reinforced Polypropylene

The impact test bars were compression-molded from glass-fiber-PP prepreg tapes (Fiberod; Polymer Composites Inc.). Since thermoplastic matrix alone (PP) usually exhibits an increase in impact energy with an increase in temperature, this trend is opposite to the expected effects of thermal residual stresses that would dcrease with increasing temperature. A study of fracture energy in relation to temperature should provide additional information on the effects of thermal stresses.

Scanning Electron Microscopy (SEM)

Selected samples from the light microscope examination group and those from the impact test are further examined using SEM (Model ARM-1000 and ISI-40). The samples were cut into small sections, mounted on specimen holders, and coated with a thin layer of Au:Pd (60/40 ratio) to avoid charging problem. Fractured surfaces from the impact test were examined in order to provide information about the failure mechanisms.

RESULTS AND DISCUSSION

Fiber Pull-out

Data obtained for the PP fiber-epoxy matrix systems are shown in Figure 1, both indicating that the strength of the fiber-matrix bond increases with increasing cure temperature. Since the propylene molecules are relatively nonpolar they are not expected to form strong chemical bonding with epoxy resin. The mechanical bond due to residual thermal stress may therefore play a significant role in contributing to the interfacial adhesion. The possibility of chemical bonding was further reduced by coating the fiber surface with a layer of silicone oil which did somewhat decrease the bond strength. However, the bond strength still increased with increasing cure temperature (higher $\Delta T = T_c - T_g$). These results appear to be at least qualitatively consistent with Eq. 25 which suggests that the pressure exerted by the matrix on the fiber is proportional to ΔT.

For the experiments where the samples were cured at different temperatures, it was necessary to make sure that the only variable was thermal mismatch and to eliminate extraneous variables. It was required that the degree of cure in the resin be a constant, no matter what the cure temperature is, so that the resin's viscoelastic properties would be constant. A dynamic mechanical thermal analyzer (Polymer Lab, Inc.-DMTA) was used to check the viscoelastic properties of the epoxy resin after various cure times at selected temperatures. When the relative rigidity and damping characteristics of the test resins were similar, the degrees of cure were considered to be equivalent.

The monofilament pull-out results of fiber-thermoplastic matrix, as depicted in Figure 2, are more difficult to interpret. These specimens were prepared by embedding the Nylon-6 single fiber in a high density polyethylene (HDPE) matrix which was allowed to crystallize at different temperatures. It was revealed that the debonding load decreased with increasing temperature. Since very little chemical bond exists between Nylon fiber and PE matrix the debonding load and hence the transverse pressure are dependent on three variables: (1) The differential thermal contraction, (2) Different crystallization temperatures resulting in various degrees of crystallinity and hence different levels of volume shrinkage, (3) High crystallization temperatures act as an annealing process to relieve residual thermal stresses and pressure.

The Nylon-6 fiber was found to have a greater thermal expansion coefficient than that of PE. This should result in less adhesion at the interface with a higher crystallization temperature. Therefore, differential thermal contraction played a decreasing role with increasing temperature (the first term in the numerator of Eq. 20B being negative). The mechanical interaction between Nylon fiber and PE matrix is induced solely by volume shrinkage during crystallization of PE. The degrees of crystallinity for PE solidified at 125, 100, 80, and 50°C may not be much different. Further, the thermal stresses at higher solidification temperatures may be reduced due to the annealing effect. The observation that the bond strength was lower at a higher T_c may well reflect the possibility that the effects of d_c are overshadowed by the annealing effect and the differential thermal contraction effect.

The results of the fiber pull-out tests appear to be in support of our analysis of thermal stresses. This elasticity approach of stress analysis will then be used later to estimate the residual thermal stresses in the composite laminates composed of advanced fibers.

Impact Energy of Irradiated E-glass Fiber-Epoxy

The impact energies of Group A composite laminates at both room and liquid N_2 temperature as a function of radiation dosage are presented in Figure 3. The impact load was applied in a direction parallel to the laminae of a laminate (hereafter referred to as "z-direction") and the lamination planes are therefore vertical. When unidirectional glass fiber/epoxy specimens were loaded the specimen often delaminated laterally and high energy aborption resulted. The failure mechanism in this case is transverse buckling and delamination [50] as shown in Figure 4a. This failure initiates on the compression side of the beam and results from the fact that weak planes are created in the vertical direction and there is no restraint preventing these planes from delaminating. In other words, there is no compressive stress normal to the planes as there would be if the planes were horizontal or normal to the load (referred to as "y-direction" loading). The results of impact tests following different loading directions may be compared in Figure 5 where group B of irradiated samples were involved. The "z-direction" loaded samples again showed the transverse buckling and delamination mode while the "y-direction" loaded samples showed a combination of main crack propagation and interfacial delamination or delamination alone (Fig. 4b).

When a crossply or isotropic laminate is loaded along the z-direction the main crack propagation ("cut" type) is always a dominant mode of failure. The energy needed to propagate a crack through the cross section is much lower than the energy need to form a great deal of delaminations between the layers as the crack advances or pushes through the cross section [50]. In the case of crossply laminate, the crack front is not straight as there are weak layers in the thickness where it can propagate easily. These weak layers let the crack surround the other layers and fracture the fibers without arresting the crack propagation. This explains why crossply and isotropic laminates, when loaded in z-direction, did not show a high level of energy absorption. All samples loaded in y-direction do show varying degree of delamination. Sometimes delamination does take place at the compression side but it is restricted to a few layers while in the case of z-direction loading of unidirectional laminates it starts with many layers and propagate downward, thus absorbing a large amount of energy.

Of uttermost interest to us is the observation that all samples impact loaded at -196 C always have impact energy greater than identical samples tested at 23°C. This higher impact energy seems to come hand-in-hand with a greater degree of macroscopic delamination and a larger amount of microdelamination or microcracking. They seem to be closely related to the residual thermal stresses that existed before external loading. Those residual stresses tend to promote microcracking and they should be of higher magnitudes at lower temperatures.

The Effects of Temperature and Nitrogen Environment

The data listed in Table 1 show that the liquid nitrogen did not seem to be an effective environmental stress cracking agent for the glass-epoxy composite. In fact, the impact energy of each composite system studied

appears to decrease a bit after one hour exposure to the liquid nitrogen (as compared to the sealed materials) with an concomitant slight reduction in the degree of delamination. The reason for this reduction is unclear. Also revealed in Table 1 is the fact that all glass fiber-epoxy composites show a higher impact energy at lower temperature than at room temperature. This again can be explained in terms of thermal residual stresses. For the biaxial laminates of graphite fiber system studied no appreciable effect of thermal stresses could be found. The reduction of impact energy for Kevlar fiber-epoxy biaxial systems loaded at liquid nitrogen temperature may be attributed to Kevlar fibers having a higher transverse thermal expansion coefficient than epoxy resin.

The Effects of Moisture and Temperature

A careful optical microscopic examination reveals that very few apparent microcracks could be found in all samples exposed or unexposed to moisture attack (before impact loading). This implies that the thermal stresses and/or the moisture-induced stress (if any) are not sufficient to cause microcracking at room temperature. A microscope cold stage is being designed and will be used to observe if microcracking will occur at -196°C.

The impact strength in this phase of study is measured at three different temperatures: -196°C, 23°C, and 100°C, and with or without the presence of moisture. As shown in Table 2, most composites studied, impact energy recorded is higher at -196°C than 23°C. In general, the impact strength at 100°C is still smaller. However, a few specimens loaded in z-direction at 100°C did possess a higher impact strength than at 23°C. The reason is not clear at the present time.

The impact strength of a continuous fiber reinforced polypropylene was also measured over a wide spectrum of temperatures ranging from -196°C to +100°C. The data obtained, as summarized in Figure 6, show a slow but definite increase in impact strength with decreased test temperature. This is also consistent with the post-failure observation that the degree of delamination appears to be greater at lower test temperature.

Estimation of Thermal Stresses

The differential thermal stresses for single fiber-epoxy systems are shown in Figure 7-9 where both hoop and radial stresses are plotted against the normalized radial distance (R/R_f) for ΔT=154°C (cooling from 177°C to 23 C) and ΔT=373°C (cooling from 177°C to -196°C). The maximum stresses, both hoop and radial, are found to exist near the fiber-matrix interface. The maximum values of residual stresses in each case are listed in Table 4. It is clear from this table that (1) the thermal residual stresses are much greater at -196°C than in 23 C in any system, (2) the magnitudes of these stresses are largest in the glass fiber-epoxy system followed in order by graphite- and Kevlar fiber systems, and (3) the maximum hoop stresses are compressive in nature due to the transverse thermal expansion coefficient of Kevlar fiber being greater than that of epoxy. These observations appear to support our hypothesis that the high fracture energy at low test temperature may be attributed to the greater prestresses that have to be added to the stresses caused by the external load when considering microcracking or microdelamination phenomena. The results of stress calculation are also in agreement with our experimental observation that the Kevlar-epoxy composites appear to show a positive trend in impact strength with increasing test temperature.

It may be noted that within a group of fibers the stress fields may show even higher maximum magnitudes although the peak values may exist at locations other than fiber-matrix interface. The residual thermal stresses can therefore promote microfailure processes near fiber-matrix interface (interfacial debonding) or in the matrix (matrix cracking). Both microfailure mechanisms should lead to a greater degree of delamination and thereby dissipating a greater amount of strain energy.

It may be noted that the previous treatment considered the fiber ends to be free to move. This is not quite true in real composite materials. Most advanced reinforcing fibers have longitudinal thermal coefficient of expansions which differ from that of the epoxy with the magnitude of difference varying with the type of fibers. Graphite fiber with zero to slightly negative thermal expansion along the fiber axis represent the most extreme case. Cooling from 177°C to -196°C represents an extreme thermal excursion in which the matrix tends to compress the fibers along their axes, and the fibers in turn tend to stretch the resin matrix causing shear stresses to develop at the interface longitudinally. These should add to the possibility of microcracking.

The fabrication curing stresses due to thermal expansion coefficient difference between two laminae with different fiber orientations may also have important influence on the response of composite laminates. Of particular significance is the effect of these stresses on the failure of composite laminates under subsequent applied stresses or environmental conditions or both, such as moisture and low- or high-imposed temperatures [52]. In some cases, the curing stresses were shown to be sufficiently large to cause fracture of layers within a laminate, even at room temperature [12]. This effect should be aggravated at -196 C. Hahn and Pagano [51] have proposed an analytical formulation to predict thermal stresses in which the material response is assumed to be elastic with temperature dependent moduli. By following this approach and assuming the maximum stress criterion the same workers went on the calculate the predicted applied stress at first ply failure [52]. According to these calculations, the effect of curing stresses in say graphite fiber-epoxy composites at room temperature is to reduce the laminate initial failure stress by a factor of approximately two. Such a marked reduction, if further aggravated at -196 C, should readily lead to a great degree of microcracking and delamination. Although the impact loading in the present case is expected to yield a much complex stress field the above arguments should remain qualitatively true. In other words, a lower test temperature should promote the occurrence of a more extensive microfailure process, leading to a large damage size but dissipateing a greater amount of fracture energy.

CONCLUSION

A simple thermomechanical analysis was presented to estimate the residual thermal stresses on cooling from cure/crystallization temperature to an end-use temperature (23°C and -196°C). The fiber pull-out tests used to estimate the mechanical bond between a fiber and matrix seems to yield results

consistent with the prediction that the fabrication stress be high with a larger temperature differential. An extensive impact loading program was carried out to study the fracture resistance as a function of temperature and environment. In general, the lower the test temperature the higher the impact energy, characterized by a greater level of microcracking and delamination which are believed to be promoted by the higher residual stresses. Slight exposure to moisture or liquid nitrogen environment did not affect the composite impact response. However, exposure to Gamma radiation tends to degrade the composite integrity by weakening the fiber-matrix interfacial bond as well as the cohesive strength of epoxy matrix.

ACKNOWLEDGEMENT

Financial support for this project was provided by Auburn University EES and Grant-in-Aid (Energy Research) Programs. This support is gratefully acknowledged.

References

1. A. F. Clark, R. P. Reed, and G. Hartwig, eds. "Nonmetallic Materials and Composites at Low Temperatures", Plenum Press, New York, 1979.
2. G. Hartwig and D. Evans, eds. "Nonmetallic Materials and Composites at Low Temperatures, II", Plenum Press, New York, 1982.
3. F. W. Clinard and G. F. Hurley, J. Nuclear Mater. 103/104 (1981) 705.
4. E. L. Stone, L. O. Elmarazki, and W. C. Young, in Ref. 1. p 283.
5. R. L. Tobler and D. T. Read, J. Composite Material 10 (1976) 32.
6. D. W. Chamberlain, B. R. Lloyd, and R. L. Tennant, "Determination of the Performance of Plastics Laminates at Cryogenic Temp." Report No. ASD-TDR-62-794, Part 2 or N64-24212 (1964).
7. M. B. Kasen, R. E.Schramm, and D. T. Read, ASTM STP 636 (1977) 141.
8. B. Kneifel, in Ref. 2, P. 125.
9. C. J. Long, R. H. Kernoban, and R. R. Coltman, Jr., in Ref. 1 p. 141.
10. D. Hull, An Introduction to Composite Materials, Cambridge University Press, 1981.
11. C. C. Chamis, Mechanics of Load Transfer at the Fiber Matrix Interface, NASA TN D-6588 (1972) Nat. Aeronaut. and Space Administration.
12. D. R. Doner and R. C. Novak, Ann. SPI Conf. 24th, Sec. 2-D, 1969.
13. J. Haener, N. Ashbaugh, C. Y. Chia, and M. Y. Feng, Investigation of Micromechanical Behavior of Fiber Reinforced Plastics, USAAVLABS-TR-67-66, AD-667901, 1968.
14. T. Koufopoulos and P. S. Theocaris, J. Compos. Mater. 3 (1969) 308.
15. A. W. Leissa, W. E. Clausen, and G. K. Agrawal, Int. J. Numer. Methods Eng., 3 (1971) 89.
16. T. F. MacLaughlin, J./ Compos. Mater. 2 (1968) 44.
17. R. H. Marloff and I. M. Daniel, Three Dimensional Photoelastic Analysis of A Fiber Reinforced Composite Model, 1968 SESA Fall Meeting, Paper 1435. San Francisco, CA.
18. R. H. Marloff and I. M. Daniel, Exp. Mech. 9 (1969) 156.
19. P. S. Theocaris and E. Marketos, Fibre Sci. and Technol. 3 (1970) 21.
20. J. O. Outwater, Jr. Modern Plast., 33 (1956) 156.
21. H. T. Corten, Ch. 2 in Modern Composite Materials, J. L. Broutman, H. R. Krock, Eds. Addison-Wesley, Inc. Mass. (1967).
22. C. C. Chamis, Mechanics of Load Transfer at the Interface, Composite Materials, Vol. 6, ed. E. P. Plueddemann, Academic Press, New York (1974) pp. 31-77.
23. J. A. Nairn and P. Zoller, J. Mater. Sci. 20, (1985), 355.
24. F. R. Jones, M. Mulheron, and J. E. Bailey, J. Mater. Sci., 18, (1983), 1533.
25. J. E. Bailey, P. T. Curtis, and A. Parvizi, Proc. R. Soc. Lond. A., 366, (1979) 599.
26. F. R. Jones, A. R. Wheatley, and J. E. Bailey, in "Composite Structures," p. 415, ed. by I. H. Marshall, Applied Science Publishers, Barking (1981).
27. J. E. Bailey and A. Parvizi, J. Mater. Sci., 16, (1981) 649.
28. J. E. Bailey, T. M. W. Fryer, and F. R. Jones, "Advances in Composite Materials," Vol. 1, pg. 514, edited by A. R. Bunsell, C. Bathias, A. Martenchar, D. Menkes, and G. Verchery, Pergamon, Paris, (1980).
29. H. Poritsky, Physics, 5, (1934) 406.
30. H. Poritsky, Phil. Mag. 24, (1937) 209.
31. B. E. Gatewood, Phil. Mag., 32, (1941) 282.
32. B. E. Gatewood, Quart. Appl. Math., 6, (1984) 84.

Table 1: The effects of temperature and liquid nitrogen environment on the impact energy of composite.

Impact Temperature and Environment	Glass fiber-Epoxy unidirectional		crossply	isotropic	Graphite-Epoxy biaxial	Kevlar-Epoxy biaxial
23°C	34.7	41.4*	24.5	23.7	12.8	23.3
-196°C; sealed	49.7	70.0*	34.0	24.5	12.9	18.7
-196°C; N_2 contact for 5 mins.	48.2	67.3*	30.9	29.8	12.2	15.9
-196°C; N_2 contact for 1 hr.	47.0	55.5*	29.2	20.9	10.1	16.6
23°C -196°C 23°C	36.2	53.0*	27.5	24.8	11.7	12.7

* : loaded in y-direction; otherwise: loaded in z-direction

Table 2: The impact strength of composites at various temperature and moisture conditions

Fiber Orientation	Impact direction	Moisture condition	Testing temperature 100°C	23°C	-196°C
Unidirectional	Z	dry	65.8	57	72
		wet	59.5	60.2	59.1
		control	64.5	61.2	70.4
	Y	dry	32.1	33.3	58.7
		wet	31.9	33.3	45.6
		control	33.0	36.0	53.5
Crossply	Z	dry	29.6	27.8	38.7
		wet	27.2	26.0	
		control		20.8	39.6
	Y	dry	29.4	30.7	35.5
		wet	25.1	29.5	33
		control		33.3	38.4

Table 3: Engineering constants used in the calculation of thermal stresses

Materials	Young's modulus (GPA)	Poisson Ratio	Thermal Expansion Coefficient (10^{-6}/°C)	Comments
Graphite Fiber	14	0.25	18	Transverse Properties
Kevlar 49 Fiber	20*	0.27*	59	Transverse Properties
Glass Fiber	76*	0.25*	4.9	Transverse Properties
Epoxy Resin	4.3	0.34	40	*=Estimated

Table 4: Maximum hoop/radial stresses near an isolated fiber embedded in an epoxy resin.

Type of Fiber	Temperature Differencial T= 154°C	T=373°C
	Hoop/Radial (PSI)	Hoop/Radial (PSI)
Glass	+2430/-2430	+5950/-5950
Graphite	+1350/-1350	+3250/-3250
Kevlar-49	-1200/+1200	-3000/+3000

33. R. A. Strub, Tans ASME, 75, (1953) 73.
34. W. Schneider, Kunststoffe, 61, (1971) 273.
35. J. A. Nairn, Polymer Composites, 6 (1985) 123.
36. C. T. Wang, Applied Elasticity, Wiley, New York, 1969, p. 54.
37. L. J. Broutman and B. D. Agarwal, Polym. Eng. and Sci., 14, (1974) 581.
38. J. G. Morley and R. S. Millman, J. Mater. Sci. 9, (1974) 1171.
39. J. H. William, Jr. and P. N. Kousiounelos, Fibre Sci. and Technol. 11, (1978) 83.
40. D. G. Peiffer, J. Appl. Polym. Sci., 24, (1979) 1451.
41. G. Marom and R. G. C. Arridge, Mater. Sci. and Eng. 23, (1976) 23.
42. R. G. C. Arridge, Polym. Eng. Sci., 15, (1975) 757.
43. D. G. Peiffer and L. E. Nielsen, J. Appl. Polym. Sci., 23, (1979) 2253.
44. C. C. Chamis, "Residual Stresses in Angle-plied Laminates and their Effects on Laminate Behavior," NASA TM-78835 (1978).
45. A. A. Fahmy and T. G. Cunningham, "Investigation of Thermal Fatigue in Fiber Composite Materials," NASA CR-2641 (1976).
46. A. Molcho and O. Ishai, "Thermal Cracking of C.F.R.P. Laminates," National SAMPE Tech. Conf. (1978) 255.
47. J. L. Camahort, E. H. Rennhack, and W. C. Coons, "Effects of Thermal Cycling Environment of Graphite/Epoxy Composites," ASTM STP 602 (1976) 37.
48. L. J. Broutman, Proc. of the 25th SPI/RP Anu. Tech. Conf. Paper 13 D, Soc. of Plastics Ind. New York, 1970.
49. L. Penn, F. Bystry, W. Karp, and S. Lee, in"Molecular Characterization of Composite Interfaces", H. Ishida and G. Kumar, eds, Plenum Press, 1985. P.93.
50. L.J. Broutman and A. Rotem, in "Foreign Object Damage to Composites", ASTM 1975, PP.114-133.
51. H.T. Hahn and N.J. Pagano, J. Comp. Material, 9 (1975) 91.
52. N.J. Pagano and H.T. Hahn, in "Comp. Mater. :Testing and Design (Fourth Conf.)", ASTM STP 617, ASTM, 1977, PP.317-329.

FIGURE CAPTIONS

Fig. 1. Average debonding load vs. cure temperature for (Epoxy/PP) specimens with no lubricant.
Fig. 2. Average debonding load vs. crystallization temperature for (PE/Nylon 6) specimens.
Fig. 3. The impact energy of E-Glass fiber/Epoxy composite laminate (Scothply 1003) irradiated at various dose.
Fig. 4. The fracture photographs of unidirectional E-Glass fiber/Epoxy laminate impacted along (A) z-direction, (B) y-direction.
Fig. 5A. The Impact energy of unidirectional E-Glass/Epoxy laminate measureed at different loading direction and temperature.
Fig. 5B. The impact energy of crossply E-Glass /Epoxy laminate measured at different loading direction and temperature.
Fig. 5C. The impact energy of isotropic E-Glass/Epoxy laminate measured at different loading direction and temperature.
Fig. 6. The impact strength of continuous fiber reinforced PP measured from -196°C to 100° C.
Fig. 7A. The calculated hoop stress and radial stress as a function of R/R_f for Glass fiber/Epoxy system, T=154°C.
Fig. 7B. The calculated hoop stress and radial stress as a function of R/R_f for Glass fiber/Epoxy system, T=373°C.
Fig. 8A. The calculated hoop stress and radial stress as a function of R/R_f for Graphite fiber/Epoxy system, T= 154 C.
Fig. 8B. The calculated hoop stress and radial stress as a function of R/R_f for Graphite fiber/Epoxy system, T= 373°C.
Fig. 9A. The calculated hoop stress and radial stress as a function of R/R_f for Kevlar fiber/Epoxy system, T=154° C
Fig. 9B. The calculated hoop stress and radial stress as a function of R/R_f for Kevlar fiber/Epoxy system, T=373°C

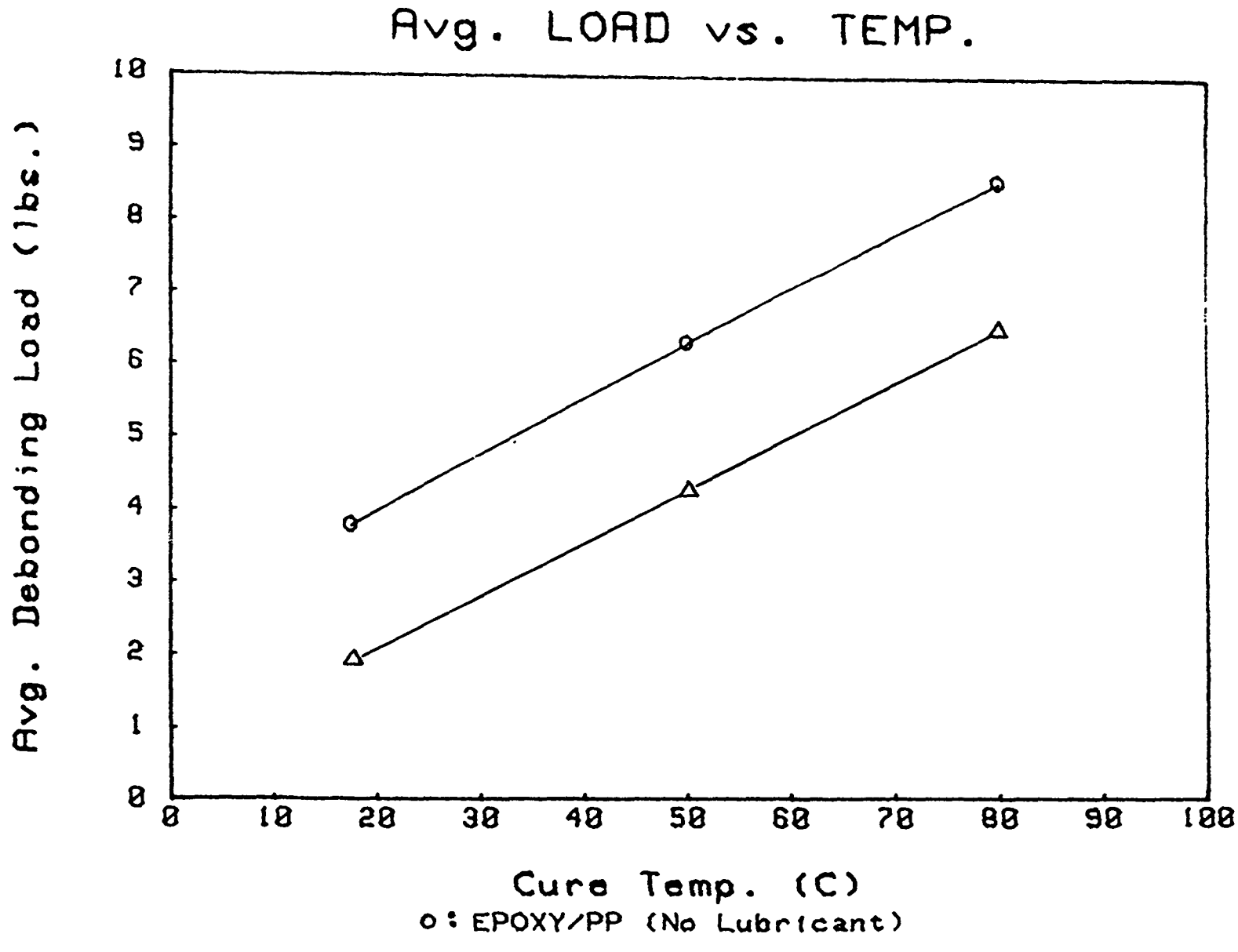

Fig. 1. Average debonding load vs. cure temp. for (epoxy/PP) specimens with no lubricant.

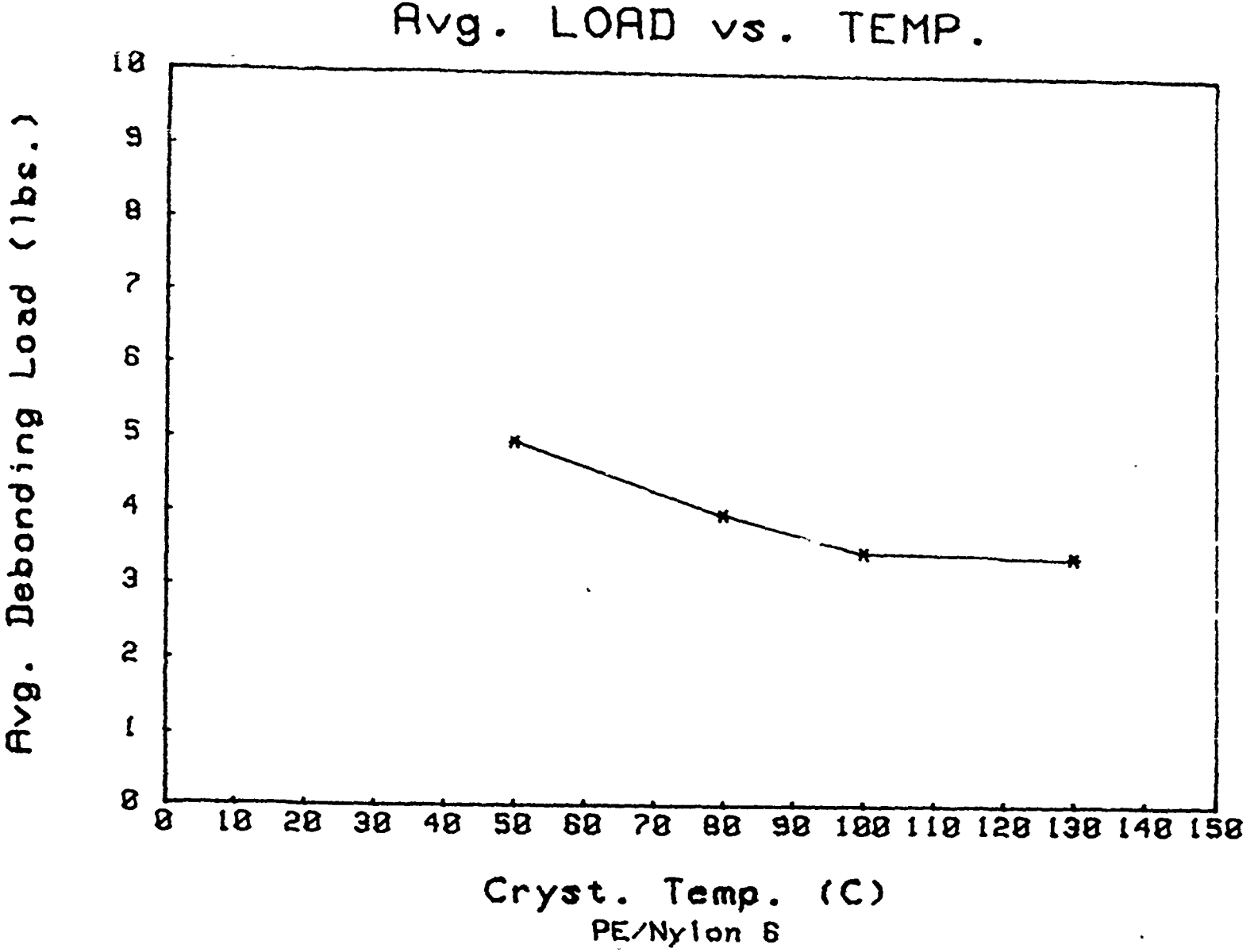

Fig. 2. Average debonding load vs. crystallization temp. for (PE/Nylon 6) specimens.

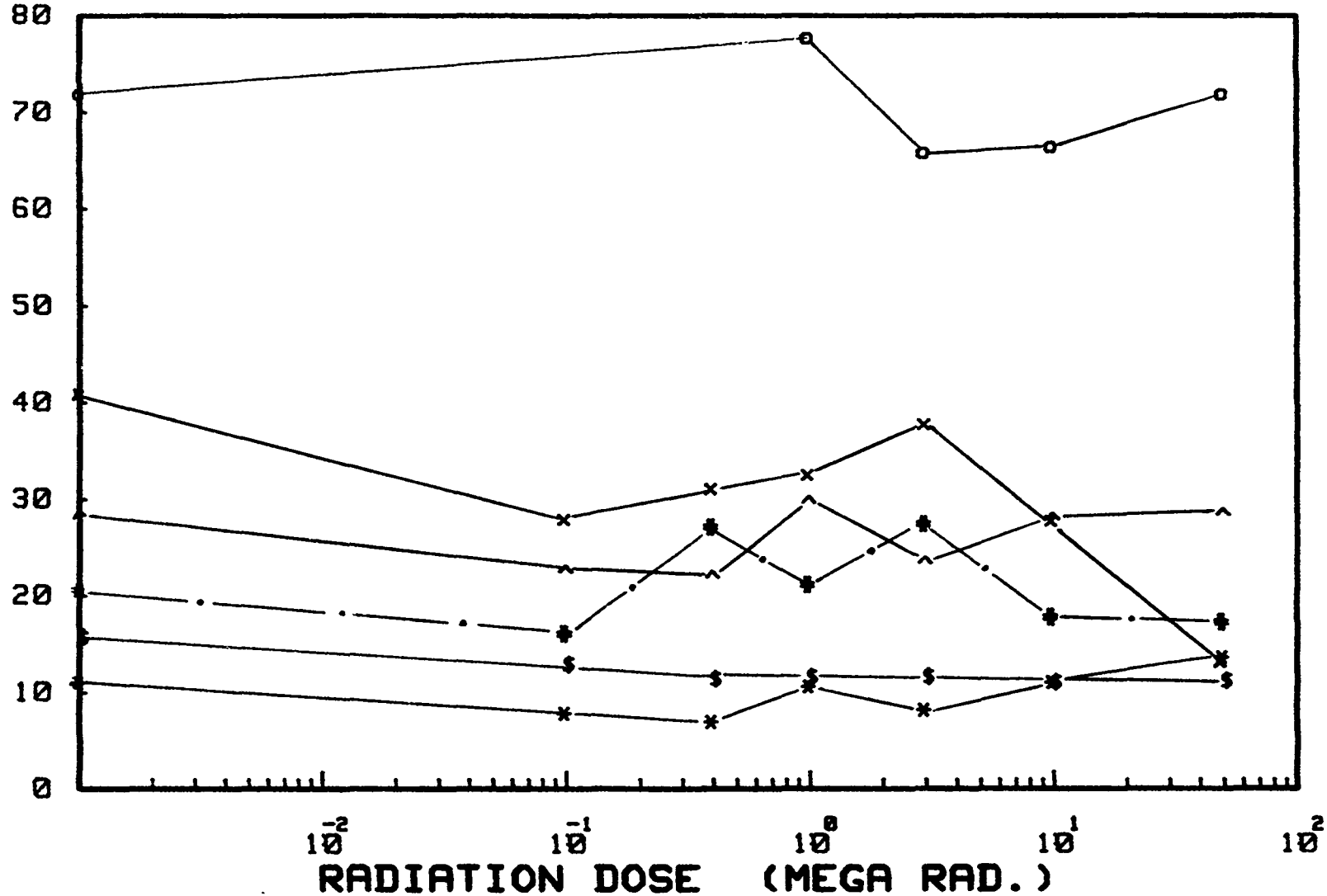
80
70
60
50
40
30
20
10
0
IMPACT ENERGY (FT-LB)
10^-2
10^-1
10^0
10^1
10^2
RADIATION DOSE (MEGA RAD.)
x/o: unidir.(23C/-196C); */*: cross.(23C/-196C); $/^: iso.(23C/-196C)

Fig 3

Fig. 4

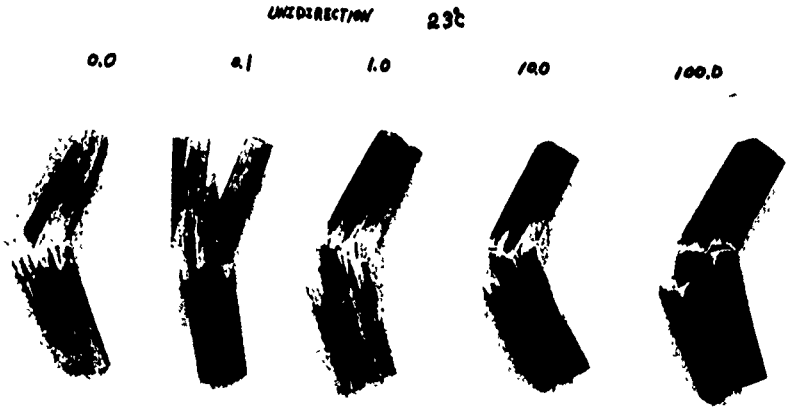
UNIDIRECTION
23℃
0.0
0.1
1.0
10.0
100.0
Z

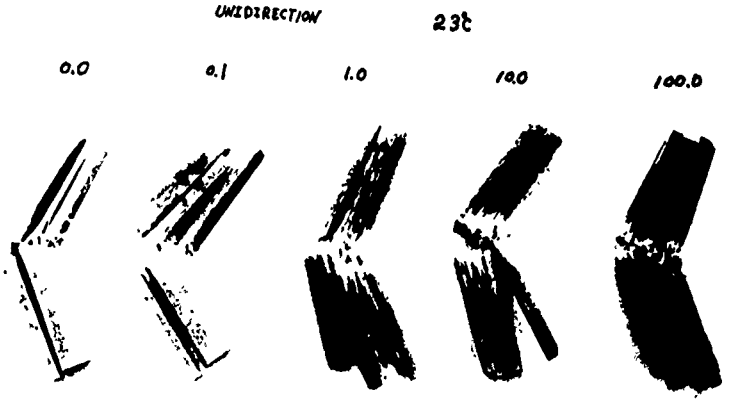
UNIDIRECTION
23℃
0.0
0.1
1.0
10.0
100.0
Y

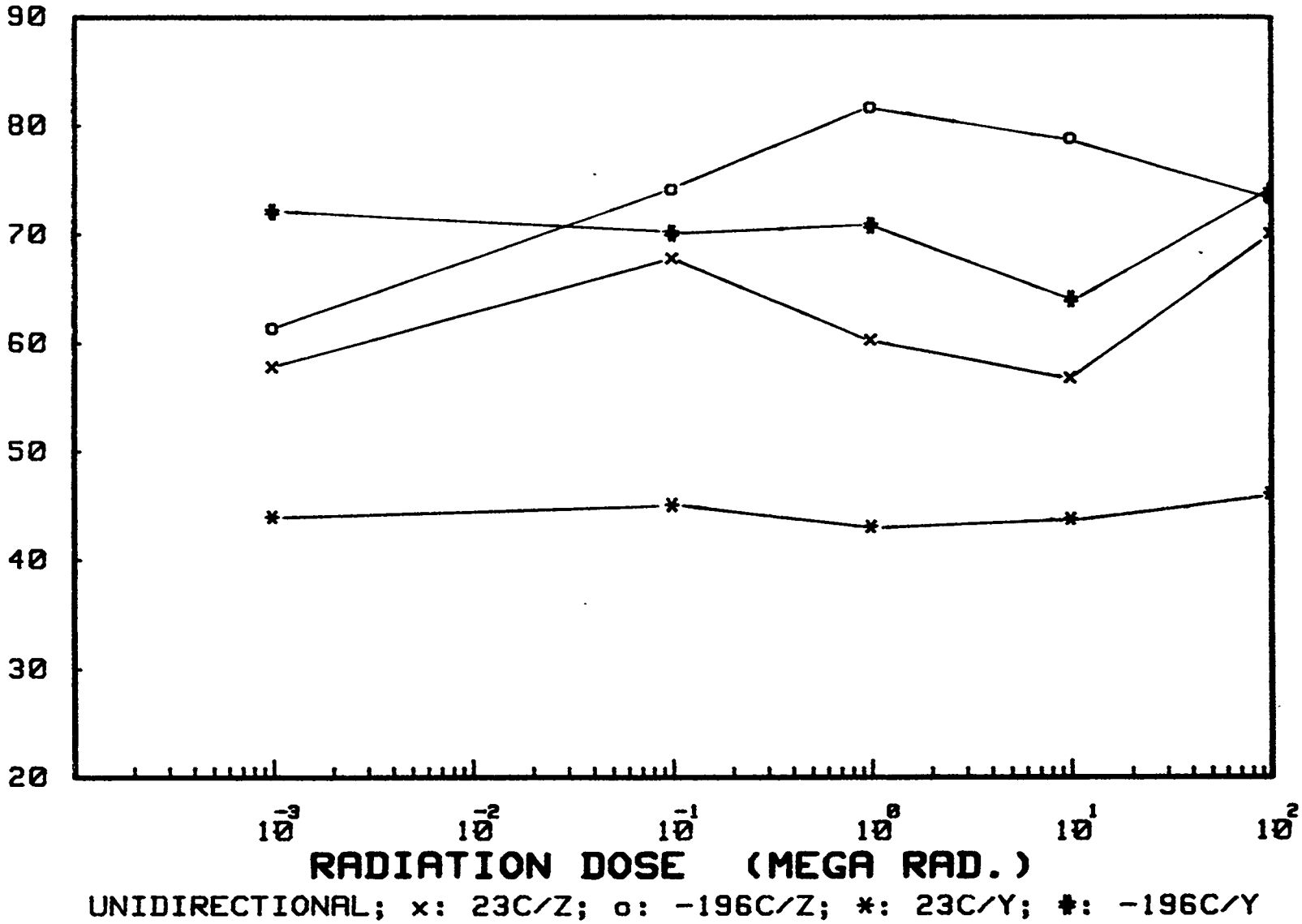
90
80
70
60
50
40
30
20
IMPACT ENERGY (FT-LB)
10^{-3}
10^{-2}
10^{-1}
10^{0}
10^{1}
10^{2}
RADIATION DOSE (MEGA RAD.)
UNIDIRECTIONAL; x: 23C/Z; o: -196C/Z; *: 23C/Y; #: -196C/Y

Fig. 5a

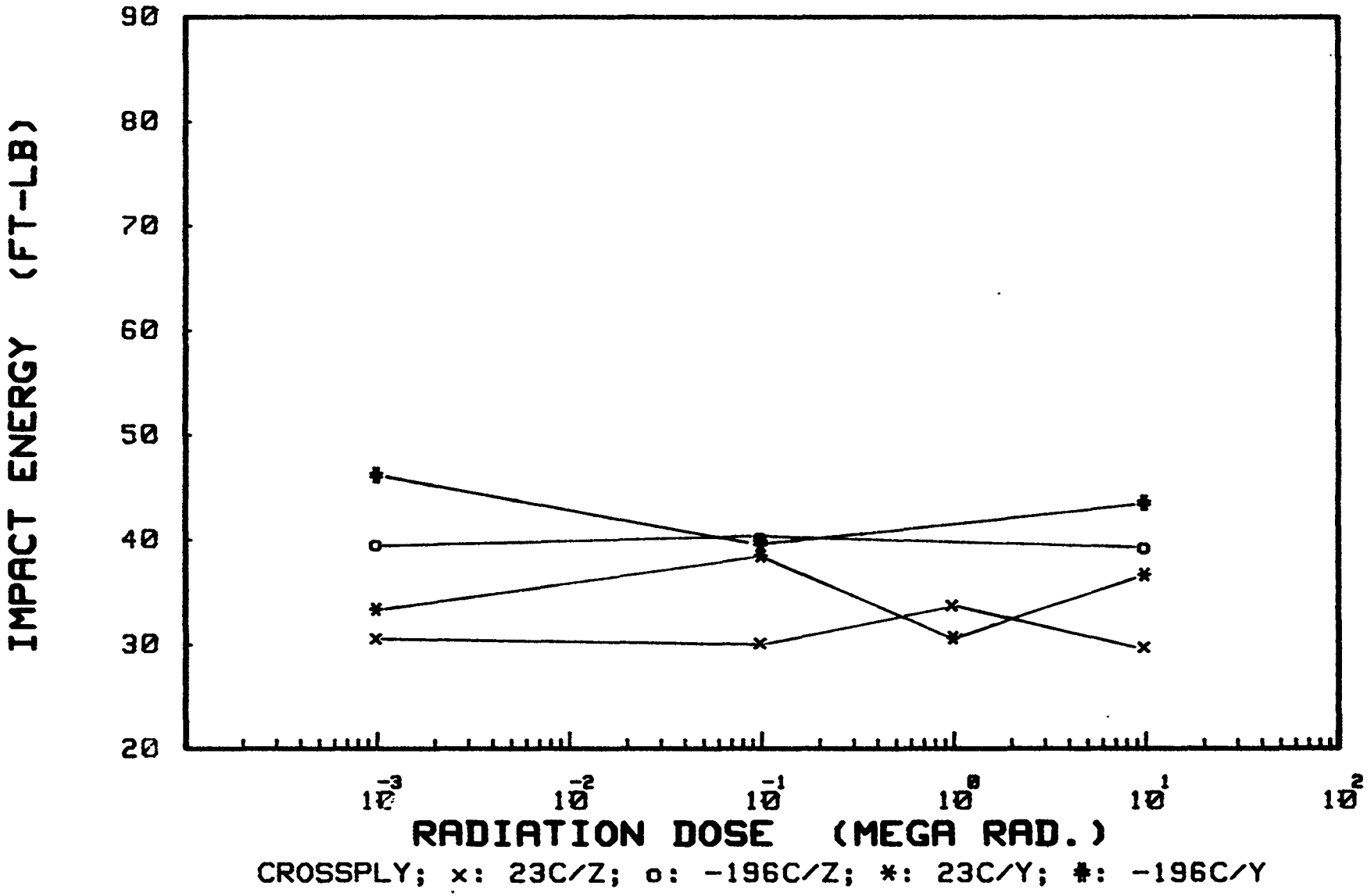
IMPACT ENERGY (FT-LB)
90
80
70
60
50
40
30
20
10^{-3}
10^{-2}
10^{-1}
10^{0}
10^{1}
10^{2}
RADIATION DOSE (MEGA RAD.)
CROSSPLY; x: 23C/Z; o: -196C/Z; *: 23C/Y; #: -196C/Y

Fig 5b

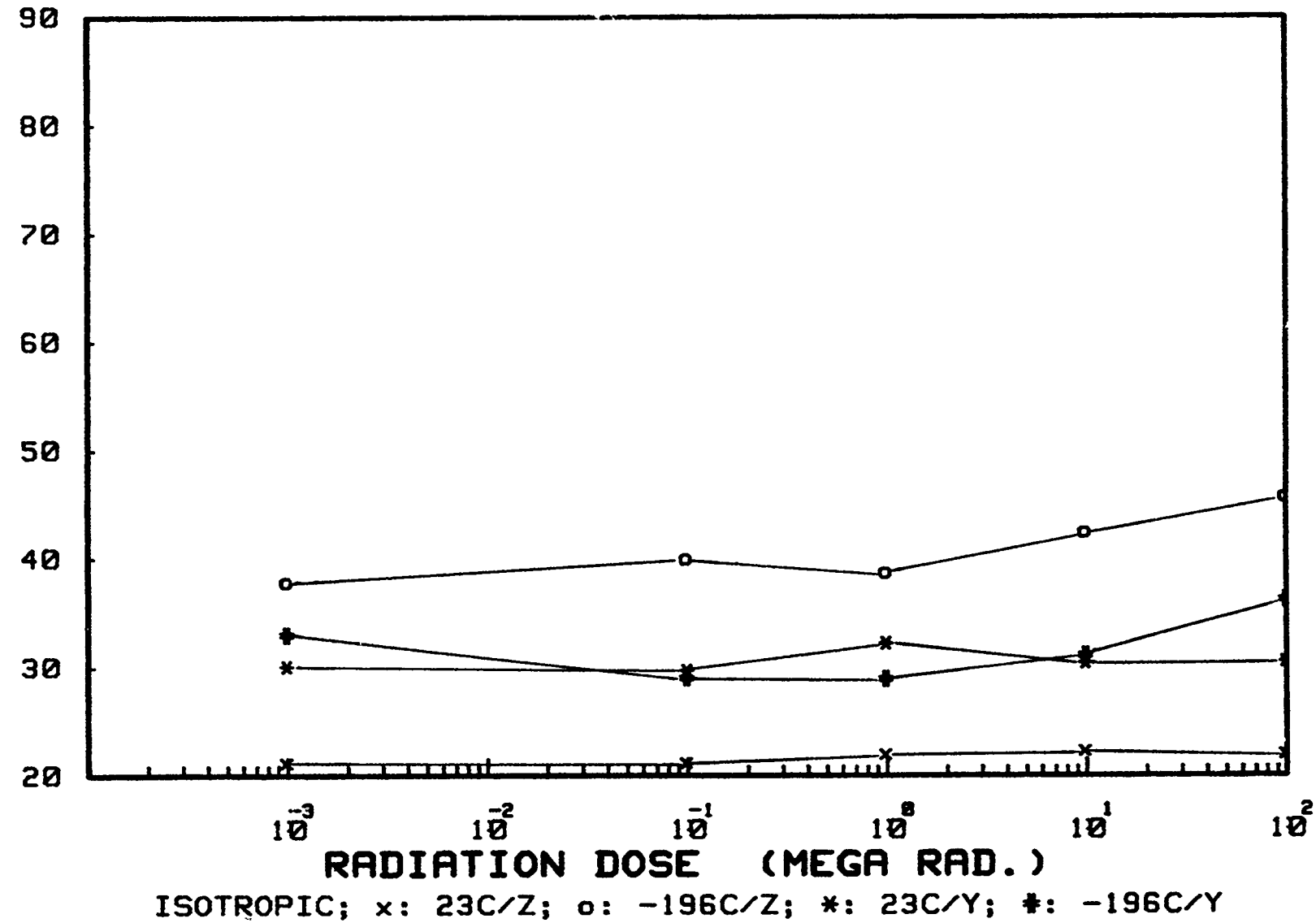
IMPACT ENERGY (FT-LB)
90
80
70
60
50
40
30
20
10^{-3}
10^{-2}
10^{-1}
10^{0}
10^{1}
10^{2}
RADIATION DOSE (MEGA RAD.)
ISOTROPIC; x: 23C/Z; o: -196C/Z; *: 23C/Y; #: -196C/Y

Fig. 5C

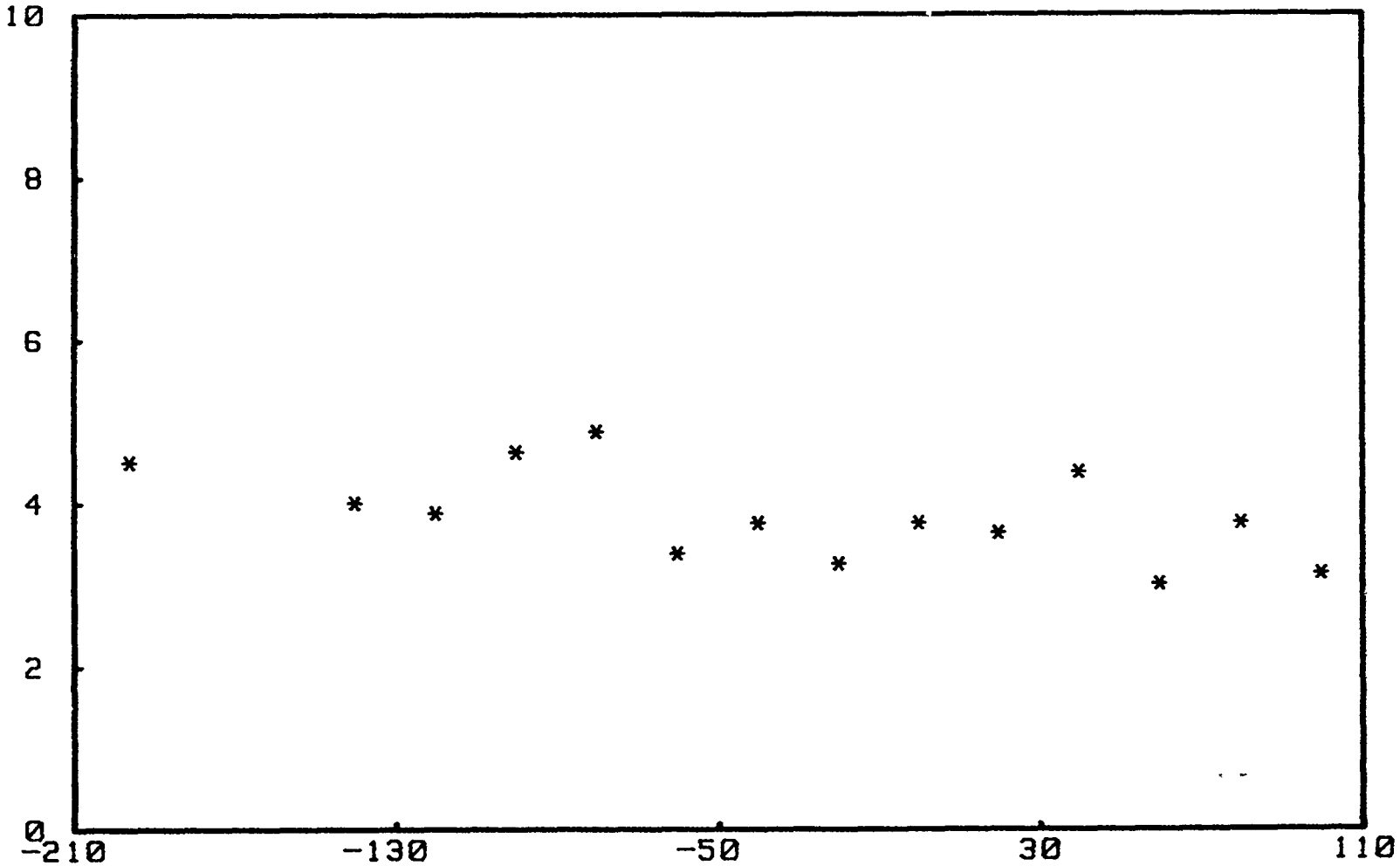
Impact Strength (ft-lb)
10
8
6
4
2
0
-210
-130
-50
30
110
Temperature (C)
PP with Continuous Fibers (Cross-Ply)

Fig. 6

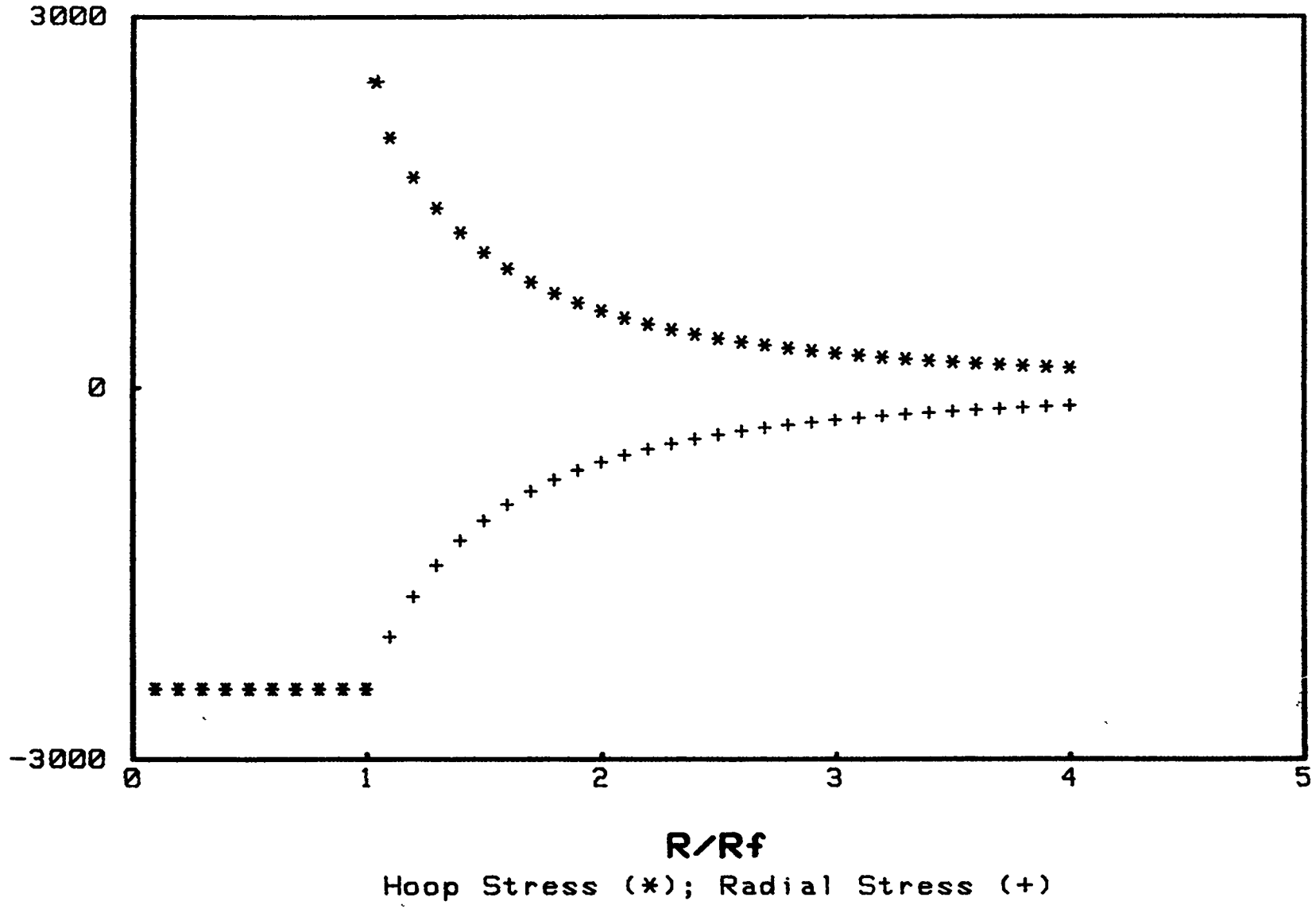
Glass Fiber/Epoxy (Temp. Changed =154 C)
3000
0
-3000
Stress (psi)
0
1
2
3
4
5
R/Rf
Hoop Stress (*); Radial Stress (+)

Fig 7a

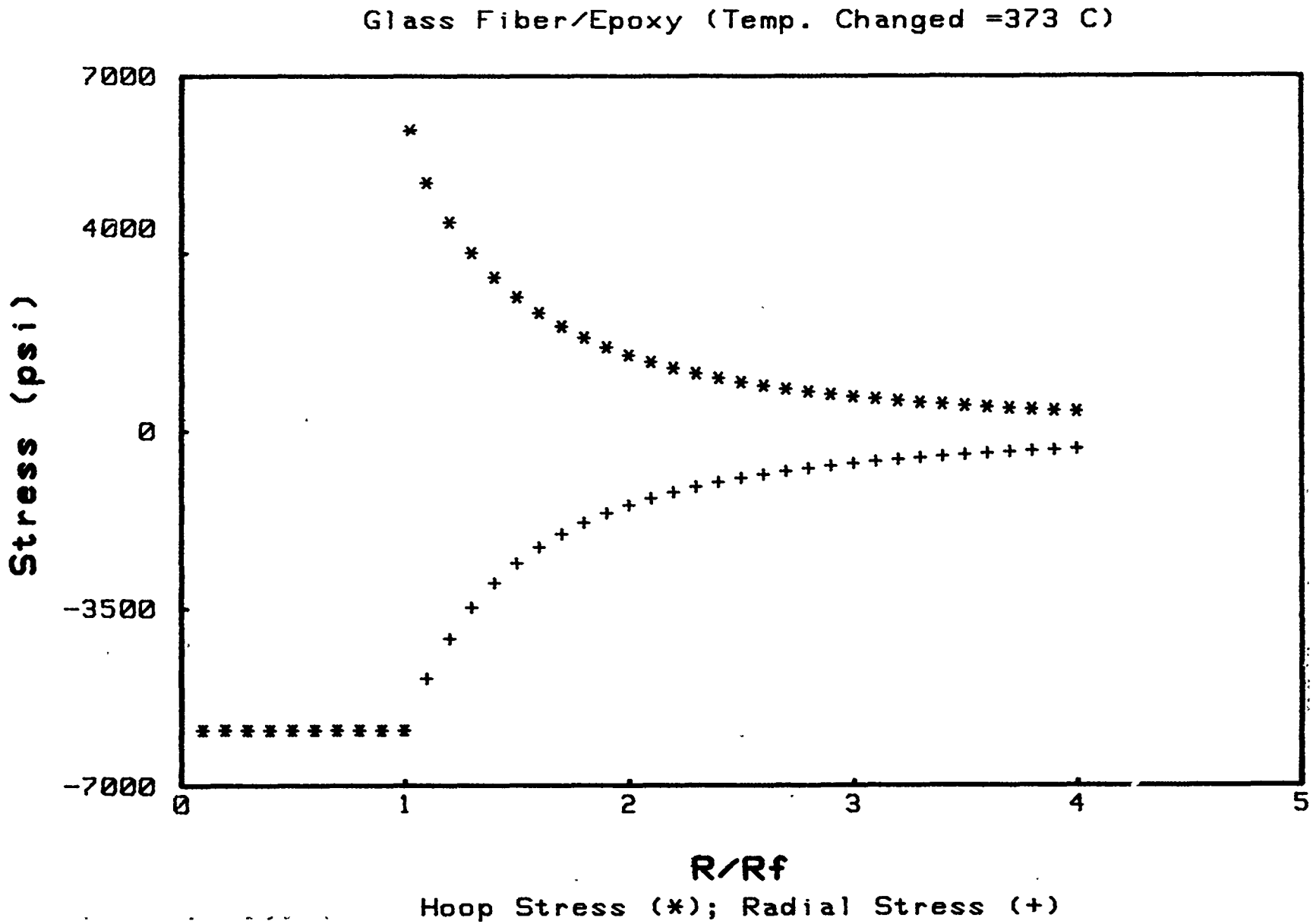
Glass Fiber/Epoxy (Temp. Changed =373 C)
7000
4000
0
-3500
-7000
Stress (psi)
0
1
2
3
4
5
R/Rf
Hoop Stress (*); Radial Stress (+)

Fig 7b

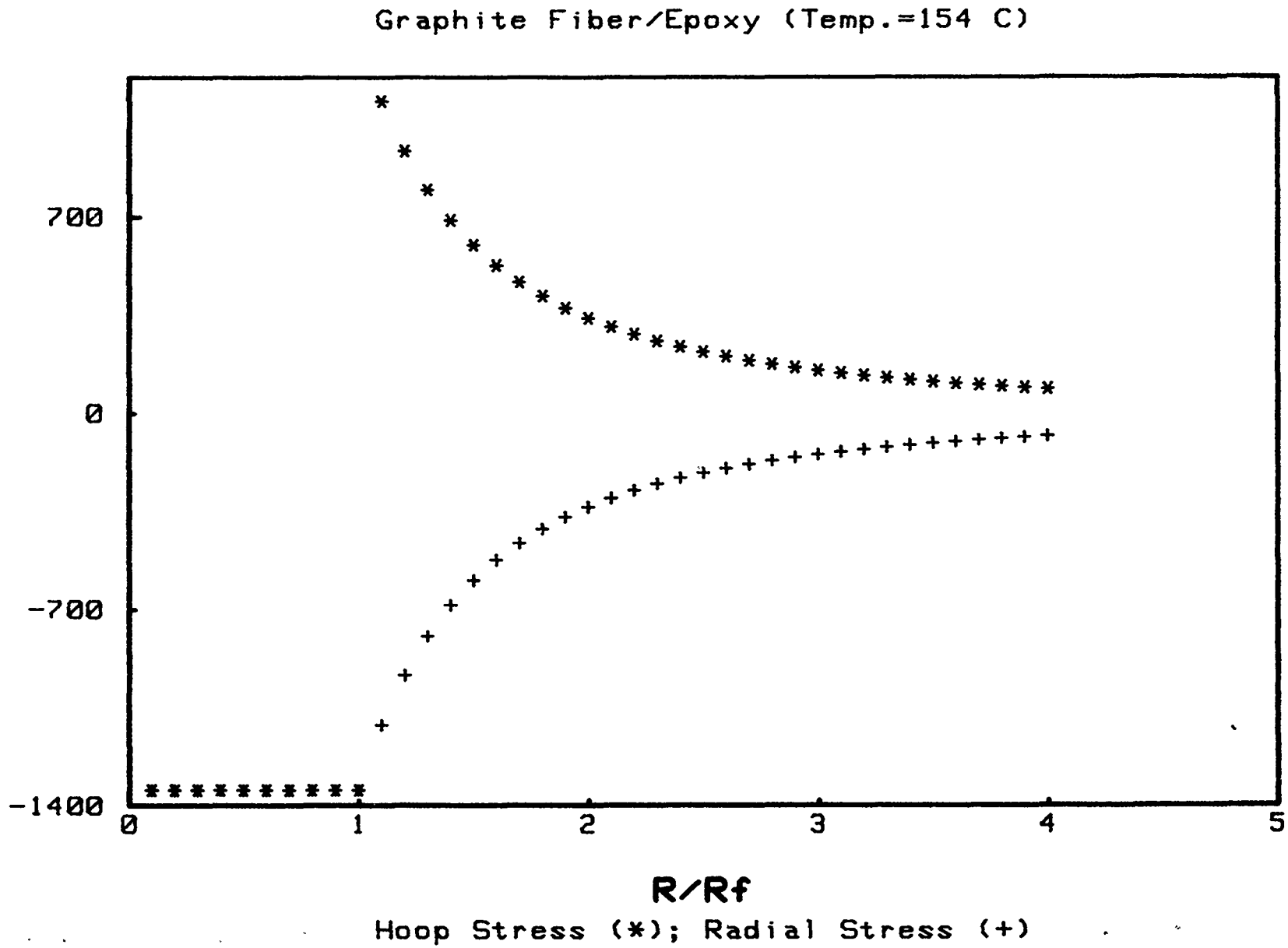
Graphite Fiber/Epoxy (Temp.=154 C)
700
0
-700
-1400
Stress (psi)
0
1
2
3
4
5
R/Rf
Hoop Stress (*); Radial Stress (+)

Fig. 8a

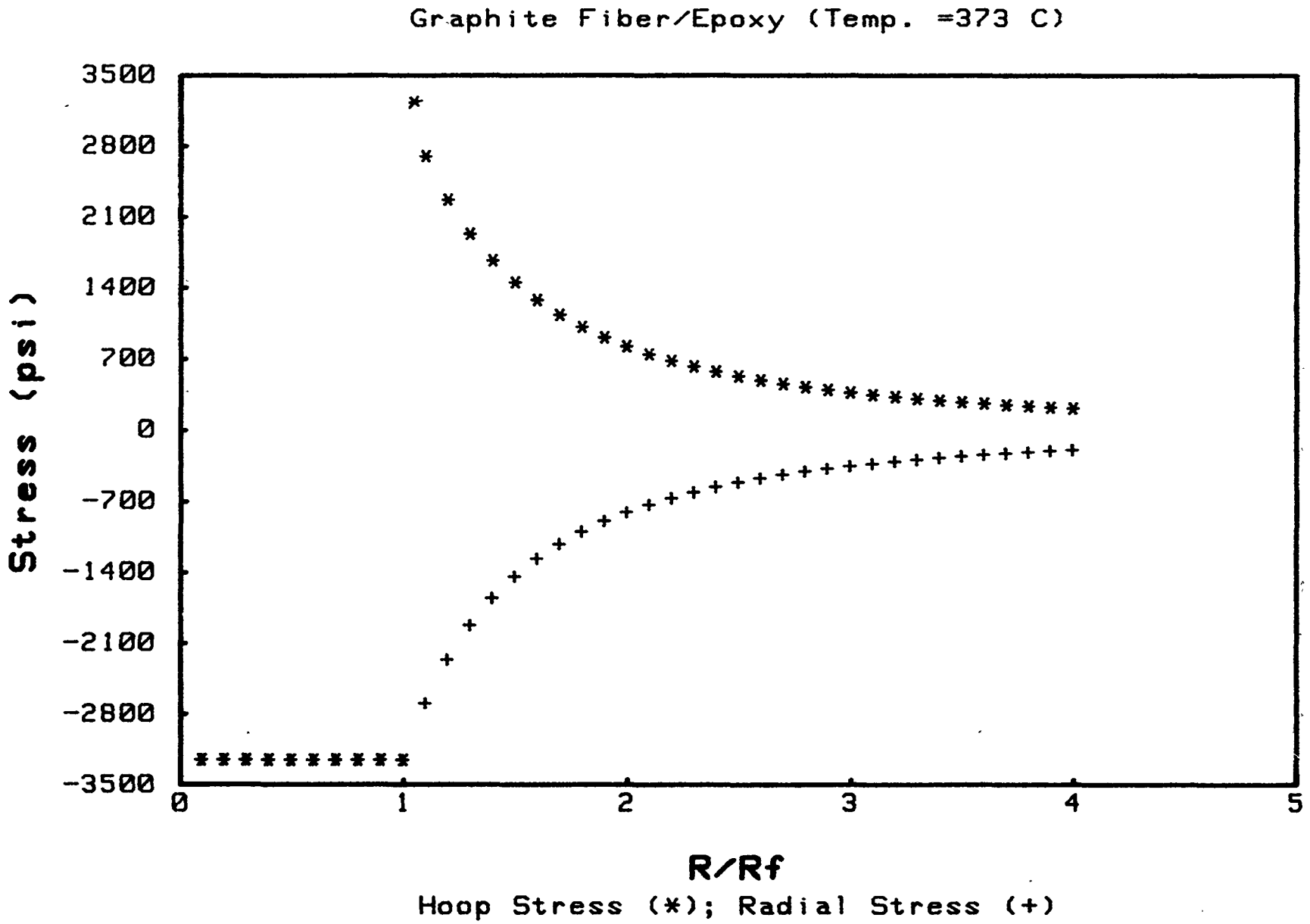
Graphite Fiber/Epoxy (Temp. =373 C)
3500
2800
2100
1400
700
0
-700
-1400
-2100
-2800
-3500
Stress (psi)
0
1
2
3
4
5
R/Rf
Hoop Stress (*); Radial Stress (+)

Fig 8b

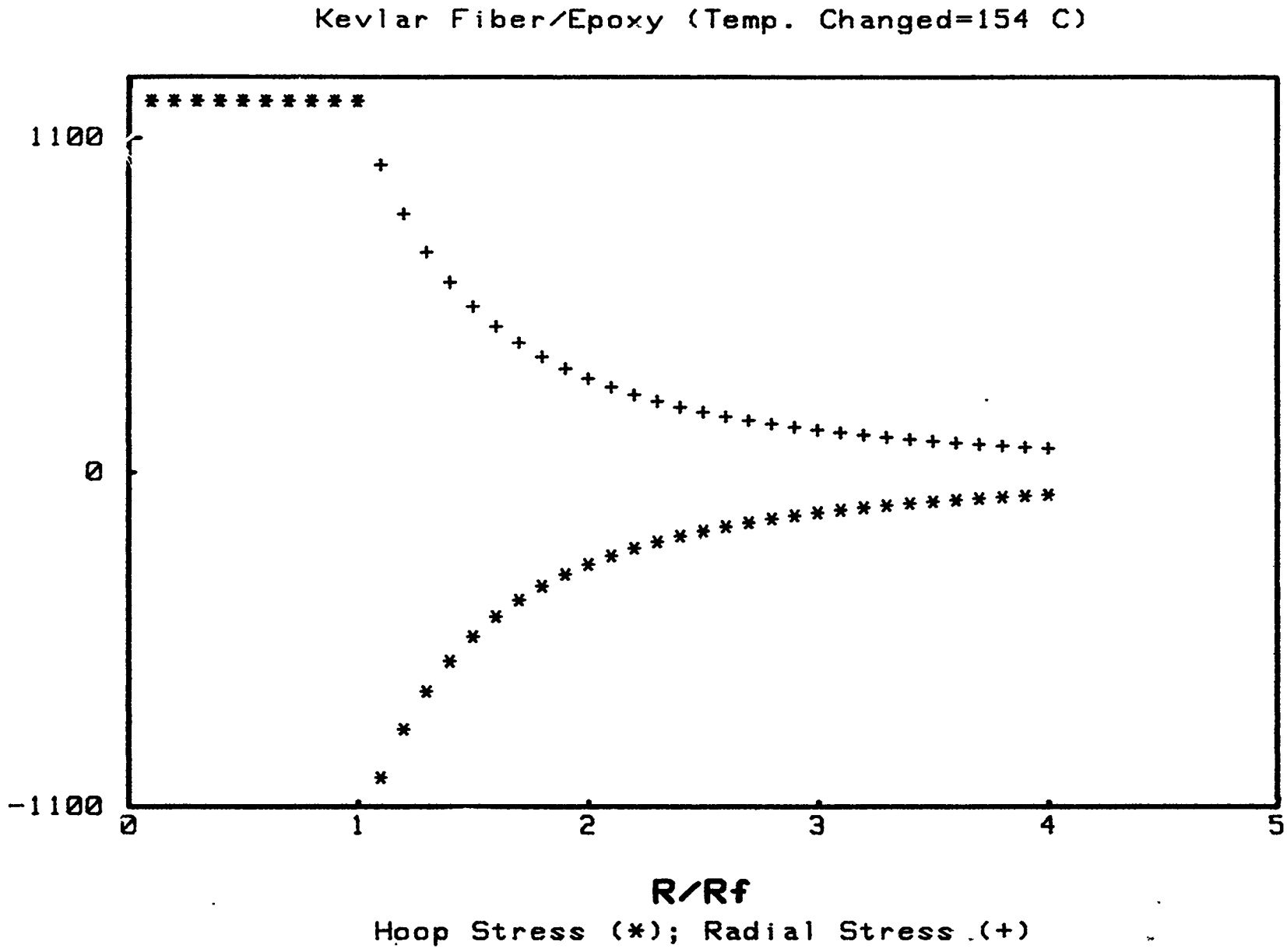
Kevlar Fiber/Epoxy (Temp. Changed=154 C)
1100
0
-1100
Stress (psi)
0
1
2
3
4
5
R/Rf
Hoop Stress (*); Radial Stress (+)

Fig. 4a

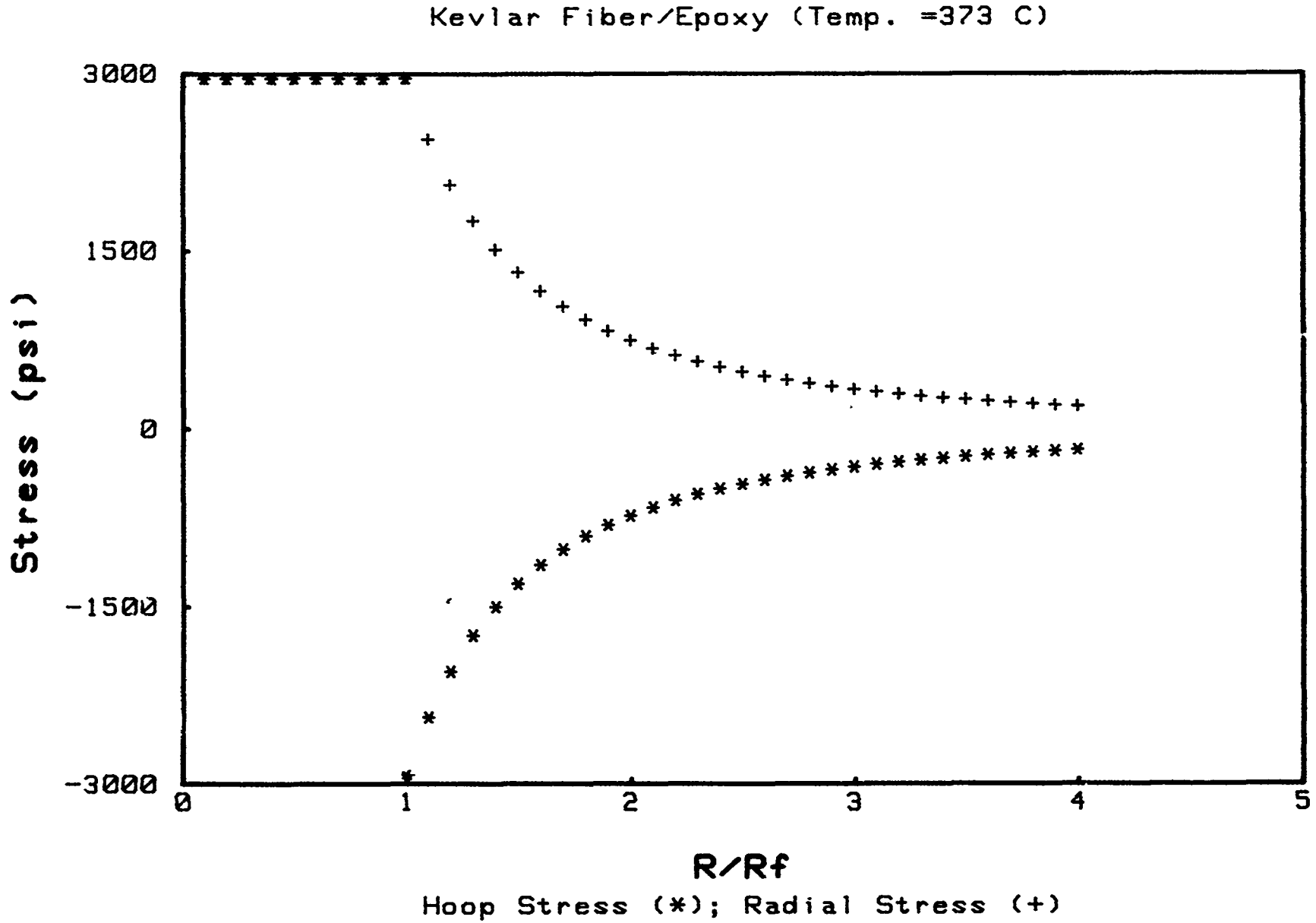
Kevlar Fiber/Epoxy (Temp. =373 C)
3000
1500
0
-1500
-3000
Stress (psi)
0
1
2
3
4
5
R/Rf
Hoop Stress (*); Radial Stress (+)

22-32

Fig. 9b

APPENDIX

In this section, the method of solving for residual stressses in a fiber composite is outlined. First, we consider a well-known classical elasticity problem i.e., the calculation of stress and strain fields in a thick cylinder under uniform pressure. Using such a thick cylinder model (TCM) we will proceed to calcualte the residual stresses established in a model single fiber-epoxy system and in a model composite system consisting of a rubber-coated fiber embedded in an epoxy matrix. Both room temperature and liquid nitrogen temperature will be considered when estimating the thermal stresses. This section will conclude with a discussion of the effects of thermal stresses due to difference in thermal expansion coefficients between laminae.

The Thick Cylinder Model (TCM)

Let us consider a thick cylinder submitted to uniform pressure on the inner and outer surfaces, as illustrated in Fig.A1. Let a and b be the inner and outer radii of the cylinder and P_i and P_e be the internal and external pressures, respectively. A consideration of the stress-strain relations, compatibility equations, and boundary conditions, using a procedure similar to that suggested by Wang [36], leads to the following stress components and radial displacement:

$$\sigma_r = \frac{1}{b^2-a^2}\left[a^2\left(1-\frac{b^2}{r^2}\right)P_i - b^2\left(1-\frac{a^2}{r^2}\right)P_e\right] \tag{1}$$

$$\sigma_\theta = \frac{1}{b^2-a^2}\left[a^2\left(1+\frac{b^2}{r^2}\right)P_i - b^2\left(1+\frac{a^2}{r^2}\right)P_e\right] \tag{2}$$

$$\sigma_z = \frac{2\nu(a^2P_i-b^2P_e)}{b^2-a^2} + E\varepsilon_z \tag{3}$$

$$\tau_{r\theta} = 0 \tag{4}$$

$$u = \frac{(1+\nu)(1-2\nu)}{E}\frac{a^2P_i-b^2P_e}{b^2-a^2} + \frac{1+\nu}{E}\frac{a^2b^2}{(b^2-a^2)r}(P_i-P_e) - \nu\varepsilon_z r \tag{5}$$

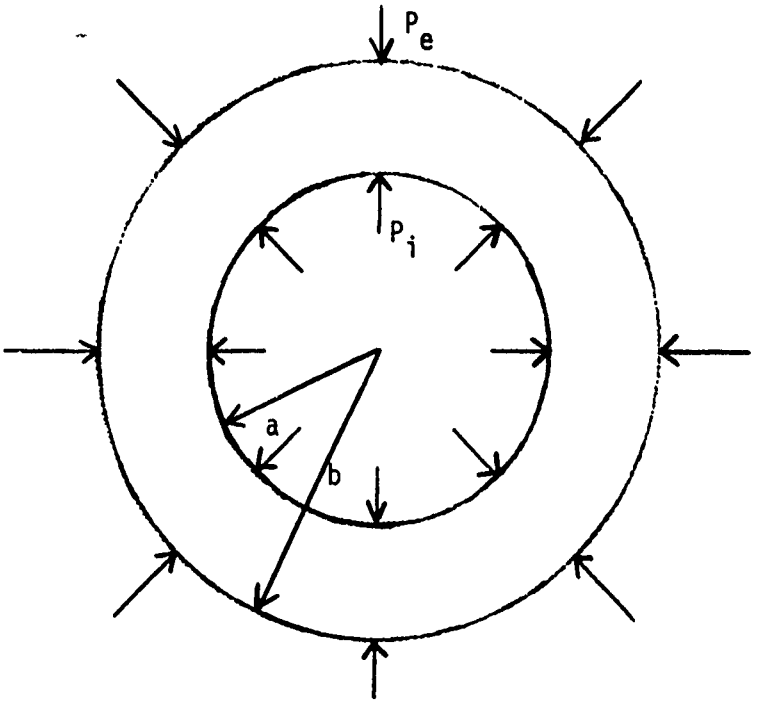

Fig. A1. Cross-section of a thick cylinder under uniform pressure.

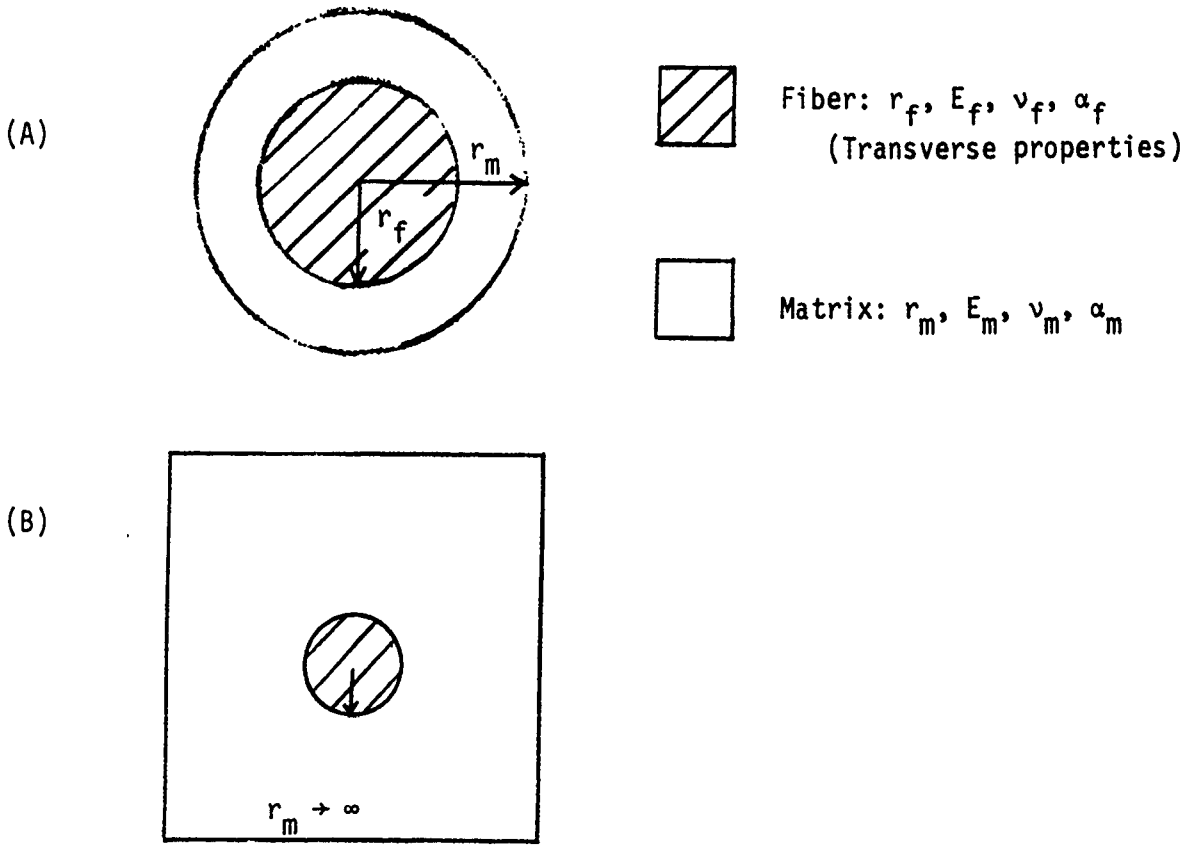

Fig. A2. A model composite consisting of a single fiber embedded in
(a) a hollow cylindrical matrix and in
(b) an infinitely large matrix.

If the ends of the cylinder are fixed, then $\varepsilon_z=0$ and the final term in both Eqs. (3) and (5) vanishes. If the ends of the cylinder are free to expand, then $\sigma_z = 0$ and Eqs. (3) and (5) simplify to, respectively,

$$\varepsilon_z = -\frac{2\nu}{E}\frac{a^2P_i-b^2P_e}{b^2-a^2} \tag{6}$$

$$u = \frac{1-\nu}{E}\frac{a^2P_i-b^2P_e}{b^2-a^2}r + \frac{1+\nu}{E}\frac{a^2\cdot b^2}{(b^2-a^2)r}(P_i-P_e) \tag{7}$$

Consider a special case where there exists only internal pressure P_i (P_e = 0). The stress components simplify to

$$\sigma_r = \frac{a^2P_i}{b^2-a^2}\left(1-\frac{b^2}{r^2}\right) \tag{8}$$

$$\sigma_\theta = \frac{a^2P_i}{b^2-a^2}\left(1+\frac{b^2}{r^2}\right) \tag{9}$$

and, if assuming free ends,

$$(u)_a = \frac{1}{E}\left(\frac{a^2+b^2}{b^2-a^2}+\nu\right)aP_i \tag{10}$$

$$(u)_b = \frac{2}{E}\left(\frac{a^2b}{b^2-a^2}\right)P_i. \tag{11}$$

For a second special case where there exists only external pressure P_e (P_i = 0), we have

$$\sigma_r = -\frac{b^2}{b^2-a^2}\left(1+\frac{a^2}{r^2}\right)P_e \tag{12}$$

$$\sigma_\theta = -\frac{b^2}{b^2-a^2}\left(1+\frac{a^2}{r^2}\right)P_e \tag{13}$$

$$(u)_a = -\frac{2}{E}\frac{ab^2}{b^2-a^2}P_e \tag{14}$$

$$(u)_b = -\frac{1}{E}\left(\frac{a^2+b^2}{b^2-a^2} - \nu\right) bP_e \tag{15}$$

where it is again assumed that the cylinder ends are free.

A. Single Fiber-Epoxy System

Consider a single fiber embedded in an epoxy matrix as shown in Fig.A 2(a). The system was cured at $T = T_2$ and then gradually cooled to an end-use temperature $T = T_1$. Due to differential thermal contraction a contact pressure P will be developed at the fiber-matrix interface. The fiber in the present case may be regarded as being submitted to an external pressure $P_e = P$ at $b = r_f$ and no internal pressure ($P_i = 0$ and $a = 0$). Eq. (15) therefore reduces to

$$u_f = -\frac{(1-\nu_f)}{E_f} r_f P \tag{16}$$

where u_f is the radial displacement of fiber at the fiber-matrix interface. The matrix is subjected to only internal pressure $P_i = P$ at $a = r_f$ ($P_e = 0$ and $b = r_m$) and Eq. (10) reduces to

$$u_m = \frac{1}{E_m}\left(\frac{r_f^2 + r_m^2}{r_m^2 - r_f^2} + \nu_m\right) r_f P \tag{17}$$

Compatibility at the fiber-matrix interface requires that

$$u_m - u_f = (\alpha_m - \alpha_f) \cdot r_f \cdot \Delta T \tag{18}$$

where $\Delta T = T_2 - T_1$. Combination of Eqs. 16, 17, and 18 yields

$$P = \frac{(\alpha_m - \alpha_f)\,\Delta T}{\frac{1}{E_m}\left(\frac{r_f^2 + r_m^2}{r_m^2 - r_f^2} + \nu_m\right) + \frac{1-\nu_f}{E_f}} \tag{19}$$

In an infinitely large matrix, $r_m \to \infty$ and thus

$$P = \frac{(\alpha_m - \alpha_f)\Delta T}{\frac{1+\nu_m}{E_m} + \frac{1-\nu_f}{E_f}} \tag{20}$$

The stress components in the matrix are, from Eqs. (8) and (9),

$$(\sigma_r)_m = \left(\frac{r_f}{r}\right)^2 (-p) \tag{21}$$

$$(\sigma_\theta)_m = \left(\frac{r_f}{r}\right)^2 p \tag{22}$$

while those in the fiber are, from Eqs. (12) and (13) with a = 0,

$$(\sigma_r)_f = - p \tag{23}$$

$$(\sigma_\theta)_m = - p \tag{24}$$

It may be noted that the second term in the denominator of Eq. 20 is usually negligible for advanced fibers compared to the first term. Therefore

$$\frac{P}{\Delta T} \approx (\alpha_m - \alpha_f) \frac{E_m}{(1+\nu_m)} . \tag{25}$$

This equation indicates that the residual stress per unit degree of temperature decrement is dictated by the thermal expansion coefficient difference $\Delta\alpha = \alpha_m - \alpha_f$, and the matrix engineering constants E_m and ν_m. The residual thermal stresses therefore can be reduced by adding plasticizer or a rubbery phase in the epoxy matrix that will decrease the magnitude of E_m and increase that of ν_m; both factor leading to a reduction in $P/\Delta T$. Eqs. 21-24 are plotted in Fig. 7, 8, 9 for graphite fiber-epoxy, Kevlar fiber-epoxy, and E-glass fiber-epoxy system, respectively.

B. Composite Consisting of Fiber-Matrix Interlayers

There has been a great deal of interest in exploring the feasibility of improving the transverse strength and the fracture resistance of composites through the introduction of an interlayer between the fibers and the matrix [37-43]. Understanding the residual thermal stresses in such a three-phase system will enhance our confidence in controlling its mechanical properties.

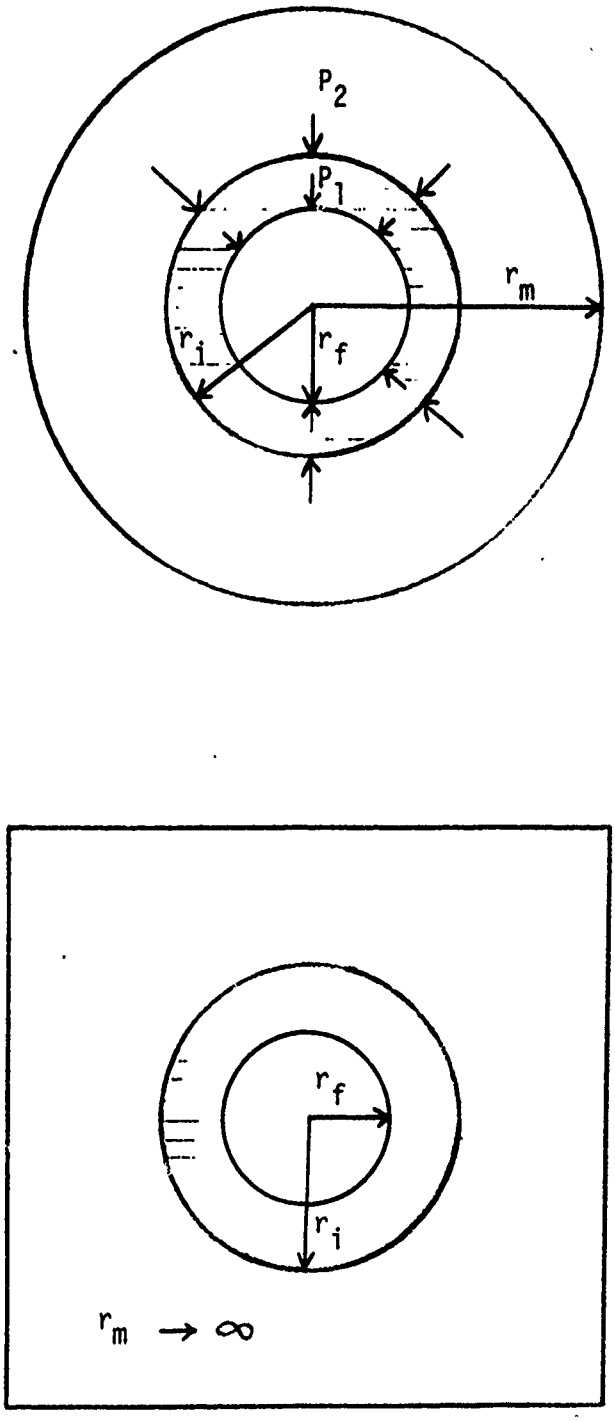

Fig. A3. A fiber-interlayer-matrix system.

Consider a three-phase system, as shown in Fig.A3, where the radii of the three phases are r_f, r_i, and r_m, respectively. Since the interlayer is subject to both the internal (P1) and external pressure (P_2) at a =

r_f and b = r_i, respectively, Eq. (7) may be rewritten as

$$U_i(r) = \frac{1-\nu_i}{E_i} \frac{r_f^2 P_1 - r_i^2 P_2}{r_i^2 - r_f^2} r + \frac{1+\nu_i}{E_i} \frac{r_f^2 r_i^2}{(r_i^2 - r_f^2)} (P_1 - P_2) \tag{26}$$

for $r_f \leq r \leq r_i$. Since the fiber is only submitted to an external pressure (in this case, a → 0, b = r_f, and $P_b = P_1$), Eq. (15) reduces

$$U_f(r_f) = -\frac{1}{E_f}(1-\nu_f) r_f P_1. \tag{27}$$

Similarly, the matrix is under a uniform internal pressure $P_i = P_2$ (a = r_i, b = r_m) and Eq. (10) becomes

$$U_m(r_i) = \frac{1}{E_m}\left(\frac{r_i^2 + r_m^2}{r_m^2 - r_i^2} + \nu_m\right) r_i P_2 \tag{28}$$

The boundary conditions at the two interfaces are

$$U_i(r_f) - U_f(r_f) = (\alpha_i - \alpha_f) r_f \cdot \Delta T \quad \text{at } r = r_f \tag{29}$$

and

$$U_m(r_i) - U_i(r_i) = (\alpha_{m-\alpha_R}) r_i \cdot \Delta T \quad \text{at } r = r_i. \tag{30}$$

Combining Eqs. (26) to (30), we have

$$P_1 = \frac{D(\alpha_i - \alpha_f)\Delta T - B(\alpha_m - \alpha_i)\Delta T}{AD - CB} \tag{31}$$

$$P_2 = \frac{A(\alpha_m - \alpha_i)\Delta T - C(\alpha_i - \alpha_f)\Delta T}{AD - CB} \tag{32}$$

where

$$A \equiv \frac{\nu_i}{E_i} + \left(\frac{r_f^2 + r_i^2}{r_i^2 - r_f^2}\right) \frac{1a}{E_i} + \frac{1-\nu_f}{E_f} \tag{33}$$

$$B \equiv \frac{-2}{E_i}\left(\frac{r_i^2}{r_i^2 - r_f^2}\right) \tag{34}$$

$$C \equiv \frac{-2}{E_i}\left(\frac{r_f^2}{r_i^2 - r_f^2}\right) \tag{35}$$

$$D = \frac{-\nu_i}{E_i} + \left(\frac{r_f^2 + r_i^2}{r_i^2 - r_f^2}\right)\frac{1}{E_i} + \frac{1}{E_m}\left(\frac{r_i^2 + r_m^2}{r_m^2 - r_i^2} + \nu_m\right) \tag{36}$$

With a large volume fraction of matrix, $\nu_m \to \infty$, we have

$$D = \frac{-\nu_i}{E_i} + \left(\frac{r_f^2 + r_i^2}{r_i^2 - r_f^2}\right)\frac{1}{E_i} + \frac{1+\nu_m}{E_m} \tag{37}$$

The stress components in the three phases are given as follows:

(1) In the matrix (with $r_m \to \infty$):
Eqs (8) and (9) may be rewritten as

$$\sigma_r = -\frac{r_i^2}{r^2} P_2 \tag{38}$$

$$\sigma_\theta = \frac{r_i^2}{r^2} P_2 \tag{39}$$

Near the interlayer-matrix interface, $r \to r_i+$, therefore

$$\sigma_r \to -P_2 \tag{40}$$

$$\sigma_\theta = P_2 \tag{41}$$

(2) In the fiber:

$$\sigma_r = -P_1 \tag{42}$$

$$\sigma_\theta = -P_1 \tag{43}$$

(3) In the interlayer:

$$\sigma_r = \frac{1}{r_i^2 - r_f^2}\left[r_f^2\left(1 - \frac{r_i^2}{r^2}\right)P_1 - r_i^2\left(1 - \frac{r_f^2}{r^2}\right)P_2\right] \tag{44}$$

$$\sigma_\theta = \frac{1}{r_i^2 - r_f^2}\left[r_f^2\left(1 + \frac{r_i^2}{r^2}\right)P_1 - r_i^2\left(1 + \frac{r_f^2}{r^2}\right)P_2\right] \tag{45}$$

Near the interlayer-fiber interface, $r \to r_f+$, and

$$\sigma_r \to - P_1 \tag{46}$$

$$\sigma_\theta \to \frac{(r_f^2 + r_i^2)\, P_1 - 2\, r_i^2\, P_2}{(r_i^2 - r_f^2)} \tag{47}$$

Near the interlayer-matrix interface, $r \to r_i-$, and

$$\sigma_r \to - P_2 \tag{48}$$

$$\sigma_\theta \to \frac{2r_f^2 P_1 - (r_i^2 + r_f^2) P_2}{r_i^2 - r_f^2} \tag{49}$$

Session V

COMPOSITE POST FAILURE ANALYSIS
APPROACHES AND EXPERIENCES

AN OVERVIEW OF THE FRACTOGRAPHY/FAILURE ANALYSIS METHODOLOGY USED AT NORTHROP FOR CHARACTERIZING FAILURES IN FIBER/RESIN COMPOSITES

R.J. Kar and R.T. Kessler
Northrop Corporation
Aircraft Division
Hawthorne, California

NB 85-253
JULY 1985

AN OVERVIEW OF THE FRACTOGRAPHY/FAILURE ANALYSIS METHODOLOGY USED AT NORTHROP FOR CHARACTERIZING FAILURES IN FIBER/RESIN COMPOSITES

By

R.J. KAR

R.T. KESSLER

To

INTERNATIONAL CONFERENCE:
POST FAILURE ANALYSIS TECHNIQUES
FOR FIBER REINFORCED COMPOSITES
3 JULY 1985

NORTHROP

Aircraft Division
Aircraft Group
Northrop Corporation

One Northrop Avenue
Hawthorne, California 90250

INTRODUCTION

FIBER/RESIN COMPOSITES ARE PRIMARY MATERIALS IN CURRENT AND NEXT GENERATION AIRCRAFT STRUCTURES

- HIGHER STRENGTH/WEIGHT RATIOS THAN METALS
- EXCELLENT FATIGUE PROPERTIES

FIBER/RESIN FORMULATIONS USED IN SEVERAL MILITARY AND COMMERCIAL AIRCRAFT

- AS4/3501-6 (F/A-18)
- T300/5208 (F-16)
- T300/934 (LEAR AVIA)
- HEXCEL F593 (BOEING 757)

(RESIN FORMULATIONS ARE GENERALLY PROPRIETARY)

85-51785
11C

INTRODUCTION (CONT)

URGENT NEED FOR COMPOSITE FRACTOGRAPHY/ FAILURE ANALYSIS DATA

- **CRITICAL FOR DESIGN-DEVELOPMENT AND CERTIFICATION TEST ARTICLES**
- **INVALUABLE FOR ADDRESSING POTENTIAL IN-SERVICE PROBLEMS**
  - **MANUFACTURING DEFECTS (POROSITY, RESIN-RICH AREAS)**
  - **IN-SERVICE DAMAGE (IMPACT, DELAMINATION)**

85-51786
11C

CRITICAL ISSUES IN FRACTOGRAPHY/FAILURE ANALYSIS OF COMPOSITES

- COMPOSITES ARE HETEROGENEOUS AND BRITTLE ON A MACROSCOPIC SCALE
- CONTINUOUS FIBER-LAMINATED COMPOSITES ARE HIGHLY ANISOTROPIC
- FRACTURE CHARACTERISTICS ARE NOT THE SAME AS FOR METALS
  - NO UNIQUE "INITIATION" EVENT
  - "LOCAL FRACTURE EVENTS" GIVE RISE TO REGIONS OF "ZONAL DAMAGE"
  - INDIVIDUAL PLY FAILURE MAY NOT RESULT IN FINAL FAILURE
  - CATASTROPHIC FRACTURE IS A HIGH-ENERGY EVENT (BRITTLE FRACTURE)

85-50623A
10E

CRITICAL ISSUES (CONT)

- FRACTURE CHARACTERISTICS KNOWN TO VARY WITH:
  - APPLIED STRESS STATE
  - TYPE OF FIBER
  - SURFACE TREATMENT OF FIBER
  - FIBER STACKING SEQUENCE (0^o, $\pm 45^o$, 90^o)
  - TEMPERATURE AND HUMIDITY
- ARE FRACTURE CHARACTERISTICS OF ONE COMPOSITE SYSTEM APPLICABLE TO ANOTHER FORMULATION ? ? ?

85-50624A
10E

METHODOLOGY USED AT NORTHROP FOR FRACTOGRAPHIC FAILURE ANALYSIS OF Gr/Ep COMPOSITES

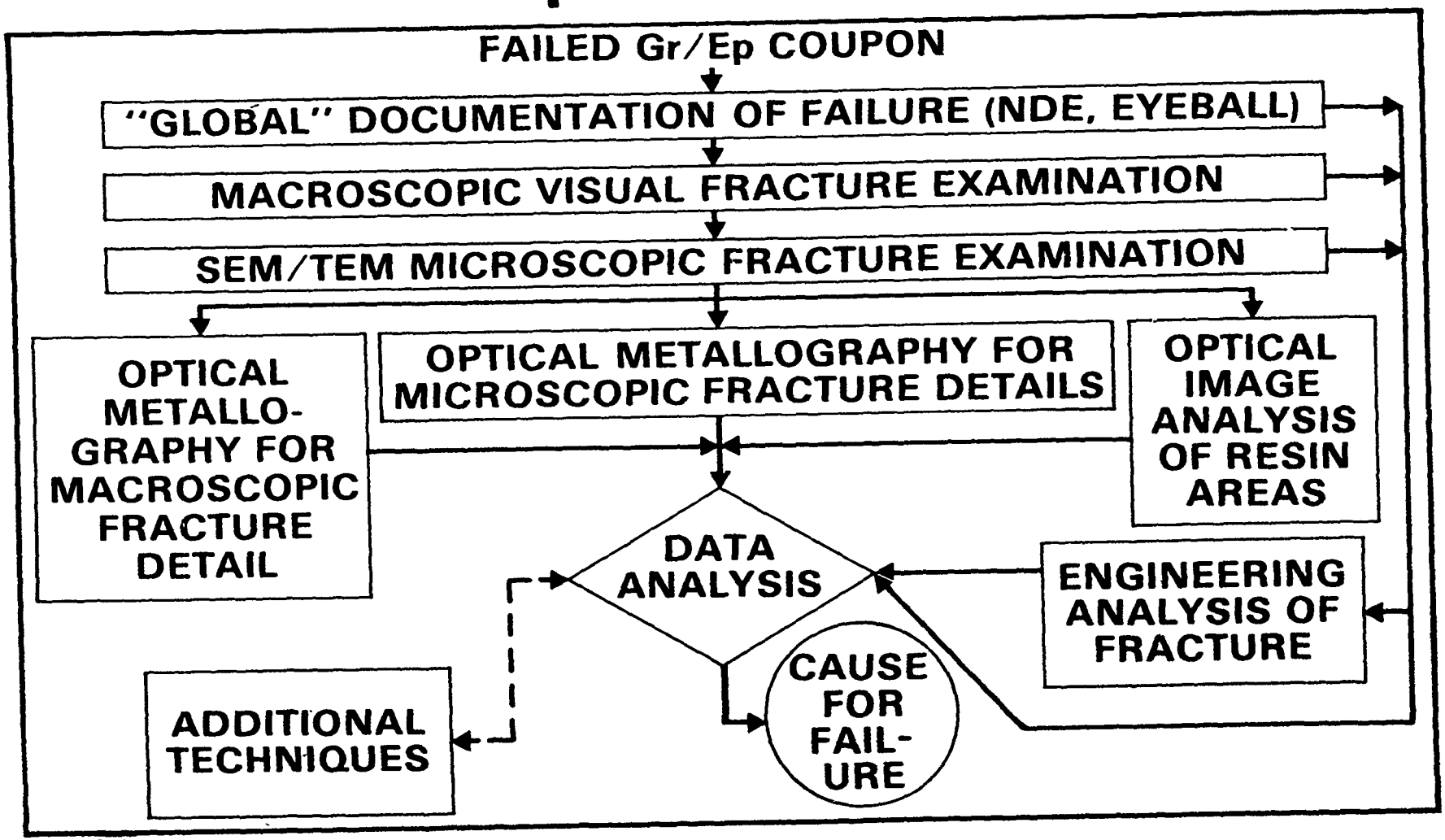

84-12506A
10E

NORTHROP ANALYTICAL CAPABILITIES FOR COMPOSITE FRACTOGRAPHY/ FAILURE ANALYSIS

- BACKGROUND INFORMATION
  - SPECIFICATIONS, DATA SHEETS
  - DESIGN REQUIREMENTS
  - MECHANICAL TEST DATA
  - FABRICATION PARAMETERS (LAY-UP SEQUENCE, CURE TEMPERATURE/CYCLES)
  - FIBER, NEAT RESIN PROPERTIES (RESIN FORMULATION IF AVAILABLE)
- PRE-AND POST-FAILURE NDE RESULTS
  - C-SCANS, A-SCANS
  - DIB/TBE ENHANCED X-RAY RADIOGRAPHY

85-51787
10E

NORTHROP ANALYTICAL CAPABILITIES FOR COMPOSITE FRACTOGRAPHY/ FAILURE ANALYSIS (CONT)

- CONVENTIONAL METALLURGICAL LABORATORY EQUIPMENT
  - STEREOMICROSCOPE
  - MACRO-PHOTOGRAPHY EQUIPMENT
  - OPTICAL METALLOGRAPHS
  - SEMS
- ACCESS TO SPECIALIZED LABORATORY EQUIPMENT
  - MICROCHEMICAL ANALYSIS INSTRUMENTATION (SAM/ESCA, GC-FTIR, DMA, DSC, RDS)
  - TEM/AEM
  - QUANTITATIVE IMAGE ANALYZERS
- "TRAINED" PERSONNEL

85-51788
10E

SEM EXAMINATION OF COMPOSITES

- INTELLIGENT SELECTION OF SAMPLES FOR SEM EXAMINATION NECESSARY
- ELECTRICALLY NON-CONDUCTING NATURE OF COMPOSITES NECESSITATES VACUUM SHADOWING WITH AU OR AU/PD PRIOR TO SEM EXAMINATION
- ARTIFACTS CAN BE PRODUCED IN SPECIMENS DUE TO LOCALIZED HEATING OF RESIN FROM THE EB – MINIMIZED BY USE OF LOW SEM OPERATING VOLTAGES (750 mV - 5 KV)
- MACROSCOPIC SEM FRACTURE EXAMINATION OF "GLOBAL FAILURE" MUST PRECEDE MICROSCOPIC SEM FRACTURE EXAMINATION

85-50627A
10E

EXAMPLES OF COMPOSITE FRACTOGRAPHY/FAILURE ANALYSES PERFORMED AT NORTHROP

85-51789
10E

STATIC COMPRESSION FAILURES IN OPEN-HOLE COUPONS

- AS6/5245C AND CE12000/5245C MULTI-PLY LAMINATES
- STATIC COMPRESSIVE PROPERTIES (RT/DRY) DIFFERENT
- OBJECTIVE OF ANALYSIS – DETERMINE IF DIFFERENCES IN PROPERTIES RELATED TO DIFFERENCES IN FAILURE MODES

85-51790
10E

MACROPHOTOGRAPHS OF OPEN-HOLE COMPRESSION COUPON FRACTURES

AS6/5245C

3mm

85-02726

CE12000/5245C

3mm

85-02726

- MACROSCOPIC DIFFERENCES IN FRACTURE SURFACE APPEARANCE
- NO MACROSCOPIC INDICATIONS THAT FRACTURES INITIATE AT OPEN HOLES

85-51791
10E

SEM FRACTURE CHARACTERISTICS OF AS6/5245C COUPON

DELAMINATIONS & FIBER BUCKLING

85-02725

FIBER BUCKLING

85-02725

FIBER WETTING BY RESIN

85-02725

FIBER BUCKLING

85-02725

SEM FRACTURE CHARACTERISTICS OF CE1200/5245C COUPON

DELAMINATION & HACKLES (ARROW)

85-02723

CLUMPING OF FIBER BUNDLES

85-02723

BUCKLING OF FIBER BUNDLES

85-02723

INTRA-PLY CRACKING

85-02723

85-51793
10E

OPTICAL METALLOGRAPHY OF AS6/5245C LAMINATE

0° 2mm 85-51794

45° 2mm 85-51794

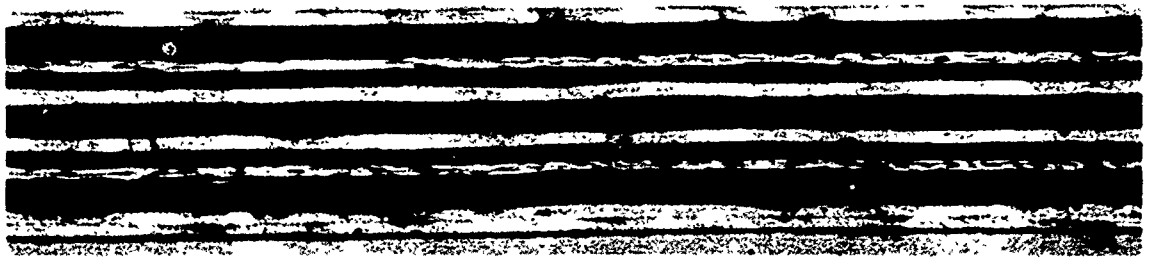

90° 2mm 85-51794

85-51794
10E

OPTICAL METALLOGRAPHY OF CE12000/5245C LAMINATE

0° 2mm 85-02730

45° 2mm 85-02730

90° 2mm 85-02730

FAILURE CHARACTERISTICS OF OPEN-HOLE COUPONS

- COMPRESSIVE PROPERTY DIFFERENCES RELATED TO DIFFERENCES IN MICROSCOPIC FRACTURE CHARACTERISTICS
- UNIQUE FRACTURE INITIATION SITES COULD NOT BE UNEQUIVOCALLY ESTABLISHED

85-51796
10E

FAILURE ANALYSIS OF A LOW COMPLEXITY STRUCTURAL COMPONENT

85-51797
10E

FAILURE ANALYSIS OF STRUCTURAL COMPONENT

- AS4/3502 GR/EP TEST PANEL CONTAINING POROSITY
- PANEL TESTED TO FAILURE IN STATIC COMPRESSION
- OBJECTIVE OF ANALYSIS – DETERMINE IF FRACTURE INITIATES AT REGIONS OF POROSITY

85-51798
10E

C-SCAN EXAMINATION OF PANEL PRIOR TO TESTING

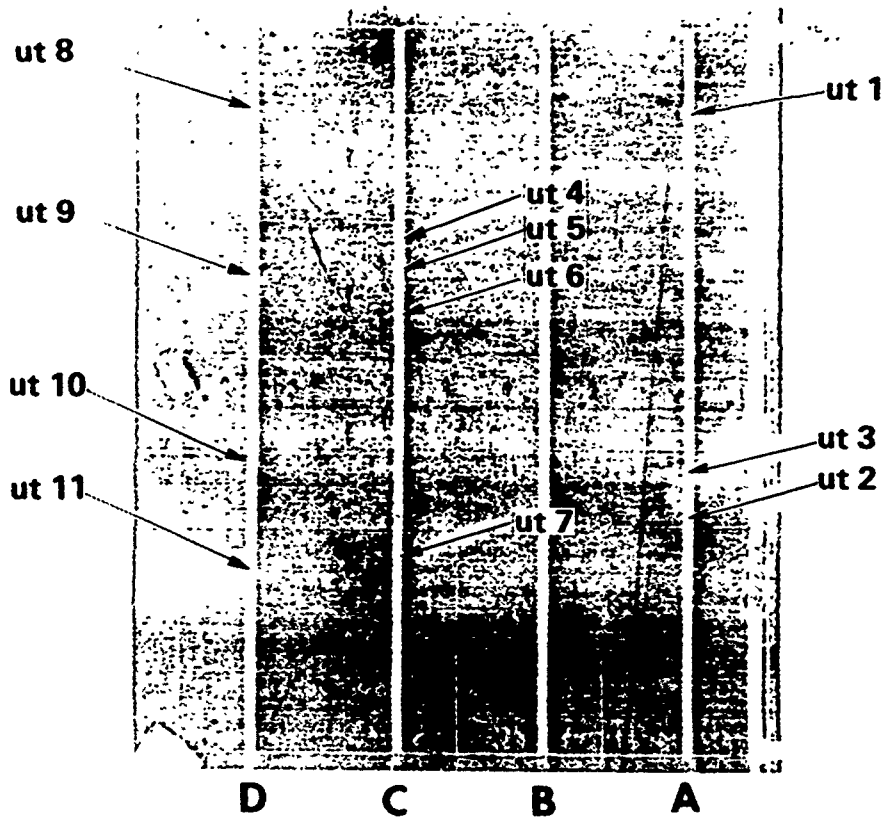

85-02724

- UT1-UT11 INDICATE REGIONS OF POROSITY IN PANEL
- A, B, C, D INDICATE BLADES

85-51799
10E

POST-FAILURE C-SCAN EXAMINATION OF PANEL

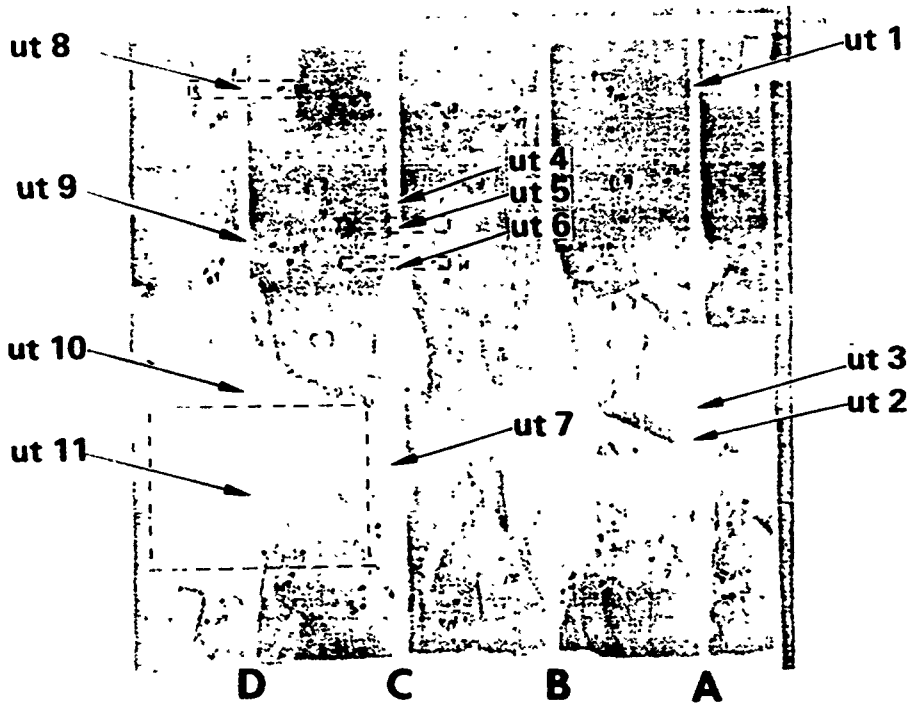

85-02728

- EXTENSIVE DAMAGE TO PANEL DURING COMPRESSION TESTING
- BOXED REGIONS USED TO PERFORM FAILURE ANALYSIS

MACROPHOTOGRAPHS OF SECTIONS OF FAILED TEST PANEL

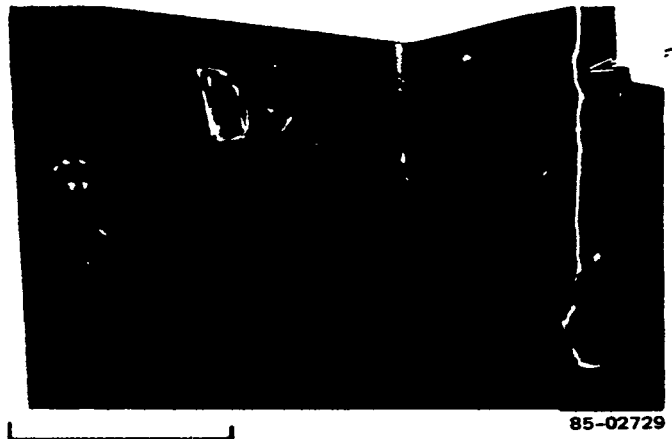

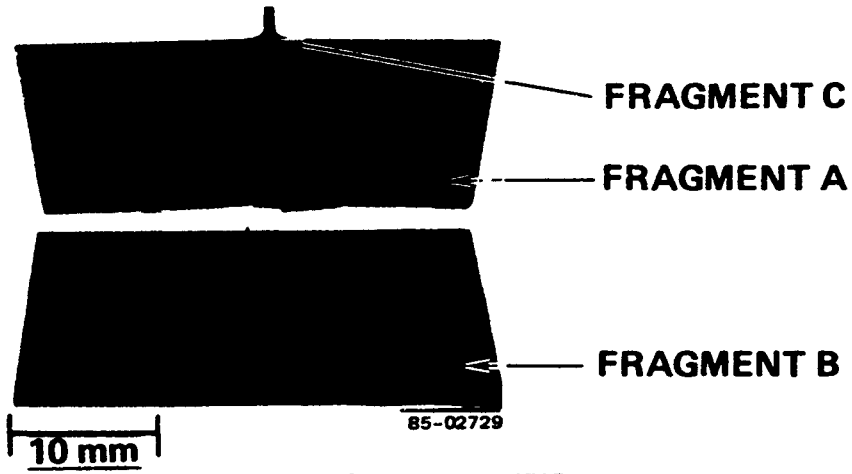

FRACTURE SURFACE FRAGMENTS

85-51801
10E

SEM FRACTURE EXAMINATION OF TEST PANEL

- FRACTURE PROGRESSION MAPPED BY DIRECTION OF "RIVER-PATTERNS" ON EPOXY RESIN

- SEM EXAMINATION INDICATES:
  - FRACTURE INITIATED AT BLADE FILLET REGIONS
  - POROSITY DID NOT PARTICIPATE IN FAILURE

85-51802
10E

OPTICAL METALLOGRAPHY OF TEST PANEL

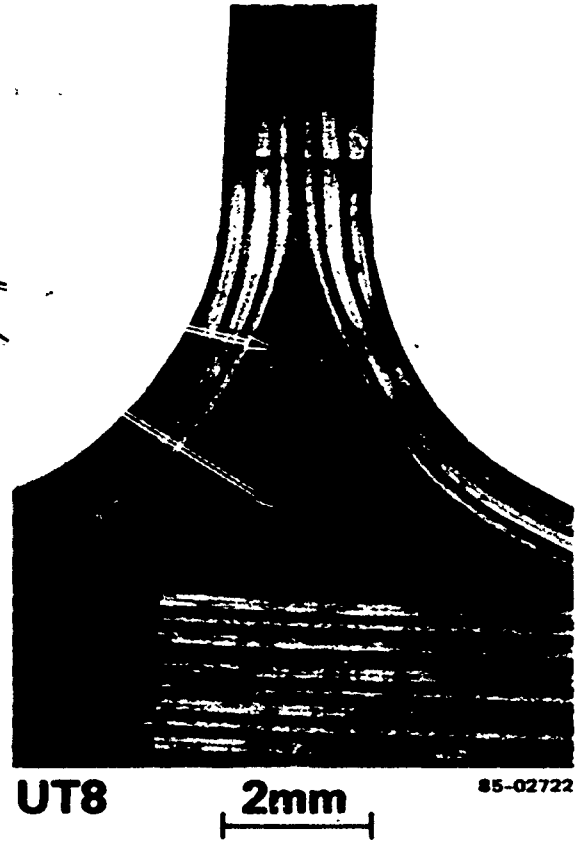

- SECTION TAKEN WELL AWAY FROM PRIMARY FAILURE INDICATES FRACTURE INITIATED AT FILLET
- POROSITY DID NOT CONTRIBUTE TO FAILURE

85-51804
10E

SEM EXAMINATION OF FRAGMENT

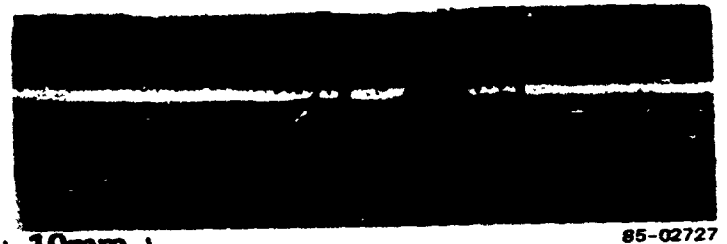

MACRO-PHOTOGRAPH

GENERAL DIRECTION
OF RIVER PATTERNS

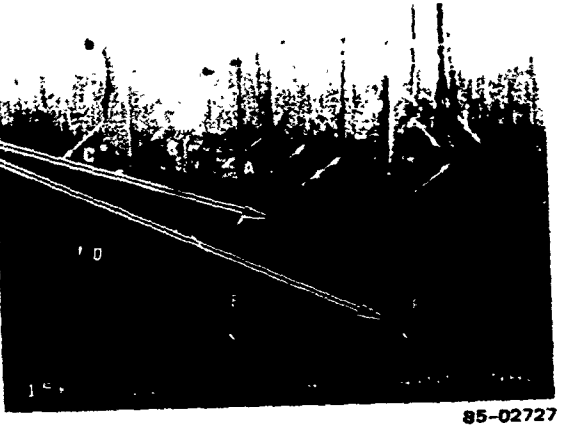

LOW MAGNIFICATION
SEM PHOTOGRAPH

RIVER PATTERNS
ON EPOXY

HIGH MAGNIFICATION
SEM PHOTOGRAPH

23-25

85-51803
10E

SUMMARY

- FRACTURE CHARACTERIZATION OF FIBER/RESIN COMPOSITES CAN BE A CHALLENGE

- FRACTOGRAPHIC FAILURE ANALYSIS OF COMPOSITE STRUCTURES CAN BE SUCCESSFULLY PERFORMED
  - ADEQUATE BACKGROUND INFORMATION
  - ACCESS TO STATE-OF-THE-ART-INSTRUMENTATION
  - "TRAINED" PERSONNEL

85-50631A
10E

COMPOSITE POST FAILURE ANALYSIS EXPERIENCES AS RELATED TO A DEVELOPING AND EVOLVING CPFA METHODOLOGY

B.W. Smith
Boeing Materials Technology
Boeing Commercial Airplane Company
Seattle, Washington

Composite Post-Fracture Analysis Experience As Related To A Developing And Evolving CPFA Methodology

Presented by: Brian W. Smith, Ray A. Grove and Thomas E. Munns

1.0 Introduction

When unanticipated failures occur there is a need to identify the causes and understand the circumstances involved so that improvements in future designs, or appropriate corrective actions can be made which are both effective as well as rationally based. In metallic structures the capability to carry out an accurate failure analysis has been fairly well established since the mid-1950's. Analyses of fractures have been influential in the selection of materials, and identification of critical design details, processes and operating conditions which must be controlled to prevent failures. Currently, composite materials are becoming increasingly competitive with conventional aircraft alloys. As a result, composites are being incorporated into a large number of weight critical aircraft structures. With the expanded use of these materials in major structural applications, the ability to identify the cause(s) of unanticipated failures in both in-service and prototype components is becoming an item of increasing interest. By identifying the sources of such fractures, vital feedback can be given to both designers and engineers thereby guaranteeing improvements in both current and future advanced composite structures.

In this paper, the Boeing Commercial Airplane Company's experience in the development and implementation of a post-failure analysis methodology for composites is reviewed. The following review considers first the fundamental sources from which fracture may occur, thus establishing a basis for developing a logical sequence of investigative steps for performing a failure analysis. Recognizing that a substantial portion of investigations may involve detailed fracture examinations, the following discussions also review Boeing's development efforts in the area of fractography. These capabilities and the aforementioned investigative framework are illustrated in an applied example: the analysis of a fractured box structure. Finally, the current Air Force Failure Analysis program (ref. 1) is reviewed and its relationship to Boeing's established capabilities discussed.

2.0 Sources of Fracture

Determination of the cause(s) of fracture for both in-service and prototype components can represent a relatively complex task. One of the primary sources of this complexity is that fracture may occur from a multitude of diverse causes. Many of the potential sources of fracture can be anticipated based on existing experience with non-composite components with similar designs and end-use applications. The sources of fracture can be grouped into three basic catagories (ref. 1) which are:

1) Design Deficiencies or Material Misapplications. These include inadequate assessment of normal service conditions and the improper selection of materials. In metallic structures, the selection of 7079-T6 aluminum and the later discovery of its susceptability to stress corrosion cracking, represents a classic example within this category. For composite materials, potential causes may include poor design details; oversimplification of loads and load paths; and inadequate assessment of the combined effects of load, environment, and damage.

2) Manufacturing and Process Discrepencies. Typical causes in this group include manufacturing and processing errors. While these processes are controlled by specifications, the complexity of controlling all aspects of manufacturing and inspection are such that out-of-compliance conditions occasionally occur. For composites, these errors may include incomplete cure, use of equipment or materials which do not meet specification requirements, mistakes in layup, and out of tolerance defect conditions such as voids or contaminants.

3) Anomalous Service Conditions. Included in this category are load, environmental, and damage conditions beyond those to be reasonably anticipated in the normal range of part function and use. In many cases, these causes are related to individual operator usages and practices. Examples of fracture causes typical of this group include improper maintenance and repair procedures as well as load conditions associated with use outside the design envelope.

3.0 Post-Failure Investigation Sequence

In carrying out a post-failure analysis, identifying the logical sequence of steps by which to carry out an investigation is often a complex and difficult process. Sufficient information must be gathered and evaluated so that the cause of fracture may be determined from positive supporting evidence rather than simply by a process of elimination. In many instances, the development of a coherent set of positive evidence is often complex since 1) numerous potential cause(s) exist and 2) multiple contributary factors may be involved. In order to accurately identify the cause of fracture, each of these potential causes and their potential contributary factors must be taken into consideration. Identifying the cause of fracture and related contributory factors without examining each and every

conceivable cause requires an organized investigation sequence. Developing this plan of attack is further complicated by the fact that many investigative steps may be destructive to remaining evidence. Consequently, adequate documentation to record existing evidence, as well as the logical flow of information from one analysis to another must be be considered.

In order to assist investigators in developing a logical plan of attack, an organizational framework was developed during Boeing's initial fracture analysis research efforts. This investigative framework was based upon well established procedures utilized in the failure analysis of metallic structures (ref. 2-5). The framework considers each major failure category, potential interrelationships, and the premature destruction of evidence. Because composite materials differ in many respects from metals, the specific operations involved were modified to address those characteristics specific to composites. The final framework developed consists of five basic investigative operations arranged around intermediate decision points. The approach is aimed at simplifying and streamlining the number and complexity of analysis steps involved. The five major investigative operations are:

1) Collection and review of background history and information

2) Nondestructive inspection

3) Evaluation of the part conformity to specified requirements

4) Detailed fractographic examinations

5) Stress analysis

The overall application sequence of these five operations are illustrated in Figure 1. The sequence illustrated is organized in a manner which emphasizes the initial use of simple, inexpensive examinations followed by progressively more detailed analyses at later stages. During the initial stages of investigation, information regarding fabrication, loads, environment, and service history are collected and reviewed. This review is aimed at building a familiarity with the component, its operation, environment, as well as areas of concern. After this initial familiarization, nondestructive inspections are performed. These examinations are aimed at identifying and defining the extent and nature of fracture and documenting it for later reference. This operation generally forms much of the groundwork needed to plan more detailed examinations as well as destructive sectioning. Following this operation, the part is evaluated for conformity to specified drawing, material and process requirements. Each of these initial examinations are directed toward identifying items of significant impact early in the investigative process. Through this feedback, the number of steps can often be minimized and directed towards items of interest.

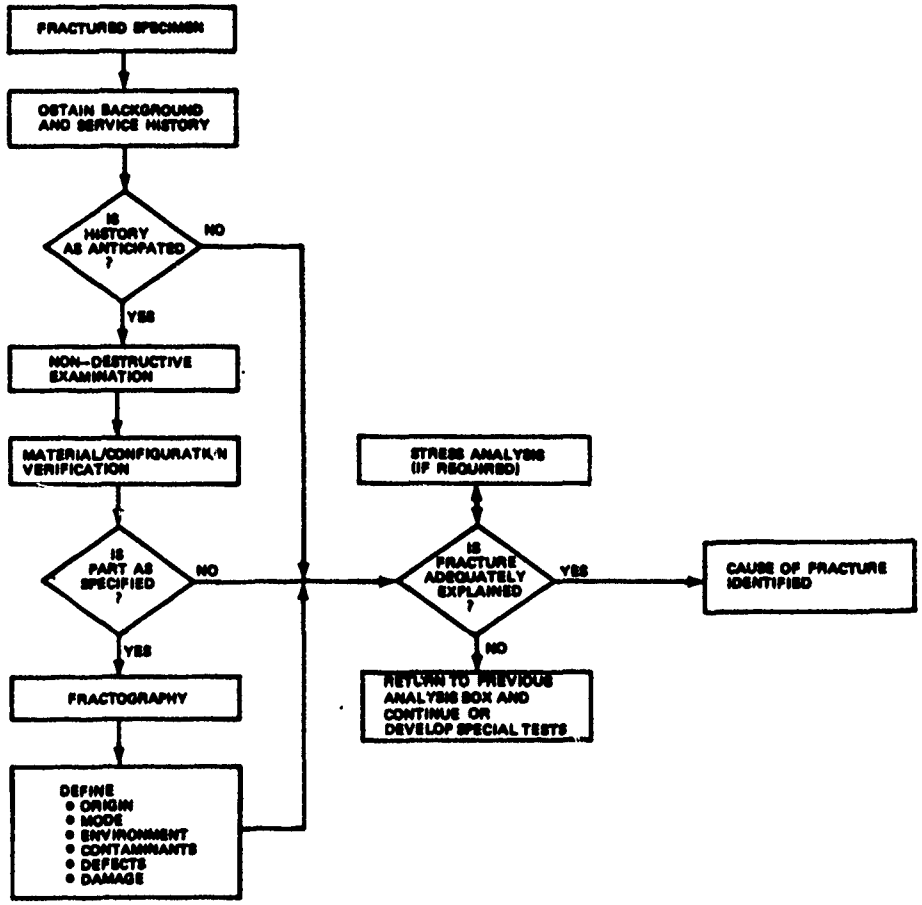

Figure 1. Simplified Investigative Framework

Beyond these initial stages, detailed fractographic and stress examinations usually form the next analysis steps. These operations are aimed at identifying more specific details and assessing their significance. Typically, fractographic examinations are performed prior to detailed stress analyses. Fracture examinations are principally directed toward identifying the specific origin and load conditions involved in failure. In many cases, one of the main benefits of this operation is the identification of defects or anomalies associated with fracture. Through the identification of these factors sufficient information may exist to identify either 1) a specific cause, or 2) a point of interest (i.e., origin) for subsequent analyses. Given this information, stress analyses may be performed to evaluate localized stress states, out-of-compliance conditions, or the criticality of any identified defects. In those cases where questions may remain, additional specialized tests may be required to model indeterminant conditions.

Through internal Boeing experience, a significant amount of detail has been added to the the investigative framework illustrated in Figure 1. This version, shown in Figure 2, establishes a more detailed path for potential investigators. While not fully complete, this flowchart delineates many of the more widely used techniques, usage points, and related decisions involved in carrying out an analysis.

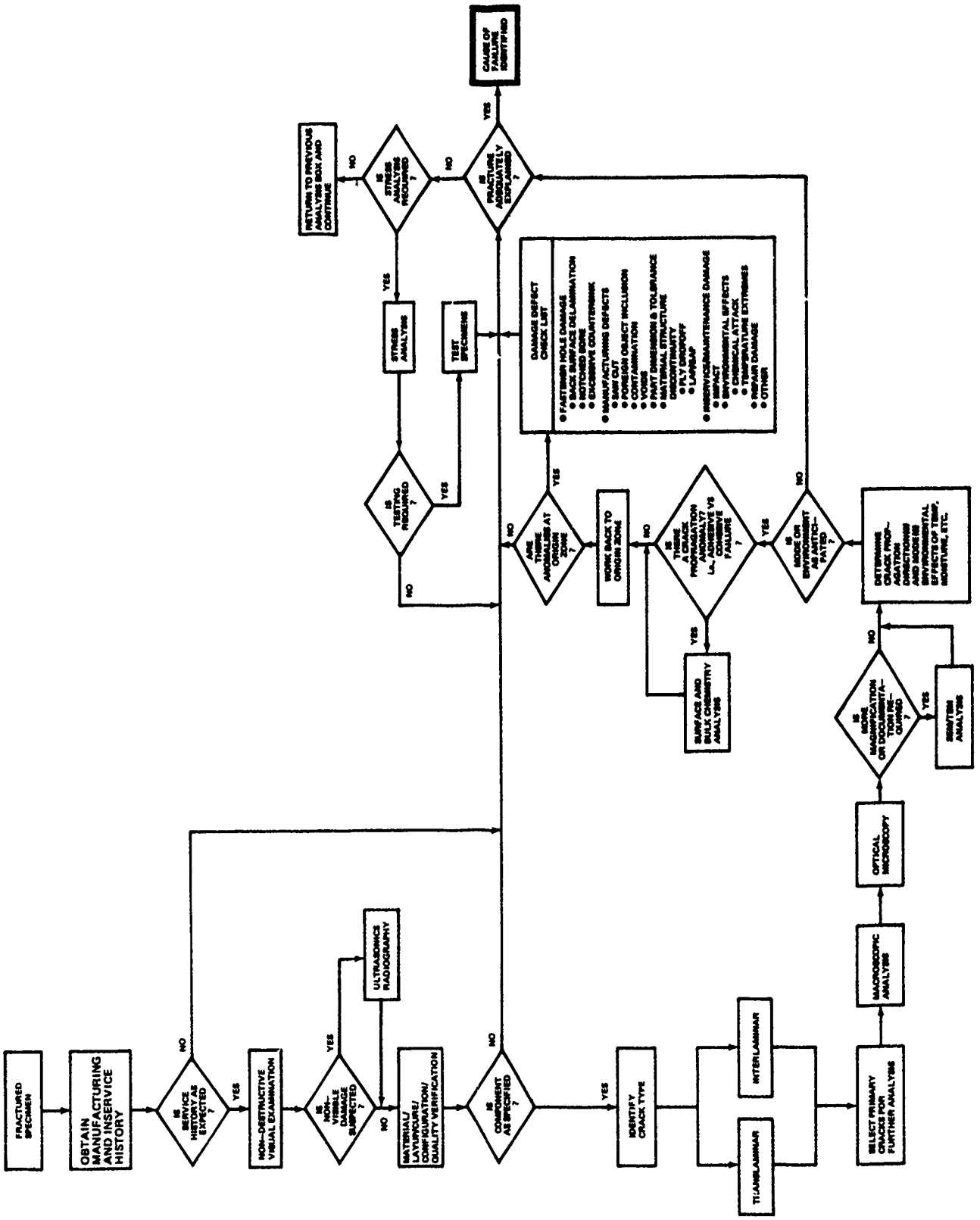

Figure 2. Detailed Investigative Framework

4.0 Fractographic Capability Development

As illustrated in Figure 1, the post-fracture analysis of failed components relies heavily on knowledge gained as a result of detailed fracture surface examinations. Information typically available as a result of such examinations can expedite and directly contribute to the identification of the cause of fracture. However, as a result of the topographical complexity of composite fracture surfaces, the ability to identify significant aspects of fracture has lagged significantly behind other analysis techniques. Consequently, one of the prime objectives of Boeing's fracture analysis program has been to develop fractographic methods applicable to composites in order to identify:

1) the origin location and direction of fracture

2) the load state involved in fracture

Fracture surfaces in composites tend to be relatively complex in appearance. However, two basic fracture modes, translaminar or interlaminar, can be defined based on the orientation of fracture with respect to the laminate. Crack surfaces oriented through the laminate thickness represent translaminar fractures, whereas those occurring within the laminate plane represent interlaminar fractures. Under actual conditions, fractures in composites tend to occur by a combination of both of these fracture types. The classification of fractures into these two categories represents a logical simplifying division. This division is similar to that used in metals where fractures are classified as either transgranular or intergranular.

Interlaminar Fracture (Delamination)

Because of their low in-plane toughness, interlaminar fractures represent a relatively common fracture mode in composite materials. Fractures along this plane typically exhibit both interfacial fiber/matrix separation as well as regions of cohesive resin fracture. These fractures may occur under a wide variety of load conditions ranging from pure tension to pure shear. In the case of fractures generated under pure interlaminar tension, Boeing has found that the overall fracture surface typically exhibits a flat topography consisting of both fiber/matrix separation and cohesive resin fracture. In general, the size and shape of cohesive resin fracture areas tends to be dictated by the cross-ply orientation between which fracture occurs. As illustrated in Figure 3, separation between adjacent 0 degree plies yields long parallel regions of resin fracture. In contrast, fractures produced between 0/90 and +45/-45 interfaces exhibit blockier regions of resin fracture as illustrated in Figures 4 and 5. Upon higher magnification examination, these cohesive resin fracture areas were found to exhibit pronounced river patterns and somewhat more subtle conditions of resin microflow. These features appear similar to river markings and chevron patterns commonly recognized in the fracture of metals and unreinforced polymers. Each of the fractographs illustrated in Figures 3 through 5

were generated on specimens in which the direction of crack propagation was controlled. Examination of these specimens revealed that the coalesence of river patterns and direction of expanding microflow coincides with the local direction of crack propagation. These conditions are particularly well illustrated in Figure 4 where both the direction of microflow and river pattern coalescence are readily apparent. In actual practice, these features have been found to provide a viable means by which to determine the load state, and direction of crack propagation.

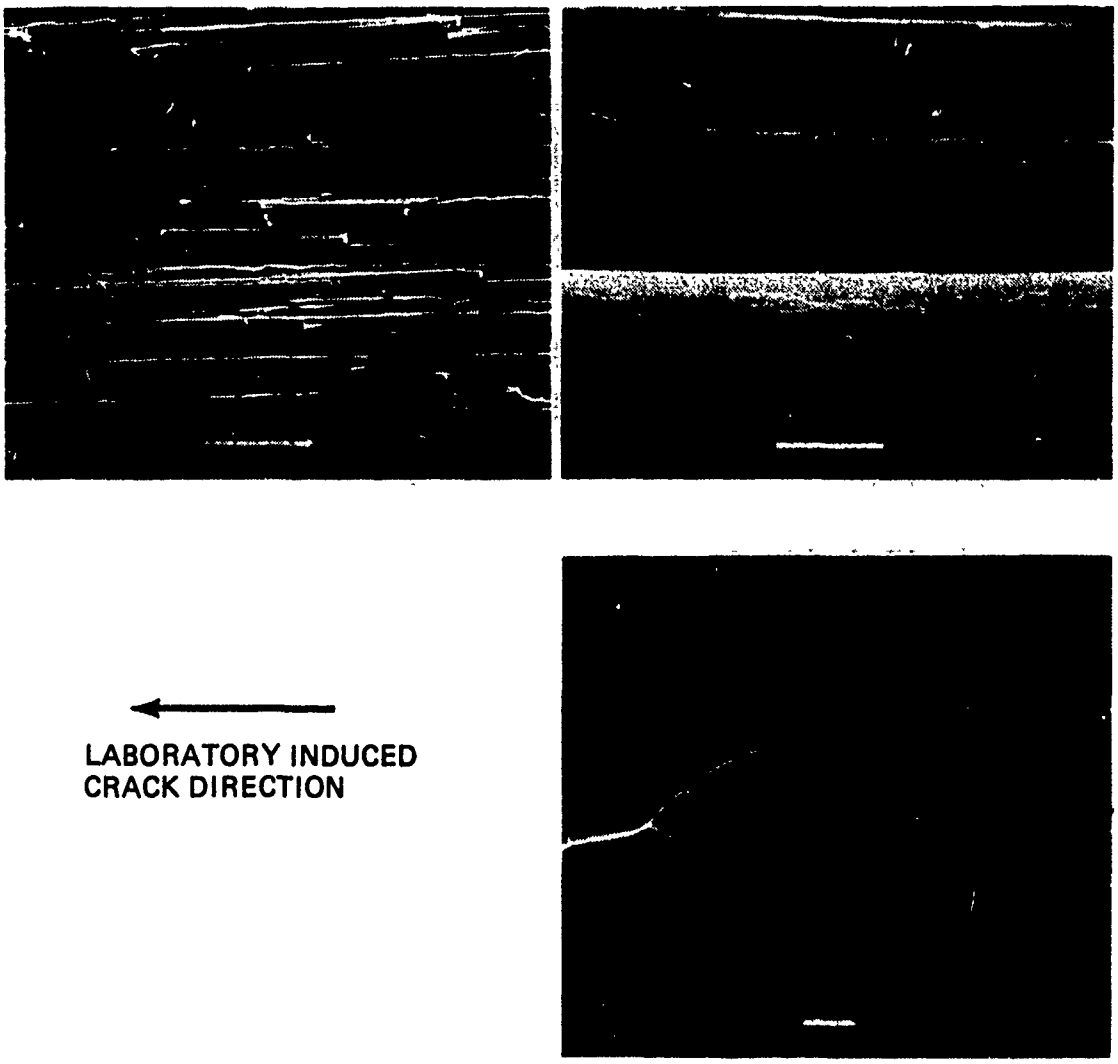

Figure 3. SEM Micrographs of Interlaminar Tension Fractures Between Adjacent 0 Degree Plies

Fractures produced under interlaminar shear conditions can be readily differentiated from tension fractures based on their overall topography. As illustrated in Figure 6, Boeing has found that shear fractures generally exhibit both a greater extent of fiber/matrix separation and rougher cohesive fracture morphology. These differences are perhaps best illustrated in comparing Figures 3 and 6, in which numerous inclined platelets (hackles) of fractured epoxy are visible under shear conditions. While the analysis of these hackles has not been well established, studies within Boeing suggest that their formation occurs through the coalesence of numerous microcracks inclined at approximately 30 to 60 degrees to the fracture plane. This tilt suggests that microcrack formation occurs normal to the resolved tension component of applied shear (ref. 5). As such, the identification of hackles and their tilt has been found to provide a means of identifying fractures generated under shear as well as its orientation with respect to the interlaminar plane (clockwise or counterclockwise).

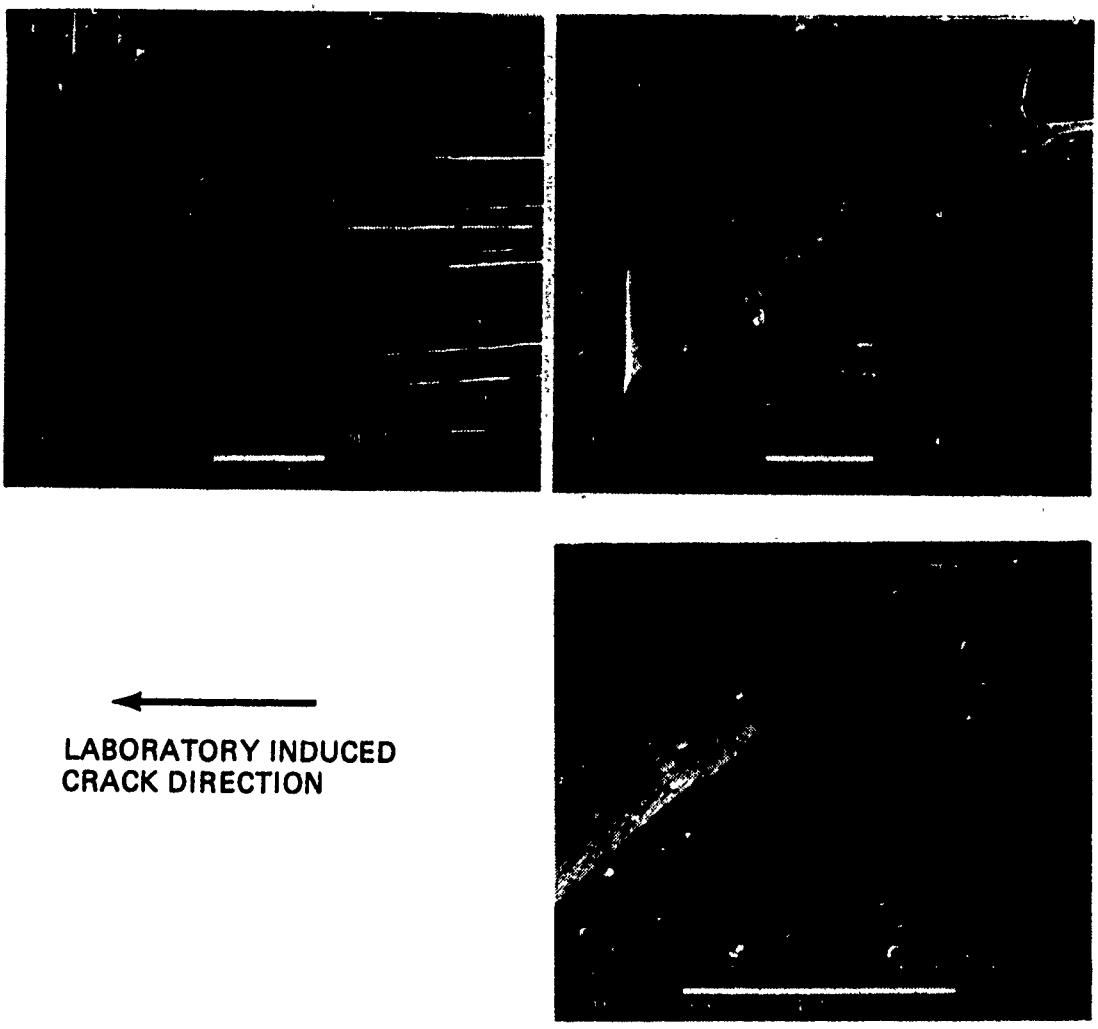

Figure 4. SEM Micrograph of Interlaminar Tension Fracture Between 0 and 90 Degree Plies

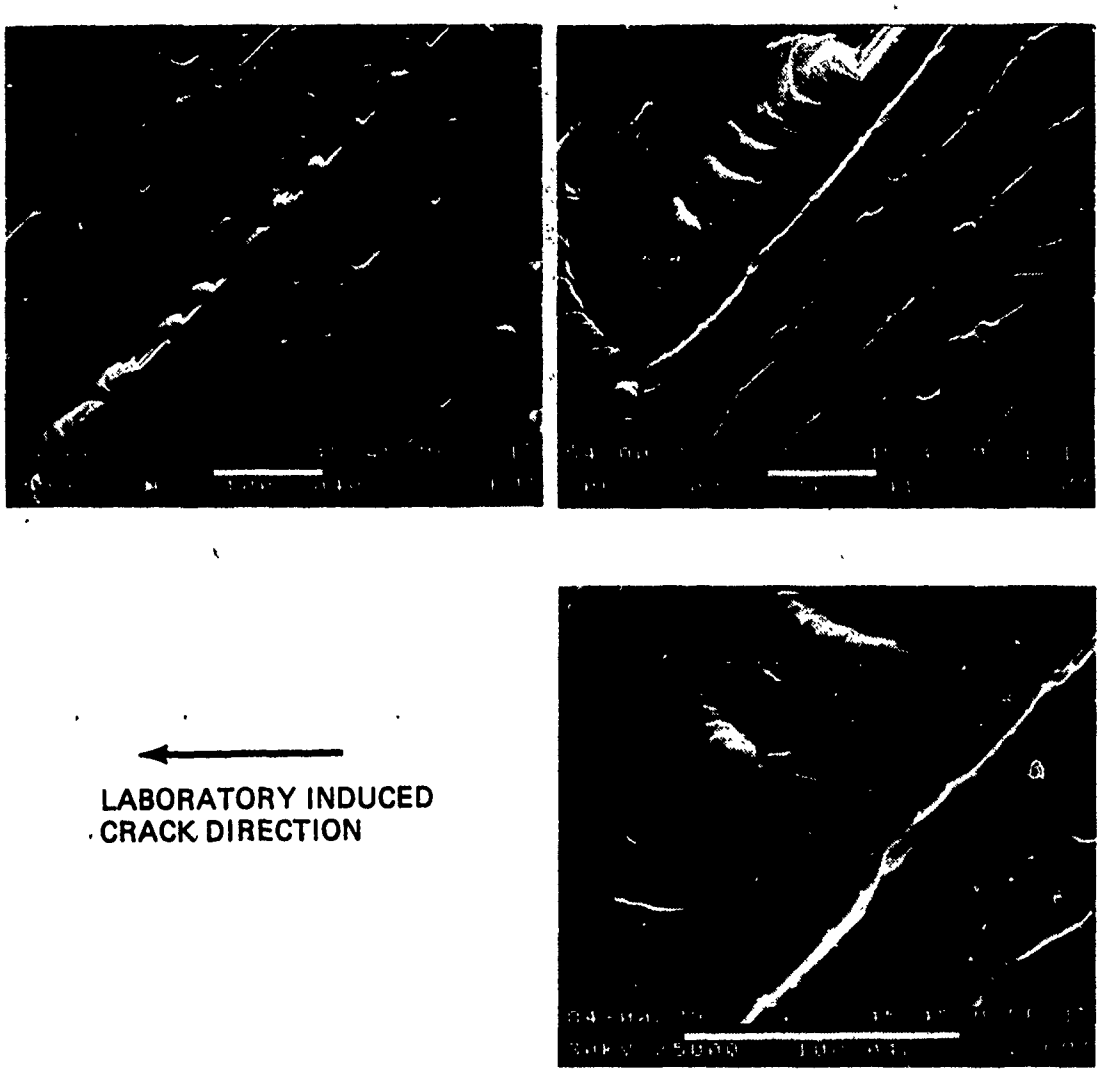

Figure 5. SEM Micrograph of Interlaminar Tension Fracture Between +45 and -45 Degree Plies

The relationship of hackles to the direction of crack propagation under shear loading has been of particular interest within Boeing. When the direction of crack propagation has been controlled, hackles have been found to occur predominantly on one side of the fracture surface (except for fracture between adjacent 0 degree plies) such that the tilt of the majority of hackles coincides with the direction of crack propagation. While a detailed discussion of the mechanism involved in hackle separation is beyond the scope of the current paper, this finding illustrates a positive correlation between hackle tilt and the direction of crack propagation. This finding suggests that hackle orientations may be of potential use in determining crack propagation directions.

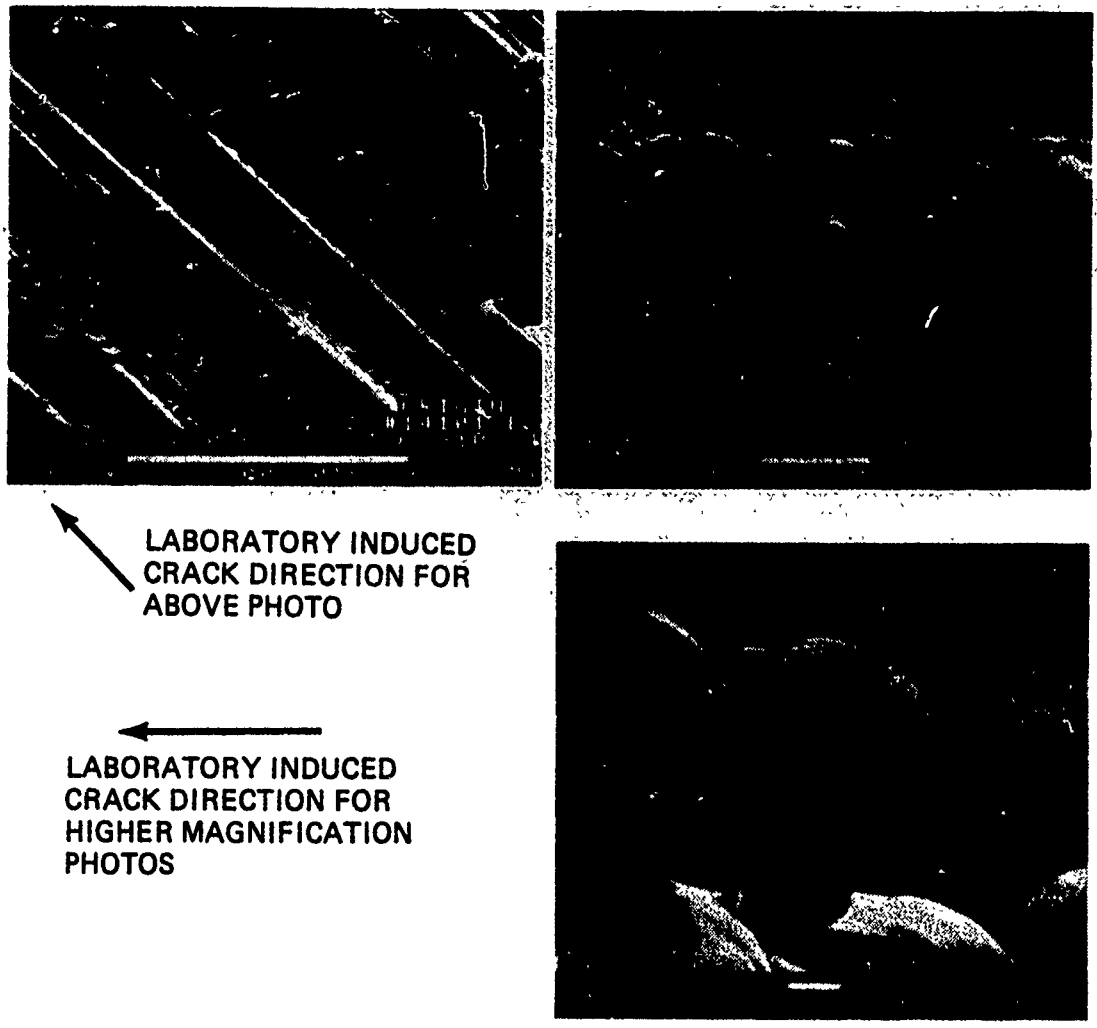

Figure 6. SEM Micrograph of Interlaminar Shear Fracture Between Adjacent 0 Degree Plies

Translaminar Fractures

While interlaminar fractures tend to be relatively planar, translaminar fractures are principally fiber dominated because through-thickness separation involves extensive amounts of transverse fiber fracture. Because of the relatively high toughness of this fracture mode a considerable amount of gross damage typically occurs. As with fractures in metallic structures, this macroscopic damage has been found to generally reflect the condition of imposed load at fracture. In contrast to interlaminar fractures, load states can generally be identified by examining the displacement of each fracture surface and surrounding damage. Typically, fractures produced under tension exhibit significant amounts of fiber pull-out and relatively little surface damage, Figure 7. Compression fractures on the other hand, have been found to typically exhibit gross post-buckling and fracture surface compression damage, as illustrated in Figure 8.

Figure 7. Translaminar Tension Fracture Produced at 70°F, Dry

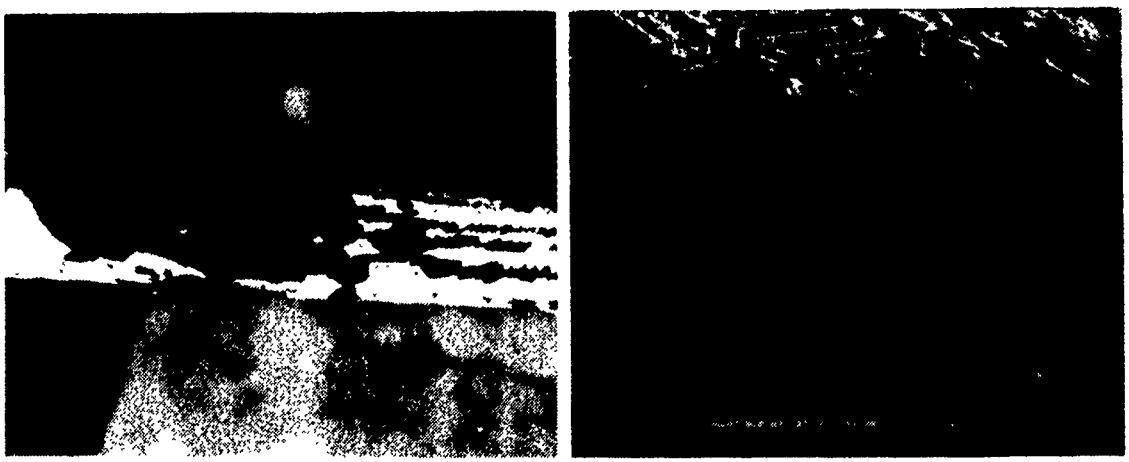

Figure 8. SEM Micrograph of Translaminar Compression Fracture Illustrating Gross Buckling and Fracture Surface Compression Damage

In the case of compression fractures, post-compression damage of the fracture surface (see Figure 8) typically precluded establishing of the direction of crack propagation. On the other hand, fractures produced under tension exhibited a mixture of fiber pull-out, transverse fiber fracture and surrounding matrix fracture. As illustrated in Figure 9, examination of fractured fiber ends typically revealed a radial topography emanating from localized internal defects or adjacent fiber fractures. In most cases, the overall fracture surface topography can be roughly modelled as a set of discontinuous fracture microplanes, each with their own individual origins and crack propagation directions. Examinations carried out on specimens with known directions of cracking revealed that the direction of overall propagation can be determined by mapping the direction of individual fiber fractures, as shown in Figure 10.

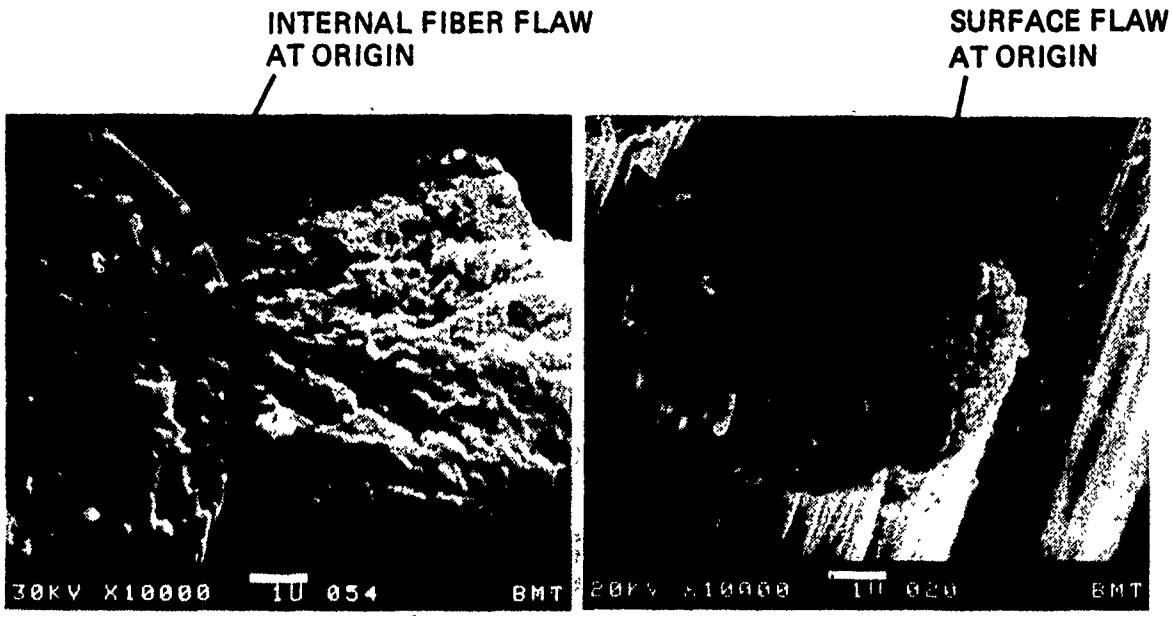

Figure 9. SEM Micrograph Illustrating Radial Topography and Origins

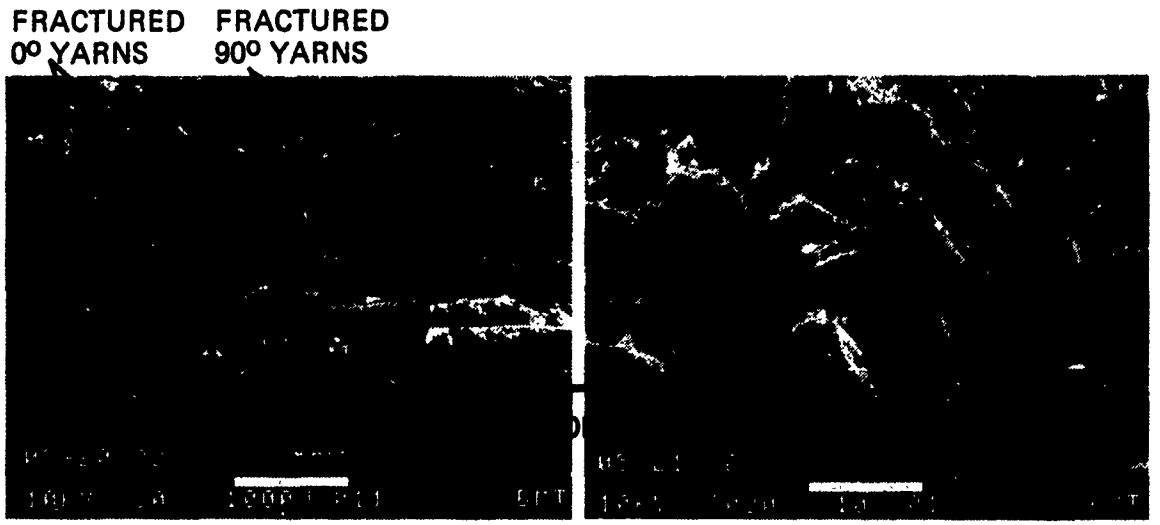

Figure 10. SEM Micrograph Illustrating Direction of Propagation on Each Fiber End

In the above discussions a variety of Boeing's fractographic capabilities have been reviewed. The main intent of these investigations have been to develop the ability to identify the direction and load state under which fracture occurred. As presented, major differences in the load state at fracture (shear versus tension) can be identified for delaminations. Furthermore, for fractures produced under interlaminar tension, the direction of crack propagation can be identified. In the case of interlaminar shear fractures, several features exist by which the direction of crack propagation appear to be identifiable, however, further investigative studies are required to verify the interpretation of these features. With regard to translaminar fractures, the load state at fracture can be identified through the macroscopic appearance of the overall fracture. As discussed, the direction of cracking can be identified for translaminar tension fractures through more detailed examinations. These capabilities provide much of the basic fractographic technology necessary to successfully carry out a post-failure analysis investigation.

5.0 Fracture Analysis Example

At this point it is valuable to examine a typical composite fracture analysis case history. The following example provides a basic illustration of the sequence, procedures and decision processes involved in a typical investigation. In this case, collection and review of background information, nondestructive inspection, materials verification, fractography and stress analysis all contributed to the determination of the cause of fracture.

Figure 11 illustrates a portion of a graphite/epoxy tapered box structure which fractured during test. This graphite/epoxy box consisted of two honeycomb skin panels fastened to a spanwise spar with intermediate chordwise ribs. A review of the test history revealed that premature fracture occurred during hingeline deflection of the front spar, as shown in Figure 11. Initial nondestructive visual inspection of the fractured box revealed through-thickness cracks in the forward and trailing edges of the compression loaded skin panel. Upon further examination, some localized buckling of the skin panel was evident between each of these through-thickness fractures. To define areas of nonvisible damage, i.e. delamination, a nondestructive evaluation was performed utilizing through transmission ultrasonics (TTU). This analysis revealed a roughly four inch wide band of delamination between the areas of through-thickness skin fracture at the front and rear spar.

Following the definition of the type and extent of fracture, tests were performed to determine if any major material discrepancies existed in either fabrication or processing. Accordingly, sections of the skin, spar and rib panels were examined to verify the lay-up and determine the overall panel quality. In addition, thermomechanical analyses (TMA) were performed to verify the extent of cure. Since Boeing uses both 250F and 350F curing prepregs, this analysis was also performed to confirm the specified use of 350F curing prepregs. Dimensions of panel, spar and rib details were also measured and checked against required dimensions and tolerances. For each of these analyses, the spar, ribs, and skin panels were found to be in compliance with the drawing requirements.

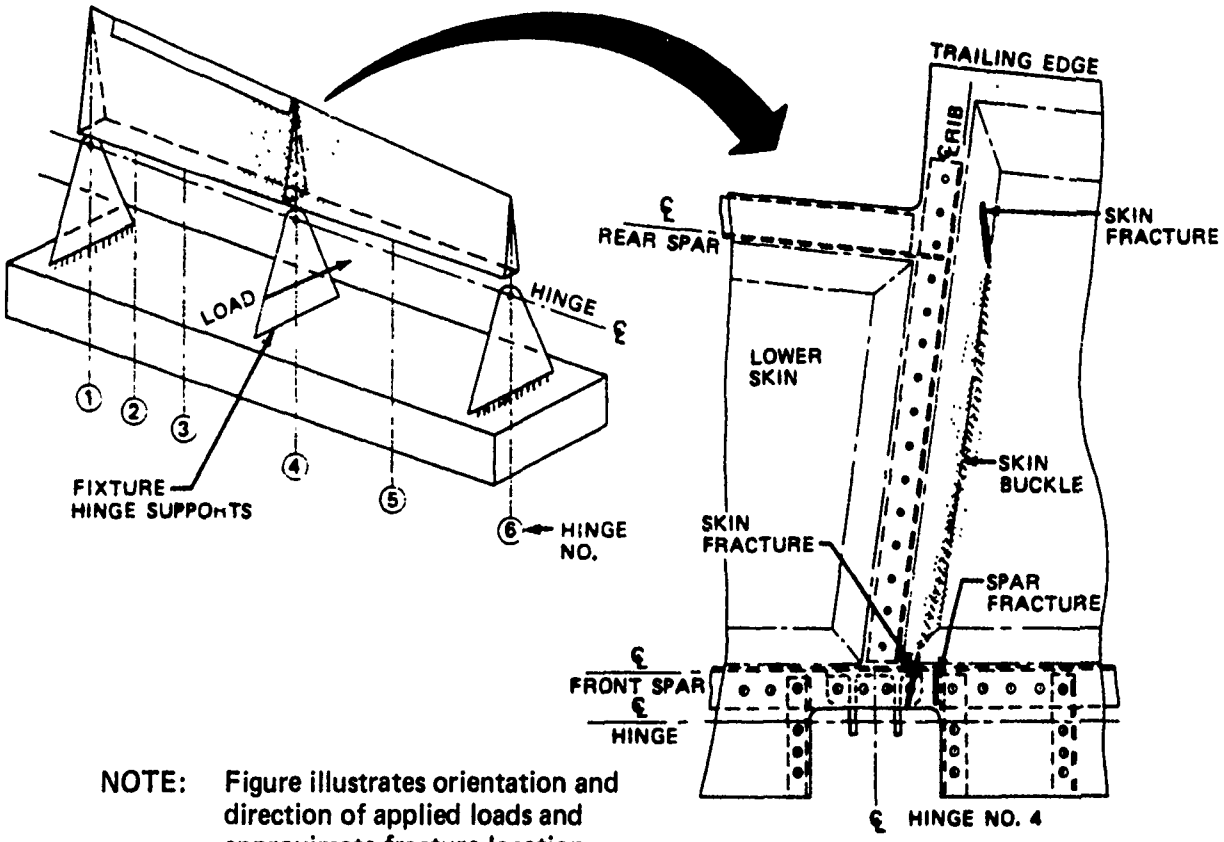

Figure 11. Schematic Illustration of Fractured Component Showing Orientation and Direction of Applied Load and Approximate Fracture Location

Since no discrepancies were identified in the above analyses, fractographic examinations were selected as the next investigative operation (see the framework shown in Figures 1 and 2). Primary emphasis was placed on identifying the direction of crack propagation, origin, and any anomalous conditions that could be associated with fracture. In order to facilitate examination, fractured areas of the panel were sectioned into roughly 6 inch by 6 inch squares and examined optically. These optical examinations were performed at 400X which provided a rapid and efficient means of identifying characteristic fracture features. Scanning electron microscopy (SEM) was performed on selected areas of interest to examine and document specific

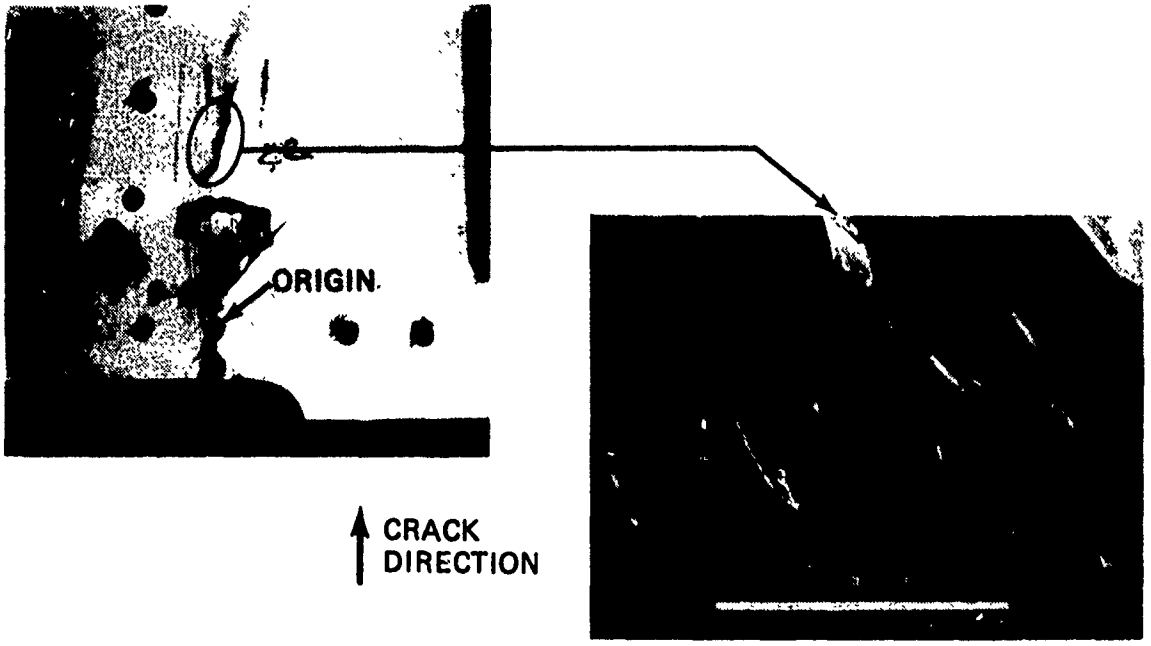

Figure 12. Crack Propagation Direction Identified on Fractured Component

fracture surface features. The orientation of river patterns and resin microflow (Figure 12) observed on the fracture surface generated a map of the local directions of crack propagation over the fracture surface. By reconstructing the fracture process it was discovered that crack initiation occurred at the periphery of a fastener hole located at the front spar. Subsequent propagation occurred chordwise across the compression loaded skin panel. Inasmuch as no anomalies were identified at the origin area which might explain premature fracture, detailed stress analyses of this area were initiated. These analyses evaluated both the basic in-plane panel strains, as well as the buckling stability of the origin area. These analyses revealed that premature skin buckling occurred under compression loading in this area. This unanticipated condition occurred because of the relatively large fastener spacing in this local area. As a result of these analyses, further attention was paid to this design detail and fastener spacing was reduced to prevent the buckling mode that precipitated fracture.

6.0 AF PROGRAM

Currently, Boeing is participating with the Air Force in a program aimed at developing a fracture analysis capability for composite materials. Completion of the investigative tasks and studies involved in this program should provide the specific results, information, and technology necessary to develop and establish three main objectives. These three objectives are:

1) Establish, verify and demonstrate analytical techniques necessary to perform a failure analysis.

2) Define a logical network describing a rational analysis sequence.

3) Establish a compendium containing the above logic network and analytical methods.

The attainment of each of these specific objectives should ultimately provide a capability similar to that which exists for metal structures whereby the causative factors of failure can be accurately determined. This program represents a necessary step to meet a longer term objective of having a widely disseminated handbook.

The subject program consists of five tasks structured around verifying, refining and expanding Boeing's existing capabilities. The fundamental approach of this program is to utilize the framework already developed to identify the techniques necessary to perform a failure analysis. In tasks 1 thru 5 (see Figure 13) these diagnostic techniques will be compiled, reviewed and evaluated for their overall utility and maturity. Techniques requiring further development will be evaluated on specimens failed under controlled conditions in tasks 2 and 3. In these tasks, fractographic results presented within this paper will be used to provide a comparative data base. Based on the results of tasks 1 through 3, Boeing's initial framework will be modified to incorporate additional techniques as appropriate. This information will then be combined into a compendium in task 4, using a format similar to ASM handbook Vol 10 (ref. 2). This compendium will be demonstrated by analyzing three failed composite structures submitted by the Air Force in task 5.

7.0 Summary

In summary, the above discussions have presented several of the salient features of Boeing's experience gained in the development of a post-fracture analysis capability for composite materials. Since the application of fracture analysis techniques to composite materials is relatively recent, these discussions have examined several of the more basic considerations required to accurately determine the cause(s) of fracture.

First, the fundamental sources from which fracture may occur were examined and separated into three basic catagories. Next, a logical framework by which to guide investigators in the evaluation of each of these potential source(s) was established. While other investigative sequences may exist, the framework presented within this paper is organized to give priority to those less costly, simple operations which have the strongest potential impact on the direction and efficiency of later analyses. Since the developed framework relies heavily upon information made available as a result of detailed fracture surface examinations, Boeing has placed primary importance on the evolution of this capability. Accordingly, in the above discussions the salient fractographic features of composite materials have

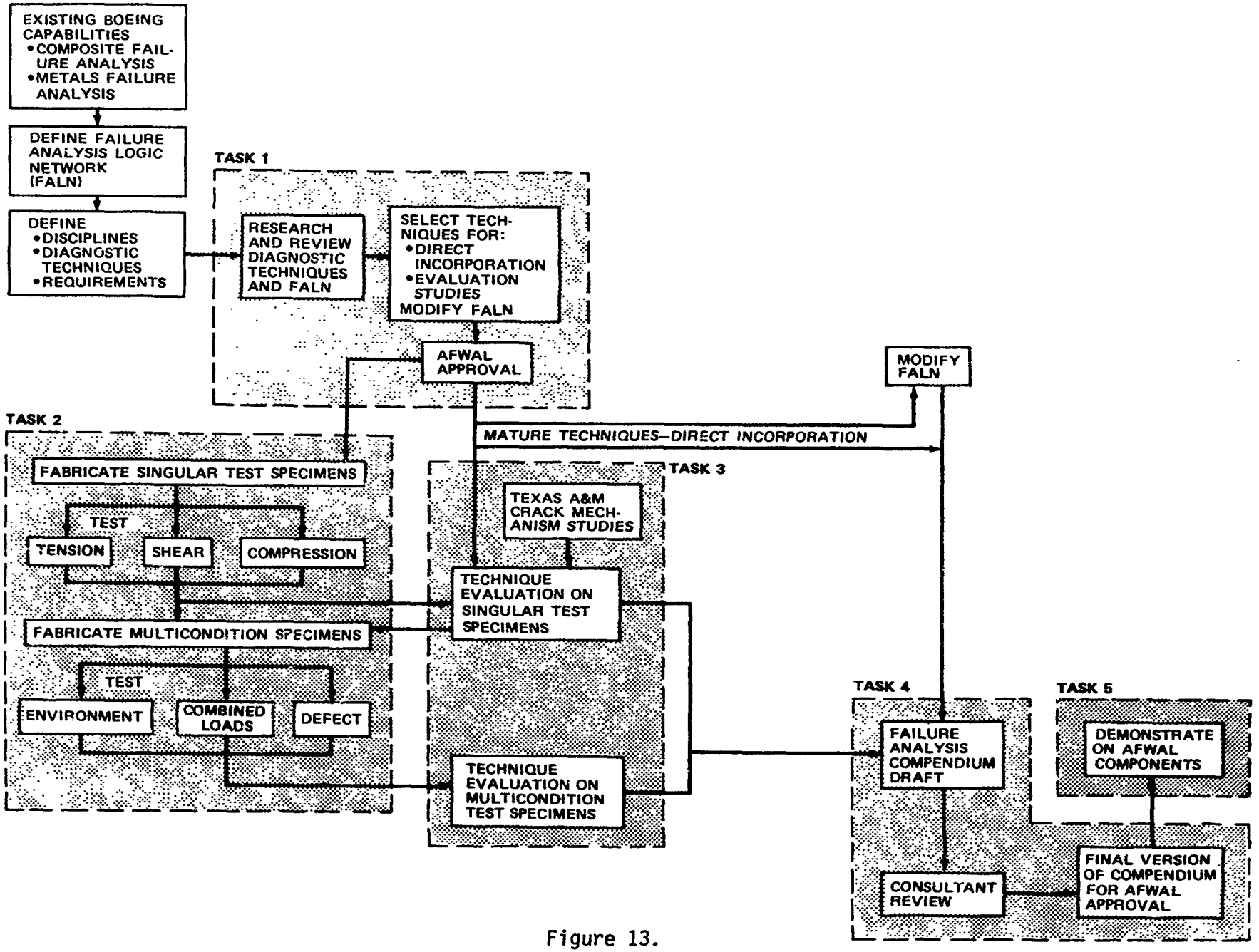
EXISTING BOEING CAPABILITIES
•COMPOSITE FAILURE ANALYSIS
•METALS FAILURE ANALYSIS
DEFINE FAILURE ANALYSIS LOGIC NETWORK (FALN)
DEFINE
•DISCIPLINES
•DIAGNOSTIC TECHNIQUES
•REQUIREMENTS
TASK 1
RESEARCH AND REVIEW DIAGNOSTIC TECHNIQUES AND FALN
SELECT TECHNIQUES FOR:
•DIRECT INCORPORATION
•EVALUATION STUDIES
MODIFY FALN
AFWAL APPROVAL
MODIFY FALN
MATURE TECHNIQUES–DIRECT INCORPORATION
TASK 2
FABRICATE SINGULAR TEST SPECIMENS
TEST
TENSION
SHEAR
COMPRESSION
FABRICATE MULTICONDITION SPECIMENS
TEST
ENVIRONMENT
COMBINED LOADS
DEFECT
TASK 3
TEXAS A&M CRACK MECHANISM STUDIES
TECHNIQUE EVALUATION ON SINGULAR TEST SPECIMENS
TECHNIQUE EVALUATION ON MULTICONDITION TEST SPECIMENS
TASK 4
FAILURE ANALYSIS COMPENDIUM DRAFT
CONSULTANT REVIEW
TASK 5
DEMONSTRATE ON AFWAL COMPONENTS
FINAL VERSION OF COMPENDIUM FOR AFWAL APPROVAL

Figure 13.

been reviewed. Typical results which are discussed include the relationship of specific interlaminar and translaminar features with the direction and load state of fracture. These capabilities, and their relationship with other analytical disciplines were demonstrated in an applied example in which the investigative framework was used to successfully identify the cause of fracture.

Finally, the structure of the current Air Force program, aimed at developing a post-failure analysis capability for composite materials, was presented. Under this program, results described within this paper will be verified, refined and significantly expanded. The resulting compendium and information generated from this program should provide investigators with the capability to determine the cause of fracture for most components. Ultimately, through this capability, vital feedback will be given to engineers and designers concerning the cause(s) of fracture for the continued improvement of composite material structures.

References;

1. "Failure Analysis for Composite Structure Materials," Contract F33615-84-C-5010; Air Force Systems Command, Aeronautical Systems Division/PMR RC, Wright Patterson AFB, 1984.

2. Dolan, T.J., "Analyzing Failures of Metal Components", Metals Engineering Quarterly, Nov. 1972.

3. "Failure Analysis and Prevention", American Society for Metals, Handbook Vol. 10, 1975.

4. Croucher, R.T., "D layed Static Failure", Metals Engineering Quarterly, Nov. 1964.

5. Ogden, P., "Case Histories of Materials Failure", Metals Progress, July 1963.

ATTENDEE RESPONSE TO THE QUESTION: What activities should the Air Force support to accelerate the maturation of the CPFA methodology?

DESCRIPTION OF THE ATTENDEE PARTICIPATION SESSION

Description of Attendee Participation Session

The final session of the conference was organized to provide the attendees an opportunity to; 1) respond to the question "What activities should the Air Force support to accelerate the maturation of the Composites Post Failure Analysis methodology?", and 2) address any other issues they considered germaine to the overall conference subject matter. Moderator of this session was Mr. Frank Fechek. He was assisted by a panel comprised of: Mr. Theodore Reinhart, Chief, Materials Engineering Branch, and Mr. Thomas Cooper, Chief, Materials Integrity Branch, both within the Systems Support Division of the Materials Laboratory, Air Force Wright Aeronautical Laboratories, and Mr. Joseph Tilson, Flight Safety Engineer, U. S. Air Force Inspection and Safety Center, Norton Air Force Base, California.

A tape recording was made of the discussions which occurred during this session. The transcript, produced from this recording, has been edited by the session moderator in an attempt to condense the information presented into a reasonable length text. Some of the shorter comments have been quoted verbatim. Concerning those longer comments which have been condensed, the moderator wishes to apologize to any of those participants whose comments or ideas he may have misinterpreted, either in content or emphasis.

An executive summary of this edited transcript has also been composed which contains the session chairman's tabulation of those topics and comments he considered significant along with his interpretation of attendee consensus and/or conclusions.

EXECUTIVE SUMMARY OF EDITED TRANSCRIPT OF ATTENDEE PARTICIPATION SESSION

EXECUTIVE SUMMARY OF EDITED TRANSCRIPT OF ATTENDEE PARTICIPATION SESSION

The overall objective of this meeting was summarized to the attendees by Mr. Frank Fechek, the session chairman. He stated that it was organized to provide an open forum for the presentation of composite post failure analysis concepts, research work results, and in-the-field experiences related to the technology of conducting a post failure analysis on a composite structure.

It was his observation that the meeting succeeded in its objective to provide a forum for the open exchange of information among a diverse, broad cross section of the international technical community. The attendee organizational representation was 35% industry, 49% government and 16% academia. Twenty nine percent of the formal presentations were authored outside the United States and 14% of the attendees represented eight countries other than the host nation.

He stated that the presented papers also covered a broad spectrum, from analytical predictive techniques for composite behavior, through testing technique development and controlled environmental exposure and the study of its effect, to the descriptions of ongoing programs aimed at laying the groundwork upon which this technology will be able to grow.

The major issues, observations and comments by the attendees during this session are listed below:

WHAT IS A COMPOSITES POST FAILURE ANALYST? Since many of the papers contained data on composite fractures obtained by a fractographer using a scanning electron microscope, and many of the attendees were experienced metallurgists, the question arose as to the role of the fractographer in deciding how and why a structure had failed. Whereas some thought he should only decide if the failure was a result of static overload or fatigue, others stated he should be (and in fact is, in many organizations) an interdisciplinary coordinator of selected specialists. Much emphasis was placed, during these discussions, upon the role of the stress analyst. It was generally concluded that many specialists might be required to participate in a composite post failure analysis, (CPFA), depending upon the circumstances. Many agreed that the stress department should be brought into a CPFA early to assure that the customer received all the information and data he required. The point was very well made that failure analysis is a service function which merely provides information to the person (organization) which makes policy decisions; i.e., ground the aircraft, replace, modify, etc., and this customer often has information and data about the incident not available to the composite failure analyst.

WHAT WORK YET REMAINS TO BE DONE? Some of the attendees observed that the impression was being given that CPFA was in its infancy, whereas in fact there had been considerable work done during the past twenty years. However, these past efforts resulting in considerable experience had not been coordinated very well. The Air Force representative described their attempt, in the mid-seventies, to develop a composites fractography handbook, which had not resulted in anything significant because the technology at that time was not sufficiently mature.

There was considerable discussion as to the applicability of simple versus complex specimens or structures to develop this technology. Most agreed that it would be appropriate to follow the historical precedent of metals where data was obtained from simple fractures, obtained under controlled conditions regarding fracture mode, direction and environment. Additional work on more realistic structures exposed to realistic environments prior to failure is needed, however.

Other observations were, in any follow-on work, additional fundamental work, i.e. in fatigue, fatigue spectrum effects, material types, environmental effects, etc., should be emphasized. If we could better understand these effects, now, it would reduce the requirement for "involved" testing for certification, etc., in the future. Cyclic loading, superimposed on fixed stressed specimens, would contribute to developing a data base for propulsion applications. Instructions and information for the in-the-field personnel on what to do and what is significant are needed.

THE CURRENT AIR FORCE PROGRAM. Most observed that the current program is taking a proper approach, that being one of developing the fundamental fracture characteristics using the building-block approach, i.e. first failing simple specimens under controlled conditions prior to proceeding to more complex configurations and conditions. The attendees thought that the program product, a "compendium" of information describing the techniques applicable to conducting a CPFA along with information of the significance of fracture characteristics, will be a useful document, especially to those metallurgists being "converted" into the field of composites failure analysis.

COMMENTS ABOUT THIS MEETING. The comments were varied. Many appreciated the opportunity to mix with technologists of very varied perspectives. They thought that this meeting was a necessary start to getting this needed technology developed. Some were disappointed that the emphasis was so great on fractography and that other problems and techniques were not addressed. It was explained that the meeting philosophy was not to address those techniques which are already quite adequately developed (chemical characterization, material property measurements, etc.) or disciplines which already had an established forum for information exchange (micromechanics, stress analysis, etc.). The in-the-field people expressed some frustration that their esoteric problems were not sufficiently addressed, either as reported solutions, or even as problems to be solved.

CONCERNS OF THOSE WHO WORK IN-THE-FIELD. These people were disappointed that it appeared that the technology was not yet mature enough to give them the help they want. They were impressed with the fundamental data which was presented but were seeking a document which would tell them how to decide what kind of failure they were observing and what to do with the physical evidence. They expressed a need for an in-the-field-usable "one x" magnification technology to obtain significant failure mode information. They also stated they do not know what data is available or even where to go to find the experts who might have the information they need. They recommended that such information as is available should be incorporated into revisions of documents such as the FAA Advisory Circular 20-107.

T concluded that perhaps the field investigators from the military safety rs, the ALC's, the NTSB, the FAA and the airframe manufacturers should get together, define their common problems, collect and coordinate their experience base, and then bring that to the research community for confirmation and verfication.

TRAINING. It seems that those companies who build and fly the parts are more motivated to develop inhouse capabilities than others, and they have done so. Meanwhile, the others are relatively helpless. A need exists for a mechanism to conduct appropriate training. In some of the schools which train the accident investigators, etc., they get a smattering of composite information. They need more.

INFORMATION DISSEMINATION. There are lots of technical societies. Each seems to be incorporating a bit of this information in their activities. How do we coordinate this technology with (through) them so we know where to look for the information which we need? Since some people can have only limited access to society meetings (and, often, the in-the-field people can have no access at all to the fundamental, scientific activities), this proliferation of dissemination vehicles is beginning to create an awkward situation.

One comment was made describing that the ASM has decided to produce and publish a new series of documents on "engineered materials", the first of which will address composites. It should contain some post failure analysis information and is scheduled for publication in November, 1987.

A HANDBOOK. This question was put to the attendees, "Are we ready for a handbook yet?" The replies were varied. They were; "The technology is not ready to give a cookbook of 'truths' to the person in-the-field about CPFA"..... "It is premature at this time, we have to understand the fundamentals before you write the 'Bible'".---"If you do not understand the fundamentals, you will not be successful at 'one x'"---Not ready yet for a handbook. Many techniques ought yet to be evaluated".

A philosophical statement was offered: There seems to be two approaches. 1) study specimens failed under controlled conditions, and 2) study real-life events. Both take time---and dedicated, intuitive people. Perhaps this process cannot be accelerated.

But the other side of the issue was also expressed: "There is considerable experience out there. Several companies, both in the United States, and overseas, have already established quite experienced composite failure analysis organizations."

The final appropriate statement seemed to be this one: "You can do three things when faced with any situation-- The right thing, the wrong thing, or nothing at all. If you do the right thing, you solve the problem. If you do the wrong thing, you stimulate others to tell you where you are wrong, and to then, themselves, address the problem, and perhaps, solve it. If you do nothing at all, no progress is made. Thus better a bad 'strawman' document now than no handbook at all."

COMPLETE TRANSCRIPT OF ATTENDEE PARTICIPATION SESSION

COMPLETE TRANSCRIPT OF ATTENDEE PARTICIPATION SESSION:

"International Conference: Post Failure Analysis of Fiber Reinforced Composites"

Stouffers Dayton Plaza

1-3 July 1985

Frank Fechek, Session Chairman, AFWAL: Before I open this session for your first question or comment, I would like to restate the objective we had in organizing this meeting, our plan for the formal, presentation portion of it, and what we have hoped to gain from it. Our objective was to provide an open forum presenting your post failure analysis concepts, research work results, and in-the-field experiences related to the technology of conducting a post failure analysis on a composite structure. The meeting has been planned as an international, open meeting in order to encourage a maximum amount of information exchange among as diverse a technical community as possible. Toward this end, in reviewing the attendance list, I find that we have had 14% of the attendees represent eight countries other than the United States. The attendee organizational representation has been 35% industry, 49% government and 16% academia. I think the formal portion of the program, composed of 7 papers out of 24 being authored outside the United States, demonstrated a fine participation by the international technical community. The breakdown of these papers, by organization of origin, was 42% industry, 4% government and 42% academia. This also represents a reasonable proportion of participation by the technical community. However, enough of the numbers.

You have heard in these presentations topics covering the spectrum from analytical predictive techniques for composite behavior, through testing techniques development and controlled environmental exposure and its effects, to the descriptions of ongoing programs aimed at laying the groundwork upon which this technology will be able to grow.

In the final paper on the program you received a progress report of an ongoing program the Materials Laboratory is sponsoring, which will culminate in a verification of the post failure analysis logic network being developed, and the publication of a composites post failure analysis compendium. We envision this document will be the initial primer in this area, and will contain descriptions of which techniques are applicable for conducting a post failure analysis, suggested logic paths to follow in order to conduct a CPFA to a successful conclusion using a minimum of resources, and some examples of CPFA's which have been conducted.

So, this brings us to the end of the formal part of this meeting and into the informal portion, which we have structured to provide everybody with an opportunity to provide us with your input so we might intelligently proceed with our future plans. We, in our longer term planning, have set aside some funds for a follow-on program to take the output of the Boeing program and grow it into a more specific guide and eventually a handbook. So, the major reason we are here this morning is to receive your input based upon what you know from your past experiences and what you have heard from others' experiences in the last two and one half days and to have you advise us on what efforts we should point ourselves toward, define and fund, so that we might make our follow-on program more meaningful in a timely fashion to your needs. I am hoping that we will get some inputs from all the categories; the theoretical, the research, the applied laboratory and from those people in the field who have to go out and pick up the pieces of failed parts.

Our eventual objective is to be able to provide good counseling to the aircraft owner. So, the purpose of this question which I put in our original preliminary agenda is to have you feed us your response. To help me in responding to your comments or questions, we have up here at the table on my far left, Mr. Ted Reinhart, who is our Branch Chief in the Systems Support Division, Materials Engineering Branch. His responsibilities are to transfer the technology and also develop some of the applied technology which will help us in what we call our supportability efforts for the composite technology to our users. On his right is Mr. Tom Cooper, he is the branch chief of our Materials Integrity Branch and the people in his organization will be expected to have the inhouse capabilities to take a composite "cadaver" and work backward using whatever techniques are necessary, to define the cause of failure under whatever the circumstances might have been. Last on our panel is Mr. Joe Tilson from the Air Force Safety office at Norton Air Force Base. He has a lot of input into defining, h· Air Force regulation and our regulation documents, what procedures the Air Force personnel must go through when they go on an accident investigation. In a lot of respects we are going to depend upon his inputs to provide them with good guidance when there are composites involved. So, with that, I would like to open this session to any questions and comments which you have. Please use the microphones as we are attempting to record these happenings so we may more precisely summarize them as a part of our proceedings. I am open for questions or comments.

SAM DASTIN, GRUMMAN AIRCRAFT COMPANY: (edited) I believe in every new science there is an audience who can see the thrust and give compliments to the originator, but they will also provide one or two negative comments. Although I must admit that everything I saw was both very scientific and necessary, I believe it might be misleading as well. I saw expert fractographers trying to do a failure analysis, where materials characteristics, processing procedures, and stress analyses may have contributed to the cause of failure, and then trying to interpret which, or which combination, of these was causal. I think the fractographer has but one job, to decide if the fracture was static overload or fatigue, and other experts in his organization should address those other disciplines. I also think there should be a greater emphasis on failures in real structures, where the loads and loading modes are more realistic, and perhaps more complex. It would be beneficial to show pictures of such failures, annotating them with the load at failure, design margin of safety, assumptions of the structural analysis, etc. This would be helpful for a fractographer who would be looking at failed test elements of structural components of advanced systems concepts.

TED REINHART, AFWAL: (edited) I heard it differently. What I heard today was that composites post failure analysis is really an interdisciplinary activity and you bring in everybody, and no one individual says that this is exactly what happened.

SAM DASTIN, GRUMMAN AIRCRAFT COMPANY: (edited) But I feel you need a structural analyst, from the stress office, in the decision making loop, and I didn't hear about him in the description of the Boeing program.

BRIAN SMITH, BOEING AIRCRAFT COMPANY: (edited) Well, I have to agree to a certain extent. At Boeing, our practice is that the fractographer tends to be a sort of interdisciplinary coordinator. He tends to handle the fractography, the

materials characterization, and identification of defects and unidentified service conditions and those kinds of things. If he can identify them from the part, he does. Generally, within our company, we do, in fact, call in the stress group, because airplane parts tend to be complex, so, Sam, you are right in that regard. The stress analysis is done by a specific group of individuals experienced in that technology, and in the aircraft industry, by and large, stress analysis is, I'll go ahead and admit it, is too complex for a single individual who is not aware of the intricacies of that component to carry out. So, in this program, what we are planning to do is to review at what point in a failure analysis investigation is stress analysis appropriate to fit in with the investigative sequence that I have shown here and what are the procedures that are commonly utilized. We feel that an analysis of a failed part requires too much knowledge for a fractographer, or a general analyst like myself, to carry out a stress analysis. For this to happen one has to understand all the loads involved in the part, and this requires a specialist. We are not proposing, in this program, to bring in a person and really expand that section, and thus provide a document which tells an analyst like myself how to do a stress analysis. We are telling him, instead, when do you ask for stress analysis help, what you are going to get out of it, what types of techniques are available, and the primary reason that we are not including a stress analysis person into this program is that, the program is not sufficiently financially scoped to bring that kind of technology into the program. I do feel strongly that a follow-on program in that area makes a lot of sense, especially if we feel that we will be asking the analyst, like myself, to do some rudimentary stress analyses. If the decision of the board and the other people here is that that really belongs in a stress analysis group, as it does in my company and perhaps in your company, then maybe we'll decide that just an overview and a presentation of the techniques is adequate.

SAM DASTIN, GRUMMAN AIRCRAFT COMPANY: (edited) Say, looking through the stress analyst's eyes, if he is not brought in early and becomes part of the data gathering activity, when the "negotiation" between the failure analysts and the stress analysts take place, the latter may be harder to convince. And his endorsement is necessary, because my company, and probably yours, will not send a report of findings to the customer (in this case, the Air Force) without the stress department's endorsement. But even if this were not the case, the customer wants the stress department's opinion, so they may as well be involved early in every post failure analysis investigation.

I would summarize by saying--continue to do the academic work, train us to be smarter in the future, but, simultaneously, do the practical things necessary so we'll have realistic data on today's structures failed under realistic conditions.

BRIAN SMITH, BOEING AIRCRAFT COMPANY: I guess I have one comment and that is, in regards to fractography, typically, in metals and other systems, the approach in fractography is to start with, if you will, the academic fractures, the ones you can control and you know what is going on, and try to describe those features. In metals, you know, there was quite a bit of hasseling around a few years ago on those features. But it is from that singular failure mode geometry, if you will, the MODE I, MODE II, that we established the basis by which to approach the more complex failures. In this particular program, starting this next month, we will be starting to look at more complex multi-mode failures, and as the program flow chart indicated, will eventually be looking at three failed components. I feel in agreement with you, that stress analysis needs to be built into this program and looked at a little more closely. At this point, I almost feel that that is worthy of a separate effort.

SAM DASTIN, GRUMMAN AIRCRAFT COMPANY: But to try to use a stress analysis that is now used for aircraft parts, not a new one.

BRIAN SMITH: Yes, how to tie it in.

TED REINHART: I think we ought to go on to the next question.

HOWARD HEINEKE, GENERAL ELECTRIC, EVENDALE, OHIO: I've got to have some sympathy for what he says, but it is the job of the failure analyst to identify discrepancies, if they exist, but nevertheless, we in the engine business at General Electric, are kind of new to the business of a failure analysis of composites, and we are just learning to crawl. We haven't yet learned to walk. But we have started an exploratory program, with IR and D money, with similar aims as Boeing's. But, to address some of the things that Sam was saying, but for my customer, who is the design engineer, and is usually concerned as to whether it is an overload or a cyclic failure, our problems really come into play in trying to recognize and understand the character of the evidence of, in terms I don't like, i.e. high cycle fatigue, low cycle fatigue. I prefer low stress fatigue and high stress fatigue, in those terms, but also, what he refers to as sustained peak low cycle fatigue, that is, high strain fatigue with a sustained hold time on it. I don't know that this is addressed in these programs I have seen today. I'm not sure that these products are intended for that type of application. They may be and I think that Sam is hinting at that. They are stretching on, extending on the limits of how these products are employed and we may have to look at such things as hold time and high stress fatigue.

TED REINHART: Did I understand you are saying, more like spectrum fatigue? Some of the Falstaff and some of the other fatigue programs we are using?

HOWARD HEINEKE: I am not sure what you are referring to, but we employ complex loading where we impose, say, a vibratory load on a sustained, steady state load.

TED REINHART: Yes, this is exactly what I am talking about. You have your landings, your takeoffs, your flight gusting, yes, and you go through that cycle,, yes, hey, that is a good idea, it is something that could be built in...thank you.

DICK BAKER, DENVER OFFICE, NATIONAL TRANSPORTATION SAFETY BOARD: I guess I am the ranking employee here of the NTSB, so I thought it would be beholden upon me to say thank you for the invitation to this seminar which has been over my head much of the time and I think I speak for them too, when I say it was over their heads most of the time. But we did pick up words and ideas and things like hackles, and hackles and hackles. One thing I would like to say is that we have been looking from our standpoint of accident investigations and failures and the gentleman was talking a little while ago about failures, static, or stress failure, or overload, as we call it, or fatigue, and we are still interested in that sort of thing. Composites are something new. I have to stop and think of the word to use it. But they are coming. And, we are going to be looking at those too, from a standpoint of fatigue or overload, and therefore I look forward to this manual that you're are putting out. Maybe NTSB can get a copy of it, but I would like to be able to get a look at it from a standpoint of, am I looking at a stress failure or am I looking at fatigue...and we will look forward to that manual in the future. Again, thank you for the invitation.

TED REINHART: Dick, I thank you for the comment. There's one thing I wanted to talk about and maybe this is a good time to do it. It was mentioned that the field inspector, and some Air Force guys, also, who are going to need some training. It is going to be a little different kind of training than we are talking about for the fractography experts. I wonder how we could get together with the people here, maybe with NTSB and maybe decide on what should go into such training and how we should bring it about.

DICK BAKER, NTSB: Well, I second the motion. I'm sure we all need it, especially in our field, we will need it.

BACKGROUND COMMENT: "Don't forget the Navy, too..."

SAM DASTIN, GRUMMAN AIRCRAFT COMPANY: (edited) I'd like to make a comment on that. I think you bring up a very interesting and very important point. I say, in addition to studying the fracture at 2000 x, we ought to be able to learn significant information at "one x". I believe that when you are looking at a structure measured in feet, the prime issue is to define the "hot spot", using "one x". But since large composites can distribute loads differently and better than a small coupon, there is a danger in using high magnification too early in the post failure analysis investigation. I think you have to provide some history to the folks in the field, using "one x", i.e. some way to characterize a major load in compression or tension. I think that would be helpful to the field person.

JOE TILSON, AIR FORCE SAFETY OFFICE, NORTON AIR FORCE BASE, CALIFORNIA: I'd like to make a comment at this time. Back in 1975 I drafted a letter which was signed by the Air Force Director of Safety to Mr. Chuck Tiffany back here at Wright-Patterson. In essence, the letter said, "The system program offices are developing and implementing composite materials, at a rather high rate. But out there in the field, our investigators don't know how to work with them, our maintainers don't know how to maintain them and our NDI people don't know how to NDI them. But they're coming out in the aircraft. Can you give us some guidelines to go by whereby our investigators can help run some of this down, and find out whether it was a design failure, a manufacturing failure, a maintenance failure, or just plain abuse?" Several people here, NTSB people, FAA people, have expressed concern, as I have, too...I am a stress analyst, and I'm concerned about the big picture, too. The first thing we do on a mishap investigation, when we get the accident investigation board out there, is to tell them to keep their hands off the wreckage. Walk around it, spend a couple of hours digesting it, look at it at "one x", and give it a little time before you start getting into the micro level and start messing up the evidence. We're going to work very hard and I'm very relieved to see this conference come off as successfully as it has. When I talked to Frank Fechek some time back, I was delighted to see what was going on here. To the best of my knowledge, this is the first time anybody has tried to have a conference on this subject, and it takes a little guts to stand up there and say, "Well, I've done this work and this is what I think I see". I haven't seen any evidence that the stress analyst was being left out. I haven't seen any evidence that the fractographer was making all the decisions, either. It looks to me like we're building a straw man at this point, and any help that we can get out there would be greatly appreciated. When I review a mishap report that comes through the Air Force

Center for final approval, I'm not for one minute going to stand still and figure that some fractographer has pronounced the failure as stress overload, or fatigue or stress corrosion cracking, or some such thing as that. So we're going to expect to see all of the technical disciplines that the Air Force has at its disposal brought into play. I am relieved to see this first meeting kick off like this, and I want to maintain, for the Air Force Safety Center, a close liason with the folks back here at Wright-Patterson to make sure that we're delivering tangible material to the field. We publish, at Norton Air Force Base "Flying Safety Magazine", "Maintenance Magazine", and "Inspector General Briefs". I have access to all of those publications. If you have any messages you want to get to those people, the maintenance folks, the managers, through the Inspector General Briefs, the operators through Flying Safety Magazine...if you want to write an article and get it published and tell somebody what to do and what not to do, about these materials, contact me. If you have an idea you want to express and don't feel like writing the article, contact me. We'll write the article and review it with you and we will publish it. My job will certainly be to see that the investigator out there in the field gets as much tangible material that he can hang his hat on as possible, and that he doesn't destroy the evidence before it gets to you, you the people in the laboratory. But, as a stress analyst, I certainly am not going to stand still and see the stress people left out of the picture. Thank you.

TED REINHART: Before the next comment, let me bring up something else that has been bothering me. I know that there are a lot of other societies and organizations involved in this kind of work. I understand that there was a D-30 meeting in Houston, Texas. My comment here is that, "What is the thinking here of maybe putting together a steering group or a blue ribbon panel to help guide the Army, Navy and Air Force and maybe the NTSB and NASA, on what our activities should be in the area, or maybe the area really should be given over to ASTM? "I think we're open to all kinds of thought here, and I'm not sure which is the best way to go, if there is a best way to go. So, let me throw that out for some thought and some future comment.

BERT CHESTERFIELD, DEPARTMENT OF TRANSPORTATION: We have in Oklahoma City the Accident Investigation school that many NTSB and most FAA people attend. I put a few copies of our catalog out there and I see that some of you have seen it. I'll mail you copies of that catalog if you did not get a copy. But to address the question that George Baker and a couple of other people brought up, concerning training, at the Transportation Safety Institute, that is the name of the unit that I work in and I am the program manager for, the Aviation Safety Program, we have a couple of things we are working on. Mike Cervilli, with Bell Helicopter, came with us to develop a special helicopter course in which we hope to have four hours...maybe eight hours, of composite aircraft investigation technology taught in that course. We presently teach an hour in our course. It is just scratching the surface and we are neophites in this area so I am happy to attend this conference. I have talked to Brian Smith from Boeing and Patricia Stumpff from the Materials Laboratory and have a lot of ideas. If I haven't talked to you, I encourage you to contact me and I'll let you know more about our school. There are some things going on in the training area. We're gearing up to teach this. If you are interested, I would love to hear from you. Thank you.

UNIDENTIFIED SPEAKER: I was expecting to see a bit more on materials characterzation. You know, a lot of failures that occur out in the field are not necessarily due to stress. They are due to something being wrong with the material. I come from the metals end of things, and this happens quite often in metals. It is heat treated wrong, stress corrosion cracking, there are a lot of things that can go wrong. I guess that Brian touched on it a little bit, with talking about DSC, and Ramish Kar had a lot of techniques listed for doing materials characterization of a failed part. But, perhaps nobody submitted papers, regarding how to do a DSC to see an undercure, for example...I have heard some comments around here about a micro-micro hardness tester that you mount inside a scanning electron microscope so you can do hardness, say, on a scale of a couple microns in size. So, with that I'll just comment that, if I had a negative comment, it would be that the focus was a little narrow on fractography and probably a bit more was needed on materials. Otherwise, I'd say I learned a lot about fractography in composites.

FRANK FECHEK, AFWAL: Well, to respond to your comments about other methods, maybe one thing that Brian did not bring out strongly enough was that he has done some work on assessing the applicability of various techniques and methods and procedures and processes that could be used in composites. He evaluated them for their potential for giving good data, high, medium or low, and we have instructed him not to develop new procedures and processes, or test techniques, but to only define the usefulness of those already existing methods and techniques. We have directed him not to attempt to develop new procedures and processes, over the broad range, but certainly to give us an assessment of existing ones' potential so that we could see if there are any deficiencies--some are critical and some are not. Given that those which are developed, say it is the wet chemistry technique, then users of his compendium would be able to go to the source of that development and bring themselves up to proficiency in it. So, his charter, by us, is to give us a stepping stone and a plan, and a basis, for entering into running an analysis. I realized when we put this meeting together that we could not deliver, especially to the people out in the field, a cookbook which would say, "here's what to do, and you will have the answer", because we don't have that information. Someone earlier today asked me, "Why don't you tell the people how to package a failed component, i.e. what to do when you go out to a 'smoking hole'?" I couldn't tell them, I would just be creating an answer out of the blue sky, because I don't know if you should package it in an inert atmosphere, I don't know if you want to package it in foam, how much abrasion will affect it, other than a wire brush, and part of the basics which Brian is doing, is to find out the effect of the environment on what causes fracture, but also, on the fracture surface after it has been sitting around so that you can make a documented, recommendation of what we found and where it came from. We are trying to put building blocks together in this program. I don't know if that answered your question, because I rambled a bit.

SAM DASTIN, GRUMMAN AIRCRAFT COMPANY: (edited) What is coming out now is what I tried to say in my elegant manner, and couldn't. There is a lot of reaction, that I see here, that this is the only composite activity in the free world. Let me tell you that advanced composite structures are on our twentith year, and the R and D expenditures over that period have been considerable. And, this work has generated considerable experience.

TED REINHART: Thanks Sam. I wanted to say that that previous gentleman's comment was very perceptive. The conference, by design, did not get into the analytical portion, because we thought we had enough for two and one half days, and we don't want to keep people here for three days. The second thing is, we have been in close touch with Ramesh and a whole lot of the rest of the industry, along with our own analytical group, and they felt very confident that the techniques and equipment exist to pin down the exact chemical composition of the resin, just like we do in metals, and, if there is any microstructure, that is what we wanted to look at here. So, that was by design, not without any forethought.

FRANK ROAN, GENERAL ELECTRIC, LYNN, MA: We are an engine manufacturer. I think it has been a very interesting seminar. Basically, I am a metalurgist by trade and also do a lot of failure analyses. I think my personal opinion is that this symposium, or this community, or this conference is in some sort of growing pain. As I can see it, there is tremendous interest, at least from our point, to know, or to understand, how to handle the failure analysis of composite parts. I think a lot of the people here share the same general feeling. I would say, also, that what Boeing is doing is pretty good. I think we have to establish some basic rules, some basic knowledge about this phenomenon. But, also I share the same feeling as Sam, maybe we are not going quick enough, going fast enough, doing as much as we should. We should be doing something more than we are doing. I think my specific comment is, "The problem is we have to broaden the representation from this industry". For example, chemistry. I seem to sense a missing link, in the materials and processing, and chemical part of it. Now, for example, if I have a failed part and that was due to contamination in handling, or probably the bagging material was not removed during the curing process, and we have the parts open up, and I am not sure what the fractographer would tell me. It is a material and chemistry problem. The question is what tools do I have available today, to tell me now, this is because of contamination, oil or whatever? But what do we do in terms of materials and processing? I see that failure analysis is more than just fractography and we have to address more of these types of issues. I heard mentioned by Northrop about the "ESGAR" (unintelligible), about FTIRs, and some other chemical analizer. Those are useful tools to the metallurgical community. But, I wonder if those tools will still be applicable to the composite failure analysis or not? I think that that question will have to be addressed by this community. Thank you.

BRIAN SMITH, BOEING: (edited) I would like to respond to that. I showed a framework that we use at Boeing, a general one. One of the things which I haven't shown, but Frank has gotten in a couple of monthly reports on, are framework diagrams which say, "What do you see, fractographically, that makes you suspect a contaminent?" What are the logical steps and analysis techniques to go through? Due to time, we didn't bring them out today. I guess I agree with you, we had an experience where we cleaned the surface prior to bonding, with MEK, and it turned out that the bottle of MEK had freecoat release agent in it. Upon drilling, the parts fell apart. I, fortunately was involved in this post failure analysis, and using ESKA, identified the problem. So, I'm keenly aware of that kind of problem and we are going to try to incorporate that type of information in the program, with a flowchart of how you go about a chemical analysis.

LEONARD JOHN, DEHAVILLAND AIRCRAFT OF CANADA: (edited) Although a lot of the current work is military application driven, the technology will find its way into the commerical sector. This sector not only has to respond to FAA 20-107A, but those U.K. and European requirements also. Although there are currently some attempts to standardize these requirements, there remain many areas where the required testing is very different. Since we are a relatively small company, and also considered as a foreign source, detailed information exchange becomes complicated. In some instances, these regulations are tending toward involved testing (i.e. hot/wet, then much fatigue, then limit load, then impact, then more fatigue, etc.) because of a lack of understanding of the basic failure mechanisms or the interaction of environmental effects with residual properties. If more of these environments could be incorporated, now, in this area, it would save the industry a lot of testing in future years.

TED REINHART, AFWAL: (edited) Yes, your comment is appreciated. Yes, we are from the Air Force and we are more interested in Air Force problems than we are in civil problems. In planning this meeting, we talked to the NASA people in depth, and we asked for a strong NASA participation, because we knew this question would arise. We were only able to get participation from NASA Langley and NASA Lewis.

TOM COOPER, AFWAL: I'd like to make one comment here before we go on to the next question. Since Sam has raised an issue which seems to be coming up again and again, maybe we ought to have a few comments about just what the function and what the role of a failure analysis group is, and just what role they should play in our technology. We have been involved in conducting failure analyses for the Air Force for a long time, more than twenty years, Sam, more than whenever composites were first considered. And I got the impression, and I hope I am wrong, but I got the impression that the failure analysis group at Grumman is a very potent group that really controls final decisions to ground airplanes. Well, I want to assure you that it is not that way in the Air Force.

SAM DASTIN, GRUMMAN AIRCRAFT COMPANY: I said the reverse, it is the structural analysts who ground the airplane.

TOM COOPER, AFWAL: I guess that is not the impression that we have gotten. I think that we ought to point out that a failure analysis group is merely a service group. When we do a failure analysis, we normally are doing it for someone at their request. Normally, in the Air Force, we conduct a failure analysis at the request of a specific accident investigation board who has had a problem. Sometimes it is a SPO, sometimes a Depot, if it is not an aircraft crash. But our role, and our function, and what I constantly emphasize to my people is, we are only a small part of that team. We don't have access to all the information, all the background, that is relative to that failure, and therefore, let us not speculate. Let us provide that board what we can technologically say is our interpretation of what we see, based upon the evidence as presented to us, and that is as far as we go. There are stress analysts, there are people who look at what the pilot ate the night before,what kind of fuel they put on the airplane, and what the weather was, and all those other factors, that all have to be brought together by somebody else, a board president, before he decides, we DO NOT...repeat...DO NOT, make the final decision. And I have heard some misunderstandings about that....

SAM DASTIN: That is exactly what I was saying.

TOM COOPER: You were saying just the opposite, at least, I thought you were saying just the opposite.

SAM DASTIN: Oh no!!! I must be "dumb-like"!

TOM COOPER: Well, the other thing is, I have not heard any comments that this group ought to attempt to take over composite technology in the country, that is not the purpose of the meeting.

SAM DASTIN: No, but it sounded that way. Because everyone is inventive, and they are inventing "ghosts" and the "ghosts" are holding back this business... the "ghosts, beware the "ghosts"....

TOM COOPER: I think they'll get the "ghosts" out of the system, but they have to start somewhere, though, that is the point I want to make.

SAM DASTIN: (edited) Oh, I have to add something else about my company...It is not only the stress office, it's the stress office on the program, and you're allowed to have differences of opinion, and the last point, maybe you didn't hear, negotiation...between the fractographer and the analysis person, and similar with the regulating agency or customer. It's a fight, a big fight, and I'm not even bringing in the lawyers. OK? This is without the lawyers. All I was trying to tell Ted and Frank is that, in addition to getting the fundamental information, since failure occurs in structures under complex conditions at the "hot spots"--as the structural analyst knows. So, have the failure analyst go to the stress analyst and ask him "what makes the margin 30% instead of 5%", so he can better understand and we can then move the industry along. That's the part I am saying was missing. I'm saying, "We have to bring that up fast".

TOM COOPER: We are all in agreement now that the failure analyst is a member of a team and, now, let's put that issue to rest.

TED REINHART: Sam, thank you. Let me pose a question to the audience. It was alluded that the Air Force was going to have a follow-up program. That is exactly true, we do have funding for a FY-86 program to do something more in this area. We are leaning toward the idea that maybe we are ready to put together what we would call an official handbook. Frank Fechek has some serious questions as to whether the technology is ready. I'd like to ask some of the people in the audience to comment on this specifically. Because one of the things we wanted out of this conference was some direction to help us spend intelligently our fiscal year 86 dollars.

DICK ROBERTSON, FORD RESEARCH CENTER: Well, I'm standing here, so I might as well comment on that. I think that it may be a bit premature. What I was going to say earlier, that is my reason for standing here, was to say, the most important thing, perhaps, that the Air Force can do, is what it has done in having

this meeting. Obviously, we've all come with our preconceived notions, and it takes more than two days, or three days, to change them. But, you can be sure, that I, perhaps representing the furtherest from reality, am considerably influenced by this rubbing shoulders with people on the other side. And so, I never will think quite the same thoughts as I did before I came and expressed my prepared remarks. Let me say that the fundamental side has had a problem. I have worked in fractography of composite materials for half a dozen years. There has never really been an ongoing opportunity to exchange ideas. This exchange of ideas that we have had here this last two or three days is almost a first. Several years ago, John Masters tried to put in a tag-along session on fractography of composites with the ASTM. It fizzled. Nobody was interested, it never occurred. Five years ago, or so, at a national ASM meeting in Cincinnati, they tried to do something with nonmetallics. We put together a sysmposium, got everybody we could find, there were three or four of us, the thing fizzled. There was never a recall, never an attempt to put together something like that again. I am speaking this year at the American Physical Society, I will speak again this fall at the American Chemical Society. These are singular symposia, these are never repeating symposia. People who happen to be in the country at the time, they exchange ideas, then they go away and then nothing ever is said. So in addition to the interchange of ideas between people on different aspects of a failure that this meeting has allowed, it has also allowed this exchange of controversy on the fundamental side, and, honestly, I don't think you can really understand failure at the eyeball level if you don't understand it at the fundamental level.

BILL BASCOM, HERCULES, INC. MAGNA, UTAH: I would like to respond to Ted's question. I don't think we have done enough work, at least that is the impression I got from this conference, to be writing a handbook, or compendium. Most of the work that has been done that I have seen that we have done is, we will look at broken surfaces and look at river markings and other things. There are other techniques, one of which we tried to talk about on Monday, and that is of slicing and microscopy. There are sophisticated accoustic techniques to examine damage, and I'm sure that there are many others that I cannot think of standing up here. I am sure that there are a lot of techniques that could be brought to bear on this problem, yet to be funded, yet to be looked into, and when put into combination, offer a stable of tools for the fractographer. I don't think we have established that stable fully yet. I'd like to make a philosophical comment: My experience with metals is extremely limited. I know that when I was at NRL, there was a man named Beech. He spent his career funded by the Navy, looking at fractured metal surfaces, much in the same way as we're doing here. When the SEM came out, he thought he had gone to heaven. But he established an enormous background over a period of more than fifteen years of what a fracture surface looks like and the things that you can look for. That's one side of what I see as a dichotomy. The other side is a gentleman I met at Cranfield Institute in England. He had a large room, in which he had piles of broken bits from Britrail and other companies. His job was to look at these and decide how they failed. He did this, not because he was a stress analyst, or because he was a physist. He was clever at doing this simply from shear experience. He had done it for years, and years, and years. How you fund, or how you generate that kind of individual, or individuals, for the composites industry, I do not know. I think, eventually, that is where we have to come out. We have to come out with people who have enough experience, and enough intuitive wisdom to look at a fracture or failure and say, "I think this is what happened", then go to the stress analyst, then to the ESKA people, then somewhere else to confirm it all. I think you have to get individuals who have an intuitive

sense of how things break, specializing in composites, or polymers. How you develop these people, other than by evolution, I don't know. Thank you.

JOE TILSON, AIR FORCE SAFETY OFFICE: I'd like to comment on that. I agree with you in principle, but I was really relieved to hear that they were going to attempt to publish a handbook. Relieved from the standpoint that I represent Air Force Safety. There are thousands, thousands of aircraft out there flying today, with people's lives depending upon them, with materials which are pretty much a mystery to us. I'm relieved that, this document, whether it is any good or not, will be attempted. The first publication of this document is going to be a strawman that the Reinharts and the Dastins and the Tilsons can all take a shot at. You know, there are three things you can do, the right thing, the wrong thing, and nothing at all. The right thing, that is easy. The wrong thing, and fifty thousand people stand up and tell you, "Hey, you are doing the wrong thing"!! Then you are going to turn around and do the right thing. The worst is to do nothing at all. So, at the risk of publishing a bad document, we are going to get a lot of shots taken at that thing, and maybe in the process, we will awaken some other people in the community, and the Air Force Commanders will stop believing, "Oh, we have solved all our fatigue problems, now that we have composites and we will never have fatigue problems again". There are an awful lot of commanders out there who do not understand how grey this area really is. I'm relieved to see something get on paper that everybody else can take a shot at, whether it is good or not. (Applause).

BRIAN SMITH, BOEING AIRCRAFT COMPANY: You stole my words....

TED REINHART: Let me interrupt you, Brian. I want to take issue with what Bill said, also, by stating that Boeing has really reduced a lot of this to practice. Northrop has, and I know that there are people overseas, Dornier and MBB, who have also reduced this to practice within their community. The name of the game, Bill, like Joe said, is to reduce technology to practice and get something out in the field. Excuse me, Brian, please go ahead.

BRIAN SMITH: At Boeing we have successfully analyzed quite a few parts and I guess the proof of the pudding is the fact that we have been able to go back and retest parts and remedy the problem successfully. To hold back that technology from the people in the field at this point, seems a little bit foolish, in my estimation. I realize that if we put out a compendium or handbook (worse?), we are building a strawman but, I think the important thing is it is going to become a forum for improved technologies and discussions, and this is really the mechanism which was used in metals in the last thirty years, to end up with volume ten of the ASM handbook or the metals fractography handbook. From that standpoint, either a compendium or handbook is important. I'm not sure what the Air Force sees which one is going to go out and become the handbook, or this forum. I would like to have some thought from them on that. The other thing, as far as that handbook goes, is, a lot of people have talked about fatigue and other things. In our current program, we are only doing a "walk-before-you-run" study. We are trying to find the origins, locate the modes, and if you really look where metal technology is, and you can do striation counts, and all those great things, then we're really still in the infancy stages. So, in a follow-on program, the areas that I see we really need to look at, perhaps harder, are,

some fatigue, and some fatigue spectrum work. I hope that this program that I've got will get us far enough that we can start that.

The other thing is wreckage analysis. In our program we haven't really addressed that, and of course, the third area, which has been brought up pretty extensively, is stress analysis.

GEORGE SENDECKYJ, AFWAL/FDL (edited) As I remember it, John Masters, in conjunction with ASTM D-30, a few years ago, sent out a survey requesting people to send in typical fractographs of composite failures, along with as much information on their loading, etc., when they were formed. He got a mixed response from government and industry, with some responses and some nonparticipation, and the project sort of expired due to a lack of continuing interest. ASTM has continued, however, to include this topic in their conferences, and, for example, has a meeting scheduled in Nashville, TN in November which is sponsored by ASTM F-8, the fractography group, and D-30. This history strikes at a very important problem in the whole area, i.e. the lack of the communication of the technology. It seems we are now repeating work which was done ten and fifteen years ago. Maybe it is important to do it over again because we know a little more about failure origins investigation for a laminate has been around, in a lot of companies, for the last ten years or so. Not acknowledging that work at this meeting is doing a disservice to the accident investigation people, I think by giving them the impression that the field for failure analysis of composites is in its infancy. I have not seen anything surprisingly new except maybe the data at elevated temperature and after moisture conditioning.

TOM COOPER, AFWAL/MLSA: George, I agree with the impression that people may have gotten from what has happened at this conference. You may recall that, back in the middle seventies, we went out on a program, specifically, to produce a handbook of composite fractography, and we had a contract with General Dynamics. We were not in that contract very long before we realized that the state of the art just wasn't ready for that. John Masters was the person who ended up with the program. We gave it what I would call a good shot at the time and, I guess what we have to now accept is that it is still an evolving technology. We gave it a try and we just weren't ready for it. So, I see what is happening now is that we are not ignoring what happened in the past. It looks to me like the efforts are being revitalized, and for a lot of good reasons. I don't think that anyone wants to, in any way, shape, or form suggest that things haven't been done over the years and put down the people that did it at all.

GEORGE SENDECKYJ: You have been around in the field and you know the background. There are a lot of people here, in this audience, who don't know what has been done in the past. I would suggest that they find out what's been around and don't rediscover the wheel.

FRANK FECHEK, AFWAL/MLSE: My response to that, George, is, we did find out what was around, and those people had the opportunity to bid and compete for our program. But the point that is important to me is; if there are several experts, or capabilities, in this country, and they are all on an airplane coming to this conference, for example, and it crashes, then, without any documentation, teaching

procedures, or a way to pass this information on and expand it to other practitioners, then we don't have a technology. I believe you cannot have something, and use it, unless it is available, reproducible, and communicable. A few people with the wisdom of a lot of experience, which is not documented and transferrable, is impractical, in my viewpoint.

TED REINHART: I would like to make another comment. You know, our thrust in this meeting was not in trying to analyze composites that have seen gross structural overload that you get in a crash, but more the kind of service and test problems that Brian and Ramesh talked about. When something crashes and you have a big pile of straw out there, that is a tough job. That is something we decided not to attack here. But our direction here is, how we analyze a part, how we feed that back to the designer, how it gets improved, and the interaction that Sam was talking about. That was really the thrust of this meeting, as opposed to the field accident investigation.

SPEAKER UNIDENTIFIED: Aren't we mature enough to bring this down to the practical level that the accident investigator can start to use it? At least to know when to call a specialist...when to ask for the services of those of you who are in the research and scientific community who have these valuable techniques. Up to now, we haven't spread the word to the field investigator, the investigation community, the NTSB, the FAA, the Air Force, the Navy... I think the field investigators are out there groping in the dark because they don't know that these services are available. If we've matured that far, let us get the word back out to those people who kick the tin..or the fibers, or whatever... the resin kickers. It looks like to me maybe we are mature enough to divide this august body into two groups, the research scientists who are doing things at the five thousand magnification, and the rest of us that are out there, kicking the resin. Maybe, in your FY-86 program, Frank, you could take some of your funds and put on a seminar for the FAA people, and the NTSB people, and the Navy people, and the Air Force people, and bring them together in a group and discuss the practical aspects. For example, the FAA advisory circular 20-107 is badly in need of revision. We need to get some of these words out to some of these authors, the people responsible for rewritng that advisory circular. But, they are not in attendance here today. Are we not mature enough to divide this group up and have two seminars next year? And make one a very practical seminar?

BRIAN SMITH: Maybe it should be a combined seminar, I'm not really sure...

SAME UNIDENTIFIED SPEAKER: Well, I thought this was going to be a combined seminar, and we are outnumbered, two or three to one, here.

BRIAN SMITH: (edited) I agree. Another thing I wanted to comment on is, one of the things that really forced us at Boeing to push our technology was the fact that we have had our planes flying, and, all of a sudden, we started having hardware come back. By having people out there like the FAA or the NTSB start to take part and send the parts back in, we are going to actually force people in industry to come up with a fracture analysis technology. What I have seen in some other companies that don't have a product, or that they are not pushing a

product, is that they fail a component of a panel in test, they are not flying it, so the requirement to identify the cause is not as great as what we have in Boeing. If a part fails, you have to believe that we are going to put in two or three months of effort in finding out why it failed..er, fractured, excuse me... (laughter). Oh boy, no Boeing guys left here??? (at Boeing, we use only the word "fracture"). So, to that extent, I think it is a good idea to start to get people, the users of the parts, who have broken parts, involved in this, and, maybe get the information disseminated so we can start to force ourselves to deal with the problem, rather than wait and do more academic studies.

JOHN MEININGER, McCLELLAN AIR FORCE BASE: I am a metallurgist in our failure analysis group at McClellan and, it is occuring to me from coming here that a lot of people who are involved are people with a metallurgical background. If we are going to work toward the final product of a handbook, what I would like to see, coming from my own background, is, what are the sorts of things which can go wrong when you are building composites? Obviously, Brian has talked about some of these, but I would really like to see some emphasis placed on that. I have some intuitive, gut level feelings about that with metals, but I don't have any sort of comparable feelings with composites.

WARREN WANDEL, NTSB: I had originally addressed the question about field recognition, field investigation techniques to Brian during his talk, and I think we have pretty much beat it to death. On reconsideration of my question, I'm not sure, that this is the community, or the forum, for the development of those techniques. I think we have people here, who could be very actively involved in another level forum, the field investigators from the military safety centers, from the ALC's, from our organization, from the FAA, from airframe manufacturers, who have their own investigators. I think we should probably try to communicate among ourselves. Now, we have limited knowledge in composite structures, we have limited exposure, at this point. The Army, Navy and Air Force are gaining more knowledge every day from each accident that they do in composite structures. Yet, individually, we don't have any knowledge. Collectively, if we could get ourselves together and sit down and review what knowledge we do have, perhaps, then that would be the step toward developing the methodology. Once we do that, then bring that methodology to this forum, and have it confirmed.

WILLIAM FEENEY, GRUMMAN AIRCRAFT COMPANY: I'm a fractographer at Grumman. This meeting has really hit home. It has addressed the needs that I had, as a metallurgist, 15 to 18 years in metals fractography and failures. When you get to the SEM, and you try to understand what you are looking at, there have really been tremendous roadblocks, and (unintelligible) is really going to be helpful. There are other people, certainly the stress people, that have other problems, and have other forums. But the metals handbook created by McDonnell Douglas proved, in the long run, to be really helpful. I am sure that, Boeing trying to create this work right now in fractography, is going to be very useful, especially if the fatigue area starts to be emphasized, because that could be the real problem. The basic work has been done and I'm sure that this meeting, with the focus on the fractographer, that that problem can be licked. And, somebody else can have a forum for Sam's problem...Sam has a significant problem.

UNIDENTIFIED SPEAKER: We at the Army depots feel like we're almost at the end of the communication pipeline, as far as technology is concerned. We feel like the only people below us is the user out in the field. I'm a chemist by my background, so I'm going to sound a little bit biased. But, I see ASM going more and more into composites and I ask, why are the metals folks going into organics? It just seems strange. Of course, I'm always telling our metallurgists that we're going to put them out of business. So, apparently they have decided to join us, but to go through their own organizations. But I really feel that with SAMPE, the SAE, ASM--that you've got too many of these various organizations. Where are we going to put information? How do I know who is going to cover the particular topic I need, and in what journal? And, then, as for symposia..we're production facilities, and they are not going to let us go to these academic symposia. But I think that we really need to define where the channel of communciation is going to be, so that the user will know where to look, instead of having it scattered over the various societies.

TOM COOPER, AFWAL: I have to respond to his comments about ASM and its forays into various areas. The reason I feel an obligation to respond is I am currently chairman of the handbook committee for ASM. As some of you may or may not know, the Board of Directors of the American Society for Metals, within the last couple of years, has made a firm decision that the society will expand into all engineered materials. And, in fact, for years and years, ASM has had the trademark on "American Society for Materials". So it is a fact that ASM is going to expand its horizons into organic materials, and in fact, as part of that activity, the handbook committee is already stepping out briskly. We are going to publish the metals handbook, which we are in the ninth edition now. It will be composed of seventeen volumes. Then we will start the tenth edition. We made a decision some time ago, and have recently implemented an action, to establish a series of handbooks called engineered materials. The first volume will be on composites. Ted Reinhart has accepted the job of serving as orgnaizer for that handbook. We had a meeting in Denver last week of a number of leaders in the composites business, to help get that started. I think it is off to a great start. We have a target date of November, 1987 to publish that handbook. One of the things that ASM is really good at is publishing good technical documents. And so, if we get the right technical leadership from the industry, the document will be an excellent one. We have the right kind of people in this activity, and I just mentioned to Ted that he has to include in his handbook volume a chapter on fractography.

FRANK FECHEK, SESSION CHAIRMAN, AFWAL/MLSE: And with that, I want to express my thanks and appreciation, and I know that I speak also for the Air force Wright Aeronautical Laboratories, for your attendance and very alert and active participation in this, the First International Conference: Post Failure Analysis of Fiber Reinforced Composites. This meeting is hereby adjourned. Thank you.